Vol. 173, July 1, 1985
Complete in one issue

ISSN 0003-2670

ANALYTICA CHIMICA ACTA

International journal devoted to all branches of analytical chemistry

ELSEVIER

ANALYTICA CHIMICA ACTA

International journal devoted to all branches of analytical chemistry
Revue internationale consacrée à tous les domaines de la chimie analytique
Internationale Zeitschrift für alle Gebiete der analytischen Chemie

PUBLICATION SCHEDULE FOR 1985

	J	F	M	A	M	J	J	A	S	O	N	D
Analytica Chimica Acta	167	168	169	170/1 170/2	171	172	173	174	175	176	177	178

Scope. *Analytica Chimica Acta* publishes original papers, short communications, and reviews dealing with eve aspect of modern chemical analysis both fundamental and applied.

Submission of Papers. Manuscripts (three copies) should be submitted as designated below for rapid and efficie handling:

Papers from the Americas to: Professor Harry L. Pardue, Department of Chemistry, Purdue University, West Lafayett IN 47907, U.S.A.

Papers from all other countries to: Dr. A. M. G. Macdonald, Department of Chemistry, The University, P.O. Box 36 Birmingham B15 2TT, England. Papers dealing particularly with computer techniques to: Professor J. T. Cler Universität Bern, Pharmazeutisches Institut, Baltzerstrasse 5, CH-3012 Bern, Switzerland.

Submission of an article is understood to imply that the article is original and unpublished and is not being considere for publication elsewhere. Upon acceptance of an article by the journal, authors will be asked to transfer the copyrig of the article to the publisher. This transfer will ensure the widest possible dissemination of information.

Information for Authors. Papers in English, French and German are published. There are no page charge Manuscripts should conform in layout and style to the papers published in this Volume. Authors should consu Vol. 170 for detailed information. Reprints of this information are available from the Editors or from: Elsevier Editori Services Ltd., Mayfield House, 256 Banbury Road, Oxford OX2 7DH (Great Britain).

Reprints. Fifty reprints will be supplied free of charge. Additional reprints (minimum 100) can be ordered. An ord form containing price quotations will be sent to the authors together with the proofs of their article.

Advertisements. Advertisement rates are available from the publisher.

Subscriptions. Subscriptions should be sent to: Elsevier Science Publishers B.V., Journals Department, P.O. Bo 211, 1000 AE Amsterdam, The Netherlands. Tel: 5803 911, Telex: 18582.

Publication. *Analytica Chimica Acta* appears in 12 volumes in 1985. The subscription for 1985 (Vols. 167–178) Dfl. 2400.00 plus Dfl. 264.00 (p.p.h.) (total approx. US $986.70). All earlier volumes (Vols. 1–166) except Vols. 2 and 28 are available at Dfl. 215.00 (US $79.60), plus Dfl. 15.00 (US $5.60) p.p.h., per volume.

Our p.p.h. (postage, packing and handling) charge includes surface delivery of all issues, except to subscribers in th U.S.A., Canada, Japan, Australia, New Zealand, P.R. China, India, Israel, South Africa, Malaysia, Singapore, Sou Korea, Taiwan, Pakistan, Hong Kong and Brazil who receive all issues by air delivery (S.A.L. — Surface Air Lifted) no extra cost. For the rest of the world, airmail and S.A.L. charges are available upon request.

Claims for issues not received should be made within three months of publication of the issues. If not they cannot b honoured free of charge.

For further information, or a free sample copy of this or any other Elsevier Science Publishers journal, readers in th U.S.A. and Canada can contact the following address: Elsevier Science Publishing Co. Inc., Journal Informatic Center, 52 Vanderbilt Avenue, New York, NY 10017, U.S.A., Tel: (212) 916-1250.

ANALYTICA CHIMICA ACTA
VOL. 173 (1985)

ANALYTICA CHIMICA ACTA

International journal devoted to all branches of analytical chemistry

ELSEVIER Amsterdam–Oxford–New York–Tokyo

Anal. Chim. Acta, Vol. 173 (1985)

0003-2670/85/$03.30

Printed in The Netherlands

Analytica Chimica Acta, 173 (1985) 1
Elsevier Science Publishers B.V., Amsterdam — Printed in The Netherlands

Editorial

As a new service to its readers, *Analytica Chimica Acta* will implement a new section:

Software Available from Authors.

As the name implies, the section will give authors of computer programs the opportunity to announce software that they are willing to share with their colleagues. The program descriptions will be very short, giving only the title and purpose of the program, the hardware requirements, the exchange media offered, and the name and address of the author to be contacted. Anyone interested in a particular program must contact the author named directly to obtain further information about the program and the mode of exchange. Letters sent to the editors or to the publisher will **not** be forwarded.

The programs included in this section will not be refereed in any way, and neither the publisher nor the editors will take any responsibility for the software offered. Anyone interested in placing program announcements in this new section should write to J. T. Clerc (address on inside cover) who will provide a standard entry form to be filled in.

The editors of *Analytica Chimica Acta* hope that this new service will give authors of programs an easy way to disseminate information about the software that they have available, and will allow analytical chemists to avoid unnecessary programming efforts by gaining access to programs already developed elsewhere.

J. T. Clerc

Analytica Chimica Acta, 173 (1985) 3—21
Elsevier Science Publishers B.V., Amsterdam — Printed in The Netherlands

OPTOSENSING AT ACTIVE SURFACES - A NEW DETECTION PRINCIPLE IN FLOW INJECTION ANALYSIS

JAROMIR RŮŽIČKA and ELO H. HANSEN

Chemistry Department A, Technical University of Denmark, Building 207, DK-2800 Lyngby (Denmark)

(Received 10th February 1985)

SUMMARY

Reflectance spectrophotometry is applied to flow-injection measurements of pH and the assays of ammonia and urea with the aim of demonstrating the principle and testing the performance of optosensors integrated into microconduits. A novel injection approach, the split-loop technique, is applied. For pH measurements, detection is based on commercial non-bleeding acid-base indicator papers situated in the flow stream at the tip of the fibre optic. Measurements of pH in the range 4—10 are possible at a rate of 120 h^{-1}. Special attention is given to the physiological pH range; the standard deviation is 0.004 at pH 7.2. For the determinations of ammonia and urea (via urease), a bromothymol blue stream is used with a miniature gas-diffusion device.

When the development of flow injection analysis (f.i.a.) over the last ten years is reviewed, several patterns emerge, the trend towards miniaturization and the introduction of new flow-through detectors being the most striking. While the first flow-injection system [1] used more than 10 ml of reagent and 0.5 ml of sample for a single measurement, the contemporary integrated systems require ten to twenty times smaller volumes of solutions yet yield more reproducible results [2]. This advance has been achieved through integration of detectors into the manifolds for f.i.a.; it has become feasible to place the detector exactly into that section of the flow channel where dispersion of the sample zone is optimal to suit best the requirements of the intended assay. Because conventional flow-through detectors are far too bulky to be integrated into flow-injection microchannels, the existing detection techniques have had to be modified by using optical fibres or miniaturized electrodes [2].

The present work is a step further in this direction. A novel group of detectors, based on interaction of radiation with a surface situated in a flowing stream is introduced. Such optosensors will exploit absorbance, reflectance, or fluorescence of visible and/or u.v. light as it is changed by chemical reactions taking place at, or in close proximity to, a surface surrounded by a flowing solution. This surface may be a solid fibrous structure, a diffusion membrane, a gas-permeable membrane, an ion exchanger, or a

0003-2670/85/$03.30

water-immiscible liquid. These materials may contain covalently-bound reagent(s) and associated dyes, which by changing colour or fluorescence intensity allow optosensing of the chemical reactions that occur. The flow of solutions through the cell serves two purposes: to transport the sample zone through the detector in the f.i.a. mode, and to renew the reagents which cannot be immobilized within the optosensor. For both these purposes, the flow of solutions may be continuous, or intermittent, depending on the desired mode (e.g., stopped-flow for kinetic measurements) and on the desired reagent economy.

Flow-through optosensors based on the above principles will allow miniaturization of the great majority of assays which utilize colorimetric reagents and enzymes. Those reagents that cannot be immobilized or are not reversible, can be replenished within the optosensor by intermittent pumping of microlitre volumes. Assays that rely on separation processes, like dialysis, gas diffusion, ion exchange and liquid-liquid extraction, can be miniaturized and executed within the optosensor. On-line preconcentration within a small volume of a suitable reagent located in the flow-through optosensor will allow a substantial increase in sensitivity of measurements based on the above technique. Clearly, such a wide range of possibilities will have to be examined gradually and carefully. It is therefore intended to do so and to describe the results obtained in a series of papers similar to those initiated in this journal ten years ago [1, 3]. As then, it is not possible to anticipate the scope or application of this new concept, yet the preliminary results described below, as obtained with flow-through optosensors utilizing reflectance spectrophotometry, certainly justify further exploration of this field.

Reflectance spectrophotometry

Reflectance spectrophotometry has traditional applications such as evaluation of paints, printing materials and textiles, but it has recently found use in two other areas. In rapid diagnostics [4], it is used for quantitative evaluation of test strips designed for assays of urea and glucose in urine or blood. The test strips, with solid-phase reagents, may be conceived as the modern extension of the traditional litmus paper principle which is finding its way back into the clinical laboratory in two novel modifications: (a) as a fibre-based system where reagents and their combinations are covalently bound to cellulose; and (b) as a multilayer film system where reagents and associated dyes are located in gelatine-based layers sandwiched together. Though designed exclusively for one-time use and batchwise operation, some of the commercially produced strips contain strongly-bound reversible reagents and are therefore perfectly suited to become sensing surfaces in flow-through optosensors. Another area in which reflectance measurements have found application is in construction of optical probes (optrodes) for continuous monitoring. Peterson et al. [5] made the pioneering contribution by designing a probe for continuous monitoring of pH of blood in vivo, and their work was later extended to monitoring of oxygen, glucose and other species. An excellent review by

Seitz [6] and contributions by Kirkbright et al. [7, 8] are very useful sources of information about the technology of fibre optics and the methods of incorporating reagents and/or dyes onto the tip of optical fibres. None of this work, however, was conducted with the aim of incorporating the optrodes into f.i.a. In fact, only the pH probe designed by Kirkbright et al. [8] was tested in a flow-through mode, yet its response is too slow for f.i.a. applications (99% of steady state is reached within 5 min). In the same work, normalized reflected radiation intensity was used to measure the response of the probe. There is, however, generally some uncertainty above which mode is most appropriate for the presentation and interpretation of reflectance measurements on reactive media, and it seems useful to review briefly the principles of reflectance measurements as relevant to the present purpose.

Absorbance and reflectance spectrophotometry are interrelated and for f.i.a. applications a spectrophotometer can be used for both methods (although requiring different designs of the flow through cells), thus it is useful to review their principles by comparison. In absorptiometry, the radiation intensity I_0 entering the flow cell is related to the intensity of the transmitted radiation, I_T, by the transmittance T: $T = I_T/I_0$. In reflectance measurements the reflected radiation, I_{Re}, is related to the incident radiation, I_0, by the reflecting power, R: $R = I_{Re}/I_0$. Evidently, both T and R can reach values between 0 and 1. As long as the content of the flow cell is transparent, the concentration C of the absorbing species can be expressed by Lambert—Beer's law

$$-\log (I_T/I_0) = A = \epsilon C d \tag{1}$$

where ϵ is the molar absorptivity and d is the thickness of the absorbing solution. For reflectance measurement, the situation is much more complex, because radiation scattering, the nature of the reflecting medium, the geometry of illumination and of radiation collection play important roles [9—11]. Therefore several equations have been proposed to describe the relation between R and C. For opaque layers, the Kubelka—Munk function [10] applies

$$f(R_\infty) = C\epsilon s^{-1} \tag{2}$$

where R_∞ is the reflectance of an opaque (and infinitely thick) layer and s is the scattering coefficient. It can be shown [10] that A and $f(R_\infty)$ are equal at $R_\infty = T = 0.44$, and that for the same ϵ value, $C_T d = C_{Re} s^{-1}$. Furthermore, it has been shown [10] that error curves for both Eqns. 1 and 2 have minima in the range 0.2—0.6, yet the reflectance concentration function has a lower slope, shorter linear range and larger errors at both extremes.

Transparent layers on a white opaque background, if suitably illuminated (so that light scattering of the transparent layer as well as gloss are eliminated), will yield a reflectance/concentration dependence which resembles Lambert—Beer's law, except that because the radiation traverses the absorbing layer at least twice (if not more, by multiple internal reflection), the

thickness of the absorbing layer is equal to $2d$ (Eqn. 1). Mirror-like reflectance (gloss) will cause negative deviations at low R values, and excessive back-scattering, owing to poor geometry of illumination and of reflector, will result in loss of sensitivity.

Thus, in principle the following operational conclusions may be made. Reflectance by an opaque layer is independent of its thickness, d, provided that a certain minimum d value has been reached. Reflectance by a transparent layer will be at least twice as high as its absorbance. The interdependence of R and C as described by the Kubelka—Munk function is a nonlinear function (a combination of a straight line and a hyperbola) which within a short range of concentrations close to the point of minimum error will resemble Lambert—Beer's law. Therefore, all reflectance measurements in this work will be treated as if absorbance had been measured, yet to indicate that the intensity of the reflected light has been measured, A_R will be used for the flow cell with a transparent solution layer and a white diffuse reflecting background, while A_r will designate measurements made in a cell with an opaque reflecting layer. While this approach would not be feasible in classical (i.e., discrete) applications of reflectance, it is practical in flow-through applications because f.i.a. allows calibration of the optosensor by means of standard solutions while the geometry of illumination, of light collection, and of the position of the reflecting surfaces within the flow cell remain strictly constant during series of measurements. The resulting calibration curve will be linear within a limited range in favourable cases while at higher concentrations it will exhibit a negative deviation.

To test the performance of optosensors with transparent and opaque layers, a model system was chosen, the common feature of its components being the optosensed reaction, namely, the colour change of an acid-base indicator. The three methods examined, measurement of pH and assays of ammonia and urea, are among the most frequently required assays, and therefore their miniaturization is of general interest.

Flow-through optosensors

The flow-through optosensor for pH measurement (Fig. 1) uses a commercially available fibrous cellulose material to which acid-base indicators are covalently bound and through which the carrier stream C may freely pass so that the change of reflectance of the incident light, led to the fibrous pad by a bifurcated optical fibre (o), may be measured at the distant end by means of a conventional spectrophotometer. If the pad thickness (d) were to be sufficiently great, the use of a reflector (r) would not have been necessary because each cellulose fibre, being white, serves as a diffuse reflector. Yet for reasons of miniaturization (the channel thickness being 2 mm) an "infinitely thick layer" was not viable. Several acid-base indicators covalently bound to the surface of cellulose fibres were tested with the aim of optimizing the reproducibility of a series of pH measurements, maximum range and maximum sensitivity of pH measurements (i.e., pH/A_r slope), the reproducibility

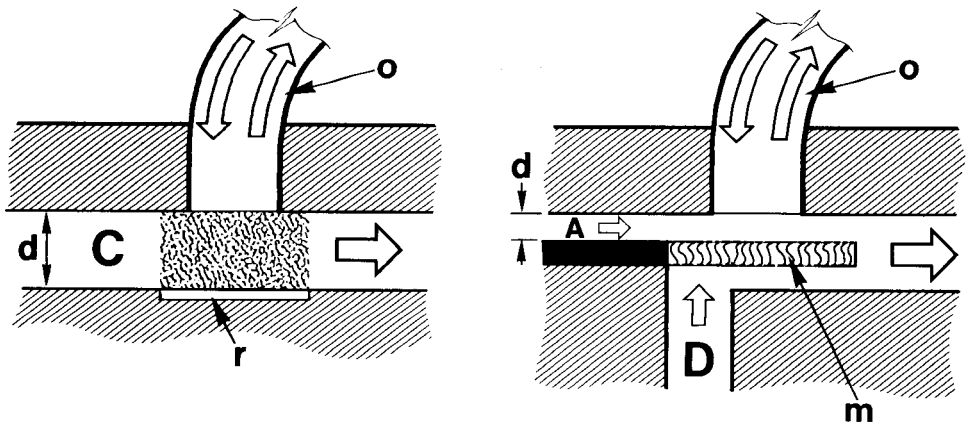

Fig. 1. Optosensor with fibrous flow-through structure on the surface of which a pH indicator is covalently bound. C, Carrier stream; d, thickness of indicator-containing cellulose pad; r, reflector; o, optical fibre.

Fig. 2. Optosensor with a gas-diffusion membrane (m) separating a donor stream (D) and an indicator-containing acceptor stream (A), the membrane being situated in that section of the channel which is monitored by the optical fibre (o).

of the optosensor preparation, and the long-term stability of the optosensor calibration curves, as well as the possible influence of colour, refractive index and air bubbles in the measured sample solution.

The flow-through optosensor for gas measurements (Fig. 2) utilizes the same bifurcated optical fibre (o) and associated instrumentation, yet the ammonia emanating from the donor stream (D; cf. Fig. 5) penetrates a porous hydrophobic membrane (m), thus changing the pH of the acceptor stream (A) and so the colour of the acid-base indicator present in it. The incident light is reflected by the hydrophobic membrane which is opaque and white, thus serving as an ideal reflecting layer for an indicator reaction in its vicinity. The indicator solution is transparent and the incident light traverses the acceptor stream twice (the path length being $2d$). The small portion of the acceptor stream (ca. 1 μl) in which the pH and the indicator colour change, is renewed periodically after each measuring cycle. The main purpose in designing and testing the gas optosensor was to miniaturize the gas-diffusion unit, which in conventional form [12—14] is bulky and awkward to assemble. A further aim was to test how the reflectance measurement of a transparent layer of a dye solution compares with the absorbance measurement of the same dye (here, bromothymol blue), how the sensitivity of ammonia measurements by such an optosensor compares with conventional gas-diffusion f.i.a., and to evaluate the reproducibility of the gas measurement and the lifetime of the gas optosensor.

Measurement of urea by the well known method based on enzymatic degradation of urea by urease, yielding ammonia which is then sensed by the

approach outlined above, was chosen as the last component of the present model system, because it provides a link to a number of biochemical applications and enzymatic tests. As both the ammonia and the urea assay require that a sequence of chemical reactions must take place prior to the diffusion of ammonia into the indicator acceptor stream, the mutual dispersion of sample and reagent zones had to be controlled between the injector and the detector. Because miniaturized f.i.a. requires extremely precise control of such a merging process, a novel approach based on split-loop injection was designed for this purpose.

Common to all three systems investigated is that the pH is sensed via a colour change of an acid-base indicator

$$pH = pK_{a_{Ind}} + \log [b_{Ind}]/[a_{Ind}] = pK_{a_{Ind}} + \log x_{b_{Ind}}/x_{a_{Ind}} \quad (3)$$

where $x_{b_{Ind}}$ and $x_{a_{Ind}}$ are the molar fractions, and where either the alkaline (b) or the acid (a) form of the indicator can be selected for monitoring. Depicted in a Bjerrum diagram, $x_{b_{Ind}}$ (or $x_{a_{Ind}}$) as a function of pH will yield a sigmoidal curve which can be shown to approximate a straight line in the pH range $pH = pK_{a_{Ind}} \pm 0.6$. Thus, if b_{Ind} is the component to be monitored, then within this pH range the equation valid will be

$$pH = k_1 x_{b_{Ind}} + k_2 = 2x_{b_{Ind}} + (pK_{a_{Ind}} - 1) \quad (4)$$

Isolating $x_{b_{Ind}}$ from Eqn. 4 and inserting $x_{b_{Ind}} = [b_{Ind}]/C_0$, where C_0 is the stoichiometric concentration of indicator, gives

$$[b_{Ind}] = 1/2C_0(pH - pK_{a_{Ind}} + 1) \quad (5)$$

In all indicator-based reflectance measurements, the indicator concentration and hence the pH value is measured relative to the initial conditions. For measurements of the reflectance A_R in cells with a transparent solution layer and a white diffuse reflecting background, the initial conditions are fixed by the indicator concentration, $[b_{Ind}]_0$, in the acceptor stream, whereas for measurements of A_r, referring to measurement of reflectance in cells with an opaque reflecting layer, the baseline pH value, pH_0, is governed by the pH of the carrier stream. If the $[b_{Ind}]$ and pH values corresponding to the presence of a sample in the flow-through cell are called $[b_{Ind}]_x$ and pH_x, i.e.,

$$pH_0 = (2[b_{Ind}]_0/C_0) + pK_{a_{Ind}} - 1; \; pH_x = (2[b_{Ind}]_x/C_0) + pK_{a_{Ind}} - 1$$

the recorded change in pH as the result of injection of a sample will be

$$\Delta pH = pH_x - pH_0 = (2/C_0)([b_{Ind}]_x - [b_{Ind}]_0) = (2/C_0)\Delta[b_{Ind}] \quad (6)$$

For measurements of A_R, as used for the flow-through cell based on diffusion of gas through a gas-permeable membrane, $\Delta[b_{Ind}]$ will be proportional to the amount of gas diffused, i.e., $\Delta[b_{Ind}] = k_d C_s$, where C_s is the sample concentration and k_d is a constant the value of which depends on the characteristics of the membrane, the cell geometry and the residence time of the sample in the cell. Combined with Eqn. 1, this yields

$$(2/C_0)\Delta[b_{Ind}] = (2/C_0)k_d C_s = (2/C_0)k\Delta A_R$$

or

$$\Delta A_R = k_d C_s/k = k' C_s \quad (7)$$

where k is proportional to $1/(\epsilon 2d)$. Thus, provided that the indicator concentration is sufficient to fulfil the conditions of Eqn. 7 (i.e., in excess) the measured signal will be independent of C_0.

For measurements of A_r, the recorded signal will be, according to Eqn. 2, a function of the population of indicator molecules in the b-form, i.e., $A_r = k[b_{Ind}]$(Area), where Area refers to the area of indicator layer which is observed by the detector system (the optical fibre). Combined with Eqn. 6, this gives

$$\Delta pH = (2/C_0)\Delta[b_{Ind}] = 2\Delta A_r/kC_0(\text{Area})$$

or

$$\Delta A_r = \Delta pH\, k' C_0(\text{Area}) \quad (8)$$

where k' will be proportional to ϵ. Thus, if one imagines the indicator pad consisting of sandwiched layers, each consecutive layer will add, to a gradually diminishing extent, to the population of indicator observed by the optical fibre. Therefore, eventually the reflectance R_∞ (Eqn. 2) is reached, and is independent of the pad thickness d.

The conditions on which Eqns. 7 and 8 are based are essential for both pH measurements and indicator-based assays, if linearity of response is to be maintained. The slope of the response plot is unconditionally and directly proportional to ϵ and d (or Area). Yet, for pH measurements all molecules of the indicator (i.e., the population) have to be equilibrated with the sample pH (i.e., fully reacted with the sample solution), whereas for the assay of ammonia or urea, the indicator concentration C_0 must always be in excess compared to the millimoles of base diffusing from the donor stream across the membrane to the acceptor stream. This means that in order to achieve maximum sensitivity of measurement, the indicator must have the highest possible ϵ value as well as a suitable pK_a value. Further increase in sensitivity can be achieved for the pH measurements by increasing the amount of indicator immobilized within the illuminated area, provided that a sufficiently large buffering capacity and/or large volume of sample solution is being contacted with the immobilized indicator, so that all indicator molecules will become equilibrated with the sample solution. For assay of ammonia (or urea), in contrast, an increase in indicator concentration in the acceptor stream will not yield higher sensitivity, but will increase the upper linear range if the indicator is not already present in sufficient excess, provided that other limiting factors (e.g., deviations arising from reflectance measurements or from limited gas diffusion) do not play a role.

EXPERIMENTAL

Instrumentation

All experiments were done with two Bifok-Tecator FIA-5020 Flow Injection Analyzers. The manifolds with integrated flow-through detectors were constructed by the microconduit technology as described earlier [2]. As a novel feature, a miniaturized injection valve, provided with an external sample loop to allow for injection of variable sample volumes, was integrated into the microconduit (cf. Fig. 3); this allowed the volume of the channel connecting the sample loop and the detector to be minimized (to 10 μl for the pH unit shown in Fig. 3). Optical communications were made by means of plastic optical fibres (DuPont Crofon fibre 1610, 2.6 mm; Optronics, Cambridge, England) consisting of 32 individual acrylic strands which were randomly bifurcated at the remote end to allow connection to a light source and to the spectrophotometer.

Microconduits were accommodated in a cassette furnished with a gear box which allowed the arm of the miniaturized valve to be operated by the valve motor of the FIA-5020 analyzer. For delivery and aspiration of liquids, both peristaltic pumps (P1 and P2) of the analyzer were used. The automated sequential operation of the pumps, and the timing of the valve functions, were controlled by the microprocessor of the FIA-5020.

Reflectance measurements were done by either one of two conventional spectrophotometers: the Bausch and Lomb Mini-20 spectrophotometer used was furnished with a home-made logarithmic signal converter and a home-made external high-intensity light source (20 W) powered by a variable

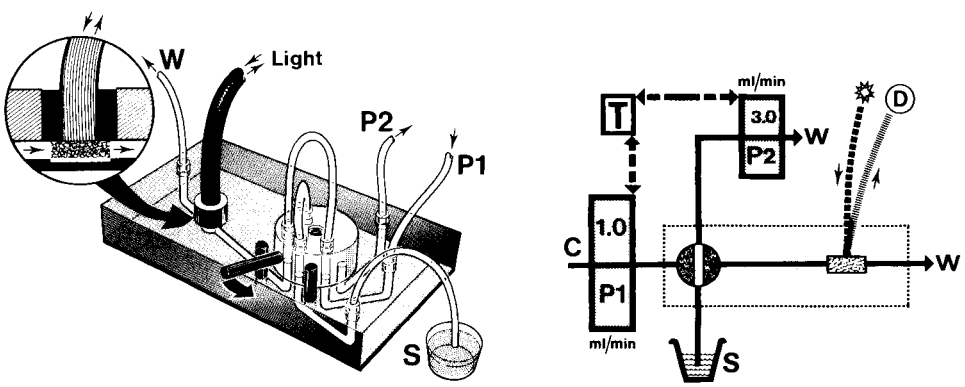

Fig. 3. Integrated microconduit for measurement of pH comprising injection valve and optosensor. S, Sample solution; P1 and P2, tubes leading to the peristaltic pumps (cf. Fig. 4); W, waste tube. The insert shows a cross-section of the optosensor (cf. Fig. 1).

Fig. 4. Manifold for pH measurement comprising two peristaltic pumps (P1 and P2), a timer (T) and the microconduit shown in Fig. 3 (comprising the components within the boxed area). S, Sample; C, carrier stream; W, waste. The flow-through cell communicates with a light source and a spectrophotometer (D) through optical fibres.

power supply (4—8 V); the Bifok-Tecator FIAstar 5023 scanning spectrophotometer used was modified by removing the 400—700-nm blue filter and by increasing the voltage of the light source lamp to 6.4 V in order to increase the light intensity. The conventional flow-through cuvette of the instrument was then replaced by a black plastic block which held in appropriate positions the two bifurcated ends of the multistrand plastic fibre so that the light from the internal light source could be piped into the microconduit and then the light reflected from there could be piped back into the spectrophotometer. Because the white opaque reflector of the flow-through cell used reflected only 10% of the light, the signal of the unattenuated reference beam had to be balanced electronically by means of the built-in adjustment potentiometers.

Both spectrophotometers yielded identical results, but the FIAstar 5023 allowed automated recording of reflectance spectra. Further operational details of spectrophotometry/reflectance measurements seem unnecessary here, but it should be noted that the intensity of the polychromatic light as supplied by the home-made unit, and subsequently made monochromatic and measured by the Bausch and Lomb Mini-20, was so high that the microconduits could be made from transparent PVC without any danger that changes in ambient illumination would affect the measurement. The light source of the FIAstar 5023, after being boosted, allowed reflectance measurements to be made, but the microconduits had to be made of black PVC to avoid any influence by ambient illumination. All fibre bundles were protected from ambient light by black PVC sleeving. The measurements of reflectance (A_r or A_R) were automatically recorded on the printer of the FIAstar 5023 and were digitally displayed on the FIA-5020, and concurrently fed to a recorder (Radiometer Servograph REC-61, furnished with a REA-112 high-sensitivity interface). When the Bausch and Lomb spectrophotometer was used, the transmittance signal was first fed to the logarithmic converter and then to the Radiometer recorder, and from there to the FIA-5020. Results were displayed digitally on the FIA-5020 and also recorded on an attached printer (Alphacom Sprinter 40).

Microconduits

The microconduits consisted of 70 × 45 × 10-mm PVC blocks into which appropriate channel patterns were impressed or engraved. When closed by a transparent plate with the aid of pressure-sensitive polymeric glue, the channels formed conduits of semicircular cross-section with an internal area of 0.8 mm^2. Introduction of liquids into the channels and their withdrawal were effected through small perpendicular holes drilled at appropriate positions and furnished with externally communicating tubes.

The microconduit and manifold for pH measurements are shown in Figs. 3 and 4, respectively. Details of the flow-through cell are shown in Fig. 1, the cell compartment being ca. 3 mm in diameter (d = 2.0 mm), comprising a circular pad (ca. 2.9 mm in diameter) containing the covalently bound

acid-base indicator dye on cellulose support, which in the swollen state was ca. 1.8 mm thick.

The manifold for the gas-diffusion system is outlined in Fig. 5. For convenience, it was made of two microconduits, one containing the injection valve and the split-loop system, and the other one comprising the mixing coil M and the flow-through cell. Details of the gas flow-through cell are shown in Fig. 2. The donor stream (D) flows in a channel, 1.5 mm wide, 0.3 mm deep and 4 mm long, engraved into the microconduit, while the acceptor stream (A) is guided through a channel, 1.5 mm wide, 0.13 mm deep (d) and 7 mm long, the two channels being separated by the gas-permeable membrane, m (Celgard 2500 microporous film; Celanese Fibers Operations, U.S.A.), but sharing a common outlet in order to eliminate pressure differences across the membrane.

Reagents and materials

For the pH measurements, the non-bleeding indicator papers (Merck) designated as Universal (pH 0—14; cat. no. 9535), Neutralit (pH 5—10; cat. no. 9533), Spezial (pH 4—7; cat. no. 9542), and Spezial (pH 6.5—10; cat. no. 9543) were selected. A circular section (2.9 mm in diameter, 0.1 mm thick) of cellulose fibres with covalently bound indicator was sliced off the supporting plastic backing with a lancet and was placed into the flow-through cell to face the end of the optical fibre (see insert of Fig. 3).

The carrier stream (C, Fig. 4) used for wide-range pH measurements was 5×10^{-4} M hydrochloric acid; for narrow pH ranges, a 5×10^{-4} M phosphate buffer adjusted to pH 6.50 was used. Both carrier solutions contained surfactant (0.01% Brij) and were degassed before use. The standard buffers used in this work contained phosphate, citrate, borate and appropriate amounts of either hydrochloric acid or sodium hydroxide. Their exact compositions are described in Tables 10.25, 10.43 and 10.45 in the monograph by Perrin and Dempsey [15].

The carrier stream (C) for the ammonia determinations (Fig. 5) was a (1 + 99) dilution of a stock solution containing 1.2 M potassium dihydrogenphosphate and 0.59 M disodium hydrogenphosphate, pH 6.50. The reagent solution (R) was 0.1 M sodium hydroxide. For urea determinations (Fig. 5), the carrier stream (C) was 0.1 M tris(hydroxymethyl)aminomethane (Tris) adjusted to pH 8.32, while the reagent stream (R) was 0.1 M Tris to which per 100 ml buffer (pH 8.32) was added 100 mg of urease (nominally 51 U mg^{-1}; Worthington 3886 URC 30S956A). The acid-base indicator solution (Ind) consisted in both cases of 0.04% (w/v) bromothymol blue in a 25:75 (% v/v) ethanol/water mixture, the pH being adjusted so that 5–10% of the indicator was in the alkaline form. The blue form of the indicator was monitored at 620 nm. Ammonium chloride standards in the range 1–20 mg l^{-1} ammonia and urea standards in the range 1–10 mmol l^{-1} were prepared by aqueous dilutions of stock solutions.

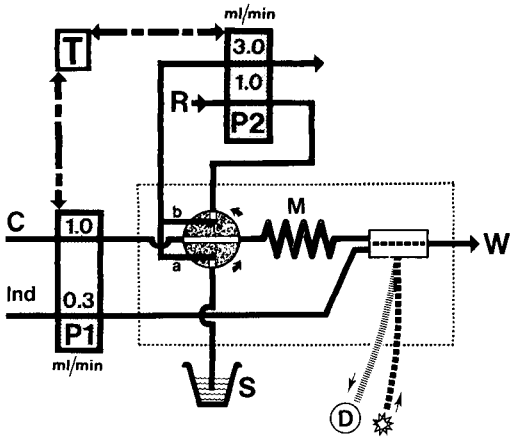

Fig. 5. Manifold for assay of ammonia and of urea, comprising two peristaltic pumps (P1 and P2), a timer (T), reagent (R), carrier (C) and indicator (Ind) channels, mixing coil (M, 70 μl), sample channel (S) and a valve furnished with a split-loop configuration comprising sample (a) and reagent (b) sections. The optosensor (cf. Fig. 2) is connected to a light source and a spectrophotometer (D) by means of optical fibres. W leads to waste. The boxed area includes the components within the microconduit.

Split-loop injection procedure

The split-loop injection approach may be explained by referring to Fig. 5; the principle is that the normally used external sample loop, the length and internal diameter of which fixes the injected sample volume, is divided (split) into two sections sharing a common outlet. Thus, when the valve is in the load position (as shown on Fig. 5) sample and reagent solutions are simultaneously being aspirated by means of pump P2, filling sections a and b, respectively. When the loading has been completed pump P2 is stopped and the valve is turned in the direction of the arrow so that both zones are injected into the manifold by carrier stream C propelled by pump P1, zone b (reagent) following immediately on zone a (sample) through the mixing coil M. The dimensions of this coil govern the dispersions of the two zones and hence their mutual overlap before entering the flow-through cell.

In practice, the common outlet and a portion of each volumetric section a and b were imprinted into the microconduit, adjacent to the injection valve; the connecting tubes between the valve and the imprinted channels thus fix the volumes of zone a and b. By varying the length and internal diameter of these connecting tubes, the injected volumes of reagent and sample could readily be changed.

RESULTS AND DISCUSSION

Measurement of pH

Measurements of pH were made in the manifold with integrated valve and optosensor (Fig. 4). The programming sequence of the FIA-5020 was

00-00-00-08-1-6 which resulted in sample aspiration (S by pump P2) for 8 s during which the sample loop (volume 50 μl) was washed and filled with sample solution. After a 2-s delay the valve was turned, and the sample zone was injected into the carrier stream which was pumped continuously by pump P1, reached the optosensor after 1 s and passed through the sensor during the next 20 s (cf. Fig. 7, curve e). Because sample aspiration and sensor wash-out partially overlapped, a sampling frequency of 120 h^{-1} could be maintained.

The indicator pads, cut from the Merck strips, were chosen to change from yellow (acid form) to blue (alkaline form), thus yielding minimum reflectance (maximum A_r) in the alkaline form in the vicinity of 610 nm. In order to cover different pH ranges, pads were selected according to the manufacturer's instructions (from the Universal indicator series, a section covering pH 5—10 was selected). Typical recordings obtained with these cellulose-bound indicators and standard buffers are shown in Fig. 6. The same pad could be used for several weeks and for thousands of measurements without any deterioration of response characteristics (i.e., slope of calibration curve, speed of response). Because of the excellent homogeneity of the commercial materials and the reproducible geometry of the pad in the flow cell, a pad could be replaced, or an entirely new microconduit fabricated, with such repeatability that identical calibration curves were obtained with new and old devices.

In order to investigate the reproducibility of pH measurements at the maximum sensitivity achievable within the linear range of the indicator

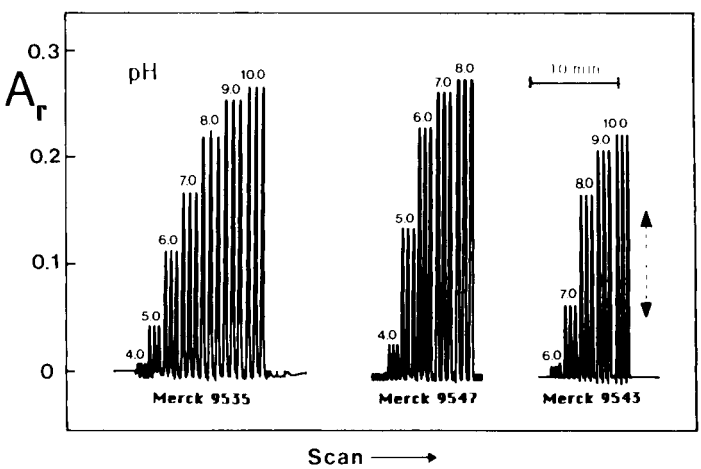

Fig. 6. The pH responses of the optosensor furnished with the following immobilized indicators: Universal (Merck 9535), Spezial (Merck 9547), and Spezial (Merck 9543), recorded by injecting standard buffer solutions into a 5×10^{-4} M HCl carrier stream and monitoring the reflectance as increased absorbance (A_r) at 610 nm. The arrow at the far right indicates the pH range investigated in Fig. 7.

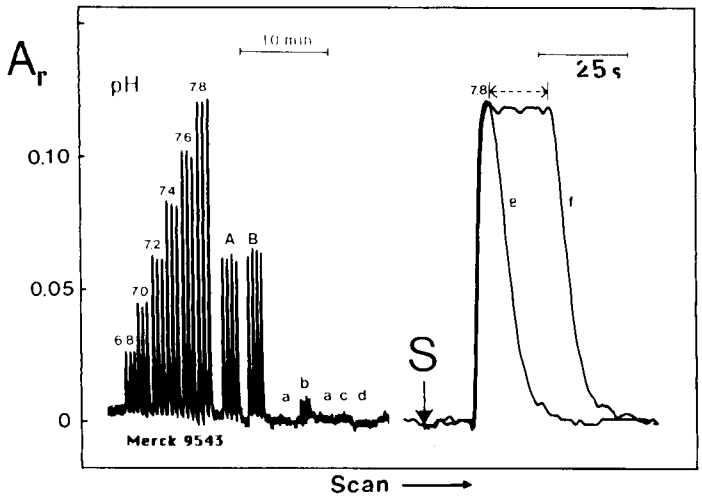

Fig. 7. Response of the optosensor within the pH range 6.8—7.8 using immobilized indicator (Merck 9543) with a phosphate-based carrier stream of pH 6.5. Standard buffer solutions were injected in triplicate, then (A) the standard buffer of pH 7.20 was injected in quadruplicate followed by (B) the standard buffer of pH 7.20 containing 0.4% methyl red injected in quadruplicate. Further injections (all in triplicate) were: (a) carrier solution; (b) carrier solution with 0.4% methyl red; (c) air; (d) 60% (w/v) glucose in carrier solution. Recorded at high paper speed to the right are: (e) the buffer pH 7.80; (f) as (e) but with a stop period of 17 s (indicated by the arrow on top of the peak). S is the point of injection.

response, a Spezial indicator strip (cat. no. 9543, pH 6.5—10.5) was selected and used together with a phosphate-based carrier stream, the pH of which was chosen to fulfil the conditions stipulated by Eqns. 4 and 8, so that linearity of response and reproducibility of measurement could be evaluated. The recording obtained (Fig. 7) yielded a calibration line with the equation $pH = 6.580 + 0.003A_r$ ($r^2 = 0.9995$) while the standard deviation for 7 repeated injections of the pH 7.2 buffer (peaks marked 7.2 and A on Fig. 7) corresponded to 0.004 pH.

Surprisingly, the injection of air, carrier solution containing a red dye or containing 60% glucose (Fig. 7, a, b, c, d) had little or no effect on the baseline, though one would intuitively expect that reflectance, absorbance or schlieren effects would result in distortion of the signal read-out.

Fast detector response is crucial for all applications of f.i.a. and the optosensor described above fulfils this requirement, as seen from Fig. 7 where Δt, as measured from baseline to baseline, is 20 s while $t_{1/2} = 1$ s. For the reasons described earlier [16], the present system was designed and the sample volume was selected to yield limited dispersion ($D = 1.008$). Therefore the above response times reflect the linear velocity of the liquid and the rate of sample zone wash-out from the optosensor. This conclusion is supported by the stopped-flow experiment (Fig. 7, f) which shows no change in A_r and pH

value when the forward motion of the carrier stream is stopped, because the covalently-bound indicator throughout the pad thickness has been equilibrated with the flowing solution.

The compositions of the indicators immobilized on the pH strips used are proprietary information; but from the information available [17], all the indicators used here are substituted azo-dyes covalently bound to cellulose by the Remazol process [18, 19]. This process, mainly used in the textile industry, is based on the following scheme

$$D{-}SO_2{-}CH_2{-}CH_2{-}O{-}SO_3H + 2\,NaOH \rightarrow D{-}SO_2CH{=}CH_2 + Na_2SO_4 + 2\,H_2O$$

$$D{-}SO_2{-}CH{=}CH_2 + HO{-}[Cell] \rightarrow D{-}SO_2{-}CH_2{-}CH_2{-}O{-}[Cell]$$

where **D** is the Remazol azo-dye backbone molecule, tailored to have one or two pK_a values and suitable colour transition(s) to serve as an indicator. Because the dyes are covalently bound to the surface of white reflecting fibres forming a loose structure, within which the turbulent flow allows rapid interaction between solution and surface, fast response is achieved, in contrast to the less favourable geometries used earlier where an indicator was impregnated into polystyrene spheres or retained on absorbing materials behind a diffusion membrane [5—8] with the result that diffusion (and rediffusion) of solute takes a long time while the indicator is more loosely retained and less uniformly distributed. The Remazol process is also applicable to nylon and some other polymers, and it would be interesting to construct optosensors with smooth (nonporous) reflecting surfaces covered with a thin layer of covalently-bound indicator and compare their performance with that of fibrous structures. Because covalently-bound indicators are said [17] to be free from protein error, and because the present work demonstrates the excellent reproducibility of f.i.a. for pH measurements within the physiological range, further research along these lines appears to be justified.

Assays of ammonia and urea

Determination of ammonia. For the assay of ammonia, the manifold shown in Fig. 5 and the optosensor depicted schematically in Fig. 2 were most suitable. While the chemistry of this assay is the same as that used in previously described flow-injection methods for ammonia [12] the experimental arrangement differs from the conventional techniques in the following respects: (a) the gas diffusion unit is miniaturized and integrated with the detector to form an optosensor; (b) the valve, mixing coil and optosensor are integrated by using the microconduit technology; (c) the use of the split loop ensures highly reproducible merging of the sample and reagent zones.

With the manifold recommended and the FIA-5020 unit, the integrated microconduit was operated by using the following sequence: 18-16-00-09-1-6. This means that the measuring cycle was initiated by a 9-s aspiration period during which the sample loop a (20 μl of ammonium chloride solution) and

the reagent loop b (35 μl of 0.1 M sodium hydroxide) were filled; pump P2 was then stopped, and after a delay period of 1 s the valve was automatically turned, the two zones passing through the mixing coil M towards the optosensor, propelled by the phosphate carrier stream. The dispersion in the mixing coil is sufficiently large to ensure an alkaline milieu over the entire length of the sample zone, and ammonia is liberated from each segment of the zone. If, however, both the indicator and the carrier streams were pumped continuously, the residence time in the small flow-through cell would be so short that only minute amounts of ammonia would diffuse across the membrane from the donor stream to the acceptor (Ind) stream. When the two streams are stopped after a prepicked delay period following cycle initiation, a suitable section of the mutually dispersed zones can be selected and contained within the flow-through cell whereby the diffusion of gas across the membrane is enhanced. In this manner, the sensitivity of measurement can be increased, the length of the stop period governing the degree of transfer of the ammonia available within the entrapped segment of sample zone. The ammonia is then sensed via the colour change of the indicator. In Fig. 8 is shown the output for a series of calibration solutions in the range of 1—20 mg l^{-1} ammonia, the stop period being 16 s. All peaks were recorded during stop intervals commencing at a delay time of 18 s after cycle initiation, corresponding to the point of maximum concentration of ammonia on the sample zone gradient. With the 16-s stop period, approximately 70% of the ammonia within the optosensor was transferred into the acceptor stream. For shorter or longer delay times than 18 s, corresponding to segments on the ascending or descending parts of the sample zone gradient, smaller but equally well reproducible peaks were obtained. As seen from Fig. 8, the experimental conditions used resulted in a small response even for the injection of blank solution. Thus the lower limit of detection for the ammonia detection with the present system is ca. 0.3 mg l^{-1} ammonia.

Assay of urea. For the urea determinations, the manifold and split-loop configuration were used as for the ammonia determinations. The carrier stream consisted of diluted Tris buffer of pH 8.32 and the reagent solution was the same Tris buffer containing urease. This operational pH value was chosen as a compromise between the optimal pH for the enzymatic degradation procedure and a sufficient degree of liberation of ammonia. As the reagent zone (enzyme) follows the sample zone, the peak maxima of the two gradients are spatially displaced and therefore the enzyme concentration at the peak maximum of the sample zone will be relatively low, while over part of the descending gradient of the sample zone, the enzyme concentration will be increasing. Thus the optimal point for measurement, corresponding to the highest sensitivity, is found at a delay time longer than the 18 s measured above to correspond to the peak maximum of the sample zone. In the present configuration, the optimum delay time was found to be 22 s. For a 16-s stop period (i.e., the programming of the FIA-5020 was 22-16-00-09-1-6), a series of urea standards in the range 1—10 mM were run. A typical output is reproduced in Fig. 8.

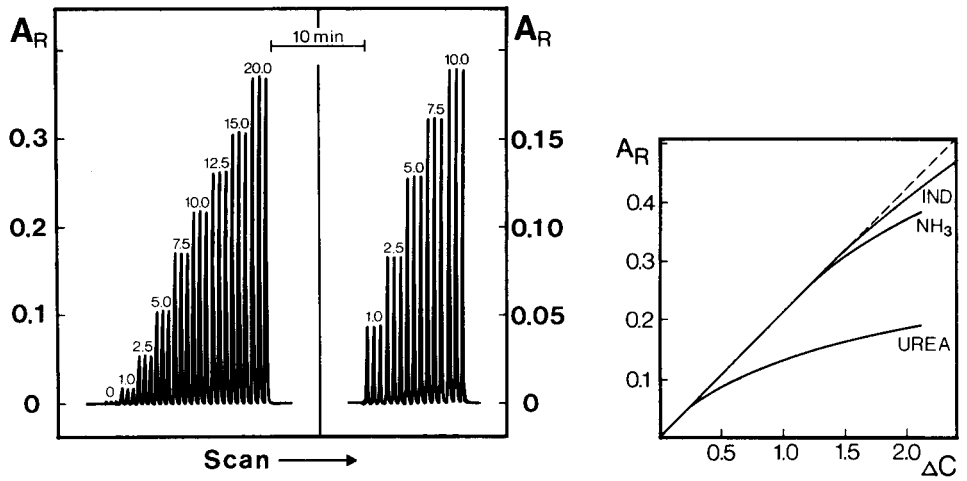

Fig. 8. Recordings for the assay of ammonia and urea with the manifold depicted in Fig. 5. To the left are shown the responses for a series of ammonium chloride standards in the range 0—20 mg l^{-1} ammonia. At the right are shown the responses for 5 urea standards in the range 1—10 mM. All samples were injected in triplicate. For details, see text.

Fig. 9. Calibration graphs for bromothymol blue, ammonia and urea, obtained with the optosensor in Fig. 2 and the manifold of Fig. 5. For comparison, the values on the abscissa were normalized, so that C = 2.0 corresponds to 10 mM urea or 20 mg l^{-1} ammonia.

Linearity of response. When the calibration graphs for ammonia and urea are plotted from the responses shown in Fig. 8, a negative deviation from linearity is observed at high analyte concentrations. Because such a deviation could be due to the nature of reflectance measurement on the transparent layer, it was decided to test the performance of the optosensor by means of serially diluted solutions of bromothymol blue which were all adjusted by means of sodium tetraborate to pH 9.2. Because the same indicator was used in both the ammonia and urea assays, it was possible to evaluate in which range of A_R the optosensor responds linearly (Fig. 9). By normalizing the concentration units on the abscissa (through the respective stoichiometries of the reactions involved), it was possible to accommodate all calibration curves in one graph. Obviously, A_R closely follows Lambert—Beer's Law versus bromothymol blue concentrations up to a value of 0.35 A_R. In the case of ammonia, the negative deviation at higher ammonia contents is due to limited diffusion of ammonia through the membrane. This was confirmed by an additional experiment in which higher indicator concentrations were used in the acceptor stream; there was no increase of the linear range. The even larger deviation from linearity in case of urea assay is primarily due to limitations in the enzymatic degradation of the substrate, e.g., lack of activity of the urease used.

Gas diffusion units. The units used previously were designed according to the original device of Baadenhuijsen and Seuren-Jacobs [20] and/or the commercial unit available from Bifok-Tecator [14]. All have channel/membrane interface areas of approximately 2 mm × 100 mm. Surprisingly, with the same membrane material and with identical chemistry, the optosensor yielded similar sensitivity and limit of detection as the conventional gas diffusion units in spite of the fact that the active membrane area in the optosensor is at least 50 times smaller. Additionally, as the physical thickness of the acceptor channel is 0.13 mm, the transparent reflecting layer is effectively only 0.26 mm thick, i.e., 40 times shorter than a conventional detector light path of 10 mm. These attenuating factors arising from miniaturization are, however, offset by the gains produced by the following features: (a) better transport of solute towards the membrane surface because of the wall-jet geometry of the optosensor; (b) absence of dispersion within the optosensor; and (c) preconcentration of analyte from a larger volume of sample solution into a smaller volume of acceptor (indicator) solution.

Close inspection of Fig. 2 shows that the donor stream is directed to impinge on that section of the membrane which is directly opposite the sensing range of the optical fibre. This geometry of flow, similar to the design of electrochemical wall-jet detectors, brings the solute material into close contact with the diffusion membrane by promoting turbulent flow and eliminating the concentration profiles formed by radial dispersion.

Because detection occurs in the layer of the stationary indicator solution situated at the surface of the membrane directly opposite the wall-jet position, and because there is no dispersion of the resulting coloured zone, much larger colour changes are optosensed than in conventional units where dispersion of analyte occurs during three consecutive steps: (a) during passage of sample through the donor channel; (b) during collection of elements of diffused material in the acceptor channel; and (c) during transfer of diffused and collected analyte through the transmission tubing which connects the gas diffusion unit to the detector. Recently, detailed theoretical and experimental studies on gas diffusion and dialysis have been published [13, 21]; it was shown that the tanks-in-series model predicts higher transfer of analyte than the plug or laminar flow models. The present design may be described by a single tank model on the donor side and a quiescent diffusion unit on the acceptor side of the membrane, and will thus be easier to solve mathematically than the model describing the conventional gas diffusion unit with constantly flowing streams of donor and acceptor solutions.

Finally, it should be mentioned that the gas diffusion experiments described above did not, owing to the limitation in the programming of the FIA-5020 unit, involve preconcentration of analyte within a smaller volume of indicator. It is likely that such preconcentration would allow further increase in sensitivity and improvement of the detection limit of the optosensor beyond that of conventional devices.

Conclusion

While this work describes only the beginning of research into optosensing devices, the results provide interesting information within both technological and conceptual areas. On the technological side, microconduits proved to be an excellent tool for fabricating optosensors and integrating them into miniaturized flow-injection manifolds. The optosensor and microconduit technologies are admirably compatible. Next, covalent binding of reversible reagents on a suitable support proved to be thoroughly suited for applications of f.i.a. Further, renewal of a reagent phase within an optosensor proved to be a technique which allowed highly reproducible regeneration of the optosensor function prior to each measuring cycle. This is an invaluable feature in situations where either back-diffusion into a donor stream (ammonia in the present case) would take a long time, or where the reagent used is irreversible or becomes consumed during the measuring cycle. Another important feature of this work is the introduction of the split-loop technique which proved to be a highly reproducible means of applying the merging zones principle. It is remarkable that this split-loop approach is being introduced only now, more than 10 years after the first f.i.a. experiment was designed.

On the conceptual side, it is important to realize that the use of fibre optics is only a convenient means of directing radiation to and from the optosensor. What is new is the optosensing at a second phase in the detector area through which a stream of sample and of reagent are flowing. This approach allows miniaturization and results in great economy of sample and reagent materials. In addition, it will allow preconcentration of analyte from a large sample volume into a small volume of immobilized reagent thereby increasing the sensitivity of assays. Ultimately, it should allow multiple detection based on spatial rather than on time or spectral resolution.

The authors express their appreciation to Inge Marie Johansen and Eva Thale for conscientious technical assistance. Thanks are also due to Tage Frederiksen for mechanical help and to Ove Broo Sørensen for help in preparing the illustrations.

REFERENCES

1 J. Růžička and E. H. Hansen, Anal. Chim. Acta, 78 (1975) 145.
2 J. Růžička and E. H. Hansen, Anal. Chim. Acta, 161 (1984) 1.
3 J. Růžička and E. H. Hansen, Anal. Chim. Acta, 99 (1978) 37.
4 A. Zipp and W. E. Hornby, Talanta, 31 (1984) 863.
5 J. I. Peterson, S. R. Goldstein, R. V. Fitzgerald and D. K. Buckhold, Anal. Chem., 52 (1980) 864.
6 W. R. Seitz, Anal. Chem., 56 (1984) 16A.
7 G. F. Kirkbright, R. Narayanaswamy and N. A. Welti, Analyst (London), 109 (1984) 1025.
8 G. F. Kirkbright, R. Narayanaswamy and N. A. Welti, Analyst (London), 109 (1984) 15.

9 H. U. Bergmeyer, Methods of Enzymatic Analysis, Vol. 1, 3rd edn., Verlag Chemie, Weinheim, 1984, Ch. 3.3.
10 P. Kubelka and F. Munk, Z. Tech. Phys., 12 (1931) 593.
11 F. C. Williams and F. R. Clapper, J. Opt. Soc. Am., 43 (1953) 595.
12 J. Růžička and E. H. Hansen, Flow Injection Analysis, Wiley-Interscience, New York, 1981.
13 W. E. van der Linden, Anal. Chim. Acta, 151 (1983) 359.
14 J. Müller, Labor Praxis, 6 (1982) 278.
15 D. D. Perrin and B. Dempsey, Buffers for pH and Metal Ion Control, Chapman and Hall, London, 1974.
16 C. Hongbo, E. H. Hansen and J. Růžička, Anal. Chim. Acta, 169 (1985) 209.
17 K. H. Neisius, Kontakte, Merck 2/71 (1971) 15.
18 I. D. Rattee, J. Soc. Dye Chem., Jan. (1969) 23.
19 W. F. Beech, Fibre Reactive Dyes, Logos Press, London, 1970.
20 H. Baadenhuijsen and H. E. H. Seuren-Jacobs, Clin. Chem., 25 (1979) 443.
21 B. Bernhardsson, E. Martins and G. Johansson, Anal. Chim. Acta, 167 (1985) 111.

Analytica Chimica Acta, 173 (1985) 23—32
Elsevier Science Publishers B.V., Amsterdam — Printed in The Netherlands

A PREDICTIVE-KINETIC METHOD FOR THE QUANTITATION OF AMINO ACIDS WITH NINHYDRIN

YAHYA R. TAHBOUB and HARRY L. PARDUE*
Department of Chemistry, Purdue University, West Lafayette, IN 47907 (U.S.A.)
(Received 4th January 1985)

SUMMARY

The development and evaluation of a predictive-kinetic method for quantifying amino acids based on reactions with ninhydrin are described. Conditions are developed for which reactions are pseudo-first-order in the amino acid. Absorbance vs. time data from the kinetic region of the reaction (1—3 half-lives) are fitted to a first-order model to predict the total absorbance change that would occur if the reaction were monitored to completion. Computed absorbance changes vary linearly with amino acid concentration between 1×10^{-5} and 5×10^{-5} mol l^{-1}. Results are virtually independent of changes in temperature ($\pm 1°C$) and ninhydrin concentration ($\pm 3 \times 10^{-3}$ mol l^{-1}).

The determination of amino acids frequently involves a chromatographic separation followed by reaction with ninhydrin and hydrindantin with subsequent measurement of the absorbance of the reaction product. Conventional procedures involve relatively long (e.g., 20 min) reaction times during which the ninhydrin reaction approaches completion [1, 2]. By replacing the traditional equilibrium measurement approach with a kinetic approach, it should be possible to reduce substantially the time involved in the measurement step.

Traditional kinetic approaches to the measurement step have not been attractive because they frequently involve error coefficients that are much larger than the error coefficients for equilibrium methods [3]. Papers from this laboratory have described results of a curve-fitting approach that reduces error coefficients for kinetic results to values that are similar to values for equilibrium methods [4, 5]. This paper describes the results of an evaluation of this kinetic approach for quantifying amino acids via their reaction with ninhydrin.

In the proposed method, the amino acid is mixed with large excesses of ninhydrin and hydrindantin and several absorbance values measured during the first 1.25—2.5 half-lives are fitted to a first-order model to compute the absorbance change, ΔA_∞, that would occur if the reaction were monitored to completion. Results obtained for glycine, alanine, phenylalanine, leucine, and isoleucine with this "predictive" kinetic method are virtually identical to results obtained when reactions are monitored to completion. Variations in temperature and reagent composition that produced 13% and 22% changes,

0003-2670/85/$03.30

respectively, in initial-rate results produced only 1% and 0.4% changes, respectively, in results obtained by the predictive-kinetic method with data collected during the first 130 s of reaction time. These apparent errors (1% and 0.4%) are well within the random uncertainty of both the equilibrium and predictive-kinetic methods. Thus, a substantial reduction in reaction time (2 min vs. 20 min) is achieved without significant sacrifice of reliability.

EXPERIMENTAL

Instrumentation and reagents

Reactions proceeded in 1-cm cuvets controlled to ±0.1°C with circulating water. Absorbance vs. time data were monitored with a Hewlett-Packard 8450A spectrophotometer interfaced to a Hewlett-Packard 2100 minicomputer.

Ninhydrin, hydrindantin, amino acids and methylcellosolve were all from Sigma Chemical Company.

Sodium acetate buffer was prepared by dissolving 54.4 g of sodium acetate trihydrate and about 9.0 ml of glacial acetic acid in sufficient distilled water to make 100 ml of solution with pH = 5.51 ± 0.03.

Ninhydrin reagent was prepared by dissolving 500 mg of ninhydrin and 80 mg of hydrindantin in 20 ml of methylcellosolve. Then 6.7 ml of sodium acetate buffer was added to the solution. Ninhydrin reagent was prepared freshly before each experiment and was kept under high-purity nitrogen prior to its addition to the amino acid solutions.

Stock solutions (1.0×10^{-3} mol l^{-1}) of each amino acid were prepared in distilled water; the solutions were refrigerated at 4°C. Standards were prepared by diluting 1.0—5.0 ml of the stock solution to 10 ml with distilled water to give concentrations in the range $1.00—5.00 \times 10^{-4}$ mol l^{-1}.

Procedure

All reactions except those in temperature studies were monitored at 80 ± 0.1°C in a water-jacketed quartz cuvet, and all reactions except those in ninhydrin reagent concentration studies were monitored at concentrations of 4.80×10^{-2} mol l^{-1} ninhydrin, 4.30×10^{-3} mol l^{-1} hydrindantin and 0.50 mol l^{-1} acetate buffer (pH 5.50). For each run, 0.50 ml of ninhydrin reagent and 0.40 ml of distilled water were mixed in the cuvet before the reaction was initiated by adding 0.1 ml of amino acid solution at 80°C. Absorbances at 570 nm vs. a distilled water blank were recorded at 10-s intervals for the desired time period. All reactions were monitored to completion to permit comparisons between kinetic and equilibrium results. Predictive-kinetic results were obtained with a program described earlier [4].

RESULTS AND DISCUSSION

Kinetic dependencies

Although there have been extensive kinetic and mechanistic studies of this reaction system [6], inadequate kinetic data are available to permit a clear definition of appropriate conditions for the kinetic quantitation of amino acids. Accordingly, effects of temperature, and pH, as well as ninhydrin, hydrindantin, and acetate concentrations were studied. Except when the parameter was being varied, conditions for these studies were as specified in the above procedure. Glycine was the acid used in these studies.

Temperature. Effects of temperature between 40 and 100° C were studied; the results are presented in Fig. 1. The slope of the plot of ln k vs. $1/T$ is $-8.66 \times 10^3 \pm 1.5 \times 10^2$, corresponding to an activation energy of 72 kJ mol^{-1}. For reasons that will be explained later, subsequent studies were done at 80° C.

Effect of pH. Figure 2 shows the effect of pH on both the apparent first-order rate constant and the initial absorbance of the reaction solution. The apparent rate constant has a very small dependence on pH between 4.5 and 5.5 and increases gradually with pH above 5.5. The initial absorbance of the reaction solution is relatively low up to pH 5 and then rises sharply after that. As a compromise between a detrimental acid-catalyzed hydrolysis of a reaction intermediate [6] and an unacceptably large blank absorbance, pH 5.5 was chosen for subsequent studies.

Ninhydrin concentration. Figure 3 shows the effect of ninhydrin concentration on the apparent first-order rate constant. The data exhibit a very gradual curvature toward the concentration axis as ninhydrin concentration is increased. These data suggest that higher ninhydrin concentration could be used to speed the reaction, permit the use of lower temperatures and/or reduce the measurement time. However, as will be explained in more detail later, reactions for some amino acids deviate from pseudo-first-order behavior

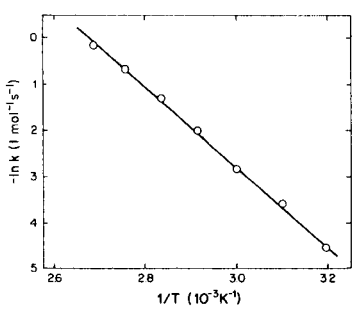

Fig. 1. Effect of temperature on the apparent first-order rate constant for glycine.

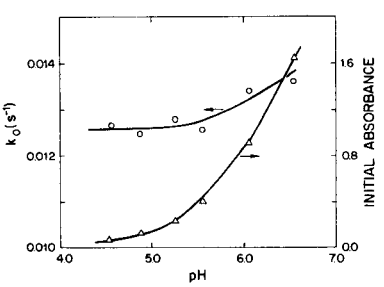

Fig. 2. Effects of pH on the apparent first-order rate constant and initial absorbance for glycine.

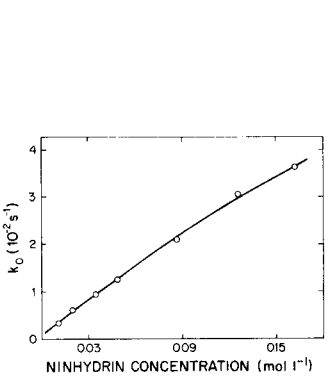

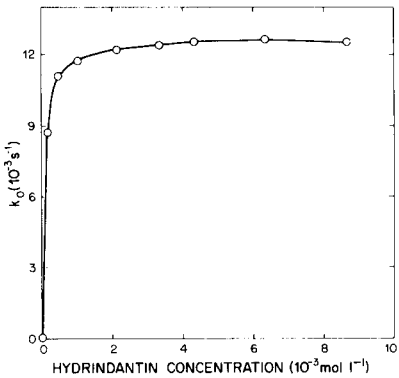

Fig. 3. Effect of ninhydrin concentration on the apparent first-order rate constant for glycine.

Fig. 4. Effect of hydrindantin concentration on the apparent first-order rate constant for glycine.

at higher ninhydrin concentration and a value of 0.048 M was chosen for subsequent studies except when stated otherwise.

Hydrindantin concentration. Figure 4 shows the effect of hydrindantin on the apparent first-order rate constant. The data show that there is no measurable color development in the absence of hydrindantin, but that the rate constant rises rapidly with small increments of the reagent and becomes independent of concentration above about 2×10^{-3} mol l^{-1}. A value of 4.3×10^{-3} mol l^{-1} was selected for the remainder of these studies.

Acetate concentration. As shown in Fig. 5, the apparent rate constant varies linearly with acetate concentration between 0.1 and 1.0 mol l^{-1}. The least-squares equation for the data is $k_0 = 7.90 \times 10^{-3}$ s^{-1} l $mol^{-1} + 7.95 \times 10^{-3}$ s^{-1}. A somewhat arbitrary value of 0.5 M acetate was chosen for subsequent studies.

Selection of reaction conditions

A major objective of this study was to develop a single set of reaction conditions that would permit a variety of amino acids to be quantified with measurement times in the range 1—2 min. A secondary objective was to use the lowest temperature that would permit the primary goals to be achieved. Accordingly, experiments were done with a relatively high (0.165 mol l^{-1}) ninhydrin concentration at 70° C.

Excellent results were obtained for glycine and leucine, with both exhibiting pseudo-first-order behavior. For example, Fig. 6A shows a set of experimental absorbance vs. time data for glycine along with results of a first-order fit based on data from the early part of the reaction. There is good agreement between the experimental (e) data and fitted (f) results, confirming desired pseudo-first-order behavior. However, response curves for phenylalanine

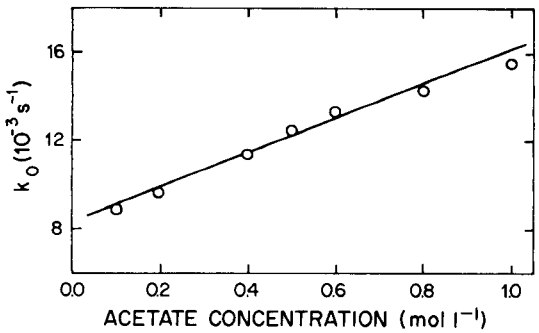

Fig. 5. Effect of acetate concentration on the apparent first-order rate constant for glycine.

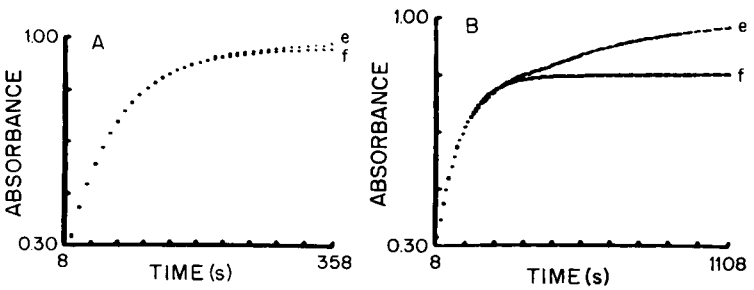

Fig. 6. Comparison of kinetic behavior for glycine (A) and phenylalanine (B) at 0.165 M ninhydrin and 70° C. Curves: (e) experimental data; (f) fitted results (first-order model). Data range, 8—88 s for glycine, 8—148 s for phenylalanine.

exhibited significant deviation from first-order behavior (Fig. 6B). The extent of deviation from first-order behavior decreased as the ninhydrin concentration was decreased. Although the reasons for this behavior are not understood, it is clear that this is not a satisfactory situation for the kinetic quantitation of amino acids. Accordingly, alternative conditions involving 80° C and 0.048 mol l^{-1} ninhydrin (and other conditions summarized above) were evaluated and shown to be applicable to a wide range of concentrations of several amino acids. With these conditions, the behavior of each amino acid examined was similar to that illustrated for glycine in Fig. 6A. Accordingly, these conditions were used for further work.

Quantitative evaluation

Three different data-processing options were compared for glycine. In a rate method, glycine concentration was evaluated from the linear least-squares slope of absorbance vs. time data between 8 and 58 s. In an equilibrium method, the glycine concentration was evaluated from absorbance measurements after 7—8 half-lives. In the predictive kinetic method, concentration was evaluated from values of initial absorbance ($\hat{A}_0$) and equilibrium

absorbance ($\hat{A}_\infty$) computed by fitting A vs. t data between 8 and 128 s to a first-order model [4] as illustrated in Fig. 6A. These plots are atypical of most obtained in this study in that the computed value of $\hat{A}_\infty$ usually tends to be slightly larger than the measured value, A_∞. Because the effect is relatively small, reasons for it were not investigated. However, it is known that the reaction mechanism is quite complex [6] and it is not surprising that it does not follow exact first-order kinetics.

In the following discussion, all uncertainties are reported at ±1 standard deviation.

Comparison of data-processing options. Figure 7 includes calibration plots for rate ($\Delta A/\Delta t$), predictive kinetic ($\Delta\hat{A}_\infty = \hat{A}_\infty - \hat{A}_0$), and equilibrium ($\Delta A = A_\infty - \hat{A}_0$) data. Rate data vary nonlinearly with concentration but both predictive-kinetic and equilibrium data vary linearly with concentration. The slight offset between the latter plots results from the apparent deviation of the reaction from exact first-order behavior (Fig. 6A). Least-squares statistics for these two plots, included as the first two rows in Table 1, show that the difference between the intercepts (0.019 − 0.017 = 0.002) is relatively small in comparison with the uncertainty in the intercepts (0.006) and the standard error of the estimate (0.012). Although the curve-fitting process tends to over-estimate the A_∞ value in most cases, the systematic error is relatively small in comparison with the random scatter about the calibration plots. A linear least-squares fit of predictive kinetic data ($\Delta\hat{A}_\infty$) vs. equilibrium data (ΔA_∞) gave

$$\Delta\hat{A}_\infty = (1.014 \pm 0.006)\Delta\hat{A}_\infty - 0.003 \pm 0.004$$

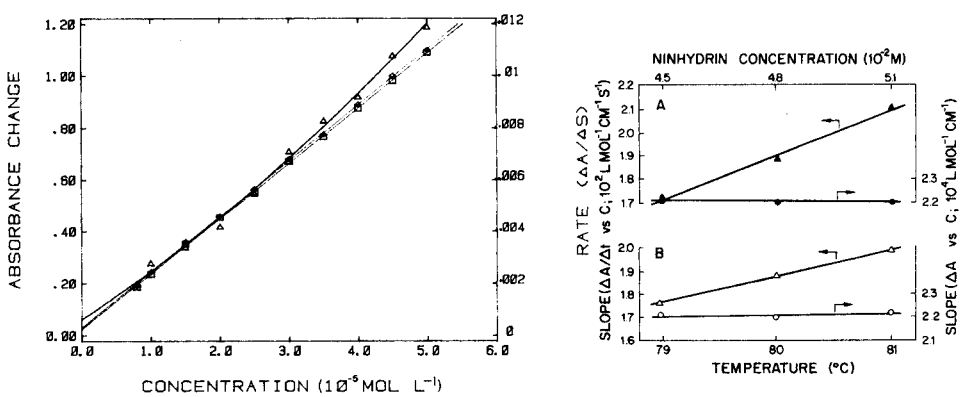

Fig. 7. Calibration data for glycine with different data-processing methods: (△) rate; (□) equilibrium; (◇) predictive-kinetic.

Fig. 8. Comparison of error dependencies for rate and predictive-kinetic methods: (A) ninhydrin concentration; (B) temperature. Data-processing method: (△, ▲) rate; (○, ●) predictive-kinetic.

TABLE 1

Least-squares statistics for absorbance change vs. concentration of glycine[a]

Data range (s)	Half-lives	Slope[b] (10^4 l mol^{-1} cm^{-1})	Intercept[b] (Absorbance)	Std. error est. (S_{yx})	Correlation coefficient
Equilibrium	7.5	2.17 ± 0.02	0.019 ± 0.006	0.011	0.999
8—128	2.3	2.20 ± 0.02	0.017 ± 0.007	0.013	0.999
8—188	3.3	2.19 ± 0.02	0.015 ± 0.006	0.011	0.999
8—148	2.7	2.19 ± 0.02	0.017 ± 0.007	0.012	0.999
8—108	1.95	2.22 ± 0.03	0.020 ± 0.010	0.018	0.998
8—98	1.75	2.24 ± 0.04	0.020 ± 0.013	0.023	0.996
8—88	1.6	2.29 ± 0.05	0.020 ± 0.016	0.029	0.995

[a]Four replicates at each of nine equally spaced concentrations of glycine from 1.0×10^{-5} to 5.0×10^{-5} mol l^{-1}; the absorbance range of each data set is about 0.3—1.4. [b]With standard deviations.

with $S_{yx} = 0.008$ and $r = 0.9996$. These statistics confirm good agreement between results obtained with the predictive-kinetic and equilibrium approaches.

Effects of data range. Table 1 includes least-squares statistics for $\Delta\hat{A}_\infty$ values computed over different data ranges vs. concentration. Predictably (see Fig. 6A), some statistics are degraded as the data range is decreased. Thus, it is possible for a user to make a trade-off between reliability and the time involved in the measurement step. Noting that it will usually be necessary to include a calibration step, it is probable that a data-processing range as short as 90 s could be used for glycine without substantial degradation of results.

Error coefficients. Because the predictive kinetic method computes the absorbance change expected if the reaction were monitored to completion, this method is expected to have variable dependencies and error coefficients that are much closer to those for equilibrium methods than for more conventional rate methods. To check this, error dependences were evaluated for variations in the temperature or the ninhydrin concentration. Results are presented for the rate and predictive-kinetic methods.

Triplicate runs were made at 79, 80, and 81° C on each of four equally-spaced glycine concentrations from 2.0×10^{-5} to 3.5×10^{-5} mol l^{-1}. Average values of rate constants at the three temperatures were 1.11×10^{-2}, 1.25×10^{-2}, and 1.43×10^{-2} s^{-1}. Least-squares slopes of rate data ($\Delta A/\Delta t$) and predictive-kinetic data ($\Delta\hat{A}_\infty$) vs. concentration were computed at each temperature and results are plotted in Fig. 8B. Slopes for rate data exhibit the expected increase with temperature with a temperature coefficient of about 6% per degree. In contrast, the slopes for the predictive-kinetic data are virtually independent of temperature corresponding to a temperature coefficient near zero (less than the random uncertainty of the points). It should be

noted that the temperature coefficient of the rate data is only about half the value that might be expected from the 12—13% temperature coefficient of rate constants given above. The smaller value is obtained because the "rate" data computed in this work are chords computed over about one half-life of the reaction rather than initial rates which would have error coefficients equivalent to the temperature coefficients for the rate constants. Even so, the predictive-kinetic method exhibits substantial improvement in the temperature coefficient relative to the rate method. The temperature coefficient for equilibrium data is virtually identical to that of the predictive kinetic data.

Triplicate runs were also made at 4.5×10^{-2}, 4.8×10^{-2}, and 5.1×10^{-2} mol l^{-1} ninhydrin on each of four equally-spaced glycine concentrations from 2.0×10^{-5} to 3.5×10^{-5} M glycine. Average values of rate constants at the three ninhydrin concentrations were 1.06×10^{-2}, 1.25×10^{-2}, and 1.42×10^{-2} s^{-1}. Calibration slopes ($\Delta A/\Delta t$ vs. C and $\Delta \hat{A}_\infty$ vs. C) computed as described for the temperature data are plotted vs. ninhydrin concentration in Fig. 8A. Whereas the rate data change by about 20% for this change in ninhydrin concentration, the predictive kinetic data change less than the random scatter among the points.

Thus, the predictive-kinetic method has systematic error coefficients that are virtually zero for both temperature and ninhydrin concentration. Similar results are expected for other variables that do not affect either the pseudo-first-order behavior or the equilibrium absorbance.

Other amino acids. Four other amino acids (alanine, phenylalanine, leucine, and isoleucine) were studied. All behaved similarly to glycine with apparent first-order rate constants of 4.1, 6.9, 8.2, and 3.9×10^{-3} s^{-1} for alanine, phenylalanine, leucine and isoleucine, respectively.

Selected quantitative data for these four acids are summarized in Table 2. The data confirm good agreement between the predictive-kinetic and equilibrium results and reflect the good linearity of $\Delta \hat{A}_\infty$ vs. concentration. As with glycine, better results are obtained when data ranges of 2—2.5 half-lives are used in the fitting process. However, reasonable reliability is achieved when data ranges of 1—1.5 half-lives are used.

Effects of variables such as temperature and reagent concentration were not evaluated for these acids; however, there is no reason to expect that error coefficients would be different than those obtained for glycine (Fig. 8).

The slopes in Tables 1 and 2 represent the apparent molar absorptivities (assuming complete reaction) for the reaction products for the different amino acids. For the five acids examined here, the absorptivities differ by less than 5%. It should be noted that apparent absorptivities for products of other amino acids differ from the ones studied here [1].

DISCUSSION

To ensure proper perspective for this study, it is emphasized that the focus has been on the measurement and data-processing steps and that it is

TABLE 2

Least-squares statistics for absorbance change vs. concentration[a] for four amino acids processed by the equilibrium and predictive-kinetic methods

Data range (s)	Half-lives	Slope[b] (10^4 l mol^{-1} cm^{-1})	Intercept[b] (Absorbance)	Std. error est. (S_{yx})	Correlation coefficient
Alanine					
8—1248	7.5	2.28 ± 0.02	0.011 ± 0.007	0.009	0.999
8—368	2.2	2.27 ± 0.02	0.007 ± 0.007	0.009	0.999
8—208	1.25	2.34 ± 0.05	0.001 ± 0.016	0.026	0.997
Phenylalanine					
8—748	7.5	2.20 ± 0.02	—0.003 ± 0.007	0.010	0.999
8—238	2.4	2.21 ± 0.02	—0.006 ± 0.007	0.008	0.999
8—118	1.2	2.30 ± 0.04	—0.014 ± 0.012	0.016	0.998
Leucine					
8—548	7.5	2.24 ± 0.02	0.002 ± 0.005	0.007	0.999
8—208	2.45	2.26 ± 0.03	0.005 ± 0.009	0.011	0.999
8—108	1.3	2.27 ± 0.07	0.007 ± 0.024	0.033	0.996
Isoleucine					
8—1328	7.5	2.26 ± 0.04	0.005 ± 0.013	0.013	0.999
8—398	2.25	2.26 ± 0.02	0.005 ± 0.003	0.011	0.999
8—208	1.15	2.28 ± 0.04	0.005 ± 0.014	0.019	0.998

[a]Three replicates at each of five equally-spaced concentrations between 1×10^{-5} and 5×10^{-5} mol l^{-1}; absorbance ranges are about 0.3—1.5. [b]With standard deviation.

expected that the proposed approach will be combined with suitable separation methods as is the equilibrium measurement approach. The results show that the predictive-kinetic method offers an alternative to the more traditional equilibrium procedure without sacrificing reliability as is the case with commoner kinetic methods [3].

One potential advantage of the kinetic measurement approach is the substantially reduced time required for the measurement step. A second advantage is that the kinetic method compensates for any blank absorbance of the sample because the A vs. t data are projected to zero time so that the initial absorbance, A_0, is calculated as part of the process. A third potential advantage involves the possible use of rate constants generated by the fitting process to confirm identifications based on chromatographic retention times. A potential disadvantage of the kinetic approach is the need for multiple data points for each sample. This problem could be alleviated with the aid of any one of a variety of sample-processing systems developed recently that permit several samples to be monitored simultaneously and repeatedly. One such sample processor is the so-called "centrifugal analyzer" that uses centrifugal force to mix many different samples simultaneously with aliquots of

reagent and then to spin the different mixtures past a detector rapidly for repeated measurements as the reaction proceeds. There are other types of "parallel" sample processors that permit multiple samples to be processed simultaneously. Most of these could make it feasible to adapt the predictive-kinetic measurement step to the chromatographic separation process. The resulting combination could offer some advantages relative to the commoner approaches without the problem of reduced reliability that characterizes more conventional kinetic methods.

This work was supported by Grant No. CHE 8319014 from the National Science Foundation.

REFERENCES

1 S. Blackburn, Amino Acid Determination Methods and Techniques, M. Dekker, New York, 1968, pp. 69—80.
2 K. M. Jonker, H. Poppe and J. K. Huber, Chromatographia, 11 (1978) 123.
3 H. A. Mottola and H. B. Mark, Anal. Chem., 54 (1982) 62R.
4 G. E. Mieling and H. L. Pardue, Anal. Chem., 50 (1978) 1611.
5 G. E. Mieling, H. L. Pardue, J. E. Thompson and R. A. Smith, Clin. Chem., 25 (1979) 1581.
6 P. J. Lamothe and P. G. McCormic, Anal. Chem., 45 (1973) 1906.

Analytica Chimica Acta, 173 (1985) 33—41
Elsevier Science Publishers B.V., Amsterdam — Printed in The Netherlands

SPECTROPHOTOMETRIC DETERMINATION OF MICRO AMOUNTS OF THIOSULFATE BY LIBERATION OF THIOCYANATE FROM MERCURY(II) THIOCYANATE

YASUYUKI MIURA and TOMOZO KOH*

Department of Chemistry, Faculty of Science, Tokai University, Hiratsuka-shi, Kanagawa 259-12 (Japan)

(Received 21st November 1984)

SUMMARY

The proposed determination of thiosulfate is based on the liberation of thiocyanate by the reaction of thiosulfate with mercury(II) thiocyanate and spectrophotometric determination of the thiocyanate with iron(III). The reaction of thiosulfate with mercury(II) thiocyanate is elucidated with reference to a system containing phosphate buffer; the phosphate is shown to participate directly in the reaction, and a balanced chemical equation is given. Optimum conditions are described for the stoichiometric formation of 3 mol of thiocyanate from 1 mol of thiosulfate. The method can be applied to the determination of thiosulfate in the range 3×10^{-6}—1.4×10^{-4} M (1.7—78.5 μg thiosulfate in 5 ml).

The accurate determination of sulfur compounds in their mixtures causes many problems. Sörbo [1] showed that copper(II) catalyzes the conversion of thiosulfate to thiocyanate, and reported a method for the determination of thiosulfate by spectrophotometric measurement of the thiocyanate formed. The copper(II)-catalyzed cyanolysis of thiosulfate has played an important role in the development of methods for the analysis of mixtures of polythionates [2—6]. In a different method, Utsumi [7] determined thiosulfate by quantifying the thiocyanate released in the reaction of thiosulfate with mercury(II) thiocyanate. However, the chemical composition of the precipitate yielded in the reaction, its identity, and also the stoichiometric reaction were not established.

It was found here that thiosulfate reacts with mercury(II) thiocyanate to yield thiocyanate in the following manner

$$4\ S_2O_3^{2-} + 6\ Hg(SCN)_2 + HPO_4^{2-} + 16\ H_2O = Hg_6S_4(OH)_2HPO_4 + 4\ SO_4^{2-} + 10\ H_3O^+ + 12\ SCN^- \quad (1)$$

The purpose of this study is to establish the optimum conditions under which this reaction proceeds to stoichiometric completion and to clarify the reaction with special reference to the determination of thiosulfate.

0003-2670/85/$03.30

EXPERIMENTAL

Reagents and apparatus

All chemicals used, except mercury(II) thiocyanate, were of analytical grade and were used without further purification. A thiosulfate solution was prepared by dissolving sodium thiosulfate pentahydrate in freshly boiled and cooled redistilled water containing a small amount of sodium carbonate, and standardized by iodimetry a week after preparation. Working standard thiosulfate solutions were prepared by appropriate dilution. A stock solution of thiocyanate was standardized by Volhard's method [8], and working standards were prepared by suitable dilution. These standards were used to confirm the stoichiometry and completion of the reaction of thiosulfate with mercury(II) thiocyanate.

Mercury(II) thiocyanate was synthesized by adding 250 ml of 0.4 M potassium thiocyanate to 250 ml of 0.2 M mercury(II) nitrate in 1.5 M nitric acid, in small portions and with vigorous stirring. The white precipitate of mercury(II) thiocyanate formed was filtered off by suction with a sintered-glass filter (3SG4), washed with distilled water and small amounts of methanol, and then air-dried at room temperature.

A methanol solution of mercury(II) thiocyanate (3.5×10^{-3} M) was prepared by dissolving 280 mg (accurately weighed) of the mercury(II) thiocyanate in methanol and diluting the mixture to 250 ml with methanol.

Buffer solutions as required for adjusting the pH of reaction solutions to 2.7—8.1 were prepared by mixing phosphoric acid (0.11 M) with sodium dihydrogenphosphate (0.11 M), acetic acid (0.2 M) with sodium acetate (0.2 M), sodium dihydrogenphosphate (0.11 or 0.2 M) with sodium monohydrogenphosphate (0.11 M) or sodium hydroxide (0.2 M) and boric acid (0.2 M) with sodium tetraborate (0.05 M), respectively, in various volume ratios. The buffer solution of pH 7.4 used in the procedure given below was obtained by mixing 50 ml of 0.2 M sodium dihydrogenphosphate with 39.5 ml of 0.2 M sodium hydroxide. A solution of iron(III) nitrate in perchloric acid was prepared by dissolving 306.1 g of iron(III) nitrate nonahydrate in 217.6 ml of 60% perchloric acid and diluting to 500 ml with redistilled water to give a 1.5 M iron(III) nitrate in 4 M perchloric acid.

All spectrophotometric measurements were made at 460 nm with a Hirama Model 6B spectrophotometer with 10-mm glass cells. The precipitate formed by the reaction of thiosulfate with mercury(II) thiocyanate was collected on the interface between aqueous and organic phases with a Kokusan Model H-100B1 centrifuge. Desired temperatures were controlled by a Taiyo Coolnit CL-15 thermoregulator. pH was measured with a Hitachi-Horiba Model M-7 pH meter.

Procedure

Pipette 1 ml of 0.2 M phosphate buffer solution (pH 7.4), 5 ml of thiosulfate solution up to 1.4×10^{-4} M, and then 1 ml of 3.5×10^{-3} M mercury-

(II) thiocyanate in methanol into a 15-ml glass-stoppered tube. The pH of the solution is whereby brought to 7.7. Allow the mixture to stand at temperatures ranging from 15 to 30°C for 10 min, to drive the reaction to completion. In this case, the reaction solution becomes turbid owing to the formation of a yellow precipitate. To this mixture, add 2 ml of 1.5 M iron(III) nitrate in 4 M perchloric acid and about 1 ml of carbon tetrachloride. Shake the mixture vigorously by hand, and centrifuge it in order to collect the precipitate formed on the interface between the aqueous and organic phases. Measure the absorbance of a clear aqueous solution of the iron(III) thiocyanate complex formed against distilled water at 460 nm.

RESULTS AND DISCUSSION

Calibration graphs

A series of standard solutions of thiosulfate and thiocyanate were treated as in the above Procedure. The resulting plots are shown in Fig. 1. If thiosulfate is completely and stoichiometrically converted into thiocyanate according to Eqn. 1, the calibration graph for thiosulfate should coincide with that for thiocyanate when the molar concentration scale for thiosulfate is drawn to three times the scale for the thiocyanate concentration. Figure 1 thus proves that the reaction had proceeded to stoichiometric completion. Positive deviation from a straight line in the lower concentration range is attributed to the thiocyanate yielded as a result of slight dissociation of the mercury(II) thiocyanate.

The precision was estimated from 11 results for 5-ml aliquots containing 0.505 μmol of thiosulfate. The present method gave a mean value of 0.505 μmol of thiosulfate with a standard deviation of 0.0013 μmol and a relative standard deviation of 0.27%.

Effects of varying experimental conditions on the reaction

Rate of the reaction of thiosulfate with mercury(II) thiocyanate at different temperatures. The rate of the reaction was investigated at pH 7.7 and at various temperatures ranging from 10 to 30°C. The absorbance for 8×10^{-5} M thiosulfate reached that for 2.4×10^{-4} M thiocyanate, which is the expected value, in 60 min at 10°C, in 10 min at 15°C, in 8 min at 22°C and in 5 min at both 25 and 30°C, and then remained constant. These results reveal that the reaction can proceed to completion, as long as the reaction is carried out for 10 min at temperatures ranging between 15 and 30°C. Thiosulfate was therefore allowed to react with mercury(II) thiocyanate under these conditions.

Effect of pH. Preliminary studies showed that the monohydrogenphosphate produced from the phosphate buffer added for pH adjustment participated directly in the reaction of thiosulfate with mercury(II) thiocyanate. Therefore in the presence of the same amounts (0.11 mmol) of phosphate as those used in the Procedure, the influence of pH on the reaction was

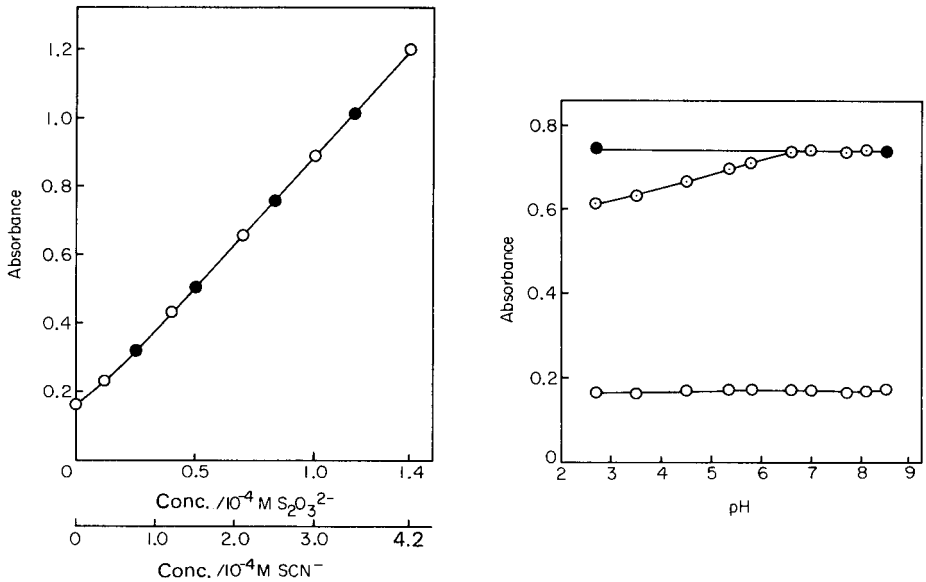

Fig. 1. Calibration graphs for thiosulfate and thiocyanate. (○) $S_2O_3^{2-}$; (●) SCN^-.

Fig. 2. Effect of pH on the reaction of thiosulfate with mercury(II) thiocyanate at 22°C in the presence of 0.11 mmol phosphate: (⊙) 8×10^{-5} M $S_2O_3^{2-}$; (●) 2.4×10^{-4} M SCN^-; (○) reagent blank.

examined over the pH range 4.5—8.5. The results are summarized in Table 1. At pH 4.5 where the fraction present as monohydrogenphosphate is quite negligible, the absorbances obtained for thiosulfate did not reach the expected value, though they are very reproducible. Over the pH range 6.6—8.5, where monohydrogenphosphate can exist, each reaction went to completion in 8 min and the absorbances at pH 7.0, 7.7 and 8.1 reached the relevant expected value, confirming that the thiosulfate was stoichiometrically converted to thiocyanate according to Eqn. 1, while the reaction at pH 6.6 did not follow Eqn. 1 completely, owing to the inadequate fraction present as monohydrogenphosphate. At pH 8.5, however, poor and variable results were obtained presumably because of some interaction between the thiosulfate and the hydrolysis product of mercury(II) thiocyanate. The pH range 6.8—8.1 was therefore optimal for the reaction of thiosulfate with mercury(II) thiocyanate under the recommended conditions (Fig. 2). A decrease in absorbance below pH 6.8 was caused by a decrease in the fraction of monohydrogenphosphate, the pK_{a_2} of phosphoric acid being 7.2.

Effect of amount of mercury(II) thiocyanate. To establish the optimal amounts of mercury(II) thiocyanate in the conversion of thiosulfate into thiocyanate, 1-ml portions of methanol solutions of mercury(II) thiocyanate of various concentrations were used. Figure 3 shows that the reaction was incomplete with 1 ml of 5×10^{-4}—2.7×10^{-3} M mercury(II) thiocyanate because the amount was inadequate. But when 1 ml of 3×10^{-3}—5×10^{-3} M

TABLE 1

Effect of phosphate on the reaction of thiosulphate with mercury(II) thiocyanate at various pH levels and 22°C

Time	Absorbance[a]					
	8×10^{-5} M $S_2O_3^{2-}$					
	pH 4.5	pH 6.6	pH 7.0	pH 7.7	pH 8.1	pH 8.5
	0.581[b]	0.582[b]	0.579[b]	0.577[b]	0.573[b]	0.567[b]
2	0.484	0.532	0.535	0.537	0.545	0.571
5	0.484	0.564	0.562	0.568	0.563	0.576
8	0.477	0.568	0.576	0.575	0.569	0.598
10	0.484	0.570	0.578	0.576	0.575	0.589
15	0.482	0.566	0.579	0.573	0.577	0.604
20	0.478	0.571	0.578	0.576	0.573	0.582
30	0.474	0.575	0.578	0.575	0.574	0.605

[a]Against the reagent blank. [b]Absorbances for 2.4×10^{-4} M SCN^-, which are the expected values.

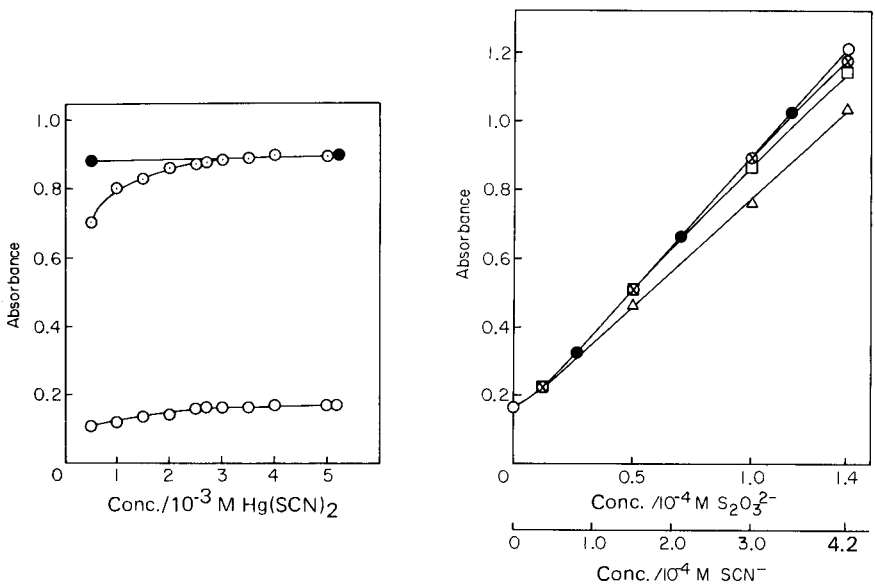

Fig. 3. Effect of concentration of mercury(II) thiocyanate (1-ml portions) on the reaction of thiosulfate: (⊙) 1×10^{-4} M $S_2O_3^{2-}$; (●) 3×10^{-4} M SCN^-; (○) reagent blank. Other conditions as in the Procedure.

Fig. 4. Effect of amounts of phosphate buffer on the reaction of thiosulfate with mercury(II) thiocyanate: (△) $S_2O_3^{2-}$ in the absence of phosphate buffer (tetraborate buffer was used for pH adjustment); (□) $S_2O_3^{2-}$ with 0.05 M phosphate buffer; (⊗) $S_2O_3^{2-}$ with 0.1 M phosphate buffer; (○) $S_2O_3^{2-}$ with 0.15—0.3 M phosphate buffer; (●) SCN^- with tetraborate buffer or 0.3 M phosphate buffer (expected graph). (The volume of buffer solutions employed was 1 ml.)

mercury(II) thiocyanate was used, the absorbances for thiosulfate were in exact agreement with the expected values obtained for thiocyanate. Therefore, 1 ml of methanol solution of 3.5×10^{-3} M mercury(II) thiocyanate was used in the Procedure.

Effect of amount of phosphate buffer. As mentioned during the discussion of pH, the monohydrogenphosphate arising from the phosphate buffer used for pH adjustment participated directly in the reaction of thiosulfate with mercury(II) thiocyanate. In establishing the optimal amounts of the buffer, thiosulfate was treated with mercury(II) thiocyanate in the presence of various concentrations of phosphate buffer (pH 7.4) prepared by mixing equimolar solutions of sodium dihydrogenphosphate and sodium hydroxide in a volume ratio of 50:39.5 ml; 1-ml portions of each buffer tested were used. The resulting graphs are shown in Fig. 4. In the absence of the phosphate buffer, where tetraborate buffer solution (pH 7.8) was used for pH adjustment, the calibration graph for thiosulphate gave the greatest negative deviation from the expected graph. When 0.05 or 0.1 M phosphate buffer was used, thiosulfate was not quantitatively converted to thiocyanate according to Eqn. 1 because of insufficient phosphate. But the graph for thiosulfate was in exact accordance with that for standard thiocyanate when the phosphate buffer used was 0.15—0.3 M. Therefore, 1 ml of 0.2 M phosphate buffer (pH 7.4) sufficed for quantitative reaction.

Reaction of thiosulfate with mercury(II) thiocyanate in the presence of phosphate

In order to establish the stoichiometric relationship of thiosulfate to mercury(II) thiocyanate, the reaction was investigated by the method of continuous variations. For application of this method, $4x$ (x = mole fraction of thiosulfate) ml of 5×10^{-4} M thiosulfate and $4(1 - x)$ ml of 5×10^{-4} M mercury(II) thiocyanate in methanol were used with a varying mole ratio of thiosulfate to mercury(II) thiocyanate. In this case, $4x$ ml of methanol and $4(1 - x)$ ml of distilled water also were added in order to keep the volumes of water and alcohol constant, because the alcohol tended to increase the absorbance; 1 ml of 0.2 M phosphate buffer (pH 7.0) was used to adjust the pH to the optimum range of 6.8—8.1. Then the absorbances of a series of solutions were measured at 460 nm against water. Figure 5 shows the plots of absorbance vs. mole fraction of thiosulfate, in which the $Hg(SCN)_2$ blank in the region $x < 0.4$ and the $Hg(SCN)_2$-free blank in the region $x > 0.4$ were subtracted. The two curves intersected at a point indicating a 0.4 mole fraction of thiosulfate. This signifies that 4 mol of thiosulfate apparently reacted with 6 mol of mercury(II) thiocyanate in the recommended procedure.

A yellow precipitate which is soluble only in aqua regia was formed in addition to the thiocyanate as a result of the reaction of thiosulfate with mercury(II) thiocyanate. An attempt was made to elucidate the reaction by determining the mercury, sulfur, and phosphorus in the precipitate.

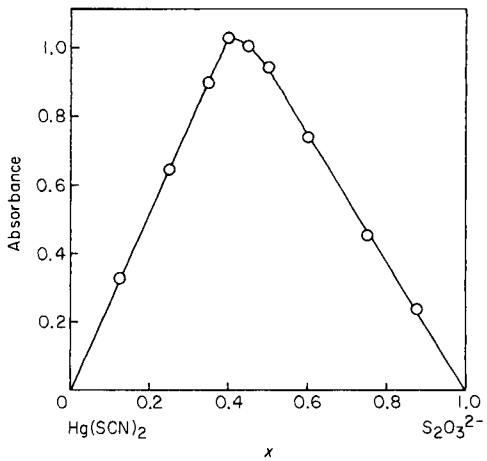

Fig. 5. Continuous variations plot for the $S_2O_3^{2-}$—$Hg(SCN)_2$ reaction in the presence of phosphate.

Some of the precipitates obtained in the Procedure were dissolved in a small volume (3—4 drops) of aqua regia by heating, and then the solution was diluted with water as required. The solutions so obtained were used for the determination of mercury by atomic absorption spectrometry and for the spectrophotometric determination of phosphorus [9]. For the determination of sulfur contents, the precipitate was mixed with tin(II)/strong phosphoric acid, and the mixture was heated at about 280° C for 15 min [10]. The evolved hydrogen sulfide was absorbed in 1 M zinc acetate; the fixed sulfide was determined by iodimetry. The results are shown in Table 2. The ratio of the number of atoms for Hg, S, and P in the precipitate was thus calculated to be 5.94:3.95:1.00. The precipitate could, therefore, be $Hg_6S_4(OH)_2HPO_4$; the percentages of Hg, S, and P found are extremely close to those calculated for this chemical formula (see Table 2).

It was concluded that the reaction proceeded to completion according to Eqn. 1 under the conditions given in the Procedure on the basis of the following findings: (1) 4 mol of thiosulfate react with 6 mol of mercury(II) thiocyanate (Fig. 5); (2) 1 mol of thiosulfate produces 3 mol of thiocyanate (Fig. 1); (3) the monohydrogenphosphate from the phosphate buffer participated directly in the reaction (Table 1 and Fig. 4); and (4) the above element percentages fit the formula of $Hg_6S_4(OH)_2HPO_4$ (Table 2).

Effect of diverse ions

Aliquots (5-ml) of solutions containing 44.8 μg of thiosulfate and various amounts of diverse ions were treated as in the Procedure. The amounts of diverse ions that caused errors below 3% are listed in Table 3. Ammonium, chloride, bromide, iodide, cyanide, sulfide gave positive interferences even when present in small amounts, because they reacted with mercury(II) thiocyanate to liberate thiocyanate. Metal ions such as Mg(II), Ca(II),

TABLE 2

Determination of mercury, sulfur and phosphorus in the precipitate

Precipitate taken (mg)	Element found (mg)	Element found in precipitate (%)	Element calculated for $Hg_6S_4(OH)_2HPO_4$ (%)
Mercury			
10.82	8.84	81.7	82.3
9.30	7.60	81.7	
Sulfur			
12.56	1.09	8.68	8.77
10.68	0.93	8.70	
Phosphorus			
49.59	1.05	2.12	2.12
53.09	1.13	2.13	

TABLE 3

Effect of diverse ions on the determination of 44.8 μg of thiosulfate

Ion	Added as[a]	Amount (μg)	$S_2O_3^{2-}$ found (μg)	Ion	Added as	Amount (μg)	$S_2O_3^{2-}$ found (μg)
Na^+	$NaNO_3$	5000	44.8	Al^{3+}	$Al_2(SO_4)_3$	50	43.8
K^+	KNO_3	5000	44.6			1000[b]	43.7
NH_4^+	NH_4NO_3	5	44.6	F^-	NaF	5000	45.2
Mg^{2+}	$MgSO_4$	500	43.4	Cl^-	NaCl	2.5	45.6
		1000[b]	43.6	Br^-	KBr	5	45.9
Ca^{2+}	$Ca(NO_3)_2$	50	44.1	I^-	KI	5	45.9
		1000[b]	43.5	NO_3^-	$NaNO_3$	5000	44.1
Mn^{2+}	$MnSO_4$	2500	43.4	NO_2^-	KNO_2	5000	46.0
		5000[b]	43.5	CN^-	NaCN	0.5	45.4
Cu^{2+}	$Cu(NO_3)_2$	500	44.1	CO_3^{2-}	Na_2CO_3	500	44.3
		1000[b]	43.5	S^{2-}	Na_2S	0.5	46.1
Zn^{2+}	$Zn(NO_3)_2$	50	43.4	SO_3^{2-}	$NaHSO_3$	25	44.1
		100[b]	43.4	SO_4^{2-}	Na_2SO_4	5000	44.3
Cd^{2+}	$CdSO_4$	50	44.3	$HAsO_4^{2-}$	Na_2HAsO_4	5000	44.3
		100[b]	43.4	CH_3COO^-	CH_3COONa	5000	43.8
Pb^{2+}	$Pb(NO)_3$	500	43.8	borate ion	H_3BO_3	5000	44.3
		1000[b]	43.6				

[a]Water of hydration is omitted for brevity. [b]1 ml of 0.5 M phosphate buffer was used in place of 0.2 M phosphate buffer.

Mn(II), Cu(II), Zn(II), Cd(II), Pb(II), and Al(III) gave negative interference caused by a decrease in the fraction of monohydrogenphosphate owing to the formation of their insoluble phosphates. The interferences of these metals could be reduced or eliminated by increasing the amount of phosphate buffer (see Table 3).

REFERENCES

1 B. Sörbo, Biochim. Biophys. Acta, 23 (1957) 412.
2 P. J. Urban, Z. Anal. Chem., 180 (1961) 110.
3 T. Koh and I. Iwasaki, Bull. Chem. Soc. Jpn., 39 (1966) 703.
4 D. P. Kelly, L. A. Chambers and P. A. Trudinger, Anal. Chem., 41 (1969) 898.
5 T. Mizoguchi and T. Okabe, Bull. Chem. Soc. Jpn., 46 (1975) 1799.
6 T. Koh, Y. Aoki and I. Iwasaki, Analyst (London), 104 (1979) 41.
7 S. Utsumi, Nippon Kagaku Zasshi, 74 (1953) 301.
8 I. M. Kolthoff, E. B. Sandell, E. J. Meehan and S. Bruckenstein, Quantitative Chemical Analysis, 4th edn., Macmillan, London. 1969, p. 798.
9 D. F. Boltz and M. G. Mellon, Anal. Chem., 20 (1948) 749.
10 T. Kiba, I. Akaza and N. Sugishita, Bull. Chem. Soc. Jpn., 30 (1957) 972.

Analytica Chimica Acta, 173 (1985) 43—49
Elsevier Science Publishers B.V., Amsterdam — Printed in The Netherlands

KINETIC SPECTROPHOTOMETRIC METHOD FOR THE SIMULTANEOUS QUANTITATION OF AMINO ACIDS IN TWO- AND THREE-COMPONENT MIXTURES

YAHYA R. TAHBOUB[a] and HARRY L. PARDUE*
Department of Chemistry, Purdue University, West Lafayette, IN 47907 (U.S.A.)
(Received 22nd January 1985)

SUMMARY

The development and evaluation of a kinetic method for the simultaneous quantitation of two- and three-component mixtures of amino acids are described. The method is based on reaction with ninhydrin. Multipoint kinetic data collected during one or more half-lives of the slower-reacting component are processed with a nonlinear regression program to resolve the data into the concentrations of the individual components in the mixture. Results demonstrate good linearity between prepared and calculated concentrations of each component and total amino acid in the mixture (10—50 μM). Slopes of least-squares fits of calculated vs. prepared concentrations vary from 0.98 to 1.13 and intercepts vary from —0.1 to 2.9 μM with standard errors of the estimate (S_{yx}) between 0.67 and 1.7 μM.

Differences in the kinetic behavior of components that undergo the same or similar reactions have been used to resolve quantitatively the individual components in mixtures for several years. Earlier methods were based on graphical or simple computational procedures [1—4]. More recent papers have described multipoint curve-fitting methods to resolve mixtures with kinetic data [5—8]. Some of the curve-fitting methods were based on non-linear regression methods [5, 7] while others were based on so-called multiple-linear regression methods [6, 8]. Also, all the curve-fitting methods have involved the use of data collected during 7—8 half-lives of the slowest reacting component. Although this latter approach is satisfactory for the fast reactions used as models in the earlier studies, it is less satisfactory for slow reactions for which measurement time can present a problem.

The primary objective of this study was to evaluate the utility of the curve-fitting methods to resolve mixtures of amino acids based on reactions with ninhydrin. Secondary objectives were to compare the two curve-fitting approaches and to evaluate the feasibility of utilizing data ranges shorter than 7—8 half-lives to resolve mixtures. Conclusions are that the curve-fitting methods can be used to resolve selected two- and three-component

---

[a]Present address: Department of Chemistry, Oklahoma State University, Stillwater, OK 74078, U.S.A.

0003-2670/85/$03.30

mixtures of amino acids, that the two curve-fitting methods yield virtually identical results, and that satisfactory results can be obtained with data processed over as little as two half-lives of the more slowly reacting component.

EXPERIMENTAL

Principles and procedures involved in the curve-fitting methods were described earlier [5, 6, 8]. Briefly, signal vs. time data collected for a fixed period of time are fitted to a mathematical model that describes the kinetic behavior of the mixture. In the present study, the model involved two or three simultaneous pseudo-first-order reactions monitored by absorbance changes. The computed value of the absorbance change, $\Delta\hat{A}_\infty$, for each component that gave the best fit to the experimental model was used to compute the concentration of the component.

Experimental conditions required for first-order behavior for amino acids were described earlier [9]. Briefly they involve a reaction medium consisting of 4.8×10^{-2} M ninhydrin, 4.3×10^{-3} M hydrindantin, 0.5 M acetate buffer at pH 5.5, and a temperature of 80°C. The acetate buffer was prepared by dissolving 54.4 g of sodium acetate trihydrate in water, adding 9.0 ml of glacial acetic acid, and diluting to 100 ml with water. A composite reagent was prepared daily by dissolving 500 mg of ninhydrin and 80 mg of hydrindantin in 20 ml of methylcellosolve (all from Sigma Chemical Co.) and adding 6.7 ml of acetate buffer.

For each sample, 0.50 ml of the composite reagent and 0.40 ml of water were mixed in a cuvet and 0.1 ml of sample containing amino acids was added after the solution in the cuvet had reached 80°C. Absorbance was monitored at 10-s intervals at 570 nm with a distilled-water blank. Absorbance/time data were processed with regression programs described earlier [5, 6, 8].

RESULTS AND DISCUSSION

Uncertainties for all quantitative results are quoted as one standard-deviation unit. Unless stated otherwise, reported results were obtained with the nonlinear least-squares curve-fitting method [5].

Response curves

Figure 1A shows response curves for three amino acids (histidine, isoleucine, and leucine). Figure 1B is a response curve for an equimolar mixture of these three components. The pseudo-first-order rate constant and absorptivity of the product for each component are computed from data such as those in Fig. 1A. Then, the experimental values of rate constants are used in the curve-fitting programs to compute values of $\hat{A}_0$ and values of $\hat{A}_\infty$ for each acid that give the "best" (least-squares) fit of A vs. t data to the model for three simultaneous first-order reactions with known rate constants.

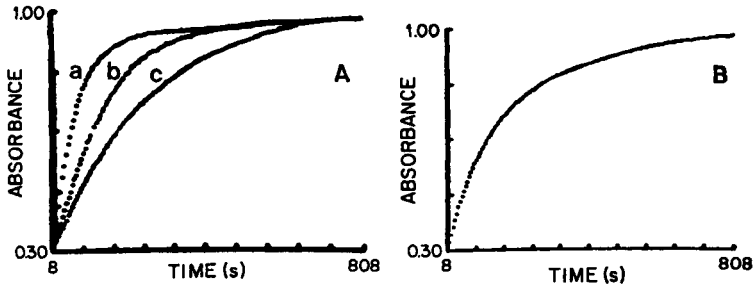

Fig. 1. Response curves for selected amino acids: (A) 30 μM histidine (a), leucine (b), and isoleucine (c); (B) mixture containing 10 μM each histidine, leucine, and isoleucine.

The concentration of each component is computed from the absorbance change, $\Delta\hat{A}_\infty = \hat{A}_\infty - \hat{A}_0$, by using a known value of absorptivity for the reaction product. The fitting process involves assumptions that there are no synergic effects among the amino acids and that all acids produce products with the same absorptivities.

Absorptivities/rate constants

Molar absorptivities for all amino acids examined except lysine are 2.24×10^4 l mol^{-1} cm^{-1}; the value for lysine is slightly larger at 2.37×10^4 l mol^{-1} cm^{-1}. Pseudo-first-order rate constants for the five amino acids included in this study were 16.0, 12.5, 8.2, 6.8, and 3.9×10^{-3} s^{-1} for histidine, glycine, leucine, lysine and isoleucine, respectively. It is of course important that these rate constants be independent of amino-acid concentration. For amino-acid concentrations between 10 and 50 μM, least-squares slopes of experimental values of rate constants vs. concentration (μM) were 2.6, 2.9 and 5.8×10^{-6} for glycine, leucine, and isoleucine, respectively, confirming the required low dependence on concentration. For isoleucine, the complete least-squares equation was

$$k = 5.8 \times 10^{-6}\, C^0 + 3.9 \times 10^{-3}$$

For the lowest and highest concentrations (10 and 50 μM), computed values of k were 3.958×10^{-3} and 4.19×10^{-3} s^{-1}, corresponding to a maximum difference of 0.23×10^{-3} s^{-1} or 6%. This is the worst-case value; all other slopes and relative "errors" were smaller and well within the random uncertainty in experimental value of rate constants.

Concentration data

Results are reported here for two- and three-component samples processed with different data ranges and with the different curve-fitting approaches [5, 6, 8].

Two-component samples. Samples contained 10—50 μM total amino acid and 5—45 μM of each component so that concentration ratios varied between 9:1 and 1:9. The two different sets of mixtures evaluated were glycine with

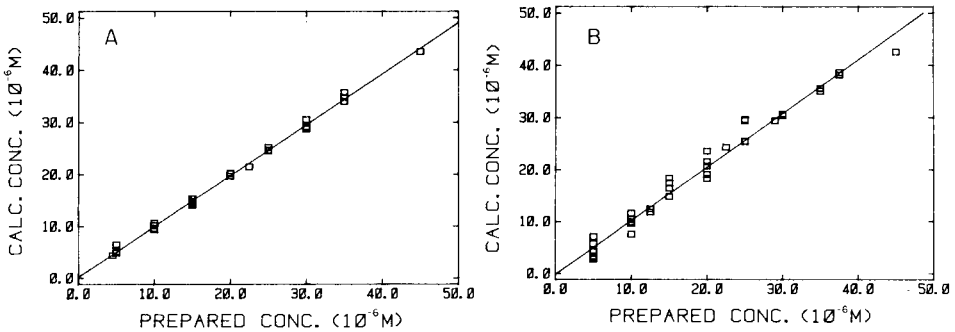

Fig. 2. Comparison of computed vs. prepared concentrations for two-component mixtures: (A) glycine with a fitting range of 7.4 half-lives; (B) isoleucine with a fitting range of 1.15 half-lives.

isoleucine, and leucine with isoleucine, involving ratios of rate constants of 3.2:1 and 2.1:1, respectively. Best-case and worst-case results for the glycine/isoleucine mixture are presented in Fig. 2. Reproducibility was evaluated for fixed amounts of each component in the presence of variable amounts of the other component(s). For 5, 20 and 35 μM each of the acids, standard deviations were 0.51, 0.39 and 0.41, respectively, for glycine and 0.84, 0.81 and 0.40, respectively, for isoleucine with data ranges of 8—408 s for glycine and 8—608 s for isoleucine. More complete results are presented as pooled stan-

TABLE 1

Least-squares statistics for calculated vs. prepared concentration of glycine, isoleucine and total amino acid in glycine/isoleucine mixtures[a]

Data range (s)	Number of half-lives	Pooled s.d.[b] (μM)	Slope ± s.d.[a]	Intercept ± s.d.[a] (μM)	S_{yx}[a,c] (μM)	r[d]
Glycine						
8—408	7.4	0.51	0.99 ± 0.01	0.12 ± 0.21	0.64	0.999
8—248	4.5	0.71	1.01 ± 0.01	—0.25 ± 0.26	0.78	0.997
8—208	3.8	0.95	0.01 ± 0.02	—0.26 ± 0.35	1.05	0.995
Isoleucine						
8—608	3.4	0.69	1.00 ± 0.01	0.32 ± 0.21	0.67	0.999
8—248	1.4	1.21	1.02 ± 0.02	—0.19 ± 0.33	1.09	0.995
8—208	1.15	1.51	1.03 ± 0.02	—0.01 ± 0.49	1.61	0.990
Total amino acid						
8—608	—	0.43	1.00 ± 0.01	0.14 ± 0.21	0.45	0.999
8—248	—	0.75	0.99 ± 0.01	0.36 ± 0.41	0.64	0.999
8—208	—	0.91	0.99 ± 0.01	0.43 ± 0.45	0.95	0.996

[a]30 samples; 5—45 μM glycine, 5—45 μM isoleucine, and 10—50 μM total amino acid. [b]Seven groups with 5, 5, 4, 4, 4, 3, and 3 samples, respectively. [c]Standard error of estimate. [d]Correlation coefficient.

TABLE 2

Least-squares statistics for calculated vs. prepared concentration of leucine, isoleucine and total amino acid in leucine/isoleucine mixtures[a]

Data range (s)	Half-lives (s)	Pooled s.d. (μM)	Slope ± s.d.	Intercept ± s.d. (μM)	S_{yx} (μM)	r
Leucine						
8—608	7.05	0.76	1.03 ± 0.02	—0.32 ± 0.36	0.67	0.998
8—408	4.75	1.26	1.00 ± 0.03	—0.10 ± 0.60	1.00	0.996
8—308	3.60	0.94	0.95 ± 0.04	—0.24 ± 0.46	0.86	0.996
Isoleucine						
8—608	3.4	0.69	1.07 ± 0.02	—1.20 ± 0.33	0.67	0.998
8—408	2.3	1.68	1.05 ± 0.03	—0.36 ± 0.71	1.45	0.992
8—308	1.75	2.24	0.98 ± 0.05	—2.20 ± 0.98	2.00	0.983
Total amino acid						
8—608	—	0.71	1.02 ± 0.02	—0.43 ± 0.55	0.69	0.999
8—408	—	0.98	1.00 ± 0.02	0.32 ± 0.81	1.00	0.998
8—308	—	1.26	1.02 ± 0.03	0.39 ± 0.98	1.25	0.997

[a]30 samples; 5—45 μM leucine, 5—45 μM isoleucine, and 10—50 μM total amino acid.

dard deviations and least-squares statistics for fits of computed vs. prepared concentrations in Tables 1 and 2 for these two-component mixtures. In each case, best results were obtained for the faster-reacting component with data processed over longer times and worst results were obtained for the slower-reacting component with data processed over shorter times.

To provide a basis for comparison, single-component samples were processed over similar data ranges by the predictive kinetic method described earlier [9]. The least-squares statistics for a fit of computed concentration ($\hat{C}^0$) vs. prepared concentration (C^0) of glycine were

$$\hat{C}^0 = (1.007 \pm 0.003)C^0 - 0.16 \pm 0.21$$

with a standard error of the estimate (S_{yx}) of 0.35 μM and correlation coefficient of 0.9996. All results for two-component samples are degraded relative to those for the single-component sample. However, when the standard error of the estimate is used as a measure of the scatter about the best fit to the data, results are degraded by little more than a factor of 2 as long as ratios of rate constants are 2:1 or larger, and the data range includes three or more half-lives of the slower-reacting component. Shorter reaction times can be used with a corresponding increase in uncertainty.

Three-component mixtures. Results obtained for two sets of three-component samples are summarized in Table 3. To obtain reasonably reliable results with these mixtures, it was necessary to process data over some 4.5 half-lives of the slower-reacting component. Results are substantially degraded relative to results for single-component samples and the best results for two-components mixtures but are similar to those for two-component

TABLE 3

Least-squares statistics for calculated vs. prepared concentration of individual and total amino acid in three-component mixtures[a]

Amino acid	Pooled s.d.[b] (μM)	Slope ± s.d.	Intercept ± s.d. (μM)	S_{yx} (μM)	r
Histidine/lysine/isoleucine					
Histidine	1.12	1.02 ± 0.03	−1.02 ± 0.50	0.93	0.99
Lysine	1.66	1.04 ± 0.06	−0.70 ± 0.56	1.70	0.98
Isoleucine	1.25	1.09 ± 0.04	0.20 ± 0.60	1.30	0.99
Total amino acid	0.98	1.03 ± 0.02	−0.64 ± 0.68	1.05	0.99
Histidine/leucine/isoleucine					
Histidine	1.21	0.11 ± 0.04	−2.90 ± 0.60	1.10	0.99
Leucine	1.85	1.02 ± 0.06	−0.32 ± 1.00	1.82	0.97
Isoleucine	1.35	1.13 ± 0.04	−0.32 ± 0.59	1.02	0.99
Total amino acid	0.86	1.03 ± 0.03	−0.72 ± 0.65	1.05	0.99

[a]25 samples, concentration of each component 5 to 30 μM, and total amino acid 15 to 50 μM, data range 8—808 s. [b]Six groups with 4, 6, 6, 4, 3 and 2 samples, respectively.

mixtures when reduced data ranges are used. Longer monitoring times approaching 6—8 half-lives for the slower-reacting component would likely yield some improvement. However, such long times would not be practical unless some type of multichannel sample-processing system were used.

Comparison of data-processing methods

The two data-processing methods reported previously [5, 6, 8] were used to process data sets for selected two- and three-component samples. For eighteen different combinations of samples and data ranges, the two methods yielded results for $\Delta\hat{A}_\infty$ that differed by less than 0.001. A linear least-squares fit of computed absorbance changes for the multiple-linear regression ($\Delta\hat{A}'_\infty$) and nonlinear regression ($\Delta\hat{A}_\infty$) methods yielded the equation

$$\Delta A'_\infty = 1.0002\ \Delta A_\infty - 0.0004$$

with $S_{yx} = 0.002$ and $r = 0.99995$, indicating excellent agreement between the two fitting methods.

Conclusions

It is apparent from the data presented above that, for ideal samples, there is a real loss in reliability as one proceeds from one- to two- to three-component samples. If it were possible to do separations without any loss or cross-contamination, then clearly, best results would be obtained with complete separations so that measurements would be made on single-component aliquots of the sample. However, when allowance is made for the nonideal nature of separation processes, it may be possible to exploit the multi-component kinetic data-processing methods to resolve incompletely separated

samples with substantially less net loss of reliability than might be implied by the results presented above.

This work was supported by Grant No. CHE 8319014 from the National Science Foundation.

REFERENCES

1 H. B. Mark and G. A. Rechnitz, Kinetics in Analytical Chemistry, Interscience, New York, 1968.
2 H. A. Laitinen and W. E. Harris, Chemical Analysis, McGraw-Hill, New York, 1975, p. 389.
3 J. B. Pausch and D. W. Margerum, anal. Chem., 41 (1969) 226.
4 D. W. Margerum, J. B. Pausch, G. A. Nyssen and G. F. Smith, Anal. Chem., 41 (1969) 233.
5 B. G. Willis, W. H. Woodruff, J. R. Frysinger, D. W. Margerum and H. L. Pardue, Anal. Chem., 42 (1970) 1350.
6 G. M. Ridder and D. W. Margerum, Anal. Chem., 49 (1977) 2098.
7 J. B. Landis and H. L. Pardue, Clin. Chem., 24 (1978) 1700.
8 R. S. Harner and H. L. Pardue, Anal. Chim. Acta, 127 (1981) 23.
9 Y. R. Tahboub and H. L. Pardue, Anal. Chim. Acta, 173 (1985) 23.

Analytica Chimica Acta, 173 (1985) 51—62
Elsevier Science Publishers B.V., Amsterdam — Printed in The Netherlands

A SIMPLE, INEXPENSIVE COMPUTER-CONTROLLED SLEW-SCAN ATOMIC FLUORESCENCE FLAME SPECTROMETER FOR MULTI-ELEMENT DETERMINATIONS

LORI A. DAVIS, R. J. KRUPA and J. D. WINEFORDNER*
Department of Chemistry, University of Florida, Gainesville, FL 32611 (U.S.A.)
(Received 29th January 1985)

SUMMARY

The system consists of a continuum xenon arc lamp source, a chopper, an argon-separated air/acetylene flame atomizer, a high-throughput, medium-resolution grating monochromator under Apple II+ wavelength control, a photomultiplier detector, and a photon counter with an Apple II+ for data collection and statistical treatment. The computer-controlled system is shown to give semiquantitative results (within ±50%) for 19 elements at two wavelengths each (one wavelength for 7 elements) in less than 15 min; quantitative results (within ±5%) for each element at a selected wavelength were obtained in about 5 min. The system was characterized by determining 10 and 14 elements in synthetic mixtures and by determining a number of elements in NBS standard reference materials (orchard leaves and two steels).

Presently, graphite-furnace and flame atomic absorption spectrometry and inductively coupled plasma atomic emission spectrometry are the most commonly used atomic spectrometric methods for the determination of the concentration of elements in a variety of samples; atomic fluorescence spectrometry (a.f.s.) is less widely used. Presently there is only one commercially available atomic fluorescence spectrometer, the Baird ICP AFS-2000 [1].

While atomic absorption spectrometry (a.a.s.) provides low limits of detection, it has a relatively small linear dynamic range, approximately one to three decades [2]. Multi-element a.a.s. with individual hollow-cathode line sources is also time-consuming, especially with the conventional single-channel instruments. Modern atomic absorption flame spectrometers are capable of rapidly measuring 2, 6 or 12 elements sequentially and rapidly with no changes in instrumentation, such as hollow-cathode lamps. The xenon source, wavelength modulated, echelle, flame/furnace atomic absorption spectrometric system of Harnly et al. [3] allows up to 20 elements (wavelengths) to be measured simultaneously.

While a.f.s. has been noted as a valuable tool in multi-element determinations, it has not been commonly used [2, 4]. However, it has several potential advantages over a.a.s. Detection limits by a.f.s. are generally equal to or better than a.a.s., and a.f.s. has a linear dynamic range of three to six decades.

0003-2670/85/$03.30

Just as in a.a.s., a.f.s. has high selectivity. The presence of chemical (matrix) interferences depend on the atomizer used. Because of the high spectral selectivity, a multi-element atomic fluorescence spectrometer is easy to operate and can be constructed at a relatively low cost.

Several years ago, Ullman et al. [5] proposed the use of a wavelength-modulated computer-controlled atomic emission/fluorescence spectrometer for multi-element determinations [5]. Based on this design, our system, a computer-controlled, slew-scan, multi-element atomic fluorescence spectrometer (m.e.a.f.s.), was constructed at a low cost and for ease of operation. An Eimac (Cermax) xenon arc lamp, which is a continuum source of radiation, was used as the excitation source. This eliminated the need for a different source for each element which is measured, and thus eliminated the normally long warm-up time for individual lamps. The m.e.a.f.s. system in the present case sequentially slew-scans to thirty-one different fluorescence wavelengths, and determines the presence of and concentrations of nineteen elements in a water matrix. The scanning of the monochromator and the data acquisition are all under computer-control. The signal data are converted to concentrations by using calibration curves stored within the computer programming. The system was designed for ease of operation, time efficiency, wide applicability, and low cost while yielding semi-quantitative results (results within a factor of 2X the known results).

EXPERIMENTAL

Instrumental system

A block diagram of the system is shown in Fig. 1. Much of this system was based upon systems previously described [5, 6]; a list of instrumental components is given in Table 1. A 300-W Eimac (Cermax) xenon arc lamp (the excitation source) was focused onto an argon-separated air/acetylene flame. The optical train consisted of an *f*/4,4-in. focal length Suprasil lens focusing

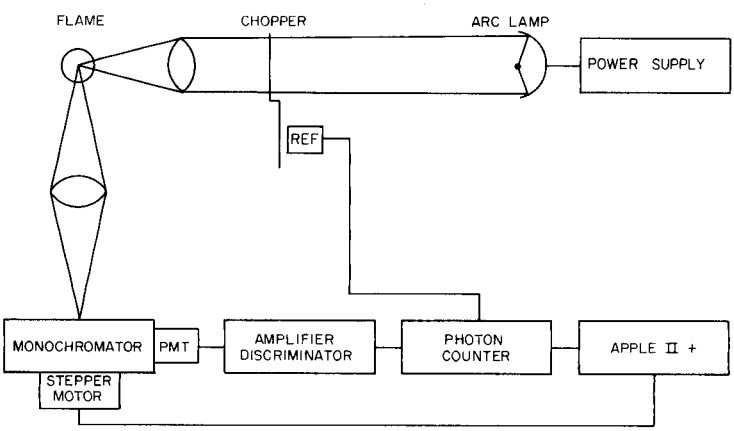

Fig. 1. Block diagram of the m.e.a.f.s. system.

TABLE 1

Components of the m.e.a.f.s. instrument

Component	Model No.	Company
Monochromator	218	GCA McPherson
Photomultiplier	EMI 9789QB	Thorne
Photomultiplier power supply	244	Keithley
Photomultiplier housing	1151	SSR Instruments
Photon counter		
Amplifier/discriminator	1120	SSR Instruments
Digital synchronous computer	1110	SSR Instruments
Nebulizer	303-0110	Perkin Elmer
Capillary burner		Laboratory-made
Xenon arc lamp	300 UV	EIMAC, Div. of Varian
Lamp power supply	PS300-1	EIMAC, Div. of Varian
Computer	II$^+$	Apple
Interfaces		Laboratory-made
Video terminal		Zenith
Printer	V300-25	Vista Computer Co.
Dual disk drives	Disk II	Apple
	Elite I	Rana
Stepping motors	M063-FC06 C2	Superior Electric Co.
Translator module	STM 101	Superior Electric Co.
Chopper	382 B	Ithaco

the light from the xenon arc lamp onto the flame and an $f/5.3$,2-in. focal length Suprasil lens in a $2f$ configuration focusing a 1:1 image onto the entrance slit of the monochromator. The fluorescence signals were amplitude-modulated by means of a chopper placed between the xenon arc lamp and the first lens.

Several precautions were also taken to reduce scattered light reaching the monochromator. Two sets of cylindrical snouts, painted with flat black paint, enclosed the light path. The first set of snouts was placed between the xenon arc lamp and the first lens, enclosing the light path. These snouts were also purged with nitrogen gas to reduce the formation of ozone. A 1-in. aperture (diameter of the collimated beam emitted by the xenon arc lamp) was placed on the end of one snout prior to the first lens. The second set of snouts enclosed the light path from the flame to the monochromator. A second aperture was placed prior to the second lens and was 0.75 in. to match the angle of acceptance of the monochromator.

The pre-mixed argon-separated air/acetylene flame was fuel-rich to reduce the background in the OH region [7]. A laboratory-constructed stainless-steel capillary burner was used. Both the air and acetylene gas flows were doubly regulated to reduce fluctuations in the flame. Nupro fine-metering valves were also placed after the rotameters to adjust and set the gas flows to the burner. The gas can, thus, be shut off from the burner at the rotameters

without changing the flow settings. The argon sheath was also used around the flame to minimize entrainment of air into the flame.

Several precautions were taken to reduce radiofrequency (r.f.) noise. In addition to a photomultiplier housing which was magnetically and r.f. shielded, a doubly shielded coaxial cable was constructed for the high voltage cable to the photomultiplier tube. All other cables were wrapped in aluminum foil and electrical tape and grounded to reduce r.f. pickup. The Eimac xenon arc lamp was also housed in a ventilated, grounded, aluminum box. The photon counter was mounted in a bench which was surrounded on three sides with grounded copper screen acting like a Faraday cage. These precautions helped reduce r.f. noise and thus lowered the background count rate.

An Apple II^+ microcomputer controlled the sequential slew scanning of the monochromator by means of a stepping motor attached to the grating drive lead screw [6]. The slew scan (ca. 16 nm s^{-1}) was controlled by an assembly language program. Acquisition of the fluorescence signal from the photon counter was also under computer control. The experimental parameters (used with SEMI-QUANT) chosen to reduce noise and fluctuations in the system are given in Table 2.

Computer system and programming

A listing of the computer programs is available from the authors on request. Two programs, SEMI-QUANT and QUANT are written in BASIC for use with the m.e.a.f.s. system. The SEMI-QUANT program also used an assembly language program, which is callable from BASIC, to control the sequential slew scan.

The QUANT program is a modification of an LOD program written by Long, based on a propagation-of-error approach to limits of detection [8].

TABLE 2

Experimental conditions used with the SEMI-QUANT program

Component	Condition
Monochromator	0.3-m Czerny-Turner, $f/5.3$; 600 grooves/mm grating blazed at 300 nm; 90-μm slit width; 1-cm slit height; 0.4-nm spectral bandpass
Source	
power	300 W
arc voltage	15 V
arc current	19.6 A
Chopper frequency	141 Hz
Photon counter	Chop mode; difference display select; preset N = 1410 (10 s); chopper sampling time = 3.2 ms
Flame gases (l min^{-1})	Air atomization = 5.6; air auxiliary = 0.8; acetylene = 1.2; argon = 8.5
Nebulizer aspiration rate	5 ml min^{-1}
Observation height	1.8 cm above burner

In this program, calibration graphs for an element at a single wavelength are obtained. Upon completion of the calibration graph, the limit of detection (LOD) for k values of 2 and 3, a propagation-of-error LOD, and the equation for the calibration graph are printed out. Finally, samples are introduced, the fluorescence signal at the specific fluorescence line used for the calibration curve is measured and converted by means of the program into an analyte concentration, and the results (concentrations) are printed. To use the QUANT program at a single wavelength requires about 5 min for determination of concentration (±5%).

The SEMI-QUANT program is written to allow rapid sequential slew scanning to 31 fluorescence wavelengths and to facilitate collection of data for both qualitative and semi-quantitative analysis of 19 elements using stored (up to 6 months) calibration data. The experimental conditions for use with this system (see Table 2) are chosen to reduce noise and fluctuations in the system over time. The SEMI-QUANT program resulted in slew scanning of the monochromator to each wavelength and in the collection of two measured signals; each measured signal is the number of counts in a 10-s integration period. The first signal is compared to the sum of three times the standard deviation of the blank signal plus the average blank signal, i.e., $3s_b + \bar{x}_b$, based on the IUPAC definition of limit of detection [9]. If the first measured signal is less than the value of $3s_b + \bar{x}_b$, then the second value is not collected. Otherwise, the two measured signals are averaged, and the average is stored. These averages are then compared to the stored log-log calibration graphs and concentrations are calculated. For the concentrations to be accepted, they must fall within the previously established linear dynamic ranges at each wavelength. A table of the elements detected, their wavelengths, and the concentration calculated at that wavelength is then printed out. The program was also adapted to the collection of blank signals and/or standard signals prior to running a sample.

The m.e.a.f.s. system was found to be background shot-noise limited. Thus, the standard deviation of the fluorescence signal is equivalent to the square root of the sum of the fluorescence and emission of the flame [10]. The values for the square root of the sum at each wavelength were also stored within the program. The sum of the blank signal plus three times the square root of the background is then used for each line of each element as the minimum signal with which to compare the measured signals for qualitative and semi-quantitative measurement.

The fluorescence signal of one standard solution (located in the middle of the calibration data) collected at each fluorescence line is used to correct the intercepts of the log-log calibrations. Blank signals and standard signals may be collected as often as necessary (in this case, once every two weeks). The slopes of these log-log calibrations are very close to unity (1.00 ± 0.05). By periodically measuring blank signals and signals of standard solutions, the m.e.a.f.s. system can thus be corrected for long-term drift.

Reagents

The 1000 μg ml^{-1} stock solutions of each element were prepared by dissolving the pure metal or reagent-grade salt in dilute acid, and diluting with deionized water which was further purified using a Barnstead Nanopure filtration system (14 MΩ cm^{-1} resistivity). Volumetric dilutions of the stock solutions were made to obtain standard solutions of the desired concentrations. Two multi-element solutions were also prepared to evaluate the instrument. One such solution, a ten-element mixture called 10M, was prepared by dissolving the metals in nitric acid. An aliquot of this solution was then diluted to be within the linear dynamic range of the system. The second solution, a fourteen-element mixture called 14M, was prepared by taking aliquots of standard solutions and diluting them in a volumetric flask. This solution was also diluted further to be within the linear dynamic range of the instrument. Solutions of National Bureau of Standards (NBS) Standard Reference Materials (SRM) were prepared by established procedures [11]. Aliquots of these solutions were then diluted so that the concentration of all major constituents was 100 μg ml^{-1} or less, to approximate a water matrix. Water was used as the blank in all cases.

RESULTS AND DISCUSSION

Detection limits

In Table 3 are listed limits of detection obtained under optimized conditions (applicable to the QUANT program) and constant conditions (Table 2, applicable to the SEMI-QUANT program) for all lines of all elements studied. Two lines were used for each element when possible to increase the reliability of the results. The linear dynamic ranges are also indicated in Table 3; this range corresponds to the range of concentrations for which the slope of the log-log plot is 1.00 ± 0.05. It should be noted that the linear dynamic range for sodium at 589.6 nm is only one decade; this is caused by a high background and the maximum count rate of 85 MHz for the photon counter used.

In Tables 4 and 5, the recoveries of 10 and 14 elements, respectively, in two synthetic solutions are given. Except for iron (at 252.285 nm), all elements are recovered within ±16% in the case of the 10M synthetic mix. Except for Au, Pt, Tl, and Rh (at 350.252 nm), all elements were measured within ±23% in the case of the 14M synthetic mixture. In the 10M mixture, the high iron result at 252.285 nm may be due to a spectral interference by cobalt at 252.136 nm. In the 10M mixture, the somewhat low result for copper occurs at both copper lines, indicating a non-spectral interference. In the 14M mixture, the low results for thallium may have been the result of thallium(I) chloride precipitating out of solution, because of a high concentration of hydrochloric acid before dilution. The very high results for gold at 267.595 nm and platinum at 265.945 nm are certainly due to spectral interferences. The system also does not sufficiently resolve the cobalt and gold lines at 242.493 nm and 242.795 nm, respectively.

TABLE 3

Limits of detection (LOD) and linear dynamic ranges obtained by the m.e.a.f.s. system

Element	Wavelength (nm)	LOD[a] (μg ml^{-1})		Upper conc.[b] (μg ml^{-1})	LOD a.a.s.[c] (μg ml^{-1})
Cd	228.800	0.01	(0.01)	1	0.03
Ca	422.673	0.002	(0.004)	1	NA (0.003)
Cr	357.869	0.007	(0.009)	5	0.02
	359.349	—	(0.01)	10	
Co	240.725	0.03	(0.06)	10	0.07
	242.493	—	(0.09)	10	
Cu	324.754	0.005	(0.008)	5	0.01
	327.396	—	(0.02)	5	
Au	242.795	0.3	(0.3)	40	0.17
	267.595	—	(0.3)	100	
In	303.936	—	(0.2)	50	—
	451.131	0.05	(0.08)	10	
Fe	248.327	0.02	(0.05)	100	0.07
	252.285	—	(0.07)	100	
Pb	283.306	—	(0.2)	50	0.1
	405.783	0.2	(0.2)	50	
Mg	285.213	0.0003	(0.0006)	1	0.001
Mn	279.482	0.003	(0.005)	10	0.01
Ni	232.003	0.04	(0.06)	5	0.07
	352.454	—	(0.1)	10	
Pt	265.945	1.0	(1)	100	1
	306.471	—	(5)	1000	
Rh	343.489	0.08	(0.2)	100	0.07
	350.252	—	(1)	100	
Ag	328.068	0.004	(0.004)	5	0.007
	338.289	—	(0.007)	5	
Na	589.592	0.06	(0.1)	1	0.003
Sr	460.733	0.003	(0.01)	5	NA (0.03)
Tl	276.787	—	(0.2)	50	0.1
	377.572	0.04	(0.04)	50	
Zn	213.756	0.02	(0.02)	1	0.07

[a]Values obtained for optimized flame conditions; values in parentheses were obtained for m.e.a.f.s. SEMI-QUANT experimental parameters. [b]Concentration at which linearity of calibration curve has changed by 5% (see text). [c]Values taken from O'Haver [12] for simultaneous multi-element atomic absorption flame spectrometry. NA means nitrous oxide/acetylene flame; all other values are for air/acetylene flames. The upper concentration for linear response is obtained by combining several calibration lines obtained at different points on the absorption profile during wavelength modulation. Those upper concentrations are usually 10^4—10^5 the limits of detection.

TABLE 4

Determination of ten elements in a synthetic mixture (10M) with the SEMI-QUANT program

Element	Wavelength (nm)	Concentration ($\mu g\ ml^{-1}$)		Error[a] (%)
		Actual	Found	
Cd	228.802	0.433	0.378	−12.7
Ca	422.673	0.290	0.292	0.7
Co	240.725	2.38	2.35	−1.0
	242.493		2.50	5.5
Cu	324.754	0.669	0.574	14.2
	327.396		0.573	−14.3
Fe	248.327	5.03	5.61	11.5
	252.285		6.41	27.5
Pb	283.306	2.75	2.77	0.8
	405.783		2.79	1.6
Mn	279.482	0.858	0.722	−15.8
Ni	232.003	2.01	1.86	−7.6
	352.454		2.17	8.0
Ag	328.068	0.135	0.121	−10.4
	338.289		0.129	−4.4
Zn	213.856	0.157	0.163	3.8

[a]Error = ((conc. found − actual conc.)/actual conc.) × 100.

TABLE 5

Determination of fourteen elements in a synthetic mixture (14M) with the SEMI-QUANT program

Element	Wavelength (nm)	Concentration ($\mu g\ ml^{-1}$)		Error[a] (%)
		Actual	Found	
Cd	228.802	0.100	0.097	−2.9
Ca	422.673	0.100	0.103	3.0
Cr	357.869	1.00	0.969	−3.1
	359.349		1.00	0.3
Co	240.725	1.00	0.956	−4.4
	242.493		(0.988)[b]	(−1.2)[b]
Au	242.795	1.00	(3.13)[b]	(21.3)[b]
	267.595		0.701	−29.9
In	303.936	5.00	4.91	−1.8
	451.131		5.00	0
Mg	285.213	0.0500	0.0439	−12.2
Mn	279.482	0.100	0.100	0
Pt	265.945	10.0	22.0	120
	306.471		<LOD[a]	—
Rh	343.489	5.00	4.87	−2.6
	350.252		7.07	41.4
Na	589.592	0.500	0.386	−22.8
Sr	460.733	1.00	1.03	3.5
Tl	276.787	5.00	2.30	−54.0
	377.572		1.94	−61.2
Zn	213.756	0.100	0.096	−4.2

[a]See Table 4. [b]The monochromator does not have sufficient resolution fully to separate these lines. [c]<LOD means concentration was below limit of detection resulting in a signal-to-noise ratio below 3.

It must be stressed that the results in Tables 4 and 5 were obtained by using the SEMI-QUANT approach, involving stored calibration curves. A 19-component mixture can be processed in about 15 min. By means of a faster stepping motor and by decreasing the integration time to 5 s, a 19-component mixture (at 31 wavelengths) could be processed in 3.5 min but the imprecision is doubled. If greater precision is needed, then the QUANT program must be used involving the preparation of fresh calibration data for each line of each element prior to sample processing. Table 6 shows a comparison of the recoveries for the SEMI-QUANT and QUANT approaches; the superior accuracy of the QUANT approach is apparent. However, the QUANT approach is considerably more time-consuming as discussed above.

Analysis of reference materials

In Table 7, the concentrations of several elements in three NBS-SRMs (Orchard leaves and two carbon steel samples) measured by the m.e.a.f.s./SEMI-QUANT approach are given and compared with certified values. For most elements, the results are reasonable, especially when viewed from the semi-quantitative aspect. In all cases, the concentrations are within a factor of two of the certified values.

Reproducibility

The 10M and 14M synthetic mixtures were used to obtain estimates of the relative standard deviation (RSD) for measurements taken over a period of time (ranging from a week to a month). In Table 8, the RSD values are given for all elements, except for platinum and gold (at 267.595 nm) which were not reproducibly detected. These measurements were all obtained by using the SEMI-QUANT approach (with constant input blank and standard values and therefore no recalibration). The average RSD for all lines is 10.7%. It is obvious that the reproducibility of the m.e.a.f.s. system in the SEMI-QUANT program mode is considerably better than the accuracy (especially if Table 7 is considered).

TABLE 6

Comparison of recoveries for m.e.a.f.s. with the SEMI-QUANT and QUANT approaches

Element	Wavelength (nm)	Actual conc. (μg ml^{-1})	SEMI-QUANT (μg ml^{-1})	Error[a] (%)	QUANT (μg ml^{-1})	Error[a] (%)
Cd	228.802	0.100	0.100	0	0.107	0
Ca	422.673	0.100	0.098	−2	0.103	3
Cr	357.869	0.100	0.054	−46	0.106	6
Co	240.725	1.00	1.14	14	1.15	15
Au	267.595	1.00	1.18	18	1.05	5
Pt	265.945	10.0	2.91	−71	9.41	−6
Zn	213.756	0.100	0.094	−6	0.112	12

[a]See footnote to Table 4.

TABLE 7

Analysis of NBS standards by m.e.a.f.s. and the SEMI-QUANT approach

Element	Wavelength (nm)	Concentration (μg ml^{-1})	
		Actual	Found
SRM 1571 (Orchard Leaves)[a]			
Ca	422.673	1.20	0.677
Mg	285.213	0.267	0.267
SRM 361 (High Carbon Steel)[b]			
Cr	359.349	1.40	0.94
Cu	324.754	0.086	0.113
	327.396		0.124
Fe	248.327		>LDR[c]
	252.285		69.0
Mn	279.482	1.35	1.31
Ni	232.003	4.08	5.10
	352.454		5.34
SRM 364 (High Carbon Steel)[d]			
Cr	359.349	0.07	0.12
Cu	324.754	0.293	0.266
	327.396		0.284
Fe	248.327	118	85
	252.285		69
Mn	279.482	0.305	0.353
Ag	328.068	0.008	0.010
	338.289		<LOD

[a]Concentration (μg g^{-1}) of analyte in orchard leaves is calculated as the concentration (μg ml^{-1}) of analyte measured × 250 ml of solution × 100-fold dilution/0.8609 g of sample. [b]Concentration (μg g^{-1}) of analyte in SRM 361 is calculated as the concentration (μg ml^{-1}) of analyte measured × 250 ml of solution × 50-fold dilution/2.5596 g of sample. [c]>LDR means concentration is above the range of linear response. [d]Concentration (μg g^{-1}) of analyte in SRM 364 is calculated as concentration (μg ml^{-1}) of analyte measured × 250 ml of solution × 100-fold dilution/3.0515 g of sample.

Conclusions

The m.e.a.f.s. system with the SEMI-QUANT program based on stored calibration curves gives reasonable precision and accuracy for low concentrations. The QUANT program improves the accuracy and precision but at the expense of speed. For samples such as steel, the accuracy is degraded because the matrix causes spectral interferences in some cases. The m.e.a.f.s. system is simple to operate and easy to adapt to specific problems, because of the use of a flame atomizer. The system could be improved by better r.f. shielding to reduce the background even more, by a photon counter with a higher maximum counting rate, by a higher-resolution grating in the monochromator and by a more powerful light source. For higher light levels, as are found in nitrous oxide/acetylene flames, a lock-in amplifier could be used rather than the photon counter.

TABLE 8

Reproducibility (RSD for concentration) of the SEMI-QUANT mode over a period of time

Element	Wavelength (nm)	RSD (%)	Wavelength (nm)	RSD (%)
Cd	228.802	8.3		
Ca	422.673	17.8		
Cr	357.869	22.8[a]	359.349	8.1[a]
Co	240.725	10.6	242.493	7.7
Cu	324.754	5.5	327.396	5.5
Au	242.795	2.9[a]	267.595	—[b]
In	303.936	4.9[a]	451.131	9.7[a]
Fe	248.327	4.3	252.285	4.8
Pb	283.306	9.4	205.783	14.3
Mg	285.213	8.4		
Mn	279.482	10.6		
Ni	232.003	7.5	352.454	4.6
Pt	265.945	—[a]	306.471	—[b]
Rh	343.489	11.9[a]	350.252	1.0[a]
Ag	328.068	5.7	338.289	11.8
Na	589.592	33.2[a]		
Sr	460.733	20.7[a]		
Tl	276.787	12.2[a]	377.572	9.5[a]
Zn	213.856	26.7		

[a]These values are based on three readings taken over a week for solution 14M. The other values are based on six readings taken over a month for solution 10M. [b]Concentrations not reproducibly detected.

The authors acknowledge the help of Dr. Benjamin W. Smith and Dr. Edward G. Voigtman in the design of this system. This work was supported by AF-AFOSR-F49620-84-C-0002.

REFERENCES

1 D. R. Demers and C. D. Allemand, Anal. Chem., 53 (1981) 1915.
2 J. D. Winefordner, J. J. Fitzgerald and N. Omenetto, Appl. Spectrosc., 29 (1975) 369.
3 J. M. Harnly, N. J. Miller-Ihli and T. C. O'Haver, Spectrochim. Acta, 39B (1984) 305.
4 J. D. Winefordner, in K. Fuwa (Ed.), Recent Advances in Analytical Spectroscopy, Pergamon Press, New York, 1982, pp. 151—164.
5 A. H. Ullman, B. D. Pollard, G. D. Boutilier, R. P. Bateh and P. Hanley, Anal. Chem., 51 (1979) 2382.
6 P. Wittman, J. Bower, J. J. Horvath, A. Ullman and J. D. Winefordner, Can. J. Spectrosc., 26(5) (1981) 212.
7 K. Fujiwara, A. H. Ullman, J. D. Bradshaw, B. D. Pollard and J. D. Winefordner, Spectrochim. Acta, 34B (1979) 137.
8 G. L. Long and J. D. Winefordner, Anal. Chem., 55 (1983) 712A.
9 Nomenclature, Symbols, Units and Their Usage in Spectrochemical Analysis — II, Spectrochim. Acta, 33B (1978) 242.

10 B. D. Pollard, A. H. Ullman and J. D. Winefordner, Anal. Chem., 53 (1981) 330.
11 R. Mavrodineanu (Ed.), Procedures Used at the NBS to Determine Selected Trace Elements in Biological and Botanical Materials, NBS Spec. Pub. 492, Department of Commerce, Washington, DC, 1977.
12 T. C. O'Haver, Analyst (London), 109 (1984) 211.

Analytica Chimica Acta, 173 (1985) 63—75
Elsevier Science Publishers B.V., Amsterdam — Printed in The Netherlands

ANALYTICAL CHARACTERISTICS OF AN OPTIMIZED MINIATURE INDUCTIVELY-COUPLED PLASMA SOURCE FOR ATOMIC EMISSION SPECTROMETRY

R. REZAAIYAAN and G. M. HIEFTJE*
Department of Chemistry, Indiana University, Bloomington, IN 47405 (U.S.A.)
(Received 1st November 1984)

SUMMARY

The inside dimensions of a miniature (13 mm i.d.) inductively-coupled plasma (i.c.p.) torch were optimized in an attempt to reduce further the r.f. power and argon gas required to sustain an i.c.p. As found earlier with a conventional-sized (18 mm i.d.) torch, the annular spacing between the plasma (intermediate) and coolant (outer) tube was shown to be the most critical design parameter. However, the optimized miniature i.c.p. could not necessarily be operated at lower r.f. power and argon flow rate than the optimized 18-mm torch or at lower argon flow rate than the original 13-mm torch. Moreover, although the detection limits and working-curve linearity of the optimized mini-i.c.p. were comparable to those of a conventional-sized torch, the errors caused by classical vaporization interferents were somewhat greater.

Despite its great popularity and broad application [1, 2], world-wide acceptance of the inductively-coupled plasma (i.c.p.) has been hindered by high initial expenditure and continuing operating cost. Several approaches have been taken to overcome these limitations [3—14]. Each, however, has its own drawbacks: e.g., detection limits deteriorate [6, 7], interferences are increased [5], the load coil must be modified [7, 8], or in some cases the emission must be viewed through the quartz torch [8]. Only recently has it been shown possible to sustain a low-flow i.c.p. which overcomes the above limitations [15, 16].

In an earlier study [16], it was shown that the torch of a conventional-sized i.c.p. can be optimized so that a stable, analytically useful discharge can be sustained at coolant gas flows as low as 3.5 l min^{-1} and at radio-frequency (r.f.) powers down to 125 W. To demonstrate the utility of the optimized torch for the analysis of samples, an NBS standard reference material (SRM 1573, tomato leaves) was examined.

In the present work the same optimization procedure was applied to a miniature i.c.p. torch (13 mm i.d.) similar to the one developed by Savage and Hieftje [3, 4]. The purpose is to combine the optimization and miniaturization of the torch to reduce power and argon flow consumption further. However, the optimized mini-torch cannot be operated at r.f. powers or

0003-2670/85/$03.30

argon flows appreciably lower than the conventional-sized torch. Moreover, although detection limits and working-curve linearity equal those of a conventional plasma, vaporization and ionization interferents are more pronounced. Possible reasons for this behavior are offered.

EXPERIMENTAL

Instrumentation

A 2.5-kW, 40.68-MHz crystal-controlled generator (model HFP 2500D, Plasma-Therm, Kresson, NJ) with an automatic impedance matching unit (model PT/AMN/RCM, Plasma-Therm, Kresson, NJ) were used to supply r.f. power to the torch. In contrast to the previous work which used a two-turn small-sized coil, a conventional-sized, water-cooled three-turn load coil was used in this work mainly because it was easier to ignite the plasma. With both sizes of coil, however, the coupling of r.f. power into the mini-plasma was relatively inefficient, probably because the present impedance-matching module used only one capacitor for automatic tuning. In our experience, the older double-tuning-capacitor units were superior when used with a miniature plasma [3, 4]. The sample-introduction system for all experiments except interference studies consisted of a pneumatic, concentric (glass) nebulizer (made in this laboratory) and a spray chamber with impact surface similar to type 2C in Fig. 2 described by Schutyser and Janssens [17]. For interference studies, a commercial (Plasma-Therm) pneumatic, concentric nebulizer and a Scott-type [18] spray chamber were employed. All the measurements for "plasma stability" curves were made with water aspirated into the plasma at a flow rate of 1 ml min^{-1}. The nebulizer and plasma (intermediate) argon flow rates were held at 0.5 l min^{-1} in these experiments unless stated otherwise.

To optimize torch parameters, as in the previous work [16] "plasma stability" curves were developed. These curves give the minimum r.f. power and coolant gas flow under which an ignited plasma can be sustained. To generate the plasma-stability curves, the plasma is first ignited and stabilized at conventional flow and power levels, after which the coolant argon flow or r.f. power is gradually decreased until the plasma spontaneously quenches. The power at which the plasma extinguishes is then plotted vs. the coolant flow rate. With this procedure, the dimensions of the torch were first optimized for low-flow, low-power operation. Afterward, the "optimized" torch was used for measurements and, in these measurements, plasma variables (flow, power, observation height) were optimized for highest S/B and lowest interferences.

The optical and readout systems for measuring detection limits were as previously described [3]. Interferences, however, were studied by using a silicon-intensified target (SIT) vidicon detector in an optical arrangement similar to that described earlier [19]. A blank signal obtained during introduction of distilled water into the i.c.p. was subtracted from each analyte spatial profile.

Operating procedure for detection-limit determinations

To obtain a set of operating conditions for the optimized miniature i.c.p., the critical variables (i.e., r.f. power, coolant flow, plasma flow and aerosol carrier flow) were varied one at a time while keeping the other three constant. The observation height was optimized for each combination of variables; the criterion for optimization was signal-to-background ratio (SBR).

Detection limits were measured for several elements under optimized operating conditions (Table 1); observation heights were optimized individually for maximum signal-to-background ratio for each element. Five measurements of signal and blank (water) were used in these measurements. Signal-to-noise ratios were taken from these measurements and detection limits were calculated as in the procedure described by Winefordner et al. [20].

Reagents. Stock solutions were prepared as suggested by Dean and Rains [21], from reagent-grade salts and acids. Analyte solutions were prepared by suitable dilution. For interference studies, sodium was added as the reagent-grade chloride, phosphorus as phosphoric acid, and the aluminum solution was prepared from the metal.

TABLE 1

Operating conditions optimized for signal-to-background ratio in the miniature-i.c.p. system (see Fig. 4)

R.f. power	450 W (<50 W reflected)
Gas flows (l min^{-1})	
coolant (outer)	7.5
plasma (auxiliary)	0.3
aerosol carrier (nebulizer)	0.48
Monochromator slits	width 50 μm (0.02-nm spectral band width), height 5 mm
Sample uptake rate	1 ml min^{-1}
Time constant	1 s

RESULTS AND DISCUSSION

Plasma-stability curves for mini-torch

Figure 1 shows the effect on the plasma stability curve of the annular spacing between the plasma and coolant tubes. Clearly, this spacing has a dramatic effect on the power and flow required to sustain the plasma; a 0.2-mm change in annular spacing causes a 58% change in the coolant flow and a 44% change in the r.f. power required to sustain the plasma. In the mini-torch, just as in the conventional-sized torch, the optimized value of this parameter was found to be 0.5 mm. Spacings smaller than 0.5 mm were not explored because of the difficulty in fabricating symmetric, concentric torches.

The effect of the length of the flared portion of the plasma tube and of the extension of the coolant tube beyond the plasma tube was found to be not very critical in the design of a miniature i.c.p. torch.

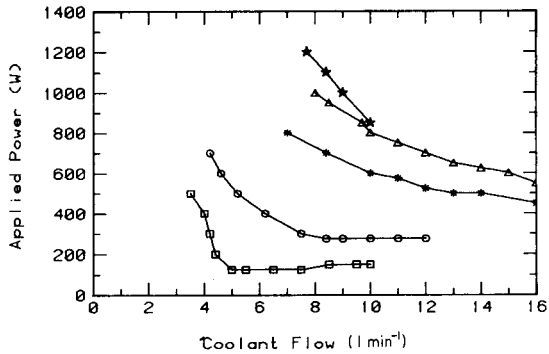

Fig. 1. Effect of annular spacing between the flared portion of plasma (intermediate) and coolant (outer) quartz tubes. (○) 0.5 mm annular spacing; (*) 0.7 mm annular spacing; (△) a non-optimized miniature torch with 1.0-mm annular spacing. (Length of coolant tube, 17 mm; length of flared portion of plasma tube 15 mm; vertical spacing between aerosol and plasma tubes, 3 mm; aerosol tube inner diameter, 0.75 mm.) (★) Non-optimized conventional-size (18 mm o.d.) torch; (□) optimized conventional-size torch (see [16]).

The influence of the inner diameter of the aerosol injection tube and its recession below the flared plasma tube on plasma stability was also studied (Figs. 2 and 3). It appeared that these two parameters have a significant effect on the performance of the torch. The optimized values for the various parameters of the mini-torch are cited in Table 2.

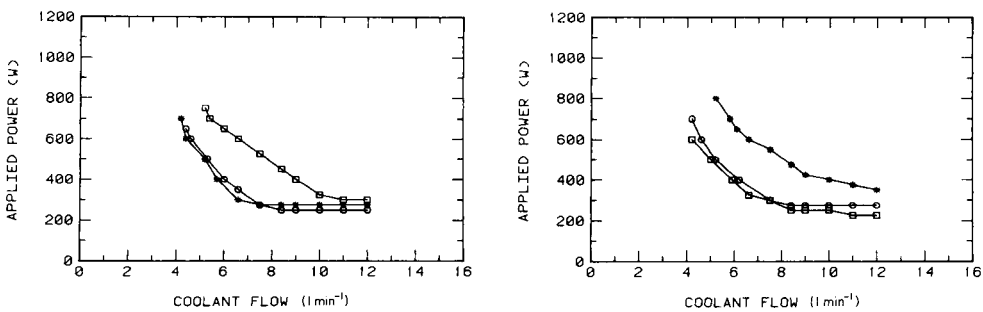

Fig. 2. Plasma stability curves illustrating the influence of inside diameter of aerosol injection tube on plasma stability curves: (□) inner diameter 1 mm; (○) inner diameter 0.75 mm; (*) inner diameter 1 mm and tapered length of flared portion of plasma tube 7 mm. Annular spacing between plasma and coolant tubes 0.5 mm; all other dimensions are the same as in Fig. 1.

Fig. 3. Effect of recession of capillary injection tube below rim of plasma tube; (*) aerosol tube terminated 7.5 mm below plasma tube rim; (□) aerosol tube terminated 5 mm below plasma tube rim; (○) aerosol tube terminated 3 mm below plasma tube rim. Annular spacing between plasma and coolant tubes 0.5 mm; all other dimensions as in Fig. 1.

Comparison of the minimum argon flow rate required for operation of the mini-i.c.p. with that of an optimized conventional-sized low-flow, low-power i.c.p. [16] indicates that it is not possible to sustain a discharge at even lower coolant gas flow rates by reducing the external diameter of the torch. This finding agrees with the recent predictions of Angleys and Mermet [22]. Apparently, if the annular spacing between the coolant and plasma tubes is larger than a limiting value (0.27 mm for an 18 mm i.d. torch), this spacing rather than the internal diameter of the torch will limit the minimum coolant-gas flow rate required for a plasma. Therefore, in the present situation only a very small reduction of the coolant-gas flow rate is realized by miniaturizing the i.c.p. torch.

Effect of operating conditions on SBR in the optimized-miniature i.c.p.

Figure 4 shows that the applied r.f. power and aerosol carrier (nebulizer) gas flow rate are the most critical parameters in governing SBR in the new i.c.p. Coolant flow and plasma flow have a comparatively slight effect on SBR. These results are in good agreement with those reported by Ebdon et al. [23]. The optimized operating conditions extracted from these plots are compiled in Table 1.

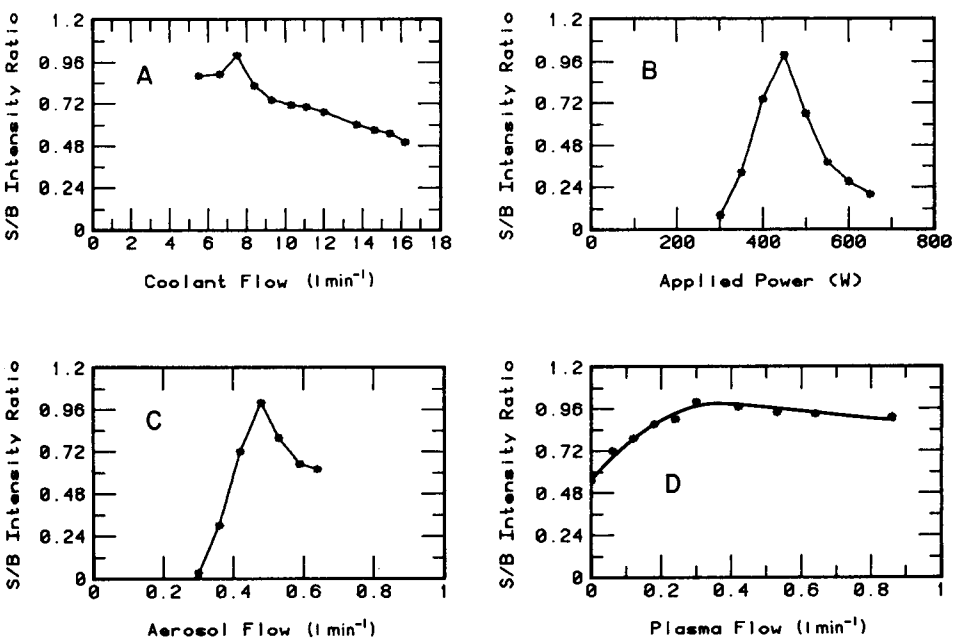

Fig. 4. Influence of operating conditions on signal-to-background ratio of Ca II (393.4 nm). (A) Effect of coolant-gas flow rate; r.f. power 450 W, plasma gas and nebulizer gas each at 0.5 l min^{-1}. (B) Effect of r.f. power; coolant flow rate 7.5 l min^{-1}, nebulizer gas and plasma gas each at 0.5 l min^{-1}. (C) Effect of injector-gas flow rate, r.f. power 450 W, coolant gas flow rate 7.5 l min^{-1}, plasma gas = 0.5 l min^{-1}. (D) Effect of plasma-gas flow rate, nebulizer gas flow 0.48 l min^{-1}; other variables as in (C).

TABLE 2

Optimized miniature i.c.p. torch dimensions

Parameter	Optimal value (mm)
Annular spacing between plasma and coolant tubes	0.5
Coolant inlet port diameter	1
Length of flared portion of plasma tube	7
Length of coolant tube extending beyond plasma tube	17
Recession of aerosol injection tube below rim of plasma tube	2—5
Inner diameter of aerosol injection capillary tube	0.75

Detection limits

The analytical capability of the optimized miniature torch was evaluated by measuring detection limits for several elements, reported in Table 3. The right hand columns in Table 3 give the detection limits reported for a miniature i.c.p. operated at higher power, for a conventional-sized i.c.p. [3], and for a low-flow, low-power i.c.p. [24]. Detection limits for the optimized miniature i.c.p. obtained here are not significantly different from those obtained with the other torches.

Matrix interferences in the optimized miniature i.c.p.

Although earlier reports indicated that the i.c.p. is free from matrix (interelement) effects [1, 25, 26], later studies [27—31] disagreed. The exact nature and mechanisms of these interferences are known [32—36] to be complex and so far it has not been possible to explain them satisfactorily. However, it has been demonstrated [4, 37, 38] that interferences can be minimized through proper choice of operating conditions (i.e., applied r.f.

TABLE 3

Comparison of detection limits offered by several i.c.p. torch designs

Element	Spectral line (nm)	Detection limits (ng ml^{-1}) with i.c.p.			
		Optimized mini	Mini- [3]	Low-flow, low-power [24]	Conventional [3]
Al	396.15	8	3	16	5
Ca II	393.37	0.2	0.07	0.19	0.04
Cu	324.75	5	8	5.4	2
Fe	371.99	30	10	21	12
Mg	285.21	3	6	3	2
Na	588.49	1.5	0.7	2.5	0.2
Ni	352.45	24	4	12	15
Pb	405.78	83	33	—	40
Zn	213.86	25	71	15	23

power, nebulizer and chamber type, nebulizer gas flow, and observation height in the plasma tail flame).

Figure 5 shows the rather strong effect of classical matrix interferents on Ca II (393.4 nm) emission under the operating conditions optimized for SBR listed in Table 1. In all emission profiles, curve A represents a 5 mg l^{-1} calcium (analyte) solution and curve B the same solution but with interferent added at an appropriate concentration. In Figs. 5—11 the scales are the same within one frame but are different from frame to frame. Figure 5 shows that aluminum suppresses the Ca II emission to a greater extent than sodium or phosphate. In an attempt to identify a set of operating conditions under which the calcium signal is free from interferences, the effect of applied r.f. power and nebulizer gas flow were further studied.

Vaporization interferences on calcium. Figure 6 and 7 show the effect of added aluminum and varying nebulizer gas flow on the spatial profiles of Ca I (422.7 nm) and Ca II (393.4 nm), respectively. At larger nebulizer flow rates, the magnitude of the aluminum interference on Ca II (393.4 nm) emission increases. The spatial shift in the emission profile of Ca I (422.7 nm) also becomes larger as the nebulizer gas flow is raised. Figure 6 (a—d) demonstrates that the interference of aluminum on Ca I (422.7 nm) can be minimal if proper operating conditions are selected.

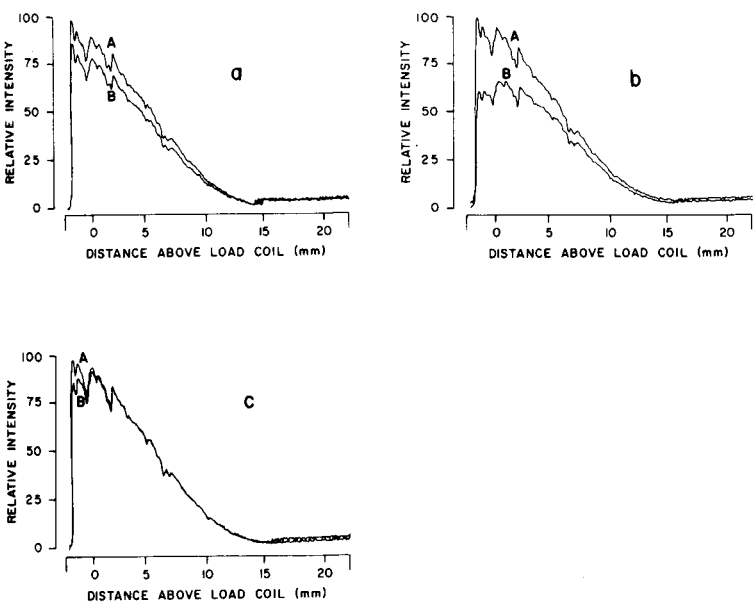

Fig. 5. Effect of several classical interferents on Ca II (393.4 nm) emission intensity profiles under the optimized operating conditions listed in Table 1. Interferent: (a) phosphate, 1470 mg l^{-1}; (b) Al, 1200 mg l^{-1}; (c) Na, 1400 mg l^{-1}. Curve A represents analyte (5 mg l^{-1} Ca) signal and curves B analyte plus interferent. The intensity scales are the same within one frame but vary from frame to frame.

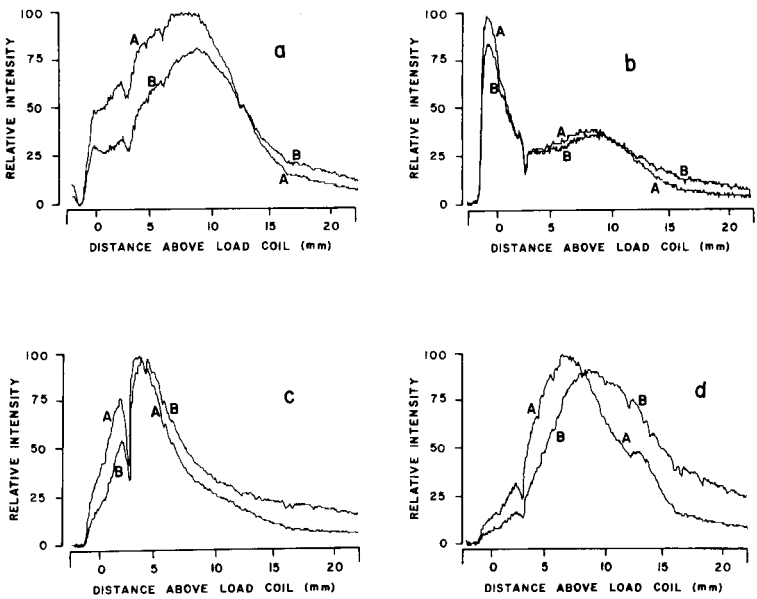

Fig. 6. Effect of added aluminum and varying nebulizer gas flow rate on the spatial emission profile of Ca I (422.7 nm) (r.f. power 450 W). Curves A represent the analyte (5 mg l^{-1} Ca) signal and curves B analyte plus interferent (1200 mg l^{-1} Al). Nebulizer gas flow rate (l min^{-1}): 0.48; (b) 0.59; (c) 0.67; (d) 0.8. Intensity scales are the same as in Fig. 5.

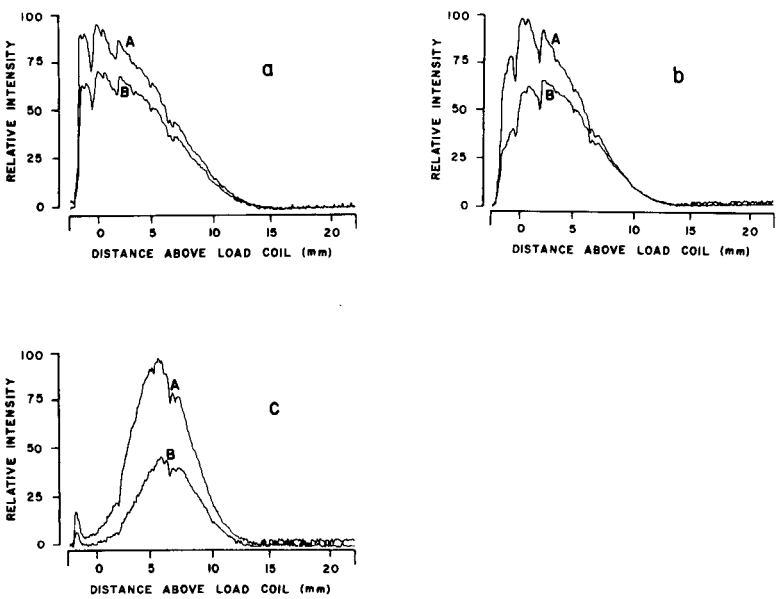

Fig. 7. Effect of aluminum on Ca II (393.4 nm) emission profile with changing nebulizer gas flow rate (r.f. power = 400 W; <10 W reflected). Nebulizer gas flow rate (l min^{-1}): (a) 0.48; (b) 0.53; (c) 0.64. A and B as in Fig. 6.

Figure 8 illustrates the influence of an aluminum matrix on the spatial emission profile of Ca II (393.4 nm) at different r.f. powers. At 400 W the interferences are severe; as the power is increased, the effect of aluminum on the profile is reduced. Unfortunately, the interference cannot be eliminated entirely by increasing the power input to the plasma. Savage and Hieftje [4] observed the same effect using a mini-i.c.p. and 1-kW r.f. power. The caption to Fig. 8 indicates that as the power was increased, the coolant flow rate had also to be increased to prevent torch melting.

The spatial emission profiles of Ca I (422.7 nm) and Ca II (393.4 nm) at different powers and nebulizer gas flows were studied also in the presence of phosphate. The effect of phosphate on Ca I (422.7 nm) was very similar to that of aluminum (cf. Fig. 6). The effect of r.f. power on the Ca II (393.4 nm) emission profile in the presence of a phosphate matrix is shown in Fig. 9. Surprisingly, there is an increase in the magnitude of the calcium-phosphate interference as the r.f. power is increased. Savage and Hieftje [4] observed the same behavior.

Effect of an easily ionized species on calcium emission. The effect of an easily ionized element (sodium) on the Ca II (393.4 nm) emission profile at various powers is shown in Fig. 10. The operating conditions for these plots are identical to those in Fig. 8. Interestingly, the magnitude of sodium interference on Ca II is relatively small compared to that of a vaporization interference (i.e., from Al and phosphate). The interference of sodium on Ca II

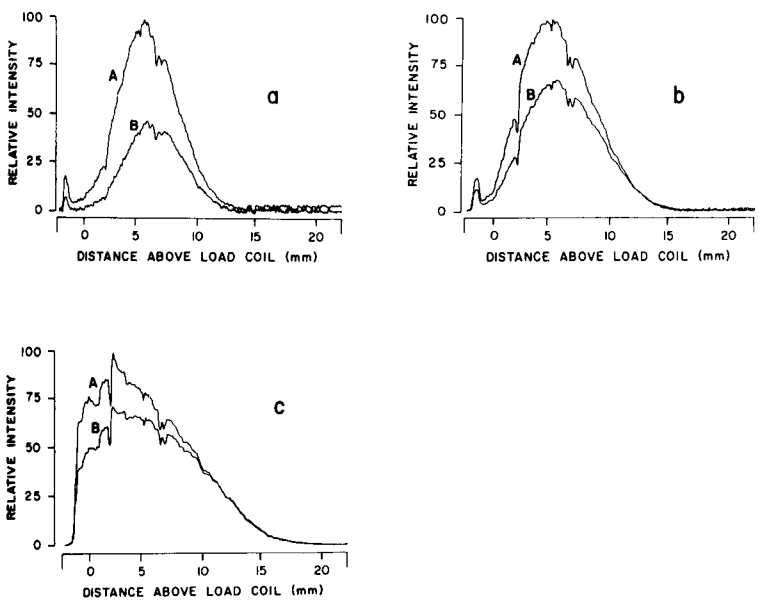

Fig. 8. Influence of aluminum matrix on spatial emission profiles of Ca II (393.4 nm) as a function of r.f. power. (a) R.f. power 400 W, coolant flow 6 l min^{-1}; (b) r.f. power 500 W, coolant flow 6.5 l min^{-1}; (c) r.f. power 750 W, coolant flow 7.5 l min^{-1}. Nebulizer gas 0.64 l min^{-1}. Intensity scales are the same as in Fig. 5; curves A and B as in Fig. 6.

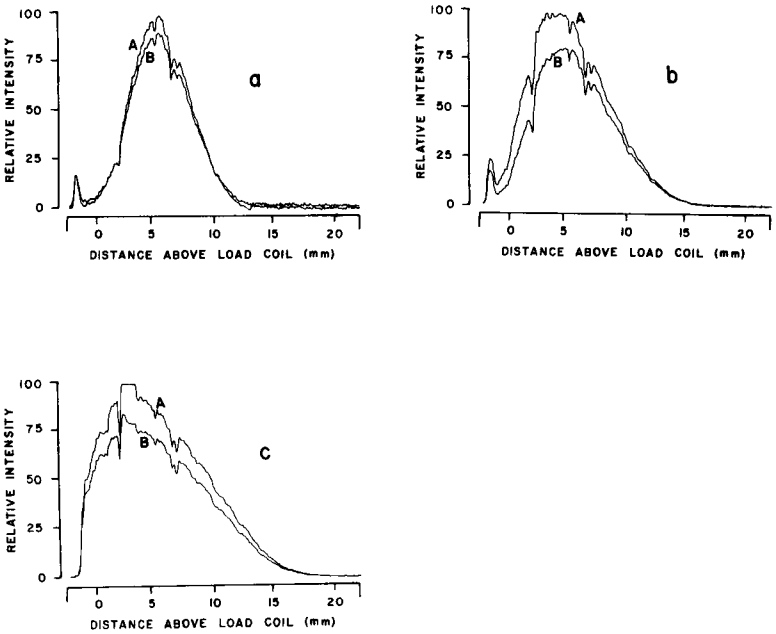

Fig. 9. Effect of phosphate interference on Ca II (393.4 nm) spatial emission profile with changing r.f. power. Curves A represent analyte (5 mg l^{-1} Ca) and curves B analyte plus interferent (1470 mg l^{-1} phosphate). The operating conditions for (a—c) are the same as in Fig. 8; for intensity scales, see Fig. 5.

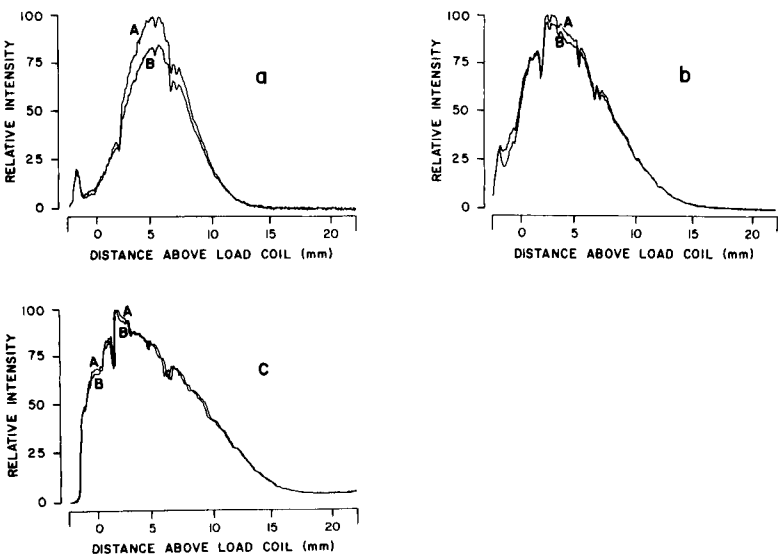

Fig. 10. Influence of sodium on the Ca II (393.4 nm) emission profile at various r.f. power levels, obtained under the same operating conditions as Fig. 8. Curve A represents analyte (5 mg l^{-1} Ca) and curve B analyte plus interferent (1400 mg l^{-1} Na); for intensity scales, see Fig. 5.

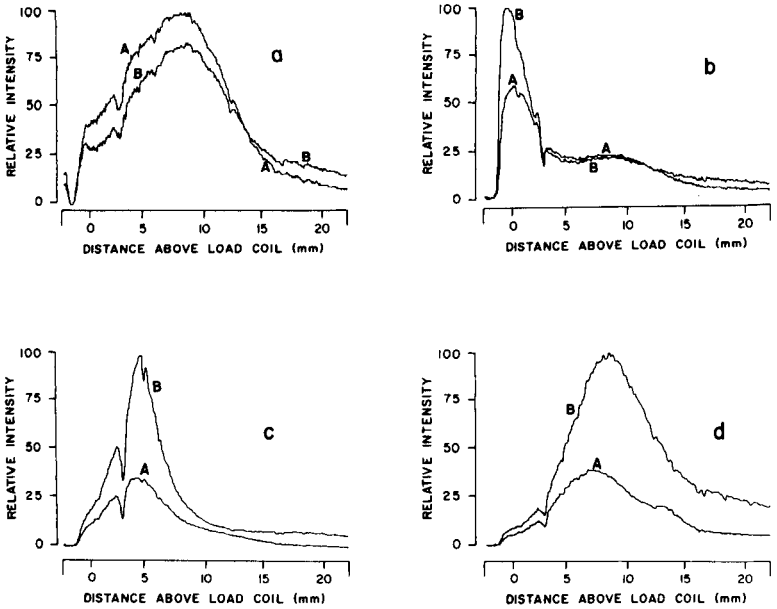

Fig. 11. Effect of sodium matrix on the Ca I (422.7 nm) emission profile at different nebulizer-gas flow rates; the nebulizer-gas flows and powers are the same as in Fig. 6.

increased with a decrease in nebulizer-gas flow from 0.59 l min^{-1} to 0.3 l min^{-1}.

Figure 11 illustrates the effect of sodium on the Ca I (422.7 nm) emission profile at several nebulizer (aerosol carrier) gas flow rates. At higher aerosol-gas flows an enhancement in the entire emission profile of Ca I (422.7 nm) is observed in the presence of the sodium. Significantly, the magnitude and direction of the interference are changed as the nebulizer flow is reduced. At lower powers (250—450 W), the profile develops two peaks, the most intense occurring very low in the plasma. The second peak, like Fig. 11(a), occurs higher in the tail flame. In addition, at higher nebulizer flows the peak in the emission profile shifts upward in the plasma in the presence of the sodium matrix, possibly indicating both a vaporization and ionization interference. The magnitude of this interference increases as the r.f. power is raised.

Conclusion

The torch parameters of a miniature-i.c.p. can be optimized, so that the plasma can be operated at somewhat lower gas flows and r.f. powers although the decrease is less dramatic than in conventional-sized i.c.p. torches. Under the optimized operating conditions for best SBR, matrix interferences were found to be pronounced. A detailed study of vaporization (phosphate, aluminum) and ionization (sodium) interferences on Ca I (422.7 nm) and Ca II (393.4 nm) emission profiles indicated that it is not possible

to obtain operating conditions (i.e., r.f. power, nebulizer gas flow, and observation height) under which interferences can be entirely eliminated.

This work was supported in part by the National Science Foundation through grants CHE 82-14121 and CHE 83-20053 and by the Office of Naval Research.

REFERENCES

1 S. Greenfield, I. L. Jones and C. T. Berry, Analyst (London), 89 (1964) 713.
2 R. H. Wendt and V. A. Fassel, Anal. Chem., 37 (1965) 920.
3 R. N. Savage and G. M. Hieftje, Anal. Chem., 51 (1979) 408.
4 R. N. Savage and G. M. Hieftje, Anal. Chem., 52 (1980) 1267.
5 C. D. Allemand, R. M. Barnes and C. C. Wohlers, Anal. Chem., 51 (1979) 2392.
6 A. D. Weiss, R. N. Savage and G. M. Hieftje, Anal. Chim. Acta, 124 (1981) 245.
7 C. R. Kornblum, W. Van der Waa and L. de Galan, Anal. Chem., 51 (1979) 2378.
8 P. A. M. Ripson, L. de Galan and J. W. de Ruiter, Spectrochim. Acta, Part B, 37 (1982) 733.
9 P. A. M. Ripson and L. de Galan, Spectrochim. Acta, Part B, 38 (1983) 707.
10 C. D. Allemand and R. M. Barnes, Appl. Spectrosc., 31 (1977) 434.
11 J. L. Genna, R. M. Barnes and C. D. Allemand, Anal. Chem., 49 (1977) 450.
12 M. D. Lowe, Appl. Spectrosc., 35 (1981) 126.
13 H. Kawaguchi, T. Ito, S. Rubi and A. Mizuike, Anal. Chem., 52 (1980) 2440.
14 H. Kawaguchi, T. Tanaka, S. Miura and A. Mizuike, Spectrochim. Acta, Part B (supplement), 38 (1983) 176.
15 A. Montaser, G. R. Huse, R. A. Wax, Shi-Kit Chan, D. W. Golightly, J. S. Kane and A. F. Dorrzapf, Jr., Anal. Chem., 56 (1984) 283.
16 R. Rezaaiyaan, G. M. Hieftje, A. Anderson, H. Kaiser and B. Meddings, Appl. Spectrosc., 36 (1982) 627.
17 P. Schutyser and E. Janssens, Spectrochim. Acta, Part B, 34 (1979) 443.
18 R. H. Scott, V. A. Fassel, R. N. Kniseley and D. E. Nixon, Anal. Chem., 46 (1974) 75.
19 R. Rezaaiyaan, J. Olesik and G. M. Hieftje, Spectrochim. Acta, Part B, 40 (1985) 73.
20 J. D. Winefordner, P. A. St. John and W. J. McCarthy, Anal. Chem., 39 (1967) 1495.
21 J. A. Dean and T. C. Rains, in J. A. Dean and T. C. Rains (Eds.), Flame Emission and Atomic Absorption Spectrometry, Vol. 2, M. Dekker, New York, 1971, Ch. 13.
22 G. Angleys and J. M. Mermet, Appl. Spectrosc., 38 (1984) 647.
23 L. Ebdon, M. R. Cave and D. J. Mowthorpe, Anal. Chim. Acta, 115 (1980) 179.
24 R. Rezaaiyaan and G. M. Hieftje, Anal. Chem., 57 (1985) 412.
25 V. A. Fassel, Proc. 16th Coll. Spectrosc. Int. Heidelberg 1971: Plenary Lectures and Reports, Hilger, London, 1972, p. 63.
26 V. A. Fassel and R. N. Kniseley, Anal. Chem., 46 (1974) 1110A, 1155A.
27 P. W. J. M. Boumans, F. J. De Boer, F. T. Dahmen, H. Noelzel and A. Meier, Spectrochim. Acta, Part B, 20 (1975) 449.
28 G. F. Larson, V. A. Fassel, R. H. Scott and R. N. Kniseley, Anal. Chem., 47 (1975) 238.
29 P. W. J. M. Boumans and F. J. De Boer, Spectrochim. Acta, Part B, 31 (1976) 355.
30 J. M. Mermet and J. P. Robin, Anal. Chim. Acta, 70 (1979) 271.
31 S. R. Koirtyohann, J. S. Jones, C. P. Jester and D. A. Yates, Spectrochim. Acta, Part B, 36 (1981) 49.
32 G. R. Kornblum and L. de Galan, Spectrochim. Acta, Part B, 32 (1977) 455.
33 G. F. Larson, V. A. Fassel, R. H. Scott and R. N. Kniseley, Anal. Chem., 47 (1975) 238.

34 W. H. Gunter, K. Visser and P. B. Zeeman, Spectrochim. Acta, Part B, 37 (1982) 571.
35 M. W. Blades and G. Horlick, Spectrochim. Acta, Part B, 36 (1981) 881.
36 J. P. Rybarczyk, C. P. Jester, D. A. Yates and S. R. Koirtyohann, Anal. Chem., 55 (1982) 2162.
37 G. Horlick and M. W. Blades, Appl. Spectrosc., 34 (1980) 229.
38 H. Kawaguchi, T. Ito, K. Ota and A. Mizuike, Spectrochim. Acta, Part B, 35 (1980) 199.

Analytica Chimica Acta, 173 (1985) 77—87
Elsevier Science Publishers B.V., Amsterdam — Printed in The Netherlands

THE DETERMINATION OF GOLD IN GEOCHEMICAL SAMPLES BY NON-DISPERSIVE ATOMIC FLUORESCENCE SPECTROMETRY

P. L. LARKINS

CSIRO Division of Chemical Physics, P.O. Box 160, Clayton, Victoria 3168 (Australia)

(Received 15th January 1985)

SUMMARY

Non-dispersive flame atomic fluorescence spectrometry is a very sensitive method for the determination of gold, with a limit of detection in aqueous solution of about 0.5 ng ml^{-1}. However, the application of the technique to aqua regia digests of geochemical samples is limited by large scatter signals which are due mainly to aluminium. The use of an auxiliary lamp to provide correction for scatter is suitable for samples containing low concentrations of elements which form refractory compounds in the flame or for samples where the full sensitivity of the fluorescence technique is not required. To obtain both high accuracy and sensitivity, gold must be separated from the scattering matrix and this can be achieved by a simple extraction with a 0.1% (w/v) solution of a trioctylmethylammonium salt (Aliquat-336) in di-isobutyl ketone. The use of fluorescence avoids the need for a large extraction ratio and a subsequent washing step to remove iron, as is normally required for atomic absorption measurements.

Flame atomic absorption spectrometry is well established for the determination of gold in a wide range of samples. However, it is not sufficiently sensitive to provide direct determinations on an acid digest of many geochemical exploration samples. The use of carbon rod or furnace atomisation provides a significant improvement in sensitivity but the complex matrix usually associated with gold in rock and soil samples can result in high background absorption values for which adequate correction is difficult.

Gold can be concentrated from dilute solutions by a variety of methods including coprecipitation with tellurium [1, 2] or mercury [3] with tin(II) chloride or hypophosphorous acid as the reducing agent. Although very sensitive, such methods are lengthy and involve a substantial amount of sample processing.

A commoner method of improving the sensitivity for gold is the use of liquid-liquid extraction with large extraction ratios. Numerous solvents and complexing agents have been used and good summaries of these have been provided [4, 5]. The commonest method involves extraction of gold(III) from a hydrochloric or hydrobromic acid solution with methyl isobutyl ketone (MIBK) or di-isobutyl ketone (DIBK). The distribution coefficient for the HCl/MIBK system is greater than 1000 [6] for acid concentrations above about 1.5 M. Some complexing agents interfere with this extraction

and, in addition, gold(I) is not readily extracted. However, Groeneweld [7, 8] has shown that the cyanide complex of gold(I) and the cyanide and chloride complexes of gold(III) can be extracted by using a solution of the commercial trioctylmethylammonium salt, Aliquat-336, in DIBK. This solvent was used [7] because it has lower volatility and water-solubility than MIBK together with suitable flame characteristics.

Although flame atomic fluorescence spectrometry with boosted-output hollow-cathode lamps has been shown to be a very sensitive method for the determination of gold [9, 10], there has been no thorough investigation of the application of this method in the analysis of complex samples. As the previously reported detection limit of 5 ng ml^{-1} is near the minimum level of interest in geochemical exploration, the atomic fluorescence technique was investigated more thoroughly to establish its suitability for this type of sample.

EXPERIMENTAL

Apparatus

Atomic fluorescence. Measurements were made by using the non-dispersive technique described previously [10] but with the optical system modified slightly as discussed later. The light source was a boosted-output gold hollow-cathode lamp which was made in this laboratory and was of the type described by Lowe [11]. The sample was atomised in a stoichiometric air/acetylene flame which was separated by a nitrogen sheath [12].

Scatter was corrected by using the auxiliary light source method described by Larkins and Willis [13]. This technique involves the use of a second light source (of an element known to be absent from the sample or incapable of being atomised by the flame) to provide a measure of the amount of scatter. The auxiliary lamp used in this work was a Philips OZ-4W mercury germicidal lamp. A comparison of lamp intensities for scatter calculations was obtained by aspirating aluminium solutions which were prepared by dissolving Specpure aluminium in hydrochloric acid or a 1:1 hydrochloric/nitric acid mixture. Correction provided by this technique was expected to be especially reliable for two reasons: first, the main mercury lamp emission is at 253.7 nm which is mid-way between (and close to) the two main gold fluorescence lines at 242.8 and 267.6 nm; second, the major source of scatter in the sample solutions was expected to be aluminium.

The lamps were operated by appropriate current-regulated power supplies as described previously [10]. The fluoresced and scattered radiation was detected by a single photomultiplier (Hamamatsu TV; Type R166), the output of which was fed via a preamplifier/buffer to two phase-sensitive amplifiers in parallel (Techtron Model IM1). One of the amplifiers (gold channel) was operated at the standard 285 Hz while the other (mercury channel) was altered to operate at 313 Hz. Synchronizing signals were available from the amplifiers to permit modulation of the power supplies.

The output signals from the amplifiers were further amplified, to provide 5 V at full scale, and passed to an OKI-if800 Model 10 computer fitted with an eight-input multiplexed 12-bit A/D converter. Data were collected and processed by using programs written in BASIC.

Atomic Absorption. A Varian-Techtron Model AA6 atomic absorption spectrometer was used but the AA6 amplifier was replaced by the dual amplifier system used for scatter-corrected fluorescence measurements. A standard 10-cm slot burner was used and background absorption was measured simultaneously with a deuterium arc lamp (Hamamatsu TV) in a manner similar to that of commercial systems. The lamp currents were adjusted to provide similar signal intensities, and data collection and processing were again done by computer.

Sample preparation

A sample (30 g) of finely ground rock chip was roasted, if necessary, to destroy sulphides, slurried with distilled water to prevent caking and then digested for about 1 h with 60 ml of concentrated hydrochloric acid and 25 ml of concentrated nitric acid. After cooling, the sample was diluted to 300 ml and allowed to settle. Gold was then quantified on the clear liquid, either directly or after liquid-liquid extraction.

For most extraction work, the following simplified procedure was used. A portion (3 ml) of the sample solution was extracted by shaking for about 1 min in a small glass vial with a 0.1% (w/v) solution of Aliquat-336 in DIBK. After the two layers had separated, the DIBK layer was aspirated into an air/acetylene flame and the gold was quantified by atomic absorption or fluorescence spectrometry. Gold standards were extracted in the same fashion. Solvent was aspirated between samples and the acetylene flow rate was adjusted to provide an approximately stoichiometric flame.

The proposed fluorescence method was evaluated for solutions of rock chip samples which had been treated by the following more extensive extraction procedure: 200 ml of sample solution was extracted with 10 ml of 5% (v/v) Aliquat-336 in DIBK. The DIBK layer was washed with 50 ml of 10% (w/v) nitric acid, to remove iron, and then aspirated into an air/acetylene flame for the determination of gold by atomic absorption spectrometry in the usual manner.

RESULTS AND DISCUSSION

Detection limit

One of the main attractions of non-dispersive atomic fluorescence, compared with other atomic spectrometric methods for the determination of gold, is its low detection limit. In accordance with common usage [14], the detection limit is defined here as that concentration which gives a signal equal to twice the standard deviation of ten measurements on a solution with a concentration near the detection limit. For the determination of detection limits in the present work, all signals were obtained by integration for 10 s.

Detection limits were evaluated for both atomic absorption and fluorescence by using the same nebuliser and spray chamber assembly and aqueous solutions of gold in 2 M hydrochloric acid. The results are given in Table 1 together with values reported in the literature for some other spectrochemical techniques. It can be seen that flame fluorescence is a much more sensitive method than the others listed except for a.a.s. with furnace atomization. For flame fluorescence the detection limit varies slightly with height of observation in the flame. The value quoted was obtained at 36 mm above the burner top but at 22 mm the value was 0.001 μg ml^{-1}. This variation is due to increasing flame gas emission (and the associated shot noise) with decreasing height. The value given in Table 1 for flame atomic fluorescence shows a significant improvement over the result of earlier work [10]. Although part of this change is due to the adoption of the definition of detection limit quoted above, the balance is due to improvements in the light source and the optical system.

The detection limit given for furnace a.a.s. depends directly on the sample volume and could be improved by the use of a larger volume. However, in a practical situation the presence of large quantities of matrix materials can produce very high background absorbances which cannot be corrected by the standard deuterium-arc correction systems. The use of much smaller sample volumes or less concentrated solutions can alleviate the background problem but raises the detection limit. The use of platform furnaces and Zeeman background correction is claimed [18] largely to overcome these problems.

The result for non-dispersive fluorescence with plasma atomization was obtained with a pulsed hollow-cathode lamp. The use of a boosted-output hollow-cathode lamp, of the type employed in the present work, may produce a substantial improvement in that technique.

Linear range

The upper linear limit (5% departure from linearity) was evaluated for flame atomic fluorescence and found to be 20 μg ml^{-1}. This value varies slightly with the angle of observation and is best at small angles. Thus, the method has a linear range, from detection limit to upper linear limit, of four

TABLE 1

Comparison of detection limits for gold by various spectrometric methods (all values are for simple gold solutions and are given in μg ml^{-1})

	Fluorescence		Absorption		Emission
	Flame[a]	I.c.p.[b]	Flame[a]	Furnace[c]	I.c.p.[d]
Detection limit	0.0005	0.01	0.015	0.0002	0.01

[a]This work. [b]Ref. 15. [c]From Ref. 16 assuming a 50-μl sample size. [d]Ref. 17.

and a half decades, which is comparable to linear ranges found in inductively-coupled plasma emission.

Although atomic fluorescence is a very sensitive technique for the determination of gold, there are two major limitations which have previously discouraged its use in this application. The first is the lack of availability of a suitable light source. Apart from lasers, which are still very expensive, the best light source for gold is the boosted-output hollow-cathode lamp [11, 19]. Although previously unavailable, these are now being made commerically in both sealed (Photron Pty., Dandenong, Victoria, Australia) and demountable [20] (SGE Pty., Ringwood, Victoria, Australia) styles. Both should give similar results to those obtained in this work. The second (and more difficult) problem is that of scatter [13].

Scatter

The acid digestion technique used to dissolve the gold from the rock samples also dissolves materials such as aluminium which can form refractory particles in the flame and scatter the incident radiation. For a given sample the ratio of scatter to fluorescence depends on several factors, in particular the measurement angle and the height of observation in the flame.

Measurement angle. Most previous work on fluorescence has used an angle of 90° between the incident and fluoresced radiation. Preliminary investigations for the present work showed that both the fluorescence intensity and the scatter-to-fluorescence ratio vary with the angle of observation as shown in Figs. 1 and 2 (an angle of 0° represents scatter or fluorescence back

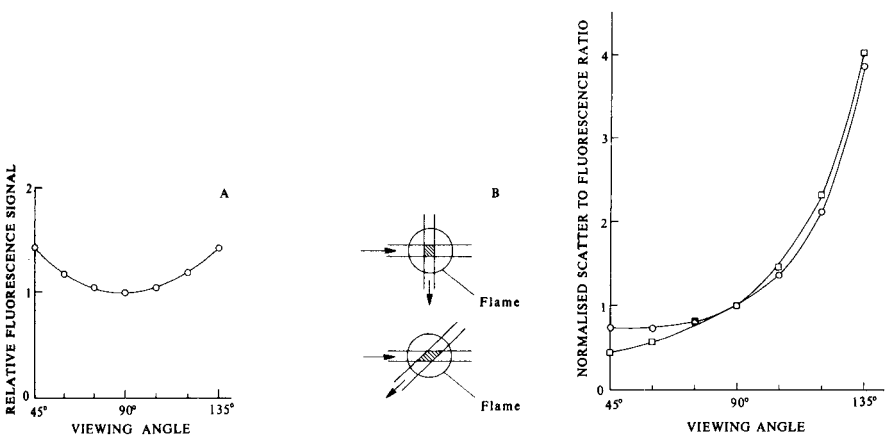

Fig. 1. (A) Variation of fluorescence intensity with viewing angle. (B) Diagrams showing the increased flame volume from which fluorescence is collected when the viewing angle is changed from 90° to 45°.

Fig. 2. Variation of scatter to fluorescence ratio with viewing angle: (○) 500 μg ml^{-1} aluminium solution; (□) 25 μg ml^{-1} aluminium solution. Both graphs have been normalised to 1 at 90° for direct comparison.

towards the light source). The increase in fluorescence intensity is a geometric effect resulting from the fact that both the incident light beam and the observation path are narrower than the flame. Changing the direction of observation can, therefore, change the fraction of the illuminated flame volume from which fluorescence is gathered, as indicated in Fig. 1B. The change in fluorescence signal was exactly as expected from this effect. The change in scatter-to-fluorescence ratio with angle is slightly dependent on the concentration of the scatterer but is always much worse in the forward than in the reverse direction. All fluorescence intensities were therefore measured by using an angle of 45° between the lamp and the photomultiplier as shown in Fig. 3. A similar dependence of scatter on viewing angle has also been found by other workers [21—23] and shows that the scatter is not of the simple Rayleigh type [24] for which scattering is minimal at 90° and increases symmetrically in the forward and reverse directions.

Height of observation. In addition to the effect on signal-to-noise ratio noted earlier, there is a small variation in both scatter and signal levels at different heights in the flame. The variation in the scatter level depends on the nature of the scatterer. For pure aluminium solutions and also for most rock samples, the scatter increases slightly with height. For example, increasing the height of observation from 22 to 36 mm above the burner top resulted in an increase in scatter of between 1% and 10% for a range of rock samples and approximately 3% for a 2000 μg ml^{-1} aluminium solution. However, the scatter from one rock sample and from a 1000 μg ml^{-1} calcium solution decreased by 7% and 23%, respectively. The latter effect is probably due mainly to the scattering particles being less refractory than aluminium oxide and evaporating significantly as they pass up the flame. The cause of the increase in scatter is not obvious. The gold fluorescence decreased slightly (about 3%) for the same increase in height and this is probably due to slight dilution of the flame gases by the nitrogen sheath.

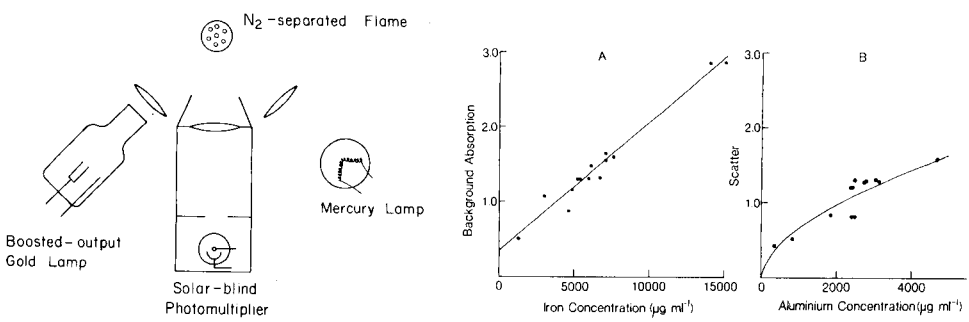

Fig. 3. Schematic diagram of the optical system.

Fig. 4. Diagrams showing correlation, for rock chip samples, of (A) background absorption in flame a.a.s. with iron concentration and (B) scatter in flame fluorescence with aluminium concentration. Background absorption and scatter are both given in terms of equivalent gold concentrations in μg ml^{-1}. The solid lines are curves of best fit showing a linear fit on graph A and a logarithmic fit on graph B.

Of more importance for the proposed method of scatter correction by using an auxiliary light source is the fact that the ratio of the scatter signals from gold and mercury lamps also varied with height and the variation was different for different samples. When a 2000 $\mu g\ ml^{-1}$ aluminium solution was used to provide the lamp intensity ratio, the best correction for scatter from the rock samples was obtained low in the flame (22 mm above the burner) and so scatter-corrected measurements were made at this height. At greater heights, the scatter measured with the mercury lamp generally resulted in over-correction and low or negative results.

Scatter-corrected fluorescence

The extent of scattering by typical geochemical samples and the ability of the auxiliary lamp technique to provide adequate scatter correction was further evaluated by analysing a range of rock chip samples. The results are shown in Table 2 together with results obtained by background-corrected atomic absorption. Also included in Table 2 are the results which were provided with the samples and which were obtained by the liquid-liquid extraction/washing/a.a.s. procedure outlined earlier. Results were not provided for samples 9—12 but the gold content of these samples is sufficiently high for the results by background-corrected atomic absorption to provide a reasonable reference. In addition, the results for these four samples are in good agreement with those determined by the simple liquid-liquid extraction

TABLE 2

Determination of gold in acid digests of rock samples by using scatter/background correction (all results are given in $\mu g\ ml^{-1}$)

Sample no.	Atomic fluorescence			Atomic absorption			Given value[b]
	Total signal	Scatter[a]	Net signal	Total signal	Background[a]	Net signal	
1	1.348	1.308	0.040	1.12	1.09	0.03	0.031
2	0.844	0.838	0.006	1.44	1.33	0.11	0.013
3	1.525	1.503	0.022	1.67	1.65	0.02	<0.003
4	0.519	0.514	0.005	0.97	0.89	0.08	0.007
5	1.238	1.275	−0.037	1.24	1.17	0.07	0.005
6	1.233	1.284	−0.051	1.35	1.32	0.03	<0.003
7	0.419	0.431	−0.012	0.54	0.51	0.03	<0.003
8	1.593	1.574	0.019	1.53	1.49	0.04	0.004
9	1.653	1.213	0.440	2.06	1.60	0.46	—
10	1.585	1.201	0.384	1.96	1.57	0.39	—
11	1.527	0.814	0.713	3.56	2.86	0.70	—
12	1.501	0.809	0.692	3.55	2.87	0.68	—
13	1.342	1.304	0.038	1.31	1.31	0.00	0.006
14	1.333	1.290	0.043	1.34	1.31	0.03	0.010

[a]Expressed as equivalent gold concentration in $\mu g\ ml^{-1}$. [b]Value provided with the samples and obtained by a liquid-liquid extraction a.a.s. procedure as detailed in the text.

procedure described later. All concentrations are given as $\mu g\ ml^{-1}$ in the solution analysed and scatter and background signals are expressed as equivalent gold concentrations.

It can be seen from Table 2 that the signal caused by scatter in fluorescence is comparable with that produced by background absorption in a.a.s. However, these signals were found to be due to different causes; the background absorption gave good correlation with the iron content of the solutions, while scatter in atomic fluorescence gave reasonable correlation with the aluminium concentration. This is not surprising as iron, which is a major constituent of these samples, produces only minor scatter but has been observed by Fleming [25] to give molecular absorption in the wavelength region around the gold 242.8-nm resonance line. The correlation between scatter and the aluminium concentration was slightly better for a logarithmic fit than for a linear one and this is consistent with the results of an earlier study of scatter [13]. In addition to aluminium, the samples were found to contain between 100 and 1300 $\mu g\ ml^{-1}$ calcium, which is also known to produce significant scatter. Although aluminium was the major contributor to scatter, a slight improvement to the correlation with the scatter signal could be obtained by including an allowance for the calcium concentration. The samples were also tested for silicon but none was found to contain more than 50 $\mu g\ ml^{-1}$, which would give a negligible scatter signal compared to the aluminium and calcium. The correlations of background absorption with iron concentration and of scatter with aluminium concentration are shown in Fig. 4. The iron, aluminium, calcium and silicon were determined by normal atomic absorption measurements with an air/acetylene flame for iron and a nitrous oxide/acetylene flame for the others.

For flame atomic fluorescence measurements, the minimum relative standard deviation of a single measurement was found to be about 0.5% but was sometimes higher, depending on the type of sample. When scatter correction is used, gold is determined as the difference of two measurements and therefore the detection limit will be no better than about 1% of the scatter signal. A scatter level equivalent to more than about 0.1 $\mu g\ ml^{-1}$ gold will result in a poorer detection limit than that obtained with pure gold solutions and so, for the samples in Table 1, the detection limit will be no better than 0.004—0.016 $\mu g\ ml^{-1}$. Thus, the auxiliary lamp method can only be expected to provide reliable correction for reasonably low levels of scatter. In addition, when a mercury lamp is used for correction, the presence of mercury in the sample, even at low concentrations, will result in overcorrection and give low or negative gold values. However, the samples used here were checked for mercury by using a cold-vapour technique, similar to that described by Ebdon et al. [22], and all were found to have negligible mercury levels ($<0.05\ \mu g\ ml^{-1}$).

Several samples, notably 5, 6 and 7, show an error in excess of that expected from the level of scatter. This indicates that these samples give a slightly different ratio of scatter signals for gold and mercury radiation than

that given by the pure aluminium solution used as a reference. Thus, on the basis of these results, the correction provided by this technique may be in error by as much as 4% of the scatter signal or 0.06 $\mu g\ ml^{-1}$ of gold, although most results were in error by less than 0.03 $\mu g\ ml^{-1}$. Therefore, this method is suitable for samples containing low levels of materials which form refractory compounds in the flame or where the accuracy required is no better than about 0.06 $\mu g\ ml^{-1}$. The accuracy of the scatter correction obtained here is better than that found by Naranjit et al. [23] who used a similar auxiliary lamp scatter correction method for a number of elements in a multi-element fluorescence system. They used tellurium as a reference lamp and applied the technique with a range of observation angles. The good results obtained in the present work are probably due to the closeness of the mercury and gold spectral lines and the use of the same observation angles for both scatter and fluorescence.

Liquid-liquid extraction/atomic fluorescence

The problem of large scatter signals together with low gold concentrations can be best overcome by use of liquid-liquid extraction. As fluorescence is already very sensitive, it is not necessary to use large extraction ratios and, because iron is not expected to produce any significant molecular fluorescence or scatter, a washing step should not be necessary. The extraction procedure can therefore be much simpler than that used for atomic absorption measurements. DIBK was chosen as the extraction solvent for the reasons mentioned earlier; in addition, its flash point is above room temperature and it is therefore less of a fire hazard.

The simplest procedure is to use pure DIBK and extract the gold chloro-complex from an aqua regia digest of the sample. Therefore, initial trials were done with this solvent and solutions of gold in hydrochloric acid. Particular attention was paid to the rate of extraction and the effects of hydrochloric acid and gold concentrations on the extraction efficiency.

With the small volume ratios used in this work (3 ml of gold solution to 2 ml of DIBK), extraction was found to be extremely rapid and was practically complete within 15 s which is consistent with the findings of Groenewald [7].

Extraction efficiency was evaluated by direct atomic fluorescence measurement of the residual gold in the aqueous phase after extraction. At hydrochloric acid concentrations greater than 1 M, about 95% of the gold was extracted from a 1 $\mu g\ ml^{-1}$ solution but at lower acid concentrations the efficiency was less and at 0.05 M was only 80%. When the same extraction procedure was used, MIBK was found to extract about 99.9% of the gold from a 2 M hydrochloric acid solution (this poorer extraction efficiency of DIBK does not appear to have been noted previously). Not only is extraction by pure DIBK significantly less than 100% but it tends to be variable and influenced by the presence of other ions in solution, e.g., in the presence of

1000 μg ml^{-1} iron(III) ion and 2 M hydrochloric acid, the extraction efficiency was about 97.5%. However, the presence of a small quantity of Aliquat-336 in the DIBK was sufficient to increase the efficiency to about 99.9% and also improved the reproducibility. All further work was therefore done with 0.1% (w/v) Aliquat-336 in DIBK and with the gold solutions 2 M in hydrochloric acid.

Gold concentration was found to have no effect on the extraction efficiency when 0.1% Aliquat in DIBK was used but with pure solvent the percent extraction appeared to drop slightly for gold levels below 0.1 μg ml^{-1}.

Analysis of rock samples. Extractions with 0.1% Aliquat-336 in DIBK were done on the set of aqua regia digests of rock chip samples used previously for scatter-corrected fluorescence measurements. The results are given in Table 3 together with the results by atomic absorption after the same extraction procedure. The fluorescence results have been corrected for a small amount of scatter (equivalent to about 0.001 μg ml^{-1} gold) as discussed below. The precision of the atomic absorption measurements was about $\pm$0.02 μg ml^{-1} and there was no significant background absorption. The agreement between the fluorescence and absorption results is therefore within experimental error.

The small scatter signal in the fluorescence measurements appears to be due to co-extracted iron. When a higher concentration (1%) of Aliquat-336 in DIBK was used for the gold extraction, the solvent layer was noticeably more yellow and the results for gold were higher by about 0.003 μg ml^{-1}. The scatter signal also increased to about 0.004 μg ml^{-1}. However, provided

TABLE 3

Determination of gold in acid digests of rock samples with the simple solvent extraction procedure (all results are given in μg ml^{-1})

Sample no.[a]	Atomic fluorescence	Atomic absorption	Given value[a]
1	0.026	0.04	0.031
2	0.009	0.01	0.013
3	0.000	0.01	<0.003
4	0.004	0.02	0.007
5	0.001	0.02	0.005
6	0.000	0.02	<0.003
7	0.003	0.01	<0.003
8	0.005	0.03	0.004
9	0.425	0.43	—
10	0.367	0.38	—
11	0.716	0.71	—
12	0.712	0.70	—
13	0.007	0.02	0.006
14	0.013	0.03	0.010

[a] As for Table 2.

that the Aliquat concentration is low and the hydrochloric acid concentration is no greater than about 2 M there should be no need to check for scatter and the resulting error should be negligible.

In addition to the conditions noted above, it is necessary to observe the normal precautions recommended by instrument manufacturers regarding the use of organic solvents. In particular, the spray chamber assembly should be cleaned and dried prior to the use of solvent or a complete assembly should be reserved for this use. Provided that these precautions are observed, the simple liquid-liquid extraction procedure can be used together with atomic fluorescence to measure the concentration of gold in solutions of complex samples down to 0.001 $\mu g\ ml^{-1}$, which is equivalent to 0.01 $\mu g\ g^{-1}$ in the solid sample.

Solutions of rock chip samples were kindly supplied by Mr. A. Knowles of Anaconda Australia, Kalgoorlie, Western Australia.

REFERENCES

1 C. M. Elson and A. Chatt, Anal. Chim. Acta, 155 (1983) 305.
2 J. B. McHugh, At. Spectrosc., 4 (1983) 66.
3 E. Kontas, At. Spectrosc., 2 (1981) 59.
4 N. R. Das and S. N. Bhattacharyya, Talanta, 23 (1976) 535.
5 M. S. Cresser, Solvent Extraction in Flame Spectroscopic Analysis, Butterworth, London, 1978, p. 114.
6 F. W. E. Strelow, E. C. Feast, P. M. Mathews, C. J. C. Bothma and C. R. Van Zyl, Anal. Chem., 38 (1966) 115.
7 T. Groenewald, Anal. Chem., 40 (1968) 863.
8 T. Groenewald, Anal. Chem., 41 (1969) 1012.
9 J. Matousek and V. Sychra, Anal. Chim. Acta, 49 (1970) 175.
10 P. L. Larkins, Spectrochim. Acta, 26B (1971) 477.
11 R. M. Lowe, Spectrochim. Acta, 26B (1971) 201.
12 R. S. Hobbs, G. F. Kirkbright, M. Sargent and T. S. West, Talanta, 15 (1968) 997.
13 P. L. Larkins and J. B. Willis, Spectrochim. Acta, 29B (1974) 319.
14 W. J. Price, Spectrochemical Analysis by Atomic Absorption, Heyden, London, 1979, p. 142.
15 D. R. Demers and C. D. Allemand, Anal. Chem., 53 (1981) 1915.
16 W. Slavin and D. C. Manning, Prog. Anal. At. Spectrosc., 5 (1982) 243.
17 G. F. Kirkbright and H. M. Tinsley, Talanta, 26 (1979) 41.
18 W. Slavin, G. R. Carnrick, D. C. Manning and E. Pruszkowska, At. Spectrosc., 4 (1983) 69.
19 J. V. Sullivan and A. Walsh, Spectrochim. Acta, 21 (1965) 721.
20 G. S. Lomdahl, T. Norris and J. V. Sullivan, Am. Lab., 15(3) (1983) 66.
21 N. Omenetto, L. P. Hart and J. D. Winefordner, Appl. Spectrosc., 26 (1972) 612.
22 L. Ebdon, J. R. Wilkinson and K. W. Jackson, Anal. Chim. Acta, 128 (1981) 45.
23 D. A. Naranjit, B. H. Radziuk, J. C. Rylaarsdam, P. L. Larkins and J. C. Van Loon, Appl. Spectrosc., 39 (1985) 128.
24 H. C. Van De Hulst, Light Scattering by Small Particles, Wiley, New York, 1957.
25 H. D. Fleming, Anal. Chim. Acta, 59 (1972) 197.

Analytica Chimica Acta, 173 (1985) 89—95
Elsevier Science Publishers B.V., Amsterdam — Printed in The Netherlands

SIMULTANEOUS DETERMINATION OF GERMANIUM, ARSENIC, TIN AND ANTIMONY BY MOLECULAR EMISSION CAVITY ANALYSIS AFTER HYDRIDE GENERATION AND GAS CHROMATOGRAPHIC SEPARATION

E. HENDEN

Chemistry Department, Faculty of Science, University of Ege, Bornova, Izmir (Turkey)

(Received 29th November 1984)

SUMMARY

Arsenic (0.1—5 μg), antimony (1—40 μg), tin (0.5—10 μg) and germanium (0.2—10 μg) are determined simultaneously by reduction to their hydrides with sodium tetrahydroborate(III), followed by gas chromatographic separation on a column of 10% E-301 silicone gum rubber on Porapak Q, and measurement of the emissions at 490 nm in an oxygen/hydrogen flame within a cavity. Detection limits for 1-ml samples are 35 ng As, 400 ng Sb, 85 ng Sn and 100 ng Ge. A more sensitive determination of arsenic (0.05—3 μg) and antimony (0.1—5 μg) in binary mixtures is also described; the detection limits are 15 ng As and 40 ng Sb.

The determination of arsenic, antimony, tin and germanium by generation of their volatile hydrides and measurement by atomic spectrometry is very popular [1]. Several metal ions interfere [2] and the alleviating effect of EDTA on these interferences has been reported [3, 4]. The elements which form volatile hydrides also mutually interfere [2] and some of these interferences are believed to occur during atomization. The separation of the volatile hydrides and development of a sensitive detector for their measurement is, therefore, of importance. It would also provide a means of determining more than one element in a single run. For this purpose, a thermal conductivity detector has been used [5] to detect arsenic, antimony and germanium hydrides separated by gas chromatography. Kadeg and Christian [6] determined arsenic, antimony, tin and germanium hydrides with a gas chromatography/mass spectrometry system. Both techniques, however, required a precollection step. Sequential determination of arsenic, selenium, germanium and tin as their hydrides by gas chromatography with an atomic absorption detector has also been described [7].

Applications of molecular emission cavity analysis (m.e.c.a.) to the determination of arsenic and antimony [8, 9] and tin [9, 10] as their hydrides were described earlier. The emissions, attributed to oxides, were obtained by using an oxy-cavity. Gas chromatographic separation and simultaneous determination, at a single wavelength, of arsenic and antimony as

0003-2670/85/$03.30

their hydrides by m.e.c.a. was achieved [9]. Down to 0.2 μg of arsenic and 0.7 μg of antimony could be detected. Tin hydride could also be determined simultaneously. Determination of germanium by injection of its solution directly into the m.e.c.a. cavity and measurement of GeCl emission has been reported [11], but it seems that the m.e.c.a. determination of germanium based on hydride generation has not been described.

The m.e.c.a. oxy-cavity, which is used for producing oxide-based emissions, involves a small flow of oxygen into the cavity held in a hydrogen/nitrogen diffusion flame [8]. It was previously shown [12] that such oxide emissions could also be obtained if the entire flame is generated within the cavity. This cavity eliminates the need for the burner system required by the oxy-cavity, and because of the relatively small flows of gases used, it is more economic. The present paper reports the further development of this cavity and its application to the simultaneous determination of arsenic, antimony, tin and germanium after generation and gas-liquid chromatography (g.c.) of their hydrides. The limits of detection were about ten times lower than those obtained with the m.e.c.a. oxy-cavity [9].

EXPERIMENTAL

Instrumentation

A Pye Unicam SP90A flame spectrometer, with a 1.4-mm slit (bandwidth at 400 nm = 45 nm) was used to measure the emissions. The output was recorded on a Varian G-2500 chart recorder (response time 0.5 s for full-scale deflection). A cavity-holding assembly was attached to the top of the instrument. A stainless steel cavity without water cooling (4-mm diameter, 10 mm deep; Fig. 1) was used. Three stainless steel tubes (one of 0.8 mm i.d. for nitrogen as the carrier gas and the other two of 0.3 mm i.d. for introducing oxygen and hydrogen into the cavity) were connected via three drilled holes to the rear of the cavity at tangents to the cavity wall. All the gas tubes were fixed to the outer wall of the cavity by welding.

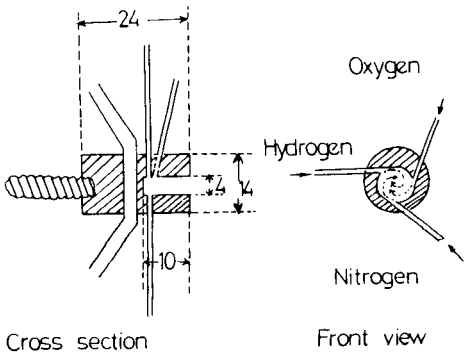

Fig. 1. The cavity, which contains the flame (dimensions in mm).

The volatilization and g.c. system was similar to that described earlier [9], with a glass reaction vessel (12.5 cm long, 1.5 cm in diameter). The chromatographic column for the separation of arsine and stibine was a PTFE tube (3 mm i.d., 13 cm long) packed with 10% E-301 silicone gum rubber on Porapak Q (80—100 mesh). The column was connected by means of PTFE tubes to the reaction vessel through a drying tube, packed with anhydrous calcium sulphate powder, and to the stainless steel tube (0.8 mm i.d.) in one of the rear openings of the cavity. The column temperature was controlled at 17 ± 0.5°C by immersion in water contained in a Dewar flask. For the separation of the hydrides of arsenic, antimony, tin and germanium, a PTFE column (55 cm long, 3 mm i.d.) was packed as above and operated at 15 ± 0.5°C.

Reagents

All chemicals used were of analytical-reagent grade unless otherwise stated. Stock solutions (1 mg ml^{-1}) of arsenic(III), antimony(III), tin(II) and germanium(IV) were prepared from arsenic(III) oxide, antimony(III) oxide, tin(II) chloride and germanium(IV) oxide, respectively. All the final stock solutions were 2 M in hydrochloric acid. The working solutions were prepared daily by dilution of the stock solutions.

Sodium tetrahydroborate(III) solution (5% w/v) was prepared, as required, by dissolving an appropriate amount of the powder (BDH Chemicals, laboratory-reagent grade) in 0.01 M sodium hydroxide.

Measurement of emissions

The oxygen/hydrogen/nitrogen (carrier gas) flame was kept on throughout a series of experiments. A 0.5-ml portion of the sodium tetrahydroborate(III) solution was pipetted into the reaction vessel and the volatilization system was closed. The system was deaerated for 20 s with nitrogen carrier gas and the chart recorder was turned on. A 1-ml portion of the test solution was injected and the resulting emissions from oxide-containing species were recorded at 400 nm, for arsenic and antimony only, or at 490 nm for the determination of arsenic, antimony, tin and germanium in mixtures. Peak-height measurements were made for arsenic and germanium (which gave sharper peaks) and peak-area measurements for tin and antimony (which gave the later, broader peaks) unless stated otherwise. Peak areas were measured by triangulation.

Because the emission intensities varied with time as the hydrides were eluted from the g.c. column, it was not possible to obtain an emission spectrum with the present system. In order to obtain a spectrum, the g.c. column was replaced by a PTFE tube. Germanium solution (500 μg ml^{-1}, 0.1 M in hydrochloric acid) was injected slowly at a constant rate from an automated burette into the reaction vessel containing 3 ml of 5% sodium tetrahydroborate(III) solution. The emission intensity was constant for more than 15 min during which the spectrum was scanned. The emission spectra of the other elements were obtained in the same way.

RESULTS AND DISCUSSION

Optimization of conditions

The water-cooled cavities required relatively high flow rates of the flame gases in order to reach high enough temperatures for the emissions to be obtained. Because the background flame emission also increased with increasing gas flow rates, the cavity used in this work was not water-cooled, but came into thermal equilibrium by conducting heat to the cavity holder assembly and to the surroundings. When thermal equilibrium was reached, which usually took ca. 15 min, the emission readings became repeatable.

It was observed that the sequence in which the gas tubes entered the cavity affected flame stability and the background emission. When the hydrogen and oxygen tubes (Fig. 1) were exchanged, a much higher oxygen flow rate was required in order to obtain a stable flame vortex within the cavity, under which conditions the background emission increased and varied more. This may be attributed to changes in the mixing efficiency of the gases within the particular cavity used. In the present work, the sequence shown in Fig. 1 was used.

The emission intensities and retention times for tin and germanium were slightly changed when the acid concentration of the solution was increased from 0.1 M to 0.3 M, as was previously found for arsenic and antimony [9]. Therefore all the working solutions were prepared in 0.1 M hydrochloric acid.

The flow rates of the flame gases determine the shape, volume, temperature and composition of the flame and the length of time spent by the analyte in the cavity. The emission intensities are therefore affected by changes in the gas flow rates. The flow rates were chosen in order to obtain relatively high emissions for all the elements in the mixtures. A flame from 55 ml min^{-1} oxygen, 85 ml min^{-1} hydrogen and 55 ml min^{-1} nitrogen was used for the determination of arsenic and antimony in binary mixtures, but for mixtures of all four elements, the flame used was from 40 ml min^{-1} oxygen, 70 ml min^{-1} hydrogen and 45 ml min^{-1} nitrogen.

Arsine and stibine were well separated on the 13-cm long g.c. column under the recommended conditions. The retention times were 69 s for arsine and 222 s for stibine. The separation of the germanium, arsenic, tin and antimony hydrides on the 55-cm long column is shown in Fig. 2.

Emission spectra

The emission spectra of arsenic, antimony and tin were similar to those obtained with the m.e.c.a. oxy-cavity [8, 10], and were attributed to oxide emitters. The emission of germanium was blue where oxygen entered the cavity and so the flame was rich in oxygen, whereas it was intense red in the other parts of the cavity; the red emission might have masked some of the blue emission. The red emission may be attributed to GeH [13]. The detector used was insensitive to red and, therefore, the red emission was not util-

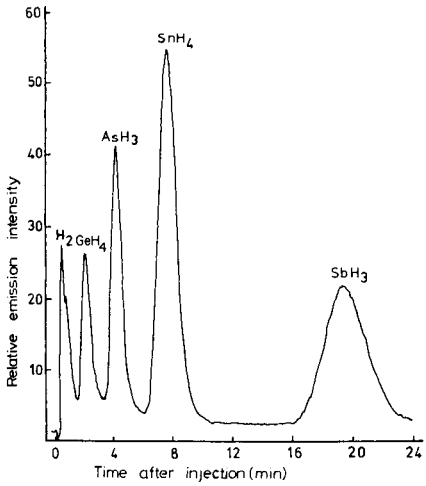

Fig. 2. Separation of germanium (5 μg), arsenic (3 μg), tin (10 μg) and antimony (20 μg) hydrides under the recommended conditions.

ized for the determination of germanium. The broad-band spectrum of the blue emission, with maximum intensity at 470 nm, was used instead (Fig. 3). This is also likely to arise from an oxide of germanium [13].

The determination of germanium, arsenic, tin and antimony in admixtures

Linear calibration graphs (Fig. 4) were obtained for 0.2—10 μg of germanium, 0.1—5 μg of arsenic, 0.5—10 μg of tin and 1.0—40 μg of antimony. The emission of 20 μg of tin showed strong apparent self-absorption at the peak maximum, resulting in a double peak. Similar effects were also observed when very intense emissions of the other elements were measured. The amount of an element for which self-absorption was observed depended on the flame composition.

The mutual effects of the four elements were studied. The calibration graph for each element was found to be unaffected by the presence of 50 μg of each of the other three elements. The relative standard deviations (n = 8) for the determination of 2 μg of germanium, 1 μg of arsenic, 2 μg of tin and 10 μg of antimony in admixture were 3.8, 4.1, 4.5 and 4.9%, respectively. These standard deviations could undoubtedly be decreased by better control of the column temperature [9]. The limits of detection (signal equal to twice the background noise) under the recommended conditions were 100 ng, 35 ng, 85 ng and 400 ng for germanium, arsenic, tin and antimony, respectively. The detection limits could be greatly improved for a particular element, if required, though at the expense of the other elements. Thus, for example, 30 ng of tin could be detected when the emissions were measured in the flame from 90 ml min^{-1} hydrogen, 35 ml min^{-1} oxygen and 45 ml min^{-1} nitrogen. Under these conditions the calibration graph was linear only up to 2 μg of tin.

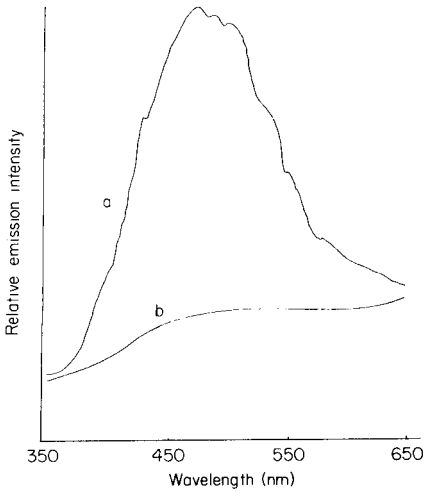

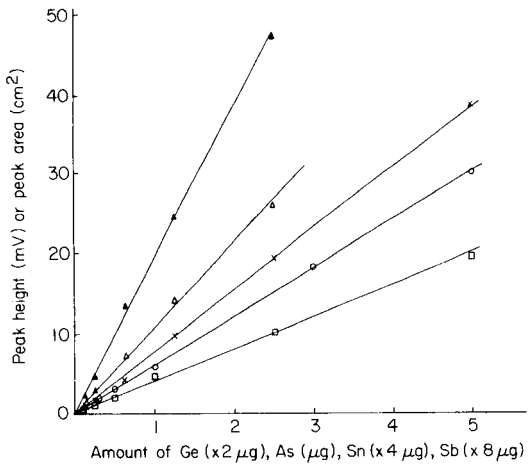

Fig. 3. Emission spectra: (a) GeH_4; (b) flame background. (Slit = 0.1 mm, ≡3.2 nm at 400 nm.)

Fig. 4. Calibration graphs: (□) 0.2—10 μg of germanium; (○) 0.1—5 μg of arsenic; (△, ▲) 0.5—10 μg of tin, by peak height (△) and by peak area (▲); (×) 1.0—40 μg of antimony.

The determination of arsenic and antimony in binary mixtures

As the calibration ranges and the detection limits vary with the wavelength and flame composition, the determination of arsenic and antimony in binary mixtures was investigated in order to increase the sensitivity of the technique for these elements. Under the recommended conditions for such binary mixtures, stibine was well separated from the other three hydrides on the 13-cm column, but the peaks of germanium, arsenic, and tin overlapped to some extent. However, the limits of detection for tin (0.5 μg) and germanium (2 μg) were poor, so that no spectral interference was expected from these weights of tin and germanium in the determination of arsenic.

Linear calibration graphs were obtained for 0.05—3.0 μg of arsenic and 0.1—5.0 μg of antimony. The relative standard deviations (n = 11) for the determination of 0.4 μg of arsenic and 1.0 μg of antimony in a mixture were 3.8% and 4.5%, respectively. The limits of detection were 15 ng for arsenic and 40 ng for antimony.

REFERENCES

1 R. G. Godden and D. R. Thomerson, Analyst (London), 105 (1980) 1137.
2 A. E. Smith, Analyst (London), 100 (1975) 300.
3 R. Belcher, S. L. Bogdanski, E. Henden and A. Townshend, Analyst (London), 100 (1975) 522.
4 E. Henden, Analyst (London), 107 (1982) 872.

5 R. K. Skogerboe and A. P. Bejmuk, Anal. Chim. Acta, 94 (1977) 297.
6 R. D. Kadeg and G. D. Christian, Anal. Chim. Acta, 88 (1977) 117.
7 M. H. Hahn, K. J. Mulligan, M. E. Jackson and J. A. Caruso, Anal. Chim. Acta, 118 (1980) 115.
8 R. Belcher, S. L. Bogdanski, S. A. Ghonaim and A. Townshend, Anal. Chim. Acta, 72 (1974) 183.
9 R. Belcher, S. L. Bogdanski, E. Henden and A. Townshend, Anal. Chim. Acta, 92 (1977) 33.
10 I. Z. Al-Zamil, Ph.D. thesis, Birmingham University, 1978.
11 S. A. Al-Tamrah, A. Z. Al-Zamil and A. Townshend, Anal. Chim. Acta, 143 (1982) 199.
12 S. L. Bogdanski, E. Henden and A. Townshend, Anal. Chim. Acta, 116 (1980) 93.
13 R. W. B. Pearse and A. G. Gaydon, The Identification of Molecular Spectra, 3rd edn., Chapman and Hall, London, 1965.

Analytica Chimica Acta, 173 (1985) 97—104
Elsevier Science Publishers B.V., Amsterdam — Printed in The Netherlands

DETERMINATION OF GOLD BY ATOMIC ABSORPTION SPECTROMETRY AFTER EXTRACTION INTO THE NON-DESULPHURIZED FRACTION OF CRUDE OIL DISTILLATE

KAREL JAKUBEC*, ZDENĚK ŠÍR and JAN VILÍMEC

Institute of Chemical Process Fundamentals, Czechoslovak Academy of Science, Rozvojová 135, Praha 6 (Czechoslovakia)

(Received 14th December 1984)

SUMMARY

The extraction of gold from aqueous chloride solutions into non-desulphurized fractions of crude oil distillates, especially paraffin oil, is described. The fraction boiling at 150—220°C exhibited optimum properties. The extraction is tested for solutions containing chlorides, dissolved chlorine and 0.1—3 M hydrochloric acid. Nitric acid should be absent. The distribution coefficient of gold varies from 400 to 900. Extracts containing ≤ 0.3 g l^{-1} gold are stable for at least 12 months. The organic extract is sprayed into a lean acetylene/air flame with measurement at 242.8 nm (background correction). The calibration graph has linear portions over the ranges 0—2.5 and 2.5—16 mg l^{-1}. The limit of detection is 0.03 mg l^{-1} gold in the extract (0.001 mg l^{-1} in the aqueous phase). The minimum measurable concentration for gold in auriferous rocks and ores is 0.018 g per ton with 25-g samples.

The determination of gold by atomic absorption spectrometry (a.a.s.) is now widely used because of its high sensitivity and its lack of complication from interference effects [1]. Nevertheless, the direct determination of gold by a.a.s. in solutions obtained by wet decomposition of ores and rocks or in leach liquors from gold-containing raw materials is often difficult or even impossible because of high salt concentrations or low gold content. Liquid/liquid extraction of gold from such samples overcomes these difficulties. The extractants used most frequently for this purpose are methyl isobutyl ketone [2, 3] and various organic sulphides [4—6].

This paper reports on an efficient and selective gold extraction with the use of non-desulphurized crude oil distillates. The extracts obtained are directly suitable for a.a.s.

EXPERIMENTAL

Chemicals and instrumentation

All the chemicals used were of p.a. purity, except for iron(III) chloride (technical grade). The standard gold(III) chloride solution was prepared from

0003-2670/85/$03.30

a known amount of pure gold sheet (Safina, Vestec) in the usual way; it contained 1.660 g l^{-1} gold and 1.0 M hydrochloric acid.

Non-desulphurized crude oil distillates were commercial samples (CHZ ČSSP Litvínov).

An Atomspek H-1580 atomic absorption spectrometer (Rank-Hilger) was used. A 9825A desktop computer equipped with a 9885M flexible disk memory (Hewlett-Packard) was used for treatment of data.

Preparation of standard organic extracts

In preliminary experiments, the suitability of the crude oil and of a series of non-desulphurized crude oil distillates (obtained by distillation at atmospheric pressure and in vacuum) as extractants for gold from aqueous chloride solutions was investigated. The properties of the extractants were evaluated with respect to their extraction capacity and their behaviour during extraction. On the basis of these experiments, two fractions obtained by atmospheric distillation of the crude oil were used in further work: the fraction boiling at 90—160° C and containing 200 mg l^{-1} sulphur (lacquer petroleum, designated further as I) and the fraction boiling at 150—220° C, containing 0.2% sulphur and 19% aromatic hydrocarbons (primary paraffin oil, extractant II). The crude oil itself and the other fractions of the distillate were found to have either low extraction capacity or to form a dark precipitate at the interface during extraction.

Two series of standard extracts I and II with defined gold concentration were obtained as follows. Into 50-ml separating funnels, appropriate volumes of the standard gold solution were pipetted, diluted to ca. 20 ml with 2M hydrochloric acid and extracted with four 20-ml portions of extractant I or II (about 1 min of intense shaking for each extraction step). The combined extracts were diluted with the extractant to 100.00 ml. The concentration of gold in these standards was 0.20, 0.50, 1.00, 2.50, 5.00, 10.00 and 16.00 mg l^{-1}.

Quantitative extraction was checked by the sensitive test with Rhodamine B [7] which has a detection limit of 0.1 μg of gold (limiting dilution 1:500 000). For testing, the aqueous phases after the fourth extraction were evaporated to $\leqslant$1 ml. In none of the residual aqueous solutions was the presence of gold detected.

Instrument settings

Optimum values of the a.a.s. parameters were established for a standard extract of gold (16 mg l^{-1}) in extractant II and for the extractant itself. The 242.8-nm line with a slit width of 235 μm and a current intensity of 8 mA for the hollow-cathode lamp were found satisfactory. For all measurements, background correction and an integration time of 10 s were used. The optimum ratio of the gases for the air/acetylene flame was established for extractant II. The signal of the extractant increased as the amount of acetylene in the mixture was increased (Table 1) so that the flame should be kept

TABLE 1

The dependence of the blank absorbance signal on the air/acetylene ratio (242.8 nm)

Ratio	10:1	10:1.5	10:2	10:2.5	10:3	10:3.5
Signal	−0.0015	−0.0005	0.007	0.045	0.132	0.221

as lean as possible. The height of the burner top with respect to the horizontal axis of the beam was also important. For the instrument used, the optimum value was ca. 8 mm. Obviously, these parameters would require adjustment for other sorts of spectrometer.

Recommended procedures

Leach liquors. A total of 100 ml of the leach liquor containing 0.008—2.4 mg l^{-1} gold, a maximum of 1 mol l^{-1} iron and 0.1—3 M hydrochloric acid is extracted with three 5.00-ml portions of extractant II. The combined extract is used for a.a.s. in the acetylene/air (1.5:10) flame at 242.8 nm. The gold content in the sample is evaluated from the calibration graphs plotted for the concentration ranges 0—2.5 and 2.5—16 mg l^{-1} by using standard gold extracts in the same extractant.

For leach liquors containing 0.001—0.008 mg l^{-1} gold, larger volumes of sample, e.g., 500 ml, and the same procedure are recommended.

Auriferous rocks and ores. A weighed portion (25.00 g) of the milled sample ($\leqslant$0.07-mm particle size) is heated with 20 ml of concentrated nitric acid and 60 ml of concentrated hydrochloric acid to boiling for 1 h in a covered beaker and left aside for 24 h at ambient temperature. Then, it is diluted with 150 ml of distilled water and filtered on fine filter paper. The residue on the filter is washed with 100 ml of hot 2% (v/v) hydrochloric acid, 1 g of sodium chloride is added to the filtrate, and the solution is evaporated nearly to dryness. The residue is dissolved in 10 ml of 6 M hydrochloric acid saturated with chlorine and subjected to another evaporation until nitric acid is completely removed. The residue is then dissolved in 10 ml of 6 M hydrochloric acid saturated with chlorine, the solution is diluted with 50 ml of distilled water and filtered, and the residue on the filter is washed with 50 ml of hot 2 M hydrochloric acid. The filtrate is cooled, placed in a separating funnel and extracted with three 5.00-ml portions of the extractant II. The extract is then completed as in the preceding case.

RESULTS AND DISCUSSION

Calibration

The parameters of the calibration plots were calculated by linear regression. Over the range of gold concentrations examined (0.20—16 mg l^{-1}), two linear portions were found at 0—2.5 mg l^{-1} and 2.5—16 mg l^{-1}; for these ranges, the correlation coefficients were better than 0.999. The preliminary experiments

showed that extractant II is more suitable for analytical purposes, because its extraction capacity and its ignition temperature are higher. Accordingly, extractant II was preferred for further measurements. With one sample of extractant II, more than 30 calibration plots were obtained over about 13 months, as described above. For the calibration equation $A = a + bc$, where A is the absorbance and c is the gold concentration (mg l^{-1}), a for the lower concentration region varied from −0.005 to +0.004 and b changed from 0.073 to 0.090; similarly, for the higher concentration region, a varied from +0.013 to +0.030 and b from 0.064 to 0.081. There was no observable time/stability dependence of the standard gold extracts prepared under the conditions described. This indicates that extracts of gold (0.2—16 mg l^{-1}) in extractant II are stable at least for one year, which is a great advantage compared to other a.a.s. methods for gold. The stability of extracts in extractant I was tested only for 4 months. The a and b values remained nearly constant during this period.

From these data for the a.a.s. determination of gold with extractant II, the limit of determination was calculated as 0.050 mg l^{-1} and the detection limit as 0.030 mg l^{-1}.

Extraction of gold from chloride solutions

Extraction capacity. The extraction capacities of extractants I and II were evaluated as follows: 10 ml of the extractant was shaken with 10 ml of aqueous gold standard (1.66 g l^{-1} Au, 2 M hydrochloric acid) for 30 min and after phase separation, 1.00 ml of the organic phase was diluted with an appropriate volume of the pure extractant for a.a.s. The remaining organic phase was shaken with another 10 ml of the gold standard. This procedure was repeated until the composition of the organic phase remained unchanged. Three steps were found to be necessary for extractant I and five steps for extractant II. The calculated values of the extraction capacity were 0.18 g l^{-1} gold for I and 4.85 g l^{-1} for II.

Stability of extracts. Gold-saturated extracts in both extractants were found to deposit pale to dark yellow sediments on the walls of glass flasks even after several hours, which indicates their low stability.

In order to evaluate the stability of concentrated gold extracts in extractant II, three standard extracts containing ca. 1.00, 0.75 and 0.31 g l^{-1} gold were prepared. These standards were stored in closed Erlenmeyer flasks at ambient temperature in sunlight; 0.50-ml portions of the extracts were diluted at given time intervals to 50.00 ml with extractant II and subjected to a.a.s. As shown in Table 2, the gold extracts obtained from chloride solutions by using extractant II are remarkably stable. After ca. 6 months, the gold content decreased from the initial value of 1.0 g l^{-1} by about 7% and from the initial value of 0.75 by about 4%, while the extract containing 0.3 g l^{-1} was stable. As mentioned earlier, extracts containing 0.2—16 mg l^{-1} gold were stable for at least 13 months.

Distribution coefficient. The value of the distribution coefficient of gold can be affected significantly by the composition of the aqueous phase that

TABLE 2

Stability of gold extract in extractant II with time

Time (days)	0	7	14	21	30	45	150
Au found[a]	1.006	0.965	0.956	0.952	0.956	0.937	0.935
($g\ l^{-1}$)	0.746	0.736	0.723	0.717	0.712	0.729	0.717
	0.314	0.316	0.313	0.314	0.318	0.310	0.313

[a]Gold concentrations taken were 1.00, 0.75 and 0.31 $g\ l^{-1}$, respectively.

can vary in different samples. For that reason, aqueous phases of the following composition were examined: 2 M hydrochloric acid, 1 M iron(III) chloride in 0.5 M hydrochloric acid, 0.5 M iron(III) chloride in 1 M hydrochloric acid, and 1.5 M calcium chloride in 0.5 M hydrochloric acid. All the aqueous phases contained 0.15 mg l^{-1} gold. In each case, 1 l of the aqueous phase was extracted with four 10.00-ml portions of extractant II and after phase separation, each portion was subjected to a.a.s. The values of the distribution coefficient ranged from 400 to 900 with no significant dependence on the aqueous phase composition.

It is evident that for analytical purposes, it is sufficient to extract 100 ml of the aqueous phase with three 5-ml portions of extractant II; if necessary, 1 l of the aqueous phase should be extracted with three 10-ml portions of the extractant.

The effect of nitric acid. Nitric acid is an essential component of almost all solutions obtained by wet decomposition of solid gold-containing samples, and its removal is time-consuming. Therefore, the possibility of extracting gold from aqueous solutions containing nitric acid by extractant II was examined as follows. To 50.00 ml of 0.5 M iron(III) chloride containing 0.5 M hydrochloric acid and 0.53 mg l^{-1} gold were added different volumes of 65% nitric acid, and each solution was extracted with three 10.00-ml portions of extractant II. The extracts were subjected to a.a.s. The results in Table 3 show that the extraction of gold is affected significantly even by low nitric acid concentrations.

The effect of dissolved chlorine. The leaching of auriferous rocks is usually done with chloride solutions containing dissolved chlorine in varying concentrations. The effect of the dissolved chlorine on the gold extraction was examined under several different conditions. In the first set of tests, 60 ml of aqueous phase containing 26.5 μg of gold, 0.25 M iron(III) chloride, 1.58 M hydrochloric acid and 1 g l^{-1} chlorine were extracted with three 10.00-ml portions of extractant II. The following results were obtained: 22.5 μg of gold in the first extract, 5.1 μg of gold in the second, and none in the third. The total yield of gold thus corresponds to 104.1% of the theoretical value. The overall time of contact of both phases in the three extraction steps was ca. 15 min.

TABLE 3

Effect of nitric acid on the extraction of gold (26.5 μg) with extractant II

HNO_3 in aq. phase (M)	0.3	1.5	2.5
Au found (μg) in			
extract 1	28.5	28.6	17.3
extract 2	0	8.6	3.2
extract 3	0	4.1	0
Total Au found (μg)	28.5 (+7.6%)	41.3 (+56%)	20.5 (−22.6%)

In the second set of tests, equal volumes of extractant II and an aqueous phase of the same composition as above were shaken for 10 h. After phase separation, 102.8% of the gold was found in the organic phase. In the third set of tests, equal volumes of extractant II and 7 M hydrochloric acid containing 5 g l^{-1} chlorine were shaken for 15 h or 48 h. After phase separation, the extractants were used for one-step extraction of an aqueous standard containing 0.53 mg l^{-1} gold. The yield of the gold extraction was 24% in the former case and 0% in the latter. Finally, the portion of extractant II which had been deactivated in the third experiment by shaking for 48 h was stirred with an equal volume of 5% (w/v) tin(II) chloride solution in 5 M hydrochloric acid in the presence of 100 mg of tin foil for 5 min. The recovered extractant exhibited the same properties as the original extractant for gold.

These experiments show that dissolved chlorine degrades the extraction properties of extractant II. The rate of this reaction is, however, slow enough for the extractant to be used in the analysis of chlorine-containing aqueous gold solutions, provided that the time of the contact between the two phases is not too long.

The valence of gold. The chloride solutions of gold contain two chloro complexes, the proportion of which is given by the equilibrium constant [8] of the reaction

$$AuCl_4^- + 2e^- \rightleftharpoons AuCl_2^- + 2Cl^- \quad (E_0 = 0.921\ V)$$

How the two forms of gold behave during extraction with extractant II was therefore studied. As already mentioned, the distribution coefficient of tetrachloroaurate(III) which is practically the only form of gold present in solutions containing dissolved chlorine varied from 400 to 900. In another series of experiments, extraction was done from solutions containing iron(III) and iron(II) ions in different mole ratios. Distribution coefficients were calculated as described above. The results are presented in Table 4. It was calculated that the solutions with a $c_{Fe(III)}/c_{Fe(II)}$ ratio of 10 contain gold exclusively in the form of $AuCl_2^-$. This indicates that the distribution coefficients of both chloro complexes are sufficiently high for analytical purposes.

TABLE 4

The dependence of the distribution coefficient ($D = c_{org}/c_w$) of gold on the ratio Fe(III)/Fe(II) in extraction with extractant II (for 1 M total iron)

Ratio Fe(III)/Fe(II)	300	200	100	50	10
D	630	750	400	340	270

Acidity. To establish the effect of acidity on the distribution coefficient, the concentration of hydrochloric acid was changed within the 0.1—3 M range. In all cases, the gold concentration was 26.5 mg l^{-1} and the iron(III) chloride was 0.3 M. The distribution coefficient, evaluated as in the preceding experiments, was found to lie within the 400—800 region, without any significant dependence on the acidity of the aqueous phase.

On the basis of all these experiments, the procedures given under Experimental are recommended for determining gold in chloride leach liquors of auriferous rocks and in the rocks or ores themselves.

Precision and reproducibility

Leach liquors from auriferous rocks containing 0.3—1.0 M iron(III) chloride and 0.5—1.0 M hydrochloric acid were analysed by a.a.s. in three laboratories. In two laboratories, gold was extracted with dibutyl sulphide and in the other the primary paraffin oil (extractant II) was used as the extractant. The results are summarized in Table 5.

In further tests, the process of leaching gold from rock was examined; the solution used contained 1 M iron(III) chloride and 0.5 M hydrochloric acid. The gold contents in the leach liquors and solid phases were determined by the recommended procedure. The results are given in Table 6.

From these results, it becomes evident that there is very good agreement between the procedure recommended in the present work and the frequently

TABLE 5

The determination of gold in leach liquors of rocks after extraction into dibutyl sulphide (Labs. 1 and 2) and into extractant II (Lab. 3)

Sample	Gold found (mg l^{-1})		
	Laboratory 1	Laboratory 2	Laboratory 3
1	0.010	0.006	0.008
2	0.037	0.033	0.040
3	0.046	0.037	0.045
4	0.054	0.053	0.055
5	0.060	0.060	0.070
6	0.106	0.092	0.102
7	0.250	0.231	0.233

TABLE 6

The balance of a complete leaching process of auriferous rock analysed by the recommended procedures

Gold found (mg kg^{-1})			Balance (%)
Primary rock	Rock after leaching	Leached gold	
2.790	2.035	0.904	+5.3
2.807	1.962	0.845	−0.7
2.470	1.969	0.560	+2.6

used extraction of gold with dibutyl sulphide and also satisfactory consistency in the analysis of the solid and liquid samples.

REFERENCES

1 I. Rubeska and B. Moldan, Atomic Absorption Spectrophotometry, Iliffe Books, London, 1969.
2 M. C. Graves, Nature (London), 199 (1963) 552.
3 F. M. Tindall, At. Absorpt. Newsl., 4 (1965) 339.
4 V. G. Torgov and A. A. Khlebnikova, Zh. Anal. Khim., 32 (1977) 960.
5 V. G. Torgov, T. M. Korda and I. G. Yudelevich, Zh. Anal. Khim., 33 (1978) 2341.
6 I. G. Yudelevich, G. A. Vall, V. G. Torgov and T. M. Korda, Zh. Anal. Khim., 25 (1970) 870.
7 F. Feigl, Spot Tests in Inorganic Analysis, Elsevier, Amsterdam, 1958, p. 445.
8 J. Pouradier, M. C. Gadet and H. Chateau, J. Chim. Phys., 62 (1965) 203.

Analytica Chimica Acta, 173 (1985) 105—116
Elsevier Science Publishers B.V., Amsterdam — Printed in The Netherlands

X-RAY FLUORESCENCE SPECTROMETRY WITH SYNCHROTRON RADIATION

A. KNÖCHEL*, W. PETERSEN and G. TOLKIEHN

Institute of Inorganic and Applied Chemistry, University of Hamburg, Martin-Luther-King Platz 6, D-2000 Hamburg 13 (Federal Republic of Germany)

(Received 10th December 1984)

SUMMARY

X-ray fluorescence spectrometry (x.r.f.) can be done through excitation with synchrotron radiation. This permits multi-element determinations in the trace region with improved detection limits compared to conventional x.r.f. Detection limits are evaluated and compared with theoretically calculated values. For a beam diameter of 0.5 mm and a sample of 1 mg cm^{-2}, absolute detection limits are between 0.1 and 0.4 pg. The dependence of the detection limit on the atomic number is reduced, when white synchrotron radiation is used for excitation instead of monochromatic radiation. The optimum of the limit of detection on the Z-scale can be shifted to higher atomic numbers and improved through filtration of the primary radiation by aluminium absorbers. Preparation of samples on different polymeric films is discussed in relation to blank values.

Developments in various branches of experimental science have increased the need for knowledge of the quantitative distribution of elements even at trace levels, and the demand for analytical procedures suitable for determining elements in the nanogram and picogram regions, preferably in multi-element mode [1]. The principal multi-element techniques used in trace analysis are neutron activation analysis (n.a.a.), atomic emission spectrometry (a.e.s.) and some variants of x-ray fluorescence spectrometry (x.r.f.) [2], which can quantify many elements simultaneously with different detection limits. The x.r.f. method seems to have high potential for development. Under normal circumstances, procedures based on x.r.f. reach detection limits only in the microgram region, as a result of unfavourable peak/background ratios. The background is caused mainly by scattering of the primary beam in the sample carrier and matrix.

In order to reduce background signals, recent developments include monochromatic and polarized Bragg reflectance on a single crystal [3—6], or polarized scattered rays on secondary targets of low atomic number [7]. The total intensity is, however, also greatly reduced so that little overall improvement is achieved. Very important progress in the endeavour to reduce background signals caused by scattering was made by the development of the x.r.f. method with a totally reflecting sample carrier made of quartz [8].

0003-2670/85/$03.30

However, the method requires that the measuring sample film be extremely thin with defined dimensions, and the limit of detection is strongly dependent on the atomic number, when excitation is done with a quasi-monoenergetic x-ray tube. Good detection limits are obtained when the x-ray fluorescence is induced by particle bombardment (p.i.x.e.) [9]. These methods are associated with potential systematic errors because of evaporation of some elements in the high vacuum commonly used. Owing to strong absorption of the primary beam, the samples must be very thin, and again the limits of detection show a strong dependence on the atomic number [9].

Synchrotron radiation originates from the acceleration of charged particles in the field of a deflecting magnet, which is necessary to retain the circular trajectory in a storage ring. The radiation, depending on the particle energy, can extend from the visible to the hard x-ray region, and is emitted in a narrow angular interval tangentially to the direction of the particles. Synchrotron radiation bestows the following advantages on x.r.f. methods: high photon flux density, strong collimation, high degree of linear polarization, a white spectrum free of characteristic lines, and a well-defined source.

The high flux density and the strong collimation allow the irradiated area and therefore the amount of sample to be kept small. The high degree of linear polarization improves the peak/background ratio by a factor of $1/(1 - P)$, e.g., a degree of polarization $P = 0.9$ produces a 10-fold improvement. The white spectrum, in contrast to normal tube excitation, permits nearly uniform excitation of all elements with the consequence that comparable detection limits are achieved nearly independently of the atomic number. The possibility of calculating the spectral distribution and intensity of the source indicates that, when sufficient data become available, the method might be developed into an absolute method operable without an internal standard.

The first application of synchrotron radiation for x.r.f. with soft x-rays was reported by Horowitz and Howell [10]. Later, Sparks et al. [11] attempted to detect super heavy elements with the aid of synchrotron radiation and monochromatic excitation [11]. Gilfrich et al. [12] conducted the test experiments in the SPEAR storage ring at Stanford and further such experiments are in progress elsewhere. With a graphite monochromator, the limits of detection of such a procedure were determined on the storage ring in Daresbury (G.B.) and compared with those of tube-excited x.r.f. (Mo tubes) and p.i.x.e. [13]. Results obtained by means of x.r.f. spectrometry with synchrotron radiation at the synchrotron radiation laboratory in Hamburg (HASYLAB) are reported in this paper.

EXPERIMENTAL

Equipment

The measuring arrangement is outlined in Fig. 1. The apparatus was built so that the whole arrangement up to the beryllium window of the radiation tubes can be flushed with helium. This prevents not only absorption losses

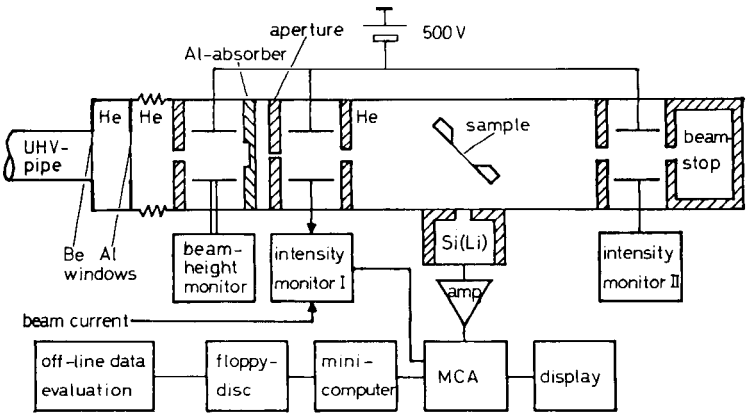

Fig. 1. The measuring arrangement. The UHV pipe leads from the DORIS storage ring at HASYLAB.

and increased scattering background resulting from the use of air, but also the risk of uncontrollable vacuum evaporation of certain elements or volatilizing of the sample material, and pressure forces on thin samples.

The whole arrangement is mounted on a goniometer head to afford remote adjustment in the beam [14]. For the purpose of correct adjustment of the sample, there are two ionization chambers, one in front and the other behind the sample chamber. They measure the radiation intensity. In order to locate the beam centre, i.e., the point of highest degree of polarization, a spatially sensitive ionization chamber was built in, consisting of two identical electrodes arranged in parallel with horizontal field. Standardization of the radiation intensity was done by obtaining the quotients of the difference and sum of the measured ionization currents with the aid of a division amplifier. The accuracy of locating the midpoint of the radiation was better than 0.1 mm. The sample is mounted in a sample holder on a goniometer, which facilitates manipulation in the x-, y- and z-directions inside the beam. The sample position is indicated through potentiometers coupled to an analog display. Over the sample holder there is a sample changer connected directly to the sample chamber.

Optimal excitation conditions for the samples are obtained with the help of a remotely controlled system of aperture and absorber. Different shutters (0.05—3 mm diameter) and absorbers of purified aluminium (0.0—12.0 mm thick) allow diverse combinations.

Owing to its ease of purification, the sample carrier is made of PTFE. Illumination of the sample spot should be only a few mm, if the aim is to operate in an area with a high degree of polarization. For this purpose, the sample carrier is equipped with a conical hole of 6-mm diameter. This permits not only the attachment of thin synthetic foils on which the sample preparation can take place but also direct preparation of thin sample films on the sample carrier. The external dimensions of the sample carrier are

30 × 30 × 2.5 mm to fit the sample changer. This size corresponds to slide frames from Minox so that cassettes and slide boxes could be used for the storage, transport and measurement of samples.

For characterization of the source, scattering experiments on defined materials (e.g., gases or special foils) were conducted to determine the degree of polarization and the spectral distribution of the excitation radiation. Figure 2 illustrates the effect of polarization on the fluorescence spectra of a xenon/nitrogen mixture taken (a) in the plane of ring (maximum polarization) and (b) perpendicular to it (linear degree of polarization $P = 0$). Spectra taken under standard conditions (uniform radiation, flux and same measuring time) show clearly the improved peak/background ratio obtained on application of polarized beam. The directed scattered rays can be drastically reduced whereas the intensity of the isotopic fluorescence rays remains constant. Evaluation of the degree of polarization yielded a value of 88—90% at an energy of 4—35 keV [15].

Sample preparation

The preparation of the sample for measurement was considered mainly from the point of view of developing an all-round sample system applicable in different methods and for diverse sample materials. The simplest arrangement for x.r.f. with synchrotron radiation is that illustrated in Fig. 1. The following conditions must be observed: (a) in order to minimize scattering effects and avoid absorption corrections, the sample carrier should be very thin and should be made of a material comprising only elements with low atomic numbers with the maximum thickness not exceeding 10 μm; (b) impurities (blank values) in the sample carrier should be below the detection limit of the method (e.g., in the case of iron, $\leqslant 10$ ng g^{-1}); (c) if the blank values are higher, they must be reproducible to allow their being considered as a constant background.

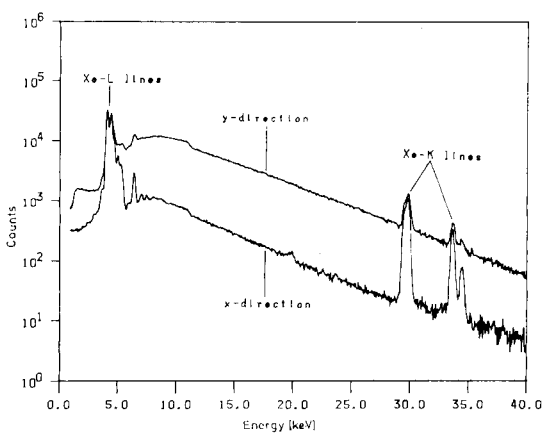

Fig. 2. Spectra of Xe/N_2 in the horizontal and vertical directions in the plane of polarization.

Possible candidates for the sample carrier are thin plastic sheets or water-soluble polymers which leave thin films behind on drying. With addition of an internal standard, these carriers are suitable for the following types of sample preparation: drying of an aliquot of the trace element solution on a suitable plastic sheet, evaporation on the plastic sheet, separation of precipitated trace elements on membrane filters, or incorporation of the trace elements in a polymer solution, from which an aliquot can be evaporated to yield a thin film. Important criteria are the mechanical strength of the prepared sample and low blank values of the substance used.

In general, solid samples are decomposed by wet digestion in the presence of an internal calibration standard and the resulting solution, after addition of a polymer, is used to fabricate the delicate films. If the solution is sufficiently dilute, the resulting sample ($\leqslant 1$ mg cm^{-2}) can be measured directly. Calibration can then be done with the help of an external multi-element standard but absolute calibration may also be possible. Aqueous solutions need no decomposition and, after addition of a standard, can be dispensed onto a suitable foil for evaporation to a film. Another method requires the (concentrated) solution to be mixed directly with a water-soluble polymer to form a hydrophilic film. A further possibility is to proceed with a chemical separation and concentration step aided by organic complexing agents, and then to treat the resulting organic solution of the trace elements with a lipophilic polymer; the solution thus obtained is used to prepare the sample film. This method is suitable for the analysis of organic solutions, after a standard has been added. Organic solutions can, of course, also be dropped directly onto the sample carrier and dried to a film.

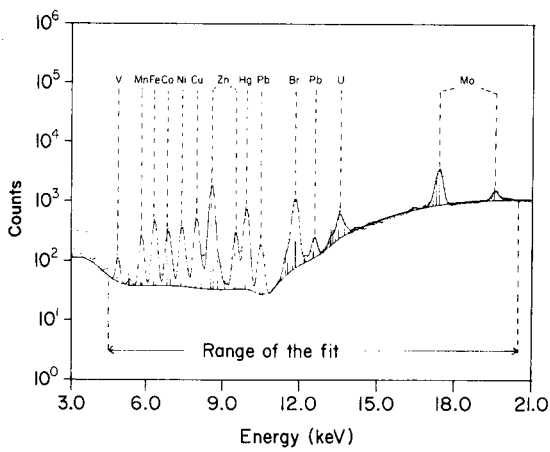

Fig. 3. Fit of the spectrum for a sea-water sample.

RESULTS AND DISCUSSION

Optimization of the sample preparation

Carrier films. Five types of film were studied. Polyester (Mylar) films are available as 2-μm thick foils and can be made thinner by stretching. Polyamide (Kapton) films are obtainable only at a minimum thickness of 7.5 μm. Polycarbonate (Makrofol) films are available as 2-μm thick foils. Formvar films were 5-μm thick. Polystyrene films were prepared to a minimum thickness of 2 μm [16]. The blank values of these various films were determined by n.a.a. and x.r.f. with synchrotron radiation. Table 1 summarizes the results.

In agreement with other authors [17], the blank values of the most frequently used Mylar films are in certain cases very high. Polycarbonate films appear more suitable, particularly because their thickness can be reduced by stretching without adversely influencing the mechanical strength. The highest purity was found for the relatively thick polyamide (Kapton) and laboratory-prepared polystyrene films. Polycarbonate and polystyrene were preferably used. The former was also used for the preparation of the calibration standard. The standards were obtained by evaporating delicate layers (2 or 50 nm) containing the elements Ti, Fe, Cu, Nb, Ag, Ta, Bi and Au. The values were checked by n.a.a.

For the separation of trace elements precipitated and collected on a membrane filter (Nucleopore), preliminary experiments showed that satisfactory yields of the trace elements were achieved only in the presence of large amounts of coprecipitants, which of course has a deleterious effect on the scattering background. In addition, the distribution of the trace elements on the filter was not homogeneous and the membrane filter shows in some cases very large blank values. This method was therefore discarded.

Preparation of sample films containing trace elements. Sample film preparation from polymer solutions containing trace elements was found to be very appropriate [18]. Especially methylcellulose and poly(vinylpyrrolidone)

TABLE 1

Blank values (μg g^{-1}) of thin films[a]

Element	Mylar	Makrofol	Kapton	Formvar	Polystyrene
K	9.5 ± 1.7	11 ± 2	<3	<3	<3
Ca	1900 ± 420(1750 ± 11)	13 ± 3(38 ± 0.7)	2.5 ± 0.4	<3	<3
Cr	5.4 ± 0.9	<0.5	<0.5	0.7 ± 0.2	0.6 ± 0.3
Fe	3.4 ± 0.5(3.8 ± 0.4)	17 ± 3(11 ± 0.7)	6.2 ± 0.9	1.2 ± 0.2	0.9 ± 0.4
Ni	<0.3(<0.3)	5.5 ± 1.1	<0.3	<0.3	<0.3
Cu	<0.5(0.38 ± 0.4)	<0.5(1.3 ± 0.5)	1.3 ± 0.5	<0.1	<0.1
Zn	60 ± 21(26 ± 0.9)	7.8 ± 2.0(0.7 ± 0.7)	<0.2	0.3 ± 0.2	0.6 ± 0.3
As	<0.6	<0.6	<0.6	0.8	<0.6
Pb	<0.2	<0.2	<0.2	0.35	<0.2

[a]Literature values [17] are given in parentheses where available.

showed favourable properties as film-forming agents. Methylcellulose has high blank values, which can be improved by purification. Table 2 shows the blank values for some hydrophilic films. As was shown by x.r.f. measurements with synchrotron radiation and spatial resolution, however, these polymers are not suitable for alkali and alkaline earth metals or for halogens. These elements tend to concentrate at the edges of the film during evaporation of the solution and thereby adversely affect the required homogeneity. For these elements, application of the essentially small irradiation diameter did not allow the acquisition of a representative section. Addition of complexing agents to speed up the drying process did not improve the situation for these elements.

Embedding the trace elements in an organic matrix is advantageous in that volatilization of elements caused by high radiation densities is avoided. For instance, when a sample containing mercury(II) chloride, potassium bromide, arsenic(III) oxide and selenium oxide was prepared with poly(vinyl alcohol), no losses were detected even after continuous irradiation for 1 h. Measurements before and after the irradiation showed (within the statistical error of 4%), no change in the sample composition.

To prepare samples from organic solutions, procedures similar to those for hydrophilic polymers are suitable. With lipophilic polymers, very good and stable films are obtained. Investigations on metal solutions complexed with dithiocarbamates or 8-hydroxychinoline showed no inhomogeneity within the films.

On the whole, embedding the trace elements in film-forming agents appears to be the most suitable procedure for sample preparation, especially when the procedure is restricted to the following steps: (a) preparation of a concentrated polymer solution; (b) addition of a definite amount of the trace element solution under investigation to a definite amount of polymer solution; (c) addition of an internal standard; (d) transfer of an aliquot of this mixture to the sample carrier placed on a polyethylene foil and drying; and (e) detachment of the sample carrier with the sample film from the polyethylene foil.

TABLE 2

Blank values ($\mu g\ g^{-1}$) for some hydrophilic polymers

Element	Methylcellulose (MC400)	Methylcellulose purified	Poly(vinylpyrrolidone)
K	11.5 ± 3.7	4.0 ± 2.3	97.8 ± 22.0
Ca	175.0 ± 17.3	1.7 ± 0.9	14.7 ± 1.8
Cr	0.9 ± 0.1	0.3 —	0.7 ± 0.5
Fe	41.0 ± 2.5	6.8 ± 1.7	36.6 ± 4.1
Ni	4.4 ± 0.1	0.63 ± 0.4	1.8 ± 0.3
Cu	1.1 ± 0.4	0.25 ± 0.1	1.6 ± 0.3
Zn	1.3 ± 0.1	0.25 ± 0.1	1.6 ± 0.2

Evaluation of the spectra

Spectra were evaluated by a program originally developed by the working group of Prof. J. Scheer and adapted to tube-excited x.r.f. [19]. In this program, the line ratios of the various elements are held constant. Because, however, the excitation conditions of the tube (monoenergetic excitation) are quite different from that of the white synchrotron beam and therefore the probabilities of exciting the L- and M-edges also differ, major changes in the program had to be made and the ratios of the excitation probabilities of all elements emitting L- or M-lines between 1.7 and 3.5 keV (i.e., all elements with $Z \geqslant 40$) had to be determined anew. For this purpose, single-element samples were prepared and the line ratios were calculated with a special variation of the spectra evaluation program. Measurements were done with five different absorbers. The intensity ratios of each line determined in this way were fitted to a fourth-degree polynomial relative to atomic number. The coefficients of these fits serve as constant parameters in the evaluation program. A maximum of 16 lines can be fitted for one element. The off-line computation of the measured spectra was done on a PDP 11/34 computer. Entry of the data sets of the elements and fixing of the background were done iteratively. The result of such a fit is illustrated in Fig. 3.

Detection limits

The sample preparation technique described above was used in evaluating experimentally the detection limits for the various elements for comparison with calculated values. The procedure involved optimization of the parameters affecting the detection limit (e.g., sample geometry), computation and coverage of the excitation radiation and its properties, and preparation of samples with known composition. By measuring the radiation intensity with ionization chambers, and through the special construction of the sample chamber with its built-in detector, it could be guaranteed that the measurement was made in the optimal region of polarization and also that the detector measured only the direct radiation of the irradiated sample spot. By means of the aperture and absorber systems, optimum excitation conditions could be adjusted and adapted to each sample.

The influence of the absorber used in the primary radiation on the peak sizes for the various elements is illustrated for a multi-element sample in Fig. 4. The figure shows a bad peak/background ratio without an absorber in the low-energy region; the ratio becomes much better with an absorber in the primary beam. Using the correct absorbers and simultaneously increasing the intensity by selecting a larger aperture can lead to a significant improvement in the detection limits for many elements.

Calculation of the detection limit was based on Currie's criterion of three times the square root of the background [20]. In each case, the background of the main lines of the element was used. The detection limits were obtained for numerous elements across the periodic system in sample matrices having negligible blank values. Experimental and theoretically calculated limits of

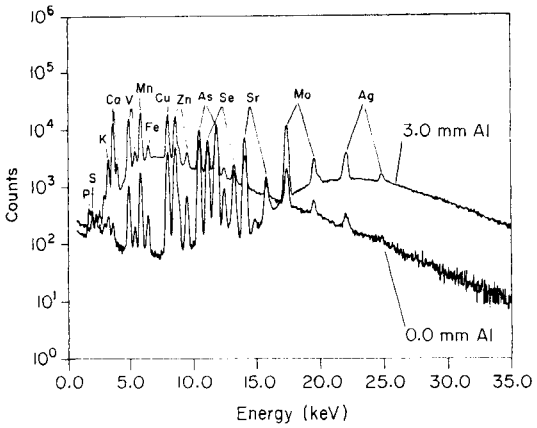

Fig. 4. Measurement of a multi-element sample without and with an aluminium primary filter.

detection are compared in Fig. 5. It can be seen clearly that the detection limits are strongly influenced by the absorbers. This happens because the low-energy part of the primary radiation is strongly reduced and so the scattering rays in this region, and therefore the background are decreased. Elements emitting fluorescence lines in the region are sufficiently excited through the high-energy portion, so that an average improvement in the peak/background ratio is achieved. By choosing the correct filter it is possible to select a region of high sensitivity for the desired elements.

The detection limits are generally in the range 0.05—0.2 $\mu g\ g^{-1}$. If a primary beam diameter of 0.5 mm and a sample of 1 mg cm^{-2} are assumed, this corresponds to an absolute value of 0.1—0.4 pg. Similar measurements for

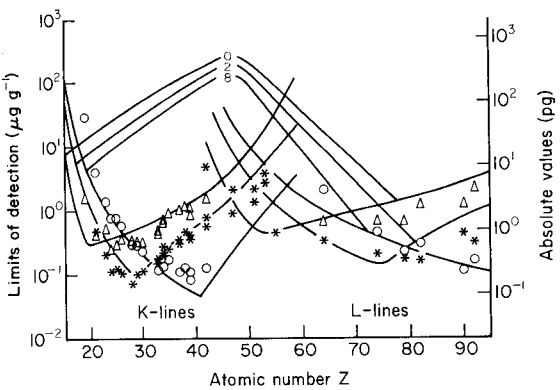

Fig. 5. Comparison of theoretical detection limits (solid lines) with experimental values. Calculated lines relate to absorber 0 (0.0 mm Al), absorber 2 (0.5 mm Al) and absorber 8 (6.0 mm Al), as indicated on the figure. For the experimental values, the sample was 1 mg cm^{-2} and the beam diameter 0.5 mm. Points: (△) absorber 0; (★) absorber 2, 0.5 mm Al; (○) absorber 8, 6.0 mm Al.

different multi-element samples showed no differences. This is valid only as long as there is no overlapping; otherwise the detection limits for the affected elements deteriorate, depending on the sample composition.

Calibration

The calibration function was evaluated with different single-element samples in a measuring series for which the peak area measured was always referred to a reference element added in constant amounts (usually about 100 $\mu g\ g^{-1}$). The concentration range varied between the detection limit for the element in question and 3000 $\mu g\ g^{-1}$. The concentrations were always altered by a factor of 3. All calibration plots showed, as expected, a linear dependence of the signal on the concentration up to a maximum value. In the case of high concentrations, however, the standard deviations were relatively high, because the concentration of the internal standard compared to the concentration to be measured was very small and because the constant total counting rate imposed relatively poor statistics. The curves broke off in the low-concentration region, because the counting statistics deteriorated near the detection limit. Figure 6 shows the calibration plots for selected elements. Corresponding multi-element samples showed similar behaviour. Problems arise only when overlapping of lines occurs. Typical examples are the Pb-L/As-K and Ba-L/Ti-K lines.

With the correct excitation conditions (absorber), lead and arsenic can be determined together up to a ratio of 20:1. At higher Pb/As ratios, values for arsenic become more erroneous, as subsidiary lines overlap with other elements. For example, the lead lines L_η and L_β are concealed behind selenium. In such cases, the analytical problem obviously depends on the sample concerned. Large concentration differences of both elements can be resolved when both are selectively excited. The L_{III}-edge of lead and the K-edge of

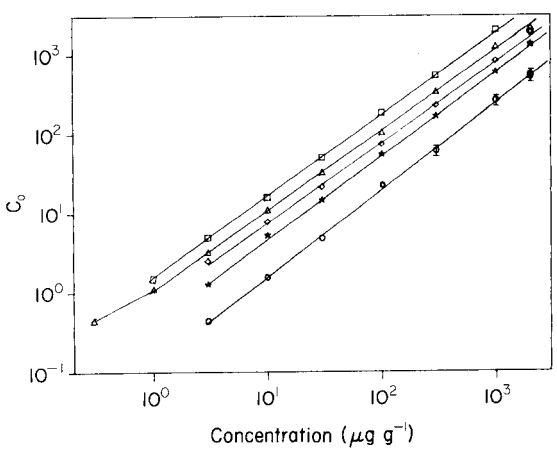

Fig. 6. Calibration plots: (△) chromium; (□) arsenic (× 1.50); (◇) yttrium; (*) molybdenum (× 0.75); (○) cesium (× 0.50). C_0 is the ratio of the countrate to the standard.

arsenic lie about 1 keV apart. This allows selective excitation with a monochromatic source (graphite broad-band monochromator) or by cutting off the high-energy component with a total reflecting mirror.

Overlapping of barium and titanium on excitation with white synchrotron radiation can be resolved by first quantifying barium through its K-lines and then calculating the contribution of the barium L-line to the titanium peak, given the K/L-line ratio of barium.

Conclusions

Compared to other sources, synchrotron radiation-excited x.r.f. has the disadvantage of being tied to one site. Advantages are that the high polarization makes it less sensitive to matrix interference and provides better detection limits. The white radiation effects a uniform excitation of all elements.

With this analytical principle, it should be possible to solve problems which previously have required tedious separation techniques. The detection limits generally attainable are in the range 0.1—0.4 pg (lower trace region).

With the help of absorbers on the primary radiation, the limits of detection can be improved for particular parts of the periodic table. In extreme cases, however, two separate spectra of the same sample are necessary: one for elements of low atomic number ($Z \leqslant 30$) and another with strong absorbers for the heavier elements.

The high photon-flux density facilitates x.r.f. measurements with spatial resolution by relatively simple manipulation (collimation). For intensity reasons, the present limit of resolution is about 10 μm. Aided by a focussing mirror and high radiation currents (for DORIS II, radiation currents up to 200 mA are planned), the resolution can be improved further.

We thank the Bundesminister für Forschung and Technologie and the Verband der Chemischen Industrie-Fond der Chemischen Industrie for financial support. We gratefully acknowledge the support of the staff of the HASYLAB, which made completion of this work possible.

REFERENCES

1 G. Tölg, Die Naturwissenschaften, 63 (1976) 99.
2 G. Tölg, Nachr. Chem. Tech. Lab., 27 (1979) 250.
3 R. H. Howell, W. L. Pickles and J. L. Cate, Adv. X-ray Anal., 18 (1975) 265.
4 L. Kaufmann and D. C. Camp, Adv. X-Ray Anal., 18 (1975) 247.
5 P. Wobrauschek and H. Aiginger, X-Ray Spectrom., 9 (1980) 57.
6 T. G. Dzubay, B. V. Jarrett and J. M. Jaklevic, Nucl. Inst. Methods, 115 (1974) 297.
7 K. Maack Bisgard, J. Laursen and B. Schmidt Nielsen, X-Ray Spectrom., 10 (1981) 17.
8 J. Knoth and H. Schwencke, Fresenius Z. Anal. Chem., 301 (1980) 7.
9 S. A. E. Johansson, T. B. Johansson, Nucl. Instrum. Methods, 137 (1976) 473.
10 P. Horowitz and J. A. Howell, Science, 178 (1972) 608.
11 C. J. Sparks, S. Raman, H. L. Yakel, R. V. Gentry and M. O. Krause, Phys. Rev. Lett., 38 (1977) 205.
12 J. V. Gilfrich, E. F. Skelton, S. B. Quadri, J. P. Kirkland and D. J. Nagel, Anal. Chem., 55 (1983) 187.

13 A. J. J. Bos, R. D. Vis, H. Verheul, M. Prins, S. T. Davies and P. K. Bowen, Third International Conference on PIXE and its Analytical Applications, Heidelberg, July 1983; Nucl. Instrum. Methods, B3 (1984) 232.
14 J. Staun Olsen, B. Buras, L. Gerward and S. Steenstrup, J. Phys. E., 14 (1981) 1154.
15 G. Tolkiehn and W. Petersen, Nucl. Instrum. Methods, 215 (1983) 515.
16 U. Waetjen, Thesis, University of Marburg, West Germany, 1963.
17 S. B. Russell, Ch. W. Schulte, Sh. Faig and J. L. Campbell, Anal. Chem., 53 (1981) 571.
18 J. Billiet, R. Dams and J. Hoste, X-Ray Spectrom., 9 (1980) 206.
19 R. Breschinsky, E. Krusch and R. Wehrse, Diplomarbeit im Fachbereich Physik, Universität Bremen (1979).
20 L. A. Currie, Anal. Chem., 40 (1968) 586.

Analytica Chimica Acta, 173 (1985) 117—127
Elsevier Scientific Publishing Company, Amsterdam — Printed in The Netherlands

A TANDEM MASS SPECTROMETRIC INVESTIGATION OF HYDROXY-AROMATIC CONSTITUENTS IN COAL LIQUIDS

K. V. WOOD

Engine Fuels Laboratory, Chemistry Building, Purdue University, W. Lafayette, IN 47907 (U.S.A.)

L. F. ALBRIGHT

Department of Chemical Engineering, Purdue University, W. Lafayette, IN 47907 (U.S.A.)

J. S. BRODBELT and R. G. COOKS*

Department of Chemistry, Purdue University, W. Lafayette, IN 47907 (U.S.A.)

(Received 12th December 1984)

SUMMARY

Preasphaltene fractions of exinite and vitrinite macerals, liquefied in tetralin, were examined by chemical ionization mass spectrometry/mass spectrometry for phenolic constituents. Recognition was based on dehydration of the protonated molecule with confirmation from daughter spectra, which in some cases could be compared with the spectra of authentic compounds. Rapid screening for homologous compounds was achieved by employing parent scans. Twelve homologous series of hydroxyaromatic compounds were identified, including phenols, naphthols, indenols, indanols, and some dihydroxy compounds. Many of the alkylated species have not been previously reported in coal liquids. While tandem mass spectrometry is an effective means of encountering new compounds, it does not provide the isomer selectivity of chromatographic methods to which it is complementary.

Mass spectrometry/mass spectrometry (m.s./m.s.) has had a wide range of applications in the analysis of complex mixtures. Its strengths include high sensitivity, lack of reliance on lengthy sample preparation, and flexibility in screening mixtures either for individual compounds or for groups of compounds having related structures [1]. These advantages are particularly suited to the characterization of fuel-related materials where there is growing interest in identifying series of compounds containing common functional groups [2].

Mass spectrometry, in many cases coupled with gas chromatography, has been used extensively for the investigation of fuels [3—7]. Several previous studies have confirmed the presence of phenols and related compounds in coal-derived materials [8—11]. The use of gas chromatography/mass spectrometry (g.c./m.s.) has greatly facilitated the characterization of these materials, even though some are difficult to chromatograph. Furthermore, as higher-molecular-weight coal-derived materials become of increased

0003-2670/85/$03.30

interest, the difficulties in utilizing g.c./m.s. increase, making an exploration of alternatives desirable. Simple phenols in coal liquids have also been investigated by other spectroscopic methods including ^{19}F-n.m.r. of hexafluoroacetone adducts of isomeric phenols [12]. Several alkylphenols have been identified in coal recycle solvents by using ultraviolet absorption and fluorescence spectroscopy of chromatographically separated fractions [13]. The combination of liquid chromatography with Fourier-transform infrared spectroscopy has also shown promise in the speciation of polar compounds including amines, ethers, and phenols in coal-derived process solvents [14].

The emphasis of the studies just mentioned is on the separation and identification of simple phenols. Tandem mass spectrometry, although incapable of distinguishing some types of isomers, is a technique which promises greatly to expand the existing range of phenolic compounds identified in coal liquids. This was indicated in an early m.s./m.s. study which showed the potential of neutral loss scans in the identification of alkyl phenols from a solvent-refined coal [15]. In the present study, attention is devoted to the identification of homologous series of the hydroxyaromatic compounds by using the complementary methods of parent and daughter spectra. The degree to which different coal macerals can be distinguished on the basis of their constituents identified by using tandem mass spectrometry is an additional object of enquiry.

EXPERIMENTAL

All spectra were obtained by using a Finnigan triple quadrupole mass spectrometer [16] with either electron-impact ionization (70 eV) or isobutane chemical ionization (0.4 torr). The triple quadrupole mass spectrometer consists of three co-axially aligned quadrupole rod assemblies; the first and third are conventional mass analyzers and the second is a focussing collision cell. A daughter spectrum is obtained by selecting a given ion in the first stage of mass spectrometry, passing it into the collision quadrupole where it undergoes collision-induced dissociation (CID) with the resulting fragments being mass-analyzed by the second mass analyzer. Argon was used as the target gas for collision-induced dissociation at an indicated pressure of 2 mtorr. Collision energy was set at 20 eV.

The two coal samples studied were hand-sorted Indiana VII macerals that were separated into exinite and vitrinite fractions under a reflected light microscope. Vitrinite purities were estimated as 99%, but the exinite contained considerable pyrite. The macerals were liquefied under high pressure at 400°C in a stainless steel bomb with tetralin as the hydrogen donor solvent. The product was washed and extracted in tetrahydrofuran in a Soxhlet apparatus. The liquid products were fractionated by liquid chromatography; pentane, toluene, and pyridine were used successively to separate maltene, asphaltene, and preasphaltene fractions. The eluted components were dried and stored in a refrigerator.

RESULTS AND DISCUSSION

The identification of phenolics and other hydroxyaromatics utilized two major types of m.s./m.s. scanning. Daughter spectra were taken for individual ions suspected to be hydroxyaromatics in order to confirm their structures through interpretation of their fragmentation patterns and, where possible, by comparison with the spectra of the authentic compounds. Parent spectra were used to characterize all ions which fragmented to specified daughter ions characteristic of a selected hydroxyaromatic skeleton (Scheme 1).

Step I. Record daughter spectra of the C_0 and C_1 members of a suspected hydroxyaromatic series and a non-member (fourteen dalton less in mass).

↓

continue if spectra reveal water loss and non-member does not

↓

Step II. Record parent spectra of the protonated C_0 and C_1 members of the suspected hydroxyaromatic series

↓

Select homologous ions

↓

Step III. Record daughter spectra of suspected higher-molecular-weight members of series

Scheme 1.

The first two members of the protonated phenol series, *m/z* 95, phenol itself, and *m/z* 109, methylphenol, as well as the *m/z* 81 ion, not a member of the series, were selected for CID. The resulting spectra were examined for water loss, as well as for other fragment ions which could be interpreted in terms of the suspected structure. The daughter spectra of authentic hydroxyaromatics without alkyl substitution exhibit a dominant loss of 18 mass units (loss of water), while alkyl-substituted phenolics yield variable amounts of water loss along with fragmentation to the hydroxyaromatic skeleton. In contrast, compounds which are not hydroxyaromatics, do not generally exhibit this type of fragmentation. The presence of higher members of the series was examined by obtaining parent spectra of ions corresponding to the lowest members of the series and tabulating the ions which satisfy the requirement for being extended alkyl analogs. Finally, daughter spectra were taken for each suspected series member to confirm the tentative structures suggested by the parent scans.

The pre-asphaltene fraction of the two liquefied macerals was chosen for this study because this fraction is the richest of the solubility classes in compounds containing polar functional groups, including hydroxyaromatics [17]. Cursory examination of the maltene and asphaltene fractions by comparison of mass spectra indicated that maceral-related differences were

small. This point was verified by tandem mass spectrometry. In both the asphaltenes and maltenes, the presence of a homologous series of alkylnaphthalenes was indicated by recording parent scans of *m/z* 141 (methylnaphthalene ion) with electron ionization. The series extended to *m/z* 254 with intense ions at *m/z* 142, 156, 170, 184, 198, 212, 226 and 240 (Table 1). The daughter spectra of the protonated forms of these ions showed intense peaks at *m/z* 128 and 129, the naphthalene ions, and in most cases, *m/z* 141 and 142, methylnaphthalene ions. A strong alkylbenzene series was also found in the asphaltenes by recording the electron-impact parent spectrum of *m/z* 91 (Fig. 1). As was done for the alkylnaphthalenes, daughter spectra of ions at *m/z* 92, 106, 120, 134, 148, 162, 176 and 190 were recorded using chemical ionization, and they indicated a common set of fragments including 106^+, 92^+, and 79^+ which represent stable aromatic ions. In each series of daughter spectra studied, a regular pattern of peaks at 14 dalton intervals was observed which extended down to the benzene or

TABLE 1

Parent scans of alkylbenzenes and alkylnaphthalenes[a]

Selected fragment (*m/z*)	Relative intensity			
	Asphaltenes		Maltenes	
	Exinite	Vitrinite	Exinite	Vitrinite
Alkylbenzenes[b] Parents of 91^+				
106	0.06	0.02	—[c]	—[c]
120	0.18	0.60	0.10	0.08
134	0.08	0.20	—[c]	—[c]
148	0.15	0.20	0.09	0.08
162	0.03	0.02	—[c]	—[c]
176	0.01	0.01	—[c]	—[c]
190	0.01	—[c]	—[c]	—[c]
Alkylnaphthalenes Parents of 141^+				
156	0.21	0.10	0.45	1.00
170	1.00	0.41	1.00	0.35
184	0.05	0.31	0.10	0.07
198	0.20	1.00	0.20	0.06
212	0.11	—[c]	0.05	0.01
226	0.01	0.30	0.03	0.01
240	—[c]	0.10	—[c]	0.01
254	0.04	0.03	—[c]	—[c]

[a]All abundances are ± 20%. [b]All intensities are relative to base peak *m/z* 131. [c]Too weak to be reliable.

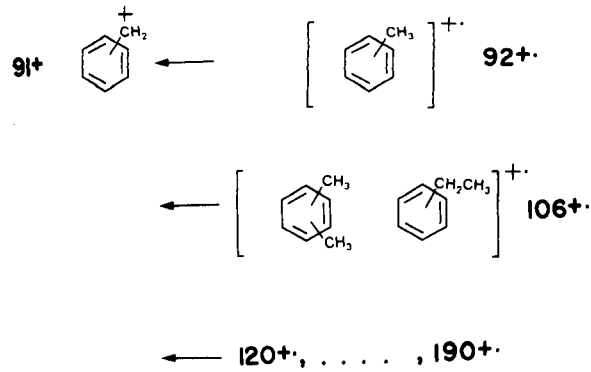

Fig. 1. Representative structures of parents that fragment to *m/z* 91 after collision-induced dissociation.

naphthalene skeleton. The alkylbenzene and the alkylnaphthalene contents were similar in both the exinite and vitrinite asphaltene and maltene samples. The expected differences between the highly paraffinic maltenes [17] and the asphaltenes were observed. In fact, the low aromatic content of the maltenes meant that reliable data on the alkylbenzenes distribution in the maltene fraction could not be obtained for either the exinite or vitrinite samples.

The less-than-encouraging indications of maceral-related differences in the asphaltenes and maltenes led to consideration of the pre-asphaltenes and of their phenolic constituents. Preliminary chemical-ionization mass spectra revealed several extremely intense solvent-related peaks that obscured the ions from hydroxyaromatics in the mass spectra. The additional selectivity of parent and daughter scans overcame this problem. The chemical-ionization data showed that at high probe temperatures ions were observed up to about 700 daltons. In obtaining m.s./m.s. data, attention was concentrated on the lower half of this range so as to deal with the overwhelmingly abundant lower members of the various homologous series.

Twelve hydroxyaromatic series were observed in the two pre-asphaltene fractions (see Table 2). The exinite fraction showed about an order of magnitude greater concentration of hydroxyaromatics, compared to the vitrinite fraction. This quantitative difference was indicated by the ion abundances in the parent ion spectra. Differences in distributions of particular compounds were not encountered, however, and in much of the remaining discussion, data for exinite macerals are referred to for convenience.

Neutral-loss spectra were recorded to select the species that lost water after undergoing collision-induced dissociation. As expected, the non-alkylated hydroxyaromatics were present in greater relative abundance than any of the substituted species. Naphthol, dihydronaphthol, tetrahydronaphthol, phenol, pyridinol and indenol were particularly intense in both the exinite and vitrinite pre-asphaltene spectra while dihydroxybenzene was also extremely abundant in the exinite sample.

TABLE 2

Hydroxyaromatic compounds identified in liquefied coal macerals

Side chain	Identification	Molecular weights[a]
C_0—C_{10}	Alkylphenols	94, 108, 122, 136, 150, 164, 178, 192, 206, 220, 234
C_0—C_1	Alkylpyridinols	95, 109
C_0—C_3	Alkyldihydroxybenzenes	110, 124, 138, 152
C_0—C_8	Alkylindenols	132, 146, 160, 174, 188, 202, 216, 230, 244
C_0—C_7	Alkyldihydronaphthols	146, 160, 174, 188, 202, 216, 230, 244
C_0—C_5	Alkylindanols	134, 148, 162, 176, 190, 204
C_0—C_4	Alkyltetrahydronaphthols	148, 162, 176, 190, 204
C_0—C_6	Alkylnaphthols	144, 158, 172, 186, 200, 214, 228
C_0—C_4	Alkylacenaphthols	170, 184, 198, 212, 226
C_0—C_2	Alkylanthracenols/phenanthrols	194, 208, 222
C_0—C_1	Alkylnaphthylphenols	220, 234
C_0—C_6	Alkyldihydroxynaphthols	160, 174, 188, 202, 216, 230, 244

[a]The ion selected for examination was always the $(M + 1)^+$ ion, viz., *m/z* 95, 109, etc.

Figure 2 is a representative set of daughter spectra used in the identification of the naphthol series. The three spectra shown include the two lowest members of the suspected series (C_0 and C_1 protonated naphthol at *m/z* 145 and 159, respectively) and the ion which has a molecular weight 14 daltons less than the C_0 analog (*m/z* 131). The ion at 131^+ effectively represents a blank and is not expected to demonstrate a significant loss of water unless it is by chance a member of a different phenolic series. Figure 2(b) is a daughter spectrum of the *m/z* 145 ion in the exinite pre-asphaltene fraction, which is consistent with the daughter spectrum of protonated 1-naphthol. The intense peak from loss of water (18 dalton) is the most striking feature of the spectrum. The ion at 117 dalton, or loss of 28 daltons, corresponds to the elimination of CO. Also indicative of aromaticity is the ion at 91 daltons which represents the $C_7H_7^+$ species. The daughter spectrum of 159^+ (Fig. 2c), representative of a protonated methylnaphthol, shows abundant fragment ions from water loss and methyl radical loss. An enhanced 91^+ ion and loss of CO are observed. The presence of other ions (e.g., 71^+) inconsistent with alkylnaphthol fragmentation indicate the occurrence of isobaric or isomeric species at *m/z* 159^+ in the pre-asphaltene sample. In contrast, the daughter spectrum of 131^+ (Fig. 2a) shows no water loss and is clearly not a member of the naphtholic series. In fact, the daughter spectrum of *m/z* 131 matches well with that of protonated dihydronaphthalene, which would be an expected component of the mixture because tetralin was used as the hydrogen donor solvent. The identity of the ion at

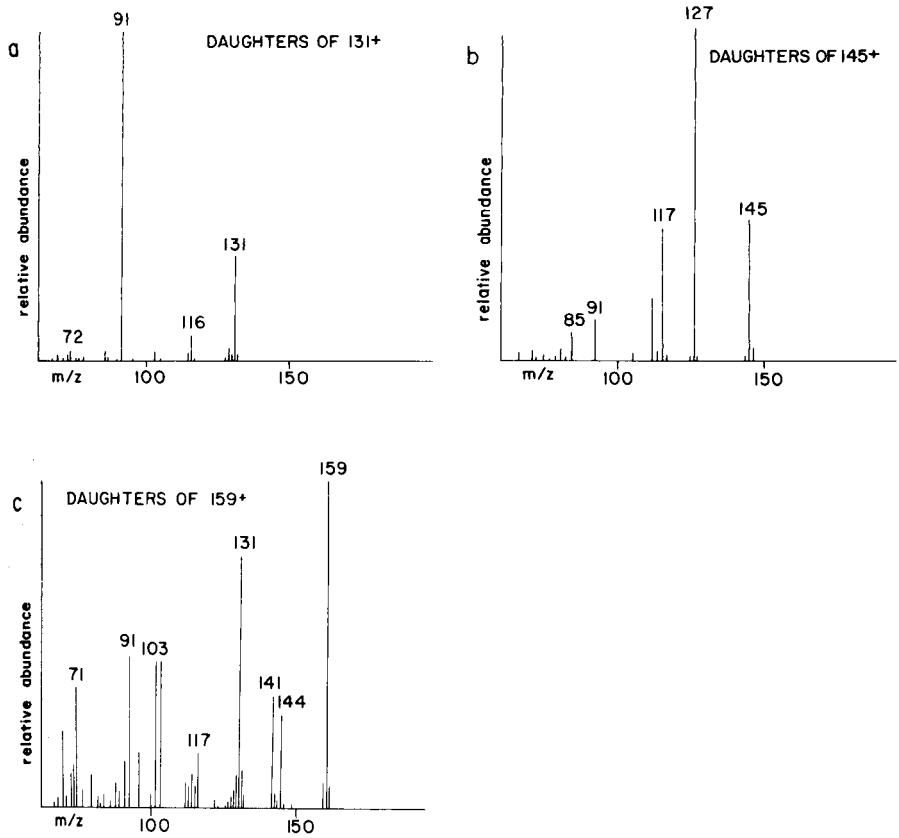

Fig. 2. Daughter spectra (chemical-ionization m.s./m.s.) of protonated molecules derived from an exinite-derived pre-asphaltene showing the first two members of the naphthol series, C_0 at 145^+ and C_1 at 159^+, and 131^+ not a member of the series.

131 is established by its facile fragmentation to the benzyl ion, its elimination of a methyl radical, and by comparison with a standard. Thus, the daughter spectra of ions 145 and 159 support the assignment to the series of naphthols while the daughter spectrum of 131 establishes the lower mass termination of the series.

To elucidate the extent of the series, parent spectra of ions 145^+ and 159^+ were used to indicate the presence of ions of higher molecular weight that yield either 145^+ or 159^+ on fragmentation. A parent spectrum of 159^+ (Fig. 3) shows the presence of additional members of the alkylnaphthol series at *m/z* 187, 201, 215, and 229, corresponding to the C_3—C_6 naphthols. The intense ions at *m/z* 174, 177 and 219 are not part of this series but rather are present as a result of facile cleavage to *m/z* 159. The ion at *m/z* 174 results from $CH_3\cdot$ loss. The ion at *m/z* 177 is observed as a result of the loss of water and is consistent with the presence of protonated

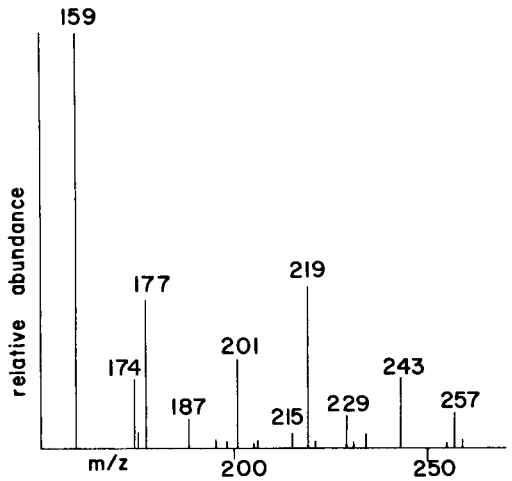

Fig. 3. Parent spectrum (chemical-ionization m.s./m.s.) of ion 159^+ (exinite pre-asphaltene) showing the extended alkylnaphthol series represented by ions at 187, 201, 215, and 229 (C_3—C_6).

C_3-alkylindanol. The daughter spectrum of *m/z* 219 suggests that it is phenolic (loss of 18 and 28). The spectrum contains evidence for alkyl substitution (loss of 15 and 16), but the ring system remains to be established.

The procedure just described for the alkylnaphthols was repeated many times over to identify the other hydroxyaromatic compounds shown in Table 2. It should be noted that each member of an alkyl hydroxyaromatic series listed in the table (excepting the unsubstituted component) does not represent a single compound, but potentially an entire set of isomers. Most previous studies in which alternative analytical methods were used, list isomers separately, but the direct analytical capabilities of m.s./m.s. enable a more extensive characterization of hydroxyaromatic compounds in coal liquids to be achieved, while it is of limited value in isomer distinctions.

To confirm the presence of hydroxyaromatics in the coal samples, standard hydroxyaromatic compounds were determined by recording their chemical-ionization daughter spectra. Isomers that differ by type of substituent, configuration of functional group, or skeletal structure are easily distinguished by their fragmentation patterns. For example, the presence of C_3-alkylnaphthol (m.w. 186; $C_{13}H_{14}O$) and the absence of biphenol (m.w. 186; $C_{12}H_{10}O_2$) in the coal samples was established by careful examination of the daughter spectra of the protonated ion, *m/z* 187, and comparison to standards. Biphenol demonstrates only three significant neutral losses, loss of 18 dalton, 46 dalton, and 72 dalton, whereas the chemical-ionization daughter spectrum of the corresponding ion, in the pre-asphaltenes, exhibits no loss of 46. Moreover, the pre-asphaltene spectrum showed abundant losses of neutral fragments of 15, 28 and 42 dalton corresponding to alkyl losses. The presence of ions consistent with alkylnaphthol behavior such as *m/z* 91, 117 and 128 dalton was also noted.

While this is an example of tandem mass spectrometry being used to distinguish skeletal structures, the interpretation of daughter spectra can also be used to assign substituent structure. Methylphenol, which has the same molecular weight (m.w. 108), molecular formula (C_7H_8O), and aromatic skeleton as anisole, can readily be distinguished in the pre-asphaltene samples by comparison to standard chemical-ionization m.s./m.s. spectra of reference compounds. Anisole does not lose water and cleaves primarily to form a stable phenyl ion (*m/z* 77). The daughter spectrum of 109^+ in the coal samples indicates strong water loss, absence of 77^+, and the presence of other ions consistent with the methylphenol standard. Similar procedures of comparison of standard daughter spectra to pre-asphaltene daughter spectra were used repeatedly to elucidate the isomeric structures of the other hydroxyaromatics.

The spectra for several positional isomers were examined to estimate the feasibility of making isomeric distinctions within the pre-asphaltene hydroxyaromatic series. Pairs such as hydroquinone and resorcinol, methylhydroquinone and 4-methylcatechol, and 1,3-dihydroxynaphthalene and 2,3-dihydroxynaphthalene, showed significant differences in the relative ratios of specific fragment ions, but the actual fragments were virtually identical. This last point made the assignment of positional isomers in the complex coal samples impossible.

Parent spectra can often establish related series if expected fragment species that are representative of a group of homologs are judiciously selected. For this reason, the basic skeletal hydroxyaromatic is chosen as the predicted common fragment of other members in a series. Thus, when parent and daughter spectra are jointly inspected, the elucidation of hydroxyaromatics becomes facile.

CONCLUSIONS

The power of tandem mass spectrometry for molecular characterization is often not fully realized. When used to its full extent, m.s./m.s. offers more than simply compound identification through fragmentation patterns of selected ions. A hierarchy of structural information can be inferred by careful inspection of the spectra, comparison with standards, and consideration of known fragmentation behavior. Significant features of the spectrum from m.s./m.s. may suggest the skeletal structure of the compound under consideration as well as the molecular formula. Commonly, this is the furthest structural level that is associated with tandem mass spectrometry. Yet the depth of available information can be expanded to include the assignment of a skeletal structure having specific substituents in specific positions through closer analysis of the spectral details (Scheme 2). Furthermore, by comparison with known standards, the configuration of side chains or other constituents can be accurately predicted, and the structures of new compounds can be assigned. Other commonly available analytical techniques have a narrower range of utility.

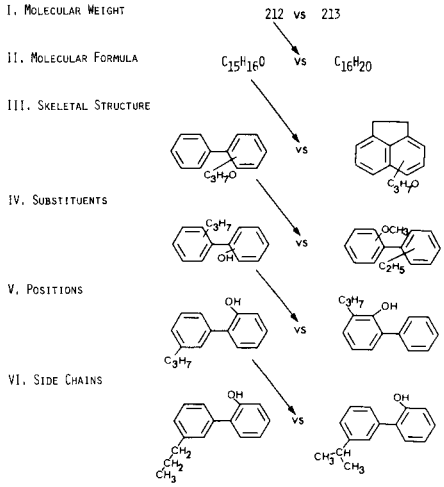

Scheme 2.

This study incorporated four levels of the structural hierarchy including the determination of molecular weight and molecular formula, skeletal structure, and groupings of substituents. This report demonstrated the utility of tandem mass spectrometry for the characterization of liquefied coal macerals for hydroxyaromatics. Substantial differences have not been observed in the types of compounds derived from different macerals, although a substantial difference in the quantity of phenolics occurs in the pre-asphaltene fractions derived from exinite and vitrinite. The method of complementary parent-daughter spectra can be applied to any investigation of components containing a common substructural unit. As an analytical technique, m.s./m.s. avoids time-consuming sample preparation while maintaining good sensitivity and flexibility for the detection of trace components of complex mixtures.

This research was supported in part by the Department of Energy (DE-FG22-82-PC50803).

REFERENCES

1 R. G. Cooks and K. L. Busch, J. Chem. Ed., 59 (1982) 926.
2 D. Bodzek and A. Marzec, Fuel, 60 (1981) 47.
3 D. W. Later, M. L. Lee, K. D. Bartle, R. C. Kong and D. L. Vassilaras, Anal. Chem., 53 (1981) 1612.
4 D. M. Parees and A. Z. Kamzelski, J. Chromatogr. Sci., 20 (1982) 441.
5 K. V. Wood, C. E. Schmidt, R. G. Cooks and B. D. Batts, Anal. Chem., 56 (1984) 1335.
6 T. Ramanowski, W. Funcke, I. Grossman, J. Konig and E. Balfanz, Anal. Chem., 55 (1983) 1030.
7 D. Zakett, V. M. Shaddock and R. G. Cooks, Anal. Chem., 51 (1979) 1849.
8 M. V. Buchanan, Anal. Chem., 56 (1984) 546.
9 W. H. McClenne, H. L. C. Meuzelaar, G. S. Metcalf and G. R. Hill, Fuel, 62 (1983) 1422.
10 C. M. White and N. C. Li, Anal. Chem., 54 (1982) 1570.

11 F. R. Guenther, R. M. Parris, S. N. Cheseler and L. R. Hilpert, J. Chromatogr., 207 (1981) 256.
12 K. D. Bartle, R. S. Matthews and J. W. Stadelhofer, Appl. Spectrosc., 34 (1980) 615.
13 J. F. Schabron and R. J. Hurtubise, Anal. Chem., 51 (1979) 1426.
13 J. F. Schabron and R. J. Hurtubise, Anal. Chem., 51(9) (1979) 1426.
14 R. S. Brown and L. T. Taylor, Anal. Chem., 55 (1983) 723.
15 J. D. Ciupek, R. G. Cooks, K. V. Wood and C. R. Ferguson, Fuel, 62 (1983) 829.
16 J. R. B. Slayback and M. S. Story, Ind. Res. Dev., (1981) 129.
17 J. F. Stephens, Fuel, 58 (1979) 489.

Analytica Chimica Acta, 173 (1985) 129—140
Elsevier Science Publishers B.V., Amsterdam — Printed in The Netherlands

LOCAL SURFACE DIPOLAR PERTURBATION OF LIPID MEMBRANES BY PHLORETIN AND ITS ANALOGUES

MICHAEL THOMPSON*, U. J. KRULL* and L. I. BENDELL-YOUNG

Department of Chemistry, University of Toronto, 80 St. George Street, Toronto, Ontario M5S 1A1 (Canada)

I. LUNDSTRÖM and C. NYLANDER

Department of Physics and Measurement Technology, Linköping Institute of Technology, S-581 83 Linköping (Sweden)

(Received 23rd December 1984)

SUMMARY

Concentration-response, electrolyte concentration and composition, and Arrhenius—Eyring energy in relation to changes in phosphatidyl choline-cholesterol membrane conductance have been studied to examine the adsorptive dipolar potential reduction caused by phloretin. The results indicate that these membranes possess weak surface binding sites for potassium ion. Calculations for a statistical local model of adsorption of phloretin molecules for each occupied cation site correlate with experimental trends. A rapid transient current resembling a capacitive charging effect was observed shortly after addition to one side of the membrane of phloretin and 2,4,6-trihydroxyacetophenone, but not for the dipolar species phlorhizin, *p*-nitrophenol or *o*-nitrophenol; the effect shows saturation characteristics.

Perturbation of the surface dipolar potential of a bilayer lipid membrane (BLM), with consequent modulation of ion flux, provides a potentially useful signal for the development of electrochemical sensors [1]. In order to probe the influence of modified electrostatic fields on the ion conductance of BLM, it is instructive to observe the effects of dipolar molecules which can adsorb to the membrane. An example of such a species is phloretin (dipole moment 5.6 D) which can bind to BLM in unionized form, producing a significant increase of ion current [2, 3]. Apparently, the molecule aligns against the established membrane dipole field with a consequent reduction in dipolar potential [4]. Such a model assumes that the alignment of the anisotropic lipid head group creates net dipolar fields which are laterally continuous across each membrane surface [5—7]. In this case, any ion passing into a membrane would always encounter a uniform electrostatic barrier regardless of lateral positioning with respect to the membrane surface. However, modification of this model may be required, because localized interactions of ions with head groups may occur and be significant with respect to the energy barrier faced by the translocating ion [8].

0003-2670/85/$03.30

A test for the validity of the local model is the Langmuir adsorption isotherm, which must exist for dipolar species capable of surface adsorption [3, 9]. In addition, the temperature dependence of transmembrane ion current can indicate the correct model. Arrhenius activation energy considerations determine whether both the pre-factor (the number of ion-conductive pathways) and the activation energy vary, which would imply that localized effects dominate, or whether surface "sheets" of dipoles cause a concentration-dependent homogeneous reduction of the activation energy. The influence of electrolyte concentration as well as the electrolyte composition coupled with the adsorption isotherm can indicate the degree of surface ion complexation and competition for surface-binding sites.

In the present paper, several aspects of the interaction of phloretin with phosphatidyl choline/cholesterol membranes are examined in order to increase understanding of the dipole-perturbation hypothesis for chemical sensing. Arrhenius—Eyring results are interpreted in terms of a statistical local model for the adsorption of phloretin at membrane binding sites that are weakly selective for potassium ion. Also, a phloretin-induced rapid, transient current minimum is discussed in terms of a charging model. Finally, current amplification through coupling of reduction of both membrane electrical and chemical potential energy barriers is demonstrated.

EXPERIMENTAL

The electrochemical cell consisted of two identical perspex blocks separated by a teflon sheet (0.1 mm thick) containing a circular aperture (1 mm diameter) used for BLM support. An external +25-mV direct potential was applied across the membrane between two Ag/AgCl reference electrodes (Orion Research) via salt bridges. The external circuitry consisted of a d.c. power supply and a microprocessor-controlled digital electrometer (Model 616B; Keithley Instruments). The solution cell and sensitive electronic equipment were isolated in a well-grounded Faraday cage.

The lipid used was phosphatidyl choline (Avanti Biochemicals, Birmingham, AL), which was prepared with cholesterol (Sigma Chemical Co.) in a 20 mg/20 mg quantity in 1.0 ml of dry n-decane. The cholesterol was partially oxidized as determined by thin-layer chromatography. The brush technique was used to introduce lipid solution into the teflon aperture, where formation of planar BLM was monitored by optical and electrical methods. Each stirred solution compartment contained 5 ml of aqueous electrolyte adjusted to pH 5. The organic agents, phloretin, phlorhizin, 2,4,6-trihydroxyacetophenone, *p*-nitrophenol, *o*-nitrophenol, and valinomycin (all from Sigma) were added as methanolic solutions by a variable-volume micropipette. The methanol concentrations in the aqueous electrolyte never exceeded 1% by volume. Experiments were done at 21 ± 1°C unless noted otherwise. An infrared heat source was used to provide elevated temperatures.

RESULTS AND DISCUSSION

Phloretin action and electrolyte dependence

For phosphatidyl choline membranes, contributions to the net perpendicular membrane dipole originate with the carbonyl and phosphorus-choline (P-N) moieties, and ordered water of hydration [10, 11]. Sterol incorporation into such membranes increases mechanical integrity and can concurrently contribute to, or alter, the electrostatic field [6, 12]. Reduction of the dipolar potential by membrane adsorption of phloretin is evidenced by the increase in positive current observed on addition of the dipolar species to 0.1 M lithium chloride on the positive high potential side of a BLM (Fig. 1). The current/time profile exhibits a relatively rapid negative transient current (see below). Adsorption of *p*-nitrophenol (dipole moment 5.4 D) produces a similar positive response although a 100-fold increase in concentration is required to elicit a response equivalent to that for phloretin because of the large difference expected for membrane partitioning between the two compounds [3, 4]. A concentration of 10^{-2} M *o*-nitrophenol (3.1 D) does not induce a response in any electrolyte for similar reasons.

Sequential bilateral addition of equal quantities of phloretin (first to the high side, then the low, with a final aqueous concentration of 10^{-5} M) generally results in two positive current increases, the second increase being generally of smaller magnitude. This is consistent with local phloretin action, but may imply the existence of an interfacial process depending on ion transfer rate and directly controlled by the phloretin concentration on the membrane face. A similar effect has been described for the case of phloretin action on valinomycin ion transport, where high concentrations of phloretin apparently reduce interfacial ion transport, limiting the magnitude of transport of the complex through the membrane [4]. Further evidence for such a property may be derived from the observation that addition of phloretin to a compartment containing 0.1 M potassium chloride held at the positive potential followed by addition to the low potential compartment results in a second current increase which is three to four times smaller than that obtained on sequential addition to the low and then the high potential electrolyte compartments. This suggests that an adsorption plane for the cation exists at one membrane/solution interface because of the applied potential and membrane capacitive properties, and is consistent with a model involving local phloretin action.

Electrolyte competition has an effect on phloretin response. (It should be noted that phosphatidyl choline/cholesterol membranes exhibit cation selectivity with respect to permeability in the order $Rb^+ > K^+ > Li^+ > Mg^{2+}$ [13].) This effect is predominantly determined by Born energy requirements. In the present work, the response to phloretin was studied for various K^+/Li^+ ratios at different ionic strengths. If permeability is only a function of ion concentration in solution and membrane partitioning (constant for any species), a simple analysis of K^+/Li^+ competition indicates that the ion

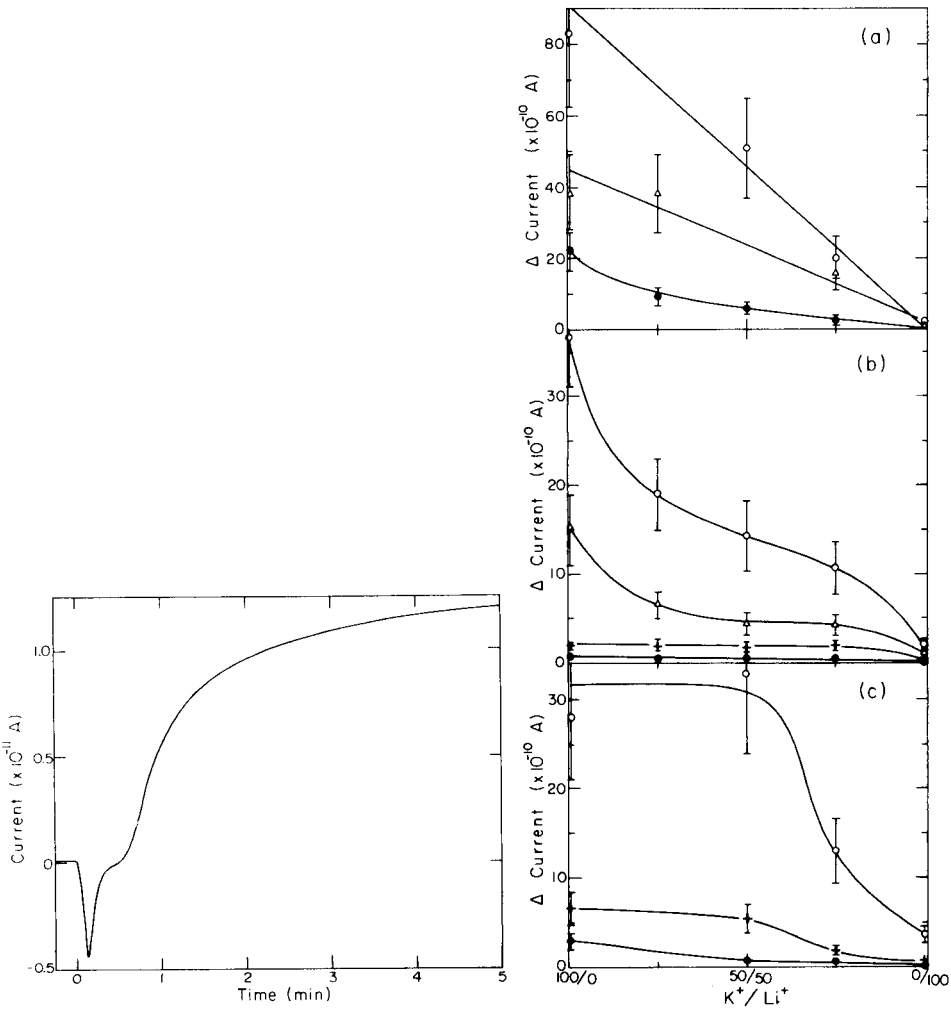

Fig. 1. Ion current/time profile observed for phloretin interaction with a phosphatidyl choline BLM. The final concentration was 1.0×10^{-5} M in 0.1 M LiCl electrolyte.

Fig. 2. Current changes for different ratios of K^+/Li^+ at constant ionic strength with different phloretin concentrations: (•) 7.0×10^{-6} M; (+) 1.0×10^{-5} M; (△) 2.0×10^{-5} M; (○) 4.0×10^{-5} M. Ionic strength: (a) 10^{-1} M; (b) 10^{-2} M; (c) 10^{-4} M.

current should remain large and drop in direct proportion to potassium ion concentration. The current generated by lithium ion permeation should become important only at high lithium ion concentration because of the large Born energy opposing membrane permeation of the latter ion and even then the current should be extremely small. These effects can be amplified to facilitate accurate measurement by the action of phloretin on the membrane, though anomalies in phloretin action may be observed at very low

concentrations where local effects apparently dominate, or at very high concentrations where a substantial proportion of the membrane surface is covered by phloretin. Figure 2(a—c) illustrates the results of these experiments, indicating that potassium ion has a greater surface affinity than lithium ion and dominates the ion current in solutions of low ionic strength except at high lithium concentrations. The BLM ion current is governed by the cation residing at the membrane-solution interface rather than by cations in bulk solution [9]. The amplification property produced by increasing phloretin concentration consistently indicates that a weak potassium ion-selective binding site is available at the aqueous interface. At high ionic strength (0.1 M), no selectivity is observed, but reduced ionic strength leads to maintenance of a large transmembrane ion flux in the presence of potassium ion. A similar result is used practically in the formation of membranes used for ion-selective electrodes [14].

Concentration and Arrhenius—Eyring analysis

Measurement of the maximum current generated by addition of phloretin to the solution compartment held at positive potential results in concentration-response curves which are different for different lithium chloride concentrations (Fig. 3). In order to rationalize these curves, it is necessary to consider the nature of perturbation of membrane dipolar potential by phloretin. Change in the potential is reflected as a function of the magnitude of the dipole, the net perpendicular adsorbed dipole component and the surface density or concentration [1, 3]. A surface sheet model, where adsorbed phloretin molecules would cause a homogeneous alteration of the surface potential, should generate current values which fit a Langmuir-like adsorption isotherm including a saturation level. It is apparent that the results of Fig. 3 do not fit this description. (Experiments with over 10^{-4} M phloretin are not included because the molecule causes membrane structural

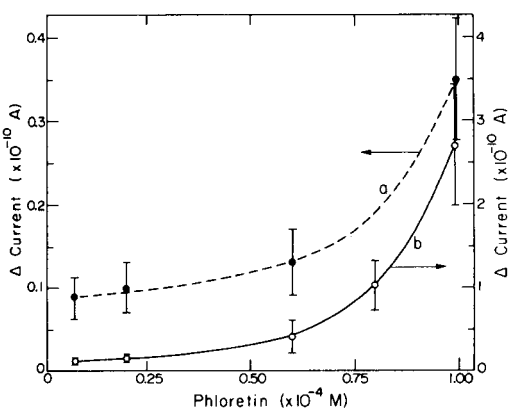

Fig. 3. Concentration-response curve for phloretin measured as a change in ion current from a background current obtained in: (a) 10^{-4} M LiCl; (b) 10^{-2} M LiCl.

changes and because the availability of interfacial ion-binding sites is reduced at relatively high concentration levels.)

An Arrhenius—Eyring analysis was then considered. This could yield both confirmatory evidence for the existence of an ion-adsorption plane at the membrane surface, and indications regarding a possible mechanism for phloretin perturbation of the surface dipolar potential. Eyring [15] has proposed an absolute rate theory of membrane permeation which treats the problem as an ion migration over a series of activation energy barriers. The relationship of the BLM residual current to temperature provides data suitable for analysis with the Arrhenius equation to determine the activation energy.

Figure 4(a) represents data in a standard graphical Arrhenius format where the slopes of the resulting linear plots are proportional to the total activation energy barriers and the intercepts are related to the Arrhenius pre-factor. Although the temperature range investigated is small, the large values of the activation energies indicate energy barrier limitation of ion transport through the membrane. The barrier can be considered as an electrical potential and for the unmodified lipid/sterol membrane this results in a calculated barrier of approximately 1200 mV. The size of this barrier indicates that ions probably pass through the membrane in a partially hydrated form. It is also interesting to note that an increase in the fraction of cholesterol in the sterol content range (60—80%) encompassed in Fig. 4(a) decreases the activation energy barrier. This may be due to an increase in polar groups in the membrane because partially oxidized sterol was used, and/or to a decreasing order caused by the heterogeneous lipid-sterol distribution which is expected at mole fraction cholesterol contents greater than 60%.

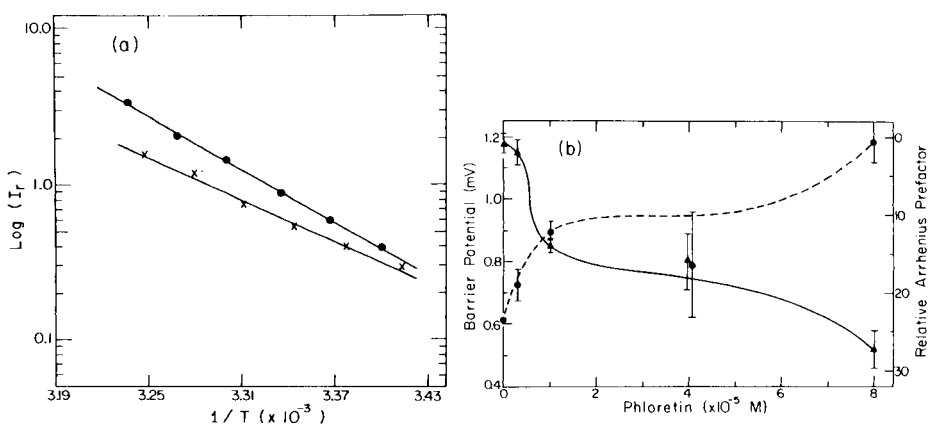

Fig. 4. (a) Standard Arrhenius plot of the logarithm of residual current (I_r) against the inverse of the absolute temperature. Cholesterol mole fraction (X_c): (•) ca. 0.7; (×) ca. 0.8. (b) Arrhenius-type temperature analysis of the phloretin-generated positive current in 0.1 M KCl: (▲) potential barrier to ion transport; (•) relative change in the pre-factor as a function of phloretin concentration.

Application of the Eyring rate theory can be used to estimate the rate constant (k_i) of transmembrane ion permeation:

$$k_i = (kt/h) \exp(-q\phi/kt) \quad (1)$$

where q is charge, ϕ is the activation energy for ion transport and the conventional kth^{-1} factor represents the number of times per second that an ion attempts to cross the energy barrier. The rate constant for an unmodified membrane can be estimated as being around 10^{-4} s^{-1}. Measurements of BLM residual current allow estimates of the number of ions which actually manage to cross the barrier (6×10^7 s^{-1} at 10^{-11} A). For a bulk electrolyte concentration of 0.1 M salt, approximately 10^{10} ions are instantaneously at the membrane/solution interface for a BLM in a 1-mm diameter aperture, so that given the Eyring rate constant, ions should permeate the membrane at a rate of about 10^6 s^{-1}. This value is 60-fold less than that actually observed and again indicates that a weak adsorption plane for permeation may exist. The most probable location of such a selective ion-adsorption plane is at the negative phosphate sites [16, 17]. If the area of each phospholipid and cholesterol molecule is assumed to be 0.5 nm^2, and if there is negligible overlap of electrostatic fields generated by individual ions, then up to 25% of the available membrane surface may be occupied by cation. This indicates that 5×10^{11} ions may reside at the membrane/solution interface, so that given the rate constant, ions should penetrate the membrane at about 5×10^7 s^{-1}, as experimentally observed. Slightly higher theoretical currents are obtained when the effect of bulk electrolyte, anion flux and the concentrated partition plane of cation are considered concurrently.

A temperature analysis of transmembrane ion-current alteration in the presence of phloretin addition to the solution compartment held at positive potential is represented in Fig. 4(b). The analysis assumes that the surface partitioning of phloretin does not vary in the temperature range 22—30° C. At concentrations above 5×10^{-6} M, it is apparent that the activation energy for ion transport is dramatically reduced. This is apparently not the case at lower phloretin concentration as indicated by the fact that the Arrhenius activation energy remains relatively constant, but the pre-factor decreases substantially.

The strong evidence for a weak selective adsorption plane for potassium ion at the membrane surface and the Arrhenius—Eyring results lead to an alternative to the surface sheet model for phloretin adsorption.

Statistical local model

The findings described above suggest that the influence of phloretin is local and not due to a general change in the membrane potential. If the existence of ion-binding sites is accepted, then phloretin molecules adsorbed close to an ion must have a larger influence than those adsorbed further away. Further, the large decrease in activation energy for ion transport accompanied by the decrease in the number of current-carrying pathways is strong

support for a local model. In order to rationalize the experimental results, a statistical local model is invoked, in which phloretin molecules are assumed to influence adsorbed ions. If there are phloretin molecules close to a cation site, the adsorbed molecules will alter the activation energy for ion transport through the membrane. It is also possible that more than one phloretin molecule influences the same ion.

To investigate the general features of such a statistical model, some simple calculations were done on the following basis. The leakage current through the membrane is

$$I_0 = k_i n_s \exp(-q\phi/kt) \tag{2}$$

where n is the density of ions in the binding sites, and k_i is a rate constant. If a large increase in permeability is obtained for ions influenced by phloretin through a decrease in activation energy $\Delta\phi_n$, then the current through a membrane can be described by

$$I \approx I_0[1 - \theta^n + \theta^n \exp(-q\Delta\phi_n/kt)] \tag{3}$$

where θ is the coverage of phloretin molecules on the membrane surface [$\theta = (C/C_0)/(1 + C/C_0)$] and n represents the number of adsorbed phloretin molecules per ion.

Calculations were made for n = 1, 2, 3 and 4 and with ϕ = 1170 mV and ϕ_n = 260 mV for all n values. Figure 5 shows the equivalent prefactor, k_{eff}, and the effective barrier height, ϕ_{eff}, calculated from

$$I = k_{eff} n_s \exp(-q\phi_{eff}/kt) \tag{5}$$

Figure 5(c) shows the expected current increase as a function of phloretin concentration, and results for the higher-order terms ($n \geqslant 2$) correlate at least qualitatively with the experimental findings. No attempt was made to fit the theory to the experimental results because several parameters are

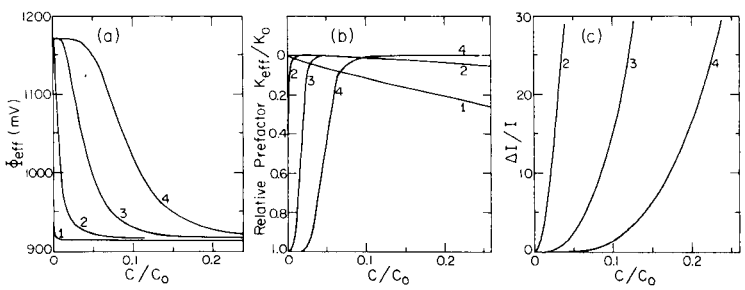

Fig. 5. Calculated current changes versus phloretin concentration for a statistical local model, where n phloretin molecules (n = 1—4) influence: (a) effective activation energy barrier; (b) relative Arrhenius pre-factor; (c) relative current change (at 300 K). The values ϕ = 1170 mV and $\Delta\phi_n$ = 260 mV, were used in the calculations. Phloretin was assumed to adsorb on the membrane in a Langmuir-like fashion with coverage θ = 0.5 at $C = C_0$.

obviously unknown at present. For example, an important question is whether all or only a fraction of the ions in the membrane binding sites (n_s) are available for interaction with phloretin. Furthermore, in a complete theory, terms with different n values would have to be added with the correct statistical weight and $\Delta\phi_n$, i.e.,

$$I = I_0 \sum_{i=0}^{n} (n_i)\theta^i(1-\theta)^{n-i} \exp(-q\Delta\phi_i/kt) \tag{6}$$

The curves in Fig. 5 represent the case when $\Delta\phi_n \gg \Delta\phi_i$ and $i < n$.

A local model has previously been proposed for the action of dipolar molecules on excitable membranes [18] and a statistical local model was suggested for the gating of nerve membranes [19, 20]. In the present case, any effect of channels or pores in the membrane is not included; instead, localized current-carrying pathways determined by a low activation energy for ion transport are considered. That the cholesterol content and lipid/cholesterol oxidation in the membrane are important factors is supported by the results in Fig. 4. Such a mechanism would depend on ion interaction with polar sites inside the membrane and "lattice" defect structures, which would be partially dependent on ion hydration properties. It is interesting to note that simple calculations indicate that the activation energy of transport of an unhydrated ion through an unperturbed lipid membrane (3 nm thick) is about 3 eV, and that of fully hydrated ion is about 0.7 eV [20].

Charging transient

A feature of phloretin interaction with BLM is the occasional evolution of a concentration-dependent initial current transient as shown in Fig. 1. Addition of phloretin to the solution compartment held at the positive potential results in a current minimum, which is always observed in the electrolytes which eliminate observable transmembrane residual current. If phloretin adsorbs to the membrane after addition to the electrolyte solution, a surface dipolar potential may build up to charge the membrane capacitance. This charging is observed as a current in the external circuit. The time constant of the charging process may be governed by the membrane adsorption kinetics of phloretin. Integration of the area under the current/time profiles for transient current evolution provides a direct measure of membrane charging, which can be coupled with an estimate of capacitance for determination of potential. Figure 6 provides a summary of data illustrating asymmetric membrane potential as a function of phloretin concentration. The rate of charging is generally independent of solution cations (K^+, Na^+, Li^+), though the evolution and extent of the transient current signal is related to the concentration of supporting electrolyte. The time constant in the charging current becomes shorter as phloretin concentration is increased, as expected for a charging current reflecting phloretin adsorption to the membrane.

The origin of the transient current is probably more complicated than a result of simple alteration of surface dipole potential. The fact that a maximum

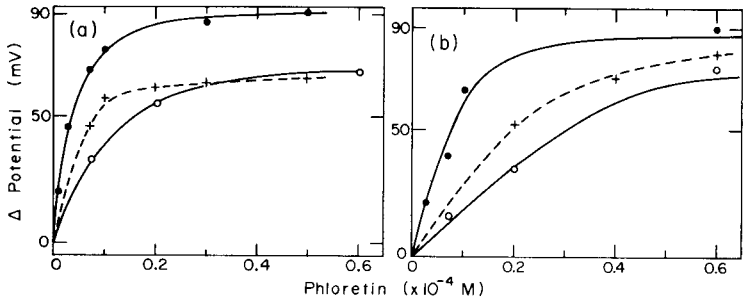

Fig. 6. Summary of the rapid change in calculated membrane potential calculated from the ion-current minimum shown in Fig. 1. Experiments were done as single additions of phloretin (a), and as sequential series of additions analogous to a titration (b). LiCl molarity: (•) 10^{-1}; (+) 10^{-2}; (○) 10^{-4} M.

charging of 70—80 mV is observed in Fig. 6 implies the existence of a saturation of the charging mechanism. This could indicate that selective binding sites for phloretin are present on these membranes or that a limited change in surface structure is caused by phloretin action. The saturation effect occurs at a concentration where Fig. 3 shows a deflection in the concentration response curve, providing supporting evidence that a significant threshold is present. Similar transient current functions were not observed for the dipolar species *o*-nitrophenol, *p*-nitrophenol and phlorhizin. However, 2,4,6-trihydroxyacetophenone proved capable of generating similar current/time profiles as were observed with phloretin. The actual binding position/location of the dipolar species may be critical for this effect to be observed. The most energetically favorable interaction of a molecule such as phloretin with membrane lipid (phloretin is electrochemically active in the absence of cholesterol) may be through dipole-dipole electrostatic binding. Such a model suggests that the charge-center distributions of phloretin and 2,4,6-trihydroxyacetophenone are very similar, and are spatially and electrostatically suitable for lipid dipole vector binding. The binding stability of phlorhizin would be limited by the large steric hindrance caused by the glucose residue. In this model, however, P-N dipole vector, bound water of hydration and underlying carbonyl dipole vector reorientation would also have to be considered.

Phloretin signal amplification

One interesting practical feature obtained through electrostatic manipulation of BLM surfaces is the ability to amplify or probe the effects of agents that act directly on the chemical potential energy barrier. Several studies have included the use of molecular membrane probes such as valinomycin to establish the nature of dipolar interaction [3, 4, 21, 22]. The addition of valinomycin to a BLM significantly increases the potassium ion flux by decreasing the chemical potential barrier involved in transmembrane ion transport. The addition of phloretin to the same membrane will decrease the

TABLE 1

Amplification of ion current for 1.0×10^{-5} M phloretin additions to membranes doped with valinomycin

Valinomycin (M)[a]	6.4×10^{-8}	3.2×10^{-7}	5.0×10^{-7}	6.4×10^{-7}	6.4×10^{-6}
Amplification[b]	1.6	2.3	5.5	8.3	16.5

[a]Concentration of valinomycin in 0.1 M KCl. [b]Amplification relative to the ion current measured for the unmodified membrane.

electrical potential barrier to carrier ion transport. These two energy changes then act in a concerted manner to produce greater potassium ion flux on addition of both valinomycin and phloretin. A standard application of phloretin resulting in a well defined final concentration will produce greater electrochemical response for membranes containing increasing concentrations of valinomycin. Table 1 shows the amplification possible when a constant phloretin concentration is added with BLM of increasing valinomycin content.

Conclusions

This work confirms earlier work [1] which showed that local perturbation of the electrical potential distribution in lipid membranes results in a valuable analytical signal. With phloretin added, the ion permeability of the BLM is influenced by local interaction of the stimulant with permions adsorbed at the membrane surface. This effect is associated with ion conduction through BLM sites that provide a low potential-energy pathway for the ion. Selective sensing mechanisms based on alteration of an intrinsic receptor/membrane dipolar potential by simple addition of a stimulant dipole and/or by surface structural effects thus seem possible. Sensitivity increases for this mechanism can be achieved if permion-binding sites are located near receptors operating on the basis of dipolar change.

The transient charging of the membrane observed on addition of certain dipolar molecules appears to be related to the adsorption of the stimulant on the membrane surface. The induction period between adsorption and the positive current increase indicates that there is not an immediate response of transmembrane ion transport to molecular adsorption. There are at least two possible reasons for this. First, the ions need time to respond to changes in the potential distribution of the membrane; for a barrier height of about 0.8 eV, this time constant is estimated to be about 10 s at room temperature. Secondly, there seems to be an extra step between the charging of the membrane with phloretin and any dipole-induced action; the evolution of large transient signals by such a mechanism has implications for receptor action.

We are grateful to the Natural Sciences and Engineering Research Council of Canada and the Ministry of the Environment, Province of Ontario for support of this work.

REFERENCES

1 M. Thompson and U. J. Krull, Anal. Chim. Acta, 147 (1983) 1.
2 M. L. Jennings and A. K. Solomon, J. Gen. Physiol., 67 (1976) 381.
3 J. Reyes, F. Greco, R. Motais and R. Latorre, J. Membr. Biol., 72 (1983) 93.
4 O. S. Andersen, A. Finkelstein, I. Katz and A. Cass, J. Gen. Physiol., 67 (1976) 749.
5 J. E. Hall, C. A. Mead and G. Szabo, J. Membr. Biol., 11 (1973) 75.
6 D. A. Haydon, N.Y. Acad. Sci. Ann., 264 (1975) 2.
7 B. A. Pethica, M. Mingins and J. A. G. Taylor, J. Colloid Interface Sci., 55 (1976) 2.
8 W. B. Kleijn, L. J. Bruner, M. M. Midland and J. Wisniewski, Biochim. Biophys. Acta, 727 (1983) 357.
9 S. McLaughlin, in F. Bonner and A. Kleinzeller (Eds.), Current Topics in Membranes and Transport, Academic Press, New York, 1977, p. 71.
10 F. Paltauf, H. Hauser and M. C. Philips, Biochim. Biophys. Acta, 249 (1971) 539.
11 K. C. Sehgal, W. F. Pickard and C. M. Jackson, Biochim. Biophys. Acta, 552 (1979) 11.
12 R. Benz and D. Cros, Biochim. Biophys. Acta, 506 (1978) 256.
13 A. Scarpa and J. De Grier, Biochim. Biophys. Acta, 241 (1971) 789.
14 A. J. Bard and L. R. Faulkner, Electrochemical Methods, Wiley, New York, 1980, p. 73.
15 P. Lauger and B. Neumke, in G. Eisenman (Ed.), Membranes, Vol. 2, M. Dekker, New York, 1972, p. 31.
16 P. Narayaman, E. Ramirez, T. McCaffrey, W. F. Chaw and J. F. Marecek, J. Org. Chem., 43 (1978) 24.
17 H. Hauser, M. C. Philips, B. Levine and R. J. P. Williams, Nature, 261 (1976) 390.
18 I. Lundström and C. Nylander, J. Theor. Biol., 88 (1981) 671; Periodicum Biologorum, 85 (1983) Suppl. 2, 53.
19 C. Nylander and I. Lundström, Proc. 5th Nordic Meet. Medical Biological Engineering, 2 (1981) 586.
20 I. Lundström and C. Nylander, Int. J. Quantum Chem., 23 (1983) 1269.
21 H. P. Ting-Beall, D. J. Benos, J. E. Hall and D. C. Tosteson, Biophys. J., 15 (1975) 308a.
22 N. R. Clement and J. M. Gould, Biochemistry, 20 (1981) 1539.

Analytica Chimica Acta, 173 (1985) 141—148
Elsevier Science Publishers B.V., Amsterdam — Printed in The Netherlands

ACID—BASE EQUILIBRIA IN ORGANIC SOLVENTS
Part 1. Evaluation of Solvent Basicity by Cyclic Voltammetry

SALVATORE DANIELE, PAOLO UGO and GIAN-ANTONIO MAZZOCCHIN

Dipartimento di Spettroscopia, Elettrochimica e Chimica Fisica, Università di Venezia, Dorsoduro 2137, 30123 Venezia (Italy)

GINO BONTEMPELLI*

Istituto di Chimica Analitica, University of Padova, via Marzolo 1, 35131 Padova (Italy)

(Received 3rd December 1984)

SUMMARY

Cyclic voltammetry is applied to evaluate the relative basicity of some organic polar solvents of electroanalytical interest (nitromethane, acetonitrile, tetrahydrofuran, 1,2-dimethoxyethane, dimethylformamide, dimethyl sulphoxide and pyridine). For this purpose, anhydrous perchloric acid is electrogenerated in these solvents and the half-wave potentials of the redox couple H^+/H_2 are recorded by referring them to a reference system independent of the nature of the solvent. The proton-basicity scale so obtained is compared with previous basicity series and the observed analogies and differences are discussed. The same procedure is also applied to evaluate, in the solvents mentioned, the relative strengths of some bases which can be used as titrants in nonaqueous media.

Several attempts to rank organic solvents on the basis of their relative basicity have been reported in the literature [1]. Different experimental techniques, such as n.m.r., u.v. and i.r. spectroscopy, calorimetry and liquid chromatography, have been applied. Full agreement between the scales obtained is not observed. This is probably a consequence both of the different nature of the acid-base reactions considered for evaluating the solvent basicity and of the reaction parameter (ΔH or ΔG) measured. As to the nature of the acid-base reaction, the reference acid and the solvent can interact with each other, leading either to a real proton-transfer reaction or to the formation of a molecular adduct with or without hydrogen bonds, depending on the reference Lewis acid used. In particular, in the latter case, steric hindrance may also play quite an important role.

Although the definition of basicity with reference to the proton is of prime interest in gaining insight into the correct fulfilment of acid-base titrations in nonaqueous solvents, relatively few data are available with respect to reactions of bulk solvents with hydrogen ion.

To date, these reactions have been studied by using the potentiometric approach [1] in which a solvent-independent reference electrode involving stable redox couples and a hydrogen electrode are required; both of these

0003-2670/85/$03.30

imply experimental difficulties that are hard to overcome. These reactions can also be studied by voltammetric techniques which make it possible to use an easier experimental approach. In this paper, the bulk solvent basicity is evaluated by using cyclic voltammetry to measure the reversible half-wave potential of the redox couple H^+/H_2 in some organic polar solvents of electroanalytical interest. The solvents investigated are pyridine (Py), dimethyl sulphoxide (DMSO), *N,N*-dimethylformamide (DMF), 1,2-dimethoxyethane (DME), tetrahydrofuran (THF), acetonitrile (AN) and nitromethane (NM). The strengths of some bases which can be used as titrants are also evaluated in these solvents.

EXPERIMENTAL

Chemicals

All the chemicals used were of reagent-grade quality. Reagent-grade solvents were further purified by procedures reported in the literature [2] and were stored over 0.4-nm molecular sieves under a nitrogen atmosphere.

The supporting electrolyte, tetrabutylammonium perchlorate (TBAP), was recrystallized from methanol and dried under vacuum at 50° C. Stock solutions of anhydrous perchloric acid in all the organic solvents examined were obtained by anodic oxidation on a platinum electrode of hydrogen gas bubbled through the solvents containing the appropriate amount of supporting electrolyte.

Nitrogen used to remove dissolved oxygen from the working solutions and hydrogen were previously passed through sulphuric acid to remove traces of water and then equilibrated to the vapour pressure of the solvent.

Apparatus and procedure

Voltammetric experiments were conducted at 20° C in a three-electrode cell. The working electrode was a platinum disc mirror-polished with graded alumina powder prior to each voltammetric scan. This preliminary surface activation made it possible to record cyclic voltammetric responses as reproducible as those obtained by using the activation method proposed recently [3] which requires pre-anodization. The polishing procedure with alumina is preferable for this work, in any case, because anodization is precluded when the ferrocene reference system is present in the solution (see later).

In the cell, the working electrode was surrounded by a platinum spiral counter electrode. Its potential was measured against a Luggin capillary-reference electrode compartment, the position of which could be adjusted by mounting it on a syringe barrel. An aqueous SCE was used as the actual reference electrode, but all the potentials reported in this paper are referred to the half-wave potential, $E_{1/2}$, of the ferricinium/ferrocene (Fc^+/Fc) system. This was measured by cyclic voltammetry after addition of ferrocene to the H^+-containing solutions in the different solvents, following the

procedure recommended by IUPAC [4]. The Fc^+/Fc system was chosen because its $E_{1/2}$ is independent of the nature of the solvent; it was found to be reversible in all the solvents investigated at the scan rate generally used (0.050 V s^{-1}).

Perchloric acid was electrogenerated in an H-shaped cell with cathodic and anodic compartments separated by a sintered glass disc. The working electrode was a platinum gauze and a nickel spiral served as the counter electrode; again, the reference electrode was an aqueous SCE. The solutions thus obtained were then transferred to the voltammetric cell under nitrogen with a degassed syringe.

The voltammetric unit was a three-electrode system assembled with MPI-System 1000 equipment in conjunction with a function generator (PAR 175 universal programmer). The recorder device was either a Hewlett-Packard model 7040 A X-Y recorder or a Tracor Northern NS-570A digital storage oscilloscope/wave form digitizer with analog output for an X-Y recorder, depending on the scan rate applied.

In the controlled potential electrolyses, an Amel model 552 potentiostat was used and the associated coulometer was an Amel model 731 integrator. Potentiometric titrations were done in the H-shaped cell used for electrogenerating perchloric acid; a Metrohm EA-158 glass electrode was always used for nonaqueous media.

RESULTS AND DISCUSSION

Bulk solvent basicity

According to the literature [5, 6], all measurements are made on the assumption that the perchlorate ion is a weaker base than all the solvents investigated. Consequently, quantitative dissociation of electrogenerated perchloric acid is always expected, in agreement with the following general reaction (S = solvent)

$$HClO_4 + S \rightarrow HS^+ + ClO_4^-$$

The cyclic voltammetric profiles of all the perchloric acid solutions shows, in fact, a single one-electron cathodic peak arising from the reduction of H^+ to H_2, the potential of which depends on the nature of the solvent used.

The occurrence of a one-electron process was checked by comparing the height of the relevant peak with that displayed by ferrocene which is known to involve a one-electron oxidation [7]. As shown in Fig. 1, the cathodic peak is accompanied by an anodic peak reflecting the re-oxidation of hydrogen to hydrogen ion. Consequently, the observed cathodic-anodic system can be attributed to the following redox equilibrium

$$HS^+ + e^- \rightleftharpoons \frac{1}{2} H_2 + S$$

Depending on the nature of the solvent used, the separation between the associated cathodic and anodic peaks ranges from 0.060 to 0.090 V, when a

scan rate of 0.020 V s^{-1} is applied. An increase in the scan rate causes greater peak separations to be observed (e.g., 0.090—0.120 V for ΔE_p at a scan rate of 2 V s^{-1}). This dependence of peak separation on the sweep rate suggests that the process involved is not perfectly reversible; nevertheless, the cathodic-anodic couple is always centred at the same potential value for each solvent investigated. These findings indicate that a transfer coefficient α ranging from 0.3 to 0.7 characterizes the electrode process, thus allowing evaluation of the half-wave potential by the simple relationship [10] $E_{1/2} = (E_{pa} + E_{pc})/2$.

In Table 1 the solvents investigated are ranked on the basis of their increasing basicity which is reflected by the decreasing $E_{1/2}$ values measured

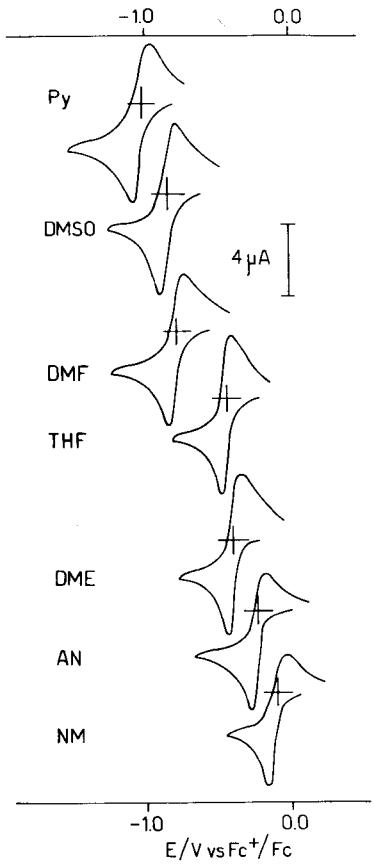

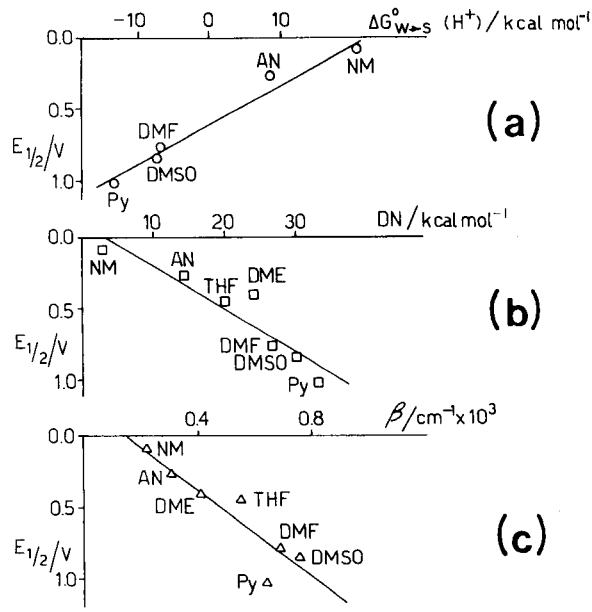

Fig. 1. Cyclic voltammograms recorded with a platinum disc microelectrode from solutions containing 6 × 10^{-3} M $HClO_4$ and 0.5 M TBAP in the solvents indicated. Scan rate 0.1 V s^{-1}.

Fig. 2. Comparison of the $E_{1/2}$ values reported in Table 1 with the following basicity parameters: (a) free energy for the transfer of H^+ from water to the organic solvent (from Benoit and Louis [1]); (b) donor number (from Gutmann [8]); (c) basicity solvatochromic parameter (from Kamlet et al. [9]).

TABLE 1

$E_{1/2}$ values for the H^+/H_2 redox couple recorded at a platinum disc microelectrode from cyclic voltammetry at a scan rate of 0.1 V s^{-1}, referred to the Fc^+/Fc system

Solvent	$E_{1/2}$ (V)	Solvent	$E_{1/2}$ (V)
NM	−0.080	DMF	−0.770
AN	−0.260	DMSO	−0.830
DME	−0.400	Py	−1.020
THF	−0.440		

against the reference redox system Fc^+/Fc. In agreement with obvious expectations, this basicity is shown to increase with the availability of unshared pairs of electrons in the solvent molecule. The reported $E_{1/2}$ values might be affected by the possible ion-pair formation ($HS^+ClO_4^-$), especially in the solvents with quite low dielectric constant. This effect, if present, would lower the proton activity leading to a more difficult reduction of the HS^+ species and hence to an "apparent" higher basicity of the solvents. Therefore, the voltammograms were recorded for solutions in which the concentration of the supporting electrolyte ranged from 0.2 to 2 M. No changes in the voltammetric profiles were observed, thus indicating that the effect of the ion-pair formation is negligible in the present experimental conditions.

A comparison between the present results and those obtained by different approaches was attempted in order to test the reliability of the basicity scale found here. For this purpose, the $E_{1/2}$ values were plotted against the parameters used in some other series. Figure 2(a) shows a good correlation with the scale based on the potentiometric determination of the free energy for the transfer of hydrogen ion from water to the generic organic solvent S ($\Delta G^0_{w\rightarrow s}(H^+)$) [1]. The following correlation equation is valid in this case:

$$E_{1/2} = -0.600 + 0.028\Delta G^0_{w\rightarrow s}(H^+) \quad (r = 0.986)$$

This equation was calculated for only five solvents because the $\Delta G^0_{w\rightarrow s}(H^+)$ values for 1,2-dimethoxyethane and tetrahydrofuran are not available in the literature. The good correlation coefficient can be explained by considering that both scales are based on measurements of free energy variations. In this connection, it may be noted, however, that the voltammetric approach simplifies the evaluation of solvent basicity compared with the potentiometric method. It enables the use of a hydrogen electrode, with all its experimental difficulties, to be avoided. Moreover, the presence in the solution of freshly prepared Fc^+ ion (not very stable) is not required.

A rather satisfactory agreement is also apparent in Fig. 2(b) with the series suggested by Gutmann [8], although it is referred to a different thermodynamic quantity. This series involves a parameter, the donor number (DN), which is coincident with the ΔH^0 involved in the formation of an adduct between the solvent and a Lewis acid (antimony(V) chloride). In this case,

the correlation equation found is $E_{1/2} = 0.111 - 0.030$ DN ($r = 0.933$). The reasonably satisfactory value for the correlation coefficient indicates that entropy variations do not play an important role in these acid-base equilibria.

The plot of $E_{1/2}$ vs. the solvatochromic parameter β [9, 11], is shown in Fig. 2(c). The correlation equation here is $E_{1/2} = 0.233 - 1.518\,\beta$ ($r = 0.911$). It must be emphasized that in this last plot, there is complete disagreement about the basicity of pyridine. This solvent is characterized by a β parameter which is intermediate between those proper for THF and DMF, whereas it is the more basic solvent examined according to the present ranking. This quite unsatisfactory agreement is probably due to the different reference reactions used for the two scales. The β parameter quantifies the solvent hydrogen-bonding acceptor ability which leads to the formation of neutral adducts. In contrast, the $E_{1/2}$ values used here refers to the net transfer of a proton to the solvent. Nevertheless, it should be emphasized that the potentials measured here can be conditioned not only by the strength of the species HS^+, but also by the formation of hydrogen bonds between HS^+ and other solvent molecules, yielding ionic adducts of the type HS_n^+.

Relative strength of some bases in organic solvents

In order to ascertain if valuable information concerning acid-base titrations in nonaqueous solvents can be gathered by the cyclic voltammetric approach described above, the strength of a series of bases was evaluated in the different solvents investigated. For this purpose, each basic compound (B) was added to the perchloric acid solution in the desired solvent and then the cyclic voltammetric responses were recorded. A base/hydrogen ion molar ratio of 2:1 was taken in all cases in order to determine the $E_{1/2}$ values relative to the HB^+/B buffers. The addition to the HS^+ solutions of compounds more basic than the solvent caused only a cathodic shift of the couple of peaks displayed by the system H^+/H_2, while no effect was observed for compounds of similar or lesser basicity, in full agreement with obvious expectations.

A quite similar approach has been described very recently [12]. In that case, however, the measurements were made under moist conditions in that the species HS^+ was generated by adding aqueous perchloric acid to the solvent. Moreover, the reference electrode used was not independent of the nature of the solvent.

Table 2 collects all the experimental data; they appear to reflect quite well the order of basicity expected from the literature [5]. Comparison of the reported potentials with those collected in Table 1 allows one to infer the potential changes expected in the relevant potentiometric titrations. To verify the reliability of the present voltammetric data, potentiometric titrations were done on perchloric acid solutions in different solvents by adding stepwise the bases mentioned in Table 2. In all cases, the potential changes obtained potentiometrically (see Fig. 3) agreed within ±0.010 V with those expected on the basis of the comparison of Table 1 with Table 2.

TABLE 2

$E_{1/2}$ values (V) for the H^+/H_2 redox couple recorded at a platinum disc microelectrode from cyclic voltammetry on solutions of some bases in different solvents (scan rate 0.1 V s^{-1}; reference system Fc^+/Fc)

Base	$E_{1/2}$ (V) in different solvents						
	NM	AN	DME	THF	DMF	DMSO	Py
AN	nd[a]	—[b]	—[b]	—[b]	—[b]	—[b]	—[b]
DME	nd	−0.250	—[b]	—[b]	—[b]	—[b]	—[b]
THF	nd	−0.270	nd	—[b]	—[b]	—[b]	—[b]
PPh_3	nd	−0.430	nd	nd	—[b]	—[b]	—[b]
DMF	nd	−0.430	nd	nd	—[b]	—[b]	—[b]
DMSO	nd	−0.440	nd	nd	—[b]	—[b]	—[b]
Py	−0.680	−0.750	−0.800	−0.800	−0.850	−0.930	—[b]
Morp[c]	−0.960	−1.040	−1.070	−1.090	−1.140	−1.230	−1.130
Pip[d]	−1.080	−1.160	−1.180	−1.200	−1.250	−1.350	−1.250

[a]Not determined. [b]Undetectable owing to the higher or comparable basicity of the solvent. [c]Morpholine. [d]Piperidine.

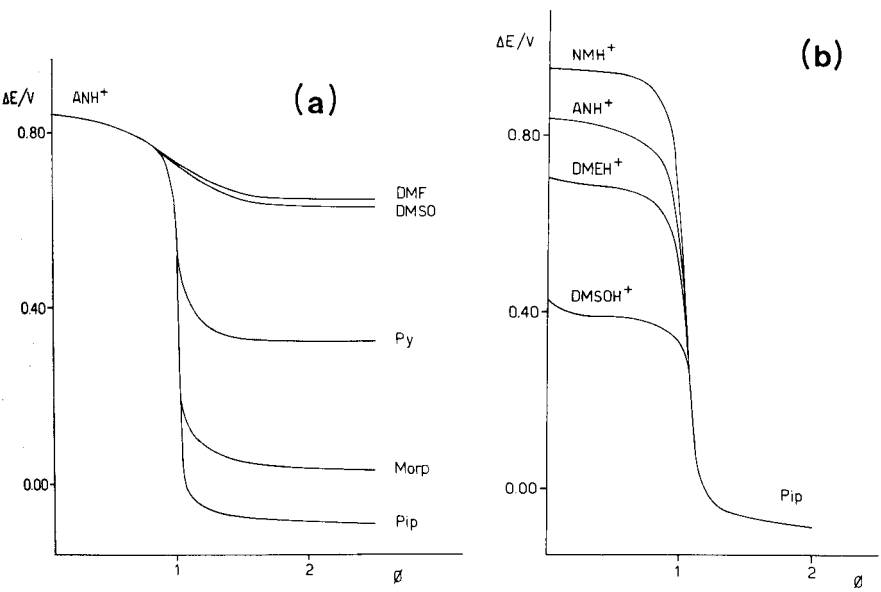

Fig. 3. Titration curves: (a) electrogenerated 6×10^{-3} M $HClO_4$ in 0.1 M TBAP solutions in acetonitrile with 0.1 M TBAP solutions in acetonitrile of the bases (1.6×10^{-2} M) indicated on the curves; (b) electrogenerated 6×10^{-3} M $HClO_4$ in 0.5 M TBAP solutions in the solvent indicated on the curves with 1.6×10^{-2} M piperidine in 0.5 M TBAP dissolved in the same solvent. (Morp means morpholine.)

The inspection of Table 2 indicates that the $E_{1/2}$ values relative to each of the reported compounds are affected by the nature of the medium, even when solvents with lesser basicity than that compound are used. In particular, it can be seen that the reduction of the acids conjugated with pyridine, morpholine and piperidine occurs at increasingly negative potential values as the basic character of the solvent increases. The only exception to this trend is given by the solvent DMSO which causes a higher cathodic shift than pyridine, although the opposite basicity order is shown in Table 1.

The dependence of the $E_{1/2}$ values on the nature of the solvent indicates that the real basicity exhibited by the compounds is conditioned by the basic character of the medium and this is strongly suggestive of the formation of hydrogen bonds between HB^+ and the solvent molecules. These bonds, mentioned also at the end of the previous section, are in fact expected to be stronger the more basic is the solvent. The effect of their formation on the "proton-basicity" measured here is the subject of a second report [13].

The authors thank C.N.R. (Rome) and the Ministry of Public Instruction for partial support. Also the financial aid of C.N.R., Project ELA, "Accumulo Elettrochimico", is gratefully acknowledged.

REFERENCES

1 R. L. Benoit and C. Louis, in J. J. Lagowski (Ed.), The Chemistry of Nonaqueous Solvents, Vol. 5A, Academic Press, New York, 1978.
2 C. K. Mann, in A. J. Bard (Ed.), Electroanalytical Chemistry, Vol. 3, M. Dekker, New York, 1969.
3 W. C. Barrette Jr. and D. T. Sawyer, Anal. Chem., 56 (1984) 653.
4 G. Gritzner and J. Kuta, Pure Appl. Chem., 56 (1984) 461.
5 G. Charlot and B. Tremillon, Les reactions Chimiques dans les Solvants et les Sels Fondus, Gauthier-Villars, Paris, 1963.
6 G. Cauquis and D. Serve, Bull. Soc. Chim. France, (1966) 302.
7 C. K. Mann and K. K. Barnes, Electrochemical Reactions in Nonaqueous Systems, M. Dekker, New York, 1970.
8 V. Gutmann, Electrochim. Acta, 21 (1976) 661.
9 M. J. Kamlet, J. M. Abboud, M. H. Abraham and R. W. Taft, J. Org. Chem., 48 (1983) 2877.
10 R. S. Nicholson, Anal. Chem., 37 (1965) 1351.
11 M. J. Kamlet and R. W. Taft, J. Am. Chem. Soc., 98 (1976) 377.
12 W. C. Barrette Jr., H. W. Johnson Jr. and D. T. Sawjer, Anal. Chem., 56 (1984) 1890.
13 P. Ugo, S. Daniele, G.-A. Mazzocchin and G. Bontempelli, Anal. Chim. Acta, 173 (1985) 149.

Analytica Chimica Acta, 173 (1985) 149—156
Elsevier Science Publishers B.V., Amsterdam — Printed in The Netherlands

ACID—BASE EQUILIBRIA IN ORGANIC SOLVENTS
Part 2. Cyclic Voltammetry in the Study of Hydrogen-bond Formation

PAOLO UGO, SALVATORE DANIELE and GIAN-ANTONIO MAZZOCCHIN

Dipartimento di Spettroscopia, Elettrochimica e Chimica Fisica, Università di Venezia, Dorsoduro 2137, 30123 Venezia (Italy)

GINO BONTEMPELLI*

Istituto di Chimica Analitica, University of Padova, Via Marzolo 1, 35131 Padova (Italy)

(Received 3rd December 1984)

SUMMARY

The cyclic voltammetric technique is used to study hydrogen-bond formation in some polar organic solvents (S) of electroanalytical interest (1,2-dimethoxyethane, tetrahydrofuran, dimethylformamide, dimethyl sulphoxide and pyridine). The cathodic shift of the proton reduction caused by stepwise addition of the solvent investigated to a solution of anhydrous perchloric acid in acetonitrile is utilized. The theoretical treatment applied produced evidence that HS^+ and HS_2^+ are the only acidic species involved, so that the relevant formation constants can be evaluated. The data obtained mostly compare well with those available in the literature. The features that condition the tendency to hydrogen-bonding and the effect of hydrogen bonding on solvent basicity are discussed.

One of the most important solvent-solvent interactions is due to the formation of hydrogen bonds when one hydrogen atom is shared between solvent molecules. There have been many experimental and theoretical studies dealing with the effect of hydrogen bonding on the solvent self-association [1—3]. Although some of these investigations have been devoted to evaluation of the solvent basicity [4, 5], no attempt seems to have been made to quantify the role played by hydrogen bonding in conditioning the proton activity in a given organic solvent.

In principle, the relevant association products, when originated by added protons, can be regarded as simple complexes of the type HS_n^+. Consequently, it is possible to characterize their stoichiometry as well as to determine their stability constants by the normal methods used to study complex formation equilibria which involve gradual changes in the concentration of the ligand S. This approach has been adopted previously in potentiometric studies of the hydrogen-bonded complexes formed by nitrogen bases in different solvents, even though only quite low concentration ranges of the added bases were used [6].

The effect on the proton activity caused by a concentration change of a basic species can easily be monitored by cyclic voltammetry which appears

0003-2670/85/$03.30

to be a valuable tool for this purpose, as was pointed out in the first part of this report [7]. Of course, these measurements must be made in a solvent which is itself incapable of forming hydrogen bonds. Because the very poor bonding ability of acetonitrile is well recognized [8], it was chosen as the reference medium in this work; another advantageous feature is that this solvent is easily purified and very stable on storage.

This paper reports the results achieved in a series of cyclic voltammetric measurements on the H^+/H_2 redox couple present in a medium obtained by mixing the reference solvent acetonitrile (R) with increasing mole fractions of some more basic solvents (S). The solvents examined were 1,2-dimethoxyethane (DME), tetrahydrofuran (THF), dimethylformamide (DMF), dimethyl sulphoxide (DMSO) and pyridine (Py).

EXPERIMENTAL

The preparation and the purification of all the chemicals as well as the electroanalytical instrumentation were described in Part 1 [7].

All measurements were made at 20°C and the total proton concentration was kept constant in order to avoid a dilution effect on the potential values recorded (see later). For this purpose, anhydrous perchloric acid solutions both in acetonitrile and in the solvent investigated (S) were freshly prepared to exactly the same concentration, by following the electrochemical procedure reported previously [7]. Subsequently, increasing amounts of the $HClO_4/S$ solution were added stepwise to the $HClO_4/CH_3CN$ solution and cyclic voltammograms were recorded after each addition. The relevant $E_{1/2}$ values were then evaluated from the well-established relationship $E_{1/2} = (E_{pa} + E_{pc})/2$. They were referred to the $E_{1/2}$ of the ferricinium ion/ferrocene (Fc^+/Fc) redox couple measured in its turn after each addition of the $HClO_4/S$ solution, ferrocene (3.0×10^{-3} M) being added at the beginning of all the measurements.

All calculations were run on a Digital model 11/23 computer.

RESULTS AND DISCUSSION

The stepwise addition to perchloric acid solutions in acetonitrile (reference solvent R) of a more basic solvent, S, containing perchloric acid at exactly the same concentration, causes a progressive shift of the H^+/H_2 cathodic-anodic system of voltammetric peaks towards more negative potentials. But there is no remarkable change in the height of these peaks.

The dependence of the relevant $E_{1/2}$ value, evaluated after each addition, on the logarithm of the concentration of S is shown in Fig. 1; in these measurements, a large change in the concentration of added solvent was explored, reaching experimental conditions in which it became the predominant medium, thus the mole fraction is preferred for expressing the concentration of S. In three cases at least, the curves obtained made it possible to identify

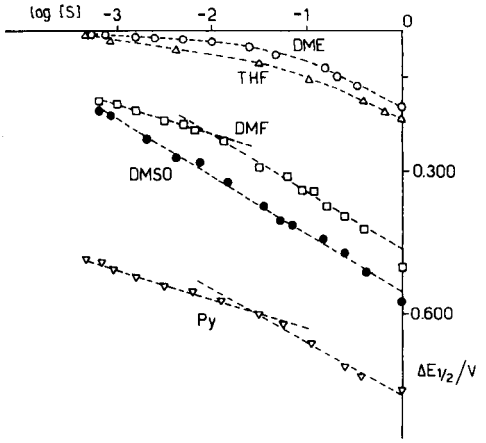

Fig. 1. Dependence of $E_{1/2}$ for the H^+/H_2 couple on the logarithm of the mole fraction of the solvent added to acetonitrile, both containing 6.0×10^{-3} M $HClO_4$, 3.0×10^{-3} M Fc (internal reference) and 0.5 M TBAP. All the potentials are measured with a platinum microelectrode at a scan rate of 0.1 V s^{-1} and referred to the $E_{1/2}$ (H^+/H_2) in acetonitrile.

linear portions; the slopes are reported in Table 1. Such trends suggest that H^+-S association equilibria are operative; their rationalization is possible on the basis of the following simple considerations.

Because the reference solvent R (acetonitrile) is unable to provide hydrogen bonds to an appreciable extent [8], its protonation can be assumed to yield only the species HR^+. The addition of a more basic solvent S to HR^+ solutions is expected to cause the formation of protonated species such as HS^+, HS_2^+, ..., HS_n^+. Consequently, the following equilibria may be operative:

$$\begin{aligned} HR^+ + S &\rightleftharpoons HS^+ + R \qquad (K_1 = [HS^+][R]/[HR^+][S]) \\ HS^+ + S &\rightleftharpoons HS_2^+ \qquad (K_2 = [HS_2^+]/[HS^+][S]) \\ HS_{n-1}^+ + S &\rightleftharpoons HS_n^+ \qquad (K_n = [HS_n^+]/[HS_{n-1}^+][S]) \end{aligned} \tag{1}$$

TABLE 1

Slopes available from Fig. 1

Solvent	Approximate mole fraction range	Slope[a]	n
DMF	0.0006—0.01	0.058	1
	0.01—1.0	0.119	2
DMSO	0.0006—1.0	0.118	2
Pyridine	0.0006—0.035	0.059	1
	0.035—1.0	0.114	2

[a]Calculated by the least-squares method.

The total concentration of protons is $C_{H^+} = [HR^+] + \Sigma_1^n[HS_j^+]$. This combines with the above equations to give the following relationship for the equilibrium concentration of HR^+

$$[HR^+] = C_{H^+}(1 + \sum_1^n \beta_j[S]^j/[R])^{-1} \quad (2)$$

where β_j is the jth overall formation constant ($\beta_j = \Pi^j K_j$). This can be inserted in the Nernst equation relative to the redox system (supposed to be totally reversible)

$$HR^+ + e^- \rightleftharpoons 1/2H_2 + R \quad (3)$$

This equation is valid if all activity coefficients are kept constant; it can be considered that the ionic strength does not change appreciably under the present experimental conditions (irrespective of the dielectric constant of the solvent used) because of the presence of the supporting electrolyte in both the mixed solutions. Thus

$$E = E^{\circ\prime} + RTF^{-1} \ln [HR^+]/[R][H_2]^{1/2} \quad (4)$$

and

$$E = E^{\circ\prime} + RTF^{-1} \ln C_{H^+}([R][H_2]^{1/2})^{-1}(1 + \sum_1^n \beta_j[S]^j/[R])^{-1} \quad (5)$$

In order to express the potential as a function of current, the following diffusion conditions can be introduced: $i = i_d - \bar{d}(C_{H^+})_0$ and $i = d_{H_2}[H_2]_0$, where $\bar{d}$ and d_{H_2} are the relevant "Ilkovič" coefficients and the subscript 0 refers to the concentrations at the electrode surface. Consequently, by imposing $i = i_d/2$, Eqn. 5 becomes

$$E_{1/2} = E^{\circ\prime} + RTF^{-1} \ln (d_{H_2}^{1/2}/\bar{d}) + RT(2F)^{-1} \ln (i_d/2) - RTF^{-1} \ln ([R]_0 + \sum_1^n \beta_j[S]_0^j) \quad (6)$$

Comparison of this equation with the half-wave potential relative to the occurrence of reaction (3) in the absence of S, i.e.,

$$E_{1/2} = E^{\circ\prime} + RTF^{-1} \ln (d_{H_2}^{1/2}/d_{HR^+}) + RT(2F)^{-1} \ln (i_d/2)$$

(the term $(RTF^{-1}) \ln [R]_0$ is omitted because its value is zero in pure R), gives the following relationship, which is valid if it can be assumed that the mean coefficient $\bar{d}$ is equal to d_{HR^+}

$$\Delta E_{1/2} = -RTF^{-1} \ln ([R]_0 + \sum_1^n \beta_j[S]_0^j) \quad (7)$$

This equation implies that the plot of the half-wave potential against the

logarithm of the concentration of the added solvent S consists either of a number of linear portions with breaks if the step formation constants K_n differ sufficiently or of a smooth curve with no breaks when these constants lie close to one another. The present experimental data appear to obey Eqn. 7, thus indicating that all the assumptions made above are satisfactory and so that the products HS_n^+ of the interaction between protons and solvent molecules can be regarded in this case as simple complex species.

Inspection of Fig. 1 and Table 1 indicates that all the solvents investigated are able to form hydrogen-bonded species of the type HS_2^+, while higher-order association products are not formed even by the more basic solvents. Different behaviours are observed, however, for the various solvents added. In particular, a slope lower than 0.058 V ($n = 1$) is shown by 1,2-dimethoxyethane and THF until a quite high molar fraction is reached. This finding indicates that the K_1 value for these solvents is not high enough to allow reaction (1) to be shifted to the right for relatively low C_S/C_R ratios. Moreover, in these cases, a slope attaining 0.116 V ($n = 2$) is observed only for a mole fraction approaching unity and no clear break in the slope is apparent, which shows that K_2 does not differ considerably from K_1.

Similar considerations lead to the conclusion that, in contrast, the solvents DMF and pyridine are characterized by relatively high values for K_1 and rather notable differences between K_2 and K_1. A different behaviour again is exhibited by DMSO, for which a straight line with a slope of 0.116 V ($n = 2$) is obtained over the entire concentration range explored. This result strongly suggests that the value for K_2 is higher than that for K_1, even though K_1 is expected to be fairly high in view of the significantly higher basicity of DMSO (S) compared to that exhibited by acetonitrile (R). The circumstance that the formation of the hydrogen-bonded species HS_2^+ for DMSO is more favoured than that of HS^+, which is at variance with the behaviour of the apparently more basic solvent pyridine, suggests that not only basic strength but also other effects (e.g., steric hindrance) can play an important role in the hydrogen-bonding ability of a basic species. However, if this ability is conditioned mainly by the basicity, then the more basic is the solvent, the lower should be the mole fraction at which the change in slope (from $n = 1$ to $n = 2$) is observed; this is in disagreement with the experimental evidence (see Fig. 1).

According to this view, the least steric hindrance among the solvents investigated is expected to be exhibited by DMSO, on the basis of simple considerations. This could account for the disagreement between the proposed "proton-basicity" scale [7] and that based on the solvatochromic parameter β which ranks the solvents simply in order of their hydrogen-bonding ability [5]. On this latter scale, DMSO is in fact more basic than pyridine, whereas the opposite order was found in the present work, as well as in some other series [9, 10]. This disagreement emphasizes that much caution must be used before basicity data can be inferred from the hydrogen-bonding capability displayed by a species.

The applicability of Eqn. 7 to the equilibria involving protons in the solvents investigated means that the formation constants K_1, K_2 and/or β_2 may be evaluated. For this purpose, a simple linear regression procedure can be used in the cases of DMF, DMSO and pyridine, where a linear trend is apparent in finite ranges of log S. Of course, for DMSO, only β_2 can be obtained from the data because the condition $K_2 > K_1$ mentioned above means that the term $\beta_1[S]_0$ in Eqn. 7 is negligible for all values of the mole fraction of S. Conversely, this method cannot be used for 1,2-dimethoxyethane and THF because smooth curves were observed; for these solvents, the formation constants K_1 and K_2 were evaluated by a modified simplex optimization procedure [11]. It is worth noting that the application of this procedure to DMF and pyridine yielded K_1 and K_2 values which agreed well with those obtained by the linear regression method. The formation constants obtained are collected in Table 2. The reliability of these data was estimated by comparing the experimental points with the $\Delta E_{1/2}$ vs. log [S] curves calculated by inserting into Eqn. 7 the formation constants reported in Table 2. This comparison is shown in Fig. 2.

The order of basicity inferred from the K_1 values agrees completely with that found in Part 1 of this work [7]. In contrast, the formation constants K_2 do not increase with solvent basicity. This strongly supports the above suggestion that other effects are also of importance in the formation of H^+-bonded solvent association species. In this regard, it must be noted that all of these effects are accounted for in the solvatochromic series [5] which indeed evaluates the hydrogen-bonding ability. Thus at variance with the present scale, the solvatochromic scale attributes a higher basicity to DMF than to pyridine; according to the present K_2 values, pyridine is in fact less prone to participate in the formation of hydrogen bonds. These arguments can also explain the unexpected increase in basicity observed for morpholine and piperidine on changing from pyridine to DMSO as solvent (see Table 2 [7]). This higher basicity is possibly due to the formation of heteroconjugated complexes of the type HBS^+ which will be more stable when S = DMSO, because of its higher tendency to hydrogen bonding (see above).

TABLE 2

Formation constants of HS^+ and HS_2^+ for the solvents investigated, referred to acetonitrile[a]

Solvent	K_1	K_2	β_2
DME	1.2×10^2	5.0	6.0×10^2
THF	6.4×10^2	1.4	9.0×10^2
DMF	5.8×10^5	110.3	6.4×10^7
DMSO	—	—	2.0×10^9
Pyridine	4.5×10^{11}	31.1	1.4×10^{13}

[a]The mole fraction is used as the concentration unit (see text).

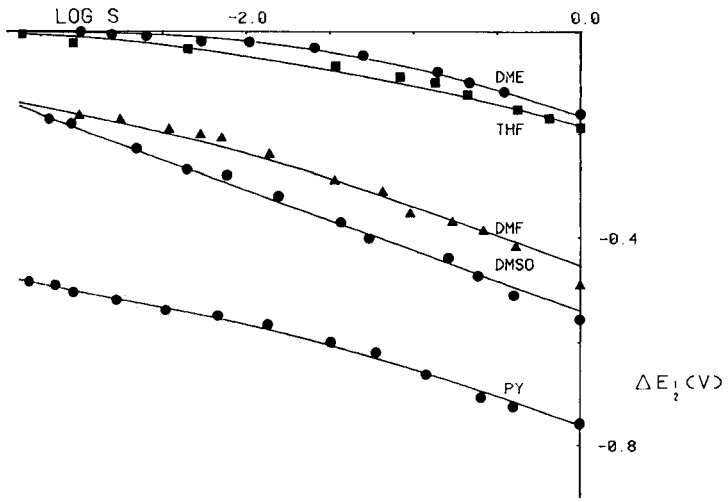

Fig. 2. Fit of the experimental points to the calculated curves.

In comparing the formation constants found here with those reported in the literature, it must be taken into account that the literature data are usually based on molarity as the concentration unit, whereas mole fractions are used here. No problem arises for K_1 in that K_1 is a dimensionless quantity in both cases; to make the K_2 values consistent, the sum of the molarities of all the species present in the solution may be used as the conversion factor. Few data are available in the literature; however, they appear to be in reasonable agreement with those found here. Only the K_1 value for THF (12.6 [12]) differs from the present value by more than one order of magnitude; this can probably be attributed to the different approaches used and to the presence in this work of the supporting electrolyte, which especially affects the measurements in solvents of lower polarity. For the K_1 values relevant to DMF (1.2×10^6 [12]) and to pyridine (2×10^{12} [13]), the agreement is better. Substantial agreement is observed also with the only available K_2 value (4 l mol^{-1} for pyridine [8]); in the mole fraction scale, this becomes about 50 when the conversion factor mentioned above is used.

Conclusions

The above findings emphasize that the strength of a base when it is used as solvent, i.e., the "bulk solvent basicity", differs from its "intrinsic basicity" (which is accounted for by K_1) by a term defining its ability to undergo hydrogen bonding (expressed by k_2). Consequently, basicity data cannot be applied indiscriminately to any experimental condition. Whether the "bulk solvent basicity" or the "intrinsic basicity" should be considered will depend on whether the solvent is used as the medium or as the basis titrant dissolved in another medium with little tendency to hydrogen bonding.

It must be noted, finally, that the formation constants found here may be affected by the presence of the supporting electrolyte. Moreover, in spite of the good agreement between the experimental results and Eqn. 7, all the simplifying assumptions required by this equation are expected to have a small but not negligible weight. Of course, the approach based on cyclic voltammetry can be applied only for polar organic solvents.

The authors thank C.N.R. (Rome) and the Ministry of Public Instruction for partial support. The financial aid of C.N.R., Project ELA, "Accumulo Elettrochimico" is gratefully acknowledged.

REFERENCES

1 I. M. Kolthoff, Anal. Chem., 46 (1974) 1992.
2 J. Emsley, Chem. Soc. Rev., 9 (1980) 91.
3 R. H. Stokes, Chem. Soc. Rev., 11 (1982) 257.
4 E. M. Arnett, E. J. Mitchell and T. S. S. R. Murty, J. Am. Chem. Soc., 96 (1974) 3875.
5 M. J. Kamlet and R. W. Taft, J. Am. Chem. Soc., 98 (1976) 377.
6 S. Kuna, Z. Pawlak and M. Tusk, J. Chem. Soc. Faraday Trans. I, 78 (1982) 2685 and references therein.
7 P. Ugo, S. Daniele, G.-A. Mazzocchin and G. Bontempelli, Anal. Chim. Acta, 173 (1985) 141.
8 J. F. Coetzee, G. R. Padmanabhan and G. P. Cunningham, Talanta, 11 (1964) 93.
9 V. Gutmann, Electrochim. Acta, 21 (1976) 661.
10 R. L. Benoit and C. Louis, in J. J. Lagowski (Ed.), The Chemistry of Nonaqueous Solvents, Vol. 5A, Academic Press, New York, 1978.
11 S. N. Deming and S. L. Morgan, Anal. Chem., 45 (1973) 278A.
12 I. M. Kolthoff and M. K. Chantooni Jr., J. Am. Chem. Soc., 95 (1973) 8539.
13 I. M. Kolthoff, M. K. Chantooni Jr. and S. Bhowmik, J. Am. Chem. Soc., 90 (1968) 23.

Analytica Chimica Acta, 173 (1985) 157—164
Elsevier Science Publishers B.V., Amsterdam — Printed in The Netherlands

GRAPHITIZED CARBON BLACK IN POLYETHYLENE AS AN ELECTROCHEMICAL SENSOR

ARNALDO LIBERTI and CINZIA MORGIA

Department of Chemistry, I University of Roma, La Sapienza, Rome (Italy)

MARCO MASCINI*

Department of Sciences and Chemical Technologies, II University of Roma, Tor Vergata, Roma (Italy)

(Received 8th January 1985)

SUMMARY

The electrochemical behaviour of a material obtained by moulding graphitized carbon black and polyethylene at 100—150°C is described. The material can be used as a pellet electrode in voltammetric procedures. As a tubular anode held in a teflon body, the material is valuable as a sensor for high-performance liquid chromatography. Its properties are comparable with those of glassy carbon with better signal-to-noise ratios. It is applied for the determination of several phenols, chlorophenols and hydroquinone in the low mg l^{-1} range or less.

Carbon materials are extensively used as electrodes in electroanalytical chemistry. Although glassy carbon has been used in very many applications, other products such as graphite, impregnated carbon and carbon paste have also been applied [1—5]. The outstanding properties exhibited by graphitized carbon black (GCB), a very homogeneous material which is widely applied in gas chromatography [6—8], suggested an examination of its use as an electrochemical sensor. If GCB is mixed with polyethylene powder and moulded at a temperature of about 120°C and a pressure of 10—15 atmospheres, the material can be obtained in any desired shape [9].

The polyethylene/graphitized carbon black (PGCB) electrode is attractive because it is easy to fabricate and machine and it is inexpensive; it can be used as a disposable electrode and discarded when it becomes fouled. The aim of this investigation was to evaluate the performance of polyethylene/graphitized carbon black electrodes for hydrodynamic voltammetry and to examine their suitability as an electrochemical sensor in high-performance liquid chromatography (h.p.l.c.).

EXPERIMENTAL

Preparation of electrodes

Graphitized carbon black was obtained as a fine powder (100 mesh; Supelco). Polyethylene (low density; Montedison, Milano, Italy) in powder

0003-2670/85/$03.30

form was mixed thoroughly with the GCB in several weight ratios (from 1:10 to 1:20), introduced into a suitable mould and moulded in a press at 10—15 atm. and 100—150°C. The pellet obtained was 4 mm in diameter and 3—8 mm in length.

For studies of electrochemical behaviour, the pellet was inserted into a polyethylene tube (7 mm external diameter, 4 mm internal diameter) and in another suitable mould with the same procedure the pellet was fixed at one end of the tube, providing a planar electrode as shown in Fig. 1(a). In order to obtain a tubular electrode for use in h.p.l.c., the pellet was drilled mechanically to give a bore in the range 0.4—1.5 mm. The pellet was introduced into a teflon holder as shown in Fig. 1(b).

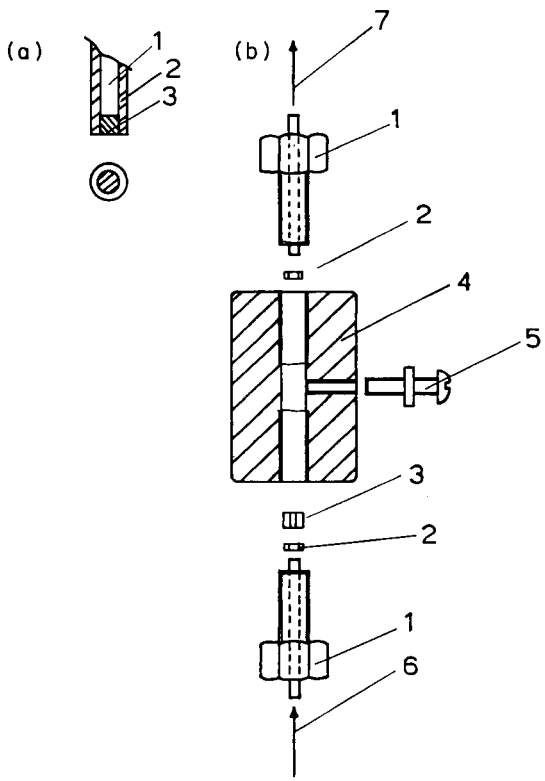

Fig. 1. Polyethylene/graphitized carbon black pellet electrodes. (a) Pellet fixed on the bottom of a polyethylene tube for characterization: (1) metal rod for contact; (2) polyethylene tube, 7 mm o.d., 4 mm i.d.; (3) PGCB pellet. (b) Pellet drilled and fixed in a tubular holder as a sensor for h.p.l.c.: (1) standard nut; (2) teflon spacers: (3) PGCB pellet drilled to give a bore of 0.4—1.5 mm; (4) teflon holder; (5) screw for contact; (6) from h.p.l.c. column; (7) to reference electrode.

Voltammetric procedures

The electrochemical behaviour was checked by comparing the performance of the pellet PGCB electrode with that of an analogous glassy carbon electrode (3 mm in diameter; Tokai Carbon Co., Tokyo, Japan).

The behaviour of the detector for h.p.l.c. was compared with that of a thin-layer glassy carbon cell (LC-17; Bioanalytical Systems, West Lafayette, IN 47907).

Voltammetric behaviour was studied with a Polarographic Analyzer Model 466 (Amel, Milano, Italy) equipped with an Amel Model 868 recorder. The linear-sweep mode was used in all studies.

The h.p.l.c. equipment consisted of a Perkin-Elmer pump connected to a standard stainless steel chromatographic column filled with Lichrosorb C8 (Merck) or Erbasil C18 (Carlo Erba, Milano). The flow rate was 1 ml min^{-1}. A Rheodyne Model 4125 rotary injection valve with a 20-μl injection loop was used. The electrochemical detector used was a model LC-4B (Bioanalytical Systems). The electrochemical cell was modified by inserting the tubular PGCB electrode as described above. The system was equipped with a Perkin-Elmer Model 561 recorder.

RESULTS AND DISCUSSION

Anodic voltammetry

Voltammetric curves obtained for hydroquinone (4.3×10^{-5} M) in 0.5 M sulfuric acid at a sweep rate of 20 mV s^{-1} with a glassy carbon electrode showed a pattern similar to that described by Gunasingham and Fleet [10]. Similar tests were run with hydroquinone concentrations of 0—4.3×10^{-5} M as shown in Fig. 2(a). It is worth observing that at zero concentration there is evidence for the existence on the glassy carbon surface of a species to which a quinoidal structure might be attributed from its oxidation pattern. This behaviour has been discussed by many authors [1—10]. Voltammograms obtained with PGCB electrodes under the same experimental conditions for hydroquinone concentrations of 0—7.5×10^{-5} M are shown in Fig. 2(b). No extra peaks are observed and, though the hydroquinone peak is less well defined than in the experiments with glassy carbon, reproducible results were obtained.

Voltammetry at the PGCB electrodes was found to be possible over a potential range of 0—2 V, which is much wider than the range available with glassy carbon (0—1 V). A higher electrochemical inertia can thus be attributed to this material. A point of major interest is obtained from Fig. 3, where the intensity of the current measured (nA) is plotted against the hydroquinone concentration. The plots for two PGCB electrodes of different sizes and one glassy carbon electrode are shown. The former plots have better correlation coefficients than the plot for the glassy carbon electrode and the plots with the PGCB electrodes start from the origin whereas the plot with the glassy carbon electrode does not. These results indicate that the PGCB surface does

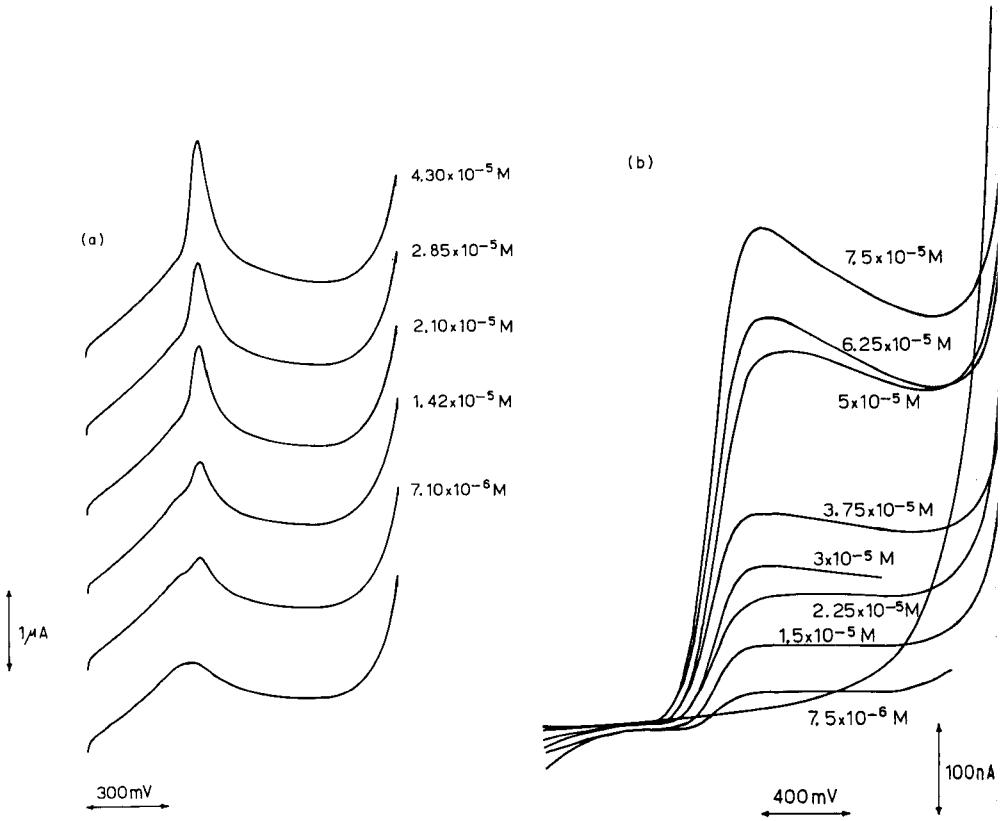

Fig. 2. Voltammetric curves for hydroquinone at different concentrations from 0 to 7.5 × 10^{-5} M: (a) on glassy carbon (0—1 V), scan rate 20 mV s^{-1}; (b) on PGCB (0—2 V), scan rate 20 mV s^{-1}.

not present species which might be oxidized and, as linear response is observed, that this material might be useful as a sensor in a flow-through cell. It is well known that polyethylene is stable in the organic solvents and mixed solvents often used as eluants in h.p.l.c.

The PGCB electrode as electrochemical detector in h.p.l.c.

The polyethylene/graphitized carbon black was examined for use as a sensor in h.p.l.c. A common configuration for an electrochemical detector in h.p.l.c. is a thin-layer cell with a glassy carbon electrode as anode. However, this can easily be replaced by a tubular anode [11] as described in Fig. 1(b). The tubular PGCB was forced into the teflon cavity and held in position with teflon spacers and flanged teflon tubes. The reference and counter electrodes (Ag/AgCl electrode and the stainless steel tube, respectively) were placed downstream in a similar teflon container.

The behaviour of the thin-layer cell with a glassy carbon electrode was compared with that of the tubular PGCB electrode by running hydrodynamic

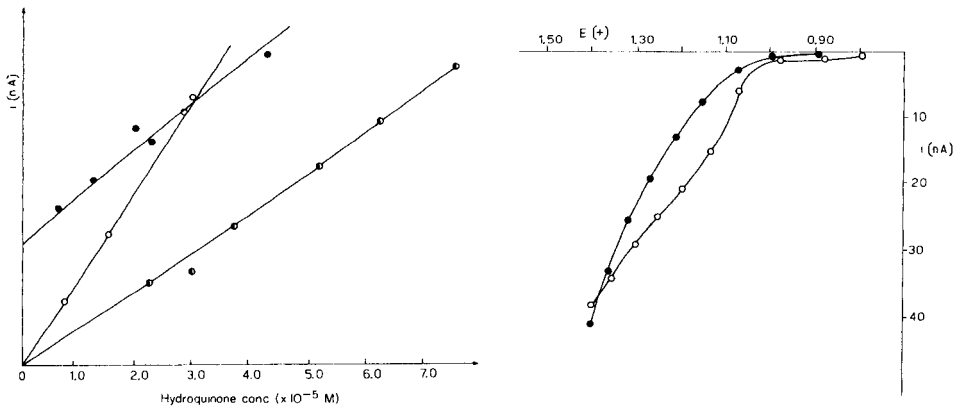

Fig. 3. Calibration plots for hydroquinone: (•) glassy carbon, correlation coefficient r = 0.98; (◐) 3-mm diameter PGCB electrode, r = 0.997; (○) 5-mm diameter PGCB electrode, r = 0.996.

Fig. 4. Hydrodynamic voltammograms for phenol (2 mg l^{-1}) obtained by using (•) PGCB and (○) glassy carbon as the detector in h.p.l.c. (Ag/AgCl reference).

voltammograms of various compounds. As an example, Fig. 4 shows the voltammograms for phenol obtained with aqueous 0.01 M phosphoric acid/acetonitrile (1:1) as eluent. In neither case was a plateau observed but the currents measured had similar values, becoming higher as the applied potential became more positive. The selected potentials were 1.1 V for the glassy carbon electrode and 1.2 V for the PGCB electrode (vs. Ag/AgCl).

It is of primary importance to evaluate the signal/noise ratio which provides a measure of the detection limits for these devices. As shown in Table 1, this ratio for the PGCB sensors is much higher than that for the glassy carbon sensor, but it is strongly affected by the length of the electrode and by the diameter of the hole through which the solution flows. The most favourable

TABLE 1

Signal/noise responses for various phenols with different anodes

Anode	Length/diameter (mm)	Signal/noise ratio[a]			
		Phenol	CP	DCP	PCP
Glassy carbon[b]	—	9	5	0.15	0.45
PGCB	3/0.8	30	22	20	5
PGCB	6/0.8	110	42	82	20
PGCB	8/0.8	60	24	45	11
PGCB	4/1	70	32	53	16

[a]Signal/noise ratios normalized to 1 mg l^{-1} concentrations for phenol, 2,4-dichlorophenol (DCP) and pentachlorophenol (PCP). [b]The BAS LC-17 cell.

TABLE 2

Detector response and elution order of halogenated phenols

Compound	Response (mm^2 ng^{-1})		Retention time (min)
	Glassy carbon	PGCB	
Phenol	1.00	1.00	2.6
p-Chlorophenol	0.36	0.165	3.4
2,6-Dichlorophenol	1.20	0.48	4.2
2,4-Dichlorophenol	0.94	0.71	4.5
3,4,5-Trichlorophenol	0.09	1.10	7.0
2,4,5-Trichlorophenol	0.14	1.60	6.4
2,3,4,6-Tetrachlorophenol	0.15	1.35	8.9
2,3,4,5-Tetrachlorophenol	0.12	0.34	9.6
Pentachlorophenol	0.19	0.75	13.8

results were obtained with a PGCB length of 6 mm and a bore of 0.8 mm diameter. The large increases obtained in the signal/noise ratios for some chlorophenols with the PGCB electrodes are remarkable. This effect is more readily appreciated from Table 2 in which response data are reported for a set of compounds; the signal is expressed as peak area (mm^2) per nanogram of each compound; all values are referred to phenol taken as standard. In several cases, the values obtained with the PGCB electrode are higher.

Artificial mixtures of phenol and chlorophenols were injected onto a reversed-phase Lichrosorb C8 column under the operating conditions outlined above. The results are shown in Fig. 5(a) and (b). The higher response of the PGCB electrode makes it possible to record signals for compounds in the low mg l^{-1} range or less.

The PGCB sensor is also suitable for the determination of other phenols; Fig. 6 shows the chromatogram for a mixture of cresol, pyrocatechol, and phloroglucinol.

The high sensitivity of the PGCB tubular anode for the determination of phenolic compounds suggested its application for the determination of this class of compounds in commercial samples of whiskies. Prior to chromatography, it was necessary to clean up the sample; in the procedure, 25 ml of the sample was adjusted to pH 12 by adding sodium hydroxide, evaporated to 5 ml and washed with dichloromethane. After acidification with 0.01 M phosphoric acid, the sample was injected onto the column. Some results are summarized in Table 3.

Conclusions

Graphitized carbon black can be moulded with polyethylene at 100—150°C under pressure to yield a material which has interesting properties for use as an electrochemical sensor in voltammetry. This material seems

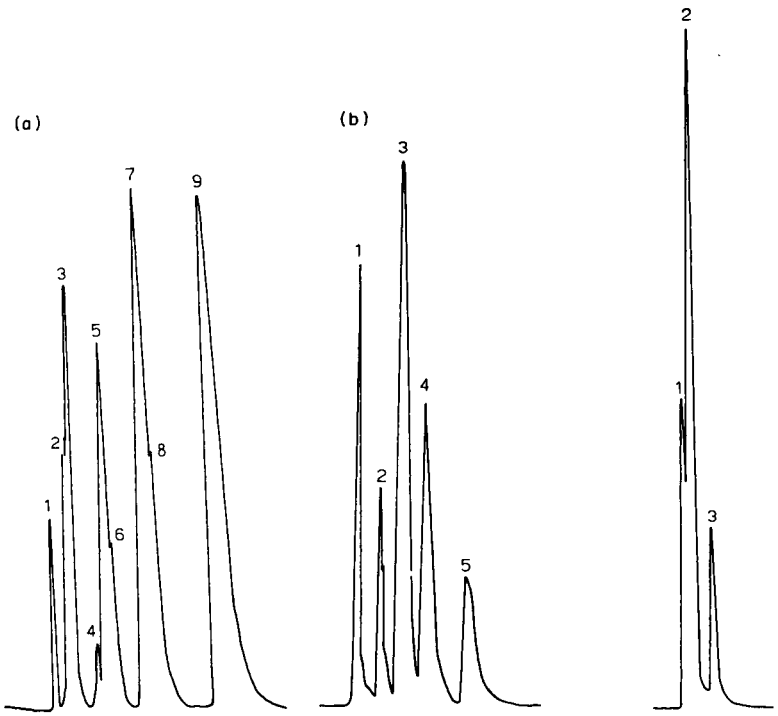

Fig. 5. Chromatograms of mixtures of phenols with the amperometric detector: (a) glassy carbon sensor; (b) PGCB sensor. Peaks in (a) with concentration injected in $\mu g\ ml^{-1}$: (1) *p*-chlorophenol, 2; (2) 2,6-dichlorophenol, 4; (3) 2,4-dichlorophenol, 8; (4) 3,4,5-trichlorophenol, 100; (5) 2,4,5-trichlorophenol, 40; (6) 2,4,6-trichlorophenol, 40; (7) 2,3,4,6-tetrachlorophenol, 40; (8) 2,3,4,5-tetrachlorophenol, 40; (9) pentachlorophenol, 40. Peaks in (b): (1) hydroquinone, 0.2; (2) *o*-cresol, 2; (3) 2,6-dichlorophenol, 4; (4) 2,3,4-trichlorophenol, 2; (5) 2,3,4,6-tetrachlorophenol, 2.

Fig. 6. Response of the PGCB sensor to a mixture of phenols, with concentrations injected in $\mu g\ ml^{-1}$: (1) phloroglucinol, 0.2; (2) pyrocatechol, 0.2; (3) *o*-cresol, 2.

TABLE 3

Determination of phenols in commercial whiskies

Brand	Concentrations found ($mg\ l^{-1}$)				
	Phenol	*o*-Cresol	*m*-Cresol	*p*-Cresol	*p*-Ethylphenol
Ballantines	0.06	0.15	—	0.04	2.35
J. and B.	0.08	0.06	0.01	0.03	2.00
Johnnie Walker	0.09	0.07	0.01	0.11	2.60

to be more inert than glassy carbon and yields a higher signal/noise ratio. A tubular electrode moulded from the material is useful as an anode in h.p.l.c. The behaviour of several compounds (phenol, chlorophenols and hydroquinone) indicates its advantages.

The PGCB electrode is attractive because it is easily prepared and cheap enough to be regarded as disposable when it becomes fouled.

REFERENCES

1 W. E. Van Der Linden and J. W. Dieker, Anal. Chim. Acta, 119 (1980) 1.
2 R. M. Wightman, E. C. Palk, S. Borman and M. A. Dayton, Anal. Chem., 50 (1978) 1410.
3 D. Armentrout, J. D. McLean and M. W. Long, Anal. Chem., 51 (1978) 1410.
4 D. E. Weisshaar, D. E. Tallman and J. L. Anderson, Anal. Chem., 51 (1981) 1809.
5 K. Stulik and V. Pacakova, J. Chromatogr., 208 (1981) 269.
6 F. Bruner, A. Di Corcia, G. Goretti and S. Zelli, J. Chromatogr., 76 (1973) 1.
7 G. Bertoni, C. Perrino and A. Liberti, Anal. Lett., 15(A12) (1982) 1039.
8 P. Ciccioli and R. Tappa, J. Chromatogr., 269 (1983) 47.
9 M. Mascini, F. Pallozzi and A. Liberti, Anal. Chim. Acta, 43 (1973) 126.
10 H. Gunasingham and B. Fleet, Analyst (London), 107 (1982) 896.
11 H. B. Hanekamp and H. J. Van Nieuwkerk, Anal. Chim. Acta, 121 (1980) 13.

Analytica Chimica Acta, 173 (1985) 165—175
Elsevier Science Publishers B.V., Amsterdam — Printed in The Netherlands

THREE-DIMENSIONAL HIGH-PERFORMANCE LIQUID CHROMATOGRAPHY BASED ON TIME-RESOLVED LASER FLUORIMETRY

KOUICHI ISHIBASHI, TOTARO IMASAKA and NOBUHIKO ISHIBASHI*
Faculty of Engineering, Kyushu University, Hakozaki, Fukuoka 812 (Japan)
(Received 7th October 1984)

SUMMARY

Microcolumn high-performance liquid chromatography is used for trace determinations of polynuclear aromatic hydrocarbons. The detector is a laser fluorimetric system with subnanosecond time resolution. The detection limit is 210 fg for perylene. In chromatography, the fluorescence decay curves are measured successively as the sample elutes by a microcomputer-controlled data-processing system. A three-dimensional chromatogram, in which retention times and delay times are displayed, is constructed after sample elution. A real sample extracted from airborne particulates is measured, and perylene, benzo(a)pyrene, and benzo(ghi)perylene are shown to be present.

Polynuclear aromatic hydrocarbons (PAHs) are produced mainly by combustion of fossil fuels from power plants and automobiles. Some of them are strongly carcinogenic and should be determined at ultratrace levels. High-performance liquid chromatography (h.p.l.c.) has been used extensively for practical applications in analysis of real samples. A laser fluorimetric detector is attractive because of its high sensitivity; the powerful radiation can be focused tightly into a small detector [1, 2]. Diebold and Zare [3] were the first to apply this technique to the determination of aflatoxins, using a continuous-wave He-Cd laser as light source and a flowing droplet instead of a detection cell. Recently, Joseffson et al. [4] determined 20 fg of fluoranthene, using an ultraviolet krypton laser and a flowing jet stream.

A fluorimetric detector based on a pulsed dye laser may be advantageous with respect to the wide tuning range and the capability of temporal discrimination of unwanted fluorescence from impurities. Richardson et al. [5] used a pulsed dye laser for the determination of PAHs in coal gasification studies. They could identify clearly the PAH species with long fluorescence lifetimes by using temporal resolution, and the limits of detection were reported to be 1—10 pg. In our previous work [6], a time-resolved fluorimeter with nanosecond resolution was constructed; the instrument consisted of a subnanosecond dye laser pumped by an atmospheric-pressure nitrogen laser, and was applied with a conventional h.p.l.c. system. It was used for the analysis of samples extracted from airborne particulates, and

0003-2670/85/$03.30

the time-resolved fluorimeter with a good time resolution was shown to be advantageous for efficient reduction of background emission [6]. Recently, Furuta and Otsuki [7] developed a h.p.l.c. system with a pulsed dye laser (pulse width of about 10 ns), which provided a sensitivity of 180 fg. They measured the content of PAHs in Lake Mashu and found the concentration of benzo(a)pyrene existing under natural conditions to be 7 pg l^{-1}.

Microcolumn h.p.l.c. has recently been developed [8, 9]. The resolution obtained with fused silica capillary columns is satisfactory even at high flow rates, so that the technique is advantageous for rapid resolution of the complicated samples [9]. Furthermore, the solvent consumption rate is very low, which is useful for routine purposes. However, it requires a very small detector with a volume of the order of nanoliters, otherwise the good resolution may be degraded. A fused silica capillary was used for the detector for this reason [4]. Hirschy et al. [10] used a flowing stream and could detect several femtograms of fluorescent dyes. Very recently, Zare [11] reported the application of laser fluorimetry to a microcolumn h.p.l.c. system with a capillary detector and achieved femtogram detection limits with a He-Cd laser.

In h.p.l.c., reliable assignment is achieved by clarifying the characteristics of the eluting component. The fluorescence technique is advantageous, because the sample species can be identified from both the excitation and fluorescence spectra. Time-resolved fluorimetry has an additional advantage. In our previous study, the chromatograms were measured several times at different delay times, and a three-dimensional chromatogram was constructed by superimposing these graphs [6]. This technique provided additional information concerned with the fluorescence lifetime of the sample, and the eluting component could be identified more reliably. But, this technique requires a long time to obtain a three-dimensional chromatogram, because the sample injection must be repeated several times for constructing the three-dimensional chromatogram.

In this study, a microcolumn h.p.l.c. system with a time-resolved laser fluorimetric detector is constructed and a microcomputer-controlled data-processing system is developed which allows the construction of the three-dimensional chromatogram after injection of a single sample. Based on three-dimensional chromatography combined with time-resolved fluorimetry, ultratrace analysis for PAHs and their reliable identifications are demonstrated. The analytical advantages of the proposed method are discussed.

EXPERIMENTAL

Apparatus

A block diagram of the equipment is shown in Fig. 1. The pumping source of the dye laser is a transversely-excited atmospheric-pressure (TEA) nitrogen laser (Nippon Dynamics, JH-500A). The dye laser is made with a quartz cuvette for conventional fluorimetry, and is operated without tuning optics; the output coupler is a quartz plate and the reflector is made of an

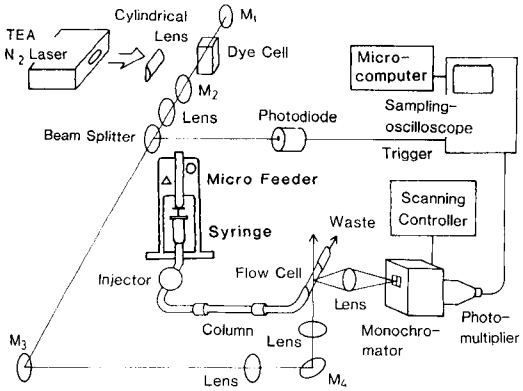

Fig. 1. Block diagram of the equipment; M indicates a mirror.

aluminum mirror. The laser dye used was 4,4''''-bis(butyloctyloxy)-*p*-quaterphenyl (BBQ), which was dissolved in a mixture of ethanol and toluene (1:1). The output power and the oscillating wavelength of the dye laser was 0.1 mJ and 386 nm, the average power being ca. 1 mW. The pulse-to-pulse variation in the pulse energy of the dye laser was 50%. The dye laser beam is split by a quartz plate, and the reflected pulse is detected by a photodiode to provide a trigger pulse for a sampling oscilloscope (Iwatsu, SS 601B, 6 GHz). The transmitted laser beam is focused by an objective lens for a microscope (Nikon, M4) into a flow cell, which is made of a fused silica capillary. The polyimide coating on the capillary was burned off by using a gas flame [4]. Fluorescence from the sample is focused by a lens (Nikon, M10) and passes through a special mask to reduce scattered emission from the surface of the capillary. The monochromator (Jasco, CT-10, dispersion 8 nm mm^{-1}) is equipped with a microchannel plate photomultiplier (Hamamatsu Photonics, R1294U-01); the dynode bias-resistance network including capacitors is installed in the photomultiplier housing. The applied voltage was typically 3000 V. In this condition, no saturation effect was observed, and the signal intensity was proportional to the fluorescence intensity. The signal is measured by the sampling oscilloscope (aperture width 60 ps). The output analog signal was amplified 10 times by a home-made amplifier and was displayed on a strip-chart recorder or introduced into the analog input interface of a microcomputer (NEC, PC9801) for data acquisition and processing. The results were drawn by a plotter (Watanabe, WX4671) controlled by the microcomputer. The time resolution of the instrument was less than 1 ns.

The h.p.l.c. pumping system is assembled from a micro feeder (Azuma-denki Kogyo, MF-2) with a 250-μl gas-tight syringe (Terumo, MS-GAN025). The typical flow rate of solvent was 2—3 μl min^{-1}. The stability of the flow rate was not always adequate and the retention times varied slightly with column conditions. A micro loop injector (Jasco, ML-422, 300 nl) was modified for use in the microcolumn h.p.l.c. system, and gave an injection

volume of 57 nl. The separation column was made of a fused silica capillary with an inner diameter of 0.35 mm and a length of 100 mm. Fine SIL C_{18}-5 (Jasco, ODS, 5 μm) was used as packing material. The column was prepared by the procedure recommended earlier [9].

Data processing

The three-dimensional chromatogram was constructed by displaying the fluorescence intensity against the retention time and the delay time. The laser was operated at a repetition rate of 20—30 Hz, and the fluorescence decay curve was recorded successively as the sample eluted. The data were stored during the measurement in the memory of the microcomputer. Data with the same delay times were combined after all the components had eluted, and a chromatogram was constructed. This procedure was repeated sequentially by the microcomputer and the three-dimensional chromatogram was displayed by the plotter. Thus, 15 chromatograms were displayed in a graph. For recording a decay curve, 15 data points at the specified retention time were combined and displayed by the plotter. The signal-to-noise (S/N) ratio of the chromatogram was improved by five-point data smoothing, and this procedure was repeated a few times, unless the chromatographic resolution became poor. A semilog plot of the decay curve was also displayed. Multicomponent analysis and calculation of the fluorescence lifetimes were done by the microcomputer.

For recording two-dimensional chromatograms, the dye laser was operated at a repetition rate of 1 Hz, and the fluorescence intensity was measured at a specified delay time. For recording a time-resolved fluorescence spectrum, the flow of solvent was stopped for a moment by a 6-way loop injector valve (Gasukuro Kogyo, MPV-3), and the fluorescence intensity was measured at a specified delay time by scanning the wavelength of the monochromator.

Reagents

Perylene, benzo(k)fluoranthene, benzo(a)pyrene, and benzo(ghi)perylene were obtained from Wako Chemicals. The PAH samples from airborne particulates and from solvent-refined coal were gifts. The methanol solvent (Kishida Chemical Co.), specified for use in h.p.l.c. was used as received. The water was doubly distilled and deionized. Oxygen dissolved in the solvent and the sample was removed by bubbling with nitrogen and by further treatment with ultrasonic agitation (Yamato, Brasonic 12).

RESULTS AND DISCUSSION

Sensitivity

In order to optimize the experimental conditions, the S/N ratio of the chromatograph peak was plotted against the delay time by using the standard PAH samples. The S/N ratio immediately after excitation was very poor because of the large background. The samples with short lifetimes

such as perylene or benzo(k)fluoranthene gave optimum delay times at around 6 ns. The optimum values were 10 ns for samples with long lifetimes such as benzo(a)pyrene and benzo(ghi)perylene. At sufficient times after excitation, the S/N ratio again decreased with increasing delay times, because the signal intensity of the sample decreased.

The detection limits achieved with the present instrument are listed in Table 1. These detection limits are apparently lower than those obtained with the h.p.l.c. system and a conventional fluorimetric detector based on a lamp excitation source. A similar detection limit (180 fg) has already been reported for a conventionally sized h.p.l.c. system with a fluorimetric detector based on high average power (15 mW) and a pulsed dye laser (10 ns) [7]. But, it should be emphasized that the present results were achieved with a very low laser power (1/15) and a low solvent flow rate (1/320) so that the system described here is more practical and versatile. Moreover, the proposed time-resolved fluorimetric system with subnanosecond resolution can be applied to the determinations of various organic substances with nanosecond fluorescence lifetimes such as drugs and metabolites. It may be noted that a large detector can be used for a conventionally sized h.p.l.c. system, and background fluorescence from the window material of the detector cell can then be more effectively removed by optical masks. A similar approach was difficult for the detector used in microcolumn h.p.l.c. A few techniques have recently been developed to reduce background emission even for the micro flow cells [12, 13], but they are complicated and were not used in this study.

In order to clarify the source of background, a time-resolved emission spectrum of the empty fused silica capillary used as the detection cell was measured. Immediately after excitation, scattered emission was dominant in the time-resolved fluorescence spectrum, whereas impurity fluorescence predominated long after excitation. The semilog plot of the decay curve indicated that the decay time of the impurity fluorescence was 3.1 ns. Two types of fused silica capillaries, which had purities of 99.99 and 99.9999%, were tested, but no appreciable difference was observed in the background intensities. Impurity fluorescence seems to originate from organic compounds formed on burning off the polyimide coating. Several ideas were

TABLE 1

Detection limits for PAH measured by microcolumn h.p.l.c.

Sample	Wavelength (nm)	Delay time (ns)	Detection limit (fg)
Perylene	443	6	210
Benzo(k)fluoranthene	420	6	290
Benzo(a)pyrene	430	10	500
Benzo(ghi)perylene	420	10	2600

tried to remove impurities on the surface of the fused silica capillaries, but they were unsuccessful. When methanol was introduced into the fused silica capillary, large background was observed at around 430 nm, which was due to Raman scattering of methanol. The Raman band was broadened because of the untuned optical configuration of the dye laser. A narrow-band dye laser is more useful for efficient reduction of unwanted scattered emission. Other solvents such as acetonitrile/water are frequently used for chromatographic separation, but acetonitrile seems to provide many Raman bands because of the large number of vibrational freedoms. Though background emission can be reduced compared to the signal by time-resolved fluorimetry, the maximum rating of the input voltage of the sampling oscilloscope was limited to 4.5 V. Therefore, the wavelength of the fluorescence monochromator should be carefully adjusted to the optimum value to give a low background signal even at $t = 0$. In the present system, the S/N ratio was limited by the drift of the sampling oscilloscope because of the limited capability in the maximum rating of the input voltage. A boxcar integrator consisting of a gated electronic circuit with a large maximum rating or a gated photomultiplier may be more useful for discrimination against the background signal.

Two-dimensional chromatography

A two-dimensional chromatogram of a standard sample containing perylene (120 pg), benzo(k)fluoranthene (180 pg), benzo(a)pyrene (1.8 ng), and benzo(ghi)perylene (13 ng) is shown in Fig. 2. Three peaks are resolved on

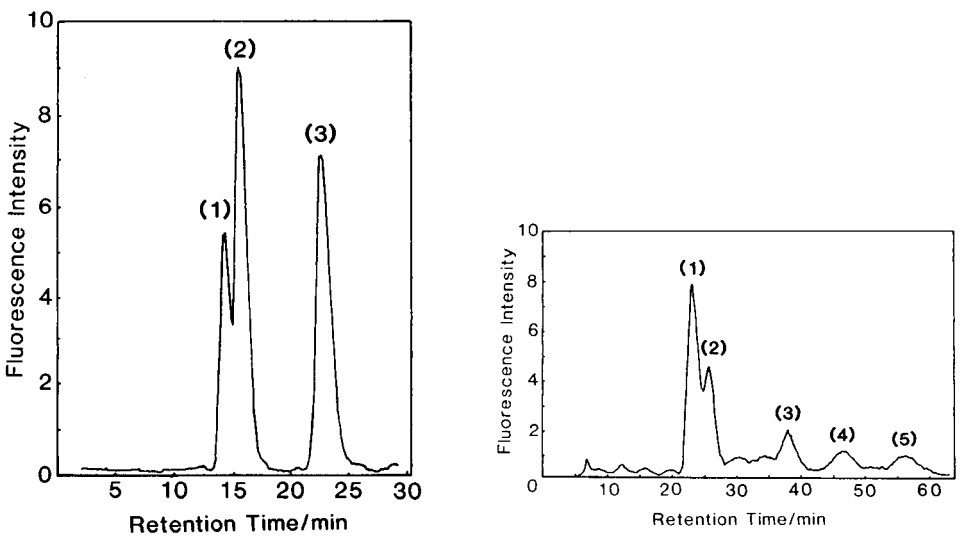

Fig. 2. Chromatogram of standard sample: (1) perylene and benzo(k)fluoranthene; (2) benzo(a)pyrene; (3) benzo(ghi)perylene. Flow rate 2.6 μl min^{-1}, λ_{ex} = 386 nm, λ_{em} = 430 nm, methanol:water = 9:1, delay time = 0 ns.

Fig. 3. Chromatogram of the sample extracted from airborne particulates. Flow rate 2.0 μl min^{-1}, delay time = 5 ns; other conditions were identical to those for Fig. 2.

the chromatogram. Peaks 2 and 3 are due to benzo(a)pyrene and benzo(ghi)-perylene, respectively. However, perylene and benzo(k)fluoranthene have similar retention times (ca. 14 min), and could not be resolved on the chromatograms. The peak resolution seems to be limited partly by the use of the methanol/water solvent instead of acetonitrile/water and partly by the dead volume in the tubing. Twofold better resolution (7000 theoretical plates) has been achieved elsewhere [9].

Figure 3 shows a chromatogram of the sample extracted from airborne particulates. In recording this chromatogram, the delay time was adjusted to 5 ns to remove scattered emission. Peak 1 may be assigned to perylene and/or benzo(k)fluoranthene. Peaks 2 and 3 seem to be due to benzo(a)-pyrene and benzo(ghi)perylene, respectively. No other standard compounds were measured in this study, so that peaks 4 and 5 remain unassigned. In two-dimensional chromatography, assignment is possible only by comparison of the retention times with those of standards. Therefore, further qualitative information is not available, unless a fluorescence spectrum is measured by stopping the flow of the h.p.l.c. system.

Three-dimensional chromatography

The above standard mixture of PAHs including perylene, benzo(k)fluoranthene, benzo(a)pyrene, and benzo(ghi)perylene, was injected into the h.p.l.c. system. The three-dimensional chromatogram obtained is shown in Fig. 4. Three peaks are apparent in the chromatogram as in the case of two-dimensional chromatography. When the fluorescence decay curve was measured for peak 1, a double exponential decay was observed. From the semilog plot of the decay curve, the shorter component was found to have a lifetime of 3 ns, the longer component being 11 ns. These components are identified as perylene and benzo(k)fluoranthene from the fluorescence lifetimes. The components providing peaks 2 and 3 have fluorescence lifetimes of 18 ns and 25 ns, which can be attributed to benzo(a)pyrene and benzo(ghi)perylene, respectively, from both the retention time and the fluorescence lifetime. It should be noted that the eluting solvent and the sample were thoroughly deaerated by bubbling with nitrogen and by ultrasonic agitation. But, sample fluorescence is partially quenched by oxygen dissolved in the solvent, which seems to be due to penetration of oxygen through the teflon tubing of the h.p.l.c. system. The use of the stainless steel tubing may be necessary to remove this effect.

Real samples

A three-dimensional chromatogram of the sample extracted from airborne particulates is shown in Fig. 5. Five components are observed in the chromatogram. The S/N ratio of the chromatogram is relatively poor, which is partly due to large fluctuations in the output power of the nitrogen laser by increasing the repetition rate and partly because of the weak fluorescence from the sample. A single exponential decay (τ = 8.6 ns) was ob-

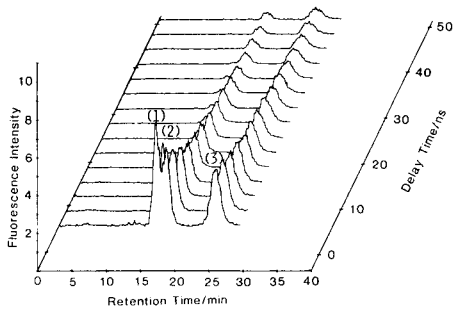

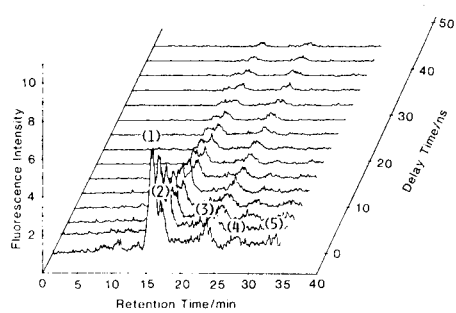

Fig. 4. Three-dimensional chromatogram of standard sample. Flow rate 2.7 μl min^{-1}; other conditions were identical to those for Fig. 2.

Fig. 5. Three-dimensional chromatogram of the sample extracted from airborne particulates.

served for peak 1, and fitting to a double exponential curve was difficult because the S/N ratio of the decay signal was poor. Perylene and benzo(k)-fluoranthene are considered to be present at this retention time. The electronic system for compensation of laser intensity variation is currently used in a dual-channel boxcar integrator system, and it might be useful to reduce noise and to resolve these components by multicomponent analysis. The use of a transient digitizer (ca. 1 GHz) combined with a signal averager may be an alternative approach to measuring the decay curve with good precision. Peak 2 provided a single exponential decay (16 ns), and was assigned to benzo(a)pyrene. A single exponential decay (24 ns) was also observed for peak 3, which was thus attributed to benzo(ghi)perylene. It is noteworthy that the proposed method allows direct identification from the fluorescence lifetime as well as the retention time. Then, it is more reliable and useful for peak assignment. Though peak 4 could not be assigned, this component was found to have a lifetime of 14 ns. If the fluorescence lifetimes were measured for many PAHs, this peak could readily be estimated from their list. Peak 5 was too weak for the fluorescence lifetime to be evaluated.

In this study, assignments were also made by measuring the time-resolved fluorescence spectrum by stopping the flow of the h.p.l.c. system. For peak 1, the fluorescence spectrum measured immediately after excitation was identical to that of perylene, so that the existence of perylene was obvious. However, the spectrum recorded at an appropriate time after excitation was not exactly identical to that of benzo(k)fluoranthene, so that the existence of benzo(k)fluoranthene was not confirmed definitely. The temporal behavior of the fluorescence spectrum for peak 2 was similar to that of benzo(a)pyrene. The time-resolved fluorescence spectrum for peak 3 is shown in Fig. 6. The spectrum measured at an appropriate time after excitation for the real sample is similar to that of the standard sample, which confirms that benzo(ghi)perylene is contained in the sample. How-

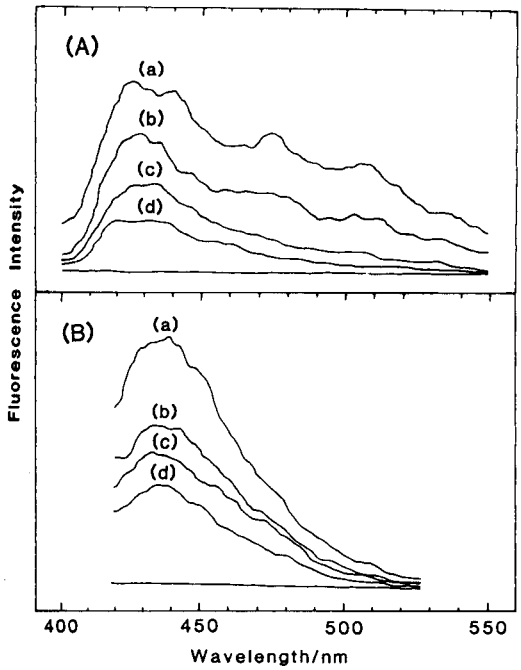

Fig. 6. Time-resolved fluorescence spectra measured at peak 3 of Fig. 5; (A) the sample extracted from airborne particulates; (B) standard sample of benzo(ghi)perylene. Delay time: (a) 5 ns; (b) 10 ns; (c) 20 ns; (d) 30 ns.

ever, peaks are observed on the spectrum at 475 nm and 510 nm immediately after excitation, so that other components with short lifetimes might be superimposed. These compounds do not appear in the chromatogram shown in Fig. 5, because it was measured at a fluorescence wavelength of 430 nm where the other components are not dominant. It should be emphasized that other spectrometric methods for measuring the absorption or fluorescence spectrum have no capability to resolve components when their retention times are identical. In contrast, time-resolved fluorimetry can separate and identify the components by monitoring the fluorescence spectrum at different delay times. Chromatograms of the solvent-refined coal sample obtained from a coal liquefaction plant were also measured by the present system. Although the components included in this sample could not be resolved fully by the column used, perylene, benzo(k)fluoranthene, benzo(a)pyrene, and benzo(ghi)perylene were found not to be present in this sample. The unresolved compounds had an average lifetime of 17 ns.

Comparison with other three-dimensional chromatographic systems

A few other types of three-dimensional chromatography are already known. A multichannel absorption detector consisting of a monochromator equipped with a photodiode array allows successive recordings of the absorp-

tion spectrum as the sample elutes. This sort of three-dimensional chromatography is not sensitive, because it is based on absorption spectrometry. However, it requires only small and cheaper components, and several commercial instruments are already available [14]. The technique is currently used in practical analysis of environmental and biochemical samples. A videofluorimeter could also be used for this purpose. For sensitive detection, an optical multichannel analyzer may be advantageous for recording a fluorescence spectrum with high sensitivity, though it is more complicated. Such analyzers are advantageous for reliable assignment of sample components because of the data available for the excitation and fluorescence spectra. However, such three-dimensional chromatography provides only limited performance in multicomponent analysis, because the shape of the spectra is strongly affected by the superimposed impurity bands.

Three-dimensional chromatography based on laser-induced time-resolved fluorimetry has several advantages. First, the laser beam can be tightly focused into a very small detector so that a very small sample cell can be used, which is essential for microcolumn h.p.l.c. Secondly, sensitivity of detection is superior than that of conventional h.p.l.c. even when a dye laser with a very low average power is used as the excitation source. Thirdly, the three-dimensional display allows visual selection of the optimum chromatogram which gives the largest S/N ratio, and time-resolved fluorimetry is useful for the reduction of scattered emission and of short-lived impurity fluorescence. The number of the components included under the chromatographic peak can be clarified by multicomponent analysis of the decay curve when the fluorescence lifetimes of the components are sufficiently different. The eluted components might be identified from the data on fluorescence lifetimes without using the retention times given for the used column, though such assignments would require fluorescence lifetime tables for many samples.

Finally, it should be emphasized that the present approach based on an atmospheric-pressure nitrogen-laser-pumped dye laser is practical because of its versatile performance, low cost, and small dimensions. Unfortunately, the stability and reliability of the laser are not very good, as yet, and radio-frequency interference noise could be more effectively reduced. These, however, are problems that could be solved for use in commercial instrumentation.

The authors thank Toyohide Takeuchi and Daido Ishii of Nagoya University for their suggestions and cooperation in preparation of the separation column and in modification of the sample injector. We also thank Yosuke Maekawa of the Governmental Industry Development Laboratory, Hokkaido, for a gift of solvent-refined coal and thank Kazumi Fukamachi of Fukuoka Environmental Research Center for a gift of the real PAH sample extracted

from airborne particulates in Omuta City. This research was supported by a Grant-in-Aid for Environmental Science and for Co-operative Research from the Ministry of Education, Science and Culture of Japan.

REFERENCES

1 E. S. Yeung and M. J. Sepaniak, Anal. Chem., 52 (1980) 1465A.
2 R. B. Green, Anal. Chem., 55 (1983) 20A.
3 G. J. Diebold and R. N. Zare, Science, 196 (1977) 1439.
4 S. Folestad, L. Johnson and B. Josefsson, Anal. Chem., 54 (1982) 925.
5 J. H. Richardson, K. M. Larson, G. R. Haugen, D. C. Johnson and J. E. Clarkson, Anal. Chim. Acta, 116 (1980) 407.
6 T. Imasaka, K. Ishibashi and N. Ishibashi, Anal. Chim. Acta, 142 (1982) 1.
7 N. Furuta and A. Otsuki, Anal. Chem., 55 (1983) 2407.
8 M. Novotny, Anal. Chem., 53 (1981) 1294A.
9 T. Takeuchi and D. Ishii, J. Chromatogr., 213 (1981) 25.
10 L. Hirschy, B. Smith, E. Voigtman and J. D. Winefordner, Anal. Chem., 54 (1982) 2387.
11 R. N. Zare, Science, 226 (1984) 298.
12 K. H. Milby and R. N. Zare, unpublished results.
13 N. J. Dovichi, J. C. Martin, J. H. Jett and R. A. Keller, Science, 219 (1983) 845.
14 S. A. Borman, Anal. Chem., 55 (1983) 836A.

Analytica Chimica Acta, 173 (1985) 177—183
Elsevier Science Publishers B.V., Amsterdam — Printed in The Netherlands

ANALYSIS OF COMMON FATTY ACID GLYCERIDES BY GAS CHROMATOGRAPHY

DENNIS A. BRENGARTNER
Owens-Illinois, Inc. One SeaGate, Toledo, OH 43666 (U.S.A.)

(Received 19th December 1984)

SUMMARY

A method is described for the determination of 25 common fatty acid mono-, di-, and triglycerides and their components and mixtures by packed-column gas chromatography after isolation and derivatization. The method is applied to two commercial materials, a polypropylene resin and a hand lotion. The glycerides along with glycerol and free fatty acids are first separated from the host by refluxing with 2-propanol containing an internal standard. The extract is derivatized and the compounds are identified and measured by gas chromatography. The chromatograms show sharp peaks, unique retention times and reproducibility in the range of 2—5%. Several positional isomers of the fatty acid glycerides were tested but found not to be resolved under the conditions used. Optical isomers and *cis-trans* isomers of unsaturated acids were not tested.

Glycerol, free fatty acids, and their ester combinations as mono-, di-, and triglycerides are widely used additives in the cosmetic, food and packaging industries. The various species are derived from the hydrolysis of animal and vegetable products which yield complex mixtures that may be used directly or may be further purified. It was necessary to develop a simple yet general method which would supply information about this class of compounds in both the package and the product that it contained. Fatty acid glycerides may be added to polyolefin resins in order to modify their handling properties. The fatty acid glycerides migrate to the surface of the plastic article where they function as lubricants and static-charge reducers (antistats). Knowledge of the fatty acid glycerides content in the package permits the correlation of the type and concentration of various fatty acid glyceride additives with changes in product performance. Knowledge of the fatty acid glycerides in the product permits the assessment of product composition and product/package interactions

It was necessary to resolve several major complications in order to develop a general analytical method for fatty acid glyceride components in a food packaging matrix. Specifically, (a) the polarity range is great; (b) the molecular weights range from 92 (glycerol) to 891 (glycerol tristearate); (c) there are isomers of the fatty acids and also fatty acid glycerides; (d) the real materials consist of mixtures of fatty acids rather than a single species; and (e) the isolation of the glyceride components from the matrix may be

0003-2670/85/$03.30

difficult. As a specific example, glycerol monostearate (GMS) is a common commercial material used as an antistatic ingredient in polyolefins. A commercial GMS sample was found to contain glycerol-1- and -2-monostearate in addition to two glycerol distearate isomers. The fatty acid portion of the material was about two-thirds stearic acid and one-third palmitic acid, with a small amount of myristic acid. Each acid may have a distribution of glyceride isomers similar to that of stearic acid. Mixed-acid esters, free acids, and free glycerol may also be present.

The general analytical approach chosen was the extraction of the glycerides and related species followed by derivatization and packed-column gas chromatography. Gas chromatographic methods for the determination of fatty acid glycerides have appeared in the literature but have not included all the species of interest [1, 2]. Methods based on capillary columns have been shown to give superior resolution [3, 4] but are not as widely used as those based on packed columns. The gas chromatographic conditions used here are similar to those reported by Sϕe [4] and provide acceptable separations of all of the species of interest.

This paper reports the separation and determination of 25 fatty acid glycerides and related materials. The species were isolated from the host material by refluxing in 2-propanol where necessary. The extract was treated with bis(trimethylsilyl)trifluoroacetamide (BSTFA) catalyzed with 1% trimethylchlorosilane to make the trimethylsilyl (TMS) derivatives. This step converted the fatty acid glycerides to the corresponding TMS ethers for gas chromatography (g.c.). The triglycerides did not appear to react with BSTFA under the conditions used (with the exception of glycerol tristearate) and could be identified and measured in a derivatized or underivatized solution. The chromatogram of the underivatized solution was obtained in all cases to check for interferences.

EXPERIMENTAL

Reagents

The glycerol, fatty acids, and fatty acid glycerides used were the best obtainable grades from several laboratory supply houses and were used without further purification. A solution of 1% trimethylchlorosilane in BSTFA was used as the derivatizing agent. The internal standard used was glycerol trioctanoate. The 2-propanol, chloroform (stabilized), and pyridine solvents used were ACS reagent grade or better.

Sample preparation

The extraction solvent, 2-propanol, was selected for its intermediate polarity and its use in the extraction of other polymeric additives [5]. It is a poor solvent for polyolefin oligomers and a satisfactory solvent for all species encountered in this work. An accurately weighed sample containing less than 100 mg of glycerides was placed in a 50-ml Erlenmeyer flask with

a 25-ml portion of 2-propanol containing 4.1 mg of the glycerol trioctanoate internal standard. Water-soluble or dispersible samples (some foods, cosmetics) were simply shaken to homogenize them. Polyolefin samples were first ground to −20 mesh, a boiling chip was added, and the sample was refluxed for 2 h. The sample was then filtered through Whatman No. 41 paper. The flask and solids were washed with a small volume of chloroform to dissolve high levels of triglycerides if present. The filtrate was immediately taken just to dryness on a hot water bath (to minimize the contact time with 2-propanol) if the sample were to be stored prior to derivatization. The dried sample was then taken up in 5 ml of 1 + 1 pyridine/chloroform. Samples for immediate treatment were derivatized directly in 2-propanol.

Derivatization and gas chromatographic conditions

Each solution was derivatized by placing 10 μl of the solution into a 2-ml crimp-top vial and adding 100 μl of the derivatizing reagent. A 50-μl portion of chloroform was added as a cosolvent for triglycerides. The vial was sealed and heated to 80°C for 10 min.

The g.c. column was selected for its ability to separate materials with large differences in volatility. The column packing used was 1% Dexsil 300 on 100/120 mesh Supelcoport in either glass or glass-lined stainless steel tubing (0.5 m long, 2 mm i.d.). The temperature program used for the most versatile conditions was a 4-min hold at 50°C followed by programming at 10°C per minute up to 380°C. Variations in the temperature-program conditions were used in cases where the highest or lowest boiling components were not to be quantified. The injector and detector temperatures were 340 and 410°C, respectively. A Varian Model 3700 gas chromatograph with a flame ionization detector was used. Helium at 30 ml min^{-1} was used as the carrier gas. A Hewlett-Packard Model 3390A integrator was used to collect data.

A Finnigan Model 4021 gas chromatograph/quadrupole mass spectrometer was used to confirm selected chromatographic peak identities. The instrument was operated in the electron-impact mode using the identical g.c. column and similar conditions.

Verification of experimental conditions

Several experiments were done to verify the suitability of the proposed experimental conditions. No further recovery of glyceride species was found by a second extraction with refluxing chloroform. There was no degradation of the internal standard during the extraction procedure. Also, no changes in response factors were observed by increasing the amount of derivatizing reagent or the reaction time at 80°C. The internal standard in the presence of the derivatizing reagent was stable for at least 24 h. The internal standard solution was stable for at least two weeks under refrigeration. The derivatized glycerides, glycerol, and free fatty acids were stable for at least 8 h. Glycerol tristearate was not stable in the derivatizing solution and was deter-

mined along with the other triglycerides without derivatization. The standard solutions in underivatized form in pyridine or pyridine/chloroform were stable for at least two weeks under refrigeration.

Glycerol, free fatty acids, and the available fatty acid glycerides were prepared as individual solutions at levels of 1 to 10 mg ml^{-1}. Triglyceride solutions were prepared in (1 + 1) 2-propanol/chloroform because of their limited solubility in cold 2-propanol. The solutions were chromatographed without derivatization to locate the peak positions of the underivatized species and impurities. Gas chromatography/mass spectrometry was used to verify the identity of selected peaks.

RESULTS AND DISCUSSION

Figure 1 shows the chromatograms obtained from a reference mixture of glycerides and related species before and after derivatization, respectively. The chromatograms were typical of those obtained in this work. The peaks were sharp and sufficiently well separated for accurate quantitation over the entire temperature range.

Table 1 lists the absolute and relative retention times of the species examined. The values given are for the derivatized form except for the tri-

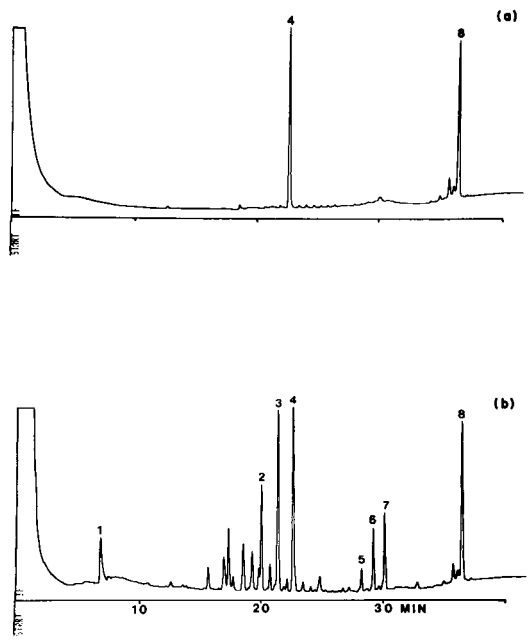

Fig. 1. Chromatograms of reference mixtures of glycerides: (a) underivatized; (b) derivatized. Peaks: (1) glycerol, (2) glycerol monopalmitate, (3) glycerol monostearate, (4) glycerol trioctanoate (internal standard), (5) glycerol dipalmitate, (6) glycerol palmitostearate, (7) glycerol distearate, (8) glycerol tristearate.

TABLE 1

Retention times (t_R) and relative retention times for glycerides

Species	t_R (min)	Rel. t_R [a]	Species	t_R (min)	Rel. t_R [a]
Glycerol	5.9	0.26	Glycerol-1,3-dipalmitate	28.3	1.25
Lauric acid	11.3	0.50	Glycerol dioleate	29.9	1.32
Myristic acid	13.4	0.59	Glycerol-1,2-distearate	30.1	1.33
Palmitic acid	15.2	0.67	Glycerol-1,3-distearate	30.1	1.33
Oleic acid	16.8	0.74	Glycerol palmitostearate	29.2	1.29
Stearic acid	17.0	0.75	Glycerol trilaurate[b]	29.4	1.30
Glycerol monolaurate	16.8	0.74	Glycerol trimyristate[b]	32.1	1.42
Glycerol monomyristate	18.3	0.81	Glycerol tripalmitate[b]	34.6	1.53
Glycerol monopalmitate	19.9	0.88	Glycerol trioleate[b]	36.7	1.62
Glycerol monooleate	20.8	0.92	Glycerol-1,3-dipalmitate-2-stearate[b]	35.3	1.56
Glycerol monostearate	21.3	0.94			
Glycerol trioctanoate	22.6	1.00	Glycerol-1,3-distearate-2-palmitate[b]	36.0	1.59
Glycerol dilaurate	23.8	1.05			
Glycerol dimyristate	26.0	1.15	Glycerol tristearate[b]	36.7	1.62
Glycerol-1,2-dipalmitate	28.1	1.24			

[a]Relative to glycerol trioctanoate internal standard. [b]Not derivatized.

glycerides which do not form TMS derivatives under these conditions. Relative retention times are given against the glycerol trioctanoate internal standard as the time reference. The internal standard has a retention index of 31.5 in the Kovats system [6]. Small differences in retention times were observed (Table 1) for selected positional isomers. These differences were considered to be too small to be of practical use in differentiating the species. Capillary g.c. and/or g.c./m.s. should be used if it is necessary to distinguish the positional isomers. Optical isomers and *cis-trans* isomers of unsaturated acids were not tested.

The overall precision of the method was within 10% of the average value for all species. This value included all sampling, preparation, derivatization and gas chromatographic steps. Standard additions were made and recovered within this value also. The accuracy of the method is thus expected to be within 10% of the true value. No better statement of accuracy can be made because standard samples were not available for testing, and because the method of standard additions is not proof of recovery for complex samples such as an intimate mixture of glycerides and polypropylene. The gas chromatographic sensitivity differed for the various species, but in all cases, submicrogram quantities were readily measurable.

When the derivatization procedure described above was used, derivatization appeared to be complete at the end of 10 min. With the exceptions of glycerol distearate and glycerol tristearate, the derivatized species were stable for at least 8 h. For glycerol distearate, the peak area increased by about 1.5 fold after 8 h while the area decreased to about 50% of the

original value for glycerol tristearate during the same period and was not reproducible. Two problems were apparent when glycerol tristearate was present in the derivatizing solution. First, a transesterification took place as evidenced by the drop in the glycerol tristearate peak and accompanying increase in the glycerol distearate derivative peak. Second, the glycerol tristearate had limited solubility in the polar derivatization solvent. A solid phase, rich in glycerol tristearate, appeared as the mixture cooled to room temperature. Both problems were solved by measuring the triglycerides before derivatization. It was necessary to obtain the underivatized chromatogram in any event to know which peaks were the result of derivatization.

The 95% confidence level variations of peak areas for derivatized glycerol monopalmitate, monostearate, dipalmitate, and distearate were 4, 5, 5, and 12%, respectively; the values for derivatized and underivatized glycerol tristearate were 50% and 2%, respectively.

Figure 2 shows the chromatograms obtained from the extract of a polypropylene resin sample containing a commercial monoglyceride antistat before and after derivatization. The clean chromatogram obtained from the underivatized solution showed that interferences, particularly from poly-

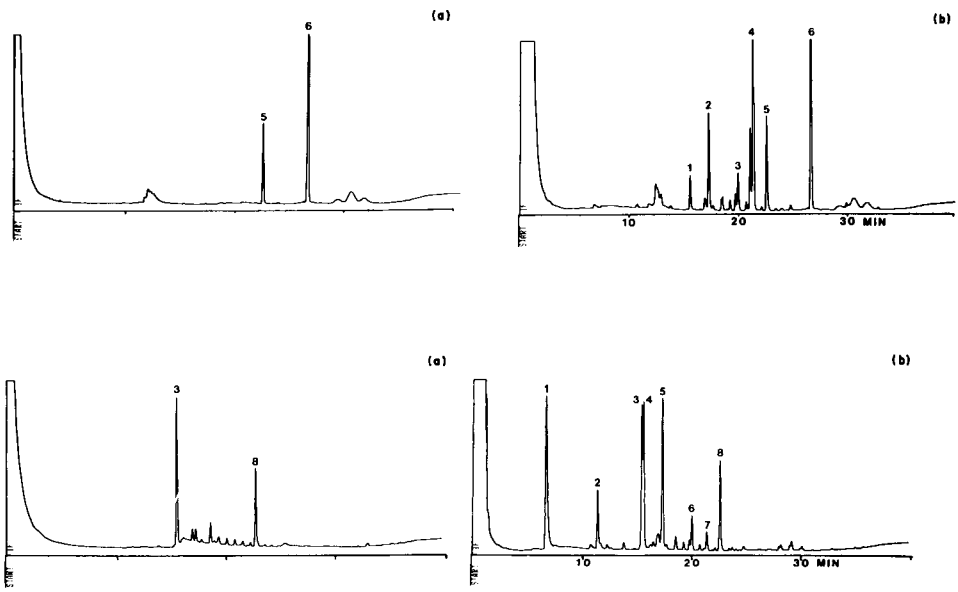

Fig. 2. Chromatograms of extract of polypropylene resin: (a) underivatized; (b) derivatized. Peaks: (1) palmitic acid, (2) stearic acid, (3) glycerol monopalmitate, (4) glycerol monostearate, (5) glycerol trioctanoate (internal standard), (6) unknown additive.

Fig. 3. Chromatograms of extract of hand lotion: (a) underivatized; (b) derivatized. Peaks: (1) glycerol, (2) unknown, (3) isopropyl myristate, (4) palmitic acid, (5) stearic acid, (6) glycerol monopalmitate, (7) glycerol monostearate, (8) glycerol trioctanoate (internal standard).

propylene oligomers, were negligible in this case. Glycerol monostearate and monopalmitate as well as free palmitic and stearic acids were found in the derivatized solution. The free acids may have been due to impurities from the antistatic agent, deliberate addition, or from metal soaps added as lubricants. Concentrations of palmitic acid, stearic acid, glycerol monopalmitate, and glycerol monostearate were 0.2, 0.5, 0.2, and 1.7% (by weight), respectively; retention times, relative to glycerol trioctanoate were 0.66, 0.75, 0.88, and 0.94, respectively. An unidentified component had a relative retention time of 1.18.

Figure 3 shows the chromatograms obtained for underivatized and derivatized extracts of a hand lotion sample. This sample illustrates the need to chromatograph unknown samples before and after derivatization. The underivatized chromatogram (Fig. 3a) shows a sharp peak (isopropyl myristate) which was not a glyceride species, and shows that there were no appreciable amounts of triglycerides present. The chromatogram of the derivatized extract added further information about the glycerol, free acids, and other glycerides. Table 2 lists the species found and their respective concentrations in the hand lotion.

TABLE 2

Qualitative and quantitative results from hand lotion extraction

Relative t_R	Species	Concentrations (% by weight)
0.30	Glycerol (TMSE)	3.0
0.50	Unknown	—
0.67	Isopropyl myristate[a]	—
0.68	Palmitic acid (TMSE)	2.9
0.77	Stearic acid (TMSE)	3.3
0.89	Glycerol monopalmitate (TMSE)	0.8
0.95	Glycerol monostearate (TMSE)	0.6
1.00	Glycerol trioctanoate	—

[a]Identified by g.c./m.s. and not determined.

REFERENCES

1 Y. Itabashi and T. Takagi, Lipids, 15 (1980) 205.
2 A. Prevot and J. -L. Coustille, Rev. Fr. Corps Gras, 29 (1982) 17.
3 R. D'Alonzo, W. Kozarek and R. Wade, J. Am. Oil Chem. Soc., 59 (1982) 292.
4 J. Sφe, Fette, Seifen, Anstrichm., 2 (1983) 72.
5 D4275-83 Test Method for Determination of Butylated Hydroxy Toluene (BHT) in Polymers of Ethylene and Ethylene-Vinyl Acetate (EVA) Copolymers by Gas Chromatography, American Society for Testing And Materials, Philadelphia.
6 E. Kovats, Helv. Chim. Acta, 41 (1958) 1915.

Analytica Chimica Acta, 173 (1985) 185—192
Elsevier Science Publishers B.V., Amsterdam — Printed in The Netherlands

DETERMINATION LIMITS IN HIGH-PERFORMANCE LIQUID CHROMATOGRAPHY OF PLANT PHENOLIC COMPOUNDS WITH AN ULTRAVIOLET DETECTOR

L. J. NAGELS*[1], W. L. CRETEN[2] and L. VAN HAVERBEKE[1]

Laboratory of Physics[1] and Laboratory of Chemistry[2], Rijksuniversitair Centrum Antwerpen, Groenenborgerlaan 171, B-2020 Antwerp (Belgium)

(Received 4th January 1985)

SUMMARY

The capabilities of high-performance liquid chromatography (h.p.l.c.) for the determination of phenolic compounds in 80% ethanol extracts from plant material are described. A reversed-phase column was used and elution was done with a linear gradient from 0.01 M phosphoric acid up to methanol. The efficiency of the method was studied via determination limits, defined as the minimum concentration of a compound (μg of compound per gram of extracted dry plant material) necessary to provide 90% probability that the relative error on the determination of the compound in an extract from a plant sample taken at random is $<10\%$. These limits take into account matrix interferences as a source of error, and were calculated with a minicomputer for the determination of 19 phenolic compounds in plant extracts. For good determinations, the concentrations of the components should be in the range 1—10 mg g^{-1} of dry plant material. Separating the extracts into different chemical groups (on ion-exchange materials) prior to h.p.l.c. decreases the determination limits about five times. The dependence of determination limits on the u.v. characteristics of the compound, the sample clean-up, and the column characteristics are discussed quantitatively by means of a simple empirical equation.

High-performance liquid chromatography (h.p.l.c.) is very popular for the analysis of plant phenolic compounds in addition to the older thin-layer and paper chromatography [1, 2]. These compounds occur in plant extracts as very complex mixtures which, when chromatographed, give rise to complex chromatographic peak patterns. In an earlier statistical study of these patterns, it was shown that even for modern chromatographic techniques, peak overlap (interference) is practically unavoidable [3]. This results in large and unpredictable errors of measurement when the plant constituents are quantified. The problem of matrix interference is inherent to the chromatographic determination of compounds in all kinds of biological mixtures. Several recent theoretical studies have dealt with such phenomena [4, 5].

It is generally accepted that the higher the relative abundance of a component in a biological mixture, the higher the chance of obtaining a good quantitative or qualitative result. In trace determinations, the minimum con-

0003-2670/85/$03.30

centration for which one has a specified probability of obtaining an accurate measurement can be called a determination limit [6], which is not to be confused with the minimum detectable concentration, or detection limit. In an earlier publication [7], the concept of determination limits was applied to predict measurement errors provoked by matrix interferences in the chromatographic analysis of plant extracts. A method was given for the calculation of determination limits DLS_e^w (see Table 1). For the present purpose, the determination limit is defined as the minimum relative abundance of a component which is needed so as to have a probability of 0.9 of doing a determination with a relative error smaller than 0.1 in a randomly chosen plant extract.

In the present study, determination limits were calculated for the h.p.l.c./u.v. determination of 19 biochemically interesting compounds (mostly phenolics) in plant extracts. The efficiency which was gained by using group separation methods prior to h.p.l.c. was evaluated quantitatively by using these calculated DLS_e^w values. The intention of the work is to provide data on concentration ranges within which these compounds can be measured accurately with the above technique.

EXPERIMENTAL

Instrumentation and chemicals

The Hewlett-Packard 1084B liquid chromatograph used was equipped with a variable wavelength detector, and a reversed-phase column (length 25 cm, internal diameter 4.6 mm) filled with Lichrosorb RP8 (Merck). It was eluted with a linear gradient from 5%B to 40%B in 20 min; solvent A was 10 mM phosphoric acid and solvent B was methanol (for more details of the method, see [8]). A HP3388A programmable integrator was used for the A/D conversion of analog signals from the h.p.l.c. and spectrophotometric

TABLE 1

Definitions of symbols

Symbol	Definition
$a_{i,\lambda}$ $a_{j,\lambda}$	Absorptivity of sample i or j at wavelength λ given as $l\ g^{-1}\ cm^{-1}$. The concentration of the sample is given as gram of dry plant material extracted per litre.
DLS_e^w	Determination limit: the minimum abundance of a component in the extract (expressed as $\mu g\ g^{-1}$ relative to the dry plant material), which is necessary to give a probability w of doing a determination with a relative error smaller than e in an extract from a plant species taken at random.
pd	Peak density: the probability that a detector response will be observed in a retention zone with central value t_R and width 4σ, when a sample is injected.

equipment. These data were transmitted to a HP1000 minicomputer for further treatment.

Most of the 19 biochemical compounds were readily available commercially in a chromatographically pure form. *p*-Coumaroylglucose, caffeoylglucose and *p*-coumaroylquinic acid were synthesized as described earlier [8, 9]. The cinnamic acids were esterified at position 1 of glucose, and at position 5 of quinic acid, i.e., they are the isomers 1-O-caffeoylglucose, 1-O-galloylglucose (glucogallin) and 5-O-*p*-coumaroylquinic acid (IUPAC numbering convention).

Plant material, extraction, and fractionation of the extracts

Sixty five different plant species were collected in the surroundings of the university. Plant leaves were extracted with 80% ethanol as described earlier [3]. This set is referred to later as the set of European plant extracts. A second set was obtained by using identical extraction and cleanup procedures for 50 plant species collected in the surroundings of the University of Ife, Ile-Ife, Nigeria. It is referred to later as the set of African plant extracts.

For fractionation of the extracts, small semi-preparative glass columns (10-mm diameter) were eluted under constant pressure. Samples (a few millilitres) were applied on top of the column, as aqueous solutions. Basic substances were first removed by passing these samples through a column filled with 10 ml of water-swollen Sephadex SP cation-exchanger (Pharmacia, Sweden) in the H^+-form, and eluting with 80 ml of distilled water. The eluent was evaporated to dryness and redissolved in a few ml of water. The latter fraction was fractionated into acidic and neutral components by using columns filled with 10 ml of water-swollen Sephadex DEAE (formate form). These columns were eluted successively with 80 ml of water (water fraction), 80 ml of 4% (w/v) ammonium formate (ammonium formate fraction) and 80 ml of 4% (v/v) formic acid (acids fraction).

The three fractions obtained were dried in vacuum and redissolved in a few ml of water, adjusted to pH 3, and stored in a deep-freeze at −18° C. Details about the use of ion-exchangers for fractionation of plant extracts are available elsewhere [9, 10].

RESULTS AND DISCUSSION

The phenolic compounds for which DLS_e^w values were calculated (Table 2) ranged from simple C6 phenolics, to C6—C1 neutral phenolics, C6—C1 carboxylic acids and C6—C3 phenylpropane acids and esters. Coumarin, naringin and indole acetic acid (IAA) were included to show that the methods are also applicable to other groups of plant constituents (coumarins, flavonoids and growth hormones). All these substances are found very frequently in plant extracts in the free form, or in combination with sugars (glycosides)

TABLE 2

Determination limits DLS_e^w for 19 plant constituents, for h.p.l.c./u.v. processing of total extracts from plant leaves (DLS_e^w extract), and of fractionated extracts (DLS_e^w fraction). The fraction in which the compounds are found is indicated in the last column

Compound	Retention time (min)	Absorptivity ($l\ g^{-1}\ cm^{-1}$)	λ_{max} (nm)	DLS_e^w extract ($\mu g\ g^{-1}$)	DLS_e^w fraction ($\mu g\ g^{-1}$)	Fraction
C6						
Hydroquinone	2.2	25.7	285	5080	3700	water
Catechol	3.7	21.3	275	7420	5400	water
C6—C1						
m-Hydroxybenzaldehyde[a]	7.9	68.4	275	3610	550	water
Salicylaldehyde	10.0	87.7	255	3750	510	water
Galloylglucose	1.5	25.7	275	6350	700	am. form.
p-Hydroxybenzoic acid	7.0	104.0	255	2370	840	acid
Vanillic acid	8.0	58.9	265	4300	1410	acid
Gallic acid	2.2	50.1	275	3120	1130	acid
C6—C3						
p-Coumaroylglucose	7.2	64.2	310	4780	730	water
Caffeoylglucose[a]	5.0	46.5	325	4200	20	am. form.
Cinnamic acid	19.2	133.0	280	3320	700	acid
p-Coumaric acid	12.8	127.0	310	2760	600	acid
Caffeic acid	9.0	88.4	325	4720	1830	acid
Sinapic acid	13.9	67.4	275	6440	1130	acid
Chlorogenic acid	8.4	44.9	325	8300	3610	acid
p-Coumaroylquinic acid	11.3	61.9	310	4980	1500	acid
Others						
Coumarin	11.8	66.7	280	5570	620	water
Naringin[a]	15.2	28.9	275	16000	2590	water
Indole acetic acid	12.0	37.7	275	11400	2030	acid

[a]The minimum determination limits were found at 255, 305 and 290 nm, respectively, for these compounds.

and non-aromatic carboxylic acids. They have been subjected to numerous biochemical, taxonomical and pharmacological studies. Because of their high u.v. absorptivities, $a_{j,\lambda}$ (Table 2, third column), and their low volatilities, h.p.l.c./u.v. methods have been used frequently for their determination.

The method for the calculation of DLS_e^w values for the determination of plant phenolics with h.p.l.c./u.v. was outlined theoretically in a previous paper [7]. This method was applied here for calculation of the determination limits which are listed in Table 2. However, the statistical equations which were derived earlier [7] were tedious as a basis for discussing the effects of sample clean-up, detector or detector wavelength, and chromatographic column, on the quality of the determination. Some simple empirical equation

would be more practical, and several equations were tried. Very good approximations of the results listed in Table 1, which were obtained with a minicomputer programmed as described earlier [7], were achieved by using the equation

$$DLS_e^w = \text{constant} \times pd \times \bar{a}_{i,\lambda}/a_{j,\lambda} \quad (1)$$

at all wavelengths λ (definitions are listed in Table 1). The value of the constant was 20.66×10^6 $\mu g\ g^{-1}$. A linear regression analysis of the 38 DLS_e^w values listed in Table 1 with values calculated via Eqn. 1, showed a correlation coefficient (r) of 0.976.

Equation 1 relates all the variables which are important in DLS_e^w predictions in a simple way. The determination limit DLS_e^w at wavelength λ is inversely proportional to the absorptivity $a_{j,\lambda}$ of compound j at that wavelength. It is proportional to $\bar{a}_{i,\lambda}$, the mean absorptivity of the sample set which is to be processed (total extracts from randomly sampled plants and subfractions thereof in this case). Figure 1 shows the frequency distributions of $a_{i,\lambda}$ values at 280 nm for extracts and subfractions, for the set of European plant extracts. [This set will be used throughout this study as being representative of plant samples.] These frequency distributions have asymmetric shapes. Obviously, the total extracts contain more absorbing material ($\bar{a}_{i,\lambda}$ = 1195 l g^{-1} cm^{-1}), while the two subfractions have similar $a_{i,\lambda}$ distributions: $\bar{a}_{i,\lambda}$ = 194 l g^{-1} cm^{-1} for the water, and $\bar{a}_{i,\lambda}$ = 220 l g^{-1} cm^{-1} for the formic acid subfraction. The distribution for the ammonium formate subfraction (not shown) had the same shape, but this fraction contained much less u.v.-absorbing material ($\bar{a}_{i,\lambda}$ = 39 l g^{-1} cm^{-1}). These distribution functions are useful for expressing the efficiency of group fractionation procedures: the more the curves are shifted to the left in relation to the curve for the total

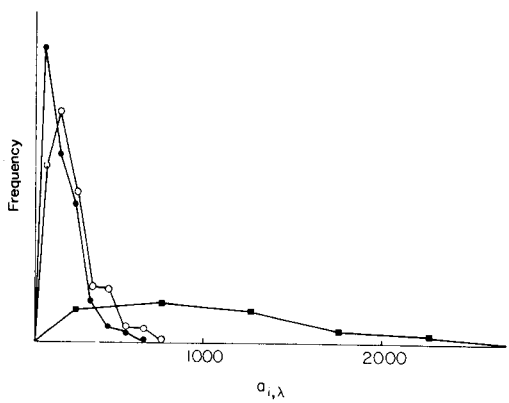

Fig. 1. Probability density functions of responses $a_{i,\lambda}$ at 280 nm: (■) for the total plant extracts; (○) for the formic acid subfraction; (●) for the water subfraction. They were obtained from the frequency distribution of the $a_{i,\lambda}$ values of the set of European plant extracts (total extracts and subfractions).

extracts, the more efficient is the group separation or clean-up (assuming that the compound of interest is quantitatively recovered, which is of course always the first prerequisite). Only the curves at 280 nm are discussed here. The calculation of determination limits (see below) was based on $a_{i,\lambda}$ data at 30 different wavelengths from 250 to 400 nm, which is the most frequently used part of the spectrum for h.p.l.c. detection. The total extracts from the set of African plants showed an $a_{i,\lambda}$ distribution pattern which was very similar to the pattern obtained for the extracts from European plants. This means that the set of 65 European plant species does not constitute a select set.

Another important feature in the calculation of DLS_e^w values is the resolving power of the chromatographic column for the sample components. As the extracts are complex mixtures, varying greatly from sample to sample, the use of "peak densities" (*pd*; see Table 1) was proposed as an evaluation parameter [7]. The peak density at retention time t_R was defined as the probability that a component response occurred within the band centred on t_R and with a width equal to 4σ (σ is the standard deviation of a Gaussian peak). Peak density was obtained here by using chromatograms from the extracts and subfractions of the set of European plants. For the total extracts of plant leaves, on the reversed-phase column with linear gradient elution and detection at 280 nm, this function has the shape shown in Fig. 2A. Figure 2(B—D) shows the distributions for the water, ammonium formate and formic acid subfractions from the model set. A comparison with results obtained from the total extracts of the African plant set again showed no significant differences.

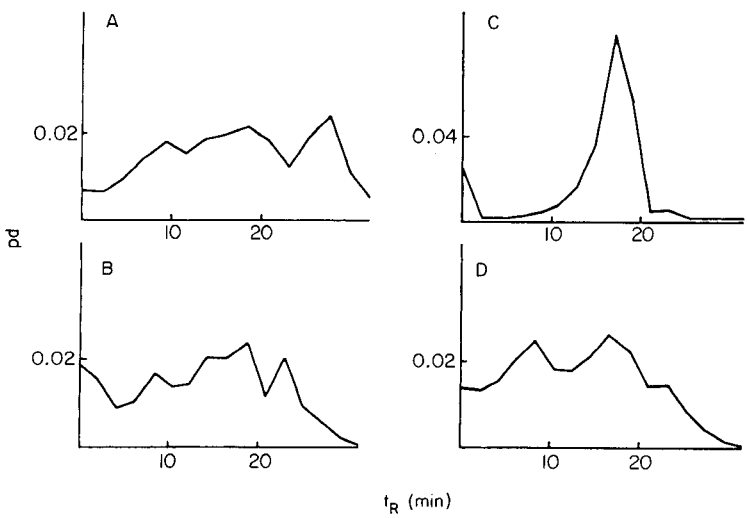

Fig. 2. Peak density, *pd*, as a function of retention time in the h.p.l.c. system: (A) for the total extracts; (B) for the water fraction; (C) for the ammonium formate fraction; (D) for the formic acid fraction. For further detail, see text.

Except for the ammonium formate fraction, peak areas were quite uniformly distributed over the chromatograms. As the samples used were 80% ethanolic extracts which were dried and redissolved in water, very apolar u.v.-absorbing compounds were not present. At high retention times (high methanol concentration in the eluent), the probability of having interference from u.v.-absorbing peaks (i.e., *pd*) becomes very low. The distribution of peaks over the chromatogram was completely different for the ammonium formate fraction. At retention times around 18 min, these chromatograms were overcrowded with u.v.-absorbing material, whereas at retention times outside the range 10—20 min, the probability of interference was very small. This means that the reversed-phase system used was not ideal for the separation of the compounds present in this subgroup. The system would not be suitable in a search for biologically interesting compounds in this subfraction, as the dispersion of the compounds was very poor. However, for the determination of u.v.-absorbing compounds with retention times outside the range 10—20 min, the system would be convenient, with a low probability of interference.

Although the DLS_e^w values were calculated by the computer for wavelengths between 250 and 400 nm [7], only the lowest value is given in Table 2, as this value is of most interest. The wavelength of the minimum determination limit was within 10 nm of the λ_{max} for the compound, except for the three compounds noted in Table 2.

For the determination of compounds in the total extracts, DLS_e^w values ranged between 2370 $\mu g\ g^{-1}$ (*p*-hydroxy benzoic acid) and 16 000 $\mu g\ g^{-1}$ (naringin). Typically, about 2—10 mg of compound per g of dry plant material extracted was needed in order to ensure correct determination of the components in the total extracts by the described h.p.l.c./u.v. method. Certain plant constituents, such as phenylpropanyl esters and glycosides, occur frequently in such high concentrations. For example, chlorogenic acid was often found in the plants in the range 5000—10 000 $\mu g\ g^{-1}$. Even for these products, it is safer however to fractionate the plant extracts into subgroups prior to h.p.l.c. On average, DLS_e^w values decreased by a factor of 3.7 and 5.5 for the acidic and water subgroups, respectively (Table 2). For chlorogenic acid, the DLS_e^w value dropped from 8300 in the total fraction to 3610 in the acid fraction.

For values below 1000 $\mu g\ g^{-1}$, more efficient group fractionations are advisable, as shown by the ammonium formate subgroup, for which $\bar{a}_{i,\lambda}$ was only 1/30 of the $\bar{a}_{i,\lambda}$ value of the total extracts. For products eluting in that fraction, a 30-fold decrease in DLS_e^w values was to be expected if the peak density were to be reasonably constant (Eqn. 1). For this subgroup, peak densities were strongly dependent on the retention time (Fig. 2C); thus, caffeoylglucose can be determined down to 20 $\mu g\ g^{-1}$, in comparison with only 700 $\mu g\ g^{-1}$ for galloylglucose.

The information given in Table 1 on determination limits will be useful for guidance on the fractions and concentrations that are practical propositions for analysis. For example, it is clear that if a method of quantifying (by

h.p.l.c./u.v.) growth hormones of the indole acetic acid type at the 0.1 $\mu g\ g^{-1}$ level is required, the formic acid subfraction will be of no interest (the predicted DLS_e^w value is 2030 $\mu g\ g^{-1}$ in that fraction), unless further purifications are done.

Conclusions

Determinations of phenolic compounds in total extracts from plant leaves by h.p.l.c./u.v. will generally be successful only for the more abundant components (2—10 mg g^{-1}). The main source of error is matrix interference from other compounds present in the extracts. The determinable concentrations are lowered by a factor of 3.5—5 when the extracts are separated into acidic and neutral subgroups. Minimum determinable concentrations vary from component to component, depending on their u.v. characteristics and retention time in the chromatographic system. Such concentrations are discussed for 19 biochemically important compounds. For determinations of these compounds at the concentrations below about 1 mg g^{-1}, more efficient group fractionations are required. The efficiency of fractionation procedures and of their combination with h.p.l.c. can be examined via DLS_e^w values calculated with a simple empirical equation based on peak density functions and $a_{i,\lambda}$ distributions.

The authors thank W. Van Dongen for writing the Fortran programs and for helpful discussions.

REFERENCES

1 M. V. Evans, J. Liq. Chromatogr., 6(S-2) (1983) 153.
2 L. J. Nagels, J. Chromatogr., 209 (1981) 377.
3 L. J. Nagels, W. L. Creten and P. M. Vanpeperstraete, Anal. Chem., 55 (1983) 216.
4 J. M. Davis and J. C. Giddings, Anal. Chem., 55 (1983) 418.
5 D. R. Reeve and A. Crozier, in J. McMillan (Ed.), Encyclopedia of Plant Physiology, Vol. 9, New series, Springer, Berlin, 1981.
6 C. Liteanu and J. Rica, Statistical Theory and Methodology of Trace Analysis, Wiley, New York, 1980.
7 L. J. Nagels and W. L. Creten, Anal. Chim. Acta, 169 (1985) 299.
8 L. Nagels, W. Van Dongen, J. De Brucker and H. De Pooter, J. Chromatogr., 187 (1980) 181.
9 L. Nagels, W. Van Dongen and F. Parmentier, Arch. Int. Phys. Biochim., 87 (1979) 585.
10 R. J. Redgwell, Anal. Biochem., 187 (1980) 44.

Analytica Chimica Acta, 173 (1985) 193—209
Elsevier Science Publishers B.V., Amsterdam — Printed in The Netherlands

SYNTHESIS OF CHROMOGENIC CROWN ETHERS AND LIQUID-LIQUID EXTRACTION OF ALKALI METAL IONS

YOSHIKI KATAYAMA, KAZUHIDE NITA, MASAHIDE UEDA, HIROSHI NAKAMURA and MAKOTO TAKAGI*

Department of Organic Synthesis, Faculty of Engineering, Kyushu University, Fukuoka 812 (Japan)

KEIHEI UENO

Department of Industrial Chemistry, Kumamoto Institute of Technology, Ikeda 4-22-1, Kumamoto 860 (Japan)

(Received 25th January 1985)

SUMMARY

New crown ethers carrying a pendent phenolic chromophore were synthesized. These crown ethers, on dissociation of the phenolic proton, provide lipophilic anions which can extract alkali metal cations into 1,2-dichloroethane by forming highly-colored uncharged metal complexes. Structural effects on the extraction were studied for possible use of these crown ethers as extraction—spectrophotometric reagents selective for alkali metals. The following factors are discussed in detail: (i) nature of the crown ether ring (ring size. aza-crown or standard crown ether), (ii) nature of the pendent phenolic group, and (iii) geometry between the crown ether center and pendent phenolic group. 15-Crown-5 or smaller ring-sized reagents favored the extraction of lithium ion when the basicity of the pendent phenolate was relatively high and a six-membered "chelate" ring was possible for the phenolate and the crown ether-bound metal. 15-Crown-5 type reagents were sodium-selective when an eight-membered "chelate" ring was possible between the phenolate and the crown ether-bound metal. 18-Crown-6 type reagents were generally potassium-selective. However, these selectivities were not absolute, and other structural parameters, steric and conformational, must be considered to explain in detail the selectivities of the individual reagents.

The synthesis of functionalized crown ether derivatives continues to be a topic of major interest in many research laboratories. Analytical applications are expanding rapidly in such fields as ion-selective electrodes and ion chromatography, but applications to spectrophotometry seem still to be limited [1]. Various chromogenic crown ethers which have pendent proton-dissociable groups on the periphery of the crown ether macrocycle have been synthesized and studied in this laboratory in the hope of developing spectrophotometric reagents selective for alkali or alkaline earth metals [2—6]. This paper describes further efforts on the synthesis of new chromogenic crown ethers and the liquid-liquid extraction of alkali metal ions by using these crown ethers. The structures of the crown ethers examined are summarized in Fig. 1.

0003-2670/85/$03.30

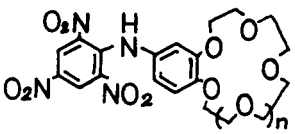

1: n=1,2; X=H, Br, NO_2

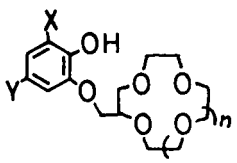

2(4): n=1; X, Y=NO_2

2(5): n=2; X, Y=NO_2

2(6): n=3; X, Y=NO_2

3(5): n=2; X=H; Y= N=N-  -NO_2

3(6): n=3; X=H; Y= N=N-  -NO_2

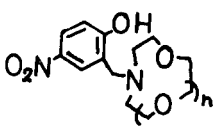

4(3): n=1

4(4): n=2

4(5): n=3

4(6): n=4

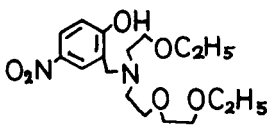

4(4,open)

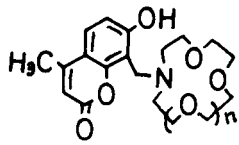

5(4): n=1

5(5): n=2

5(6): n=3

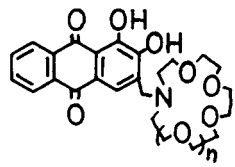

6(5): n=1

6(6): n=2

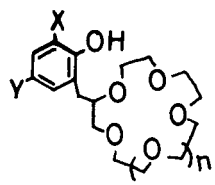

7(5): n=1; X, Y=NO_2

7(6): n=2; X, Y=NO_2

8(5): n=1; X=H; Y= N=N-  -NO_2

8(6): n=2; X=H; Y= N=N-  -NO_2

9(5): n=1; X, Y= N=N-  -NO_2

Fig. 1. Structures of the chromogenic crown ethers.

RESULTS

Synthesis of reagents

Full details of synthesis and confirmation of the compounds are given at the end of this paper. For brevity of notation, the number of hetero-atoms (oxygen and nitrogen) in the crown ether is indicated by a numeral in parentheses following the number of each crown ether.

Compounds 4(3)—4(6) were synthesized by the reaction of 5-nitro-2-hydroxybenzyl bromide (known as Koshland-I reagent) with the corresponding aza-crown ethers in the presence of triethylamine at 0°C:

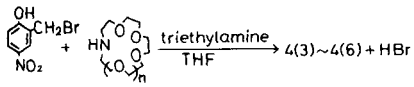

A

The yields varied within 70—90%, depending on the nature of aza-crown ethers.

Compounds 5(4)—5(6) were synthesized from the corresponding aza-crown ethers, 3-methyl-7-hydroxycoumarin and formaldehyde by Mannich reaction in the presence of triethylamine as the base:

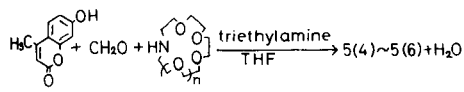

B

These preparations were successful only when the reaction was conducted in *N,N*-dimethylformamide (DMF) in combination with triethylamine. Aqueous conditions, whether alkaline or acidic, gave only poor results.

Compounds 7(5), 7(6), 8(5), 8(6), and 9(5) were synthesized as follows:

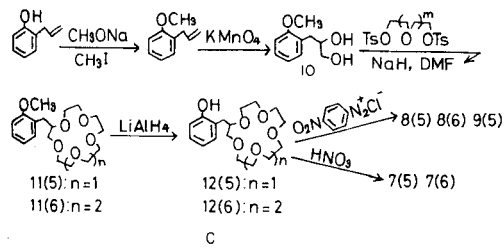

C

The key intermediate compound **12** was prepared as follows. The oxidation of 2-allylanisole with permanganate gave diol **10** in 35% yield. Compound **10** was converted to crown ethers **11** by cyclization with appropriate polyethylene glycol ditosylates in the usual manner. Reductive demethylation with lithium tetrahydroaluminate gave phenolic crown ether **12** in good yield. The demethylation proceeded most effectively in refluxing octane (ca. 125°C). At a lower reaction temperature [6] (refluxing heptane), the reaction was not complete.

Acidity constants

The proton-dissociable crown ethers and related reagents in this study are represented by HL (neutral species). Some of them carry an amino-nitrogen and form both cationic (H_2L^+) and anionic (L^-) species depending on the acidity or alkalinity of the aqueous solution. Thus, the acidity constants are defined by

$$H_2L^+ \rightleftharpoons H^+ + HL; \quad K_{H_2L^+} = [H^+][HL]/[H_2L^+] \tag{1}$$

$$HL \rightleftharpoons H^+ + L^-; \quad K_{HL} = [H^+][L^-]/[HL] \tag{2}$$

The crown ethers **6** are peculiar in that they form dianionic species by further deprotonation from L^- (dissociation of the second phenolic proton from alizarin nucleus), but the dianionic species do not play any important role in the extraction of univalent alkali metal cations. Acidity constants were measured spectrophotometrically in the usual manner [3] and are summarized in Table 1. Reagents **2**, **3**, **7**, **8**, and **9** have a single acidity constant K_{HL} which corresponds to the dissociation of the phenolic proton. For reagents **4**, **5**, and **6**, the first acidity constant $K_{H_2L^+}$ corresponds to the dissociation of phenolic proton, and the second, K_{HL}, to that of the ammonium proton.

Extraction equilibria

The crown ether reagents (HL) in the present study were substantially lipophilic, but the liquid—liquid distribution between water and 1,2-dichloroethane depended somewhat on the pH of the aqueous solution. The distribution of the reagent **9**(5) in the aqueous phase was negligible below pH 12. However, with other reagents, an appreciable fraction of the reagent distributed into the aqueous phase under strongly alkaline conditions because of the proton dissociation to form the anionic species L^-.

Figure 2 shows typical spectra of the organic phase when lithium ion in aqueous solution was extracted with crown ether **5**(5) in 1,2-dichloroethane. As the pH of the aqueous phase was raised, the absorbance maximum at 326 nm for the HL species shifted to a maximum at 376 nm corresponding to the formation of the ML complex. The process is described by

$$[HL]_o + [M^+]_w \rightleftharpoons [ML]_o + [H^+]_w; \quad K_{ex} = [ML]_o[H^+]_w/[HL]_o[M^+]_w \quad (3)$$

TABLE 1

Acidity constants in aqueous 10% (v/v) dioxane at 25°C

Reagent	$-\log K_{H_2L^+}$	$-\log K_{HL}$	Reagent	$-\log K_{H_2L^+}$	$-\log K_{HL}$
2(4)		3.03	**5**(4)	6.37	11.13
2(5)		3.16	**5**(5)	6.29	10.46
2(6)		3.27	**5**(6)	6.45	10.49
3(5)		7.51	**6**(5)[a]	4.80	9.86
3(6)		7.54	**6**(6)[a]	4.91	10.32
4(4)	5.41	9.80	**7**(5)		3.97
4(5)	5.79	9.69	**7**(6)		3.92
4(6)	5.77	9.59	**8**(5)		7.97
4(4, open)	5.11	9.11	**8**(6)		8.11
			9(5)		8.61

[a]—$\log K_{L^-} = 12.8$ for **6**(5) and 12.4 for **6**(6). K_{L^-} corresponds to the dissociation of the second phenolic proton (see text). Absorption spectra indicated that the first dissociation of the phenolic proton ($K_{H_2L^+}$) takes place at the 2-position on the anthraquinone nucleus as is usually observed with alizarin and its derivatives.

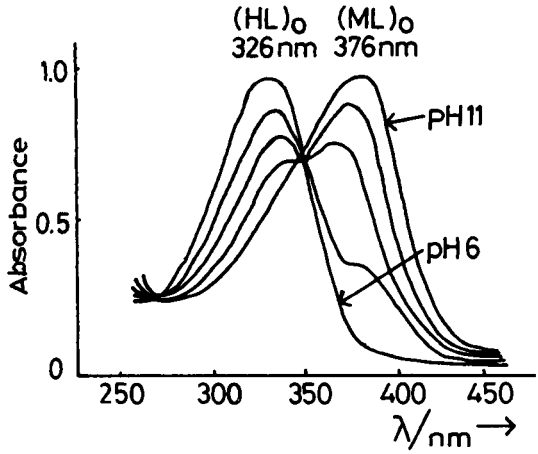

Fig. 2. Absorption spectra for extraction of lithium ion by 5(5). Conditions: 1×10^{-4} M 5(5); 1 M LiCl.

where K_{ex} is the extraction constant, and subscripts w and o denote the aqueous and organic phases, respectively. Because the crown ether reagents stay essentially in organic phase, the extraction constants K_{ex} could be determined spectrophotometrically in the standard manner. Appropriate corrections were made when the distribution of the reagent to the aqueous phase was of any importance [2, 3]. Table 2 summarizes the extraction constants of reagents 2—9 along with those reported previously.

DISCUSSION

Acidity constants

Scheme I summarizes the proton-dissociation and metal-extraction processes for aza-crown ethers. In addition to the formation of H_2L^+ species, the aza-crown reagents have another complication, in that HL can exist in solu-

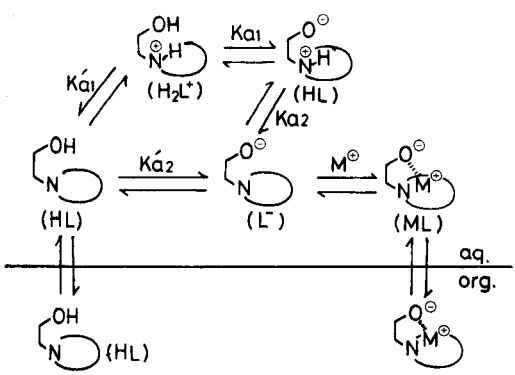

SCHEME I

TABLE 2

Extraction constants with selectivity ratios in parentheses (water/1,2-dichloroethane, 25°C)[a]

Reagent	$-\log K_{ex}$ (ratio)				
	Li^+	Na^+	K^+	Rb^+	Cs^+
2(4)	—	—	—	—	—
2(5)	5.60(0.010)	3.60(1)	4.15(0.29)	4.76(0.069)	5.60(0.010)
2(6)	4.80(0.003)	4.01(0.016)	2.22(1)	2.68(0.35)	3.76(0.029)
3(5)	9.80(0.040)	8.40(1)	9.20(0.20)	9.55(0.071)	10.0(0.025)
3(6)	8.80(0.020)	8.32(0.063)	7.11(1)	7.75(0.25)	10.0(0.001)
4(3)	—	—	—	—	—
4(4)	9.70	—	—	—	—
4(5)	9.15(1)	9.76(0.25)	9.86(0.20)	—	—
4(6)	10.29(0.033)	9.46(0.29)	8.93(1)	9.63(0.20)	10.62(0.020)
4(4, open)	11.05	—	—	—	—
5(4)	10.63	—	—	—	—
5(5)	9.70(1)	10.30(0.25)	11.50(0.016)	—	—
5(6)	11.00(0.083)	10.40(0.33)	9.90(1)	10.50(0.33)	—[b]
6(5)	8.30(1)	8.70(0.33)	9.60(0.050)	—	—
6(6)	11.00(0.002)	8.70(0.50)	8.30(1)	10.50(0.007)	—[b]
7(5)	—	5.80(0.83)	5.71(1)	6.04(0.48)	—
7(6)	—	5.05(0.051)	3.76(1)	3.90(0.71)	4.59(0.15)
8(5)	—	10.08(0.59)	9.84(1)	9.91(0.83)	10.83(0.10)
9(5)	—	10.61(0.067)	9.43(1)		10.05(0.25)

[a]Unless otherwise indicated, a dash means that the metal ion was not extracted. [b]No measurement.

tion in two tautomeric forms, i.e., nonionic and zwitterionic forms. Absorption spectra indicate that HL in aqueous solution is zwitterionic, whereas it assumes a nonionic structure in 1,2-dichloroethane. However, the coexistence of a small amount (<2—5%) of one species with the other cannot be excluded totally, and the acidity constants, $K_{H_2L^+}$, in Table 1 may safely be deemed as the sum of the acidity constants K_{a1} and K'_{a1} (Scheme I).

With regard to the effect of the acidity constants on the metal extraction, the reagents which have larger acidity constants ($K_{H_2L^+}$ and K'_{HL}, of which the latter would be the more important at the extraction step) should extract metals at lower pH, because they provide L^- species at lower pH. Comparison of the data in Tables 1 and 2 for reagents 2 and 3 or reagents 7 and 8 indicate that the larger the acidity constants, the larger are the metal extraction constants.

However, the relation just mentioned is really less simple, because the structural factors which affect proton dissociation must also influence the extractability of the resultant metal complexes. Thus, the K_{HL} values are not very different among the reagents 4, 5, and 6, and in the order, $4 > 6 > 5$, while the K_{ex} values are quite different from each other and in the order,

6 > 4 > 5. The latter order is better related to the $K_{H_2L^+}$ values (the order being 6 > 4 > 5), the constants which correspond to the dissociation of phenolic protons. Reagent 6 carries an alizarin chromophore which is reasonably expected to be more lipophilic than either the *p*-nitrobenzyl (4) or the 4-methylumbelliferone-8-methylene (5) group. Therefore, the enhanced lipophilicity of reagent 6 itself probably contributes much to the greater metal extraction constants. However, it is also possible that the more acidic alizarin chromophore produces better charge-delocalized anion, and this has led to an extractability of the resultant metal complexes.

Extraction of alkali metal cations

The crown ethers studied here can be outlined as in structure I; structural factors a—d all influence the ease of extraction of alkali metal ions. Crown ethers with the right ring size stabilize the complexes of particular metal ions

I 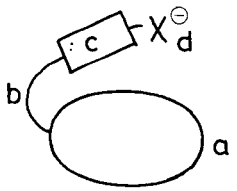

a: Crown ether ring
b: Side arm
c: Chromophore
d: Anionic center

SCHEME II

and enhance their extraction; the nature of the hetero-atom in the ring will also affect the stability of the complex (factor a), as will the length and flexibility of the side-arm (factor b). The chromophore is important not only because it provides spectral sensitivity, but also because its lipophilicity may enhance the distribution of the metal complex into the organic phase (factor c). The anionic group can neutralize the cationic charge of the metal either by coordination to the crown ether-bound metal or by formation of an intramolecular ion-pair in the organic phase, depending on the nature of the anionic group itself as well as on the structure of the remainder of the molecule (factors b and c). This schematic picture of a crown ether can be generalized to cover other crown ethers with functional groups [8]. Doubled side-arms (as well as doubled chromophores and anionic charges) provide reagents for extraction-spectrophotometry of alkaline earth metals [1, 9]. Introduction of hydrophilic side-arms with excess anionic charges leads to "crown complexones", hybrids of a crown ether and a traditional complexone [1, 10]. Use of soft hetero-atoms such as sulfur in the macrocycle causes a drastic change in metal selectivity [11].

Effect of ring size of the crown ether

It is generally accepted that an 18-crown-6 macrocycle favors K^+ complexation. In accordance with this, all the reagents of the 18-crown-6 type, 2(6)—8(6), extract potassium efficiently (Table 2). Among these reagents, 2, 3, and 7—9, which lack a macrocyclic amino-nitrogen, show the extraction selectivity order $K^+ > Rb^+ > Na^+$. In contrast, the nitrogen-containing reagents, 4(6)—6(6), display the selectivity order $K^+ > Na^+ > Rb^+$. The latter

selectivity order may indicate stabilization of the light metal complex by coordination of amino nitrogen to the metal ions of higher cationic surface charge, but this inference requires much further proof.

For 15-crown-5 derivatives, 2(5)—8(5), the extraction selectivities are somewhat different. The selectivity order $Na^+ > K^+ > Rb^+ > Cs^+$, Li^+ is observed with reagents 2(5) and 3(5), while the order $Li^+ > Na^+ > K^+ > Rb^+, Cs^+$ is shown by 4(5)—6(5). This may be explained on the basis of stabilization of a Li^+-containing 6-membered chelate ring formed with reagents 4(5)—6(5); some covalent interaction between lithium ion and the phenolate can be expected [4]. The possibility of preferred reaction of amino-nitrogen with the alkali metals of higher cationic surface charge is again indicated.

Reagents 7(5)—9(5), which lack the ethereal oxygen in the side-arm of reagents 2(5) and 3(5), display selectivity for potassium rather than sodium, in contrast to 2(5) and 3(5). This was unexpected, because a reduced rotational freedom in the side-arm of reagents 7—9 (shorter side-arm) was initially considered to stabilize a pseudo-chelate interaction between the phenolate oxygen and the metal, leading to preferred extraction of the metal ion of smaller ionic radius (i.e., sodium). However, inspection by CPK space-filling models of reagents 7(5)—9(5) suggested that a proper approach of the lone-pair electrons on the phenolate oxygen to the crown ether-bound metal is somewhat hindered in reagents 7(5)—9(5), while in reagents 2(5) and 3(5), this approach is much less hindered, effectively capping the metal-macrocycle complex. Though such an effect cannot be estimated quantitatively, this steric hindrance is probably related to the reversed Na^+—K^+ selectivity of the two series of reagents.

The 12-crown-4 derivatives, 4(4) and 5(4) extract only lithium ion, in accord with the size selectivity of this class of crown ethers. However, the 12-crown-4 type reagent, 2(4), does not extract lithium whereas the open-chain chelating extractant 4(4, open) does. These seem to suggest that a proper chelating functional group (amino-nitrogen-containing 6-membered chelate) is essential for extracting lithium ions.

It is to be noted that the lithium extraction constant of 4(4) is smaller than that of 4(5). It is also noted that the 9-crown-3 reagent 4(3) does not extract any alkali metal ions at all. These data seem to indicate that lithium ion does not assume four-coordination but is required to assume six-coordination for extraction. In the extraction with reagents 4(4) and 4(4, open), one molecule of water is thought to accompany the complex (in the first coordination sphere) to complete the six-coordination around lithium. Two molecules of coordinated water may similarly be expected in the reaction of lithium with 4(3), but such a complex must be too hydrophilic for effective transfer to the organic phase.

Effect of basicity of the anionic group

It is implicitly supposed that the phenolate anion caps the crown ether-bound metal by forming a sort of chelate ring when the metal complex is

extracted into the organic phase. The nature of the phenolate-metal interaction involved in such "chelate" formation may, however, vary from "covalent" to "ion-pair", depending on the type of both the metal ion and the phenolate. Thus, less basic, more charge-delocalized phenolates prefer the extraction of larger metal ions (which have lower cationic surface-charge density) by forming intramolecular complexes analogous to ion-pairing. In contrast, more basic, less charge-delocalized anions prefer the extraction of smaller metal ions (with higher surface-charge density) by forming covalent-like chelate complexes [12, 13]. This relationship can be seen more readily in Tables 3 and 4.

The basicity of the phenolates is in the order, monoazo- or bisazo-phenol type (3) > 7-hydroxycoumarin type (5) > nitrophenol type (4) > alizarin type (6) > dinitrophenol type (2). If the metal selectivity ratios Li^+/Na^+ are compared for reagents 2 and 3, the values for the latter reagents are always higher (Table 3). Here, reagents 3 have higher $-\log K_a$ values than reagents 2. The Li^+/K^+ and Na^+/K^+ values are also higher for 3 than for 2. The same holds for 4 and 5, though the structures of the phenolic chromophores are very different. The relationship holds even for 5 and 6 (for the most part), but it does not hold for 4 and 6; that the difference in $\log K_a$ values for the phenolic moiety is relatively large for 5 and 6 while it is small for 4 and 6 could be the reason for this different behavior.

It was unexpected that this phenolate basicity/metal extraction selectivity relationship does not hold for reagents 7 and 8 in view of the fact that the relationship holds satisfactorily for the structurally most closely related reagents 2 and 3. This again implies that factors different from the phenolate

TABLE 3

Comparison of the selectivity of metal extraction and the acidity constant, K_a, of the phenolate

Reagent	$-\log K_a$	Metal selectivity ratio[a]		
		Li^+/Na^+	Li^+/K^+	Na^+/K^+
2(5)	3.16	0.010	0.033	3.5
3(5)	7.51	0.040	0.20	5
4(5)	5.79	4	5	1.2
5(5)	6.29	4	63	16
6(5)	4.80	3	20	7
7(5)	3.97	—	—	0.83
8(5)	7.97	—	—	0.59
2(6)	3.27	0.17	0.003	0.016
3(6)	7.54	0.33	0.020	0.063
4(6)	5.77	0.11	0.033	0.29
5(6)	6.45	0.25	0.083	0.33
6(6)	4.91	0.004	0.002	0.50

[a]Ratio of extraction constants.

TABLE 4

Relation between K_{ex} and K_{a1} [a]

Reagent	$pK_{ex} - pK_{a1}$				
	Li^+	Na^+	K^+	Rb^+	Cs^+
2(5)	2.44	0.44	0.99	1.6	2.44
2(6)	1.53	0.74	−1.05	−0.59	0.49
3(5)	2.29	0.89	1.69	2.04	2.5
3(6)	1.26	0.78	−0.43	0.21	2.5
4(4)	4.29	—	—	—	—
4(5)	3.36	3.97	4.07	—	—
4(6)	4.52	3.69	3.16	3.86	4.85
4(4, open)	5.94	—	—	—	—
5(4)	4.26	—	—	—	—
5(5)	3.41	4.01	5.2	—	—
5(6)	4.55	3.95	3.45	4.05	—
6(5)	3.5	3.9	4.8	—	—
6(6)	6.09	3.79	3.39	5.59	—

[a] A dash means not determined.

basicity or the crown ether size are contributing to the selectivity of metal extraction by reagents 7 and 8 (see preceding section on the effect of crown ether ring size).

Geometry of the pendent phenolate

The reagents can be classified into three groups according to the size of the "chelate ring" formed between the pendent phenolate and the crown ether-bound metal ion. A CPK space-filling model indicates that reagents 4—6 form ideal six-membered chelates with an anionic center capping directly onto the metal from an axial direction. Reagents 7—9 formally form a seven-membered ring, but the phenolate oxygen is sterically hindered from direct interaction with the metal bound in the crown ether plane. Therefore, only indirect interaction analogous to ion-pairing seems to be feasible with this group of complexes. Reagents 2—3 form formally eight-membered chelates; the chain connecting the phenolate group is very flexible and the interaction between the metal and the phenolate oxygen could well be coordinative or ion-pair like (or even a mixture of the two) depending on the nature of the metal, the phenolate oxygen (basicity), and the crown ether. Figure 3 gives a schematic illustration of these three types of metal-phenolate interaction.

The following observations (Table 2) are in harmony with the above geometrical considerations. Lithium selectivity is achieved only with six-membered chelate-forming reagents (4—6). Reagents 2 and 3 extract lithium to only a limited extent, and reagents 7—9 do not extract lithium at all. Reagents 2 and 3 provide some selectivity for sodium ion whereas reagents 7—9 give only some selectivity for potassium ion. Selectivity to sodium ion by

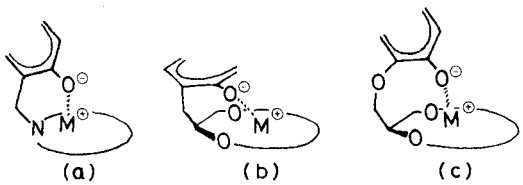

Fig. 3. Geometry and schematic illustration of metal-phenolate interaction: (a) six membered "chelate" (4—6); (b) seven membered "chelate" (7—9); (c) eight membered "chelate" (2—3).

2(5) and 3(5) seems to originate from a rather fortuitous combination of a flexible eight-membered chelate and the 15-crown-5 ring.

There is admittedly a weakness in the above simplified considerations, because six-membered chelate rings for 4—6 include an amino nitrogen while other chelate rings for 2 and 3 and 7—9 do not. In this connection, reagents which lack a benzyl methylene group in 7—9 and those in which an ethereal oxygen in the side-arm of 2 and 3 is replaced by a methylene group should be interesting. However, their synthesis has not yet proved successful in this laboratory.

Designing alkali metal-selective reagents for extraction-spectrophotometry

Based on the generalized structure I, general rules for designing alkali metal-selective chromogenic reagents may be summarized as follows. Lithium-selective reagents should be capable of forming a six-membered chelate ring through an anionic side-arm and the crown ether-bound metal. The size of the crown ether can be between 12-crown-4 and 15-crown-5. Because the extracted lithium complexes are expected to assume 6-coordination around the metal, reagents of the monoprotonic 12-crown-4 or 15-crown-5 (with two trimethylene groups in the crown ether ring) type with an extra ligating neutral side-arm could be potential candidates for lithium-selective reagents; the side-arm could fulfil the requirement of the residual sixth coordination site of the extracted lithium complex.

There seems to be no crucial requirement for attaining potassium selectivity. A combination of an 18-crown-6 and a pendent anionic side-arm (preferably forming a chelate ring with more than seven members or providing intramolecular ion-pair formation) is sufficient. An increased ion-pair character improves selectivity for potassium over sodium. In order to obtain sodium ion selectivity, some intermediate structural characteristics between those required for lithium and potassium are useful. The chelate ring would be better six-membered or larger, and the macrocycle should be 15-crown-5.

Reagents that show selectivity for rubidium or cesium according to the general formulation I have not yet been obtained. Macrocycles larger than 18-crown-6 have not been tested, and may deserve study. However, the size selectivity of such crown ethers is generally inadequate and the dehydration requirement of metal ions in the transfer from aqueous to organic solutions

is energetically not very different among the heavy alkali-metal ions. Accordingly, reagents highly selective for rubidium or cesium seem unlikely to be achieved on the basis of the reagent molecules outlined in I.

EXPERIMENTAL

Determination of acidity constants

The acidity constants of the crown ether reagents were determined spectrophotometrically in the conventional manner [3] in water containing 10% (v/v) dioxane at 25°C. The concentration of the reagent was 1×10^{-4} M. The solution was buffered with 4×10^{-3} M each of tartaric acid, MES [2-(morpholino)ethanesulfonic acid], Tricine [*N*-(2-hydroxy-1,1-bis-(hydroxymethyl)-ethyl)glycine] and boric acid, to which aqueous 0.2 M tetramethylammonium hydroxide was added dropwise to obtain the required pH.

Determination of extraction constants (K_{ex})

Portions (10 ml) of a 1,2-dichloroethane solution of the crown ether and a pH-buffered aqueous solution of the alkali metal salts were equilibrated on a mechanical shaker for 20 min at 25°C. The concentration of the reagent was 1×10^{-4} M for 2(4), 2(5), 2(6), 6(5), 6(6) and 1×10^{-5} M for 3(5), 3(6), 4(3)—(6), 5(4)—(6), 7(5), 7(6), 8(5), 8(6) and 9(5). The aqueous solution was 1×10^{-2}—1×10^{-1} M in alkali metal chloride and was buffered with boric acid, Tricine, MES and tetramethylammonium hydroxide in a similar manner to the determination of the acidity constants. The organic solution was separated by centrifuging for 10 min, and the absorption spectra were measured in a 1-cm quartz cell. Extraction constants were calculated in the conventional manner outlined previously [3].

Synthesis of reagents

N-(2-Hydroxy-5-nitrobenzyl)-monoaza-9-crown-3 [4(3)]. Monoaza-9-crown-3 (0.4 g, 3.1 mmol) and triethylamine (0.6 g, 6.2 mmol) were dissolved in anhydrous tetrahydrofuran (THF; 5 ml). The solution was cooled in ice-water, and Koshland-I reagent (2-hydroxy-5-nitrobenzyl bromide; 0.71 g, 3.1 mmol) dissolved in THF (10 ml) was added dropwise under stirring. The mixture was allowed to warm to room temperature and was stirred overnight while protected from moisture. The temperature of the bath was then raised to effect refluxing of the mixture. After 3 h, the reaction mixture was cooled and concentrated under reduced pressure. The residue was dissolved in chloroform and washed with aqueous 10% (w/v) tartatic acid solution. The chloroform solution was dried with magnesium sulfate and then concentrated under reduced pressure, to give yellow crystals. [Yield 0.5 g (57%); m.p. 89—90°C; ^{1}H-n.m.r. ($CDCl_3$, chemical shift from internal TMS) δ(ppm) = 7.8—8.1 (2H, m, aromatic H adjacent to NO_2), 6.76 (1H, d, J = 9 Hz, aromatic H), 3.95 (2H, s, Ar-CH_2), 3.6—3.9 (8H, m, OCH_2CH_2), 2.99 (4H, t, J = 5 Hz, NCH_2).]

N-(2-Hydroxy-5-nitrobenzyl)-monoaza-12-crown-4 [4(4)]. The compound was synthesized from monoaza-12-crown-4 (1.0 g 5.6 mmol) and Koshland-I reagent (1.4 g, 6 mmol) in a similar manner to 4(3). Yellow crystals were obtained. [Yield 1.3 g (71%); m.p. 82—83°C; ^{1}H-n.m.r. ($CDCl_3$) δ = 7.75—8.1 (2H, m, aromatic H adjacent to NO_2), 6.78 (1H, d, J = 9 Hz, aromatic H adjacent to OH), 3.81 (2H, s, $ArCH_2$), 3.5—3.8 (12 H, m, OCH_2CH_2), 2.76 (4H, t, J = 5 Hz, NCH_2). Found: 54.7% C, 6.5% H, 8.6% N. Calcd. for $C_{15}H_{23}N_2O_6$: 54.9% C, 6.8% H, 8.5% N.]

N-(2-Hydroxy-5-nitrobenzyl)-monoaza-15-crown-5 [4(5)]. The compound was synthesized in a similar manner to 4(3), giving yellow crystals. [Yield 91%. ^{1}H-n.m.r. ($CDCl_3$) δ = 7.9—8.3 (2H, m, aromatic H adjacent to NO_2), 6.8—7.1 (1H, d, J = 9 Hz, aromatic H adjacent to OH), 3.92 (2H, s, $ArCH_2$), 3.4—3.85 (18H, m, OCH_2CH_2), 2.8—3.1 (4H, t, J = 6 Hz, NCH_2). Found: 51.8% C, 6.6% H, 6.8% N. Calcd. for $C_{17}H_{26}N_2O_7 \cdot 3/2H_2O$: 51.4% C, 6.85% H, 7.05% N.]

N-(2-Hydroxy-5-nitrobenzyl)-monoaza-18-crown-6 [4(6)]. The compound was synthesized in a similar manner to 4(3), giving yellow crystals. [Yield 87%. ^{1}H-n.m.r. ($CDCl_3$) δ = 7.8—8.2 (2H, m, aromatic H, adjacent to NO_2), 6.8—7.1 (1H, d, J = 9 Hz, aromatic H adjacent to OH), 3.92 (2H, s, ArH), 3.4—3.8 (20H, m, OCH_2CH_2), 2.8—3.1 (4H, t, J = 6 Hz, NCH_2). Found: 53.8% C, 7.2% H, 6.4% N. Calcd. for $C_{19}H_{30}N_2O_7 \cdot 1/2H_2O$: 53.9% C, 7.1% H, 6.6% N.]

1-Chloro-3,6-dioxaoctane. 1-Hydroxy-3,6-dioxaoctane (10.0 g, 74.6 mmol), pyridine (6.2 g, 79.0 mmol) and thionyl chloride (9.3 g, 78.1 mmol) were stirred together at 110°C for 10 h. The reaction mixture was concentrated under reduced pressure, and the residual oil was treated with water and diethyl ether. The organic layer was collected and washed with water. The diethyl ether was evaporated to give pale yellowish oil. [Yield 10.5 g (92%).]

1-Iodo-3,6-dioxaoctane. 1-Chloro-3,6-dioxaoctane (10.5 g, 6.9 mmol) and sodium iodide (12.3 g, 8.0 mmol) were allowed to react for 48 h in 300 ml of refluxing acetone. The reaction mixture was concentrated under reduced pressure and the residue was dissolved in ethyl acetate. The solution was washed with aqueous 20% (w/v) sodium thiosulfate solution followed by aqueous sodium chloride solution. The removal of the solvent after drying with sodium sulfate gave a colorless oil. [Yield 13.4 g (91%).]

3,9,12-Trioxa-6-azatetradecane. 1-Iodo-3,6-dioxaoctane (13.4 g, 55 mmol) and 2-ethoxyethylamine (9.7 g, 110 mmol) were stirred together at room temperature for 1 h. The temperature was then raised to 60°C and the mixture was stirred for a further 1 h. Methanolic potassium hydroxide was added to the cooled mixture, which was then filtered, concentrated, and finally distilled under reduced pressure to give a colorless liquid. [B.p. 65°C/ 0.1 mmHg. Yield 6 g (53%). ^{1}H-n.m.r. ($CDCl_3$) δ = 3.2—3.6 (12H, m, OCH_2), 2.8—2.9 (4H, t, J = 6 Hz, NCH_2), 1.75 (1H, s, NH), 1.0—1.3 (6H, t, J = 8 Hz, CH_3).]

N-(2-Hydroxy-5-nitrobenzyl)-3,6,12-trioxa-9-azatetradecane [4(4, open)]. 3,9,12-Trioxa-6-azatetradecane (2.0 g, 9.74 mmol) and triethylamine (3.0 g,

29.22 mmol) were dissolved in anhydrous THF (5 ml) and stirred magnetically under ice-cooling. Koshland-I reagent (2.5 g, 10.71 mmol) dissolved in THF (10 ml) was added dropwise, and stirring was continued overnight at room temperature. The mixture was then heated to refluxing (3 h), cooled and concentrated under reduced pressure. The residue was taken into chloroform and washed with aqueous tartaric acid solution. The chloroform solution was concentrated under reduced pressure after drying with magnesium sulfate, giving a yellowish oil. [Yield 0.5 g (57%). ^{1}H-n.m.r. ($CDCl_3$) δ = 10.0 (1H, s, OH), 8.1—8.7 (3H, m, aromatic H), 4.0 (2H, s, $ArCH_2$), 3.7—3.3 (12H, m, OCH_2), 2.9—2.7 (4H, t, J = 8 Hz, NCH_2), 1.3—1.1 (6H, t, J = 8 Hz, CH_3). Found: 56.1% C, 7.7% H, 7.8% N. Calcd. for $C_{17}H_{28}N_2O_6$: 56.1% C, 7.65% H, 8.2% N.]

N-*(4-Methyl-7-hydroxycoumarin-8-ylmethyl)-monoaza-12-crown-4 [5(4)]*. 7-Hydroxy-4-methylcoumarin (1.1 g, 6.0 mmol), monoaza-12-crown-4 (1.0 g, 5.7 mmol), triethylamine (2.3 g, 23 mmol), and formalin (1.73 ml, 23 mmol) were dissolved in DMF (*N,N*-dimethylformamide) and stirred magnetically at room temperature under nitrogen. After 10 h of stirring, the reaction mixture was concentrated under reduced pressure. The residue was dissolved in chloroform and washed successively with aqueous tartaric acid solution and water. The chloroform solution was then concentrated under reduced pressure after drying with magnesium sulfate to give yellow crystals, which were purified by column chromatography on silica gel with chloroform/ethanol (3:1) as eluting solvent. [Yield 0.9 g (43%). ^{1}H-n.m.r. ($CDCl_3$) δ = 7.3—6.0 (4H, m, aromatic H), 4.1 (2H, s, $ArCH_2$), 3.75—3.6 (12H, t, J = 6 Hz, OCH_2), 2.9—2.7 (4H, t, J = 6 Hz, NCH_2), 2.35 (3H, s, CH_3). Found: 62.6% C, 6.95% H, 3.7% N. Calcd. for $C_{19}H_{25}NO_6$: 62.8% C, 6.9% H, 3.85% N.]

N-*(4-methyl-7-hydroxycoumarin-8-ylmethyl)-monoaza-15-crown-5 [5(5)]*. The compound was synthesized in manner similar to 5(4), giving a yellow oil. [Yield 47%. ^{1}H-n.m.r. ($CDCl_3$) δ = 7.3—6.0 (4H, m, aromatic H), 4.1 (2H, s, $ArCH_2$), 3.7—3.6 (16H, t, J = 6 Hz, OCH_2), 2.9—2.7 (4H, t, J = 6 Hz, NCH_2), 2.4 (3H, s, CH_3).]

N-*(4-Methyl-7-hydroxycoumarin-8-ylmethyl)-monoaza-18-crown-6 [5(6)]*. The compound was synthesized similarly to 5(4), giving a yellow oil. [Yield 62%. ^{1}H-n.m.r. ($CDCl_3$) δ = 7.4—6.0 (4H, m, aromatic H), 4.1 (2H, s, $ArCH_2$), 3.8—3.6 (20H, t, J = 6 Hz, OCH_2), 2.86 (4H, t, J = 6 Hz, NCH_2), 2.38 (3H, s, CH_3). Found: 57.0% C, 6.7% H, 2.9% N. Calcd. for $C_{23}H_{33}NO_8$ 0.2 $CHCl_3$: 57.0% C, 6.8% H, 2.85% N.]

N-*(1,2-Dihydroxyanthraquinone-3-ylmethyl)-monoaza-15-crown-5 [6(5)]*. The compound was synthesized by the reaction of alizarin (1,2-dihydroxyanthraquinone), monoaza-15-crown-5, triethylamine and formalin at 50°C under nitrogen in a similar manner to that of 5(4). Violet crystals were obtained. [Yield 35%, m.p. 104.2—104.6°C. ^{1}H-n.m.r. ($CDCl_3$) δ = 8.3—7.5 (5H, m, aromatic H), 4.9 (2H, s, $ArCH_2$), 3.8—3.6 (16H, m, OCH_2), 2.87 (4H, t, J = 6 Hz, NCH_2). Found: 63.55% C, 6.3% H, 2.7% N. Calcd. for $C_{25}H_{29}NO_8$: 63.7% C, 6.2% H, 3.0% N.]

N-(1,2-Dihydroxyanthraquinone-3-ylmethyl)-monoaza-18-crown-6 [6(6)]. The compound was synthesized similarly to 6(5). A violet crystalline powder was obtained. [Yield 38%, m.p. 90.2—91.1°C. ^{1}H-n.m.r. ($CDCl_3$) δ = 8.3—7.5 (5H, m, aromatic H), 4(2H, s, $ArCH_2$), 3.6—3.8 (20H, m, OCH_2), 3.0—2.8 (4H, t, J = 6 Hz, NCH_2). Found: 63.4% C, 6.5% H, 2.7% N. Calcd. for $C_{27}H_{33}NO_9$: 63.0% C, 6.45% H, 2.7% N.]

2-Allylanisole. To sodium methoxide (0.402 mol: prepared from 9.24 g of sodium) in 200 ml methanol were added under stirring 2-allylphenol (30.0 g, 0.201 mol) and methyl iodide (35 ml, 0.6 mol). The reaction mixture was refluxed for 3 h and after cooling was concentrated under reduced pressure. The residue was dissolved in chloroform and washed successively with aqueous 1 M sodium hydroxide and water. After drying with magnesium sulfate, the chloroform solution was concentrated and distilled under reduced pressure. [Yield 22.7 g (75%), colorless liquid, b.p. 96.5—98°C/12 mmHg. ^{1}H-n.m.r. ($CDCl_3$) δ = 6.7—7.4 (4H, m, aromatic H), 5.6—6.3 (1H, m, CH=C), 4.8—5.3 (2H, m, $C{=}CH_2$), 3.8 (3H, s, OCH_3), 3.3—3.4 (2H, d, J = 6 Hz, $ArCH_2$).

3-(2-Methoxyphenyl)propane-1,2-diol. 2-Allylanisole (34.0 g, 0.207 mol) was dissolved in ethanol (300 ml). A solution of potassium permanganate (32.8 g, 0.207 mol) and magnesium sulfate (51 g, 0.207 mol) in 300 ml of water was slowly added at —10°C, and the mixture was stirred for 1 h at the same temperature. Sodium hydrogensulfite (102 g, 0.98 mol) was then added portionwise under cooling, and the mixture was stirred for 1 h. Aqueous sulfuric acid (3 M) was added until the white precipitates were dissolved. The ethanol was removed under reduced pressure, and the residual solution was extracted with chloroform. The chloroform solution was washed with water, concentrated and distilled under reduced pressure to give a yellowish viscous oil. [Yield 14.4 g (38.2%), b.p. 151—153°C. ^{1}H-n.m.r. ($CDCl_3$) δ = 7.4—6.6 (4H, m, aromatic H), 5.2—4.6 (1H, m, CHOH), 3.8 (3H, s, CH_3), 3.5—3.3 (2H, m, CH_2O), 3.0—2.8 (2H, d, J = 6 Hz, $ArCH_2$). Found: 65.5% C, 7.7% H. Calcd. for $C_{10}H_{14}O_3$: 65.9% C, 7.7% H.]

(2-Methoxyphenyl)methyl-15-crown-5 [11(5)]. 3-(2-Methoxyphenyl)propane-1,2-diol (2.7 g, 14.8 mmol) was slowly added to a suspension of sodium hydride (60% in oil; 2.5 g, 63 mmol) in DMF (200 ml) under nitrogen. Tetraethyleneglycol ditosylate (7.47 g, 15 mmol) was added and stirred for 24 h at room temperature. Temperature was then raised to 60°C, and after 3 h stirring, the mixture was concentrated under reduced pressure. The residue was taken up in chloroform and washed with water. The chloroform solution was concentrated and distilled under reduced pressure to give a viscous oil. [Yield 2.36 g (47%), b.p. 173—175°C/2 × 10^{-4} mmHg. ^{1}H-n.m.r. ($CDCl_3$) δ = 6.7—7.3 (4H, m, aromatic H), 3.8 (3H, s, OCH_3), 3.6 (16H, m, OCH_2CH_2), 3.3—4.0 (3H, m, $OCHCH_2$), 2.6—2.9 (2H, d, J = 6 Hz, $ArCH_2$). Found: 62.7% C, 8.3% H. Calcd. for $C_{18}H_{28}O_6$ 1/4H_2O: 62.7% C, 8.3% H.]

(2-Methoxyphenyl)methyl-18-crown-6 [11(6)]. The compound was synthesized similarly to (2-methoxyphenyl)-methyl-15-crown-5. [Yield 41%.

Yellow viscous oil, b.p. 169—171°C/4 × 10^{-4} mmHg. ^{1}H-n.m.r. ($CDCl_3$) δ = 6.6—7.3 (4H, m, aromatic H), 3.8 (3H, s, OCH_3), 3.6 (20H, m, OCH_2CH_2), 3.4—4.0 (3H, m, $CHCH_2O$), 2.7—2.9 (2H, d, J = 6 Hz, $ArCH_2$).]

(2-Hydroxyphenyl)methyl-15-crown-5 [12(5)]. To (2-methoxyphenyl)-methyl-15-crown-5 (107.8 mg, 0.317 mmol) in benzene (5 ml) was added lithium tetrahydroaluminate (100 mg, 2.64 mmol) and heptane (20 ml). The mixture was heated to refluxing, the benzene being removed. After 10 h, the reaction mixture was cooled to room temperature and methanol was added to decompose the excess of lithium tetrahydroaluminate. Hydrochloric acid (6 M) was added, and the mixture was extracted with chloroform. The chloroform solution was concentrated to give a yellowish viscous oil. [Yield 0.94 g (91%). ^{1}H-n.m.r. ($CDCl_3$) δ = 6.7—7.4 (4H, m, aromatic H), 3.7 (16H, m, OCH_2CH_2), 3.0—4.0 (3H, m, $CHCH_2$), 2.6—2.9 (2H, d, J = 6 Hz, $ArCH_2$). Found: 62.1% C, 8.2% H. Calcd. for $C_{17}H_{26}O_6$: 62.6% C, 8.2% H.]

(2-Hydroxyphenyl)methyl-18-crown-6 [12(6)]. The compound was synthesized similarly to (2-hydroxyphenyl)methyl-15-crown-5; a yellowish viscous oil was obtained. [Yield 0.197 g (93%), ^{1}H-n.m.r. ($CDCl_3$) δ = 6.7—7.3 (4H, m, aromatic H), 3.7 (20 H, m, OCH_2CH_2), 3.0—4.0 (3H, m, $CHCH_2$), 2.8—3.0 (2H, d, J = 6 Hz, $ArCH_2$).]

(2-Hydroxy-3,5-dinitrophenyl)methyl-15-crown-5 [7(5)]. (2-Hydroxyphenyl)methyl-15-crown-5 (0.2 g, 0.62 mmol) was dissolved in 10 ml of chloroform/acetic acid (1:1 v/v) and 60% nitric acid (0.5 ml, 0.6 mmol) was slowly added at 0°C. The solution was then slowly heated to 50°C under stirring and kept at that temperature for 90 min. After cooling, the reaction mixture was diluted with chloroform (10 ml). The organic phase was collected, washed with water and concentrated under reduced pressure. The residual product was purified by column chromatography on silica gel with chloroform/ether (1:1) as eluting solvent. A yellowish viscous oil was obtained. [Yield, 0.248 g (96%). ^{1}H-n.m.r. ($CDCl_3$) δ = 8.9—9.0 (1H, d, J = 3 Hz, aromatic H adjacent to NO_2), 8.4—8.5 (1H, d, J = 3 Hz, aromatic H adjacent to $ArCH_2$), 3.7 (16H, m, OCH_2CH_2), 3.0—4.1 (5H, m, $ArCH_2$ and $CHCH_2O$). Found: 49.15% C, 5.8% H, 6.4% N. Calcd. for $C_{17}H_{24}O_{10}N_2$: 49.0% C, 5.8% H, 6.7% N.]

(2-Hydroxy-3,5-dinitrophenyl)methyl-18-crown-6 [7(6)]. The compound was synthesized similarly to 7(5). A yellow viscous oil was obtained. [Yield 56%. ^{1}H-n.m.r. ($CDCl_3$) δ = 8.9—9.0 (1H, d, J = 3 Hz, aromatic H adjacent to NO_2), 8.4—8.5 (1H, d, J = 3 Hz, aromatic H adjacent to $ArCH_2$), 3.7 (20H, m, CH_2CH_2O), 3.0—4.0 (5H, m, $ArCH_2$ and $CHCH_2$).]

[2-Hydroxy-5-(4-nitrophenylazo)phenyl] methyl-15-crown-5 [8(5)] and [2-hydroxy-3,5-bis(4-nitrophenylazo)phenyl] methyl-15-crown-5 [9(5)]. (2-Hydroxyphenyl)methyl)-15-crown-5 (0.2 g, 0.624 mmol) was dissolved in 10 ml of THF/water (1:1, v/v) in the presence of sodium hydrogencarbonate. A solution of *p*-nitrobenzenediazonium chloride (0.63 mmol) in 10 ml of THF/water (1:1, v/v) was added dropwise at 0—5°C, and the mixture was stirred continuously for 30 min. The temperature was then gradually raised

to room temperature, and the solution was stirred for 1 h. The THF was removed from the reaction mixture by evaporation, and the residue was extracted with chloroform. The chloroform solution was washed with aqueous sodium carbonate and sodium chloride followed by dilute hydrochloric acid and water. After concentration, the residue was passed through a silica-gel column with chloroform/ethanol (3:1) as eluting solvent to give two major components. Compound 8(5) was then recrystallized from water/ethanol, and 9(5) from ethanol.

For 8(5), yield 50 mg (23%), brown powder, ^{1}H-n.m.r. ($CDCl_3$) δ = 7.7—8.9 (4H, m, aromatic H adjacent to NO_2 and N=N), 7.8 (1H, d, J = 10 Hz, aromatic H adjacent to N=N), 7.7 (1H, s, aromatic H adjacent to $ArCH_2$), 6.9 (1H, d, J = 10 Hz, aromatic H adjacent to OH), 3.5—4.2 (19H, m, OCH_2CH_2), 3.1 (2H, d, J = 6 Hz, $ArCH_2$). Found: 58.5% C, 6.2% H, 9.1% N. Calcd. for $C_{23}H_{29}O_8N_3$: 58.1% C, 6.15% H, 8.8% N.

For 9(5), yield 35 mg (14%), brown powder. ^{1}H-n.m.r. ($CDCl_3$) δ = 7.9—8.6 (10H, m, aromatic H), 3.5—3.9 (19H, m, CH_2CH_2), 3.0—3.2 (2H, d, J = 6 Hz, $ArCH_2$). Found: 55.95% C, 5.2% H, 12.9% N. Calcd. for $C_{29}H_{32}N_6O_{10}$, 55.8% C, 5.15% H, 13.45% N.

[2-Hydroxy-5-(4-nitrophenylazo)phenyl] methyl-18-crown-6 [8(6)]. The compound was synthesized similarly to 8(5). [Brown powder, yield 4.8%, ^{1}H-n.m.r. ($CDCl_3$) δ = 7.7—8.5 (4H, m, aromatic H adjacent to NO_2 and N=N), 7.9 (1H, d, J = 8 Hz, aromatic H adjacent to N=N), 7.9 (1H, s, aromatic H adjacent to $ArCH_2$), 7.0 (1H, d, J = 10 Hz, aromatic H adjacent to OH), 3.5—4.2 (20H, m, OCH_2CH_2), 3.1 (2H, d, J = 6 Hz, $ArCH_2$). Found: 56.2% C, 6.6% H, 7.6% N. Calcd. for $C_{25}H_{33}N_3O_9H_2$: 55.8% C, 6.6% H, 7.8% N.]

REFERENCES

1 M. Takagi and K. Ueno, Top. Curr. Chem., 121 (1984) 39.
2 H. Nakamura, M. Takagi and K. Ueno, Talanta, 26 (1979) 921.
3 H. Nakamura, M. Takagi and K. Ueno, Anal. Chem., 52 (1980) 1668.
4 H. Nakamura, H. Sakka, M. Takagi and K. Ueno, Chem. Lett., (1981) 1305.
5 T. Yamashita, H. Nakamura, M. Takagi and K. Ueno, Bull. Chem. Soc. Jpn., 53 (1980) 1550.
6 H. Nakamura, H. Nishida, M. Takagi and K. Ueno, Anal. Chim. Acta, 139 (1982) 307.
7 B. P. Bubnis, J. L. Steger, Y. P. Wu, L. A. Meyers and G. E. Pacey, Anal. Chim. Acta, 139 (1982) 307.
8 D. M. Dishong, C. J. Diamond, M. I. Cinoman and G. W. Gokel, J. Am. Chem. Soc., 105 (1983) 586.
9 M. Shiga, H. Nishida, H. Nakamura, M. Takagi and K. Ueno, Bunseki Kagaku, 32 (1983) E293.
10 M. Tazaki, K. Nita, M. Takagi and K. Ueno, Chem. Lett., (1982) 571.
11 K. Saito, Y. Masuda and E. Sekido, Anal. Chim. Acta, 151 (1983) 447.
12 H. Nakamura, H. Nishida, M. Takagi and K. Ueno, Anal. Chim. Acta, 139 (1982) 219.
13 H. Nishida, K. Katayama, H. Katsuki, M. Takagi and K. Ueno, Chem. Lett., (1982) 1853.

Analytica Chimica Acta, 173 (1985) 211—217
Elsevier Science Publishers B.V., Amsterdam — Printed in The Netherlands

DIGITAL SIMULATION OF ELECTROCHEMICAL PROCESSES INVOLVING VERY FAST CHEMICAL REACTIONS
Part 1. A Simple General Approach

FRANCO MAGNO*, DOMENICO PEROSA and GINO BONTEMPELLI
Istituto di Chimica Analitica, Universita di Padova, via Marzolo 1, 35131 Padova (Italy)
(Received 13th November 1984)

SUMMARY

A simple approach based on the steady-state assumption and linear concentration profiles in the reaction layer is proposed to simulate electrochemical systems involving very fast homogeneous chemical reactions. The flux equations are derived in detail and the method is shown to be suitable for catalytic e.c.e. and dimerization reaction mechanism. The accuracy of the proposed method is checked by comparing the results obtained with those already available in the literature.

Digital simulation has proved to be very useful in rationalizing electroanalytical problems involving complicated reaction mechanisms [1—3] because very simple relationships can be used to represent electrochemical processes characterized by different kinetic complications. However, when very fast chemical reactions are involved, the numerical procedures described in the literature are usually no longer effective; this happens because the kinetic layer becomes much thinner than the diffusion layer so that an enormous number of time steps is required by procedures even when non-uniform space and time grids are used [4, 5].

From the mathematical point of view, this situation is characterized by values of the kinetic constants for the homogeneous reactions much greater than unity but also much lower than those proper for heterogeneous kinetic constants of the associated charge transfers, so that the overall electrochemical system cannot be considered at equilibrium. Despite its importance, only two papers have dealt with this problem in detail [6, 7]; but only the mathematical procedure relative to the c.e. mechanism was described exhaustively.

The aim of the present paper is to develop a simple but accurate general procedure, suitable for different electrochemical processes involving very fast chemical reactions. The accuracy of the procedure was checked by reproducing, with suitable parameters in the programs, the theoretical results relative to different mechanisms available in the literature. The relevant programs, available on request, were written in FORTRAN IV and the calculations were done on a MINC-11/23 minicomputer (Digital Equipment Corp.).

0003-2670/85/$03.30

THEORY

Basic concepts

The procedure described for very fast chemical reactions [6, 7] is an appropriate combination of an intermediate steady-state analytical solution and the usual finite difference approach. This treatment requires that the solution of the steady-state differential equation is used in order to build up the so-called "heterogeneous equivalent" [6, 7], i.e., a new formulation of the flux at the electrode surface. The diffusion of the reacting species is computed according to the usual "boxes" approach. However, as stated by the authors themselves [6, 7], such a solution is difficult to achieve, in many cases, particularly when other than first-order reactions have to be considered.

An easier mathematical solution to this problem should be achieved by using the approximation of a linear concentration profile in the reaction layer. A similar assumption was also adopted many years ago in polarographic studies [8]. Consequently, to verify whether this assumption is suitable for simulating correctly any kinetic complication, the data obtained by the relevant more approximate but easier procedure were compared with those calculated previously by more rigorous methods. The tests used were simulations of chronoamperometric or linear-sweep voltammetric experiments concerning some complicated electrochemical reactions. The electrochemical models were chosen on the basis of their frequent occurrence in experimental practice and of the difficulties found in their simulation by the usual procedure.

Catalytic mechanism

The mechanism for the electrochemical catalytic process is essentially

$$P + e^- \underset{}{\overset{k_{h,s}}{\rightleftharpoons}} Q; \quad Q + A \xrightarrow{k} P + B$$

for which $E^{\circ}_{P/Q}$ is the standard potential for the P/Q couple, $k_{h,s}$ is the standard heterogeneous kinetic constant for the P/Q couple, and k is the second-order homogeneous kinetic constant. If it is assumed that steady-state conditions hold for the species P and Q, then the following equations are valid:

for generation of Q, $q_{0,t} = k_{h,f}[P]_s - k_{h,b}[Q]_s$

for kinetic balance on Q, $q_{0,t} = \mu k[A]_{\mu}[Q]_s$

The flux expressed in terms of the stationary concentration of Q is

$$q_{0,t} = (D/\mu)[Q]_s \tag{1}$$

and the conservative mass balance is

$$P^* = [P]_s + [Q]_s \tag{2}$$

In these equations, $q_{0,t}$ is the flux of the depolarizer at the electrode surface, $[P]_s$ and $[Q]_s$ are steady-state concentrations, μ is the thickness of the

reaction layer (i.e., the coefficient which makes Eqns. 1 and 2 dimensionally consistent), D is the diffusion coefficient, and $[A]_\mu$ is the mean concentration of the species A in the reaction layer.

Equation 1 is the core of the approximation as it means that the gradient of Q ($\delta Q/\delta x$) is linear within the reaction layer. By suitable combination of the above relationships, one obtains $\mu = (D/k[A]_\mu)^{1/2}$, and then

$$[P]_s = [k_{h,b} + (Dk[A]_\mu)^{1/2}P^*]/[k_{h,f} + k_{h,b} + (Dk[A]_\mu)^{1/2}] \quad (3)$$

which can be inserted into the following equation of the flux, derived by combining the above equations for the generation of Q and the conservative mass balance

$$q_{0,t} = k_{h,f}[P]_s - k_{h,b}(P^* - [P]_s) \quad (4)$$

The presence in Eqn. 4 of the terms $k_{h,f}$ and $k_{h,b}$ allows the simulation of heterogeneous charge-transfer steps characterized by different degrees of reversibility, owing to the dependence of these terms on the heterogeneous standard rate constant $k_{h,s}$.

Table 1 reports the data calculated by the approach described above for a reversible and a totally irreversible process. The data agree with those reported previously [9, 10] within 0.05% and 0.5%, respectively. Figure 1 shows that the same values for the kinetic parameter, λ, lead to the same limiting currents regardless of the degree of reversibility, ψ. However, this limiting current is reached at different $E - E^\circ$ values because, for different ψ values [11], different overvoltage contributions are required for the regeneration reaction to become the rate-determining step in all cases.

TABLE 1

Calculated characteristics of the response obtained by linear-sweep voltammetry for a catalytic mechanism[a]

$\psi = 6.0 \times 10^2$ (reversible system)				
λ	5.13×10^1	5.13×10^2	5.13×10^3	5.13×10^4
FFN^∞	7.16	22.65	71.63	226.5
$E_{1/2}$	0.0	0.0	0.0	0.0
$\psi = 6.0 \times 10^{-4}$ (totally irreversible system)				
λ	5.13×10^1	5.13×10^2	5.13×10^3	5.13×10^4
FFN^∞	7.16	22.64	71.52	225.4
$E_{1/2}$	−0.452	−0.512	−0.571	−0.629

[a] $\lambda = kC_A/a$ = kinetic parameter of the homogeneous chemical reaction. $FFN^\infty = (kC_A/a)^{1/2}$ = current function for $E \to \infty$. $E_{1/2}$ = half-wave potential (V); $a = Fv/RT$; $\psi = k_{h,s}/(\pi Da)^{1/2}$ = kinetic parameter measuring the degree of reversibility of an electrode process.

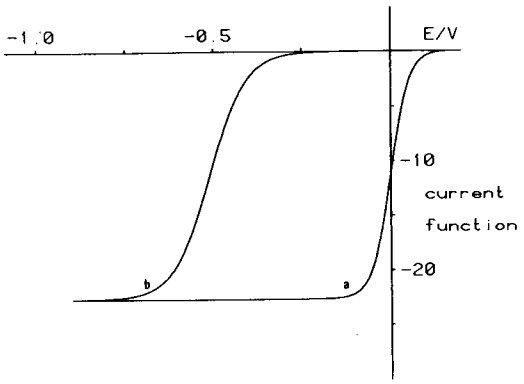

Fig. 1. Voltammetric curves for catalytic mechanisms $\lambda = 513$ with different degrees of reversibility: (a) $\psi = 6.0 \times 10^{2}$; (b) $\psi = 6.0 \times 10^{-4}$.

The e.c.e. mechanism

The usual digital simulation procedure reveals its limitations when it is applied to e.c.e. processes: $A + e^- \rightleftharpoons B$ (with $E^\circ_{A/B}$), $B \underset{k_b}{\overset{k_f}{\rightleftharpoons}} C$ (with $K_{eq} = k_f/k_b = [C]/[B]$), and $C + e^- \rightleftharpoons D$ (with $E^\circ_{C/D}$), which are characterized by K_{eq} values much lower than one and $E^\circ_{C/D} \gg E^\circ_{A/B}$.

Under these conditions, in fact, even a very large number of iteration steps cannot produce the contribution of the second electrode reaction properly, so that the fractional current increase (n_{app}) never attains the limiting value of two. This is because an insignificant value for the concentration of species C comes from the following equations used in its calculation at every step

$$K_{eq} = ([C_{j-1}] + \Delta)/([B_j] - \Delta); [C_j] = [C_{j-1}] + \Delta$$

owing to the very low value of K_{eq}. Such a difficulty is also reflected by the dependence of n_{app} on the square root of the time [$n_{app} = f(t^{1/2}k_f/k_b^{1/2})$] found for chronoamperometric conditions through the analytical solution [12]. In the simulation approach, $t^{1/2}$ is replaced by $j^{1/2}$ (j is the number of iteration steps), thus it is evident that when $\log (t^{1/2}k_f/k_b^{1/2}) \geqslant 2$, an excessive computation time is required because the k_f/k_b ratio is much less than one (see above). Conversely, when large k_f and k_b values (always under the condition $k_f/k_b \ll 1$) are handled by means of the steady-state approximation, large values of the mentioned dimensionless parameter can easily be reached in a small number of iteration steps.

The data of Amatore and Saveant [12] relative to this type of process refer to chronoamperometric experiments done under limiting conditions; the relevant equations are as follows: for diffusion of A at the electrode surface, $(q_1)_{0,t} = 2D[A]_1$, and the kinetic balance on C is

$$(q_2)_{0,t} = \mu k_f [B]_{\mu,t} - \mu k_b [C]_s \qquad (5)$$

The flux expressed in terms of the stationary concentration of C is

$$(q_2)_{0,t} = (D/\mu)[C]_s \quad (6)$$

In these equations, $[A]_1$ is the concentration of the depolarizer in the first space interval at a distance 0.5 (similar system units) from the electrode surface. Equation 6 represents again the approximation of a constant gradient in the reaction layer. The parameters used ($K_{eq} \ll 1$ and $E_2^\circ \gg E_1^\circ$) together with the chronoamperometric conditions specified make the term $\mu k_b[C]_s$ negligible in Eqn. 5, so that insertion of the residue of this equation yields

$$\mu = (D[C]_s/k_f[B]_{\mu,t})^{1/2} \approx (D/k_b)^{1/2} \quad (7)$$

That only a fraction of the species B changes into C while the remainder diffuses away from the electrode is accounted for by the relationship

$$(q_1)_{0,t} - (q_2)_{0,t} = 2D([B]_{\mu,t} - [B]_1) \quad (8)$$

Finally, combination of the reduced Eqn. 5 with Eqns. 7 and 8 gives

$$(q_2)_{0,t} = \{(k_bD)^{1/2}K_{eq}/[2D + (k_bD)^{1/2}K_{eq}]\}\{2D[B]_1 + (q_1)_{0,t}\} \quad (9)$$

which allows computation of the total faradaic flux through the obvious relationship, $q_{tot} = q_1 + q_2$.

The complete development of n_{app} from 1 to 2 was calculated in three very short simulation tests, the first using $K_{eq} = 0.1/100$, the second $K_{eq} = 1.0/1000$ and the third $K_{eq} = 10.0/10^4$. Table 2 compares the present results with those obtained by means of the relevant analytical solution [12].

Dimerization mechanism

As a further test of the general applicability of the approximation suggested, the dimerization mechanism [13] was considered

$$A + e^- \underset{}{\overset{k_{hs}}{\rightleftharpoons}} B;\ 2B \xrightarrow{k} P$$

for which $E^\circ_{A/B}$ is the standard potential for the A/B couple, and k is the second-order irreversible kinetic constant. This choice was made because analytical solutions for mechanisms involving reaction orders higher than one are generally cumbersome to achieve.

On the basis of the usual considerations, the valid equations are:

for generation of B, $q_{0,t} = k_{h,f}[A]_{0,t} - k_{h,b}[B]_s$

for kinetic balance on B, $q_{0,t} = \mu k[B]_s^2$

The flux expressed in terms of the stationary concentration of B is $q_{0,t} = (D/\mu)[B]_s$, and the diffusion of A to the electrode surface is given by $q_{0,t} = 2D([A]_{1,t} - [A]_{0,t})$. Combination of these four equations and subsequent rearrangement give

$$q_{0,t}[(2D + k_{h,f})/2D] + q_{0,t}^{2/3}[k_{h,b}/(Dk)^{1/2}] - k_{h,f}[A]_{1,t} = 0 \quad (10)$$

which allows the computation of $q_{0,t}$ by a standard iterative method.

TABLE 2

Comparison between the fractional current increases (n_{app}) calculated by two different methods[a]

log λ	Value of n_{app}		log λ	Value of n_{app}	
	From [12]	Present work		From [12]	Present work
−0.85	1.211	1.215	0.00	1.755	1.758
−0.65	1.315	1.314	+0.32	1.912	1.913
−0.50	1.408	1.406	+0.65	1.975	1.977
−0.31	1.539	1.540			

[a] $\lambda = (k_b t)^{1/2} K_{eq} = k_f t^{1/2}/k_b^{1/2}$ = kinetic parameter of the homogeneous chemical reaction.

The accuracy of this procedure was substantiated by the results obtained when Eqn. 10 was used to simulate linear-sweep voltammetric experiments. The current function $q_{0,t}/nFC_A^b D^{1/2} a^{1/2}$ ($a = nFv/RT$; v = scan rate) calculated at the peak potential was found to be 0.527, which exactly coincides with that reported for such a process [13].

DISCUSSION

The results reported indicate that the proposed method can be used profitably as a general means of simulating very fast chemical reactions coupled with heterogeneous charge-transfer steps. The assumption of a linear profile in the reaction layer introduces only small errors which are of the same order of magnitude as those typical of more rigorous treatments. The method produces solutions even for systems characterized by higher-order chemical reactions. Only one caution is required; the calculations will converge only if suitable couples of heterogeneous and homogeneous kinetic constants are inserted in the algorithm; these couples can be changed, however, over a large range to reflect not only different degrees of electrode reversibility (for reversible reactions, $\psi > 10$; for quasi-reversible reactions $10 > \psi > 10^{-3}$; and for totally irreversible reactions, $\psi < 10^{-3}$) [11] but also high rates for the homogeneous chemical reactions.

In this connection, it is worth noting that in the c.e. mechanism considered elsewhere [6], the steady-state assumption was used to simulate correctly a rather slow homogeneous chemical reaction because a very compact reaction layer is defined when the heterogeneous charge-transfer step is much faster than the homogeneous one. However, when a high value for the homogeneous constant is introduced in the equation of the flux derived for such a process with this steady-state assumption, only a diffusion-limited current can be obtained. Conversely, the correct simulation of a c.e. process in a kinetic "intermediate state" can be achieved by means of the usual finite notation, if the different kinetic characteristics of the system are taken into account by using the dimensionless parameter [9] $(Fv/RT)^{1/2} K_{eq}^{-1} (k_f + k_b)^{-1/2}$.

This work was supported by the Italian National Research Council (C.N.R) and by the Ministry of Public Education.

REFERENCES

1 D. Britz, Digital Simulation in Electrochemistry, Springer-Verlag, Berlin, 1981.
2 F. Magno, G. Bontempelli and M. Andreuzzi-Sedea, Anal. Chim. Acta, 140 (1982) 65 and references therein.
3 F. Magno, G. Bontempelli and D. Perosa, Anal. Chim. Acta, 147 (1983) 65 and references therein.
4 S. W. Feldberg, J. Electroanal. Chem., 127 (1981) 1.
5 R. Seeber and S. Stefani, Anal. Chem., 53 (1981) 1011.
6 I. Ružić and S. W. Feldberg, J. Electroanal. Chem., 50 (1974) 153.
7 I. Ružić, J. Electroanal. Chem., 144 (1983) 433.
8 J. Heyrovsky and J. Küta, Principles of Polarography, Academic Press, New York, 1966.
9 R. S. Nicholson and I. Shain, Anal. Chem., 36 (1964) 706.
10 J. M. Saveant and E. Vianello, Electrochim. Acta, 10 (1965) 905.
11 R. S. Nicholson, Anal. Chem., 37 (1965) 1351.
12 C. Amatore and J. M. Saveant, J. Electroanal. Chem., 102 (1979) 21.
13 J. M. Saveant and E. Vianello, Electrochim. Acta, 12 (1967) 1545.

Analytica Chimica Acta, 173 (1985) 219—225
Elsevier Science Publishers B.V., Amsterdam — Printed in The Netherlands

DIGITAL SIMULATION OF ELECTROCHEMICAL PROCESSES INVOLVING VERY FAST CHEMICAL REACTIONS

Part 2. A New Criterion for Determining Rate Constants of Consecutive Second-Order Irreversible Chemical Reactions

FRANCO MAGNO*, DOMENICO PEROSA and GINO BONTEMPELLI
Istituto di Chimica Analitica, University of Padova, Via Marzolo 1, 35131 Padova (Italy)
(Received 13th November 1984)

SUMMARY

Electrode reactions followed by very fast chemical reactions are considered. A simple approach, in which steady state and linear concentration profiles in the reaction layer are assumed, is proposed for the simulation of these processes when the substrate is not present in large excess. When the substrate/depolarizer mole ratio is less than one, two well-separated peaks are detected; under such conditions, working curves that enable the corresponding second-order homogeneous rate constant to be evaluated can be derived by the finite-difference simulation technique. The method is applied to elucidation of the reduction of the tetrakis(triphenylphosphine)nickel(I) complex in the presence of hydrogen ions in acetonitrile at −30°C.

Electroanalytical techniques can be used profitably not only to investigate electrode processes, but also to gain kinetic information on homogeneous chemical reactions when at least one of the reagents or products is an electroactive species. In particular, electrochemical processes of the type:

$$A + e^- \xrightarrow{k_{h,s}} B; \qquad B + S \overset{k_f}{\rightarrow} P \tag{I}$$

occur frequently in experimental practice.

Previous treatments of these irreversible mechanisms are restricted to a particular kinetic situation corresponding to a large excess of the substrate S, so that it can be regarded as constant throughout the diffusion layer. However, when the chemical step is very fast, study of these processes by the most useful criterion based on the change of the quantity i_{pa}/i_{pc} with scan rate can be no longer performed owing to the absence of response on the reverse scan. Moreover, the alternative less careful approach which takes advantage of the quantity $\delta E_p/\delta \log v$ is also unable to give the value of the homogeneous kinetic constant if $E_{1/2}$ for the uncomplicated electrode reaction is not available [1]. Therefore, in this kinetic situation, it is advisable to retard the chemical reaction by using substrate/depolarizer mole ratios (γ = S/A) less than one, so that only a fraction of the species B formed in the

0003-2670/85/$03.30

electrode step can undergo the subsequent homogeneous reaction. A further advantage offered by the use of these experimental conditions is the possibility of investigating electrochemical processes in which solubility requirements preclude the use of a large excess of substrate. Under such experimental conditions, the homogeneous reaction becomes of second-order and no theoretical treatment of this case has been reported in the literature; only a particular second-order e.c. mechanism (dimerization) has been described [2, 3].

In principle, digital simulation techniques make it possible to overcome difficulties deriving from reaction orders other than first order, but representation of extremely fast chemical reactions is time-consuming in that an enormous number of iterative steps is required in the calculations. These mathematical problems can be avoided by using the approach based on the assumption of a steady-state condition, as was emphasized in Part 1 of this work [4].

The present paper describes the mathematical approach used to represent a very fast second-order e.c. mechanism characterized by $\gamma \leqslant 1$. The relevant linear-sweep voltammetric responses are reported, together with the working curves which allow simple evaluation of the homogeneous kinetic constant. The calculations are utilized to rationalize the cathodic behaviour of the tetrakis(triphenylphosphine)nickel(I) complex in acetonitrile in the presence of protons which was encountered during an investigation of the reactivity of nickel hydrides obtained by reacting hydrogen ions with nickel(0) species [5].

EXPERIMENTAL

The electrochemical instrumentation, the experimental procedure employed and the purification of all the chemicals were described previously [5]. Explicit finite-difference programs were written in FORTRAN-IV and run on a MINC-11/23 computer (Digital Equipment Corp.) to generate current/potential curves with different boundary conditions. The relevant programs are available on request.

RESULTS AND DISCUSSION

Finite-difference simulation of the e.c. mechanism

Theoretical curves relative to mechanism I were calculated by digital simulation following two different procedures. The first, based on the usual finite kinetic relationships [6], was used to simulate e.c. processes involving not too fast chemical reactions (up to $k_f C_A/a = 5000$); for faster homogeneous steps, the steady-state assumption was utilized. In the latter case, a procedure similar to that reported in Part 1 [4] was followed. On the assumption of steady-state conditions for species B in scheme I, the following equations are valid (symbols are the same as in Part 1). Thus for generation of B,

$$q_{o,t} = k_{h,f}[A]_{o,t} - k_{b,h}[B]_s$$

The flux expressed in terms of the stationary concentration of B is $q_{o,t} = (D/\mu)[B]_s$. The kinetic balance on B is $q_{o,t} = \mu k_f [B]_s [S]_{\mu,t}$. For diffusion of A to the electrode surface, $q_{o,t} = 2D([A]_{1,t} - [A]_{0,t})$. Combination of these four equations and rearrangement gives

$$q_{o,t} = k_{h,f}(Dk_f[S]_{\mu,t})^{1/2}[A]_{1,t}/\{k_{h,b} + (Dk_f[S]_{\mu,t})^{1/2} + k_{h,f}(Dk_f[S]_{\mu,t})^{1/2}/2D\} \quad (1)$$

The correctness of this equation can easily be checked by inserting a constant value for $[S]_{\mu,t}$ (pseudo-first-order conditions). In such a way, it is possible to obtain the proper values for first-order e.c. processes characterized by different degrees of reversibility reported by Evans [7]. In this connection, it should be noted that the proposed method lowers considerably the computation times needed for high k_f/a values (from 1135 s by using a non-uniform space grid, to 113 s) while conserving the accuracy of the results. However, two main difficulties arise in the use of Eqn. 1 for representing second-order kinetic conditions (the aim of this work) owing to the inconstant value of $[S]_{\mu,t}$. This is typical of the finite-difference approach which introduces the highest error on the species at the lowest concentration (S in this case). For this reason, an iterative method was used inside every diffusion step to calculate the best $q_{o,t}$ and $[S]_{\mu,t}$ values.

The inconstancy of $[S]_{\mu,t}$ also underlies the second difficulty, because it causes the reaction layer to become broader and broader as shown by the following relationship, obtained by combining the above equations for the flux and the kinetic balance,

$$\mu = (D/k_f[S]_{\mu,t})^{1/2} \quad (2)$$

This progressive broadening implies that, after some time, the reaction layer is no longer negligible with respect to the first "diffusion box"; thus the steady-state approximation becomes no longer acceptable. This means that at this stage the algorithm must be changed to account for the fact that the chemical reaction then occurs only at some distance from the electrode surface. The discontinuity between the two algorithms reveals itself as fluctuations in the calculated voltammetric curve. An interpolation procedure based on the use of orthogonal polynomials [8] allows this difficulty to be overcome easily.

Theoretical voltammetric curves

Figure 1A shows a typical voltammetric response calculated by the above procedure. The distinctive characteristic of the curve is the presence of a well separated pre-peak resembling voltammograms appropriate to strong adsorption of the product [9]. A rather similar voltammetric profile has been described by Andrieux et al. [10] for a catalytic mechanism characterized by a very high kinetic constant and a low substrate/depolarizer mole ratio.

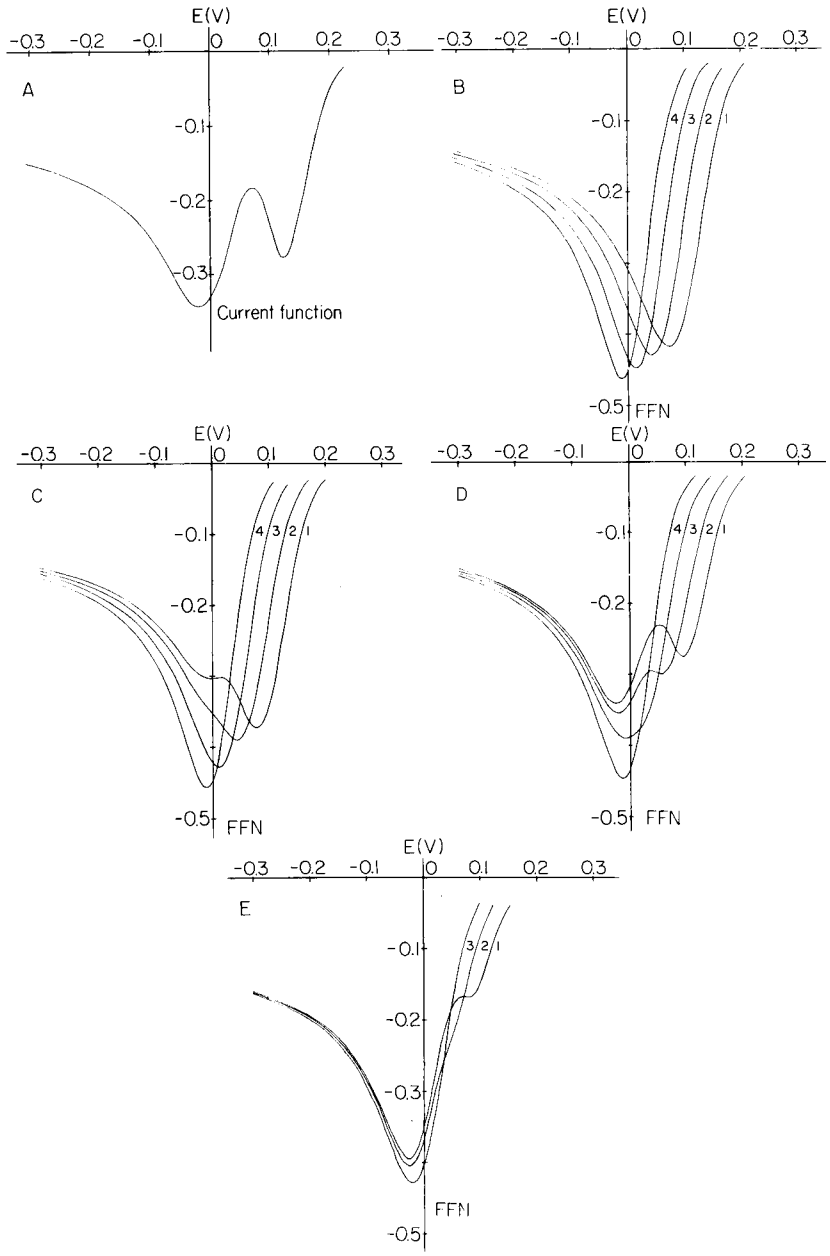

Fig. 1. Theoretical voltammetric curves for process I, calculated with different γ and k_fC_A/a values. (A) $\gamma = 0.5$, $k_fC_A/a = 50\,000$. (B) $\gamma = 1$, k_fC_A/a: (1) 2500; (2) 250; (3) 25; (4) 2.5. (C) $\gamma = 0.75$, k_fC_A/a: (1) 3336; (2) 333.6; (3) 33.36; (4) 3.33. (D) $\gamma = 0.5$, k_fC_A/a: (1) 5000; (2) 500; (3) 50; (4) 5. (E) $\gamma = 0.25$, k_fC_A/a: (1) 1000; (2) 100; (3) 10.

To verify the correctness of this unusual profile drawn by the proposed approach, voltammetric curves for intermediate situations (rather fast chemical reactions) were calculated by the earlier methods [11]. Figure 1(B—E) shows several voltammetric curves obtained in this way for different values of the kinetic parameter ($k_f C_A/a$) and different stoichiometric ratios (γ = [S]/[A]). It is apparent that decrease of γ and/or an increase of the kinetic parameter indeed cause a progressive split of the cathodic curve into two peaks.

The explanation for such behaviour lies in a typical property of the e.c. process. The occurrence of a fast consecutive chemical reaction leads generally to an anodic shift of the reduction peak [1, 7], but when $\gamma < 1$ only a fraction of the species A can be reduced at the electrode surface at a thermodynamic level lowered by the presence of the substrate S. Consequently, a real e.c. mechanism is operative only in the pre-peak; in the second peak the uncomplicated reduction of the remainder of A takes place because of the previous depletion of S at the electrode surface.

According to these arguments, the distance between the two peaks should be related to the homogeneous kinetic constant for any given value of ψ (degree of reversibility) and γ. Figure 2 shows two working curves which allow the kinetic parameter $k_f C_A/a$ to be evaluated from the experimental ΔE_p values, for a reversible and a quasi-reversible electrode process, respectively, when γ = 0.5. Previous treatments of these e.c. mechanisms in linear-sweep voltammetry were restricted to a particular kinetic situation corresponding to a large excess of substrate. The approach suggested here, based on a γ value less than one, offers the advantage of showing directly the reference potential (E_p for the uncomplicated process) and thus represents a useful extension to experimental conditions in which kinetic and/or solubility requirements preclude the use of a constant substrate concentration in the reaction layer. In the working curves (Fig. 2), the useful range of the $k_f C_A/a$ parameter is limited at the left side by merging of the peaks and at the right side by inadequate sensitivity.

As indicated above, the voltammetric response relevant to the e.c. mechanism treated in the present paper can be mistaken for that typical of adsorption reactions [9] and/or catalytic processes in which a low excess factor (γ) is used [10]. However, the dependence of the height of the pre-peak on the concentration and the potential sweep rate makes it possible to distinguish between these mechanisms. In fact, dependence on the square root of the substrate concentration is observed only for catalytic mechanisms when γ becomes sufficiently high (pseudo-first-order conditions) [12]. Conversely, adsorption and e.c. processes attain constant limiting peak heights when the substrate concentration is increased. These two last processes can be distinguished by means of their different behaviour with respect to a change in the potential scan rate; the peak current is proportional to v or $v^{1/2}$, respectively.

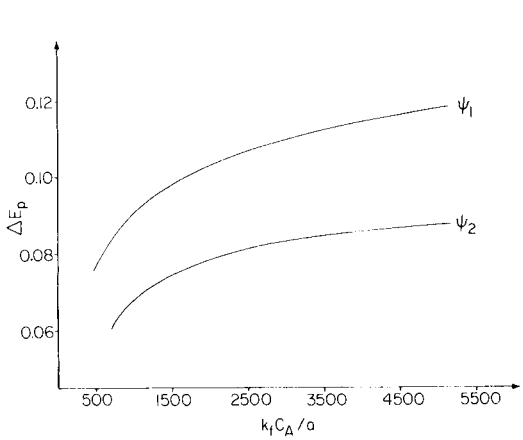

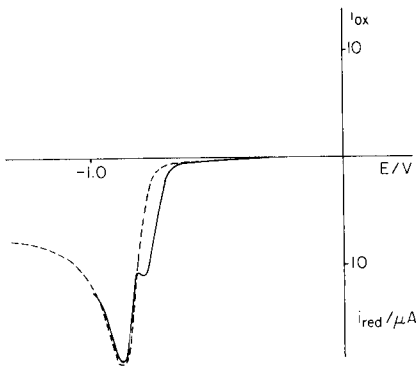

Fig. 2. Working curves for process I calculated with $\gamma = 0.5$ and two values of the charge-transfer kinetic parameter: $\psi_1 = 6025$ (totally reversible); $\psi_2 = 1.3$ (quasi-reversible).

Fig. 3. Voltammetric curves recorded at —30°C with a glassy-carbon microelectrode in a 0.1 M TBAP solution in acetonitrile/toluene (60/40 v/v) containing: (---) 2.5×10^{-3} M $[Ni(PPh_3)_4]^+$; (—) 2.5×10^{-3} M $[Ni(PPh_3)_4]^+$ after addition of 1.25×10^{-3} M triphenylphosphonium. Scan rate 0.2 V s^{-1}.

The reaction of an electrogenerated nickel(0) complex with protons

The reversible reduction of the tetrakis(triphenylphosphine)nickel(I) complex in acetonitrile containing 0.1 M tetrabutylammonium perchlorate (TBAP) as supporting electrolyte, occurs through an e.c. reaction pathway when triphenylphosphonium cations are present. The electrogenerated nickel(0) complex reacts very quickly with protons to give the corresponding nickel(II) hydride species [5]

$$[Ni(PPh_3)_4]^+ + e^- \rightarrow [Ni(PPh_3)_4]$$

$$[Ni(PPh_3)_4] + HPPh_3^+ \xrightarrow{k_f} [Ni(H)(PPh_3)_4]^+ + PPh_3$$

Figure 3 shows a typical voltammetric curve, obtained at —30°C with $\gamma = 0.5$, exhibiting two well-defined peaks as expected for an e.c. process characterized by a fast homogeneous step. By employing the criteria reported above, it was verified that such a process really is operative. Moreover, the analysis of the data obtained at different scan rates (v) and at different substrate/depolarizer mole ratios (γ) allows the second-order homogeneous constant k_f to be evaluated; the result found was 3×10^6 mol^{-1} s at —30°C.

This work was supported by the Italian National Research Council (CNR) and by the Ministry of Public Education.

REFERENCES

1 R. S. Nicholson and I. Shain, Anal. Chem., 36 (1964) 706.
2 M. L. Olmstead, R. G. Hamilton and R. S. Nicholson, Anal. Chem., 41 (1969) 260.
3 L. Nadjo and J. M. Saveant, J. Electroanal. Chem., 48 (1973) 113.
4 F. Magno, D. Perosa and G. Bontempelli, Anal. Chim. Acta, 173 (1985) 211.
5 G. Schiavon, F. Magno and G. Bontempelli, Ann. Chim. (Rome), 74 (1984) 361.
6 F. Magno, G. Bontempelli and M. Andreuzzi-Sedea, Anal. Chim. Acta, 140 (1982) 65.
7 D. H. Evans, J. Phys. Chem., 76 (1972) 1160.
8 K. J. Johnson, Numerical Methods in Chemistry, M. Dekker, New York, 1980.
9 R. H. Wopschall and I. Shain, Anal. Chem., 39 (1967) 1514.
10 C. P. Andrieux, C. Blocman, J. M. Dumas-Bouchiat, F. M'Halla and J. M. Saveant, J. Electroanal. Chem., 113 (1980) 19.
11 F. Magno, G. Bontempelli and D. Perosa, Anal. Chim. Acta, 147 (1983) 65.
12 J. M. Saveant and E. Vianello, Electrochim. Acta, 10 (1965) 905.

Analytica Chimica Acta, 173 (1985) 227—238
Elsevier Science Publishers B.V., Amsterdam — Printed in The Netherlands

COMPUTER ANALYSIS OF THE CRACKING PATTERNS OF DEUTERATED HYDROCARBONS

D. H. LENZ and WM. C. CONNER, Jr*

Department of Chemical Engineering, University of Massachusetts, Amherst MA 01003 (U.S.A.)

(Received 5th November 1984)

SUMMARY

A generalized, statistical model for calculating the mass spectral fragmentation patterns of deuterated hydrocarbons of low molecular weight is presented. Isotopic differences in bond energies and probabilities of the bond breakage of hydrogen and deuterium are included. Only a single fitting parameter is used. This parameter seems to be consistent for similar species of hydrocarbons. Small statistical deviations from observed spectra for deuterated methanes, acetylenes, ethylenes, and ethanes are obtained when this model is used.

Insights into the understanding of reaction mechanisms and specifically into heterogeneous reactions come from surface science, chemical adsorption, and reaction kinetics. Isotopic studies play an important role in each of these areas. Ozaki [1] gives numerous examples of mechanistic understandings gained from isotopic studies involving H_2/D_2 exchange reactions, olefin isomerizations, and hydrogenation/deuteration of olefins, over metal and metal oxide catalysts. For reaction-path studies and overall reaction kinetics, the mass spectrometer has proven to be a powerful and valuable tool when coupled with stable isotopes. Recently, computer programs have been developed to calculate mass spectral isotopic distributions [2—4].

The major problem noted by Ozaki as well as other authors [5—9] is due to the nature of the molecular decomposition induced by the mass spectrometer. The positive ions produced by the electron bombardment of a molecule include the parent or molecular ion as well as fragment ions. These fragment ions often interfere with the parent ion of a different molecule, making it difficult to quantify each isotopic molecular species. Though this interference is reduced by using a low ionizing voltage, it is not eliminated. The problem can be solved by calibration of the mass spectrometer with a high-purity sample of each isotopic species involved in the study. This method, however, can be very expensive and time-consuming to obtain all the isotopes for each standard run. The goal of this paper is to describe a simple generalized model for molecular decomposition in mass spectrometers which can generate these fragmentation patterns for any isotopic species in an easily usable form with a minimum amount of information.

0003-2670/85/$03.30

Schissler et al. [5] were the first to attempt a quantitative explanation for the mass spectra of deuterated methane and, to some extent, deuterated ethane. Two empirically determined weighting factors were used. With one weighting factor corresponding to the rupture of a C—H bond, a, and the other to the rupture of a C—D bond, b, good agreement between the observed and the calculated spectra was obtained. Dibeler et al. [6], in their study of the mass spectra of deuterated ethylenes, observed that the weighting factors derived from a and b occur in a regular power series type sequence (i.e., $a_2 = a_1^2$, $a_3 = a_1^3$, $a_4 = a_1^4$, $b_1 = b_4^4$, $b_2 = b_4^3$, $b_3 = b_4^2$) and that a_1 and b_4 were reciprocals. The subscripts on a_i and b_i refer to the number of deuterium atoms per ethylene molecule. A single constant, the isotopic factor K, which is analogous to the initial C—H bond rupture, was introduced from which the calculated mass spectra agreed nicely with the observed mass spectra.

Amenomiya and Pottie [8] described an empirical method for the calculation of mass spectra for deuterated ethane. The calculations were made on a statistical basis, using as few empirical rules as possible in order to minimize the number of parameters. Besides calculation of the isotopic factors, a_i and b_i, for each isotope, the hydrogen-removal mechanism was also considered. Three possible mechanisms of decomposition were identified: (A) the hydrogen molecule is removed from adjacent carbons, (B) the hydrogen molecule is removed from the same carbon, or (C) the loss is a random process involving a statistical combination of the previous two. They determined that the probability of A occurring was 0.87% and of B occurring was 0.13%. These factors were included for all fragment ion intensities which incorporated the loss of two hydrogen atoms. In an earlier paper [7], Amenomiya and Pottie had also concluded that analysis of the mass spectra of C_1 fragments indicated a reshuffling of hydrogen atoms before or during the C—C bond rupture.

Amenomiya and Pottie [8] attempted to model the degree of rearrangement of the hydrogen atoms before or during C—C bond rupture. Two models were postulated to establish whether the observed spectra for C_1 species were due to mixed isomers resulting from reshuffled hydrogen or to rearranged molecules decomposing to C_1 only and not giving rearranged C_2 ions. Unfortunately, the calculations could not distinguish between the models. In the same vein, results of Schissler et al. [5] are not in total agreement with Amenomiya and Pottie [8] concerning the hydrogen-removal mechanism. Schissler et al. [5], observed that the H_2:HD:D_2 ratio for the removal of two hydrogens from trideuteroethane was 0.06:0.71:0.23. Comparing this with the ratios obtained from each hydrogen-removal mechanism (0.0:1.0:0.0 for A; 0.5:0.0:0.5 for B; and 0.2:0.6:0.2 for C) indicates that a random process is favored over removal from the same carbon.

STATISTICAL MODEL

General

In the derivation of the proposed model, the fragmentation patterns were calculated for a variety of isotopic molecules by using a minimum amount of information. An Analog Devices Macsym 350 computer was used in the modeling and calculations, as well as the collection and analysis of all mass spectral data. The model incorporates both the probability of a hydrogen and/or deuterium atom removal from the molecule and the sequence or order in which each atom is removed. The model takes into account the isotope difference in the C—H, C—D bond breaking.

The two types of information required are the cracking patterns for the perhydro- and perdeutero-molecules, which can be standardized to the mass spectrometer used and then stored in the computer, and the number of hydrogen and/or deuterium atoms per parent molecule. The molecular ion peaks must be normalized to a parent ion peak of 1.0 or 100.0 for the input cracking patterns. As the mechanisms for both hydrogen removal and hydrogen rearrangement are ambiguous, these are not incorporated in this model.

The model creates an $N + 1$ by $2N$ matrix, where N is the number of H and/or D atoms per molecule (e.g., $N = 6$ for ethane). The first row contains the perhydro mass spectra and the last row contains the perdeutero mass spectra. The Nth element in each row is the ratio of the $(M - N)$ mass to the parent peak with mass M.

Coding

In statistically modeling the decomposition of an alkane or olefin into numerous fragment ions in a mass spectrometer, the contributions of losing just hydrogen atoms, just deuterium atoms, and all mixed orders are included. In each case, the preference for the carbon to retain hydrogen over deuterium (the isotope effect) is included. The factor for the removal of the ith hydrogen (or deuterium) is based on the cracking ratio for the removal of the ith hydrogen (or deuterium) from the perhydro- (or perdeutero-) compound. This is done in a manner similar to that of Dibeler et al. [6]. By using FFH, which is the value of the isotopic factor for the initial C—H bond rupture (the only input variable for our computer simulation), a matrix of isotopic factors is created corresponding to each specific deuterated compound. The creation of this matrix involves the following algorithms

$$\mathrm{HFF} = \mathrm{FFH}^{(M-1)} \text{ and } \mathrm{DFF} = \mathrm{FFH}^{(M-1-N)}$$

This is done in a program loop within the HFF/DFF box in Fig. 1 ($M - 1$ corresponds to the number of deuterium atoms in the molecule). Therefore, HFF is the hydrogen isotopic factor and DFF is the deuterium isotopic factor. At $M = 1$, HFF is the reciprocal of DFF at $M = N + 1$, as it should be (as outlined above, $a_1 = b_4^{-1}$).

As a molecule decomposes, its fragment ions depend on how many

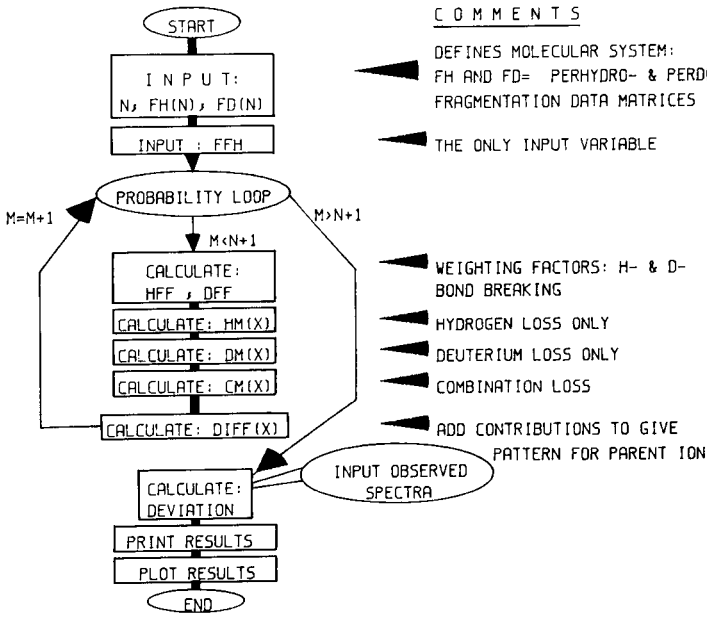

Fig. 1. Program flowsheet.

hydrogen and/or deuterium atoms are lost. For example, dideuteroethane, with a parent peak at 32 m/z, creates C_2 fragment ions at 31, 30, 29, 28, 27, 26, 25 and 24 m/z. The 31 m/z ion is due to the loss of one hydrogen atom only, while the 30 m/z ion results from the loss of either a deuterium atom or two hydrogen atoms. The 29 m/z fragment can come only from the combined loss of a hydrogen and a deuterium atom. However, the order of the loss is taken into account. It is impossible to establish whether the hydrogen atom is removed first, followed by the deuterium atom or vice versa, yet both must occur statistically and so are included. The sequencing is of greater complexity as the molecule continues to decompose. The 28 m/z ion fragment is due to the loss of either two deuterium atoms or one deuterium and two hydrogen atoms. For the latter possibility, the statistical probabilities of the loss sequence, H:D:H, H:H:D, D:H:H, are included. In each case, the bond rupture is weighted by the appropriate isotopic factor.

Computer examples

Starting with the perhydromolecule of interest, the model determines all statistically possible ways to lose hydrogen/deuterium atoms for a m/z loss of 1 until all hydrogen/deuterium atoms are removed. This is repeated as additional deuterium atoms replace hydrogen atoms until the perdeutero species is finished. A model flowsheet is shown in Fig. 1. Table 1 shows the algorithm used to determine the combination losses for each potential isotopic species. The rows indicate the m/z loss, while the columns indicate the

TABLE 1

Combination loss algorithms

m/z loss									No. of H or D
1	1H								
2	2H	1D							
3	3H	1H,1D							
4	4H	2H,1D	2D						2
5	5H	3H,1D	1H,2D						
6	6H	4H,1D	2H,2D	3D					
7	7H	5H,1D	3H,2D	1H,3D					
8	8H	6H,1D	4H,2D	2H,3D	4D				4
9	9H	7H,1D	5H,2D	3H,3D	1H,4D				
10	10H	8H,1D	6H,2D	4H,3D	2H,4D	5D			
11	11H	9H,1D	7H,2D	5H,3D	3H,4D	1H,5D			
12	12H	10H,1D	8H,2D	6H,3D	4H,4D	2H,5D	6D		6
13	13H	11H,1D	9H,2D	7H,3D	5H,4D	3H,5D	1H,6D		
14	14H	12H,1D	10H,2D	8H,3D	6H,4D	4H,5D	2H,6D	7D	
15	15H	13H,1D	11H,2D	9H,3D	7H,4D	5H,5D	3H,6D	1H,7D	
16	16H	14H,1D	12H,2D	10H,3D	8H,4D	6H,5D	4H,6D	2H,7D	8D 8

various combinations of hydrogen (H) and deuterium (D) atoms which would result in this decrease in *m/z*. Each entry in the table is a subroutine in the proposed model and the algorithm is executed showing all necessary combination losses for up to an octahydromolecule, such as propane (includes all subroutines above line 8). The simple algorithm can easily be expanded to include larger alkanes and olefins.

Some examples of the algorithms will be instructive, with back-reference to the flowsheet and Table 1. Defining some terms, HM(X) is the hydrogen loss matrix; DM(X) is the deuterium loss matrix; and CM(X) is the combination loss matrix, where X refers to the *m/z* loss number. Continuing with the dideuteroethane example, the calculation of the 31 *m/z* ion ($X = 1$) is accomplished by the following equations nested within the HM(X) loop boxed in Fig. 1 (FH(X) is the input perhydro mass spectra, $M = 1$ at this point, and I is an incremented dummy variable)

$$\mathrm{HM}(X) = \mathrm{FH}(X)$$

$$\mathrm{HM}(X) = \mathrm{HM}(X) \times (N - M - I + 2)/(N - I + 1) \times \mathrm{HFF}$$

Next, the 30 *m/z* ion ($X = 2$) could be produced by the above algorithm when $M = 2$ or by the following equations nested within the DM(X) loop boxed in Fig. 1 (FD(X) is the input perdeutero mass spectra)

$DM(2X) = FD(X)$

$DM(2X) = DM(2X) \times (M - I)/(N - I + 1) \times DFF$

Finally, the calculation of the 28 m/z ion fragment ($X = 4$) can be produced by the HM loop when $M = 4$, by the DM loop when $M = 2$, or by the Two-One subroutine of the $CM(X)$ loop with the equations, where $RH(I)$ and $RD(I)$ are matrices of the remaining atoms to be cracked off in RI is simply a constant.

$RH(I) = FH(I + 1)/FH(I)$

$RD(I) = FD(I + 1)/FD(I)$

$RI = (M - 1)(N - M + 1)/[N(N - 1)]$

For H = 2, D = 1 and $J = 4$ (J is a dummy variable)

$CM(4) = CM \times RI \times (N - M)/(N - 2)$

$FA(I) = FH(I) \quad FB(I) = FD(I)$

$RA(I) = RH(I) \quad RB(I) = RD(I)$

A and FA denote the major hydro/deutero species and B and FB denote the minor one. If H < D, which it is not here, then FH and FD, and RH and RD are simply switched.

For the Two-One subroutine (shown as 2H,1D and/or 1H,2D in Table 1)

$CM = FA(1) \times RA(2) \times RB(2)$ (for H:H:D)

$+ FB(1) \times RA(1) \times RA(2)$ (for D:H:H)

$+ FA(1) \times RB(1) \times RA(2)$ (for H:D:H)

$CM = CM \times (HFF)^{H} \times (DFF)^{D}$

In completing calculations of the fragmentation patterns for d_2-ethane, all the subroutines listed above line 6 in Table 1 will be used. A m/z ion loss of 6 ($X = 6$) requires the most subroutines (4 in this case). These are the HM(6), Four-One, Two-Two, and DM(3) subroutines.

RESULTS AND DISCUSSION

The cracking patterns for some molecules, based on the data from different instruments, were created by using the model described herein. Table 2 shows the results for methane. Experimental spectra for comparison were obtained from Schissler et al. [5], who used an all-metal, 60° sector Nier-type mass spectrometer with 75-eV bombardment and from the Atlas of Mass Spectra Data [10], for which an unspecified mass spectrometer was used at 50 eV. Experimental spectra for ethylene and acetylene obtained from Dibeler et al. [6] and Mohler and Dibeler [9], respectively, are compared with the calculated spectra in Table 3. They used a Consolidated 21-103 mass spectrometer at 70 eV.

TABLE 2

Methane spectra

Mass	CH_4 Exp.	CH_3D Exp.	CH_3D Calc.	CH_2D_2 Exp.	CH_2D_2 Calc.	CHD_3 Exp.	CHD_3 Calc.	CD_4 Exp.
Schissler et al. [5] (FFH = 1.22)								
20	—	—	—	—	—	—	—	100.0
19	—	—	—	—	—	100.0	—	—
18	—	—	—	100.0	—	36.2	36.1	72.8
17	—	100.0	—	59.0	59.2	46.3	44.8	
16	100.0	73.5	72.8	27.5	27.4	3.05	4.42	4.24
15	79.6	17.3	15.9	3.53	3.96	2.10	1.42	
14	7.91	3.52	3.28	3.56	2.12	1.91	1.83	1.60
13	2.84	1.65	1.49	0.94	0.67	0.44	0.22	
Deviation (%)			0.31		0.26		0.31	
Atlas of Mass Spectral Data [10] (FFH = 1.2)								
20	—	—	—	—	—	—	—	100.0
19	—	—	—	—	—	100.0	—	—
18	—	—	—	100.0	—	27.7	37.0	83.0
17	—	100.0	—	62.4	61.6	51.1	51.9	—
16	100.0	77.2	77.0	30.7	34.7	13.2	10.6	12.5
15	85.6	20.9	24.3	9.80	9.80	6.80	4.30	—
14	17.1	8.80	8.80	6.40	7.00	6.40	7.00	7.20
13	8.60	4.90	5.10	2.80	1.00	1.40	1.00	—
Deviation (%)			0.69		0.69		1.43	

TABLE 3

Ethyne and ethylene spectra

Mohler and Dibeler [9] (FFH = 1.2)

Mass	C_2H_2 Exp.	C_2HD Exp.	C_2HD Calc.	C_2D_2 Exp.
28	—	—	—	100.0
27	—	100.0	—	—
26	100.0	12.0	12.3	17.7
25	20.5	6.40	7.40	—
24	5.67	4.80	5.00	4.35
Deviation (%)			0.26	

Dibeler et al. [6] (FFH = 1.09)

Mass	C_2H_4 Exp.	C_2H_3D Exp.	C_2H_3D Calc.	$C_2H_2D_2$ Exp.	$C_2H_2D_2$ Calc.	$C_2H_2D_2$ *Trans* Exp.	$C_2H_2D_2$ *Trans* Calc.	C_2HD_3 Exp.	C_2HD_3 Calc.	C_2D_4 Exp.
32	—	—	—	—	—	—	—	—	—	100.0
31	—	—	—	—	—	—	—	100.0	—	—
30	—	—	—	100.0	—	100.0	—	22.7	22.0	60.8
29	—	100.0	—	41.9	41.1	40.0	40.3	40.8	41.8	—
28	100.0	55.6	55.5	39.9	41.6	41.6	41.5	38.2	39.1	63.7
27	67.9	50.6	51.8	42.6	43.9	41.5	43.9	25.8	26.8	—
26	67.5	31.0	32.1	15.0	14.8	15.5	14.9	9.80	9.30	10.4
25	13.5	7.70	8.60	4.00	4.70	4.10	4.80	1.70	2.00	—
Deviation (%)			0.37		0.40		0.43		0.27	

TABLE 4

Ethane spectra

Amenomiya and Pottie [8] FFH = 1.1

Mass	C_2H_6	C_2H_5D		$C_2H_4D_2$ (CH_2DCH_2D)		$C_2H_4D_2$ (CH_3CHD_2)		$C_2H_3D_3$ (CH_3CD_3)	
	Exp.	Exp.	Calc.	Exp.	Calc.	Exp.	Calc.	Exp.	Calc.
33								100.0	
32				100.0		100.0		49.2	52.0
31		100.0		64.2	62.4	64.2	62.4	71.6	171.8
30	100.0	72.9	70.3	258.1	251.6	206.6	251.6	337.4	271.6
29	76.2	316.7	325.9	201.6	225.2	239.7	225.2	74.1	114.3
28	388.5	153.1	165.6	98.5	86.5	100.1	86.5	53.9	60.4
27	104.3	78.2	72.5	59.7	57.8	53.3	57.8	44.3	36.9
26	68.1	44.9	40.8	25.9	18.0	19.8	18.0	12.9	13.5
25	7.80	6.70	2.60	4.90	4.20	2.60	4.20	2.80	2.80
Deviation (%)			2.42		4.01		5.25		13.59

Mass	$C_2H_3D_3$ (CH_2DCHD_2)		$C_2H_2D_4$ (CHD_2CHD_2)		$C_2H_2D_4$ (CH_2DCD_3)		C_2HD_5		C_2D_6
	Exp.	Calc.	Exp.	Calc.	Exp.	Calc.	Exp.	Calc.	Exp.
36									100.0
35							100.0		
34			100.0		100.0		18.7	21.3	73.6
33	100.0		36.5	38.5	36.5	38.5	55.2	54.8	
32	49.9	52.0	117.4	99.1	64.6	99.1	197.2	217.8	468.2
31	172.3	171.8	230.4	282.9	291.3	282.9	220.0	253.8	
30	229.5	271.6	156.5	162.6	155.2	162.6	63.6	70.1	99.2
29	107.3	114.3	54.3	61.5	62.7	61.5	41.4	36.2	
28	57.5	60.4	53.3	46.0	82.1	46.0	52.2	62.4	77.0
27	41.5	36.9	28.4	32.9	28.1	32.9	15.5	16.9	
26	12.5	13.5	7.50	8.50	8.50	8.50	6.90	0.00	7.00
25	2.80	2.80	0.80	1.00	1.70	1.00	1.00	0.70	
Deviation (%)		4.76		5.42		5.13		3.88	

Averaged spectra (FFH = 1.09)

Mass	$C_2H_4D_2$		$C_2H_3D_3$		$C_2H_2D_4$	
	Ave.	Calc.	Ave.	Calc.	Ave.	Calc.
34	—	—	—	—	100.0	—
33	—	—	100.0	—	36.5	35.8
32	100.0	—	49.6	49.2	91.0	92.5
31	64.2	60.2	122.2	158.3	260.9	272.8
30	232.4	236.3	286.8	269.6	155.9	167.9
29	220.7	228.1	91.0	116.7	58.5	61.5
28	99.3	87.3	57.5	59.5	67.7	44.7
27	56.5	57.4	41.5	37.3	28.3	34.1
26	22.9	19.2	12.5	14.1	8.00	8.60
25	3.80	4.40	2.80	2.90	1.30	1.00
Deviation (%)		1.96		5.31		2.93

The experimental spectra for ethane were obtained from three sources. The data of Schissler et al. [5] were produced by the above-mentioned Nier mass spectrometer. Amenomiya and Pottie [8] used an Atlas CH4, 60° magnetic sector mass spectrometer at 70 eV. The type of mass spectrometer used for the data from the Eight Peak Index [11] was not given. The present results are compared to the data of Schissler et al. in Table 4. Similar statistical deviations using the proposed model were found with the other experimental spectra.

For every molecule and compound, except trideuteroethane, the agreement between the observed and the calculated spectra was very good, considering the inherent error for mass spectra. This demonstrates the utility of the model for any type of mass spectrometer. The statistical deviation was obtained according to the method of Schissler et al. [5] and Amenomiya and Pottie [8] by taking the square root of the sum of the squares of the deviations, then dividing by the total number of C_2 ions produced.

Initially, the isotopic factor, FFH, was a variable. Figures 2 and 3 show the effect of including the isotopic factor into the calculated spectra for methane (Fig. 2) and ethylene (Fig. 3). An FFH value of 1.0 essentially removes the isotopic factor from the model calculations. From Tables 2—4, the observed and the calculated values can be compared for each molecule (except the perhydro and perdeutero molecules, which were input rather than calculated). The final value of FFH which gave the best fit to the reported data was reached after several iterations. Interestingly, the value of FFH which gave the best fit for all C_2 compounds, except acetylene, was independent of mass spectrometer and electron voltage (calculated as 1.09—1.1). This agrees with the value obtained by trial and error by others (Table 5). For all methanes, and also acetylene, the value of FFH which yielded the best fit was 1.2—1.22. This value for methane is in agreement with that determined by Schissler et al. [5]. A correlation between the

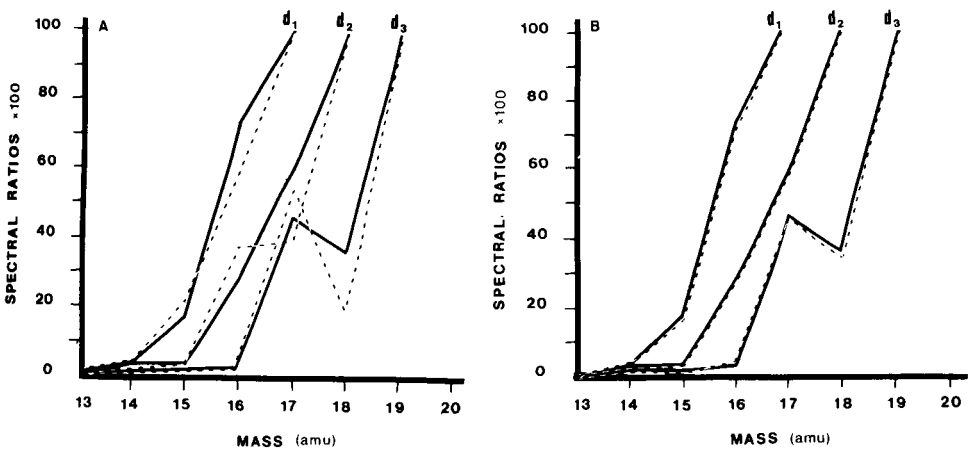

Fig. 2. Experimental spectra for deuterated methane from data of Schissler et al. (solid lines) compared with calculated values (dotted lines) using different isotope factors: (A) 1.0; (B) 1.22. Lines: (d1) CH_3D; (d2) CH_2D_2; (d3) CHD_3.

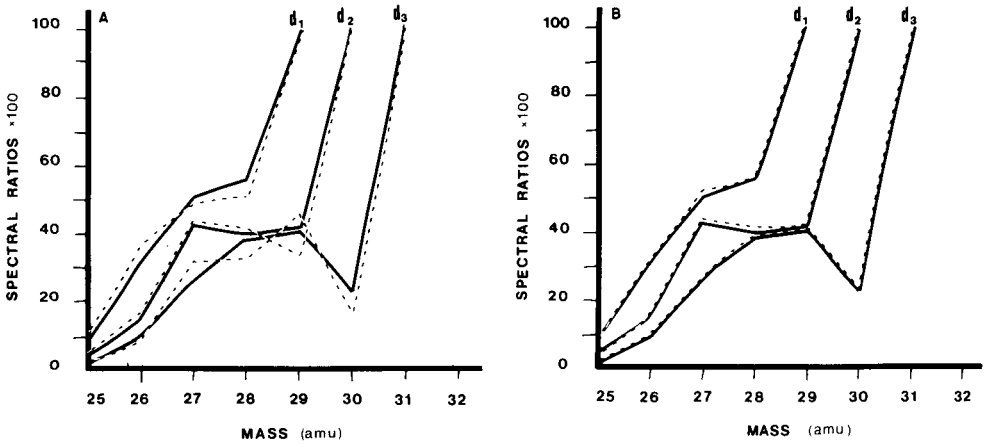

Fig. 3. Experimental spectra for deuterated ethylene from data of Dibeler et al. (solid lines) compared with calculated values (dotted lines) using different isotope factors: (A) 1.0; (B) 1.09. Lines: (d1) C_2H_3D; (d2) $C_2H_2D_2$; (d3) C_2HD_3.

number of carbon atoms of a molecule and its isotopic factor can thus be made, except for acetylene. Therefore, in actuality, this model does not depend on multiple variables or sophisticated weighting factors.

Because of the statistical coding philosophy of the model, thermodynamically preferred molecules (entropically favored; more random in combination bond positioning and rupture) are fitted better. This can best be seen with the d_2-, d_3-, d_4-ethanes in Table 4. In each case, there exist two chemically and thermodynamically stable structures. With trideuteroethane, for example, it can be seen that thermodynamically favored CH_2—$DCHD_2$ has much less statistical deviation than CH_3CD_3, which has the poorest fit. Amenomiya and Pottie [8] could not distinguish between structures for trideuteroethane and both indeed exist at the same time. But an averaged spectra for both structures gave excellent agreement with the model (Table 4).

The motivating factor in developing this model was to be able to identify the product distribution of a mixture of deuterated and undeuterated ethylenes and ethanes formed during ethylene deuteration experiments over an

TABLE 5

Isotopic factors

	This work	Ref. 5	Ref. 6	Ref. 8	Ref. 9
CH_4	1.2—1.22	1.22	—	—	—
C_2H_2	1.2	—	—	—	1.13
C_2H_4	1.09	—	1.1	—	—
C_2H_6	1.09—1.1	1.09	—	1.1	—

TABLE 6

Mixture analysis

Input mass spectra FH(X) & FD(X), FFH = 1.1				m/z	Relative areas of gas-phase mass spectra	
C_2H_4	C_2D_4	C_2H_6	C_2D_6		Run 519: $C_2H_4 + D_2$	Run 416: $C_2H_4 + D_2 + H_2$
			1.0	36	3.8	
				35	14.0	
			0.83	34		
				33	27.9	5.1
	1.0		7.14	32	89.0	18.4
				31	181.7	56.8
	0.65	1.0	2.08	30	265.7	181.5
		1.08		29	332.1	363.0
1.0	0.75	7.69	2.02	28	387.3	940.1
0.83		2.92		27	251.9	553.9
0.60	0.12	2.38	0.22	26	183.0	427.0
0.10		0.46		25	31.6	68.2
0.03	0.03	0.03	0.03	24	9.7	18.4

Isotopic algorithm analysis of above data

	Ethylene					Ethane							H (%)[a]
Run	$d0$-	$d1$-	$d2$-	$d3$-	$d4$-	$d0$-	$d1$-	$d2$-	$d3$-	$d4$-	$d5$-	$d6$-	
519	0.44	0.55	0.0	0.0	0.0	0.0	0.0	0.46	0.28	0.19	0.05	0.0	60
416	0.88	0.11	0.0	0.0	0.0	0.56	0.25	0.13	0.04	0.0	0.0	0.0	65

[a]% conversion or hydrogenation.

oxide-type catalyst. A UTI AGA-100 MUX quadrupole gas analyzer at 70 eV was used for these experiments. Some typical analyses of the product gas phase reached by this model are found in Table 6. These results are of a nature typical for oxide-type catalysts, according to Ozaki [1].

Conclusions

By using a simple, statistical model based on the probability and order of H/D-bond rupture in deuterated alkanes and olefins, and by taking into account the isotopic effect, the cracking patterns for all deuterated molecules for methane, ethane, ethylene, and acetylene can be created with a minimum amount of time and information. The model is independent of mass spectrometer, ionizing voltage, chemical species (larger alkanes and olefins can be incorporated) and can be run dynamically as part of the experimental determination. There appears to be some correlation between the number of carbon atoms of a hydrocarbon molecule and the isotopic factor for the initial C—H bond rupture.

The authors express appreciation to the donors of the Petroleum Research Fund, Grant 13703-AC7, administered by the American Chemical Society, for support of this research.

REFERENCES

1 A. Ozaki, Isotopic Studies of Heterogeneous Catalysis, Kodansha, Tokyo, & Academic Press, New York, 1977.
2 D. H. Smith, Energy Res. Abstr. (1980), Report 1979, ORNL/TM-7002.
3 J. A. Yergey, Int. J. Mass Spectra Ion Phys., 52 (1983) 337.
4 C. Strauss, CLB, Chem. Labor. Betr., 34 (1983) 556.
5 D. O. Schissler, S. O. Thompson and J. Turkevich, Discuss. Faraday Soc., 10 (1951) 46.
6 V. H. Dibeler, F. L. Mohler and M. deHemptinne, J. Res. Natl. Bur. Stand., 53 (1954) 107.
7 Y. Amenomiya and R. F. Pottie, Can. J. Chem., 76 (1968) 1735.
8 Y. Amenomiya and R. F. Pottie, Can. J. Chem., 76 (1968) 1741.
9 F. L. Mohler and V. H. Dibeler, Phys. Rev., 72 (1947) 158.
10 E. Stenhagen, S. Abrahamsson and F. W. McLafferty (Eds.), Atlas of Mass Spectral Data, Interscience, New York, 1969.
11 Eight Peak Index of Mass Spectra, 2nd edn., ICI and Mass Spectrometry Data Center, Aldermaston, England, 1974.

Analytica Chimica Acta, 173 (1985) 239—251
Elsevier Science Publishers B.V., Amsterdam — Printed in The Netherlands

EVALUATION OF ISOTACHOPHORESIS AS A METHOD OF IDENTIFICATION AND COMPARISON WITH OTHER METHODS BY INFORMATION THEORY*

E. KENNDLER

Institute of Analytical Chemistry, University of Vienna, Waehringerstr. 38, A-1090 Vienna (Austria)

(Received 11th January 1985)

SUMMARY

Information theory is applied to estimate the identification power of isotachophoresis. Two approaches are used to estimate the information content of qualitative isotachophoresis. In the first, an expression is derived for the maximum number of compounds that can be distinguished in an isotachopherogram under realistic conditions; if equal probabilities of the incidence of the compounds are assumed, the maximum information content is 6.5—7 bit. In the second approach, the information content obtained by a retrieval procedure from a library of data on 263 anionic species in eight leading electrolyte systems in the pH range 3—10 is discussed; the information content is 3.5—5.7 bit for the individual electrolyte systems. When correlation between the systems is taken into account, the information content is reduced, e.g., to an average of 3.2 bit per system for the four systems with lowest correlation. Based on the information content, isotachophoresis is compared with mass spectrometry, infrared spectrometry, gas chromatography and thin-layer chromatography. It is shown that the identification power of isotachophoresis is in the range of that of packed-column gas chromatography.

An analytical sample can be regarded as a source of information. Analytical measurements reduce the uncertainty about its composition. Decrease of uncertainty is equivalent to generation of information [1]. Information theory enables this information to be quantified and is therefore appropriate for evaluating different methods and comparing them with respect to their identification power. The decisive aspect in the application of information theory for this purpose is the possibility of quantifying information by a numerical value derived from the probability of the incidence of an event. The information content of a method, expressed in bit, is therefore a quantitative measure which can be applied to compare different analytical methods.

The goal of this study was to evaluate isotachophoresis as a method of identification on the basis of information theory, and to compare it in terms of information content with the methods already described in the literature.

*This work is dedicated to Prof. J. F. K. Huber on the occasion of his 60th birthday.

0003-2670/85/$03.30

The application of information theory is discussed here only for qualitative analysis, i.e., the identification of compounds. Such applications have been discussed in a general sense (e.g., [2—4]) as well as for particular methods such as spectrometry [5—13] and chromatography [8, 14—24].

Two approaches for the estimation of the information content are proposed here. In the first approach, the conditions of discrimination of the individual positions in an isotachopherogram are connected with information theory, and an expression is derived for the maximum number of positions or steps that can be distinguished between the leading and terminating ions. In order to calculate the maximum information content by this approach, assuming equal probabilities for the incidence of the corresponding compounds, the ionic mobilities are taken as parameters of discrimination. In the second approach, the signals relevant for identification in isotachophoresis (e.g., relative step heights) are treated by information theory in the same general manner as signals from any other information source, like mass spectra or retention indices in chromatography. If such a source produces continuous, variable signals, the information content of a measurement can be calculated from the probability density function. If this function cannot be expressed exactly, the information content can be approximated from the frequency distribution in the corresponding histograms. For this approach, a data library consisting of relative step heights (R_E values) of 263 anions in various electrolyte systems in the pH range 3—10 was used and the information content was estimated. The maximum information content as well as the information content derived from the data file were compared with the corresponding values of other identification methods. Isotachophoresis was rated on this basis.

THEORY

When information theory is applied in qualitative analysis, the information obtained by the measurement is considered equivalent to the reduction of uncertainty about the identity of a compound. In general, the measurement allows identification of one value from a set of possible values. The values can be retention indices, R_f values, capacity factors, melting points, mass spectra, i.r. spectra, etc. If the use of selective detectors is ignored, the quantity used for identification in isotachophoresis is the ionic mobility or values directly connected with it, such as relative step heights. The simplest case for evaluation of the information content is given for the selection of one value from N possible (discrete) values and equal probability P for their incidence. In this case, $P = 1/N$ and the information content reaches its maximum. The maximum information content I_0 is given by $I_0 = \mathrm{ld}\ (1/P) = \mathrm{ld}\ N$ (bit), where ld stands for the logarithm to the base 2. In isotachophoresis, the derivation of N, which is the maximum number of discrete steps that can be distinguished between the leading and terminating ions, enables I_0 to be calculated by the equation given.

If the values out of a number N of possible discrete values occur with different probabilities P_i, the maximum information content I_0 will be replaced by the information content I (bit), which is expressed by

$$I = -\sum_{i=1}^{n} P_i \operatorname{ld} P_i \tag{1}$$

with $\Sigma_{i=1}^{n} P_i = 1$. For a source producing continuous, variable signals instead of discrete ones, the sum of the probabilities P_i is replaced by the integral over the probability density function $p(x)$. The expression for the information content after the measurement consists then of two terms: one expresses the increase of information produced by the measurement, the other takes into account the remaining uncertainty from the inevitable statistical error

$$I = -\int p_m(x) \operatorname{ld} p_m(x)dx + \int p_e(x) \operatorname{ld} p_e(x)dx \tag{2}$$

where $p_m(x)$ and $p_e(x)$ are the probability density functions of the measured values and of the error, respectively. The error can usually be assumed to be normally distributed.

In isotachophoresis, identification can be done by measuring the R_E values of the unknown compound in one or several electrolyte systems and comparing them with library data (retrieval procedure). The R_E value is defined as the ratio of the effective ionic mobilities of the leading ion and the compound considered [25]. In principle, R_E can take any value within the limits given by the electrolyte systems used. Hence the signal distribution can be considered as a continuous one. If the probability density function of the measured values can be described also by a Gaussian distribution, Eqn. 2 can be converted to $I^{(G)} = 1/2 \operatorname{ld} \sigma_m^2/\sigma_e^2$, where σ_m^2 and σ_e^2 are the variances of the distribution of the measured values and the error, respectively; (G) indicates the assumption of Gaussian distribution.

No theoretical prediction can be given, however, about the shape of the distribution of the R_E values. Library data can be used to approximate the probability density by histograms, constructed from a finite number of values considered to be representative. Each histogram is divided into k intervals or classes with equal class width, Δx. Then, for the information content obtained from a histogram, Eqn. 2 can be approximated by

$$I^{(H)} = -\sum_{i=1}^{k} p_i \operatorname{ld} p_i + \operatorname{ld} \Delta x - \operatorname{ld} \sigma_e(2\pi e)^{1/2} \tag{3}$$

with $\Sigma_i p_i = 1$. Here $(2\pi e)^{1/2}$ is a constant factor, because of normal distribution, and p_i is the probability of finding an individual R_E value in class i; (H) indicates the approximation of I from a histogram.

In the case discussed so far, all measured values originated from a single (electrolyte) system, but often R_E values are measured in systems with different pH values in order to identify an unknown compound. The information

gained will be the sum of the information contents of the single systems only when the latter are totally uncorrelated. Usually, the different systems will be correlated, so that the total information content will be lower.

The influence of correlation on the information content is easily calculated if the probability density distribution functions of the R_E values are Gaussian for all electrolyte systems. The information content $I^{(G)}(1, 2, \ldots, r)$ obtained from the measurements in r systems, can then be calculated from the determinant $[COV]_m$ of the covariance matrix of the R_E values and the corresponding determinant of the error $[COV]_e$ and is given by $I^{(G)}(1, 2, \ldots, r) = 1/2 \text{ ld } [COV]_m/[COV]_e$. In case of the estimation of the information content by r-dimensional histograms from a sufficiently large data library, Eqn. 3 can be replaced by

$$I^{(H)}(1, 2, \ldots, r) = -\sum_{i=1}^{r,k} p_i(x_1, x_2, \ldots, x_r) \text{ ld } p_i(x_1, x_2, \ldots, x_r)$$

$$+ \text{ ld } [\Delta x_1 . \Delta x_2 . \ldots . \Delta x_r] - \text{ld } (2\pi e)^{r/2} \sigma_e^r \qquad (4)$$

where $p_i(x_1, x_2, \ldots, x_r)$ is the probability of finding an R_E value in one particular class of the r-dimensional histogram. In deriving Eqn. 4 it is assumed that the measuring errors are independent of the systems and are constant and equal. Depending on the value of r, very large numbers of data must be available in the library for a sufficiently good approximation.

EXPERIMENTAL

The R_E values were used for identification with isotachophoresis by retrieval. The information content was calculated based on the library published by Hirokawa et al. [26], which contains R_E values of 287 anions in 31 aqueous electrolyte systems. The data in the library are not measured values, but were calculated on the basis of measured absolute mobilities, pK_a values and the pH of the leading electrolyte. For the study presented here, 263 anions in eight electrolyte systems with different pH values of the leading electrolyte were selected. All those substances which had R_E values larger than 15 were eliminated from the library, because ions with such low mobilities are of no practical importance in isotachophoresis. The eight electrolytes chosen were those with integer pH values of the leading electrolyte. The range of pH was 3.0—10.0.

In Table 1, the leading ion, the buffering counter ion and the R_E ranges are listed for the individual electrolyte systems.

The calculations were done on a computer (Control Data Cyber 170-720) with a main memory of 131 K words of 60 bits.

TABLE 1

Leading electrolyte systems and corresponding characteristic R_E values[a]

	pH of the leading electrolyte							
	3.0	4.0	5.0	6.0	7.0	8.0	9.0	10.0
Counter ion	β-Al[b]	β-Al	Cr[c]	Hist[d]	Imid[e]	Tris	Am[f]	Eth[g]
Lowest R_E	0.96	0.94	0.89	0.88	0.88	0.88	0.88	0.88
Highest R_E	14.98	7.61	4.10	3.66	3.62	3.66	3.65	3.60
Mean R_E	5.21	3.30	2.48	2.30	2.24	2.24	2.23	2.20
s^2[h]	11.91	2.23	0.50	0.40	0.39	0.40	0.40	0.40
Width[i]	1.403	0.666	0.321	0.277	0.274	0.278	0.277	0.272

[a]The leading ion is chloride in all cases. [b]β-Alanine. [c]Creatinine. [d]Histidine. [e]Imidazole. [f]2-Amino-2-methyl-1,3-propandiol. [g]Ethanolamine. [h]Estimated variance. [i]Class width of histogram.

RESULTS AND DISCUSSION

Maximum information content, I_0

In order to calculate the maximum information content, I_0, the maximum number of discrete steps which can be distinguished in an isotachopherogram must be evaluated. The problem of estimating this number of positions in an isotachopherogram is directly connected to the question whether the axis of the qualitative parameter (ionic mobility) must be divided in equidistant intervals or in intervals increasing by a given factor. It is well known that the condition of separation is given by the ratio of the mobilities, but it was shown by Reijenga et al. [27] for signal evaluation that also the conditions of discrimination in the steady state do not follow equidistance owing to electro-osmotic disturbances.

For the estimation of the number of discrete positions for identification purposes, it is assumed that the number of positions which can be distinguished in the isotachopherogram is equal to the number of the separated compounds. Two ions i and j can be separated (and identified) when they have a sufficiently different effective ionic mobility, m_i, in the mixed zone. The condition of separation is given by the ratio r_{ij} of the effective mobilities in the transient state. It has to obey the condition $r_{ij} = m_i/m_j > 1$. Ratio r_{ij} may be termed the selectivity coefficient by analogy with chromatography. From the considerations given above, an equal, minimum value for r_{ij} is assumed for the isotachophoretic separation of all pairs of compounds to be differentiated between the leading and terminating ions. Compound 1 can be differentiated from 0, the leading ion L, under the condition $m_1 = m_0 r_{01}^{-1}$. For compound $(n + 1)$, the terminating ion T, the following relation must be valid in the general case, where r_{ij} has the assumed constant value: $m_{n+1} = m_n r_{n(n+1)}^{-1} = m_0 r_{ij}^{-(n+1)}$, which can be written as $m_L/m_T = r_{ij}^{(n+1)}$, where the index n equals N, the total number of compounds that can be separated between L and T. Then N can be derived from the preceding equation for

m_L/m_T

$$N = [\log (m_L/m_T)/\log r_{ij}] - 1 \quad (5)$$

As can be seen, the number of compounds depends on the mobility range of the leading and terminating ion and on the value of the selectivity coefficient necessary for separation. With the aid of the number of possible positions in an isotachopherogram, the maximum information content I_0 can be calculated from

$$I_0 = \mathrm{ld}\, N = \mathrm{ld}\, \{[\log (m_L/m_T)/\log r_{ij}] - 1\} \quad (6)$$

The dependence of I_0 on r_{ij} is presented in Fig. 1 for different mobility ranges m_L/m_T; I_0 varies from 2 to 8.5 bit within the ranges considered. It can be seen that the values of the function change only slightly for $r_{ij} > 1.10$ and mobility ranges >5. This is caused by the logarithmic relationship of I_0.

To estimate a realistic value for I_0, realistic assumptions must be made for the mobility range and the minimum value of the selectivity coefficient. Based on the electrolyte systems described in the literature, a value of about 15 for m_L/m_T is assumed in this calculation. To estimate a minimum value for r_{ij}, it is necessary that all pairs of compounds be separated after a migration distance d_{mig} given by the length of the separation capillary between injector and detector. This migration distance is related to the mobility ratio as described by Mikkers et al. [28] and can be expressed in a modified form for very similar mobilities and equal concentrations of compounds 1 and 2 by

$$m_2/m_1 = 1 - (2l_1/d_{mig}) \quad (7)$$

where l_1 is the zone length of compound 1 in the steady state. For realistic values of 1 mm for the zone length and 200 mm for the migration distance, a minimum value r_{ij} of 1.01 can be assumed. Because of electro-osmosis, a somewhat higher value of 1.02—1.03 can be expected. Then, according to Eqn. 6, I_0 reaches 6.5—7 bit.

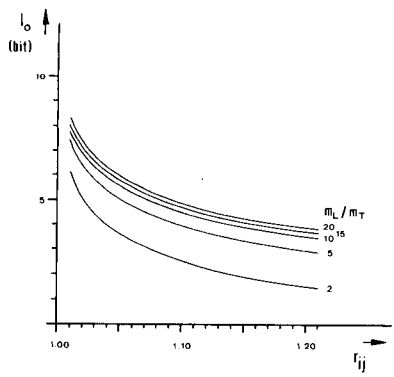

Fig. 1. Dependence of the maximum information content I_0 on the selectivity coefficient r_{ij} for different ranges of the effective ionic mobilities, m_L/m_T, of the leading ion L and the terminating ion T.

Information content

In Table 1, the highest and lowest values of R_E in the different pH systems are listed. The lowest values do not vary much. The upper values, and therefore the range of the R_E values, varies by a factor of about 4, resulting in different widths of the corresponding frequency distributions. From the data library, the information content can be estimated for the one-dimensional case (single electrolyte system) and for multidimensional data (combination of R_E values for the unknown compound in several electrolyte systems). In the one-dimensional case, the estimated information content can never exceed the maximum information content of 6.5—7 bit as calculated above.

One-dimensional data. The frequency distributions of the R_E values in the different pH systems are presented as histograms in Fig. 2. The number k of classes was chosen by $k = \mathrm{ld}\, N + 1$ [29], N being the number of compounds

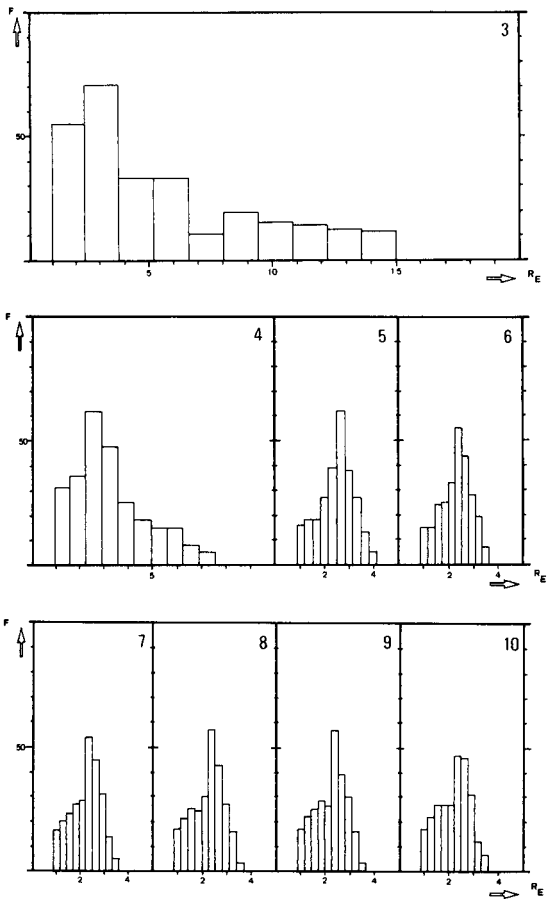

Fig. 2. Frequency distribution of the R_E values of the library for pH values of the leading electrolyte from 3 to 10. Each histogram consists of 10 classes; F = frequency.

in the library; N = 263 gave 10 classes. The histograms are presented with equal scales to make clear the varying widths of the distribution as well as those of the classes. The distribution is broadest at pH 3; the widths and the shapes, respectively, are very similar for systems with pH 5 and higher. This is also clear from the values in Table 1.

The different behaviour of the individual pH systems is plausible from a chemical point of view; most of the compounds in the library are organic acids, which usually have pK_a values in the range 3—5. The degree of dissociation and therefore the R_E value will be influenced strongly only at low pH of the leading electrolyte. At higher pH, most of the acids are totally dissociated and the R_E values are insensitive to changes in pH.

From the histograms presented in Fig. 2, the information content $I^{(H)}$ obtained from the measurement of R_E values in a single electrolyte system can be estimated according to Eqn. 3. The results are presented in Fig. 3 for pH systems 3, 4, 5 and 10. The information content depends on the precision of the measurement of the R_E value, expressed by the standard deviation σ_e of the error distribution. According to Eqn. 3, the information content decreases with decreasing precision. The remaining pH 6, 7, 8 and 9 systems, not shown in Fig. 3, give information contents close to those of 5 and 10.

The variation of $I^{(H)}$ for all pH systems is presented in Fig. 4 for two different values of the error of measurement. If the evaluation of the R_E values is relatively precise with σ_e = 0.05 [25], then the information content

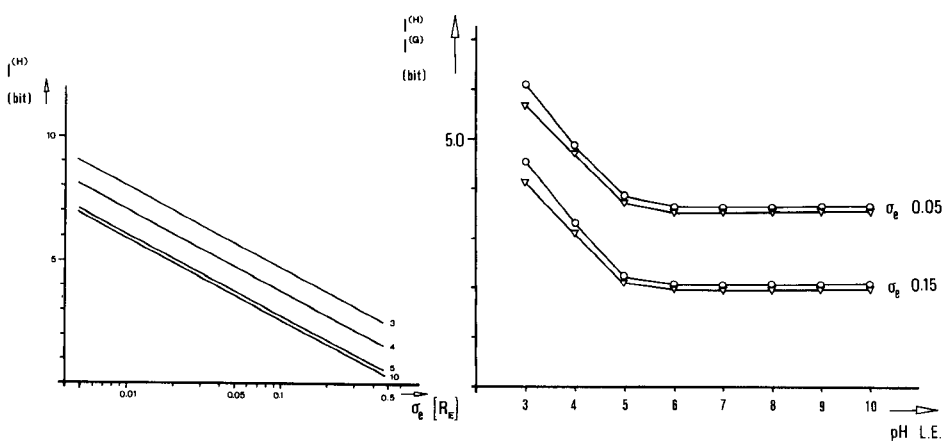

Fig. 3. Dependence of the information content $I^{(H)}$ of single electrolyte systems on the precision of the R_E measurement, expressed by the standard deviation, σ_e. $I^{(H)}$ was calculated from histograms and is shown for systems with pH 3, 4, 5 and 10.

Fig. 4. Dependence of the information content, $I^{(G)}$ and $I^{(H)}$, on the pH of the leading electrolyte for two different levels of the precision of the measurement of the R_E value. The precision is expressed by the standard deviation σ_e. The values of I were calculated in two ways: (▾) from histograms; (○) for the approximation on a Gaussian distribution.

has the highest value of 5.7 bit for pH 3, followed by pH 4 and pH 5. The difference is 1 bit between the subsequent pH systems. Above pH 5, the individual systems show a constant value of 3.6 bit. In this context, difference of 1 bit in the information content means that the number of compounds which can be distinguished differs on average by a factor of 2. From the results shown in Fig. 4, it is clear that, for the anionic substances considered, the identification potential of isotachophoresis is higher at lower pH. This result agrees with experience, but information theory enables the differences to be quantified.

In order to compare the results obtained from the histograms with those obtained by assuming normal distribution of the R_E values, the information content of individual systems was calculated with the aid of the equation $I^{(G)} = 1/2 \text{ ld } \sigma_m^2/\sigma_e^2$. The estimated variances s_m^2 are given in Table 1 and are regarded as good approximation to σ_m^2 used in this equation. $I^{(G)}$ was calculated for the same statistical error as in the calculation from the histograms (σ_e = 0.05 and 0.15 R_E units, respectively); these data are also presented in Fig. 4. The results are in good agreement for higher pH systems: from pH 5 to pH 10 the difference from the corresponding values obtained from the histograms is only 0.1 bit. The agreement is not good for pH 3 with a difference of 0.4 bit. The result is plausible considering the shape of the distributions as shown in Fig. 1, where the deviation from a Gaussian curve is highest for the pH 3 system.

The values of the information content derived for the individual electrolyte systems, ranging from 3.6 to 5.7 bit are below the theoretically predicted limit of 6.5—7 bit calculated for I_0.

Multidimensional data. The information content obtained from measurements of R_E values of an unknown compound in systems with different pH can be calculated by extension of the approximation methods discussed for one-dimensional data. The experimental data might be represented by well defined distribution curves, or by multidimensional histograms. For both methods, problems can arise from the actual structure of the file. For the histogram, the number of data in the file has to be large, especially for calculation with higher dimensions. Otherwise the approximation to the true distribution will be too erroneous. However, the quality of the results will also be inadequate if the experimental data distribution does not fit well to the model distribution.

This study was not directed towards presenting optimum selection procedures for a large number of electrolyte systems, thus the discussion of multidimensional data will be focused mainly on only two of the pH systems. As an approximate method, two-dimensional histograms are used here prior to model distribution functions. The number of compounds seems to be adequate for the former method.

In order to demonstrate the effect of correlation of data in isotachophoresis on the information content, two pairs of electrolyte systems were selected: the one with the greatest and the one with the least similarity. Similarity was

expressed by the normally used linear correlation coefficients, which are given in Table 2 for all pairs of electrolyte systems. As can be seen, especially pairs of electrolyte systems with a pH difference of one in the higher pH range are highly correlated. The two pairs of different systems with the extreme values for the correlation coefficients are systems pH 3/pH 10 (lowest value of 0.50350) and systems pH 8/pH 9 (highest value of 0.99749).

The two-dimensional histograms for the two pairs, from which the information content $I^{(H)}$ can be approximated for $r = 2$ by using Eqn. 4 are presented in Fig. 5. The two distributions are of totally different shape. For the lower correlated system pH 3/pH 10, the (finite) values of the estimated probabilities are spread over 53 two-dimensional classes of the histogram, consisting of a total of 100 classes. For the highly correlated system pH 8/pH 9, most of the (finite) probability values are concentrated in the main diagonal, as theoretically expected. From the 15 two-dimensional classes, in which probability values are finite, ten belong to the main diagonal.

With regard to the restrictions already mentioned with respect to the number of data, the estimation of the information content gives very plausible results. For an assumed constant precision of measurement, expressed by a standard deviation equal for all pH systems with $\sigma_e = 0.05\ R_E$ units, the information content estimated for systems pH 3/pH 10 is 8.60 bit. Compared to the sum of the corresponding values of the single systems, which is 9.22 bit, 0.62 bit is lost because of correlation. In contrast, the information content for the two highly correlated systems pH 8/pH 9 is 4.17 bit when correlation is considered. The sum for the single systems is 7.07 bit, thus 2.90 bit is lost. This means that the second system contributes only 0.63 bit. The information content per system is reduced from about 3.6 bit per system to 2.1 bit per system.

A similar treatment, e.g., for the data of four electrolyte systems (pH 3/pH 4/pH 6/pH 10), shows a reduction of the sum for the single systems (17.5 bit) to a value of 12.8 bit, when correlation is taken into account. Even given the problem of proper approximation, this result is probably typical for such systems.

TABLE 2

Linear correlation coefficients of the R_E values for different electrolyte systems with pH values of the leading electrolyte from 3.0 to 10.0

pH(LE)	3.0	4.0	5.0	6.0	7.0	8.0	9.0	10.0
3.0	1.00000	0.97945	0.73049	0.53309	0.51526	0.51783	0.51341	0.50350
4.0		1.00000	0.84668	0.67007	0.63953	0.63454	0.62889	0.61852
5.0			1.00000	0.94921	0.90749	0.88681	0.87838	0.86704
6.0				1.00000	0.98090	0.95995	0.95134	0.94043
7.0					1.00000	0.99528	0.98975	0.97952
8.0						1.00000	0.99749	0.98851
9.0							1.00000	0.99614
10.0								1.00000

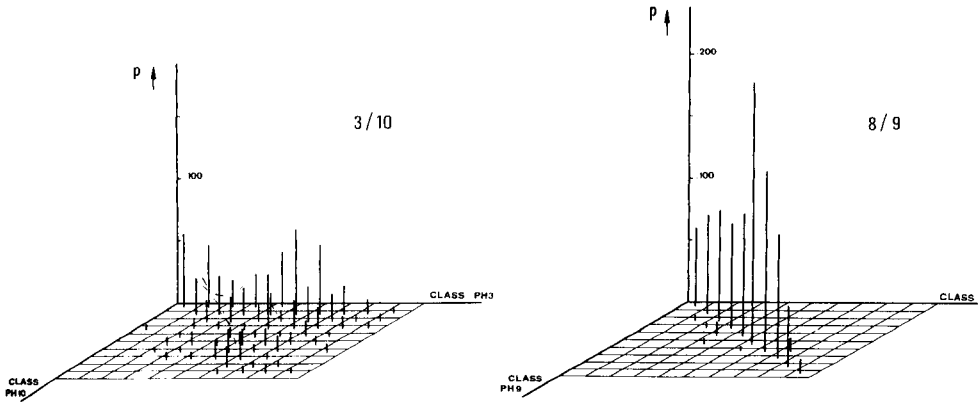

Fig. 5. Two-dimensional histograms representing the probability distribution of the R_E values of the library for two pairs of electrolyte systems with extreme similarities. Systems pH 3/pH 10 show the lowest correlation, whereas systems pH 8/pH 10 show the highest correlation from all systems considered (p = probability).

Comparison of isotachophoresis with other methods

With the results obtained above for the evaluation of isotachophoresis, a comparison with other identification methods such as mass spectrometry, infrared spectrometry, gas chromatography and thin-layer chromatography is possible on the basis of corresponding published data. From Table 3, it can be seen that the identification power of the spectrometric methods is superior to that of one-dimensional chromatographic methods and isotachophoresis, if a large variety of compounds has to be considered. Even when the high correlation of the spectrometric data is taken into account, the information content reaches about 40 bit. Only in the case of very similar compounds is the information content reduced to less than 10 bit. However, it is important to recall that the high information content of the spectrometric methods is attainable only for pure compounds, whereas chromatography and isotachophoresis can serve not only for identification but also separation, being applicable to complex mixtures. Isotachophoresis has an I_0 value of 6.5 to 7 bit and an information content I up to 5.7 bit, which lies between thin-layer and gas chromatography. The results quantify the idea that isotachophoresis is a high-performance method. From an information content of about 5 to 6 bit, it can be concluded that a maximum of about 60 compounds can be distinguished by isotachophoretic measurement under normal conditions. Because of unfavourable compositions of samples and instrumental restrictions, this value often will be lower in practice. Nevertheless, being an average value, this result of about 6 bit must be interpreted critically, because it does not guarantee the identification of one compound from 30—60. Under such conditions, if pairs of compounds cannot be distinguished, increase of detector selectivity or of separation selectivity can solve the problem.

TABLE 3

Information content of identification methods (I_0 = maximum information content; I = information content)

Method	Ref.	I_0 (bit)	I[bit] uncorr.	I[bit] corr.	Comments
Mass spectrometry[a]	5		90—150		Threshold 1% of base peak; spectra of 3000 organic substances.
	6			48	6700 spectra in library.
	7			40	Threshold 1% of base peak; 10 000 spectra in library.
	8		77	8.6	Threshold 1% of base peak; high correlation of spectra for similar compounds of real samples.
Infrared spectrometry	10		53	21	Depending on coding error and correlation; 93 wavelengths 0.1 μm wide chosen; file of about 100 000 coded spectra.
	13			15—40	Depending strongly on type of compound and on intensity threshold (5 values). Spectra coded by 140 peak positions.
Gas chromatography	14	5.1—7.7			Depending on chosen resolution, efficiency and retention time.
	15		6.5—7.0	4.3	Standard deviation of error is 2 RI[b] units; correlated value averaged from 10 columns.
	16		6.4—6.8	4.2—5.8	Standard deviation of error is 2 RI[b] units; 5 phases considered; correlated values averaged.
	8		5.1—6.0	4.1	Standard deviation of error is 5 RI[b] units; 4 phases considered; correlated values averaged.
Thin-layer chromatography	18	4.6			25 classes of R_F values with equal class widths assumed.
			0.4—3.1		Differences arising from different
	20		2.0—3.1		classes of substances and phase systems
	21		2.1—4.0		Assumed class widths: 0.05 R_F units [18, 21, 22, 24] and 0.10 R_F units [20, 21].
	22		1.5—3.6		
	23		0.6—3.0	loss of 0.1 to 0.3 bit	20 best combinations of two systems from 528 considered.
	24		3.6—4.1		
Isotachophoresis		6.5—7.0			Depending on the selectivity coefficient and the mobility range of the electrolyte system;
			3.6—5.7	3.2	Depending on the pH of the leading electrolyte; correlated value from 4 systems with different pH, averaged.

[a]Low-resolution m.s. with electron-impact ionization. [b]Retention index units.

The author is indebted to Dr. G. Reich for execution of the computation.

REFERENCES

1 C. E. Shannon and W. Weaver, The Mathematical Theory of Communication, The University of Illinois Press, Urbana, IL, 1949.

2 P. Cleij and A. Dijkstra, Z. Anal. Chem., 298 (1979) 97.
3 C. Liteanu and I. Rica, Anal. Chem., 51 (1979) 1986.
4 K. Eckschlager and V. Stepanek, Anal. Chem., 54 (1982) 1116A.
5 S. L. Grotch, Anal. Chem., 42 (1970) 1214.
6 L. E. Wangen, W. S. Woodward and T. L. Isenhour, Anal. Chem., 43 (1971) 1605.
7 G. van Marlen and A. Dijkstra, Anal. Chem., 48 (1976) 595.
8 J. F. K. Huber, E. Kenndler and G. Reich, J. Chromatogr., 172 (1979) 159.
9 G. L. Ritter, S. R. Lowry, H. B. Woodruff and T. L. Isenhour, Anal. Chem., 48 (1976) 1027.
10 P. F. Dupuis and A. Dijkstra, Z. Anal. Chem., 290 (1978) 357.
11 P. F. Dupuis, A. Dijkstra and J. H. van der Maas, Z. Anal. Chem., 291 (1978) 27.
12 F. H. Heite, P. F. Dupuis, H. A. van't Klooster and A. Dijkstra, Anal. Chim. Acta, 103 (1978) 313.
13 P. F. Dupuis, P. Cleij, H. A. van't Klooster and A. Dijkstra, Anal. Chim. Acta, 112 (1979) 83.
14 J. F. K. Huber and H. C. Smit, Z. Anal. Chem., 245 (1969) 84.
15 F. Dupuis and A. Dijkstra, Anal. Chem., 47 (1975) 379.
16 A. Eskes, F. Dupuis, A. Dijkstra, H. De Clercq and D. L. Massart, Anal. Chem., 47 (1975) 2168.
17 J. Suoto and A. Gonzalez de Valesi, J. Chromatogr., 46 (1970) 274.
18 D. L. Massart, J. Chromatogr., 79 (1973) 157.
19 D. L. Massart and H. De Clercq, Anal. Chem., 46 (1974) 1988.
20 H. De Clercq and D. L. Massart, J. Chromatogr., 93 (1974) 243.
21 H. De Clercq and D. L. Massart, J. Chromatogr., 115 (1975) 1.
22 H. De Clercq, D. L. Massart and L. Dryon, J. Pharm. Sci., 66 (1977) 1269.
23 P. Cleij and A. Dijkstra, Z. Anal. Chem., 294 (1979) 361.
24 D. L. Massart and H. De Clercq, in J. C. Giddings and R. A. Keller (Eds.), Advances of Chromatography, Vol. 16, Marcel Dekker, New York, 1978, p. 75.
25 T. Hirokawa and Y. Kiso, J. Chromatogr., 242 (1982) 227.
26 T. Hirokawa, M. Nishino, N. Aoki and Y. Kiso, J. Chromatogr., 271 (1983) D1.
27 J. C. Reijenga, W. van Iersel, G. V. A. Aben, Th. P. E. M. Verheggen and F. M. Everaerts, J. Chromatogr., 292 (1984) 217.
28 F. E. P. Mikkers, F. M. Everaerts and J. A. F. Peek, J. Chromatogr., 168 (1979) 293.
29 H. A. Sturges, J. Am. Stat. Assoc., 21 (1926) 65.

Analytica Chimica Acta, 173 (1985) 253—264
Elsevier Science Publishers B.V., Amsterdam — Printed in The Netherlands

MULTICOMPONENT SELF-MODELLING CURVE RESOLUTION IN HIGH-PERFORMANCE LIQUID CHROMATOGRAPHY BY ITERATIVE TARGET TRANSFORMATION ANALYSIS

BERNARD G. M. VANDEGINSTE*, WILBERT DERKS and GERRIT KATEMAN

Department of Analytical Chemistry, University of Nijmegen, Toernooiveld, 6525 ED Nijmegen (The Netherlands)

(Received 27th December 1984)

SUMMARY

Iterative target transformation factor analysis can provide a method for resolving elution profiles consisting of any number of compounds. The results obtained for 3-component resolution are consistent with the results obtained with conventional methods of curve resolution. The same restrictions with regard to overlap and relative signal heights of the compounds seem to apply to the conventional method of curve resolution and the proposed method. The method is tested on data from high-performance liquid chromatography with a diode-array detector obtained for polynuclear aromatic hydrocarbons and for proteins.

The introduction of diode-array detectors in high-performance liquid chromatography (h.p.l.c.) enables u.v.-visible spectra to be recorded at short time intervals (ca. 1.5 s), during elution of the components. The result is a data matrix of NS spectra measured over NW wavelengths. Typical values for a separation are 800 spectra of 80 data points, i.e., 64 000 data points per run. Many spectra are null spectra, as they have been recorded while no compounds elute from the column.

A total-component chromatogram in which all compounds contribute to the recorded signal is obtained by plotting the highest absorbance of each spectrum as a function of the spectrum number [1]. Clusters of co-eluting compounds are then easily distinguished, and their spectra can be selected for further data treatment. The complexity of the data treatment needed to obtain the required information depends on the amount of prior information on the system. In the best instance, the identity and spectra of all compounds in the cluster of co-eluting compounds are known. In that case, the individual elution profiles (in concentration units) of the co-eluting compounds are obtained by solving NS (number of spectra) systems of NW linear equations with NC (number of compounds) unknowns [2], which is multicomponent analysis (m.c.a.). When the number and identity of the compounds are unknown, m.c.a. should be preceded by a principal components analysis and factor analysis for the determination of the number of co-elut-

0003-2670/85/$03.30

ing compounds and for the estimation of their spectra. The combination of principal components analysis and factor analysis to resolve chromatographic elution profiles mathematically is generally called self-modelling curve resolution [3]. The term self-modelling emphasizes that the procedure requires no models for the peak shape.

Curve resolution was initially applicable to resolve peak clusters consisting of two compounds [2, 3]. The procedure consists of estimation of the pure spectra and calculation of the individual elution profiles. Recently, curve resolution has been extended to solve the three-component case [1]. It was demonstrated that better estimates are obtained when the individual elution profiles are estimated first, and thereafter the spectra of the compounds [1]. In this paper, an alternative and more general method for self-modelling curve resolution is presented which is based on iterative target transformation factor analysis (t.t.f.a.) [4]. The merits of the method are its simplicity compared to earlier curve-resolution methods, and its generality, because there are no limitations in principle on the number of co-eluting compounds.

The rows of the data matrix in h.p.l.c. with a diode-array detector (DAD) are linear combinations of the pure spectra of the compounds in the cluster of co-eluting compounds. The columns of the data matrix represent linear combinations of the pure elution profiles. In multivariate statistics, the pure spectra and pure elution profiles are called the true factors, the problem being to find them. The approach of t.t.f.a. [4] is to test whether or not a candidate factor or target is a true factor. This test does not require any knowledge of the other co-factors. One can test one target at a time, even though the other co-factors are unknown.

In the most general case of h.p.l.c. with DAD, however, no prior knowledge is assumed on possible candidate spectra or elution profiles, and one would exclude the use of t.t.f.a. for curve resolution. Hopke et al. [5] suggested, however, that "fake" targets may be improved in order to bring them close to one of the true factors. The target is resubmitted and modified in an iterative way until the tested target is considered to match satisfactorily one of the true factors. This is the principle of iterative t.t.f.a. In this paper, it will be shown that iterative t.t.f.a. is suitable for mathematical resolution of a data matrix from h.p.l.c. with DAD into its pure elution profiles regardless of the number of co-eluting compounds. After the pure elution profiles have been obtained, the pure spectra of all co-eluting compounds can be estimated. In this paper, attention is given to adaptaton of the targets during iteration so as to force convergence to a true factor and to prevent iteration to a linear combination of the factors.

THEORY

A (NS × NW) data matrix D of NS spectra measured at NW wavelengths is considered. The spectra are obtained during the elution of a cluster of NC co-eluting compounds, which contribute linearly to the signal. The data

matrix should be decomposed into its true factors: $\mathbf{D} = \mathbf{C}\,\mathbf{S}$, where $\mathbf{S}$ is the (NC × NW) matrix of the pure spectra of the NC compounds and $\mathbf{C}$ represents the (NS × NC) matrix of the elution profiles (in units of concentration) of the NC compounds. $\mathbf{C}$ and $\mathbf{S}$ are matrices of the true factors (chromatograms and spectra). If $\mathbf{S}$ and $\mathbf{C}$ are unknown, $\mathbf{D}$ can be decomposed in NF abstract factors by a principal components analysis (p.c.a.) which consists of the following steps: (1) calculate the (NS × NS) dispersion matrix $\mathbf{D}\,\mathbf{D}^T$; (2) calculate the NS eigenvalues and eigenvectors of $\mathbf{D}\,\mathbf{D}^T$ (the eigenvectors ($\mathbf{V}$) span a space of NS or orthonormal vectors which represent abstract chromatograms and noise, and the eigenvectors of the NW × NW dispersion matrix $\mathbf{D}^T\mathbf{D}$ are abstract spectra and noise); (3) decompose the original data matrix $\mathbf{D}$ into the abstract chromatograms by a least-squares method: $\mathbf{D} = \mathbf{V}\,\mathbf{A}$, where $\mathbf{V}$ is the (NS × NS) matrix of abstract chromatograms, and $\mathbf{A}$ is the (NS × NW) matrix of abstract spectra (factor scores) $\mathbf{A} = \mathbf{V}^T\mathbf{D}$.

The true dimensionality of the data matrix, however, equals the number of true factors (NC) [6]. Consequently, $\mathbf{D}$ can be reconstructed within the noise by including the first NC eigenvectors in $\mathbf{V}$ (the eigenvectors are ranked in the sequence of the magnitude of their eigenvalue which equals the explained variance). Thus

$$\hat{\mathbf{D}} = \mathbf{V}_C \cdot \mathbf{A}_C \qquad (1)$$

where $\mathbf{V}_C$ is the (NS × NC) matrix of abstract chromatograms, $\mathbf{A}_C$ is the (NC × NW) matrix of abstract spectra (factor scores), and NC is the number of components necessary to reconstruct $\mathbf{D}$ within the noise. The problem of estimating NC has been discussed by Malinowski and Howery [6].

The next problem is to transform the NC abstract chromatograms into true elution profiles of the NC components. It is readily seen that the cross-product of the true elution profiles will usually not be equal to zero. This means that the true elution profiles do not span an orthogonal space. The NC eigenvectors in $\mathbf{V}_C$ are, however, orthogonal. Therefore the true elution profiles cannot be found by orthogonal rotation of the eigenvector space. It has been shown [1] that the true elution profiles can be estimated by extrapolation of the factor scores ($\mathbf{A}$) to the two or three simplest elution profiles. Such an extrapolation proved useful for estimating the elution profiles for peak clusters consisting of less than four compounds.

An alternative method is to test whether a given pure elution profile, $\mathbf{T}$, the target, is a basic vector which is present in all measured chromatograms. Target testing consists of the calculation of a (NC × 1) rotation vector ($\mathbf{R}$), which rotates the (NS × 1) target $\mathbf{T}$ in the space $\mathbf{V}_C$, spanned by the first NC eigenvectors of $\hat{\mathbf{D}}$, in such a way that the sum of squares of the residuals between the rotated target and input target is minimal. Thus the equations $\mathbf{V}_C\mathbf{R} = \mathbf{T}$ have to be solved for $\mathbf{R}$, giving

$$\mathbf{R} = [\mathbf{V}_C^T\mathbf{V}_C]^{-1}\mathbf{V}_C^T\mathbf{T} = \mathbf{V}_C^T\mathbf{T} \qquad (2)$$

Thus

$$\hat{T} = V_C R \quad (3)$$

Usually the predicted target ($\hat{T}$) will differ from the input target (T). The correlation coefficient between T and $\hat{T}$ is a measure of the similarity of the target with the closest linear combination of the eigenvectors. However, every target which is a linear combination of the eigenvectors will be found to be valid, and the major problem is to formulate good targets. Focussing on the case of h.p.l.c. with DAD, this means that one should know the pure elution profiles in advance, which is, of course, the purpose of the analysis. Target transformation factor analysis would thus be applicable only if one is able to adapt any non-valid target to a better target, until a valid target has been obtained. This is the principle of iterative t.t.f.a.

The proposed method is schematically shown in Table 1. The analysis is started by a principal components analysis (Eqn. 1). Then the NC abstract factors (elution profiles) are rotated by a Varimax rotation [7], which aligns as well as possible the abstract factors along NC true but unknown factors. This procedure gives NC targets to be tested. Each of the targets is submitted to t.t.f.a. If the target fails to pass the correlation test, it is adapted according to the rules described below. Any adapted target is resubmitted to t.t.f.a.

Because all NC targets (elution profiles) are tested sequentially, no mathematical limitations are imposed on the number of compounds which are present in the peak cluster. Consequently, iterative t.t.f.a. solves the general case of curve resolution. The main part of the algorithm is the adaptation of the target from an inspection of $\hat{T}$. Obviously any resubmission of $\hat{T}$ to t.t.f.a. will return $\hat{T}$. For that reason $\hat{T}$ has to be slightly modified in order to force the t.t.f.a. to converge to a better solution (if any). At the same time, it is necessary to avoid convergence of the target to a linear combination of the elution profiles.

Useful adaptations found so far for obtaining a convergence to pure elution profiles are: (1) any element of $\hat{T}$ which is smaller than a given threshold (e.g., 0.005) is set to zero; (2) any doublet which is separated by one or more zeros is cleaned up in such a way that the main peak in the target is retained and any value of the minor peak is set to zero.

TABLE 1

Scheme of the proposed method

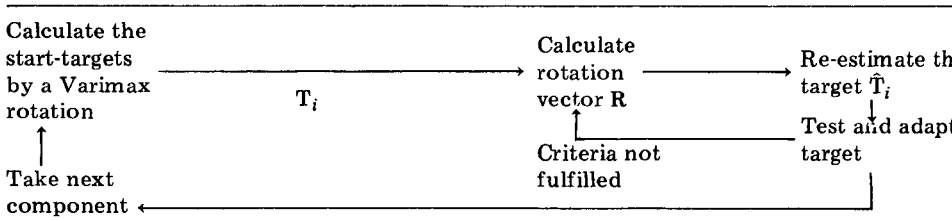

The process of iteration is ended on the first occurrence of any of the following: (1) adaptation of the target is no longer possible; (2) the correlation coefficient between the rotated and adapted target is more than 0.999; (3) the allowed maximum number of iterations has been reached (e.g., 15).

The NC elution profiles obtained at the end of the iterative t.t.f.a. are normalized on a norm = 1, as are the measured chromatograms before mathematical analysis. The elution profiles are denormalized by calculating the pure spectra of NC compounds. The norms of these spectra give the relative contributions of the compounds to the signal. When E is the (NS × NC) matrix of the NC factors (elution profiles) found in t.t.f.a., then $\mathbf{D} = \mathbf{E}\,\mathbf{S}$. The matrix of the NC pure spectra is

$$\mathbf{S} = [\mathbf{E}^T\mathbf{E}]^{-1}\,\mathbf{E}^T\mathbf{D} \qquad (4)$$

EXPERIMENTAL

Experimental data

Protein mixtures were separated by molecular-exclusion h.p.l.c. The equipment consisted of a Waters M6000-A solvent delivery system and a Serva Si-200-polyol column (9.5 × 500 mm). The eluent was 0.1 M sodium phosphate (pH 6.5) at a flow rate of 0.5 ml min^{-1}. A photodiode array detector (HP-1040) was coupled to a HP-85 microcomputer for data acquisition.

Mixtures of polynuclear aromatic hydrocarbons were separated on the system equipped with a ODS-Hypersil 5-μm (Shandon) column. Modifier concentrations of 65% acetonitrile, 80% methanol and 40% (v/v) tetrahydrofuran were used. The codes in the text refer to the peak clusters observed in the chromatogram (e.g., M80P13P2 means cluster 2 of a 13-component mixture separated with an 80% (v/v) methanol modifier).

Spectra were recorded over 80 wavelengths with an interval of 1 spectrum per second. After data collection and temporary storage on an 8-in. floppy disk by using the HP-01040-10301 software package, all data were transferred to a NAS-9040 mainframe computer for further processing.

Synthetic and semi-synthetic data

A semi-synthetic peak cluster was generated by artificially mixing four spectra of polynuclear aromatic hydrocarbons (Table 2; Fig. 1) and using the

TABLE 2

Semi-synthetic 4-component peak cluster (59 spectra, 87 wavelengths)

Peak	Component	Rel. height	Resolution
1	Phenanthrene	0.52	R_{12} 0.933
2	Pyrene	1	R_{23} 0.433
3	Fluoranthrene	0.51	R_{34} 0.702
4	Anthracene	0.86	

elution profiles of the 3-component M80P13P6 cluster (see Fig. 6), where the profile of peak 2 was used to generate the fourth compound which is peak 3 in the total profile (Fig. 5A). The data on resolution and relative signals are listed in Table 2. The noise level in the data corresponds to an absorbance of 0.12×10^{-3}.

A fully synthetic 6-component peak cluster was generated consisting of six overlapping Gaussian elution profiles from separated polynuclear aromatic hydrocarbons (Fig. 2). The data on resolution and relative signal are listed in Table 3.

RESULTS AND DISCUSSION

Curve resolution on synthetic and semi-synthetic data (4- and 6-components)

Curve resolution of a 2-dimensional data matrix from h.p.l.c. with DAD, without the inclusion of prior knowledge on the number and shape of elution profiles or pure spectra, was limited to two-component [2, 3] and three-component [1] systems. The main reason is that these methods are based on extrapolation of the purest spectra (or chromatograms), which gives a set of solutions that increases very rapidly with the number of factors: the solution of a 2-component system is a set of 2 points, the solution of a 3-component

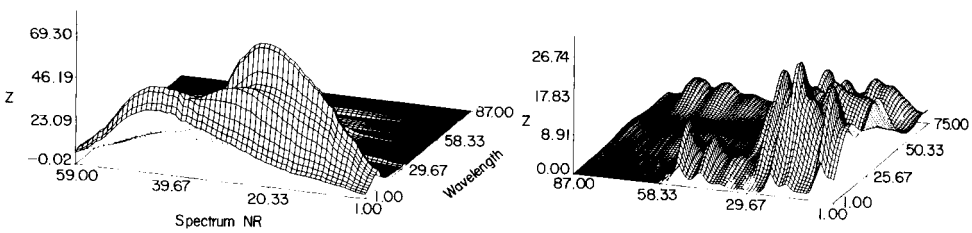

Fig. 1. Data matrix of a 4-component peak cluster of polynuclear aromatic hydrocarbons; 59 spectra measured at 87 wavelengths.

Fig. 2. Synthetic data matrix of a 6-component peak cluster of polynuclear aromatic hydrocarbons; 75 spectra measured at 87 wavelengths.

TABLE 3

Synthetic 6-component peak cluster (75 spectra, 87 wavelengths)

Peak	Component	Rel. height	Resolution
1	Benzo(k)fluoranthene	1	R_{12} 0.35
2	Chrysene	0.7	R_{23} 0.6
3	3,4-Benz(a)pyrene	0.8	R_{34} 0.32
4	Benzo(b)fluoranthene	1	R_{45} 0.4
5	Pyrene	0.5	R_{56} 1.01
6	1,2-Benzanthracene	0.9	

system is a line, of a 4-component system a plane, etc. The selection of the pure spectra (or elution profiles) from the large set of possible solutions requires the application of a number of constraints. No successful examples have been reported on $\geqslant$4-component systems. As outlined in the theoretical part, iterative t.t.f.a. imposes no limitations on the number of components present in the data matrix or peak cluster.

Six-component synthetic data. Figure 3 shows the course of a synthetic 6-component curve resolution by iterative t.t.f.a. Figure 3A gives the six first eigenvectors of the $\mathbf{D}\,\mathbf{D}^{T}$ matrix, which represent the six abstract elution profiles. These abstract elution profiles, which are orthogonal have to be transformed to non-orthogonal true elution profiles. A first step is to rotate the 6 axes in such a way that they correspond with some set of 6 axes of the original NS-dimensional space, i.e., Varimax rotation. The result of this rotation is shown in Fig. 3B. The absolute values of the 6 rotated eigenvectors correspond quite nicely with the 6 basic elution profiles with which the measured data matrix **D** can be reconstructed. However, the 6 vectors are still orthonormal and have to be transformed further. In order to retain a maximal number of degrees of freedom to let the targets converge to the pure elution profiles, the target transformation is started with a vector filled with zeros and one 1 at the position of one of the maxima found after the Varimax rotation. Figure 3C shows how the iterative target transformation of the third compound converges to a stable solution in a few steps. The target

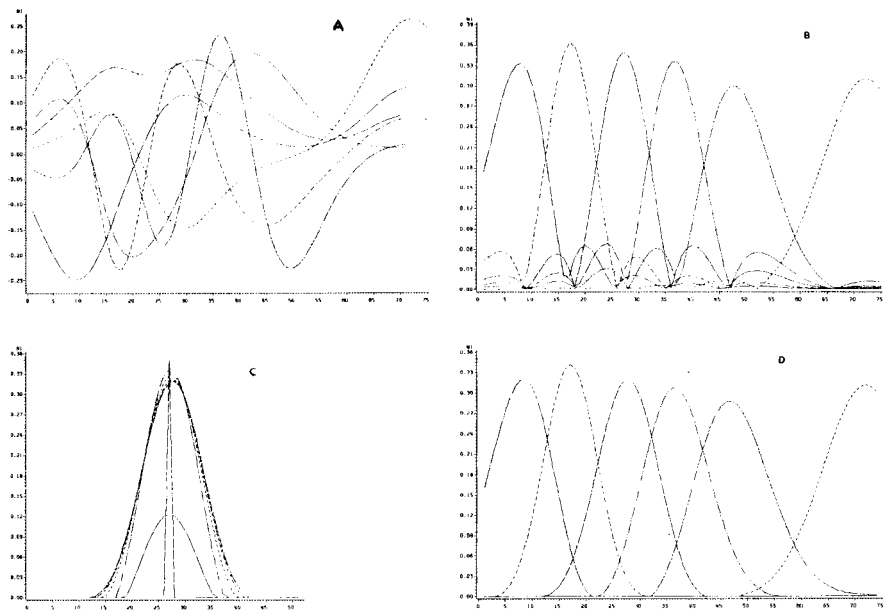

Fig. 3. (A) First 6 eigenvectors of the 6-component peak cluster of polynuclear aromatic hydrocarbons. (B) Varimax-rotated 6 first eigenvectors. (C) Iteration sequence of the target transformation factor analysis of peak 3. (D) Resolved 6-component elution profile (normalized).

TABLE 4

Successive adaptation of target 1 and correlation coefficients r (6-component system; Fig. 3)

		$r_{12} = 0.123$	$r_{23} = 0.982$	$r_{34} = 0.981$	$r_{45} = 0.994$	
Iteration	0	1	2	3	4	5
	0	0	0	0	0	0
	0	0	0	0	0	0.002
	0	0	0	0	0.004	0.007
	0	0	0	0.007	0.011	0.015
	0	0	0	0.002	0.023	0.027
	0	0	0	0.036	0.040	0.044
	0	0	0.024	0.058	0.062	0.065
	0	0.003	0.057	0.086	0.089	0.092
	0	0.020	0.100	0.119	0.121	0.122
	0	0.039	0.141	0.155	0.156	0.156
	0	0.060	0.187	0.193	0.192	0.191
	0	0.080	0.232	0.230	0.228	0.226
	0	0.097	0.273	0.264	0.261	0.256
	0	0.111	0.305	0.292	0.289	0.286
	0	0.120	0.327	0.313	0.309	0.306
	0.349	0.123	0.337	0.324	0.320	0.317
	0	0.121	0.333	0.324	0.321	0.319
	0	0.112	0.317	0.314	0.312	0.311
	0	0.099	0.289	0.293	0.293	0.293
	0	0.082	0.251	0.265	0.267	0.268
	0	0.063	0.208	0.231	0.234	0.236
	0	0.043	0.161	0.193	0.198	0.201
	0	0.024	0.115	0.154	0.160	0.165
	0	0.007	0.072	0.117	0.124	0.130
	0	0	0.036	0.084	0.091	0.098
	0	0	0.006	0.055	0.063	0.070
	0	0	0	0.032	0.039	0.046
	0	0	0	0.014	0.021	0.028
	0	0	0	0.002	0.008	0.014
	0	0	0	0	0.001	0.005

(00 . . . 1 . . . 0) is transformed to a triangle, which after resubmission becomes a Gaussian-like profile. In Table 4, successive targets are given with their corresonding correlation coefficient between successively predicted targets. Figure 3D shows the overall result found after the iteration of all 6 targets, which is the completely resolved 6-component mixture. It should be emphasized that no information was included on the shapes of the elution profiles. The proposed resolution method is thus fully self-modelling. A comparison between the obtained elution profiles and the true elution profiles is given in Fig. 4A. The corresponding spectra calculated by solving eqn. 4 are given in Fig. 4B and are in good agreement with the true spectra. The chromatographic resolution between the compounds was between 0.93 and 0.43.

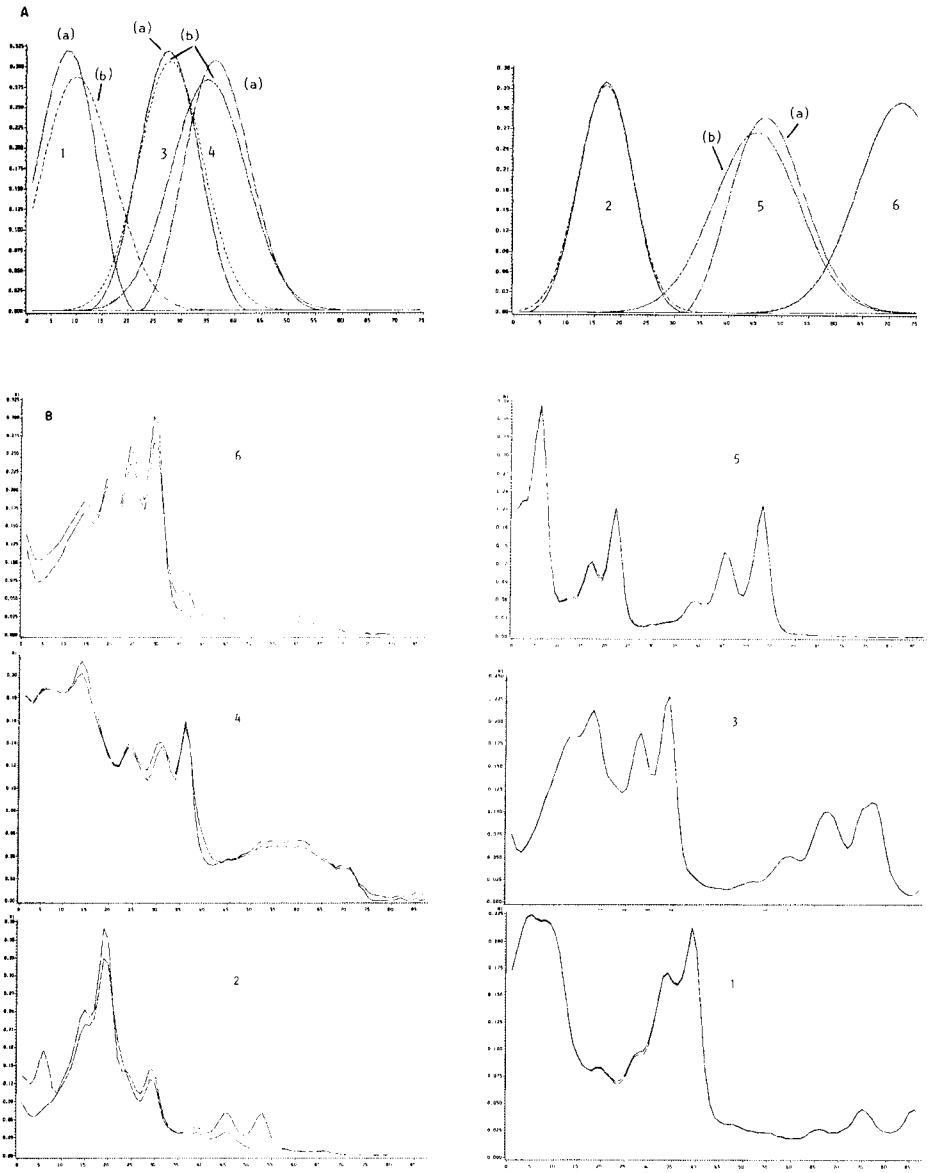

Fig. 4. Synthetic 6-component peak cluster: (A) comparison between "estimated" (a) and "true" (b) elution profiles (normalized); (B) comparison between "estimated" and "true" spectra. (For clarity the elution profiles are given in two separate figures, but are in reality superimposed.)

Four-component semi-synthetic data. The results (Fig. 5) obtained for the 4-component semi-synthetic data described in the experimental part show that self-modelling curve resolution by iterative t.t.f.a. applied on realistic systems can provide spectra of good quality. Moreover, elution profiles are

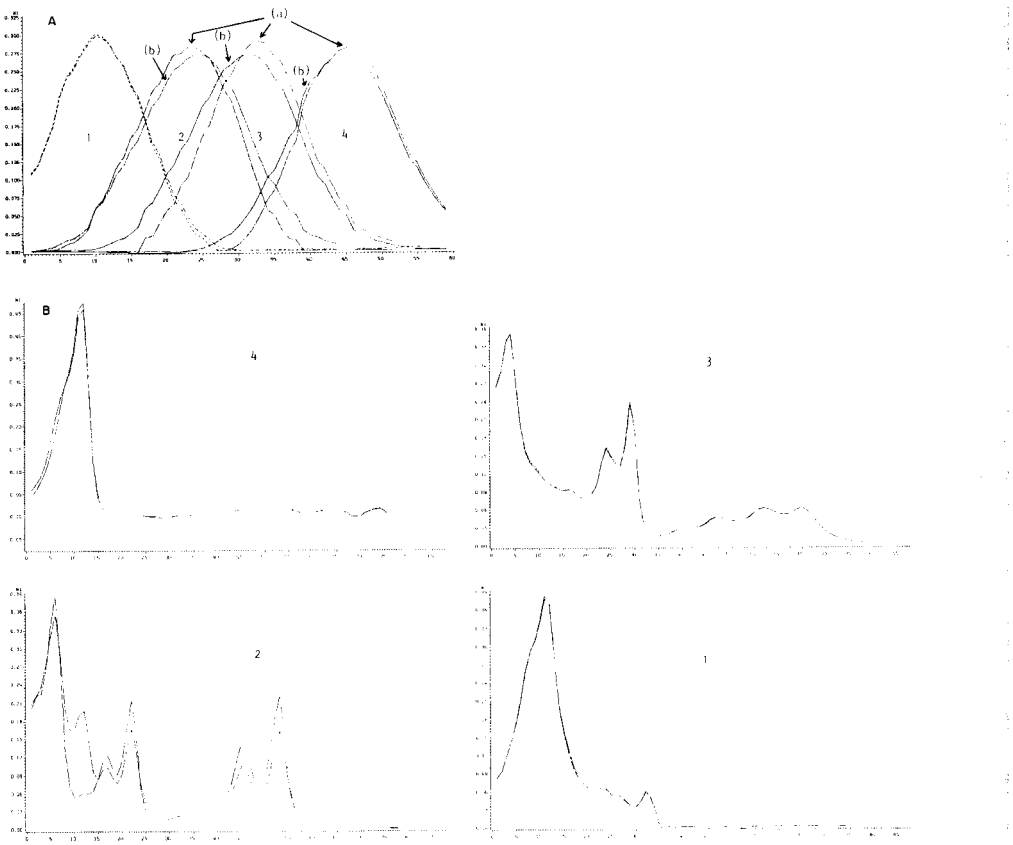

Fig. 5. Four-component curve resolution by iterative t.t.f.a.: (A) "estimated" (a) and "true" (b) elution profiles (normalized); (B) "estimated and "true" spectra.

obtained with a reasonable accuracy. From the overall-resolved elution profile (Fig. 5A), one could expect that problems would arise with compounds 2 and 3. The compounds are very poorly separated, so that their spectra are always mixed up with one or more of the other compounds. Consequently, none of the measured mixture spectra will be closely similar to the pure spectra of 2 and 3. Spectrum 3, however, is perfectly recovered, and a chemically meaningful spectrum of compound 2 is obtained.

Curve resolution on experimental data

The performance of curve resolution by iterative t.t.f.a. can be compared with the results obtained by the curve resolution based on extrapolation of the purest measured elution profiles (CR-3) [1]. Identical elution profiles and spectra were obtained by CR-3 and iterative t.t.f.a. curve resolution for the M80P13P6 3-compound cluster (see Experimental) as shown in

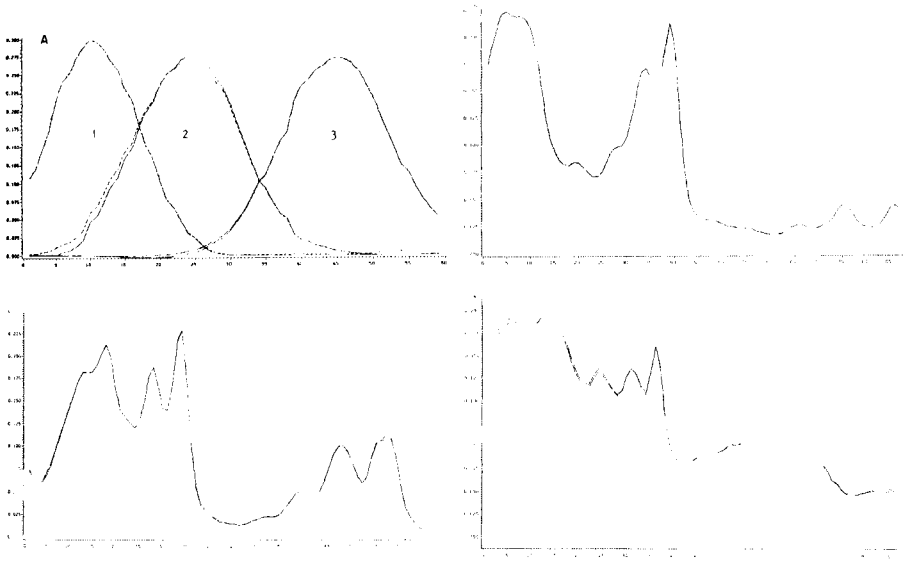

Fig. 6. Three-component curve resolution of polynuclear aromatic hydrocarbons obtained by CR-3 and iterative t.t.f.a. (A) Comparison of the "estimated" elution profiles. (B1—3) Comparison of the "estimated" spectra for the 3 components.

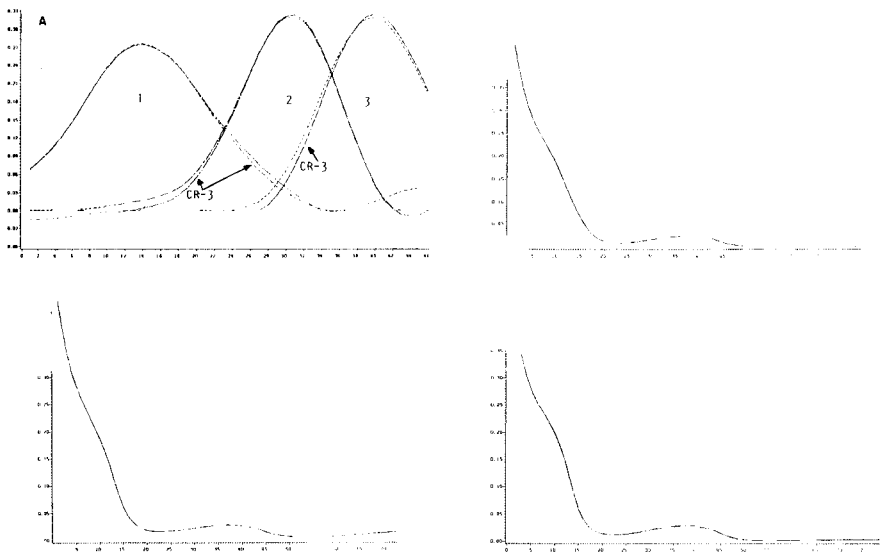

Fig. 7. Three-component curve resolution of proteins obtained by CR-3 and iterative t.t.f.a. (A) Comparison of the "estimated" elution profiles. (B1—3) Comparison of the "estimated" spectra. Compounds: (1) carbonic acid anhydrase; (2) α-chymotrypsin; (3) myoglobin.

TABLE 5

Four-component peak cluster A65P13P3

Peak number	Relative contribution of spectra to total signal (normalized spectra)	Resolution
1	25	R_{12}: 0.99
2	1	R_{23}: 0.77
3	1	R_{34}: 1.37
4	1	

Fig. 6, and for the protein separation (Fig. 7). In the latter case, the spectra of the compounds were quite similar, which demonstrates the ability of iterative t.t.f.a. to retrieve the pure elution profiles even when the spectra are quite similar. However, this method failed for a 4-component cluster with the parameters given in Table 5; it returned only two spectra of which one was allocated to three profiles. The reason is that the absorbances in the latter spectrum were much higher (25:1) than those of the other compounds. This indicates that the curve resolution of minor components (minor in the sense of having a weak signal) in the presence of a major component remains difficult, and requires further research. Equally, curve resolution becomes more difficult when the resolution of the compounds falls below 0.3. In this case, stricter rules are necessary in order to prevent the targets from converging to a linear combination of the true elution profiles.

The authors thank Hugo Billiet and Anton Drouen, Laboratory for Instrumental Analysis, Technical University of Delft, for their technical assistance in measuring the data, and Hans Frank, Department of Biochemistry, Technical University of Delft, for providing the protein data. This research was supported in part by the provision of equipment by Hewlett-Packard, The Netherlands.

REFERENCES

1 B. G. M. Vandeginste, R. Essers, T. Bosman, J. Reijnen and G. Kateman, Anal. Chem., 57 (1985) 971.
2 D. W. Osten and B. R. Kowalski, Anal. Chem., 56 (1984) 991.
3 M. A. Sharaf and B. R. Kowalski, Anal. Chem., 54 (1982) 1291.
4 B. A. Roscoe and P. K. Hopke, Comput. Chem., 5 (1981) 1.
5 P. K. Hopke, D. J. Alpert and B. A. Roscoe, Comput. Chem., 7 (1983) 149.
6 E. R. Malinowski and D. G. Howery, Factor Analysis in Chemistry, Wiley, New York, 1980.
7 P. Horst, Factor Analysis of Data Matrices, Holt, Rinehart and Winston, New York, 1965.

Analytica Chimica Acta, 173 (2985) 265—272
Elsevier Science Publishers B.V., Amsterdam — Printed in The Netherlands

A KALMAN FILTER FOR CALIBRATION, EVALUATION OF UNKNOWN SAMPLES AND QUALITY CONTROL IN DRIFTING SYSTEMS
Part 3. Variance Reduction

P. C. THIJSSEN* and G. KATEMAN

University of Nijmegen, Faculty of Science, Department of Analytical Chemistry, Toernooiveld, 6525 ED Nijmegen (The Netherlands)

H. C. SMIT

University of Amsterdam, Laboratory for Analytical Chemistry, Amsterdam (The Netherlands)

(Received 2nd August 1984)

SUMMARY

The performance of fixed-interval smoothing is investigated for a linear calibration graph with drifting parameters. When all the calibration measurements are processed on-line by the Kalman filter, the quality of the evaluated results may be improved by later off-line smoothing. It is shown that a considerable reduction in variance can be obtained.

In routine analytical laboratories, the effect of time on the quality of results can be significant. An important aim of chemometrics is to improve the accuracy and the precision of methods [1, 2]. Analytical processes have been described by a first-order autoregressive model for quality control [3, 4]. In routine practice, samples are commonly processed in batches and the well-established concepts of between-batch variance and within-batch variance are important. Within-batch effects can be controlled by placing calibration standards at fixed intervals in the sample sequence; between-batch effects can be controlled by restart of a weighted digital filter [5, 6].

A drift model can be used for processing slowly varying parameters of a linear calibration graph. After calibration, a Kalman filter estimates and predicts the parameters that change with time and are used for the evaluation of unknown samples. Given a preset precision of the final results, a control procedure recalibrates the system and assesses the next unknown [7]. On-line optimal selection from the available concentrations occurs if necessary [8]. This paper is devoted to fixed interval smoothing, an off-line estimation technique which is done after all the measurements have been collected and processed on-line [9]. The variance reduction of the analytical results in comparison with that of the Kalman filter is given particular attention.

0003-2670/85/$03.30

THEORY

State estimation

The problem of how to obtain an approximation for a state intermediate or prior to a span of imperfect measurements is handled by state estimation. In principle, no particular structure has to be attributed to the model description of the system. The state-space model investigated here is the linear discrete one. Extensions to a continuous description or a non-linear model are possible but are not discussed here.

A linear discrete system is described by

$$\mathbf{x}(k) = \mathbf{F}(k, k-1)\mathbf{x}(k-1) + \mathbf{w}(k-1)$$

$$z(k) = \mathbf{h}^t(k)\mathbf{x}(k) + v(k)$$

where $z(k)$, $\mathbf{h}(k)$, $\mathbf{x}(k)$, $v(k)$, $\mathbf{F}(k, k-1)$, and $\mathbf{w}(k)$ are the measurement, measurement vector, state vector, measurement noise, transition matrix and system noise, respectively; $k = 1, 2, 3, \ldots$ is the index denoting a sequence of fixed points, of which the time is the most commonly used variable. The system noise and measurement noise are assumed to have zero means and covariances $Q(k-1)$ and $R(k)$, respectively.

The state-space model distinguishes between two sets of equations, a state equation that models the dynamics of the state, and a measurement equation that relates the observed output to the state. A state may refer to concentrations, sensitivities or even to a curve and its derivatives. By using the state-space model in combination with available measurements, it is possible to estimate the state of the system. Any estimate of $\mathbf{x}(k)$; $k = 1, 2, \ldots$, which is based on the measurements $z(1), z(2), \ldots, z(l)$ is denoted as $\hat{\mathbf{x}}(k/l)$. Corresponding to the estimate, there is a covariance matrix denoted $\mathbf{P}(k/l)$, representing the estimation errors of the difference between the state and its estimate $\mathbf{x}(k) - \hat{\mathbf{x}}(k/l)$. Depending on the value of k related to l, the estimation algorithms can be classified: (a) prediction ($k > l$) which involves extrapolation towards future states, the estimate $\hat{\mathbf{x}}(k/l)$ occurring after the last measurement; (b) filtering ($k = l$), in which only the current state is of interest and the estimate $\hat{\mathbf{x}}(k/l)$ coincides with the last measurement; and (c) smoothing ($k < l$), which involves reconstruction of past states, i.e., the estimate $\hat{\mathbf{x}}(k/l)$ falls within the span of measurements.

Any estimate whether predicted, filtered or smoothed is defined as optimal with respect to a properly chosen criterion. For a least-squares estimate, a quadratic type of function is minimized. Based on past information and the currently available measurement, the Kalman filter combines prediction and filtering for on-line improvement of the estimate. The predicted estimate $\hat{\mathbf{x}}(k/k-1)$ and filtered estimate $\hat{\mathbf{x}}(k/k)$ are calculated [11] from

$$\hat{\mathbf{x}}(k/k-1) = \mathbf{F}(k, k-1)\hat{\mathbf{x}}(k-1/k-1) \tag{1}$$

$$\mathbf{P}(k/k-1) = \mathbf{F}(k, k-1)\mathbf{P}(k-1/k-1)\mathbf{F}^t(k, k-1) + Q(k-1) \tag{2}$$

$$\hat{\mathbf{x}}(k/k) = \hat{\mathbf{x}}(k/k-1) + \mathbf{k}(k)[z(k) - \mathbf{h}^t(k) \cdot \hat{\mathbf{x}}(k/k-1)]$$

$$\mathbf{P}(k/k) = \mathbf{P}(k/k-1) - \mathbf{k}(k)\mathbf{h}^t(k)\mathbf{P}(k/k-1)$$

$$\mathbf{k}(k) = \mathbf{P}(k/k-1)\mathbf{h}(k)[\mathbf{h}^t(k)\mathbf{P}(k/k-1)\mathbf{h}(k) + R(k)]^{-1}$$

where $\mathbf{k}(k)$ represents the Kalman gain vector. The Kalman filter predicts the state one step ahead. In order to predict more steps forward, Eqns. 1 and 2 extended by $\hat{\mathbf{x}}(k/k) = \hat{\mathbf{x}}(k/k-1)$ and $\mathbf{P}(k/k) = \mathbf{P}(k/k-1)$ can be used for each desired step. In order to start the estimation algorithm at $k = 0$, it is necessary to set the initial values of $\hat{\mathbf{x}}(0/0)$ at 0 and to initialize $\mathbf{P}(0/0)$ as a diagonal matrix with large elements in comparison to the measurement noise covariance, about $100\,R(0)$.

Fixed interval smoothing

State estimation has so far been directed towards prediction and filtering, the state space model and available measurements are used to estimate the current and future state of the system. The use of a span of measurements to estimate the history of the state is provided by smoothing. For smoothing, a further classification has been shown to be useful [10—12]: (a) fixed-interval smoothing is a data-processing scheme that uses all measurements between 1 and N to obtain an estimate $\hat{\mathbf{x}}(k/N)$ with $k < N$; (b) fixed-point smoothing yields an estimate $\hat{\mathbf{x}}(k/j)$ at a single point $k < j, \ldots$, which is useful when a previous state of a system is of particular interest; (c) fixed-lag smoothing gives an estimate $\hat{\mathbf{x}}(k/k+N)$ for $k = 1, 2, \ldots$ with a fixed period N in the past, and the incorporated delay between the current state and the available estimate is inherent to this scheme.

From an algorithmic point of view the various types of smoothers are quite similar and may easily be transformed into each other. The smoother presented here is referred to as the fixed-interval smoother. It can only be used off-line, because it must be done after all the measurements have been collected. This type of smoothing can be considered as a combination of two Kalman filters. First, a forward Kalman filter operates on the measurements, for which the filtered state and its covariance matrix [i.e., $\hat{\mathbf{x}}(k/k)$ and $\mathbf{P}(k/k)$] are stored at each step. In a similar way, a second Kalman filter operates backwards in the sequence with the prediction $\hat{\mathbf{x}}_b(k/k+1)$ and $\mathbf{P}_b(k/k+1)$, respectively. Subsequently, the smoothed estimate follows from the statistical weighting of the stored estimates by means of their stored covariance matrices. The smoothed estimates $\hat{\mathbf{x}}(k/N)$ and covariance matrices $\mathbf{P}(k/N)$ can be calculated [11] for $k = 1, 2, \ldots, N$ by

$$\hat{\mathbf{x}}(k/N) = \mathbf{P}(k/N)[\mathbf{P}(k/k)^{-1}\hat{\mathbf{x}}(k/k) + \mathbf{P}_b(k/k+1)^{-1}\hat{\mathbf{x}}_b(k/k+1)] \tag{3}$$

$$\mathbf{P}(k/N) = [\mathbf{P}(k/k)^{-1} + \mathbf{P}_b(k/k+1)^{-1}]^{-1} \tag{4}$$

For the smoothed state, all measurements between 1 and N are used, because the estimate based on measurements up to a given point k is combined with the estimate based on measurements from the final N back to

point $k + 1$ and successively retrodicted to point k. Equations 3 and 4 indicate considerable additional requirements of computer storage and time beyond that required for the Kalman filter. The algorithm can be shown to be equivalent to alternative formulations that reduce the computational effort of the matrix inversions and the storage requirements. The simplest and most elegant form of the fixed-interval smoother is the Rauch, Tung and Striebel smoother [12]. The forward run is produced by a conventional Kalman filter processing the measurements on-line. Hereafter, the backward Kalman filter and fixed-interval smoother are modified to process the stored quantities in a reversed sweep for $k = N - 1, N - 2, \ldots, 1$:

$$\hat{\mathbf{x}}(k/N) = \hat{\mathbf{x}}(k/k) + \mathbf{A}(k)[\hat{\mathbf{x}}(k + 1/N) - \hat{\mathbf{x}}(k + 1/k)] \tag{5}$$

$$\mathbf{P}(k/N) = \mathbf{P}(k/k) + \mathbf{A}(k)[\mathbf{P}(k + 1/N) - \mathbf{P}(k + 1/k)]\,\mathbf{A}^{t}(k) \tag{6}$$

$$\mathbf{A}(k) = \mathbf{P}(k/k)\,\mathbf{F}^{t}(k + 1, k)\mathbf{P}(k + 1/k)^{-1} \tag{7}$$

where for $k = N$ $\hat{\mathbf{x}}(k/N) = \hat{\mathbf{x}}(k/k)$ and $\mathbf{P}(k/N) = \mathbf{P}(k/k)$; $\mathbf{A}(k)$ refers to the smoother gain matrix. The stored estimates are processed by these equations in the same fashion as the measurements and weighted by their corresponding covariance matrices. The smoother is initialized by means of the last filtered state $\hat{\mathbf{x}}(k/k)$ and covariance $\mathbf{P}(k/k)$ of the Kalman filter. The computational effort is limited to one matrix inversion at each step; the need for storage is limited to $\hat{\mathbf{x}}(k/k)$ and $\mathbf{P}(k/k)$, because $\hat{\mathbf{x}}(k + 1/k)$ and $\mathbf{P}(k + 1/k)$ can be computed by prediction (Eqns. 1 and 2). By using the symmetry of the off-diagonal elements in the covariance matrix $\mathbf{P}(k/k)$, the storage requirements can be reduced further. A disadvantage here lies in the inversion at each step and numerical problems may arise when $\mathbf{P}(k + 1/k)$ becomes ill-conditioned. This might happen when the smoother returns to an unobservable phase, i.e., when the measurement number k is less than the dimension of the state-space model. An alternative equation similar to Eqn. 5 for the smoothed state avoids the inversion problem although some extended storage is required [10]. In the following sections, the implemented fixed-interval smoother pertains to Eqns. 5—7.

A state is said to be smoothable if the smoother provides a covariance matrix superior to that produced by a backward-operating Kalman filter. Equation 4 indicates the restriction $\mathbf{P}(k/N) \leqslant \mathbf{P}(k/k)$. Only states that are driven by the system noise $\mathbf{w}(k - 1)$ are smoothable. When the system noise covariance $Q(k - 1)$ equals the zero matrix, the results of the smoother and the Kalman filter are equivalent.

The calibration system

For a linear calibration graph with parameters drifting at random, the state-space model derived [7] is

$$\begin{pmatrix} a(k) \\ b(k) \\ \alpha(k) \\ \beta(k) \end{pmatrix} = \begin{pmatrix} 1 & 0 & 1 & 0 \\ 0 & 1 & 0 & 1 \\ 0 & 0 & 1 & 0 \\ 0 & 0 & 0 & 1 \end{pmatrix} \begin{pmatrix} a(k-1) \\ b(k-1) \\ \alpha(k-1) \\ \beta(k-1) \end{pmatrix} + \mathbf{w}(k-1) \tag{8}$$

$$z(k) = (C, 1, 0, 0) \begin{pmatrix} a(k) \\ b(k) \\ \alpha(k) \\ \beta(k) \end{pmatrix} + v(k)$$

The state refers to the parameters of a linear calibration graph $z = aC + b$, where z is the signal and C the concentration. In order to model drift with time, the slope a and intercept b are extended by α and β, respectively. The state is estimated by measuring standards with known concentrations or reference values, that are processed by the Kalman filter. For the evaluation of unknown samples, the associated signal and the predicted state are used in the formulation $C = (z - b)/a$. After each measurement, a quality-control algorithm decides whether to calibrate again or to process the next unknown. For evaluation, the preselected criterion N_{crit} is compared with the maximal relative imprecision N_{max} of the expected results. The decision to re-calibrate is followed by selecting which of the available concentration standards gives the optimal performance of the Kalman filter [8].

The calibration system with algorithms for prediction, filtering, evaluation, control and optimization operates in on-line and the results can be used directly for analytical purposes. After an entire batch of samples has been processed, and if a time delay is not detrimental, the pre-set quality of the results can be improved by smoothing. Thus smoothing provides a proper extension within the described set of algorithms.

The information $I(k) = H(k-1) - H(k)$ furnished by state estimation is given by a decrease in entropy, where the entropy H follows from the Shannon equation $H = -\int_{-\infty}^{+\infty} p(\mathbf{x}) \operatorname{ld} [p(\mathbf{x})] d\mathbf{x}$. If the probability density $p(\mathbf{x})$ is represented by a normal distribution with mean $\hat{\mathbf{x}}(k/l)$ and covariance matrix $\mathbf{P}(k/l)$ then $H(k) = 1/2 \operatorname{ld}\{(2\pi e)^n |\mathbf{P}(k/l)|\}$. The total information $I_{tot}(k)$ follows from the additive relation $I_{tot}(k) = \sum_{i=1}^{k} I(k)$. The entire data-processing scheme for state estimation gives the information yield $I(k)$:

$$I(k) = I_{pre}(k) + I_{fil}(k) + I_{smo}(k)$$

$$I_{pre}(k) = 1/2 \operatorname{ld} \{|\mathbf{P}(k-1/k-1)|/|\mathbf{P}(k/k-1|\}$$

$$I_{fil}(k) = 1/2 \operatorname{ld} \{\mathbf{h}^t(k)\mathbf{P}(k/k-1)\mathbf{h}(k)/R(k) + 1\}$$

$$I_{smo}(k) = 1/2 \operatorname{ld} \{|\mathbf{P}(k + 1/N)/\mathbf{P}(k/N)|\}$$

The information $I(k)$ is given in two parts: on-line for the $I_{pre}(k)$ and $I_{fil}(k)$ terms used by the Kalman filter, and off-line $I_{smo}(k)$ for fixed-interval

smoothing. Results have been described for on-line optimization of the experimental design [8].

The term $I_{smo}(k)$ depends exclusively on the system noise covariance $Q(k-1)$. If $Q(k-1)$ approaches the zero matrix, the information $I_{smo}(k)$ diminishes because $\mathbf{P}(k/N)$ becomes equal to $\mathbf{P}(k+1/N)$. However, the net effect for the information yield $I(k)$ is balanced with respect to the minimization of the system noise covariance $Q(k-1)$. Additionally, off-line smoothing improves the information gained on-line by the Kalman filter.

The variance reduction (VR) of the evaluated results for the smoother with respect to the Kalman filter is defined by $VR = [1 - s^2_{smo}/s^2_{kf}]\,100\%$. The experimental variances s^2_{smo} and s^2_{kf} follow from a comparison of the evaluated results with known concentration standards and with reference values that are not involved in the calibration procedure, respectively. Alternatively, the computed variance may be based on simulated concentration values.

RESULTS

The theory presented above is first illustrated with the same simulated example as given in the preceding parts of this series [7, 8]. The situation where standards are used either for the evaluation of unknowns or for calibration of the system with use of quality control and optimization is shown in Figs. 1 and 2. Figure 1(a) illustrates a drifting linear calibration graph with a slowly changing slope a (x1) and intercept b (x2); the rapidly varying drift parameters are denoted by α (x3) and β (x4), respectively. Figure 1(b) depicts the measurements including measurement noise and random drift. Figure 1(c, d) show the estimated state as produced by the Kalman filter and the fixed-interval smoother, respectively. This demonstrates the effect of smoothing on the characteristic calibration jumps of the Kalman filter. The state-space model assumes linearity between two consecutive points in the sequence. Therefore, the prediction with the Kalman filter shows linear extrapolations of the states. However, the smoother produces a non-linear interpolation between two calibrations. This behaviour provides a strong argument for the application of smoothing in practice, especially because non-equidistant measurements may be involved.

Figure 2(a, b) shows the corresponding histograms of the relative errors of the evaluated results compared with their actual values. A variance reduction of 93.5% is obtained. This implies that for the system under consideration, smoothing improves the accuracy by a factor of 4. The performance of the quality control algorithm is indicated in Fig. 2(c). Whenever the computed imprecision N_{max} exceeds the preset limit N_{crit}, recalibration is initiated. The smoother upgrades the zigzagging imprecision exploited by the Kalman filter to a constant and lower level. When a batch of samples is processed, it is advisable to terminate the run with another two calibrations. The effect on the smoothed imprecision when the last standard was omitted may be noted. This confirms the common practice with automated analyzers of recalibrating

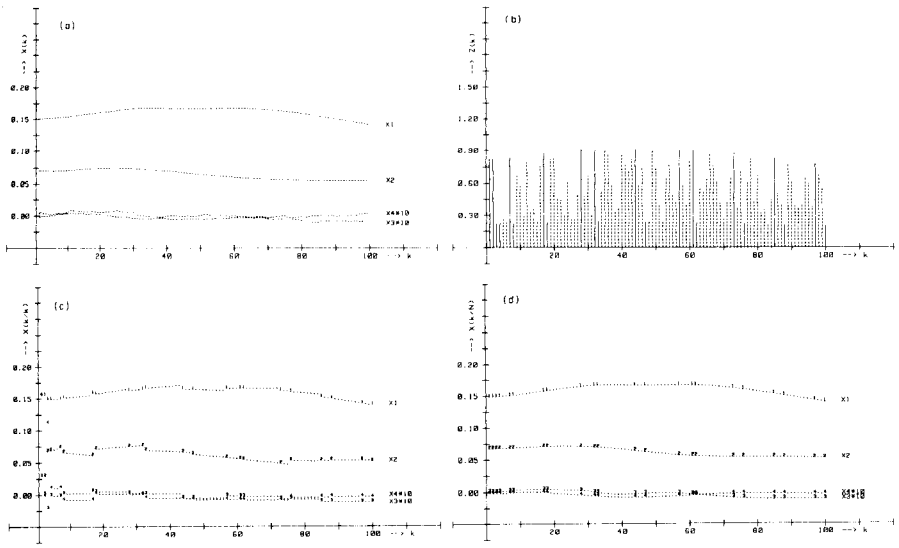

Fig. 1. The calibration system with prediction, filtering, evaluation, control, optimization and smoothing. A critical imprecision N_{crit} = 5% and calibration standards 1, 2, 3, 4, 5 are used. (a) Example of a simulated drifting state ($Q_{33} = Q_{44} = 10^{-8}$ and $R = 10^{-6}$). (b) Measurements corrupted by noise and random drift: (——) used for calibration; (— — —) used for evaluation. (c) Kalman filter estimates of the state: points 1—4 are based on calibration; (· · ·) used for evaluation. (d) Fixed-interval smoothed estimates of the state: points 1—4 are based on calibration; (· · ·) used for evaluation.

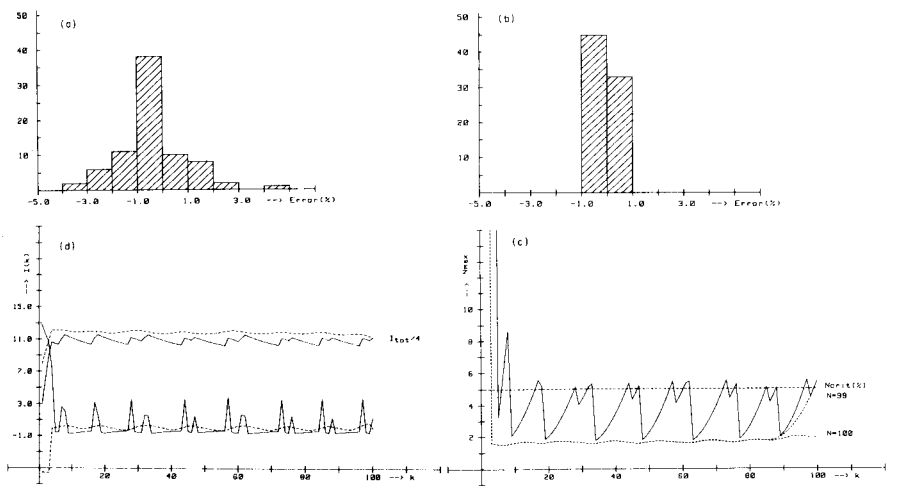

Fig. 2. Additional results of the calibration system (cf. Fig. 1). (a) Histogram of the relative errors of the evaluated results by the Kalman filter compared with their actual values: 78 entries with a mean of —0.39 and a standard deviation of 1.33. (b) Histogram of the relative errors of the evaluated results by the fixed-interval smoother compared with their actual values: 78 entries with a mean of —0.05 and a standard deviation of 0.34. (c) The resulting critical imprecisions N_{max}: (——) Kalman filter; (— — —) smoother. (d) The resulting information yields $I(k)$ and $I_{tot}(k)$: (——) Kalman filter; (— — —) smoother.

at the end of a sample run to check for disturbances. Figure 2(d) shows the information yield of combined prediction, filtering and smoothing. Each time the system calibrates on-line, a positive information yield is found. This is negative when the system evaluates unknown samples. Hereafter, the smoother yields little improvement in information around the calibration points. The total information yield, that is forced to remain above a fixed level by the applied monitoring procedure, is enhanced by the smoother.

Applicability in practice was examined for a computer-controlled flow-injection determination of chloride in aqueous samples [13]. The results obtained will be reported in the immediate future [14]

Conclusions

The application of fixed-interval smoothing for quality improvement of analytical data is demonstrated. Based on a linear calibration graph with drifting parameters, unknown samples are evaluated on-line with use of a quality control procedure. The Kalman filter produces a linear extrapolation of the predicted state, while the smoother interpolates non-linearly between two calibrations. A considerable variance reduction can be obtained by smoothing off-line, depending only on the system noise covariances encountered. This favors the practical application of smoothing, especially when non-equidistant measurements are involved. To improve the precision for batch processing of samples, each run should be terminated by a re-calibration. The entire system combines algorithms for prediction, filtering, evaluation, control, optimization and smoothing based on state estimation.

The authors thank Mr. L. T. M. Prop for making the experimental data available and Dr. F. W. Pijpers for evaluating the manuscript. This work was supported by the Netherlands Research Organisation Z.W.O.

REFERENCES

1 E. K. Harris, Am. J. Clin. Pathol., 72 (1979) 374.
2 J. K. Taylor, Anal. Chem., 53 (1981) 1588A.
3 C. B. G. Limonard, Clin. Chim. Acta, 94 (1979) 137.
4 R. P. T. Jansen and P. J. M. Bonants, Ann. Clin. Biochem., 20 (1983) 174.
5 H. N. J. Poulisse and R. T. P. Jansen, Anal. Chim. Acta, 151 (1983) 433.
6 R. T. P. Jansen and H. N. J. Poulisse, Anal. Chim. Acta, 151 (1983) 441.
7 P. C. Thijssen, S. M. Wolfrum, G. Kateman and H. C. Smit, Anal. Chim. Acta, 156 (1984) 87.
8 P. C. Thijssen, Anal. Chim. Acta, 162 (1984) 253.
9 P. C. Thijssen, H. N. J. de Jong, G. Kateman and H. C. Smit, Anal. Chim. Acta, 170 (1985) 265.
10 A. E. Bryson and Y. C. Ho, Applied Optimal Control, Blaisdell, Waltham, MA, 1969.
11 A. Gelb (Ed.), Applied Optimal Estimation, MIT Press, Cambridge, MA, 1974.
12 B. D. O. Anderson and J. B. Moore, Optimal Filtering, Prentice-Hall, Englewood Cliffs, NY, 1979.
13 L. T. M. Prop, P. C. Thijssen and L. G. G. van Dongen, Talanta, 32 (1985) 230.
14 P. C. Thijssen, L. T. M. Prop, G. Kateman and H. C. Smit, Anal. Chim. Acta, (1985) accepted for publication.

Analytica Chimica Acta, 173 (1985) 273—280
Elsevier Science Publishers B.V., Amsterdam — Printed in The Netherlands

IMINODIACETIC ACID/ETHYLCELLULOSE AS A CHELATING ION EXCHANGER

Part 1. Determination of Trace Metals by Atomic Absorption Spectrometry and Collection of Uranium

ZS. HORVÁTH, A. LÁSZTITY and O. SZAKÁCS

Institute of Inorganic and Analytical Chemistry, L. Eötvös University, PO Box 123, H-1443 Budapest (Hungary)

G. BOZSAI

Institute of Hygiene, PO Box 64, H-1966 Budapest (Hungary)

(Received 8th November 1984)

SUMMARY

A chelate-forming ion exchanger, iminodiacetic acid/ethylcellulose, is used for the separation of trace metals from waters and different organic solvents. Added uranium was collected from sea waters with recoveries of about 97%. Graphite-furnace atomic absorption spectrometry and solution spectrophotometry were used to quantify the metals. For the direct determination of trace metals in waters by the graphite-furnace method, a simple matrix-matching method is described. The detection limit for cadmium was 0.1 $\mu g\ l^{-1}$ and for lead 1 $\mu g\ l^{-1}$ in drinking water.

Chelating ion-exchange celluloses have recently become popular for the separation and preconcentration of trace metals. The chelating ion exchanger, iminodiacetic acid/ethylcellulose (IDAEC) has been prepared and characterized [2]. It is a dibasic acid with iminodiacetic functional groups (pK_{a1} = 2.65 ± 0.08, pK_{a2} = 9.1 ± 0.2) which readily forms chelates mostly with heavy metals. Chelation of the metals depends on the pH of the solution; pH 5—8 is appropriate for most of the metals. The capacity of IDAEC is in the range 1.2—1.7 meq g^{-1}, determined by potentiometric titration. The stability of the chelates approximates that of the EDTA chelates. The relative stability order is: Pb, Hg > Cu > Ni > Cd > Co > Zn > Mn > Fe(II) ⩾ Ca, Ba, Mg. Alkali metal and ammonium ions form salts with the exchanger.

For the separation of trace metals from different matrices, IDAEC is advantageous, because of the high exchange rate of the iminodiacetic groups on the cellulose skeleton and of the easy dissolution of trace metals (with 1 M acid) from the exchanger after collection. The elimination of matrix effects in flame atomic absorption spectrometry (a.a.s.) by enrichment and separation of trace metals from matrix elements in water samples and in soil extracts on this exchanger was reported earlier [3, 4].

In this paper, the use of IDAEC for the collection of trace metals from

0003-2670/85/$03.30

water and solvent samples and their determination is discussed. A special matrix-matching method was developed for the preparation of standards used in the direct determination of trace metals in water samples by graphite-furnace.

EXPERIMENTAL

Apparatus and reagents

A Perkin-Elmer Model 303 atomic absorption spectrometer with an HGA-74 graphite-furnace atomizer, deuterium background corrector, and a Hitachi-Perkin-Elmer recorder was used with Perkin-Elmer hollow-cathode lamps or electrodeless discharge lamps (for cadmium and lead). For absorption spectrophotometric measurement, a MOM model 202 spectrophotometer (MOM, Hungary) was used.

The polyethylene funnels required had 30-mm stems (10 mm i.d.) with cotton wool at the end of the stems.

High-purity water, i.e. distilled water purified with ion-exchange celluloses [5] was used. The IDAEC was prepared as described [2]. The nitric acid was double-distilled. Synthetic sea water [6] and 0.1% (w/v) arsenazo-III solution were prepared. The ammonium citrate/citric acid buffer was prepared by 500 ml of 1% (w/v) citric acid and 10 ml of (1 + 1) ammonia solution (pH 5—6) and passing the solution through an IDAEC column to remove trace metal impurities. The organic solvents used were of Reanal (analytical reagent) grade.

Procedures

Matrix-matching method. From the water samples to be analyzed, an aliquot was purified on the IDAEC column. Instead of using the standard addition method for the determination of trace metals by graphite-furnace a.a.s., standard solutions were made up to volume with the purified water aliquots. Water samples from Lake Balaton (Hungary) were filtered through a phosphate-cellulose column to eliminate the bulk of the iron(III) before the purification on IDAEC. The samples and standards were acidified with nitric acid (0.3 ml of (1 + 1) nitric acid per 100 ml).

Preconcentration of cadmium, lead and copper from drinking water. The water sample (50 ml) was buffered with ammonium acetate/acetic acid buffer to pH 5—6 and passed through 0.2 g of ammonium-form IDAEC placed in a polyethylene funnel; the flow rate was 7—8 ml min^{-1}. The exchanger was washed with 50 ml of high-purity water and then with two 10-ml portions of ammonium citrate/citric acid buffer and three 10-ml portions of high-purity water for removing alkaline and alkaline earth metal ions. The trace metals retained by the cellulose were eluted with two 2.5-ml portions of 1 M nitric acid and 5 ml of high-purity water and diluted to 10 ml. The metals were determined by graphite-furnace a.a.s. A blank solution was prepared similarly. In the model experiments, the purified water samples were spiked with

10—100 $\mu g\,l^{-1}$ zinc, iron(III) and manganese. Lead, cadmium and copper were added to the purified water in different quantities.

Graphite-furnace a.a.s. measurements. The operation of the lamps, and the drying (rate program 7)/decomposition/atomization cycles were as recommended by the manufacturer. The volume of the injected sample was 20 μl.

Determination of heavy metal impurities in organic solvents. The organic solvent (100 ml) was diluted to 200 ml with high-purity water and passed through 0.3 g of ammonium-form IDAEC in a polyethylene funnel at a flow rate of 4—5 ml min^{-1}. The metal ions retained on the IDAEC were eluted into a 25-ml volumetric flask with two 5-ml portions of 1 M nitric acid and 10 ml of high-purity water, and diluted to volume with the high-purity water. The metal ions were determined by graphite-furnace a.a.s. The organic solvents investigated were methanol, ethanol, n-propanol and acetone. The metal impurities measured included Cd, Cu, Fe and Pb.

Concentration of uranium from different waters. The water samples used were high-purity water, tap water, synthetic sea water [6] and sea water from Yugoslavia (Poreč, Korčula).

In the column experiments, 100 ml of water sample, pH 8.5—9, was spiked with 20 μg of uranium and passed through 0.3 g of the ammonium-form IDAEC in a polyethylene funnel. The flow rate was 7—8 ml min^{-1}. The IDAEC was washed with two 10-ml portions of high-purity water. The uranium was eluted with two 5-ml portions of 6 M hydrochloric acid into a 50-ml beaker and the eluate was used for the spectrophotometric determination of uranium.

Spectrophotometric determination of uranium. To the eluate were added 1—2 granules of zinc and 0.1 g of ascorbic acid. After 10 min, the solution was filtered into a 25-ml volumetric flask, 1 ml of the arsenazo-III solution was added, and the solution was diluted to volume with 6 M hydrochloric acid. The absorbance was measured at 665 nm. The blank solution was prepared similarly.

Study of pH dependence. The pH-dependence of the uptake of uranium was measured by a batch method. Synthetic sea water or other water samples (100 ml) adjusted to different pH (2, 4, 6, 8 and 9) containing 20 μg of uranium were shaken for 30 min with 0.3 g of ammonium-form IDAEC or allowed to stand for 24 h. After filtration, the uranium was eluted as described above for column experiments, and determined spectrophotometrically.

RESULTS AND DISCUSSION

Direct determination of iron and manganese in different waters by graphite-furnace a.a.s.

For this determination of the metals, a matrix-matching method was developed as described under Experimental. Passing the water samples for diluting the standards through an IDAEC column reduced the concentration of the heavy metals in the filtrate below the detection limit whereas the

concentrations of alkali metal and alkaline earth ions remained practically unchanged. Thus the matrix was essentially the same as in the original sample. When this matrix-matching method is used, standard addition can be avoided, and the time needed is shorter in the routine analysis of water samples of approximately the same hardness.

The method was used for the determination of heavy metal ions in drinking waters, and in Danube River and Lake Balaton waters. The results for Balaton water are shown in Table 1; the metal contents were measured by graphite-furnace a.a.s. in filtered and unfiltered samples, which were acidified with nitric acid. There are great differences in the iron and manganese concentrations in the filtered and unfiltered samples; the acid dissolved some metal from the suspended matter of the unfiltered sample. The concentrations of copper, chromium and lead were below the detection limit of the method in the Lake Balaton samples. Table 1 also lists the cadmium contents of the samples. Cadmium could be measured in the samples collected in

TABLE 1

Metal concentrations in Lake Balaton water on the same day (except for cadmium) in 1981[a] by direct application of graphite-furnace a.a.s.

Sampling location[b]	Concentration found ($\mu g\ l^{-1}$)			
	Iron		Manganese	Cadmium[c]
	Labile[c]	Soluble[d]	Labile[c]	October
Keszthely/Mouth of Zala River	70	3.9	13	0.26
	80	2.2	17	0.14
	30	3.0	14	0.10
Szigliget/Balatonmáriafürdö	230	3.4	17	0.05
	110	3.6	15	0.18
	125	3.0	13	0.12
Zánka/Balatonszemes	70	5.4	7.2	0.10
	30	11.0	7.8	0.28
	70	1.8	7.8	0.48
Balatonfüred/Zamárdi	70	9.0	6.8	0.12
	70	7.5	6.8	0.05
	80	6.8	5.6	0.05
Balatonalmádi/Balatonvilágos	80	3.4	4.0	0.05
	70	3.0	6.3	0.05
	90	3.4	4.4	0.05

[a]In the filtered and unfiltered water samples, the concentrations of other metals were as follows: Cu < 3 $\mu g\ l^{-1}$, Pb < 5 $\mu g\ l^{-1}$, Cr < 2 $\mu g\ l^{-1}$. [b]For each set, sampling was done at points offshore from the places mentioned, with a third sample taken in the middle of the lake between the two places. [c]Unfiltered sample: "labile" refers to the soluble fraction plus the fraction of particulate metal extracted when the sample was acidified. [d]The "soluble" fraction refers to the fraction remaining after the water had been filtered through a 0.45-μm membrane filter. The soluble manganese fraction was $<0.5\ \mu g\ l^{-1}$ in all these samples.

October but its concentration did not even reach the limit permissible in drinking water, 1 $\mu g\ l^{-1}$. Cadmium could not be detected (i.e., $<0.05\ \mu g\ l^{-1}$) in the samples collected in other seasons.

Separation and preconcentration on IDAEC

Determination of heavy metals in water samples. In hard waters with high salt content (Ca, Mg content $\geqslant 8$ meq l^{-1}), the direct determination of trace metals cannot be achieved by graphite-furnace a.a.s. because of matrix interference. In such cases, separation of the trace metals is recommended. It was shown earlier [3, 4] that chelating with IDAEC enabled many elements to be separated from alkali metal and alkaline earth metal ions and preconcentrated in the same step. By this technique, trace metals in drinking, surface, and mineral waters could be determined by flame a.a.s. [3]. This concentration method was modified for graphite-furnace a.a.s. To decrease the concentration of the alkali and alkaline earth metals in the eluate, the IDAEC column was washed with ammonium citrate/citric acid buffer before the elution of the trace elements with nitric acid. In Table 2, the accuracy and reproducibility of this method are shown for the determination of cadmium, lead and copper added to drinking water. The results were in good agreement with those from a TMDTC/MIBK extraction method but the recovery of cadmium was better by the IDAEC procedure. The detection limits, calculated as the concentration equivalent to three times the standard deviation of the background noise, were 0.1 $\mu g\ l^{-1}$ for cadmium and 1 $\mu g\ l^{-1}$ for lead and copper. The characteristic concentration and the detection limit of this method are high enough for the determination of cadmium and lead in drinking water; 10% of the permissible maximum contamination level could be detected easily. The method was used for the analysis of different drinking waters; the results are shown in Table 3.

TABLE 2

Preconcentration of metals from drinking water on IDAEC (5-fold concentration)

Metal ion	Conc. ($\mu g\ l^{-1}$)		Recovery (%)	Detection limit ($\mu g\ l^{-1}$)
	Added	Found[a]		
Cd^{2+}	2.5	2.4 (2.1)	96	
	5.0	4.8 (1.8)	96	0.1
	10.0	9.7 (1.7)	97	
Pb^{2+}	25	21 (7.0)	87	
	50	43 (6.0)	86	1.0
	100	87 (5.0)	87	
Cu^{2+}	25	22 (4.0)	89	
	50	45 (3.0)	90	1.0
	100	92 (3.0)	92	

[a]Mean of 6 determinations with relative standard deviation (%) in parentheses.

TABLE 3

Results obtained for Budapest drinking waters (from the Danube) after preconcentration of the metals on IDAEC

Sample	Conc. found ($\mu g\ l^{-1}$)		
	Cd	Pb	Cu
Intake	0.6	7.0	3.7
Clean water	0.5	<1.0	2.4
Tap water 1	0.1	1.0	2.9
2	0.3	<1.0	2.5
3	0.4	32.0	25.0
4	0.4	6.6	2.4
5	0.5	<1.0	2.5

Determination of heavy metal contaminants in organic solvents. Cellulose ion-exchangers were used previously for the purification and the determination of metal impurities in organic solvents. The method could be improved by using IDAEC. The sorption of metal ions was better in water/organic solvent mixtures than in an organic solvent alone [7]. Förster and Lieser [8], using chelating ion-exchange cellulose for the determination of the metal contaminants in solvents, had problems in the sorption of iron from acetone. When IDAEC and acetone/water mixtures were used, sorption of the metals was quantitative. The metals were determined by the graphite-furnace a.a.s. method; this had the advantage that aqueous standards could be used. Table 4 lists the metal contents found in analytical-grade organic solvents and the recoveries of added metals. Jacobs et al. [9] measured trace element concentrations in 13 organic solvents, including acetone, methanol and ethanol. The blank values for iron are in the same concentration range as the present values. The values can vary for different bottles of a given solvent.

TABLE 4

Preconcentration of metals by IDAEC from organic solvents (4-fold concentration)[a]

Solvent	Concentration found ($\mu g\ l^{-1}$)							
	Cd		Cu		Pb		Fe	
	—	0.50 added	—	5.0 added	—	5.0 added	—	50 added
Methanol	0.02	0.49 ± 0.02	0.2	5.0 ± 0.15	0.1	5.0 ± 0.16	2.0	51 ± 1.0
Ethanol	0.04	0.53 ± 0.03	1.0	5.8 ± 0.19	0.1	5.1 ± 0.15	1.5	49 ± 1.4
n-Propanol	0.02	0.48 ± 0.02	0.2	5.1 ± 0.20	0.2	4.8 ± 0.20	0.5	48 ± 1.6
Acetone	0.02	0.48 ± 0.03	0.2	4.7 ± 0.19	0.2	4.6 ± 0.21	0.5	49 ± 2.0

[a]The organic solvents were first diluted (1 + 1) with high-purity water. The data are the mean and standard deviation of six determinations.

TABLE 5

pH dependence of the collection of uranium on IDAEC in the ammonium form from synthetic sea water

pH	2	3	4	6	8	9
% Sorption (%)[a]	36	70	87	92	88	70

[a]Mean of six determinations.

TABLE 6

Percentage recovery of uranium (20 μg (100 ml) from different waters)

Water sample	Recovery (%)	
	Batch	Column[a]
High-purity	98	100 (2.1)
Drinking	98	99 (2.5)
Synthetic sea	92[b]	97 (2.8)[c]
Sea	90[b]	97 (2.8)[c]

[a]Mean of six determinations with relative standard deviation in parentheses. [b]pH 6. [c]pH 8.2.

Checking the purity of the organic solvents is especially important in the semiconductor industry.

Collection of uranium from different waters. The pH dependence of the uptake of uranium by IDAEC from synthetic sea water was measured by the batch method (see Experimental). The results (Table 5) show that the uptake of uranium is highest at pH 6; at higher pH values the uptake decreased because of the formation of uranium carbonate complexes [10]. The collection of added uranium by IDAEC was measured in various water samples by batch and column methods, with the results listed in Table 6. For the collection of uranium, the IDAEC should be in the ammonium form. The flow rate should be 5—6 ml min^{-1} for >90% uptake. The results show that IDAEC can be used for the collection of uranium from different water samples. The IDAEC was not soluble in sea water. When 0.5 g of IDAEC was left for 12 days in 200 ml of sea water, the weight loss was about 2%.

In conclusion, it can be said that the IDAEC chelate-forming ion exchanger is a good collector of trace metals from waters and solvents.

The authors thank Dr. J. Salánki, Balaton Research Institute for Limnology, Tihany, for providing Lake Balaton water samples and for his keen interest. We are grateful for the collaboration provided by Dr. K. Vörös, of the same Institute. The assistance of Mrs K. Tóth in the practical work is gratefully acknowledged.

REFERENCES

1 W. Wegscheider and G. Knapp, Crit. Rev. Anal. Chem., 11 (1981) 79.
2 Zs. Remport-Horváth and Gy. Nagydiósi, J. Inorg. Nucl. Chem., 37 (1975) 767.
3 Zs. Horváth, K. Falb and K. Fodor, Magy. Kem. Foly., 83 (1977) 254.
4 Zs. Horváth, K. Falb and M. Varju, At. Absorpt. Newsl., 16 (1977) 152.
5 Zs. Horváth, A. Lásztity and O. Szakács, Anal. Chem., 53 (1981) 1149.
6 K. Grasshoff, Methods of Sea Water Analysis, Verlag Chemie, Weinheim, 1976.
7 A. Lásztity and M. Ösy, Acta Chim. Hung., 60 (1969) 341.
8 M. Förster and K. H. Lieser, Fresenius Z. Anal. Chem., 309 (1981) 352.
9 F. S. Jacobs, V. Ekambaram and R. H. Filby, Anal. Chem., 54 (1982) 1240.
10 H. J. Schenk, L. Astheimer, E. G. Witte and K. Schwochau, Sep. Sci. Technol., 17 (1982) 1293.

Analytica Chimica Acta, 173 (1985) 281—288
Elsevier Science Publishers B.V., Amsterdam — Printed in The Netherlands

DETERMINATION OF HYDROGEN ION ACTIVITIES IN VARIOUS TERNARY WATER/METHANOL/DIOXANE SOLVENT SYSTEMS

G. PAPANASTASIOU*, I. ZIOGAS and D. JANNAKOUDAKIS

Laboratory of Physical Chemistry, Department of Chemistry, Faculty of Science, University of Thessaloniki (Greece)

(Received 19th November 1984)

SUMMARY

The practical pH values for solutions in ternary water/methanol/dioxane solvents measured by a pH meter standardized with aqueous buffer solutions do not lie on the conventional scale of hydrogen ion activity referred to the standard state in the corresponding medium (pa_H^*). These values can be converted to pa_H^* by the introduction of a correction term $\delta = E_j - \log({}_m\gamma_H)$ (where E_j is a term incorporating the liquid junction potential, which depends on the solvent composition and ${}_m\gamma_H$ is the medium effect on hydrogen ion). Values of δ were determined for various ternary solvents at 25°C and were found to be constant in each medium independent of the solute composition.

From a systematic study of the ionization of a number of weak acids in various water/methanol and water/dioxane solvents done in this laboratory [1—3], it was concluded that the ionic behaviour of a single acid was markedly different in those two mixed solvent systems. Generally, these differences can be attributed to the medium effect produced by replacement of one organic compound (say methanol) by the other (dioxane). The differences indicated that extension of the studies to the case of ternary water/dioxane/methanol systems would be useful. Therefore, the ionic behaviour of some weak acids in ternary solvent mixtures was examined and compared to their behaviour in the corresponding binary systems, in an attempt to identify the contribution of each separate organic solvent to the medium effect.

To determine the thermodynamic acidity constants, potentiometric titrations were applied, similarly to the previous work [1—3]. However, for the ternary solvent systems used, there are no literature data on buffer solutions with definite pa_H^* values (where a_H^* is the hydrogen ion activity referred to the standard state in the corresponding medium), thus these titrations were done by using a pH meter calibrated with standard aqueous buffer solutions. In such a case, the practical pH values read from the instrument do not necessarily coincide with the corresponding pa_H^* values.

However, as was first shown by Bates et al. [4], the pH readings, for the case of aqueous alcohol solutions, can be converted to pa_H^* values by the

0003-2670/85/$03.30

introduction of a correction term δ. Bates et al. found that the correction term δ is, to a first approximation, a function only of the composition of the mixed solvent and remains constant over a wide range of pH in these media. Therefore in the present work the possibility of determining a similar parameter δ was examined for the various ternary systems used. Such a possibility enables a_H^* in these complex solvent systems to be determined from pH measurements taken from a pH meter calibrated against common aqueous buffer solutions.

EXPERIMENTAL

Reagents and measurements

Conductivity water (conductance = $1.0 \times 10^{-6}\ \Omega^{-1}\ cm^{-1}$) was used throughout. 1,4-Dioxane was purified by refluxing with sodium for several days and re-distilling; the whole procedure was repeated until the sodium remained bright after several hours. Absolute methanol was distilled once and the first and last 10% fractions were rejected. All the hydrochloric acid solutions were prepared from stock solutions of known concentration (Merck, Titrisol) which were checked by potentiometric titration against silver nitrate. Solvents were mixed immediately before use.

All measurements were made by using the following cell (I):

Glass electrode	Soln. of X in partially aq. solvent	concentrated KCl or NaCl (aq.)	concentrated KCl or NaCl (aq.)	Hg_2Cl_2, Hg
		E_j		

The electrode couple (glass electrode/calomel electrode) was connected to a Beckman Research pH meter with an accuracy of 0.002 pH on the scale of the instrument.

Temperature was controlled at 25.00 ± 0.01°C by means of a Haake Ultrathermostat NBS. A nitrogen atmosphere was maintained above the working solution to avoid any contact of the solution with atmospheric carbon dioxide. A Beckman (No. 39004) glass electrode was used. The reference electrode was a saturated calomel electrode (Ingold type 303-NS-EK).

Method for determination of the correction term δ

It is known that the e.m.f. (E_x) of cell I yields a measure of the operational pH value of a partially aqueous solution X, for by definition

$$pH(X) = pH(S) + (E_x - E_s)/[(RT \ln 10)/F] \quad (1)$$

where E_s represents the e.m.f. of cell I containing an aqueous buffer solution (S). In Eqn. 1, pH(S) is the assigned pH, on a conventional activity scale in water, of the aqueous pH standard (S).

It is widely accepted that the liquid-junction potential E_j in cell I is adequately constant for aqueous solutions over a wide range of pH values [4—7].

Thus, if cell I contains an aqueous solution of X, the pH(X) value calculated by Eqn. 1 can be identified very closely with the conventional value $-\log a_H$ of the solution. However, if cell I contains a partially aqueous solution, the operational pH is still defined but it can no longer necessarily be identified with pa_H^*. In such cases, the pH numbers read from an instrument previously calibrated with an aqueous buffer solution, can be written [5] as follows

$$pH = \bar{E}_j - \log({}_w\gamma_H\, m_H) \tag{2}$$

where $\bar{E}_j$ is the residual liquid-junction potential in cell I written as a pH (namely $E_j/0.05916$ at 25°C) and ${}_w\gamma_H$ is the activity coefficient of hydrogen ion in the mixed solvent used, relative to unity in the standard state in water.

Consequently, the pH readings on a meter calibrated with a standard, aqueous buffer solution will differ from $pa_H^* = -\log a_H^* = -\log({}_s\gamma_H m_H)$, where ${}_s\gamma_H$ is the hydrogen ion activity coefficient referred to the standard state in the partially aqueous medium concerned, by

$$\delta = pH - pa_H^* = \bar{E}_j - \log({}_w\gamma_H / {}_s\gamma_H) \tag{3}$$

However the ratio of these two hydrogen ion activity coefficients is ${}_m\gamma_H$, which represents the medium effect [8, 9] when hydrogen ion is transferred from the standard state in water to the standard state in the mixed solvent concerned. This medium effect depends on the solvent composition but it is independent of the solute composition. Hence

$$\delta = pH - pa_H^* = \bar{E}_j - \log({}_m\gamma_H) \tag{4}$$

This equation shows that it is possible to convert the operational pH values to the corresponding pa_H^* values when the values of δ are known in the medium concerned. Such a conversion retains its practical significance only in solutions where δ is independent of the solute composition. It can be assumed that this condition is fulfilled in solutions where the total ionic strength (I) is not greater than 0.1 and the pH is neither very high nor very low, i.e., under conditions where $\bar{E}_j$ is independent of the solute composition [4, 5, 10].

In order to determine the values of δ in the various mixed systems and also to check the constancy of δ over a wide pH range, the following method was used. In each mixed solvent system, a series of solutions of a strong acid with an accurately known stoichiometric concentration was prepared. Hydrochloric as well as perchloric acid solutions were prepared. For these solutions, pH values were measured by using cell I, standardized against the aqueous buffer solutions recommended by the National Bureau of Standards [11]. For most of the measurements of hydrochloric acid solutions, the bridge was a saturated aqueous potassium chloride solution. A saturated bridge solution of sodium chloride was also used for certain hydrochloric acid solutions. The use of sodium chloride instead of potassium chloride gave identical results for the pH. However, when perchloric acid solutions were

used, the bridge solution was always a saturated aqueous sodium chloride solution to avoid precipitation. From the comparison of the results in each mixed solvent system, it was found that the experimental pH values (measured to a precision of 0.002 pH) of the hydrochloric and perchloric acid solutions, with equal stoichiometric concentration, were the same. For the same solutions, the corresponding pa_H^* were also calculated by means of the equation $pa_H^* = -\log({}_s\gamma_H\, m_H)$.

In these calculations, the activity coefficients ${}_s\gamma_H$ were estimated by the Güntelberg equation [12]: $\log({}_s\gamma_H) = -AI^{1/2}/(1 + I^{1/2})$. The Güntelberg equation provides sufficient accuracy only for $I \leqslant 0.01$ [13], thus care was taken to keep the concentration of the strong acid solutions used below 0.01 *m*.

The correction term δ was finally calculated from the corresponding pa_H^* (calculated) and pH (observed) values. This method is analogous to that used by Van Uitert and Haas [6] for the conversion of the pH meter readings to hydrogen concentration in water/dioxane mixtures at 30°C. The same method as that used here was also employed by Dunsmore and Speakman [14] for the determination of δ in certain water/dioxane mixtures from measurements made for a single 0.01 *m* hydrochloric acid solution.

RESULTS AND DISCUSSION

The correction term δ was determined for the following categories of ternary water/methanol/dioxane systems: (A) ternary mixtures with a volume ratio of dioxane/methanol of 7/3; (B) ternary mixtures with a volume ratio of dioxane/methanol of 3/7; (C) ternary mixtures with a constant content of 10% dioxane (by volume); (D) ternary mixtures with a constant content of 10% methanol (by volume); (E) ternary mixtures with a constant total content of 30% (by volume) of the two organic solvents; in these mixtures the composition of water can be considered, to a first approximation, as constant.

Table 1 summarizes the wt.% and vol.% compositions of all the ternary systems studied. A statement that the vol.% composition of a ternary solvent is, for example, 7% dioxane and 3% methanol, simply means that this system was prepared by mixing 7 ml of dioxane, 3 ml of methanol and adding water up to a final volume of 100 ml. Table 1 also contains the corresponding values of the correction term δ, evaluated by means of the method presented above. The correction factor δ was also evaluated for simple aqueous solutions; the mean value of δ, within the precision of these experimental measurements (i.e., 3 decimal places) was found to be zero with a standard deviation $s < 0.001$. This finding allowed the conclusion that in the acid concentration range under examination (<0.01 *m*), the Güntelberg equation is valid with satisfactory accuracy. For the application of this equation in the various ternary solvent systems, the values of the Debye-Hückel constant, A, were calculated by using dielectric constant data derived from a previous investigation [15, 16].

TABLE 1

Values of parameter $\delta = \bar{E}_j - \log({}_m\gamma_H)$ and of the dielectric constant D corresponding to various ternary water/dioxane/methanol solvent systems at 25°C

Vol.% dioxane	Vol.% methanol	Wt.% dioxane	Wt.% methanol	D	δ
Category A					
7	3	7.20	2.36	71.58	−0.004
14	6	14.36	4.72	64.56	−0.009
21	9	21.51	7.06	57.42	−0.014
28	12	28.68	9.42	50.08	−0.017
35	15	35.89	11.79	42.81	−0.022
Category B					
3	7	3.11	5.56	73.64	0.003
6	14	6.27	11.20	68.65	0.011
9	21	9.46	16.92	63.55	0.019
12	28	12.72	22.75	57.86	0.026
15	35	16.07	28.73	52.26	0.037
Category C					
	10	10.35	7.93	66.63	0.001
	20	10.49	16.08	62.82	0.013
10	30	10.65	24.48	58.94	0.026
	40	10.84	33.21	54.69	0.033
Category D					
20		20.53	7.87	57.96	−0.011
30	10	30.79	7.86	49.18	−0.023
40		40.59	7.78	40.43	−0.050
Category E					
5	25	5.30	20.32	65.40	+0.022
15	15	15.57	11.93	60.32	−0.002
25	5	25.40	3.89	55.60	−0.020

The examination of the δ parameter for the various ternary solvent systems studies showed that it is independent of the solute composition. For example, Table 2 provides the values of δ corresponding to solutions of various hydrochloric acid concentrations in the ternary system water/dioxane/methane containing 28 vol.% dioxane and 12 vol.% methanol. However, it must be said that according to literature data [6, 8, 14], hydrochloric acid can be considered as completely dissociated in dilute solutions in water/dioxane containing up to 50% dioxane ($D \approx 40$). Given that the dielectric constant of all the ternary solvents used is greater than 40, it was therefore assumed that in these media hydrochloric acid is completely dissociated. In order to justify this assumption, perchloric acid was also used for the evaluation of δ in mixtures with a high content of organic solvent; no differences were obtained.

The values in Table 1 show that the correction term δ is sometimes positive (B, C) and sometimes negative (A, D), and for category E can assume positive or negative values. In order to attempt to explain this interesting

TABLE 2

Values of pH (meter readings), pa_H^* and $\delta = \bar{E}_j - \log(_m\gamma_H)$ for various hydrochloric acid solutions in 28/12/60 (vol.%) dioxane/methanol/water at 25° C

$[H^+]$ (10^{-3} m)	pH	pa_H^*	δ	$[H^+]$ (10^{-3} m)	pH	pa_H^*	δ
1.00	3.015	3.031	−0.016	4.37	2.405	2.422	−0.017
1.49	2.846	2.863	−0.016	4.81	2.367	2.383	−0.016
2.14	2.695	2.715	−0.020	5.23	2.331	2.349	−0.018
2.46	2.639	2.656	−0.017	5.71	2.296	2.313	−0.017
2.94	2.566	2.583	−0.017	6.09	2.272	2.288	−0.016
3.32	2.516	2.533	−0.017	7.13	2.207	2.225	−0.018
3.96	2.443	2.462	−0.019				

behaviour, the behaviour of the δ parameter was examined with the same method, in the corresponding binary solvents, water/methanol and water/dioxane. The values derived are listed in Table 3. These values show that, for water/methanol mixtures, δ increases with increase in the methanol content, reaching significant values for high methanol contents. However, if, as described by Harned and Owen [8], an increase in the methanol content leads to an increase in the term $\log(_m\gamma_H)$ (the medium effect), then a study of Eqn. 4 leads to the conclusion that the increase of δ (at least up to 50% in methanol) must be accompanied by an increase in the liquid-junction potential, $\bar{E}_j$.

Similar calculations of the δ parameter were made by Ong et al. [5] in water/methanol mixtures with different compositions from those examined here. Although the methods used by Ong et al. were different from those followed here, their values are quite close to the present results (Fig. 1).

In contrast to the water/methanol mixtures, the correction term δ in all the water/dioxane solvents tested assumed negative values (Table 3). It was found that increase in the dioxane content produced a significant increase in the negative deviations of δ from the "ideal" value $\delta = 0$ which corresponds

TABLE 3

Values of $\delta = \bar{E}_j - \log(_m\gamma_H)$ for various water/methanol and water/dioxane systems at 25°C

H_2O/methanol			H_2O/dioxane		
Vol.%	Wt.%	δ	Vol.%	Wt.%	δ
10	8.01	0.011	10	10.21	−0.011
20	16.23	0.021	20	20.24	−0.019
30	24.67	0.030	30	30.15	−0.029
40	33.39	0.039	40	39.93	−0.060
50	42.50	0.081	50	49.68	−0.123

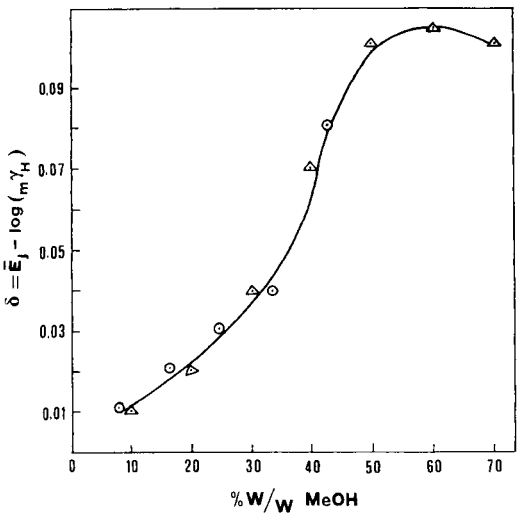

Fig. 1. $\delta = \bar{E}_j - \log({}_m\gamma_H)$ in methanol/water solvents: (△) data from Ong et al. [5]; (○) this investigation.

to simple aqueous solutions. However, this behaviour of δ in the water/dioxane mixtures did not allow any conclusion with regard to the direction of the $\bar{E}_j$ variation, because in these mixtures, the $\log({}_m\gamma_H)$ term (the medium effect) increases together with the dioxane content [8]. Similar evaluations of the δ parameter were made by Dunsmore and Speakman [14] for certain water/dioxane mixtures (20—50% dioxane). However, from their values, which are quite close to the present results, it was not possible to decide whether the δ parameter remains constant in each medium independently of the solute composition, because their values were derived by measurements in a single 0.01 *m* hydrochloric acid solution. For this reason, the work was repeated; it was found that δ was independent of the solute composition in all the water/dioxane solutions studied.

Dioxane and methanol are seen to have opposite contributions to δ values and this effect is still detected even when they coexist in ternary water/methanol/dioxane systems. For these systems, it can be said that the presence of each organic solvent compensates the influence of the other on the value of δ. Indeed, comparison of the values in Tables 1 and 3 indicates that the absolute values of the deviations of δ (from the value $\delta = 0$) are markedly smaller in the systems studied, these deviations were not greater than 0.05 whereas in the corresponding binary systems they reached 0.12 (in 50% dioxane). Actually, all these findings can be interpreted only on the assumption of some sort of competition between the contributions of the two organic solvents to the value of δ.

Examination of the δ behaviour in the various categories of ternary mixtures indicates that the δ values result from superposition of their behaviour

in the corresponding binary mixtures. Therefore when $V_{diox}/V_{MeOH} > 1$, δ behaves similarly to the case of water/dioxane mixtures where $\delta < 0$. In contrast, when $V_{diox}/V_{MeOH} < 1$, δ behaves similarly to the case of water/methanol mixtures where $\delta > 0$. In certain mixtures, the contributions of dioxane and methanol on δ are mutually compensated and the system appears to be "ideal" with $\delta \approx 0$. In such mixtures, the operational pH values obtained by the pH meter standardized against standard aqueous buffers, can be expressed by a conventional scale of hydrogen ion activity (pa_H^*) referred to the standard state in the corresponding medium. Further, mixtures having $\delta = 0$ are suitable for the indirect determination of E_j from experimental values of the medium effect, $\log({}_m\gamma_H)$, because in these mixtures the relationship $\bar{E}_j = \log({}_m\gamma_H)$ is valid. An investigation in this direction is currently in progress.

This study provides the conclusion that for the accurate determination of a_H^*, the operational pH values must be corrected by means of δ, especially for high contents of the organic solvents. If this is not done, then for the compositions studied, the relative error introduced in the value of a_H^* [$|\Delta a_H^*/a_H^*|10^2 = 2.303 \times 10^{-2} |\Delta pa_H^*| = 2.303 \times 10^2 |\delta|$] can go up to 11.5% in ternary mixtures, 18.7% in water/methanol and 28.3% in water/dioxane.

REFERENCES

1 D. Jannakoudakis and G. Papanastasiou, Chimika Chronika, 35A (1970) 1; Sci. Ann. Fac. Phys. Math. Univ. Thessaloniki, 11 (1971) 497; (Chem. Abstr., 86 (1976) 20427C).
2 D. Jannakoudakis, G. Papanastasiou and I. Moumtzis, Sci. Ann. Fac. Phys. Math. Univ. Thessaloniki, 14 (1974) 3; (Chem. Abstr., 87 (1977) 107355t).
3 G. Papanastasiou, G. Stalidis and D. Jannakoudakis, Bull. Soc. Chim. Fr., (1985) 1255.
4 R. G. Bates, M. Paabo and R. A. Robinson, J. Phys. Chem., 67 (1963) 1833.
5 K. C. Ong, R. A. Robinson and R. G. Bates, Anal. Chem., 36 (1964) 1971.
6 L. G. Van Uitert and C. G. Haas, J. Am. Chem. Soc., 75 (1953) 451.
7 R. G. Bates, Determination of pH, Wiley, New York, 1964, p. 58.
8 H. S. Harned and B. B. Owen, The Physical Chemistry of Electrolytic Solutions, 3rd edn., Reinhold, New York, 1967, pp. 453, 669.
9 E. J. King, Acid-Base Equilibria, Pergamon Press, Oxford, 1965, p. 248.
10 C. L. de Ligny and M. Rehbach, Rec. Trav. Chim., 79 (1960) 727.
11 R. G. Bates, J. Res. Natl. Bur. Stand., 66A (1962) 179.
12 E. Güntelberg, Z. Phys. Chem., 123 (1926) 240.
13 M. T. Beck, Chemistry of Complex Equilibria, Reinhold, London, 1970, p. 28.
14 H. S. Dunsmore and J. C. Speakman, Trans. Faraday Soc., 50 (1954) 236.
15 D. Jannakoudakis, G. Papanastasiou and I. Moumtzis, Chimika Chronika, New Series, 2 (1973) 73.
16 D. Jannakoudakis, G. Papanastasiou and P. G. Mavridis, J. Chim. Phys., 73 (1976) 156.

Analytica Chimica Acta, 173 (1985) 289—297
Elsevier Science Publishers B.V., Amsterdam — Printed in The Netherlands

SEQUENTIAL INJECTIONS IN FLOW SYSTEMS AS AN ALTERNATIVE TO GRADIENT EXPLOITATION

E. A. G. ZAGATTO*, M. F. GINÉ, E. A. N. FERNANDES, B. F. REIS and F. J. KRUG
Centro de Energia Nuclear na Agricultura, Universidade de São Paulo, Caixa Postal 96, 13400 Piracicaba, S. Paulo (Brasil)

(Received 4th January 1985)

SUMMARY

In flow injection analysis, several plugs can be injected simultaneously into the same carrier stream, in order to achieve overlapped zones. The potentialities of such sequential injections are studied in model systems with spectrophotometric detection; the procedure is shown to give better precision than the use of concentration gradients. The method is used with atomic absorption spectrometry to allow the determination of a wide range of manganese contents in rocks, and to facilitate the use of standard additions for the determination of copper in ethanol.

In flow injection analysis (f.i.a.) [1], the passage of the dispersed zone through the detection unit produces a transient signal proportional to the analyte concentration in the sample, which is usually recorded as a peak. For most applications, peak heights or peak areas associated with the most concentrated portion of the dispersed zone are measured. However, as the uniqueness of a dispersion pattern under fixed flow conditions is a characteristic feature of f.i.a., measurements related to other portions of the dispersed zone, where the concentration gradients are more pronounced, can also be utilized. Exploitation of gradients has expanded the range of applications of f.i.a., allowing simultaneous determinations [2], calibrations based on a single standard solution [3], reaction-rate measurements [3], gradient scanning [3], f.i.a. titrations [4], selectivity evaluations [5], and automation of the standard addition method [6—8]. In addition, with the zone-sampling approach, not only measurements related to any portion of the dispersed zone can be considered, but also that this portion can be selected, removed from the whole dispersed zone and processed further [8, 9].

The precision of measurement may deteriorate with fluctuations in flow parameters, especially in poorly designed systems with insufficient mixing. This drop in reproducibility is more severe when the measurements refer to a region of the dispersed zone with pronounced concentration gradients [8]. The difficulty of rigid control of flow parameters could be a limiting factor for precision in techniques based on gradient exploitation. This drawback

0003-2670/85/$03.30

can be overcome if all the required measurements are made in portions of the dispersed zone in which the concentration gradients are minimized. This can be achieved in a system with sequential injection [5]: several plugs of a solution are simultaneously intercalated into the same carrier stream, and then overlap strongly as a consequence of dispersion (Fig. 1). Provided that the plugs of the same solution are used, their asynchronous merging [5] results in a final dispersed zone characterized by several sites without appreciable concentration gradients, corresponding to the maximum and minimum values of the concentration/time profile (Fig. 1). Only the measurements related to these sites should be considered because the reproducibility would be less affected by fluctuations in the flow parameters. Such a system, manual or microprocessor-controlled, is of a very simple design.

This paper introduces this expansion of f.i.a.; potentialities and limitations of the approach, and the influence of the more important variables involved are discussed for model systems. Applications in atomic absorption spectrometry include the determination of manganese over a wide range in rocks and the determination of copper in ethanol by the standard addition method.

EXPERIMENTAL

Apparatus

All components of the flow-injection model system, including the spectrophotometer and accessories, the electronically operated injector-commutator and the microprocessor have already been described [8]. For analyses of real samples, a simple manually-operated injector-commutator [10] was used. Silicone-rubber pumping tubes, nylon connectors and a nylon injector-commutator were used for ethanol analyses.

The Perkin-Elmer model 306 atomic absorption spectrometer was operated as recommended by the manufacturer for maximum sensitivity with an air/acetylene flame and a damping factor of 1.3 s (TC2 setting). The flow-injection manifold was connected to the nebulizer as described earlier [10]. For ethanol analysis, the air and acetylene flow rates were 15.8 and 2.3 l min^{-1}, respectively [11].

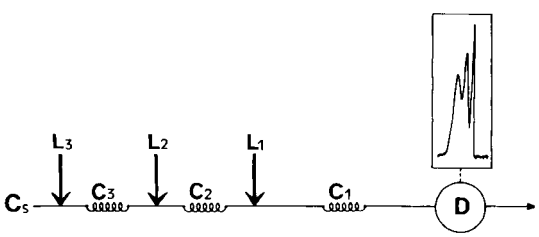

Fig. 1. Schematic representation of the sequential injection process. Symbols are explained in the text.

Reagents, standards and samples

The solutions were prepared from distilled-deionized water and analytical-grade chemicals. For the model systems, the dye solutions (0.1 and 0.01% w/v eriochrome cyanine R, pH 2.9) and the phthalate buffer solution (pH 2.9) were prepared as reported earlier [8].

For the manganese and copper stock standard solutions (1000 mg l^{-1}), 0.769 g of manganese (II) sulfate monohydrate or 0.982 g of copper(II) sulfate pentahydrate was dissolved in water, 3.5 ml of concentrated nitric acid was added and the solution was diluted to 250 ml with water. The manganese working standards (0.10—20.0 mg l^{-1}) were also 1% (v/v) in nitric acid.

The rock samples (certified reference materials, South African Bureau of Standards), were decomposed in 40-ml teflon bombs; the procedure was similar to that of Langmyhr and Paus [12]. The sample (200 mg) was mixed with 1 ml of aqua regia and left at room temperature for $\geqslant$1 h. Then 4 ml of hydrofluoric acid was added, the bomb was closed and heated in a digestor block at 130°C for 2 h. After the bomb had been cooled and opened, 1 ml of perchloric acid was added, and the bomb was replaced again in the block at 210°C. After about 2 h (evolution of white fumes), the bomb was cooled. The sample was then diluted to 20.0 ml with 1% (v/v) nitric acid solution.

Ethanol samples, from several distillation plants, were collected in 500-ml polyethylene bottles and analyzed as received.

Procedures

Sequential injection. Sequential injection is achieved simply by using several sampling loops (L_1, L_2 . . . L_N) in the proportional injector (Figs. 2 and 3). Only one aspiration line is required. When the injector is placed in the sampling position, as specified in the figures, the solution to be injected sequentially fills the sampling loops, its excess being discarded. Movement of the central sliding portion of the injector (I) to the alternative position causes all the selected plugs to be intercalated into the same carrier stream.

Model testing. Initially, the system shown in Fig. 2B was used to estimate the reproducibilities of measurements related to different portions of the dispersed zone. Eriochrome cyanine R solution (0.1%) simulating the sample, was injected into the C_S buffered sample carrier stream. After the sequential injection, the established zones were allowed to overlap before reaching the L′ resampling loop, which selected different fractions of the overlapped zone, in accordance with predefined Δt values [9], the time intervals corresponding to the time of the injector-commutator in the alternative position. These aliquots were then introduced into the C'_S carrier stream and further processed. When this zone sampling was used, the system required electronic operation. The resampling loop was kept as small as possible (3 cm) to improve the spatial resolution of the zone sampling and to emphasize any variations in the reproducibility. The other parameters were: C_1, C_2, C_3 and C_4 coil lengths, 20, 30, 40 and 100 cm; L_1, L_2 and L_3 loop lengths, 12, 20 and 20 cm; flow rates of the first and second carrier streams (phthalate buffer

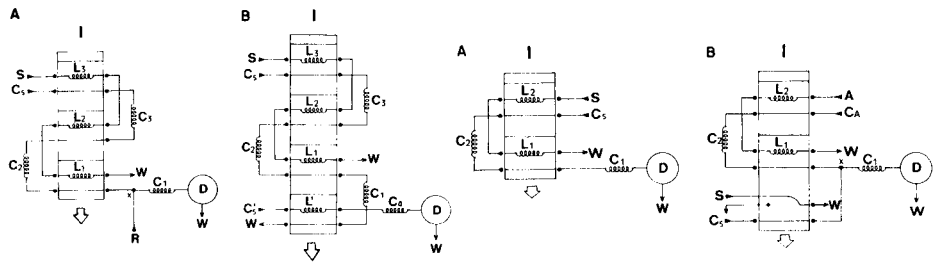

Fig. 2. Flow diagrams of the model flow-injection systems utilized for: (A) studying the main variables involved; (B) estimating the reproducibilities associated with different portions of the dispersed zone. I, Sliding portion of the injector-commutator in the sampling position; L_1, L_2, L_3, sampling loops; L', resampling loop; C_1, C_2, C_3, C_4, coils; S, sample solution; R, reagent; C_S and C'_S, first and second sample carrier streams; D, spectrophotometric detector; W, waste; x, confluence point. For dimensions, see text.

Fig. 3. Flow diagrams of the flow-injection systems utilized for: (A) manganese in rocks; (B) copper in ethanol. A, standard solution to be added; C_A, standard solution carrier stream; C_S, intermittent sample carrier stream; D, atomic absorption spectrometer. Other symbols are explained in the legend of Fig. 2. For dimensions, see text.

solution), 1.2 and 4.3 ml min^{-1}; sample aspiration rate, 2.9 ml min^{-1}; wavelength setting, 535 nm. The Δt value was varied by 0.5 s in the range 1—40 s, the total sampling period being maintained at 50 s. Within this range, the Δt scan was enough for stepwise transference of the entire overlapped zone to the second carrier stream, so that an image of the sample zone concentration/time profile near L' could be obtained (Fig. 4A). For the Δt values corresponding to maximum, minimum and inflexion points of this profile, reproducibilities were evaluated from seven replicates (Fig. 4B).

The system outlined in Fig. 2A was used to investigate the effect of variations in coil and loop lengths in the sequential injection. Any required reagent could be added via point x which was located 10 cm after the L_1 loop. A more dilute dye solution (0.01% eriochrome cyanine R), pumped at 2.9 ml min^{-1}, simulated the sample. The other parameters initially were: C_1, C_2, C_3, 50 cm; L_1, L_2, L_3, 10 cm; flow rates of C_S and R (both phthalate buffer solutions), 2.5 ml min^{-1}. To study the effect of injected volumes, either L_1 or L_2 was replaced by a 20-cm loop. After the model system had been restored to the initial conditions, the effect of C_1 length was studied by using a 100-cm coil, or an 80-cm coil was used as C_2 or C_3. For each situation, triplicate measurements were made (Fig. 5).

Determinations of manganese in rocks and copper in ethanol. The manifold outlined in Fig. 3A was used for manganese. The dimensions were as follows: C_1 = 100 cm, C_2 = 200 cm, L_1 = 100 cm, L_2 = 40 cm, C_S (0.1% v/v nitric acid solution), flow rate 6.0 ml min^{-1}, sample aspiration rate 5.0 ml min^{-1}.

The manifold shown in Fig. 3B was used for the copper determination with standard additions. This system is based on alternating streams [13] of sample and carrier solutions. Dimensions were as follows: C_1 = 75 cm, C_2 = 50 cm, L_1 = 20 cm, L_2 = 15 cm; pumping rate of the A (2.00 mg Cu l^{-1} in 96% ethanol solution) 2.5 ml min^{-1}; C_A flow rate 1.2 ml min^{-1}; pumping rate of the sample and intermittent carrier solutions 5.8 ml min^{-1}. Both C_A and C_S were 96% (v/v) ethanol.

When the injector-commutator is placed in the position specified Fig. 3B, the A standard solution is pumped to fill the L_1 and the L_2 loops, while the intermittent C_S stream is directed to the detector via point x. Manual displacement of the central sliding portion (I) to the alternative position causes solution A to be sequentially injected into C_A, and the sample solution to be directed towards the atomic absorption spectrometer. The overlapped standard zone is added to the sample at point x, mixing being improved inside coil C_1. The measurements related to the maximum and minimum values of the concentration/time profile correspond to the additions of reproducible known amounts of standard to the sample, and the measurement of the sample without addition is done after establishment of the steady state in the sample infinite-volume situation. Standard additions are thus achieved without sample dispersion and the matrix effect is constant.

The added amounts of standard were evaluated by placing a 0.2 mg Cu l^{-1} standard solution as S, and the blank solution (96% v/v ethanol) as A. If linear response is assumed, the readout may be considered in concentration units. Thereafter, C_S was placed as S, and the A solution was restored, allowing measurements of the added concentrations related to the maximum and minimum values of the recorded profile. The data were treated by linear regression, as in earlier work [8]. It should be emphasized that if the system does not provide linear response, the proposed procedure is applicable only after suitable calibration.

RESULTS AND DISCUSSION

Studies with model systems

In the zone-sampling process involving a Δt scan, the L′ resampling loop can be regarded as an intermittent pseudo-sensor. Because of this intermittent action, the Δt value may assume only discrete variations, so that the recorded profile (Fig. 4A) is chopped; in this sense, Fig. 4A is analogous to the profile shown in Fig. 1. Zone sampling, therefore, is a powerful tool for studying dead-volume effects associated with flow-through sensors, variations in the volume of the L′ pseudo-sensor being easily achieved by changing this loop length. When this loop is increased, the L′ pseudo-sensor tends to act as an integrator, and the recorded profile loses resolution. Here, a very small L′ loop (ca. 15 μl) was used to minimize averaging effects, so that any drop in the reproducibility of the measurements could be related better to particular regions of the dispersed zone. As can be seen in Fig. 4B, the reproducibility

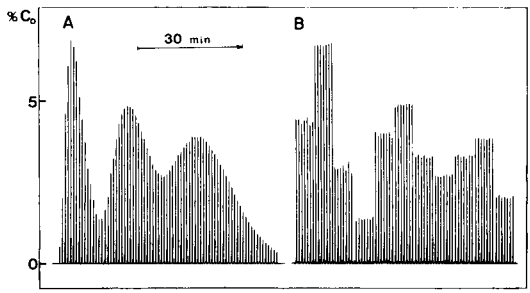

Fig. 4. Recorder output of the measurements related to different regions of the overlapped zone. (A) Image of the concentration/time profile near L′ obtained by using Δt values of 1.0, 1.5, ... 39.5, 40.0 s. (B). Replicate measurements related to maximum, minimum and inflexion points of the concentration/time profile, obtained by preselecting the corresponding Δt values.

deteriorates for regions other than the maxima and minima of the concentration/time profile. This deterioration becomes less evident as the Δt value increases, because Δt defines the mean available time for mixing before the zone sampling. Accordingly, mixing conditions and detector dead volume may become limiting factors in flow-injection procedures based on gradient exploitation, if a high degree of precision is required. In such situations, measurements related to maximum and minimum sites of the concentration/time profile typical of sequential injection should be preferred. However, selecting predefined regions implies some loss in the inherent versatility of gradient exploitation, for which infinite sites are available.

Of the various factors related to the sequential injection process, only the lengths of L_1, L_2, C_1, C_2 and C_3 were investigated, because the other parameters of the system have the same influence as in conventional systems. These loops and coil lengths govern the different path lengths associated with the several injected plugs, and the lengths of the sampling loops define the plug volumes to be intercalated into the same carrier stream. In the initial situation, with $L_1 = L_2 = L_3 = 10$ cm, the three originally identical plugs underwent different dispersions, leading to the appearance of three overlapping peaks with marked differences in heights and widths (Fig. 5a). These reflect the characteristic paths travelled by each plug. When L_1 was changed to 20 cm, the related peak increased (Fig. 5b) and the carryover effect between first and second plugs became more pronounced, thus increasing the first minimum. The other peaks were not significantly affected because the increase in L_1 provoked only a small percentage variation in their analytical paths. For the increase in L_2, similar effects were observed (compare Fig. 5a and c). Variations in the path lengths travelled caused by the sequential injection may be important when larger plugs are intercalated. Preliminary tests involving a tenfold increase in L_1 indicated that the related peak tended to reach saturation, but this marked increase in the path length increased the

dispersions of the other plugs. Consequently, the entire overlapped zone lost resolution.

Resolution also diminished when the C_1 coil was changed from 50 to 100 cm (Fig. 5d). This path increase caused a greater overlap between the injected plugs, as expected; thus sequential injection seems more applicable to systems with short analytical paths. The main effect of the intermediate coils is to enlarge the original distances between the injected plugs, thus improving the resolution of the entire overlapped zone near the detector (Fig. 5e, f). Increase in the length of the intermediate coil greatly modifies the dispersions of the plugs established after it. This is the reason why broadening can be seen in the lower peaks of Fig. 5(e, f) and in the central peak of Fig. 5(e). It is clear from Fig. 5 that the effect is more pronounced when the C_2 coil is involved. Lowering the mean concentration related to the minimum value of the concentration/time profile is, then, easily achieved by increasing the C_2 rather than the C_3 coil length.

Sequential injection is particularly attractive if its implementation does not limit the sampling rate, but this was not possible here. Study of Fig. 5 shows that under all conditions investigated, the sampling rate depended on the wash times of all peaks, not only on that of the peak related to L_1. Fortunately, parallel tests with different concentrations at the L_1, L_2 and L_3 loops indicated that it is possible for the second and third peaks to appear and disappear during the wash period related to the L_1 peak.

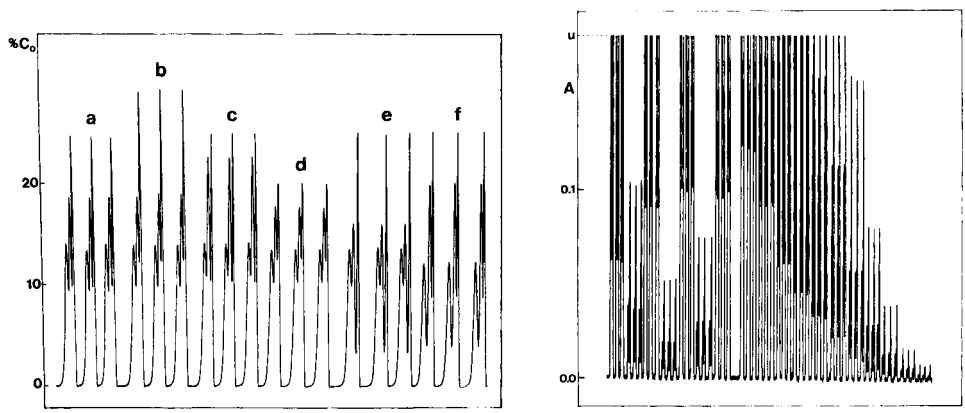

Fig. 5. Effects of coil and loop lengths. Triplicate measurements recorded with the model system of Fig. 2A: (a) initial conditions; (b) L_1 = 20 cm; (c) L_2 = 20 cm; (d) C_1 = 100 cm; (e) C_2 = 80 cm; (f) C_3 = 80 cm. For details, see text.

Fig. 6. Recorder output for the determination of manganese in rocks. From right to left: eleven standards (0.10, 0.20, 0.50, 1.00, 2.00, 4.00, 6.00, 8.00, 10.0, 15.0 and 20.0 mg Mn l^{-1}) followed by seven samples, all measurements being done in triplicate. The upper threshold (u) corresponds to the paper boundary in the recorder, above which there occurred a pronounced loss in the linearity of the response curve of the f.i.a./a.a.s. system.

Applications

The flow-injection system used for the determination of manganese in rocks is remarkably stable; even after an 8-h working period, there were only slight variations (<5%) in the coefficients of the calibration equations. The typical reproducibility of f.i.a./a.a.s. systems is maintained; for some results, calculations based on two calibration equations are feasible, so that precision can be improved. Figure 6 illustrates how a wide range of concentrations can be accommodated in useful form in one output. Similarities between results based on different calibration equations can give information on the accuracy of the procedure. The accuracy obtained was confirmed by the results for rocks (Table 1) which indicate good agreement with certified values. The suggested procedure has a sampling rate of about 100 h^{-1} at the 0.1% carry-over level. The possible concentration range may be expanded for methods with broader linear dynamic ranges and/or by using more injection loops.

For the determination of copper in ethanol, a procedure based on standard additions is easily done on a routine basis, without gradient exploitation. The proposed system is simple, manually operated and does not require a microprocessor. The sample (ca. 500 μl) is injected once, which suffices for the infinite-volume situation. The sampling rate can be improved by using different concentrations for the L_1 and L_2 plugs, as discussed above. Table 2 indicates the statistical data related to the analyses of some ethanol samples which were selected because of their high copper contents. The procedure is applicable to copper determinations for screening purposes. The copper content in most samples is not measurable by normal a.a.s.; this procedure can provide useful information about matrix effects and ethanol contents [7].

Partial support by CNPq (Conselho Nacional de Desenvolvimento Científico e Tecnológico), FINEP (Financiadora de Estudos e Projetos) and

TABLE 1

Manganese concentrations in standard reference rock materials, as determined with the f.i.a. system of Fig. 3A, (the results were based on the arithmetic mean of three repeated measurements of the same digest (Fig. 6))

Sample	Code	Manganese (mg kg^{-1})	
		Certified	Found
Pyroxenite	SARM[a]-5	1703	1588
Iron ore	SARM-11	110—115	111
Dunite	SARM-6	1704	1686
Syenite	SARM-2	80	72
Norite	SARM-4	1394	1467
Granite	SARM-1	160	164
Lujavrite[b]	SARM-3	5960	6110

[a]South African Reference Material. [b]Analyzed after a 1 + 3 manual dilution with the 1% (v/v) nitric acid solution.

TABLE 2

Statistical data related to the copper determination in ethanol with standard additions

Sample	r^2	Slope[a]	Cu found ($\mu g\ l^{-1}$)	Recovery[b] (%)
1	0.99948	114.7	267	105.0
2	0.99997	110.9	209	101.2
3	0.99999	103.5	139	100.4
4	0.99923	110.2	270	96.7
5	0.98280	128.7	463	103.3
6	0.99799	109.1	23	92.1
7	0.99896	110.9	282	101.5

[a]The slope related to an anhydrous standard solution is equal to 100.0. [b]After adding 500 μl of the 2.00 mg Cu l^{-1} standard solution to 5.00 ml of sample.

CNEN (Comissão Nacional de Energia Nuclear) is greatly appreciated. The authors express their gratitude to Dr. R. E. Bruns and Dr. H. Bergamin F° for critical comments.

REFERENCES

1 J. Růžička and E. H. Hansen, Flow Injection Analysis, Wiley, New York, 1981.
2 D. Betteridge and B. Fields, Anal. Chem., 50 (1978) 654.
3 J. Růžička and E. H. Hansen, Anal. Chem., 55 (1983) 1040A.
4 J. Růžička, E. H. Hansen and H. Mosbæk, Anal. Chim. Acta, 92 (1977) 235.
5 E. H. Hansen, J. Růžička, F. J. Krug and E. A. G. Zagatto, Anal. Chim. Acta, 148 (1983) 111.
6 J. F. Tyson and A. B. Idris, Analyst (London), 106 (1981) 1125.
7 M. C. U. Araújo, C. Pasquini, R. E. Bruns and E. A. G. Zagatto, Anal. Chim. Acta, (1985) in press.
8 M. F. Giné, B. F. Reis, E. A. G. Zagatto, F. J, Krug and A. O. Jacintho, Anal. Chim. Acta, 155 (1983) 131.
9 B. F. Reis, A. O. Jacintho, J. Mortatti, F. J. Krug, E. A. G. Zagatto, H. Bergamin F° and L. C. R. Pessenda, Anal. Chim. Acta, 123 (1981) 221.
10 A. O. Jacintho, E. A. G. Zagatto, H. Bergamin F°, F. J. Krug, B. F. Reis, R. E. Bruns and B. R. Kowalski, Anal. Chim. Acta, 130 (1981) 243.
11 E. A. N. Fernandes, M.Sc. Thesis, Piracicaba, Universidade de S. Paulo, 1981.
12 F. J. Langmyhr and P. E. Paus, Anal. Chim. Acta, 43 (1968) 397.
13 F. J. Krug, E. A. G. Zagatto, B. F. Reis, O. Bahia F°, A. O. Jacintho and S. S. Jørgensen, Anal. Chim. Acta, 145 (1983) 179.

Analytica Chimica Acta, 173 (1985) 299—303
Elsevier Science Publishers B.V., Amsterdam — Printed in The Netherlands

Short Communication

PRECONCENTRATION OF SOME PHOSPHORUS-CONTAINING ANIONS BY ADSORPTION ON HYDRATED IRON(III) OXIDE

T. HORI*

Department of Chemistry, College of Liberal Arts and Sciences, Kyoto University, Kyoto 606 (Japan)

M. MORIGUCHI, M. SASAKI, S. KITAGAWA and M. MUNAKATA

Department of Chemistry, Faculty of Science and Technology, Kinki University, Osaka 577 (Japan)

(Received 6th December 1984)

Summary. The adsorption behaviour of orthophosphate, triphosphate, pyrophosphate, monomethylphosphate, phosphite, α- and β-glycerophosphates, dimethylphosphate, and hypophosphite on hydrated iron(III) oxide precipitate is studied as a function of pH. Orthophosphate is adsorbed quantitatively at pH 4.0—8.0, triphosphate and pyrophosphate at pH 4—9.3 and the next three compounds at pH 4—6.8. The last two ions were only slightly adsorbed at any pH examined.

Hydrated iron(III) oxide is known to adsorb orthophosphate from solutions in the range pH 4—8. This adsorption has long been appreciated as a convenient method for preconcentration of orthophosphate and has been utilized variously in sensitive determinations of orthophosphate in water samples. The efficiency of adsorption is little affected by the presence of moderate amounts of neutral electrolytes such as sodium chloride and the preconcentration has also been successfully applied to sea waters [1]. During studies of the preconcentration of orthophosphate on magnesium hydroxide, Ishibashi and Tabushi [2] noted that glycerophosphate was partly adsorbed on the hydroxide along with orthophosphate. This indicated the feasibility of concentrating certain other phosphorus compounds by means of the hydrated precipitates.

In the work described here, the adsorption behaviour of triphosphate, pyrophosphate, monomethylphosphate, α- and β-glycerophosphates, phosphite, dimethylphosphate, and hypophosphite on hydrated iron(III) oxide was examined as a function of pH of the solutions. It was found that all these ions except the last two were effectively adsorbed and could later be released into a small volume of alkaline solution. Suitable conditions and procedures for the preconcentration method are presented below.

0003-2670/85/$03.30

Experimental

Reagents. Standard 0.001 M orthophosphate was prepared by dissolving potassium dihydrogenphosphate in pure water and stored in a polyethylene bottle. Similar 0.001 M solutions of triphosphate, pyrophosphate, phosphite, α-glycerophosphate, β-glycerophosphate, and hypophosphite were prepared by dissolving in water the following salts of $Na_5P_3O_{10}$ (1.4%), $Na_4P_2O_7 \cdot 10H_2O$ (0.5%), $Na_2HPO_3 \cdot 5H_2O$ (<0.1%), $HOCH_2CH(OH)CH_2OPO_3Na_2 \cdot 6H_2O$ (3.6%), $CH_2(OH)CH(OPO_3Na_2)CH_2OH \cdot xH_2O$ (<0.1%), and $Na_2H_2PO_2 \cdot H_2O$ (<0.1%). The values in brackets are the contents of orthophosphate impurity in the respective salts, which were determined by a flow-coulometric method [3] and, when necessary, were corrected for in the percent adsorption curves described later. Each phosphorus solution, after being converted to orthophosphate by using perchloric acid, was standardized spectrophotometrically against the orthophosphate standard.

The 0.001 M solutions of monomethylphosphate and dimethylphosphate were obtained by purifying their commercially available 1:1 mixture [4].

To adjust the pH for studies of adsorption equilibria, the following 0.5 M buffer solutions were prepared: acetic acid/sodium acetate (pH 4.0—5.9), 2-(*N*-morpholino)ethanesulphonic acid (MES)/sodium hydroxide [5] (pH 6.0—7.0), *N*-2-hydroxyethylpiperazine-*N'*-2-ethane sulphonic acid (HEPES)/sodium hydroxide [5] (pH 7.1—8.2), and ammonia/ammonium chloride (pH 8.3—10.2). Sodium hydroxide solutions were added to obtain pH 10.5—13.0.

The hydrated iron(III) oxide precipitate was freshly prepared for each sample by mixing in a centrifuge tube 2 ml of iron(III) chloride solution (1 mg Fe ml^{-1} in 1 M hydrochloric acid) with 2 ml of aqueous 2 M ammonia, followed by washing twice with pure water. The precipitate was then shaken vigorously with 2 ml of pure water and the resulted dispersion was used for the adsorption experiment.

General procedures for measuring per cent adsorption curves versus pH. In a 100-ml vial (40 mm i.d. × 120 mm) with a plastic screw-cap, 2 ml of 0.5 M buffer solution and 60 μl of a 0.001 M solution of the phosphorus compound to be tested (except for triphosphate and pyrophosphate), were diluted to ca. 80 ml with water. For triphosphate and pyrophosphate, 20 μl and 30 μl of the respective 0.001 M solutions were diluted similarly. With magnetic stirring, the pH of the solution was adjusted to the required value and then the hydrated iron(III) oxide dispersion was added, followed by dilution to 100 ml with water. To attain equilibrium, the solution was stirred continuously for a few more minutes and then left still for 30 min; the screw-cap prevented entry of atmospheric carbon dioxide which may disturb the pH. After pH measurement at equilibrium, the precipitate was separated by filtration on a Nuclepore membrane filter (0.4-μm pore size) and then the phosphorus compounds adsorbed were determined spectrophotometrically by a molybdenum blue method [1]. The percent adsorption for the ion was calculated from the adsorbed and initial amounts and plotted against the pH of the solution.

Results and discussion

Amounts of hydrated iron(III) oxide, concentrations of buffer, and standing times needed for adsorption equilibrium. The percent adsorption curve for orthophosphate is shown by curve 1 in Fig. 1, which was measured by using the above-recommended conditions (6×10^{-7} M) orthophosphate with 0.01 M buffer in the final solution. The curve agrees well with that reported by Ishibashi and Tabushi [1], quantitative adsorption occurring from pH 4 to pH 8. The effects of the amounts of hydrated iron(III) oxide, concentrations of buffer reagents, and standing times on the adsorption equilibrium were then examined.

At both pH 7.0 and pH 8.0, the amount of hydrated iron(III) oxide was varied from 0.2 to 5.0 mg (weight as iron), the other conditions being kept unchanged. Quantitative adsorption was achieved with more than 1 mg of iron; for safety, 2 mg of iron was used commonly in all further experiments unless specified otherwise.

Buffer concentrations of MES and HEPES were changed at the respective pH values of 7.0 and 8.0. Although these buffers are so-called "good buffers" [5] and are expected to be mostly inert to iron(III) ions, a slight decrease in the percent adsorption was observed at concentrations higher than 0.2 M. The effects, however, were not very serious and could practically be eliminated by lowering the concentrations. Here, in fact, the 0.01 M concentration was accepted throughout.

Standing times needed for adsorption equilibrium were examined at a constant pH of 7.0; it was shown that equilibrium was attained within 10 min and was little affected by further standing. As described under Experimental, subsequently, every solution was left for 30 min before filtration.

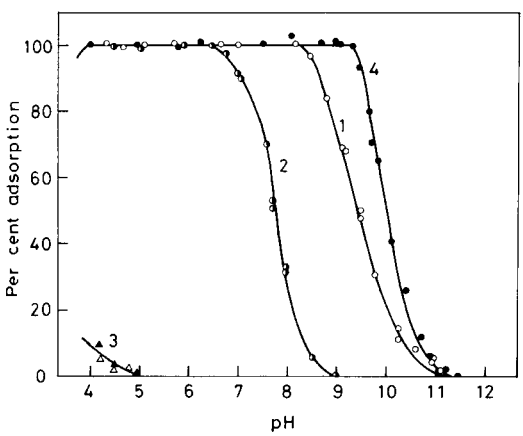

Fig. 1. Adsorption curves onto hydrated iron(III) oxide: (○) orthophosphate; (◑) monomethylphosphate; (▲) dimethylphosphate; (△) dimethylphosphate or hypophosphite; (●) pyrophosphate or triphosphate. The adsorption curves for α- and β-glycerophosphate and phosphite are represented well by curve 2. In each case, 2 mg of iron was used with 100 ml of sample solution.

Adsorption of monomethylphosphate, α- and β-glycerophosphates, and phosphite. According to the formal conditions chosen above, the percentage adsorption of monomethylphosphate was measured against pH; the result is shown by curve 2 in Fig. 1. As can be seen, this ion is adsorbed quantitatively in a range pH 4—6.8, the upper limit being shifted towards the acidic region by 1.5 pH compared to orthophosphate (curve 1). This would be useful for the differentiation of monomethylphosphate from orthophosphate.

Quite similar adsorption curves were attained for both α- and β-glycerophosphates. No practical differences between the two glycerophosphates and monomethylphosphate were observed; curve 2 in Fig. 1 represents well the adsorption behaviour of all three phosphorus compounds. This similarity seems to accord with the structures around the central phosphorus atoms of the ions: a couple of ionizable P-O corners are commonly involved in each tetrahedral structure. If the phosphorus-containing ions coordinate the iron(III) ions mainly through these P-O corners, as has been suggested [6], it would be expected that their adsorption behaviour would depend far more on the arrangement of the P-O corners than on the substituting group in each ion. Moreover, the monosubstituted phosphates have one less P-O corner than orthophosphate because of the substituent and, therefore, their tendency to coordinate with iron(III) would be weakened (cf. curves 1 and 2, Fig. 1). This view remains unproven, but such structural considerations could provide a primary indication as to whether or not a given phosphorus-containing ion could adsorb on hydrated iron(III) oxide.

The adsorption of phosphite also agreed well with that of the monosubstituted phosphates; again, the adsorption curve was essentially the same as curve 2 in Fig. 1.

Adsorption of dimethylphosphate and hypophosphite. These ions were found to be little adsorbed at any pH in the range examined here (curve 3). This precludes their concentration from water samples, but could be useful for their differentiation from the phosphorus-containing ions mentioned above, because they will remain entirely in the mother liquor above pH 5.

Adsorption of triphosphate and pyrophosphate. The adsorption curves for these condensed phosphates are represented by curve 4 (Fig. 1), which extends to more alkaline regions compared with the curve for orthophosphate (curve 1). Thus, these ions are effectively concentrated by the use of hydrated iron(III) oxide, though they could not be differentiated from each other or from orthophosphate.

Desorption of phosphorus-containing ions from hydrated iron(III) oxide. These ions, once adsorbed, could be desorbed readily into a small volume of alkaline solution either by vigorous shaking for 2 min or by applying ultrasonic agitation for 1 min, the hydrated oxide being left as a precipitate. As would be expected from curve 2, for instance, monosubstituted phosphates and phosphite can be collected (by adsorption) at pH 6 and concentrated (by desorption) into a 2-ml portion of 0.01 M ammonia buffer at pH 10. For the desorption of the condensed phosphates and orthophosphate, use of

0.01 M sodium hydroxide is recommended. The recoveries of the phosphorus-containing ions were found to be better than 90% in these procedures.

One of the authors (T. H.) thanks Dr. T. Fujinaga, Nara University of Education, for his continuous encouragement and helpful suggestions on this work.

REFERENCES

1 M. Ishibashi and M. Tabushi, Jpn. Analyst, 8 (1959) 588.
2 M. Ishibashi and M. Tabushi, Jpn. Analyst, 6 (1957) 7.
3 T. Hori and T. Fujinaga, Talanta, 30 (1983) 925.
4 T. Hori, J. Inorg. Nucl. Chem., 39 (1977) 2173.
5 N. E. Good, G. D. Winget, W. Winter, T. N. Connoly, S. Izawa and R. M. M. Singh, Biochemistry, 5 (1966) 467.
6 R. Takeshita, I. Yoshida and K. Ueno, Bull. Chem. Soc. Jpn., 52 (1979) 2577.

Analytica Chimica Acta, 173 (1985) 305—309
Elsevier Science Publishers B.V., Amsterdam — Printed in The Netherlands

Short Communication

IMINODIACETIC ACID/ETHYLCELLULOSE AS A CHELATING ION EXCHANGER
Part 2. Determination of Trace Metals by Inductively-coupled Plasma Atomic Emission Spectrometry

ZS. HORVÁTH[a], RAMON M. BARNES* and P. S. MURTY[b]

Department of Chemistry, GRC Towers, University of Massachusetts, Amherst, MA 01003-0035 (U.S.A.)

(Received 5th December 1984)

Summary. A chelate-forming cellulose, iminodiacetic acid/ethylcellulose (IDAEC), is applied to the collection of metals from ammonium citrate and acetate solutions. A method is devised for the i.c.p./a.e.s. determination of metal contaminants in magnesium by separation and preconcentration of the metals with IDAEC.

The collection and separation of trace metals by iminodiacetic acid/ethylcellulose (IDAEC) from water, solvent samples, and soil extracts was described earlier [1]. This exchanger proved to be a good collector of trace metals from matrices containing alkaline and alkaline earth metals. The metal uptake is pH-dependent, but citrate or acetate buffer provides adequate pH adjustment.

In the preparation of nuclear-grade uranium for the reduction of uranium tetrafluoride, calcium or magnesium metal is needed [2—4]. These metals should be very pure in order to prevent trace element contamination of the uranium metal during the reduction process. Jackwerth et al. [5] collected trace metals from pure magnesium and magnesium salts with activated carbon in the presence of dithizone. Of the nine elements investigated by atomic absorption spectrometry, only silver and cadmium could be enriched by more than 95%. The IDAEC does not form a chelate with magnesium while it forms chelates with many elements, mostly heavy metals [6].

Chelate-forming resins like chelate-forming celluloses can be applied to trace metal determinations and for reagent purification. Recently, Mahanti and Barnes [7] purified reagent-grade calcium carbonate solution with a poly(dithiocarbamate) resin. Barnes et al. [8] also applied a poly(acrylamidoxime) resin in the preconcentration of trace metals in high-purity

[a]Permanent Address: L. Eötvös University, Institute of Inorganic and Analytical Chemistry, P.O. Box 123, H-1443 Budapest, Hungary.
[b]Present Address: Spectroscopy Division, Babha Atomic Research Center, Trombay, Bombay 400085, India.

0003-2670/85/$03.30

aluminum. In both examples, the sample was shaken with the resin for 10—24 h. Although either of these resins can be applied for the determination of trace metals in magnesium nitrate, the rate of chelation on chelate-forming celluloses is higher. Therefore, in this paper, separation and preconcentration of metals by IDAEC from ammonium citrate and acetate and from magnesium nitrate solution is evaluated as a precursor to the determination of the trace metals in high-purity magnesium metal by inductively-coupled plasma atomic emission spectrometry (i.c.p./a.e.s.).

Experimental

Instrumentation and chemicals. The inductively-coupled plasma instrumentation and operating conditions are given in Table 1. The elements, their wavelengths, and figures of merit are summarized in Table 2. Some samples were prepared with a cool plasma asher (Anton Paar, Graz, Austria) [9]. Polyethylene chromatograph columns (0.7 mm i.d., 350 mm long; BB9194, Bolab, Lake Havasu City, AZ) with cotton wool in the end of the stem were used for the collection of metals.

Stock solutions were prepared from high-purity metals or A.C.S. reagent-grade chemicals. Distilled, deionized water and subboiling distilled nitric acid were used throughout. The 10% (w/v) magnesium nitrate solution and 2 M ammonium citrate and acetate solutions were pre-purified on an IDAEC column. The IDAEC capacity as determined by potentiometric titration was 1.3 meq g^{-1} [6].

Metal ion collection from citrate and acetate solution. Fifteen metals (10 μg of each) were dissolved in 0.1 M ammonium citrate (pH 4.9) or 0.1 M ammonium acetate (pH 5.8). The solution was passed through 0.2 g of ammonium-form IDAEC in a polyethylene column at a flow rate of 1—1.5 ml min^{-1}. The metals were eluted from each column separately with 5 ml of

TABLE 1

Instrumentation and operating conditions for i.c.p./a.e.s.

R.f. generator	Plasma Therm, Model HFS-5000D, 40.68 MHz
Load coil	3-turn copper tubing, 18 in. o.d.
Operating power	0.65 kW
Torch and nebulizer	Quartz torch with 1.5-mm i.d. orifice. Babington nebulizer with Scott-type double-barrel spray chamber (volume 200 ml). Injection method (100-μl sample)
Argon flow rates	Outer 16.0 l min^{-1}, aerosol 0.6 l min^{-1}
Spectrometer and detection	1-m Czerny-Turner monochromator (Minutemen Model 310-SMP), grating 1200 lines/mm, RCA 4832 photomultiplier tube (—1100 V), picoammeter (Keithley 414S), computer (PDP 11/23). Slit width 50 μm. Image 1:1 magnification with 2-in. diameter quartz lens, 200-mm focal length (Oriel No. A-11-661-37)
Observation zone	15 mm above induction coil and 5 mm high

TABLE 2

Wavelengths for i.c.p./a.e.s. and figures of merit

Element	Wavelength (nm)	Detection limit[a,b] (ng ml^{-1})	BEC[c] (μg ml^{-1})	Element	Wavelength (nm)	Detection limit[a,b] (ng ml^{-1})	BEC[c] (μg ml^{-1})
Al	396.1	30	1.1	La	379.5	14	0.36
Bi	223.0	34	1.8	Mn	257.6	4	0.13
Cd	226.5	2	0.10	Ni	221.6	15	0.44
Co	238.9	10	0.35	Pb	220.3	100	4.0
Cr	267.7	25	0.48	Ti	334.9	3	0.22
Cu	324.7	6	0.26	V	292.4	12	0.40
Fe	238.2	20	0.46	Zn	213.8	10	0.42
Ga	294.3	12	0.35				

[a]Calculated from three times the standard deviation of the background. [b]Injection method, 100-μl sample introduction. [c]The background equivalent concentration (BEC) is the analyte concentration equivalent to the background level at the analyte wavelength.

1.6 M nitric acid, and the solution was diluted in a 10-ml volumetric flask with distilled water.

Ashing of IDAEC on the cool plasma asher. The decomposition parameters were established for the ashing of 0.2 g of IDAEC. After collecting the metals from acetate solution, the IDAEC was dried at 70° C and transferred to the ashing chamber. The ashing without stirring was achieved in 6 h at a high-frequency power of 48 W, 4 mbar vacuum, and 3 l h^{-1} oxygen flow. The ash was dissolved in 0.5 ml of concentrated nitric acid by using a reflux heater (RFH-5). The final solution was made up to 10 ml.

Metal ions collected from magnesium nitrate. The purified magnesium nitrate was spiked with 15 test metals. The concentrations of magnesium and trace elements were chosen so that 1 g of magnesium and 10 μg of trace elements were present in 90 ml of solution. The solution contained 3.5 ml of 2 M ammonium acetate, and the solution pH was 5.80. A blank was also made. Two portions of 0.2 g of IDAEC were used in two polyethylene columns. The columns were placed one above the other. The test solution was poured on the upper column and passed through both columns. The metals were eluted from each column separately with 5 ml of 1.6 M nitric acid. The eluates were made up to 10 ml.

Results and discussion

The metal uptakes of IDAEC from citrate or acetate solutions with a ratio of citrate or acetate in iminodiacetic acid (IDA) group of 10^3:1 are listed in Table 3. In spite of the high concentration of citrate in the solution, the recovery of five elements (Cd, Co, Cu, Pb, Zn) was quantitative, because IDAEC forms highly stable chelates. Thus, IDAEC can be used for the separation of these five metals in a citrate solution. In contrast, the recovery

TABLE 3

Recovery of metals by IDAEC from citrate or acetate solutions[a]

Element	Citrate (pH 4.90)		Acetate (pH 5.80)		Element	Citrate (pH 4.90)		Acetate (pH 5.80)	
	Recovery (%)	s^b	Recovery (%)	s^b		Recovery (%)	s^b	Recovery (%)	s^b
Al	<		80	7	La	<		97	2
Bi			103	3	Mn	<		97	1
Cd	99	4	98	6	Ni	50	2	96	5
Co	93	7	99	5	Pb	100	2	101	6(4)
Cr(III)	<		52 + 47 = 99[c]	2	Ti	<		94	3
Cu	97	2	98	3	V(V)	37	2	85	7
Fe(III)	20	1(3)	85	4	Zn	99	6	99	3
Ga	<		95	0.5(4)					

[a]The ratio of citrate or acetate to IDA group was 10^3:1, and to the metals 10^4:1. The < sign means less than or equal to five times the limit of detection in Table 2. [b]Standard deviation of five determinations; if not five, the number of the determinations is in brackets. [c]52% Cr could be eluted from the IDAEC column with nitric acid; after ashing of the IDAEC, 47% more could be measured.

of 11 of the 15 metals investigated was >95% in acetate solution. Acetate should be used as a buffer if preconcentration of many metals from a solution is needed.

After elution of the metals collected from acetate solution, the IDAEC column was dried and ashed in an oxygen plasma with a cool plasma asher [9]. The aim of this test was to establish if any of the fifteen metals remained on the IDAEC after nitric acid elution. After dissolution of the IDAEC ash in nitric acid, only chromium could be measured in the solution (Table 3). The quantity of chromium eluted plus the amount found in the ash gave 99% uptake of chromium.

The IDAEC was applied to the separation of trace metals from magnesium nitrate solution from pH 5.80 acetate solution when the ratio of magnesium to metals was ca. 10^4:1. Two IDAEC columns were used, and the magnesium nitrate solution was spiked with Bi, Cd, Co, Cu, Fe(III), Mn(II), Ni, Ti and V(V). The metals were determined after separate elution from the two columns. Only bismuth was found in the eluate of the second column, which indicates that the capacity of 0.2 g of IDAEC was sufficient to retain all other elements on the first column. The recovery of the elements investigated is given in Table 4. Thus IDAEC preconcentration with i.c.p./a.e.s. can be used for the determination of the trace contaminants in magnesium nitrate. The lowest determinable concentration (LQD) values for each of these elements for 1 g of magnesium are also given in Table 4. This approach can be extended to the determination of the trace contaminants in pure magnesium. Operational convenience and sample flow rate through IDAEC columns provides an overall faster procedure for collection of appropriate trace metals from salt solutions than the poly(acrylamidoxime) [8] or poly(dithiocarbamate) [7] resins.

TABLE 4

Recovery of the metals by IDAEC from magnesium nitrate solution

Element	Recovery (%)	LQD[a] ($\mu g\ g^{-1}$)	Element	Recovery (%)	LQD[a] ($\mu g\ g^{-1}$)
Bi	100	1.7	Mn	100	0.2
Cu	98	0.3	Ni	98	0.75
Co	100	0.5	Ti	95	0.15
Cd	97	0.1	V(V)	84	0.6
Fe(III)	92	1.0			

[a]LQD is the lowest concentration that can be determined, calculated from five times the limit of detection for 1 g of magnesium in a final volume of 10 ml after IDAEC preconcentration.

This research was supported by Department of Energy Contract DE-AC02-77EV-0432 and the ICP Information Newsletter.

REFERENCES

1 Zs. Horváth, A. Lásztity, O. Szakács and G. Bozsai, Anal. Chim. Acta, 173 (1985) 273.
2 E. W. Mautz, G. G. Briggs, C. D. Bonfer and J. G. Gindel Sperger, Report No. NLCO-965, (1965) 5 pp.
3 A. Diaz Beltran, M. Diaz De Las Rivas and A. Fornes Sanchez, Energ. Nucl. (Madrid), 16(77) (1972) 295.
4 A. Perez, Electricité, 173 (1981) 31.
5 E. Jackwerth, J. Lohmar and G. Wittler, Fresenius Z. Anal. Chem., 226 (1973) 1.
6 Zs. Remport-Horváth and Gy. Nagydiósi, Inorg. Nucl. Chem., 37 (1975) 767.
7 H. S. Mahanti and R. M. Barnes, Appl. Spectrosc., 37 (1983) 401.
8 R. M. Barnes, L. Fernando, S. J. Lu and H. S. Mahanati, Appl. Spectrosc., 37 (1983) 389.
9 S. E. Raptis, G. Knapp and A. P. Schalk, Fresenius Z. Anal. Chem., 316 (1983) 482.

Analytica Chimica Acta, 173 (1985) 311—314
Elsevier Science Publishers B.V., Amsterdam — Printed in The Netherlands

Short Communication

CONTINUOUS-FLOW MOLECULAR EMISSION CAVITY ANALYSIS FOR SULPHIDE

N. GREKAS and A. C. CALOKERINOS*

Laboratory of Analytical Chemistry, Department of Chemistry, University of Athens, 106 80 Athens (Greece)

(Received 18th January 1985)

Summary. Sulphide (1—10 μg ml^{-1}) is determined by mixing the sample with an excess of orthophosphoric acid in a segmented continuous-flow system. The hydrogen sulphide evolved is swept into the cavity for generation of S_2 emission. The analysis is completely automated, requires no sample pretreatment and samples can be analyzed at 24 h^{-1}.

Sulphide can be determined by conventional molecular emission cavity analysis (m.e.c.a.) in aqueous solution [1] or in binary and some ternary mixtures [2]. Sulphide has also been determined in mixtures with sulphate, thiocyanate and thiosulphate after sequential selective removal of ions and oxidation of the remainder by hydrogen peroxide to sulphate [3]. The m.e.c.a. technique also allows the determination of sulphide in the presence of other sulphur compounds in solids [4, 5]. Alternatively, sulphide can be determined in a vaporization system in which the sample solution is acidified and the hydrogen sulphide evolved is continuously purged by nitrogen to the m.e.c.a. cavity for generation of S_2 emission [6]. Furthermore, the anion can be determined by flow injection introduction of the solution into the cavity [7].

Recently, a continuous-flow molecular emission cavity analyzer was described [8]. The sample solution is mixed with aqueous orthophosphoric acid solution and is carried by a segmented continuous-flow stream through a heated reaction coil into a debubbler where the gas evolved is swept by nitrogen into the cavity. This system was successfully used for the determination of sulphite in various samples and of sulphur dioxide in atmospheric air after fixation as disulphitomercurate(II) [8]. This communication describes the advantages of the system for determining 1—10 μg ml^{-1} sulphide.

Experimental

Apparatus. The photometer, m.e.c.a. cavity and continuous-flow system were as described previously [8].

Reagents. All reagents were of analytical grade, and deionized-distilled water was used throughout. A sulphide stock solution (500 μg ml^{-1}) was

0003-2670/85/$03.30

prepared by dissolving 1.87 g of $Na_2S \cdot 9H_2O$ (Ferak Berlin, p.a.) in 500 ml of 0.1 M sodium hydroxide/0.01 M EDTA. The exact sulphide concentration was established iodimetrically. More dilute solutions were prepared in 0.02 M sodium hydroxide/2 × 10^{-3} M EDTA by the fewest dilution steps possible. All sulphide solutions were prepared daily.

Procedure. All experimental parameters were used as optimized for sulphite [8]. The cavity was conditioned by allowing 0.5—1.0 ml of stock sulphide solution to enter into the continuous flow system and generate intense S_2 emission within the cavity. After re-establishment of the baseline, the determination was done as for sulphite [8].

Results and discussion

Analytical parameters. Figure 1 shows a typical recording for a series of sulphide standards by the proposed procedure. The calibration graph, emission intensity (I, mV) vs. μg ml^{-1} sulphide (C), was sigmoidal [9] and the log I vs. log C calibration graph was linear over the range 1—10 μg ml^{-1} sulphide ($\log I = -0.420 + 1.72 \log C$, $r = 0.9996$). The relative standard deviation for the slope of the log—log graph for six working days was 2.2%. The limit of detection (signal/noise = 2) was 0.5 μg ml^{-1} sulphide and the relative standard deviations for 2 and 4 μg ml^{-1} sulphide were 2% and 0.6% ($n = 8$), respectively. When aqueous solutions of sulphide (1—10 μg ml^{-1}) were processed, the average error was ±1.5%. Under the same experimental conditions, determination of sulphite ($\log I = -1.10 + 1.31 \log C$) [8] was less sensitive than that of sulphide.

Interferences. Interferences from anions were investigated by determining 10 μg ml^{-1} sulphide in the presence of equal and fivefold (by wt.) amounts of other anion. The responses were compared with those obtained from an uncontaminated sulphide solution. No effect was observed from thiosulphate,

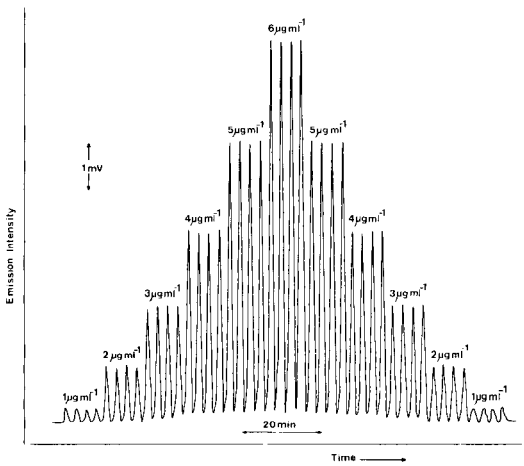

Fig. 1. Typical recording for a series of sulphide standards.

thiocyanate, cyanide, iodide, bromide or carbonate. Nitrite seriously decreased the intensity (Table 1). Reduction of nitrite to nitrogen by sulphamic acid was investigated for eliminating the interference. Aqueous solutions of sulphamic acid introduced into the analyzer did not produce any molecular emission within the cavity and left the emission intensity from pure sulphide solutions unaffected. A 0.02% (w/v) solution of sulphamic acid completely eliminated the interference from equal concentrations of nitrite on 1.0 and 5.0 μg ml^{-1} sulphide. The effect of an equal concentration of nitrite on 10 μg ml^{-1} of sulphide was eliminated by 0.04% (w/v) sulphamic acid. The interference of a fivefold concentration of nitrite on sulphide was only partially eliminated by sulphamic acid. These results are shown in Table 1.

Sulphite interferes severely with the determination of sulphide. The emission intensities from 5.0 μg ml^{-1} sulphide and 10 μg ml^{-1} sulphite were 6.0 mV and 1.6 mV, respectively, while the emission intensity from the mixture was 9.2 mV, as would be expected from the sigmoidal nature of the calibration graph. Various attempts were made to eliminate the interference of sulphite on the measurement of sulphide. Tannic acid completely removes the emission of sulphite [8] but 2×10^{-3} and 5×10^{-3}% (w/v) tannic acid also decreased the intensity from 8 μg ml^{-1} sulphide by 43% and 86%, respectively. Likewise, 0.01% and 0.02% (w/v) glyoxal decreased the intensity from 8 μg ml^{-1} sulphite by 80% and 100%, respectively, because of the formation of the addition compound. The same concentrations of glyoxal had no effect on the intensity from aqueous sulphide solutions. Nevertheless, when 0.02% (w/v) glyoxal was added to a mixture of sulphide and sulphite, the emission intensity was unaffected. This is probably due to disproportionation of glyoxal in the alkaline solution required for stabilization of sulphide.

TABLE 1

Effect of nitrite on the emission intensity from sulphide, and elimination of the interference by addition of sulphamic acid

Concentration (μg ml^{-1})		Emission intensity[a]		
Sulphide	Nitrite	Sulphamic added acid (%) (w/v)		
		0.00	0.02	0.04
10.0	0	100		
10.0	10	35.3	88.2	100
10.0	50	2.9	73.5	88.2[b]
5.0	0	100		
5.0	5.0	35.0	100	
5.0	25	0	80.0[b]	
1.0	0	100		
1.0	1.0	66.7	100	
1.0	5.0		80.0[b]	

[a]Intensities from pure sulphide solutions arbitrarily taken as 100. [b]No further decrease of interference was observed at higher sulphamic acid concentrations.

TABLE 2

Alkaline degradation of organic sulphur compounds to sulphide in 1 M sodium hydroxide

Compound	Conc. (mg ml^{-1})	Sulphide sulphur ($\mu g\ ml^{-1}$)		
		Theoretical	Found after hydrolysis[a] at:	
			30° C	100° C
Cysteamine · HCl	1.86	524.5	0(75)	1.51(75)
N-Acetyl-L-cysteine	2.55	500.4	0(60)	0.96(60)
Thiodiacetic acid	0.64	137.0	4.32(45)	5.72(60)
			4.91(95)	6.21(100)
Thioglycollic acid	13.3	4620	3.58(60)	14.88(60)
Cephalexin	0.10	9.21	0(30)	5.99(30)
	0.25	23.02	0(30)	14.93(30)

[a]The times of hydrolysis (min) are given in parentheses.

Alkaline degradation of organic sulphur compounds. The simplicity and sensitivity of the method are useful for the determination of sulphide produced by alkaline degradation of various organic sulphur-containing compounds in 1 M sodium hydroxide (Table 2). Cephalexin was found to degrade completely after 30 min at 100° C and the sulphide yields for 0.10 and 0.25 mg ml^{-1} were 65.0% and 64.9%, respectively, which are in good agreement with results obtained by Fogg et al. [10, 11]. The method was also used to determine the relatively small amounts of sulphide produced by decomposition of the other compounds.

REFERENCES

1 R. Belcher, S. L. Bogdanski, D. J. Knowles and A. Townshend, Anal. Chim. Acta, 77 (1975) 53.
2 M. Q. Al-Abachi, R. Belcher, S. L. Bogdanski and A. Townshend, Anal. Chim. Acta, 86 (1976) 139.
3 T. S. Al-Ghabsha, Ph.D. Thesis, Birmingham University, 1979; A. C. Calokerinos and A. Townshend, Prog. Anal. At. Spectrosc., 5 (1982) 63.
4 S. A. Schubert, J. W. Clayton and Q. Fernando, Anal. Chem., 52 (1980) 963.
5 J. H. Tzeng and Q. Fernando, Anal. Chem., 54 (1982) 971.
6 E. Henden, Ph.D. Thesis, Birmingham University, 1976; E. Henden, N. Pourreza and A. Townshend, Prog. Anal. At. Spectrosc., 2 (1979) 355.
7 J. L. Burguera and M. Burguera, Anal. Chim. Acta, 157 (1984) 177.
8 N. Grekas and A. C. Calokerinos, Analyst (London), 110 (1985) 335.
9 A. C. Calokerinos and T. P. Hadjiioannou, Anal. Chim. Acta, 148 (1983) 277.
10 M. A. Abdalla, A. G. Fogg and C. Burgess, Analyst (London), 107 (1982) 213.
11 A. G. Fogg, M. A. Abdalla and H. P. Henriques, Analyst (London), 107 (1982) 449.

Analytica Chimica Acta, 173 (1985) 315—319
Elsevier Science Publishers B.V., Amsterdam — Printed in The Netherlands

Short Communication

X-RAY PHOTOELECTRON SPECTROSCOPIC STUDY OF THE MECHANISM OF PALLADIUM MATRIX MODIFICATION IN THE ELECTROTHERMAL ATOMIC ABSORPTION SPECTROMETRIC DETERMINATION OF LEAD AND BISMUTH

XIAO-QUAN SHAN*
Institute of Environmental Chemistry, Academia Sinica, P.O. Box 934, Beijing (China)
DIAN-XUN WANG
Institue of Chemistry, Academia Sinica, P.O. Box 2709, Beijing (China)
(Received 30th May 1984)

Summary. The mechanism of palladium matrix modification is studied for the determination of lead and bismuth by graphite-furnace atomic absorption spectromety. The binding energies of the charring products for lead and bismuth in the presence or absence of palladium obtained at the initial stage of atomization were measured. The binding energies indicated the formation of Pb—Pd and Bi—Pd bonds, thus explaining the increase in appearance temperatures of lead and bismuth in the presence of palladium.

The introduction of matrix modification by Ediger et al. [1] was a major advance in decreasing chemical interferences in graphite-furnace atomic absorption spectrometry (a.a.s.). Chemical reagents are added to sample aliquots to alter the charring and atomization process of sample components in one of two basic ways: first, compounds such as ammonium nitrate can form more volatile species with matrix constituents to decrease or eliminate matrix interferences; second, specific modifiers allow the use of higher charring temperature by decreasing analyte volatility through the formation of more thermally stable analyte species. In addition, chemically active gases such as oxygen can be introduced into the purge gas to delay the atomization of the analyte, because of chemisorbed oxygen on the active carbon sites of the graphite furnace. Palladium matrix modification has been used for the determination of lead [2], bismuth [3], arsenic [4], selenium [5] and other elements in a variety of environmental samples. However, there is no report dealing in detail with the mechanism of matrix modification. The aim of this communication is to present the results of a preliminary study on the mechanism of palladium matrix modification for the determination of lead and bismuth by graphite-furnace a.a.s., by using x-ray photoelectron spectroscopy (x.p.s.).

0003-2670/85/$03.30

Experimental

Apparatus. A Perkin-Elmer model 4000 atomic absorption spectrometer equipped with a model HGA-400 graphite furnace and a home-made photoconductive device was used to measure the appearance temperature and to prepare the charring products of lead or bismuth in the absence or presence of palladium for the x.p.s. study. Signals for lead and bismuth absorbance obtained at 217.0 and 223.1 nm, respectively, were recorded on a Perkin-Elmer model 056 double-pen chart recorder. Hollow-cathode lamps of lead and bismuth were operated at 20 and 15 mA, respectively. The spectral bandwidth was set at 0.7 nm. A deuterium background corrector was used. A 20- or 50-μl Eppendorf pipette fitted with disposable polypropylene tips was used to introduce sample solution into the furnace.

A Kratos AEI-ES model 300 x-ray photoelectron spectrometer with a magnesium (E_x = 1253.6 eV) anode was used to measure the x.p. spectra. The power was 6 X 15 W; the widths of the entrance and exit slits were both set at 0.07 inch.

Reagents. Stock solutions of lead and bismuth (2000 μg ml^{-1}) were prepared by dissolving 0.6624 g of lead nitrate (analytical-reagent grade, Beijing Chemical Co., China) or 0.2000 g of bismuth metal (99.999% purity, Koch-Light Laboratories, England) in an adequate amount of nitric acid and diluting to 100 ml with deionized water. A palladium solution (30 mg ml^{-1}) was prepared from palladium chloride (analytical-reagent grade). All solutions for determining appearance temperatures were prepared by serial dilution with deionized water from the stock solutions.

Measurement of appearance temperatures. A laboratory-made photoconductive device and the double-pen chart recorder were used to measure the absorbance/time profiles of lead and bismuth and the temperature/time profile of the graphite furnace. The temperature scale was established by using the temperature program of the HGA-400 power supply. The heating rate setting of the atomizer was 0.1 K ms^{-1}. Samples containing 10 ng of lead, 10 ng of lead plus 2 μg of palladium, 50 ng of bismuth, or 50 ng of bismuth plus 2 μg of palladium were introduced into the atomizer, to give a maximum absorbance of 1. The temperature at which a small absorbance (0.01) appeared was defined as the appearance temperature, T_{app}.

Preparation of charring product sample. A 10-ml portion of 30 mg ml^{-1} palladium solution, 1.5 ml of 2 mg ml^{-1} lead or bismuth solution, or 12 ml of 25 mg ml^{-1} palladium and 0.33 mg ml^{-1} lead solution, or 12 ml of 25 mg ml^{-1} palladium and 0.33 mg ml^{-1} bismuth solution, were separately injected into the graphite tube with a 50-μl pipette. After drying, the residue was charred for 30 s at a temperature which was 20°C higher than the appearance temperature for lead or bismuth in the absence or presence of palladium. The atomizer was cooled to room temperature before the next sample. The injection and charring procedure was repeated many times in the same tube until each solution above had been completely introduced. The graphite tube was then removed from its holder. The interior surface graphite of the

tube where the analyte had been deposited and charred was scraped off carefully with a sharp quartz rod and collected for x.p.s.

X-ray photoelectron spectroscopy measurements. The narrow scan spectra of the components in the samples, prepared as above, were measured at 3×10^{-7} torr in the fixed retarding ratio mode. The C_{1s} signal of carbon contamination fixed at 285.0 eV was taken as a reference for the binding energy.

Results and discussion

Conditions for preparation of charring products. It has been observed that higher charring temperatures for lead, bismuth and other elements could be tolerated when microgram-amounts of palladium were added to the analyte in the graphite furnace [2—5]. This was usually ascribed to the formation of more thermally stable analyte species, but without any experimental evidence. In order to understand the mechanism of palladium matrix modification, a study of analyte species present at the initial stage of the atomization process is of importance. Therefore the appearance temperatures, T_{app}, for lead and bismuth in the absence and presence of palladium were determined. The temperature/time and absorbance/time profiles are shown schematically in Figs. 1 and 2. The average values of three replicate measurements of T_{app} are summarized in Table 1.

The temperature 20°C higher than T_{app} was arbitrarily defined as the temperature for preparation of the charring product sample, T_{cps}, the values of which are also listed in Table 1. In order to meet the sensitivity requirement of x.p.s., a large amount of lead, bismuth or palladium was introduced into the tube atomizer, as described in the experimental section. The ratio of

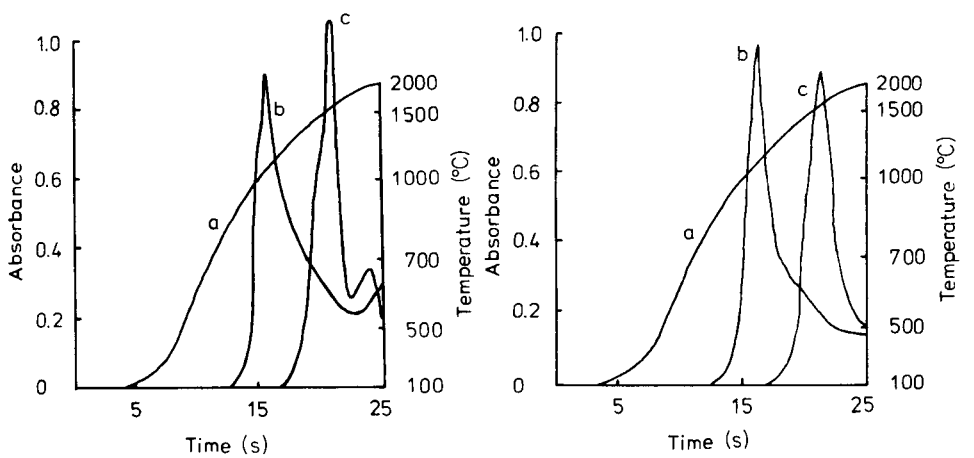

Fig. 1. (a) Temperature/time profile of graphite tube surface heated at 0.1 K ms^{-1}. (b, c) Absorbance/time profiles: (b) 10 ng Pb; (c) 10 ng Pb + 2 μg Pd.

Fig. 2. (a) As Fig. 1. (b, c) Absorbance/time profiles: (b) 50 ng Bi; (c) 50 ng Bi + 2 μg Pd.

TABLE 1

Conditions for preparation of charring products

Metal sample[a]	Lead		Bismuth	
	T_{app}[b]	T_{cps}[b]	T_{app}	T_{cps}
3 mg Pb or Bi	830	850	830	850
3 mg Pb or Bi + 300 mg Pd	1180	1200	1160	1180

[a]300 mg of palladium alone was also charred at 1200°C. [b]T_{app} = appearance temperature; T_{cps} = temperature for preparation of charring product samples for x.p.s. (both in °C).

palladium to lead or bismuth was 100:1, which is an order of magnitude lower than that used in real sample analysis [2, 3]. This was done because the deposition of increasing amounts of charring products will influence the nature of the tube surface, and thus the efficiency of matrix modification. In order to decrease the effect of charring product deposition on the properties of the tube surface and to obtain charring products representative of those present in the initial stage of atomization, several graphite tubes were used for the preparation of one sample, and no effort was made to expand the ratio of matrix modifier to analyte. Therefore, the charring product samples which contained 3 mg of lead or bismuth, 300 mg of palladium, 3 mg of lead plus 300 mg of palladium, or 3 mg of bismuth plus 300 mg of palladium were prepared by the procedure described above.

Mechanism of palladium matrix modification. There are several major pathways leading to the formation of gaseous atoms in graphite-furnace a.a.s. [6]. These include vaporization of metals, thermal dissociation of metal oxides and thermal dissociation of metal carbides. Atomization of lead and bismuth should occur by thermal dissociation of their oxides with subsequent vaporization of the metals [7]. As can be seen from Figs. 1 and 2, the appearance temperatures for lead and bismuth were shifted to higher values in the presence of palladium.

The x.p.s. spectra of the various charring products are shown in Fig. 3, and the corresponding values of the binding energies are given in Table 2. The binding energy of Pd($3d_{5/2}$) was increased by 0.8 or 1.0 eV in the charring products of a mixture of lead or bismuth plus palladium compared to that of pure palladium. It was decreased by 1.4 and 2.0 eV for Pb($4f_{7/2}$) and Bi($4f_{7/2}$), respectively, when analyte and palladium were charred together in the graphite tube. This indicates charge transfer from palladium to lead and bismuth, and, therefore, that Pb—Pd or Bi—Pd bonds may be formed. Such bonds must be broken before lead or bismuth atoms can vaporize, resulting in the increase in appearance temperatures in the presence of palladium. Although further work is required to verify the composition of the charring products and to study the atomization process of the analyte in more detail,

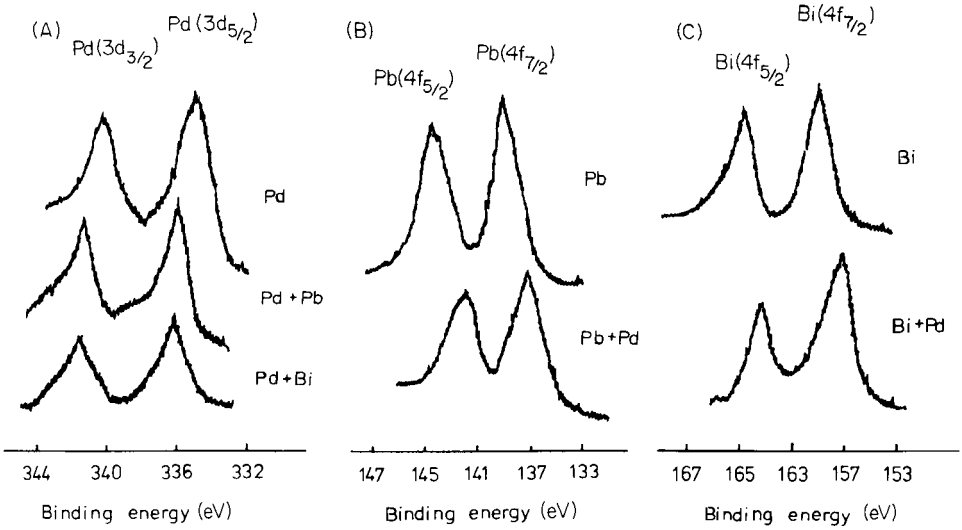

Fig. 3. Spectra for charring products. (A) Palladium 3*d* spectra in the absence and presence of analyte. (B) Lead 4*f* spectra with and without palladium. (C) Bismuth 4*f* spectra with and without palladium.

TABLE 2

X.p.s. data for charring products

Charring product	Pd	Pd + Pb	Pd + Bi	Pb	Pb + Pd	Bi	Bi + Pd
X.p.s. peak	Pd($3d_{5/2}$)			Pb($4f_{7/2}$)		Bi($4f_{7/2}$)	Pd($5d_{5/2}$)
E_b (eV)[a]	335.1	335.9	336.1	138.9	137.5	159.5	157.5

[a]Binding energy.

the present qualitative study is a step forward in understanding the mechanism of palladium matrix modification.

REFERENCES

1 R. D. Ediger, G. E. Peterson and J. D. Kerber, At. Absorpt. Newsl., 13 (1974) 61.
2 Shan Xiao-quan and Ni Zhe-ming, Can. J. Spectrosc., 27 (1982) 75.
3 Jin Long-zhu and Ni Zhe-ming, Can. J. Spectrosc., 26 (1981) 219.
4 Shan Xiao-quan, Ni Zhe-ming and Zhang Li, Anal. Chim. Acta, 151 (1983) 179.
5 Shan Xiao-quan and Hu Kai-jin, Talanta, 32 (1985) 23.
6 B. V. L'vov and G. N. Ryabchuk, Zh. Anal. Khim., 36 (1981) 2085.
7 B. V. L'vov and G. N. Ryabchuk, Spectrochim. Acta, 37B (1982) 673.

Analytica Chimica Acta, 173 (1985) 321—325
Elsevier Science Publishers B.V., Amsterdam — Printed in The Netherlands

Short Communication

MECHANISM OF INTERFERENCE ELIMINATION BY THIOUREA IN ELECTROTHERMAL ATOMIC ABSORPTION SPECTROMETRY

MASAMI SUZUKI*, KIYOHISA OHTA and KAORU ISOBE

Department of Chemistry, Faculty of Engineering, Mie University, Kamihama-cho, Tsu, Mie-ken 514 (Japan)

(Received 2nd October 1984)

Summary. The mechanism of interference elimination by thiourea in electrothermal atomization is discussed. Activation energies of atomization were measured. The experimental values for bismuth, lead, copper and cadmium were not altered in the presence of concomitants, provided that thiourea was added before atomization. These elements form complexes with thiourea which are converted to sulphides during the charring stage. Atom formation occurs from the sulphides without compound formation between analyte and concomitants.

Matrix interference effects are well known in electrothermal atomic absorption spectrometry (a.a.s.). Matousek [1] has reviewed such interferences and their elimination. For the purpose of overcoming matrix interferences, a variety of chemicals, including ascorbic acid, has been applied. Most partially overcame the interference effects. No clear account, however, has been given of the mechanism of such elimination of interferences.

Suzuki and Ohta [2] showed that thiourea improved the atomization profiles and removed the effects of different species in electrothermal a.a.s. of bismuth, antimony, copper, cadmium and lead. This reagent also proved to be effective for eliminating matrix interferences. Thiourea appears to have a different mechanism for the elimination of matrix interferences than other substances. This investigation provides some evidence about this mechanism.

Experimental

Apparatus. Atomic absorption measurements were made as described previously [3]. The output signal from the amplifier was fed to a microcomputer (Sord M223) through an AD converter (Datel ADC-HX-12BGC) and multiplexer (Datel MX-808) [3]. The signals were also monitored on a Memoriscope (Iwatsu MS5021). Light sources were hollow-cathode lamps (Hamamatsu Photonics K.K.). The wavelengths used were 233.06, 228.80, 324.75, 217.00, 328.07 and 217.59 nm for bismuth, cadmium, copper, lead, silver and antimony, respectively.

A molybdenum microtube (20 mm long, 1.5 mm i.d.) was used as the atomizer. This was machined from molybdenum sheet (0.05 mm thick;

0003-2670/85/$03.30

Rembar Co.). The microtube atomizer was enclosed in a pyrex chamber (300 ml) which had two silica end-windows to allow transmission of the light beam. The chamber was purged with argon (480 ml min^{-1}) and hydrogen (20 ml min^{-1}).

The atomizer temperature was measured with a photodiode (Hamamatsu Photonics K.K., S641) [3]. The temperature measured was corrected for non-black body emissivity by use of Planck's radiation formula. The signal from the photodiode was calibrated with an optical pyrometer and was recorded simultaneously with the absorbance signal. Samples were injected into the microtube from a 1-μl glass micropipet.

A Rigaku X-ray diffractometer was used for identification of the residues formed when metal solutions were heated with and without thiourea at 570 K before atomization.

Reagents. All reagents used were of the highest available purity. The stock solutions (nitrates) were prepared from pure metals with the exception of antimony, which was prepared from antimony(III) potassium tartrate. All working solutions were prepared just before use by dilution with deionized water.

Procedures. Atomization was achieved by heating a 1-μl sample to a final temperature of 2000—2260 K for 2 s after drying at 370 K for 10 s and charring at 570 K for 10 s. The heating rate was 1.8—3.4 K ms^{-1}. All the absorbance signals during atomization were stored in the microcomputer. Signals were smoothed after subtraction of background (noise) [3]. To determine activation energies, the slope of a logarithmic plot of the measured absorbance vs. the reciprocal absolute temperature was evaluated by least-squares analysis [4]. The precision of the measurements was $<11\%$.

Results and discussion

Information can be obtained from atomization energies which may help to elucidate the atomization process. Atomization energies, therefore, were measured in order to clarify the mechanism of the interferences and their removal with thiourea. The activation energies were determined by the method proposed by Sturgeon et al. [4]. This approach assumes that there is an analyte surface/gas phase equilibrium within the atomizer and that the rate of production of observable atoms is characterized by a unimolecular rate constant. The difference between the temperature of the gas phase in the microtube and that of the tube itself is negligible at the heating rate used [2]. Therefore, it seems reasonable to expect that the physical and chemical processes in the microtube attain equilibrium before the atoms are lost.

Silver, cadmium, copper, lead and antimony interfere in bismuth atomization [2]. Figure 1 depicts the interference of cadmium on bismuth atomization and its elimination with thiourea. The signals did not return to the baseline without thiourea. Although this tailing is characteristic of bismuth, its cause is uncertain. Thiourea greatly improved this tailing. Table 1 presents the activation energies, E_a, obtained by atomizing bismuth and concomitant

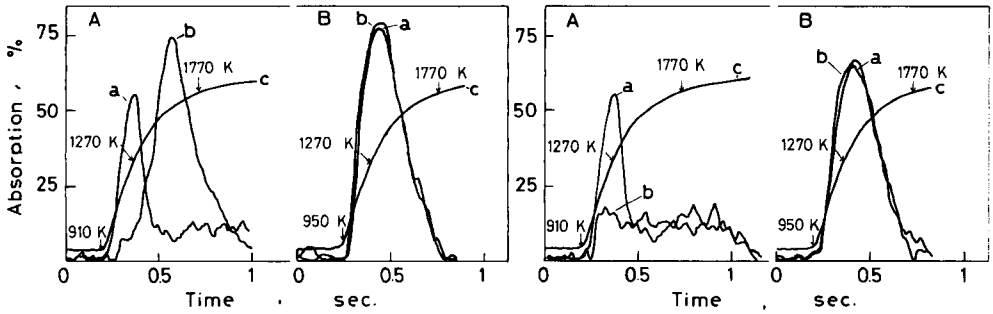

Fig. 1. Cathode-ray tube display showing the interference of cadmium on bismuth absorbance, and its elimination with thiourea: (A) no thiourea added; (B) thiourea (5 μg) added. Traces: (a) 0.25 ng Bi; (b) 0.25 ng Bi and 0.25 μg Cd; (c) temperature.

Fig. 2. Cathode-ray tube display showing the interference of magnesium on bismuth absorbance, and its elimination with thiourea: (A) no thiourea added; (B) thiourea (5 μg) added. Traces: (a) 0.25 ng Bi; (b) 0.25 ng Bi and 0.25 μg Mg; (c) temperature.

TABLE 1

Appearance temperatures and activation energies for bismuth, lead, copper and cadmium

Concomitant added[a]	Without thiourea		With thiourea	
	T_{app} (K)	E_a (kJ mol^{-1})	T_{app} (K)	E_a (kJ mol^{-1})
Bismuth				
—	910	322	950	209
Cd	925	182	920	208
Cu	910	95.7	930	206
Pb	900	141	925	205
Ag	915	196	925	209
Sb	920	248	930	204
Lead				
—	1280	401	1060	185
Bi	1200	140	1060	187
Cd	1150	200	1055	191
Copper				
—	1180	196	1325	326, 163
Cd	1325	142	1350	326, 200
Sb	1300	216	1325	323, 200
Bi	1270	101	1340	330, 191
Cadmium				
—	680	275	710	209
Pb	690	210	685	199
Cu	710	128	690	192
Bi	702	182	685	194

[a]1000-fold wt. amount with respect to the amount of the element measured (250 pg Bi, 25 pg Pb, 50 pg Cu, or 10 pg Cd).

elements in the absence and presence of thiourea. The values of E_a represent the energy required in the rate-determining step to produce metal atoms. As can be seen from Table 1, the activation energy of bismuth in the presence of concomitant elements differs from that of bismuth alone. The experimental activation energies of bismuth in the presence of lead, silver and antimony are close to the bond energies of Bi-Pb (134 kJ mol^{-1}), Bi-Ag (192 kJ mol^{-1}) and Bi-Sb (251 kJ mol^{-1}) [5]. The lack of literature values does not allow the assignment for activation energies for bismuth in the presence of copper and cadmium. The interferences from concomitant elements appear to result from the slow vaporization of compounds formed between bismuth and concomitant elements. When thiourea was present, the experimental activation energies of bismuth in the presence of concomitant elements were identical with the value for bismuth alone, which corresponded to the heat of vaporization of bismuth, Bi(l) → Bi(g) (210 kJ mol^{-1}). The atomization process for bismuth in the presence of thiourea is hydrogen reduction of bismuth sulphide followed by vaporization of the free metal [6]. The X-ray diffraction pattern showed the formation of sulphide on heating of the bismuth/thiourea complex at 570 K.

Table 1 also shows the activation energies for lead, copper and cadmium in the presence of concomitant elements. Various values were obtained, depending on the concomitant elements. But, provided that thiourea was used during atomization, the values were identical with those for the elements alone, irrespective of the concomitant elements. The E_a value of 185 kJ mol^{-1} for lead correlates well with the heat of vaporization of the element (183 kJ mol^{-1}). For copper, the two values 326 and 163 kJ mol^{-1} correspond to the heat of vaporization of Cu(s), 337 kJ mol^{-1}, and the Cu—Cu bond energy, 195 kJ mol^{-1}, respectively. This results from vaporization of copper formed by hydrogen reduction of copper sulphide [6]. The formation of the sulphide in the charring stage was identified by the X-ray diffraction pattern. An E_a value of 184 kJ mol^{-1} for cadmium correlates well with the CdS bond energy, 201 kJ mol^{-1}. The atomization process of cadmium in the presence of thiourea is thermal dissociation of cadmium sulphide [6]. The activation energies of lead, copper and cadmium in the presence of concomitants without thiourea were difficult to relate to the thermodynamic data except for Pb-Bi because of the lack of literature values.

The interference mechanism of concomitant elements may be considered as follows. The analyte and concomitant elements form compounds such as intermetallic compounds, which delay analyte vaporization. As noted above, the formation of the sulphides of analyte and concomitant elements proved to be effective for modification of interferences from concomitants. This may be due to the ready release of analyte elements from their sulphides.

In these experiments, both the analyte and concomitant elements formed thiourea complexes. The elimination of an interference from a concomitant, however, occurs if either analyte or concomitant forms a complex with thiourea. For example, a severe interference was encountered from magnesium

on the atomization of bismuth, but this interference was eliminated by thiourea, as shown in Fig. 2. Magnesium does not form a thiourea complex. The similarity of the atomization profiles in the presence of thiourea indicates that the rate of formation of analyte atoms in the microtube is not changed by the presence of concomitants. The activation energy was the same both in the absence and presence of the concomitant element.

To confirm the process of interference elimination with thiourea, atomization was tested with a microtube atomizer with double indentations [7]. First the analyte and concomitant elements were placed in one indentation and thiourea in the other. In this case, thiourea had no effect. But when analyte, concomitant and thiourea were mixed in one of the indentations, the interference was eliminated. These results suggest that the formation of a thiourea complex of the analyte has a fundamental significance for interference removal. The favorable effect of thiourea on the analyte alone was also observed when mixing was done before atomization, but not in atomization from separate indentations.

Other compounds, e.g., ascorbic acid and EDTA, have been used for elimination of matrix interferences. For ascorbic acid, Regan and Warren [8] proposed a mechanism involving the accelerated reduction of metal oxides by carbon generated in the pyrolysis of ascorbic acid. In contrast, the effect of thiourea is attributed to formation of the sulphide of the analyte or concomitant, or both, during the charring stage. This is supported by the similar effect of thioacetamide. The effect of thiourea was also observed for atomization of cadmium from a carbon surface. For this experiment, carbon was deposited on the molybdenum atomizer as a hard coating, by the thermal decomposition of acetylene added to the argon purge gas, at high temperature.

REFERENCES

1 J. P. Matousek, Prog. Anal. Atom. Spectrosc., 4 (1981) 247.
2 M. Suzuki and K. Ohta, Prog. Anal. Atom. Spectrosc., 6 (1983) 49.
3 M. Suzuki, K. Ohta and T. Yamakita, Anal. Chim. Acta, 133 (1981) 209.
4 R. E. Sturgeon, C. L. Chakrabarti and C. H. Langford, Anal. Chem., 48 (1979) 1792.
5 R. C. Weast, CRC Handbook of Chemistry and Physics, 54th edn., CRC Press, Cleveland, OH, 1979.
6 M. Suzuki and K. Ohta, Anal. Chim. Acta, 151 (1983) 401.
7 K. Ohta and M. Suzuki, Talanta, 23 (1976) 560.
8 J. G. T. Regan and J. Warren, Analyst (London), 101 (1976) 220.

Analytica Chimica Acta, 173 (1985) 327—330
Elsevier Science Publishers B.V., Amsterdam — Printed in The Netherlands

Short Communication

DETERMINATION OF ALKALI METALS LEACHED FROM GLASS AMPOULES INTO INJECTION FLUIDS

LIESELOTTE MOENKE-BLANKENBURG* and PETRA DECKER

Sektion Chemie der Martin-Luther-Universität Halle-Wittenberg, Weinbergweg 16, 4020 Halle (German Democratic Republic)

(Received 16th October 1984)

Summary. Direct determination of the alkali metal output of glass ampoules by atomic emission and absorption spectrometry is described. The methods provide suitable alternatives to acidimetric titration for characterizing the hydrolytic resistance of container glasses for pharmaceutical use.

Chemical attack on glass can ideally be described by two mechanisms, etching and leaching [1]. The etching process characteristic of alkaline attack is represented in Fig. 1A. It is a reaction that can be considered as $2NaOH + SiO_2 \rightarrow Na_2SiO_3 + H_2O$. The tetrahedra of the $[SiO_4]$ network with $Y = 4$ and three-dimensional connections is destroyed and very long chains of $R_2O \cdot SiO_2$ with $Y = 2$ and two-dimensional connections are formed [2]. This etching will leave a smooth surface if complete dissolution occurs without deposition of reaction products; otherwise, etching produces a coated or roughened surface. The leaching process characteristic of acid attack is represented in Fig. 1B. Essentially, it is a diffusion-controlled exchange of hydrogen ions for the alkali metal ions present in the glass. The network remains intact during leaching. As the leached silica layer thickens, the reaction rate decreases. Leaching will be insignificant if the thickness of the leached silica layer approaches 0.1 μm.

Glass ampoules are widely used for pharmaceutical products, especially injection fluids. The chemical constituents of brown borosilicate glass, a typical container material for parenteral drugs, are: 68% (w/w) SiO_2, 9% B_2O_3, 6.5% Na_2O, 5.5% Al_2O_3, 4% BaO, 1.5% K_2O, 0.5% CaO, 4% Fe_2O_3 and 1% MnO_2 as colouring matter. All the glass components are potentially extractable; the alkali metals are most easily extracted into acidic or nearly neutral solution [3]. The extracted element may interact with the parenteral drug in several ways. Precipitation of the free bases from an alkaloid salt solution (e.g., morphine, strychnine) is possible, as is flocculation of colloidally dissolved substances when the pH changes. Other possibilities are fission of esters and glycosides (e.g., atropine, cocaine, arecoline), rearrangement of optically active isomers, and oxidation accelerated by alkali (e.g., morphine to oxydimorphine).

0003-2670/85/$03.30

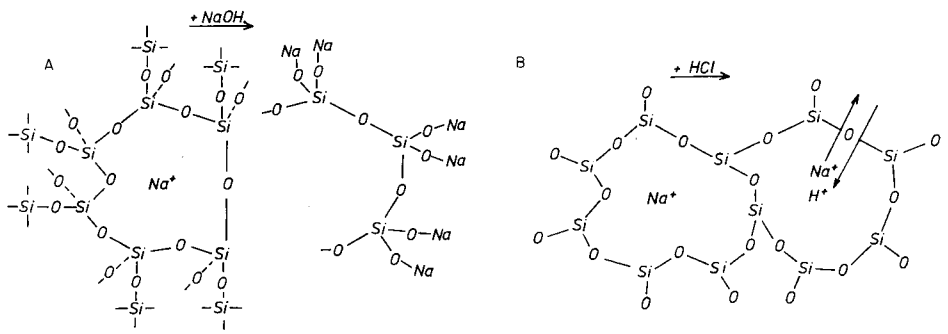

Fig. 1. Mechanisms of the etching (A) and leaching (B) of glass.

Pharmaceutical standards for testing the hydrolytic resistance of the interior surfaces of glass containers for pharmaceutical application [4, 5] depend on titration with 0.01 M hydrochloric acid, of the hydroxide leached from the glass on autoclaving (121°C) for 60 min with 100 ml of solution [4] or for 30 min with 25 ml of solution [5]. Glasses are classified as types I—III [4] or resistance classes 1—3 [5]. These titrimetric procedures can be modified by determining the alkali metal output of glasses directly. The aim of this study was to prove the validity of direct determinations of alkali metals as an alternative to titrimetry. Atomic emission spectrometry (a.e.s.) was used for the determination of the sodium and potassium contents of the autoclaved solutions; atomic absorption spectrometry (a.a.s.) was also used for determinations of sodium.

Experimental

Determination of sodium. The atomic absorption spectrometer used was a model AAS1 (VEB Carl Zeiss, Jena, D.D.R.) with an air/acetylene flame (90 l h^{-1} acetylene, 500 l h^{-1} air). For a.a.s., a three-slit burner (slit length 50 mm, slit width 0.45 mm, triple optical path) was used. The instrument settings were: lamp current 4.5 mA, slit width 0.06 mm, photomultiplier 2, intensifier 2, time constant 1 s. For a.e.s., a Mekér burner with 58 holes (1 mm diameter) was used. The instrument settings were: slit width 0.07 mm, photomultiplier 4, intensifier 3, time constant 1 s. Both absorption and emission were measured at 589.0 nm.

The calibration graphs found for both a.a.s. and a.e.s. were linear over the range 0.1—1.0 μg ml^{-1} sodium. The limits of detection (S/N = 3) were 0.03 μg ml^{-1} by a.a.s., and 0.02 μg ml^{-1} by a.e.s.

Determination of potassium. A Flapho-40 (VEB Carl Zeiss, Jena) flame photometer was used with an air/acetylene flame (40 l h^{-1} acetylene, 400 l h^{-1} air). Emission was measured at 769.9 nm (intensifier setting 10, time constant 10 s). The calibration graph was linear over the range 0.01—0.10 μg ml^{-1} potassium; the limit of detection of 0.001 μg ml^{-1}.

TABLE 1

Determination of sodium and potassium in leach water from ampoules by atomic spectrometry

Metal	Method	Type of glass	Conc. of Na or K found (μg ml^{-1})[a]	
			EP	DAB 7
Na	A.a.s.	Brown	0.549 ± 0.01	0.543 ± 0.01
		Clear	0.532 ± 0.01	0.527 ± 0.01
Na	A.e.s.	Brown	0.548 ± 0.009	0.545 ± 0.009
		Clear	0.531 ± 0.009	0.528 ± 0.009
K	A.e.s.	Brown	0.087 ± 0.0004	—
		Clear	0.016 ± 0.0004	—

[a]Mean and standard deviation of 5 measurements of leach water obtained by the EP method [4] or DAB-7 method [5].

TABLE 2

Comparison of results by titration and by a.e.s.

Glass	Volume of 0.01 M HCl needed[a] (ml)	Na + K found (μg ml^{-1})	
		By conversion of titrimetric results	By a.e.s.
Brown	0.28	0.644	0.635
Clear	0.24	0.552	0.547

[a]For titration of 100 ml of solution.

Results and conclusions

The results of the determinations of sodium and potassium in the leach waters from ampoules are listed in Table 1. The average contents are 0.546 μg ml^{-1} sodium and 0.087 μg ml^{-1} potassium for brown glass, and 0.529 μg ml^{-1} sodium and 0.016 μg ml^{-1} potassium for clear glass. Table 2 shows a comparison of the results obtained by titration and by a.e.s. and a.a.s. In the conversion of the titrimetric results to μg ml^{-1} sodium, the potassium content could not be taken into account; this was acceptable because of the low potassium content. The values for the sodium and potassium contents by a.a.s. and a.e.s. agree well with the results of titration. Therefore the direct determination of sodium and potassium contents is a real alternative to titration of the hydroxide content for classifying the quality of glasses for pharmaceutical use.

REFERENCES

1 P. B. Adams, Surface Properties of Glass Containers for Parenteral Solutions. Presented at the Annual Meeting of the Parenteral Drug Association, San Francisco, CA, November, 1976.

2 W. Vogel, Glaschemie, VEB Deutscher Verlag für Grundstoffindustrie, Leipzig, 1983.
3 R. Voigt, Lehrbuch der pharmazeutischen Technologie, VEB Verlag Volk und Gesundheit, Berlin, 1979.
4 H. Böhme and K. Hartke, Europäische Pharmacopöe, Kommentar, Wissenschaftliche Verlagsgesellschaft, Stuttgart, GOVI-Verlag, Frankfurt, 1976.
5 Deutsches Arzneibuch, 7. Ausgabe, Kommentar, Wissenschaftliche Verlagsgesellschaft, Stuttgart, GOVI-Verlag, Frankfurt, 1978.

Analytica Chimica Acta, 173 (1985) 331—336
Elsevier Science Publishers B.V., Amsterdam — Printed in The Netherlands

Short Communication

LANGMUIR — BLODGETT DEPOSITION OF LIPID FILMS ON HYDROGEL AS A BASIS FOR BIOSENSOR DEVELOPMENT

A. ARYA, U. J. KRULL*, MICHAEL THOMPSON* and H. E. WONG

Department of Chemistry, University of Toronto, 80 St. George Street, Toronto, Ontario M5S 1A1 (Canada)

(Received 22nd December 1984)

Summary. Lipid membranes composed of phosphatidyl choline and cholesterol were interfaced to polyacrylamide hydrogel by Langmuir—Blodgett thin-film deposition. The extent of lipid adsorption to the gel surface was critically dependent on the hydration of the polymer as determined by contact angle measurements. Some electrochemical transducers incorporating the deposited membrane/gel structure responded positively to phloretin and valinomycin. Limitations to the construction of this device are discussed.

In recent years, increasing attention has been paid to the development of new selective chemical sensors, biosensors and bioprobes [1, 2]. One approach examined involves electrochemical changes across lipid membrane structures induced by the selective binding of a membrane-bound receptor with a complementary liquid analyte [3—6]. Although these specialized membranes have substantial possibilities in terms of selectivity and sensitivity, their practical use has been handicapped by the fragile nature of the structure which consists of lipid molecules bound and ordered almost exclusively by hydrogen bonding and Van der Waals forces. Attempts to overcome the mechanical fragility of bilayer lipid membranes (BLM) have met with limited success. Membrane miniaturization to maximize surface effects [7, 8], and incorporation of stabilizing agents such as surfactants and polymers [9, 10] improve the strength of membranes but the structural integrity and reproducibility required of a practical device have still not been achieved.

Since the pioneering work of Langmuir and Blodgett in the 1920's, a simple method for preparing mono- and multi-layers of organized lipid films has been available [11]. A renaissance in this technology has occurred with emphasis on thin-film applications in drug encapsulation, surface coating, molecular electronics [12] and in semiconductor sensor design [12, 13]. Films can now be polymerized to yield stable structures both in situ on the trough, or on a supporting substrate. This method is tested here to prepare stable BLM, though the desirable electrochemical properties may be compromised because of alterations of lipid fluidity and receptor incorporation.

The electrochemical operation of the BLM is based on variation of the inorganic ion current through the structure as a function of membrane

0003-2670/85/$03.30

perturbation caused by receptor complexation. For this process, a reservoir of ions with the appropriate indicator electrodes must exist on either face of the membrane. Given this essential geometric configuration, and the problem of BLM stability, a first step towards preparation of practical devices consists of supporting a functional BLM on a rigid ion-conductive hydrated polymeric substrate which can act as one of the ion reservoirs. The present communication describes progress made in interfacing ordered lipid membranes to stable hydrogel substrates by film deposition techniques.

Experimental

Reagents. Acrylamide, *N,N'*-methylene-bis-acrylamide, *N,N,N',N'*-tetramethylethylenediamine (TMED) and riboflavin-5'-phosphate (Bio-Rad Laboratories) were used to prepare polyacrylamide gel. The lipids were egg-derived phosphatidyl choline (Avanti Biochemical, Birmingham, AL) and cholesterol (Sigma Chemical Co.). Epoxy resin was prepared from Epon 825 (Shell), Jeffamine D-230 (Texaco) and Silanox (Cabot Corp., Boston, MA). The electrochemical probes were phloretin [3-(4-hydroxyphenyl)-1-(2,4,6-trihydroxyphenyl)-1-propanone] and valinomycin (Sigma), prepared as methanolic solutions.

Apparatus. Langmuir—Blodgett films were prepared on a 4-cm deep teflon trough using a Wilhelmy plate pressure transducer. The electrochemical device was prepared by successive vacuum deposition of a Ti/W base and 20 nm of silver on a clean glass wafer (1 × 4 × 0.1 cm). A reference electrode surface was then prepared by either standing in aqueous 1 M iron(III) chloride or by electrolytic deposition through chloridation in 0.1 M hydrochloric acid. Partial encapsulation of the glass wafer with a hydrophobic non-conductive epoxy resin followed, so that a circular reservoir to hold the hydrogel could be formed (Fig. 1). The circuitry for electrochemical measurements consisted of an electrometer (Model 616B, Keithley Instruments), a d.c. power supply and a single-junction Ag/AgCl reference electrode (Orion Research).

Procedures. Polyacrylamide gel was prepared in the usual manner from equal volumes of a 20% (w/v) solution of total monomer containing 19:1 (w/w) acrylamide/bis-acrylamide and a 0.01% (w/v) riboflavin-5'-phosphate solution in 0.1 M phosphate buffer (pH 7). The TMED was added to a final concentration of 1% (v/v). A portion (100—200 μl) of the reaction mixture was transferred to the reservoir on the wafer (stored under nitrogen) and polymerization was induced by irradiation for 1 h at 254 nm. The wafer was then stored in 0.1 M potassium chloride for $\geqslant$1 h.

A 1:1 mixture (by weight) of phosphatidyl choline and cholesterol [3—6] was prepared in n-hexane, and a small volume was slowly spread on a 0.1 M potassium chloride subphase in the Langmuir—Blodgett trough at 20 ± 1°C. The surface film was compressed by a moving sweep boom until a pressure of at least 30 mN m^{-1} was attained. The water was then dipped at a rate of 0.5 cm min^{-1} at a fixed pressure (±0.1 mN m^{-1}) through the compressed lipid film, first being immersed into the subphase, then withdrawn and

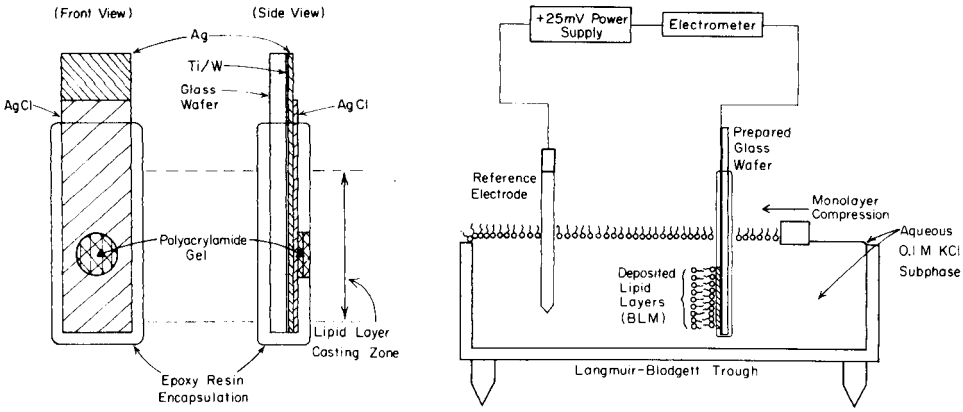

Fig. 1. Design of the substrate for support of ordered lipid films.

Fig. 2. Circuitry used to measure cation current through deposited BLM on polyacrylamide hydrogel.

finally re-immersed. A small portion of the unprocessed silver initially deposited on the wafer was used as one point of electrical connection to prepare an electrochemical circuit (Fig. 2). The phloretin and valinomycin probes were introduced to the trough subphase as concentrated methanolic solutions in the vicinity of the wafer to evaluate transducer operation.

Results and discussion

Lipid deposition. The signal obtained from a BLM transducer is the variation of transmembrane ion current as the membrane interacts with organic species. Accordingly, for film casting by the Langmuir—Blodgett process, the ordered lipid structure must be sandwiched between one electrolyte compartment and a substrate capable of ion conduction. In this work, the polyacrylamide hydrogel chosen was interfaced directly to an underlying Ag/AgCl electrode surface.

Lipid coating onto thin slabs of gel was studied in order to establish the probable orientation of successive lipid films. Surface pressure changes of the compressed monolayer as film casting proceeded were indicative of successful transfer to the gel substrate. Variation of the casting speed indicated an optimum rate of 2 mm min^{-1}. Upon removal of the gel from the trough, water droplets were placed near each end of the slab, and in the center, for contact angle measurements. When the surface pressure of the lipid monolayer in the trough was not maintained at a fixed value (always >30 mN m^{-1}) but was allowed to vary as gel dipping proceeded, contact angles were found to be of greater magnitude at the end of the gel closer to the jaws of the dipping device. Uncoated gels when hydrated produced contact angle values which were not measurable and were assigned zero values because of the flat profile of the water droplets. These results are consistent, and indicate that

the gel initially has hydrophilic character. Deposition on the gel always resulted in the outermost lipid layer having an orientation with acyl chains at the air interface on withdrawal from the trough, thus contact angles should indicate hydrophobic surface character. Deposition experiments with controlled surface pressure produced contact angles which were much more uniform over the gel surface. Unfortunately no general correlation could be established between the compressed film surface pressure and the magnitude of the contact angle, because gel surface polarity was critically controlled by the degree of hydration. As the gel dried, it became more hydrophobic, and in this condition could provide contact angles of identical magnitude to those observed for lipid-coated gels. The lack of control of hydration, and therefore the absence of an appropriate reference for comparison purposes, precluded proper correlation between individual experiments.

Electrochemical device. Surface wettability and monolayer compression characteristics, coupled with the expected hydrophilic character of the gel [14], imply that the Langmuir-Blodgett deposition routine used here created stabilized BLM. The artificial BLM used previously [3—6] have an inherent internal pressure of ca. 30 mN m^{-1} [15]. All lipid casting was therefore done at pressures of at least this value, ranging up to the monolayer collapse pressure (Fig. 3). Cast films remained stable for many hours but did not survive subphase withdrawal and re-immersion once the monolayer on the trough surface was removed.

Successful BLM casting was readily observed as a roughly 10 000-fold reduction in ion current (Fig. 4). Final current values were of the order of 10^{-9}—10^{-10} A cm^{-2}, and special electrical shielding with a Faraday cage assembly was necessary. Only a fraction of all attempts to coat electrochemically-useful BLM onto gels were successful. Once a stabilized BLM had

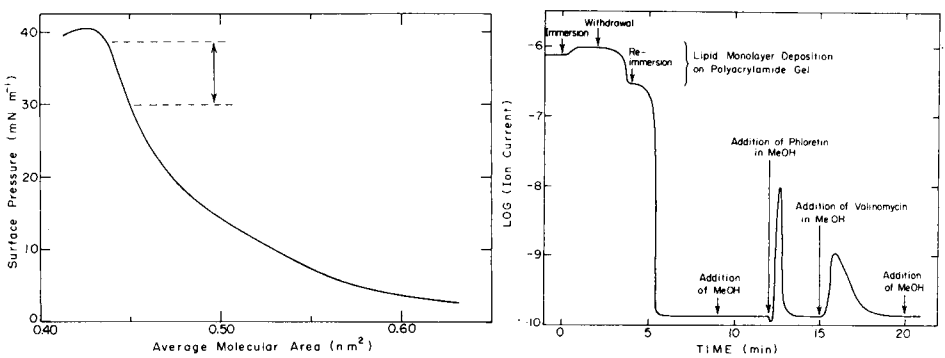

Fig. 3. Pressure/area curve demonstrating the characteristics of the phosphatidyl choline/cholesterol monolayers used in deposition experiments. Pressure range suitable for formation of functional BLM is indicated by dashes.

Fig. 4. Representative electrochemical responses of successful Langmuir—Blodgett films to phloretin and valinomycin.

been deposited on a gel surface, probing of the membrane was done with two membrane-active organic agents. Valinomycin (GMW-1111) is capable of complexing a cation into a central polar cavity surrounded by a hydrophobic peptide sheath; thus it readily dissolves into non-polar media, carrying the ion into a hydrophobic zone such as found in the interior of a BLM. This capability has been exploited widely in neutral carrier electrodes for potassium, and results in substantial increases in ion current through a BLM by reducing the Born energy requirements of ion transport. The transient ion-current increase observed in Fig. 4 on addition of a local concentrated volume of valinomycin, which rapidly dissipates into the large volume of the trough subphase, is consistent with the presence of a lipid membrane of undefined structure. A second probe of interest is the dipolar species phloretin. This small organic species (GMW-274) has a large (5.6 D) dipole moment which can align against the inherent dipolar field of a BLM [16]. This dipolar field is of an orientation which limits transmembrane cation current, so that phloretin acts to increase current (Fig. 4). The electrical activity of phloretin is important because the dipolar effect is a surface phenomenon and should be significant for only monolayer or bilayer lipid structure.

Limitations to device fabrication. Only some experiments produced successful electrochemical devices. In most cases, even repeated attempts at film deposition could not eliminate the large (10^{-6} A cm^{-2}) current characteristic of the uncoated gel device. The failures can be ascribed to the following features: (1) gel adhesion to the Ag/AgCl electrode surface or to the epoxy insulator was poor; (2) the surface morphology of the gel coated onto the electrical substrate cannot be controlled in the procedures described; (3) gel hydration is not readily controlled, and the hydrophilic or hydrophobic character will also be a function of the polymer composition and degree of cross-linking; (4) lipid adhesion to the gel, as well as the density of lipid packing on the gel surface, depends on the variable gel chemistry as well as the casting techniques; incomplete lipid coating, particularly at imperfections in boundary locations (e.g., gel contact to epoxy resin) would result in substantial leakage currents.

Conclusions

The electrical activity observed with the probes described demonstrate that it is possible, though with some difficulty, to deposit lipid monolayers successively onto an ion-conductive substrate, creating an organized structure capable of electrochemical response. This could be important in the evolution of a practical biosensor, though it is obvious that much further work is needed to improve the techniques used, particularly with respect to permanent attachment of lipid structures to optimized substrates.

We are grateful to the Natural Sciences and Engineering Research Council of Canada for support. Also, we are indebted to J. Janata and M. Levy, University of Utah, for helpful discussion and the preparation of metal-coated glass wafers, respectively.

REFERENCES

1 H. Wohltjen, Anal. Chem., 56 (1984) 87A.
2 M. Thompson and U. J. Krull, Trends Anal. Chem., 3 (1984) 173.
3 M. Thompson, P. J. Worsfold, J. M. Holuk and E. A. Stubley, Anal. Chim. Acta, 104 (1980) 195.
4 M. Thompson, U. J. Krull and P. J. Worsfold, Anal. Chim. Acta, 117 (1980) 121.
5 M. Thompson and U. J. Krull, Anal. Chim. Acta, 147 (1983) 1.
6 M. Thompson, U. J. Krull and M. A. Venis, Biochem. Biophys. Res. Commun., 110 (1983) 300.
7 J. M. Mountz and H. Ti Tien, Photochem. Photobiol., 28 (1978) 395.
8 M. Thompson, R. B. Lennox and R. A. McClelland, Anal. Chem., 54 (1982) 76.
9 P. K. Shieh and L. Packer, Biochem. Biophys. Res. Commun., 71 (1976) 603.
10 H. H. Hub, B. Hupfer, H. Koch and H. Ringsdorf, Angew. Chem. Int. Ed., 19 (1980) 938.
11 Thin Solid Films, 99 (1983).
12 G. G. Roberts, Sensors and Actuat., 4 (1983) 131.
13 J. Janata and G. F. Blackburn, Ann. N.Y. Acad. Sci., 42 (1984) 286.
14 O. Albrecht, D. S. Johnston, C. Villaverde and D. Chapman, Biochim. Biophys. Acta, 687 (1982) 165.
15 A. Blume, Biochim. Biophys. Acta, 557 (1979) 32.
16 O. S. Anderson, A. Finkelstein, I. Katz and A. Cass, J. Gen. Physiol., 67 (1976) 748.

Analytica Chimica Acta, 173 (1985) 337—341
Elsevier Science Publishers B.V., Amsterdam — Printed in The Netherlands

Short Communication

INDIRECT POTENTIOMETRIC MONITORING OF PROTEINS WITH A COPPER ELECTRODE

M. L. HITCHMAN* and F. W. M. NYASULU

Department of Chemistry and Applied Chemistry, University of Salford, Salford M5 4WT (Great Britain)

(Received 20th November 1984)

Summary. Preliminary results are given for the monitoring of proteins by indirect potentiometry with the Cu^{2+}/Cu couple in a flow system. Electrochemical cleaning of the electrode, before measurement of the potential in the presence of proteins, allows reproducible determinations of proteins at the micromolar level. The effects of pH and chloride on the measured potentials are investigated.

Potentiometric electrodes are known to show signs of poisoning in the presence of proteins [1]. One method of alleviating this problem is to use an excess of reagent such that potentials before and after addition of protein are always measured in the presence of the reagent. Alexander and Rechnitz [2] reported such an indirect potentiometric method. Proteins were dissolved in a buffer solution, pH 8.4, which was then added to buffer solution with an excess of silver(I) ions. The Ag^+ reacted with the thiol groups and the excess was measured with a silver sulphide electrode. The difference between the measured potential and the potential obtained for a blank buffer solution (ΔE) showed a linear relationship with protein concentration up to about 1.2 mg ml^{-1}. Ovalbumin has been determined similarly [3]. The indirect procedure has been extended to a continuous flow system [4]; urea denaturation of the disulphide linkages to form thiol groups, made it possible to determine proteins (e.g., albumins and globulins) down to 5—10 $\mu g\ ml^{-1}$. A continuous flow system was also reported by Diamandis et al. [5]; human serum albumin was treated with excess of picrate, the excess being measured with a picrate-selective electrode.

However, even in indirect potentiometry, problems of electrode poisoning by protein remain [1, 2]. In this communication, an indirect potentiometric method of determining proteins in a flow-injection system is outlined; an excess of copper(II) ions and a copper metal electrode are used. The procedure is adapted from the direct potentiometric determination of proteins [6] in order to improve response times and electrode behaviour.

*Present address: Department of Pure and Applied Chemistry, University of Strathclyde, Thomas Graham Building, 295 Cathedral Street, Glasgow G1 1XL, Great Britain.

0003-2670/85/$03.30

Experimental

A diagram of the system used is shown in Fig. 1(a). The apparatus was mounted on an aluminium plate that was grounded to reduce background noise. The pump was a model P3 (Pharmacia Fine Chemicals). The pulse-damping system consisted of a half-filled 10-ml bottle followed by a coil of tubing (1 m long, 0.5 mm i.d.); potentials are known to depend on flow fluctuations. All the connecting silicone-rubber tubing was 0.5-mm internal diameter and all connections were made with T2 and T3 Pharmacia connectors. A Pharmacia V7 injection valve was used to inject 200-μl volumes; the injector-to-detector distance was 30 cm. Figure 1(b) shows the design of the cell used; the electrodes were a double-junction Ag/AgCl reference electrode (Corning 00311615N) and a copper wire (99.99% purity; Goodfellow Metals) indicator electrode. A platinum wire was coiled as shown for the cleaning circuit. The pH and potential were measured with a PTI-6 Universal pH meter, to which a recorder (Pharmacia Fine Chemicals) was attached. The copper electrode was made by painting the 0.25 mm diameter wire with lacquer, inserting it through 0.5 mm i.d. tubing with only the copper tip exposed, and encasing it in a plastic holder with a silicone rubber seal.

The carrier solution consisted of a 0.05 M phosphate buffer solution (pH 7) containing a fixed level of copper(II) ions. The following amino acids and proteins (all from Sigma Chemical Co.) were used: ribonuclease A (from bovine pancreas), lysozyme (from egg white), phosvitin (from egg yolk), ovalbumin (Grade V), bovine albumin (fraction V), human albumin (fraction V), γ-globulin (human Cohn fraction II), and catalase (from bovine liver).

The effect of pH on potential response was studied in a batch system; protein solutions were prepared with an excess of 10^{-4} M copper nitrate and

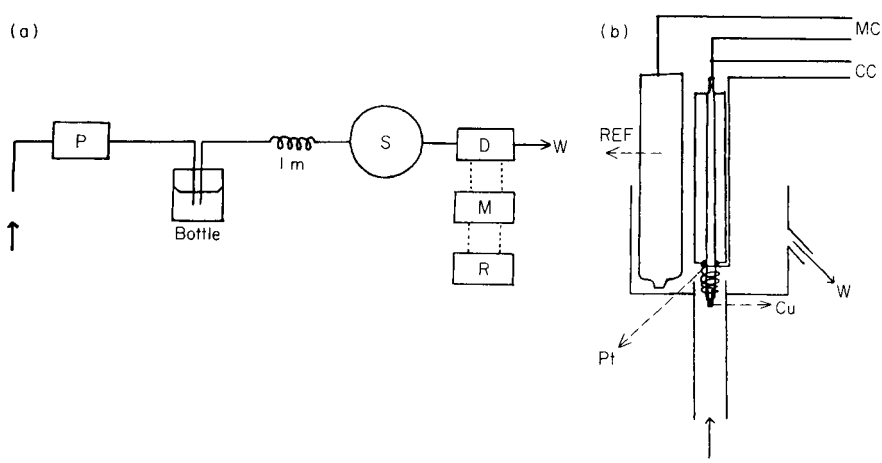

Fig. 1. (a) Diagram of the flow-injection system: P, pump; S, sample injection valve; D, detector; W, waste; M, pH meter; R, recorder. (b) Diagram of the potentiometric detector cell: MC, measuring circuit; CC, cleaning circuit; W, waste.

with 2 M sodium nitrate, to keep the ionic strength constant. The pH was then adjusted to the required value by addition of concentrated sodium hydroxide or nitric acid. Before each measurement, whether batch or flow, the electrode was usually cleaned by cathodic pretreatment for 5 s with simple d.c. circuitry (1.5 V, 250 ohm in series) and with a platinum wire as the auxiliary electrode [6].

Results and discussion

Figure 2 shows a plot of the responses obtained for the determination of phosvitin, ovalbumin and γ-globulin (human) with 10^{-5} M Cu^{2+} at a flow rate of 1 ml min^{-1}. These conditions would seem to be well suited for determinations of proteins in the 10^{-7}—10^{-6} M range. The responses are linear, following the equation $\Delta E = k[\text{protein}]/[Cu^{2+}]$, for $[Cu^{2+}] \gg [\text{protein}]$ and where k is a constant for each protein under fixed conditions. This equation will be discussed in detail in a later paper.

Table 1 gives the response indices, obtained from the least mean-square slopes, for various proteins. The detection limits obtained with the conditions indicated are also listed in Table 1; these are lower than those obtained with direct potentiometry. The above equation for ΔE shows that when determinations of lower levels of protein are required, the Cu^{2+} concentration in the carrier solution should be decreased. In these studies, the lowest level of Cu^{2+} that could be used successfully was 4×10^{-6} M, below which the copper electrode did not respond to changes in Cu^{2+} concentrations. With 4×10^{-6} M Cu^{2+}, determinations of proteins in the range 10^{-8}—10^{-7} M were possible and the response indices were 2.5 times those shown in Table 1, as predicted by the above equation. The precision attainable with the indirect potentiometric technique for human albumin and phosvitin was checked by making five potential measurements for each protein concentration; measurements were

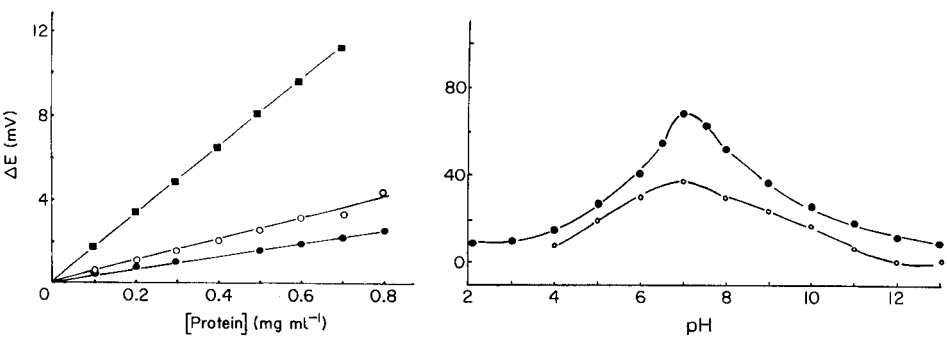

Fig. 2. Responses with proteins: (■) phosvitin; (○) ovalbumin; (●) γ-globulin. Carrier stream, 10^{-5} M Cu^{2+} in 0.05 M phosphate buffer at pH 7; flow rate, 1 ml min^{-1}.

Fig. 3. The effect of pH on potentials of Cu^{2+}/protein solutions: (●) catalase, 0.1 mg ml^{-1}; (○) human albumin, 1 mg ml^{-1}. Batch system used (see text).

TABLE 1

Summary of potentiometric determinations[a]

Protein	Response index (mV (mg ml^{-1}))	Detection limit	
		(mg ml^{-1})	(M)[b]
Human albumin	13.50 ± 0.31	0.04	5.7×10^{-7}
Bovine albumin	6.51 ± 0.20	0.09	1.2×10^{-6}
Ovalbumin	4.80 ± 0.25	0.10	2.2×10^{-6}
Phosvitin	15.89 ± 0.25	0.03	8.8×10^{-7}
γ-Globulin (human)	2.78 ± 0.18	0.20	1.7×10^{-7}
Catalase	Non-linear	0.004	1.6×10^{-8}

[a]Carrier stream, 10^{-5} M Cu^{2+} in phosphate buffer (pH 7) at a flow rate of 1 ml min^{-1}.
[b]Approximate.

TABLE 2

Values of ΔE_{mean} for human albumin (HA) and phosvitin (Ph)

Conc. (mg ml^{-1})	0.1	0.2	0.3	0.4	0.5	0.6
ΔE_{mean} (mV)[a]						
HA	1.5	2.9	4.2	5.6	7.0	8.2
Ph	2.0	3.7	5.2	6.8	8.4	10.0

[a]In each case, the error of measurement was ±0.1 mV at the 95% confidence level (n = 5).

made randomly both with respect to the actual protein being measured and to its concentration. The results in Table 2 clearly show that a sufficient level of precision exists for quantitative purposes.

Figure 3 shows the effect of pH on the potential measured. Clearly, the optimum pH for the determinations is about 7. The decline in the responses at pH > 7 is not due to the reduced complexing ability of Cu^{2+} for the proteins; it is known (e.g., from the biuret method for protein) that the higher the pH, the greater is the complexing ability. The decline is caused by precipitation of the copper(II) ions to form a colloidal solution [7] and by the response of the electrode to hydroxide ions. In the flow system, the phosphate buffer sufficed to keep the pH constant at 7.

A prominent interferent in potentiometric determinations based on the Cu^{2+}/Cu system is chloride [8]. Figure 4 shows the effect of varying the level of chloride in a 0.5 mg ml^{-1} sample of human albumin injected into the flow-injection system. The experimental conditions used were the same as those in Fig. 2. From Fig. 4, chloride interference only begins to show at concentrations $>10^{-2}$ M; this is much higher than in steady-state measurements in which interference was observed at about 10^{-5} M chloride. The improved selectivity in the flow-injection system may be due to the reduced contact time between the sample and the electrode. Similar improvements in selec-

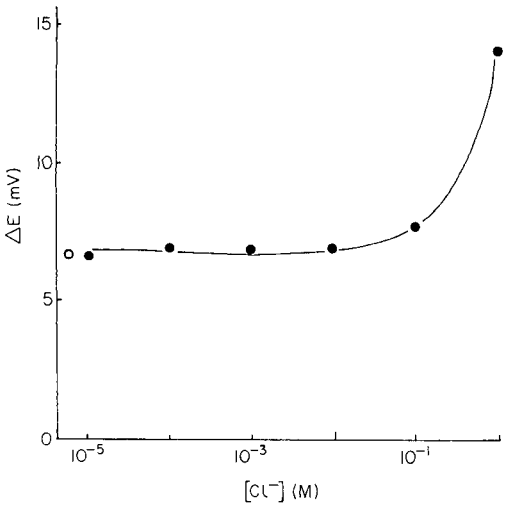

Fig. 4. The effect of chloride ion concentration on the potentials of a 0.5 mg ml^{-1} human albumin sample; (o) potential without chloride. Conditions as for Fig. 2.

tivity with other potentiometric detectors have been reported [9]. The indirect potentiometric detection reported here is currently being used in the determination of proteins eluting from a molecular exclusion chromatographic column where the Cu^{2+} is added in a post-column system.

We acknowledge a British Council training award for F.W.M.N. and Pharmacia Fine Chemicals AB, Uppsala, for the provision of materials and equipment.

REFERENCES

1 See, e.g., T. Y. Toribara and L. Koval, Talanta, 17 (1970) 1006.
2 P. W. Alexander and G. A. Rechnitz, Anal. Chem., 46 (1974) 250.
3 K. Kentaro, Y. Tetsutaro and T. Toshifumi, Bunseki Kagaku, 32 (1983) 308.
4 P. W. Alexander and G. A. Rechnitz, Anal. Chem., 46 (1974) 860.
5 L. P. Diamandis, D. S. Papastathopoulos and T. P. Hadjiioannou, Clin. Chem., 27 (1981) 427.
6 M. L. Hitchman, F. W. Nyasulu, A. Aziz and D. D. K. Chingakule, Anal. Chim. Acta, 155 (1983) 219.
7 J. Gulens, P. K. Leeson and L. Seguin, Anal. Chim. Acta, 156 (1984) 19.
8 J. C. Westall, F. M. M. Morel and D. N. Hume, Anal. Chem., 51 (1979) 1792.
9 M. Trojanowicz and W. Matuszewski, Anal. Chim. Acta, 151 (1983) 77.

Analytica Chimica Acta, 173 (1985) 343—348
Elsevier Science Publishers B.V., Amsterdam — Printed in The Netherlands

Short Communication

DETERMINATION OF SULPHUR(II) COMPOUNDS BY FLOW INJECTION ANALYSIS WITH APPLICATION OF THE INDUCED IODINE/AZIDE REACTION

JAN KURZAWA

Institute of Fundamental Chemistry, Politechnika, ul. Piotrowo 3, 60-965 Poznań (Poland)

(Received 10th December 1984)

Summary. Sulphur(II) compounds that rapidly induce the iodine/azide reaction are determined by injection of 10-μl samples into an iodine/azide solution at a flow rate of 1.4 ml min^{-1}. Iodine consumption in the induced reaction is detected by biamperometry with platinum electrodes. The linear calibration ranges depend on the concentration of iodine in the iodine/azide solution pumped. The detection limit for thiosulphate, 2-mercaptopyrimidine, 2-thiouracil, 2-thiobarbituric acid or 6-mercaptopurine is 0.1 mg l^{-1} and for sulphide, cysteine, thiourea or glutathione is 0.2 mg l^{-1} in the injected sample.

The well-known iodine/azide reaction induced by sulphur(II) compounds has found wide application in the determination of such compounds [1—8], as well as elemental sulphur [9], and traces of metals that give complexes with sulphur compounds stable enough to prevent their catalytic action [10]. Kiba and Furusawa [11] developed a flow-injection method for the determination of hydrogen sulphide by means of the iodine/azide reaction, using a continuous flow of nitrogen as carrier gas.

Sulphur compounds that induce the iodine/azide reaction differ in their induction times. Thiol compounds usually act immediately and reaction is complete in 30 s or less. In the case of disulphides and compounds possessing divalent sulphur in a heterocyclic ring (e.g., cystine, vitamin B_1, sulphathiazole), the induced reaction starts only after heterogeneous cleavage of the S—S or C—S bond by azide in the presence of triiodide and the reaction is often completed only after several hours, depending on the rate of cleavage. Only compounds causing rapid induction can be determined by a simple flow-injection method. In this study, conditions for the determination of such inductors at the nanogram level were developed.

Experimental

Reagents. A stock 0.01 M solution of iodine containing 4 g l^{-1} potassium iodide was standardized by titration with 0.01 M sodium arsenite. The stock solution of sodium azide contained 200 g l^{-1}. Iodine/azide solutions in 0.15 M potassium iodide were prepared by mixing the appropriate amounts of iodine

0003-2670/85/$03.30

and azide solutions and adding water and potassium iodide (to prevent volatilization of iodine). The required pH value of this solution was obtained by adding a suitable amount of 0.1 M hydrochloric acid; the HN_3/NaN_3 buffer system is formed and no additional buffer is needed.

The compounds examined were sodium sulphide, sodium thiosulphate, potassium thiocyanate (all from POCH, Poland), cysteine, glutathione, thiourea, 2-mercaptopyrimidine, 2-thiouracil, 2-thiobarbituric acid (all from Aldrich), and 6-mercaptopurine (Koch-Light).

Apparatus. The equipment is outlined in Fig. 1. The iodine consumed in the induced reaction was monitored by a biamperometric electrode system made in the laboratory. The injection port was made from a screw cap (Quickfit) fitted with a septum as used in gas chromatography. The detector was made from glass tubing (3 mm i.d.) into which two platinum wires (0.3 mm diameter) were sealed and bent along the tube walls to a length of 10 mm as shown in Fig. 1. These parts were consolidated by transparent resin. The distance between the injection port and the detector was varied as required. The platinum electrodes were connected to a polarograph working as a potentiostat and a recorder. A potential difference of 25 mV was applied to the platinum electrodes.

General procedure. The iodine/azide solution was pumped by peristaltic pump at a known flow rate. A suitable current sensitivity was chosen and when a steady baseline was obtained, the sample was injected with a Hamilton syringe. In all experiments, the chart speed was 400 mm h^{-1}. Wastes were collected in 2 M sodium hydroxide to avoid the liberation of toxic hydrogen azide. All experiments were done at room temperature.

Results and discussion

Flow rate of the iodine/azide solution. Flow rates were optimized with an iodine/azide solution at pH 5.9 containing 4 g of sodium azide in 100 ml of 2×10^{-4} M iodine in 0.15 M potassium iodide for 10-μl injections containing 100 ng of thiosulphate. The distance between the injection port (end of syringe needle) and the detector was 20 cm. The flow rates investigated were 0.35, 0.7, 1.4, 2.8, 5.6 and 11.2 ml min^{-1}. The highest signals were obtained at 1.4 ml min^{-1}. At higher flow rates, the signals were lower because the induced reaction did not proceed to completion (which also caused irreproducibility) and because of detector inertia; at 5.6 and 11.2 ml min^{-1}, no signal was obtained. Lengthening the path between the injection port and the detector did not improve the results for high flow rates. The signal obtained at 1.4 ml min^{-1} was not significantly affected when this distance was changed between 10 cm and 30 cm, but greater lengths caused peak broadening because of sample dispersion. Peak broadening was also noticed at flow rates <1.4 ml min^{-1}. Changes in sample volume between 2 μl and 20 μl did not affect the signals; a sample volume of 10 μl was chosen for convenience.

Determination of thiosulphate. The concentration of sodium azide and the pH of the solution are known to have a great influence on the iodine

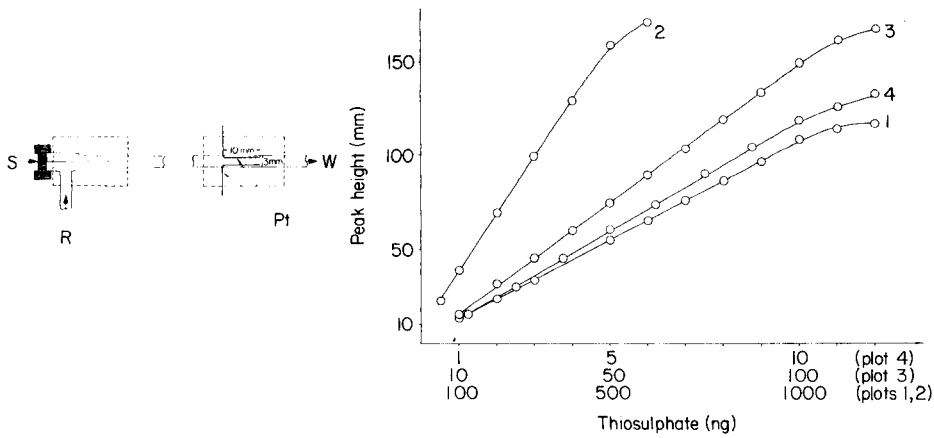

Fig. 1. Diagram of equipment: (S) Hamilton syringe; (R) pumped reagent solution; (Pt) platinum wire electrodes; (W) waste. The parts enclosed in transparent resin for stability are indicated by dashed lines.

Fig. 2. Calibration plots for thiosulphate with different concentrations of iodine: (1) 5×10^{-3} M iodine, current sensitivity 8×10^{-8} A/2.5 mm, compensation 20 μA; (2) 10^{-3} M iodine, 2×10^{-8} A/2.5 mm, 5 μA; (3) 2×10^{-4} M iodine, 1.2×10^{-8} A/2.5 mm, 2 μA; (4) 5×10^{-5} M iodine, 2×10^{-9} A/2.5 mm, 0.5 μA. Flow rate 1.4 ml min^{-1}; 10-μl injections.

consumption in the induced reaction. It was shown that increasing the sodium azide concentration in the solution above 2 g/100 ml and decreasing the pH below 5.9 improved the sensitivity of the thiosulphate determination only slightly (peak height). To check the calibrations, thiosulphate in the range 0.1—2000 ng/10 μl was determined with a reagent solution at pH 5.9 containing 2 g NaN_3/100 ml which was 5×10^{-3}, 10^{-3}, 2×10^{-4}, or 5×10^{-5} M in iodine and 0.15 M in iodide. Table 1 presents the ranges of thiosulphate concentrations for which linear relationships were found; Fig. 2 shows the calibration plots for these ranges. The lower the iodine concentration in the reagent solution, the lower the amount of thiosulphate that can be quantified. When the amount of inductor in the sample exceeded the upper limits (Table 1), negative deviations from linearity were observed (for each iodine concentration).

TABLE 1

Linear ranges for the flow-injection determination of thiosulphate

Iodine in reagent (M)	5×10^{-3}	10^{-3}	2×10^{-4}	5×10^{-5}
Linear range (ng/10 μl)	200—1000	50—500	10—110	1—10
Reproducibility[a]	500 ± 9	200 ± 7	50 ± 3	3 ± 0.4

[a]Mean (ng) and standard deviation of 7 injections for mid-range concentrations.

Figure 3 shows typical signals for 0—10 ng of thiosulphate. The limit of determination was 1 ng in 10 μl; below 0.8 ng no signals were obtained and for pure water, an increased iodine concentration was observed. Less than 1 ng of thiosulphate could be quantified in smaller samples; the lowest detectable concentration was 0.1 ng of thiosulphate in 1 μl.

Determination of other inductors. Studies similar to those described above were conducted with other rapid inductors: sodium sulphide, potassium thiocyanate, cysteine, glutathione, thiourea, 2-mercaptopyrimidine, 2-thiouracil, 2-thiobarbituric acid, and 6-mercaptopurine. Each of these has a different activity, so that the optimum conditions for their determination were established separately. In f.i.a., the various inducing activities were reflected by the different peak heights obtained for the same amount of sulphur(II) in the different compounds. It was found that all these compounds could be determined under the same conditions as thiosulphate, the differences in activity being compensated by changing the recorder settings.

2-Mercaptopyrimidine, 2-thiouracil, 2-thiobarbituric acid, and 6-mercaptopurine could be determined at concentrations of $\geqslant$1 ng/10 μl (6-mercaptopurine is shown in Fig. 4) and sulphide, cysteine, glutathione, and thiourea at $\geqslant$2 ng/10 μl. When the compound possessed very high inducing activity, the accurate determination of subnanogram amounts was possible (Fig. 4, plot 3).

Thiocyanate cannot be determined under these conditions because the induced reaction is inhibited by the iodide present [12] and there is no signal. Application of the reaction without iodide makes it possible to detect 1 ng/10 μl but the baseline is unstable, increasing with time, because the iodine concentration is decreased by hydrolysis.

Accuracy of the determinations. The results obtained for known amounts of the inductors were evaluated statistically. Calibration plots were prepared

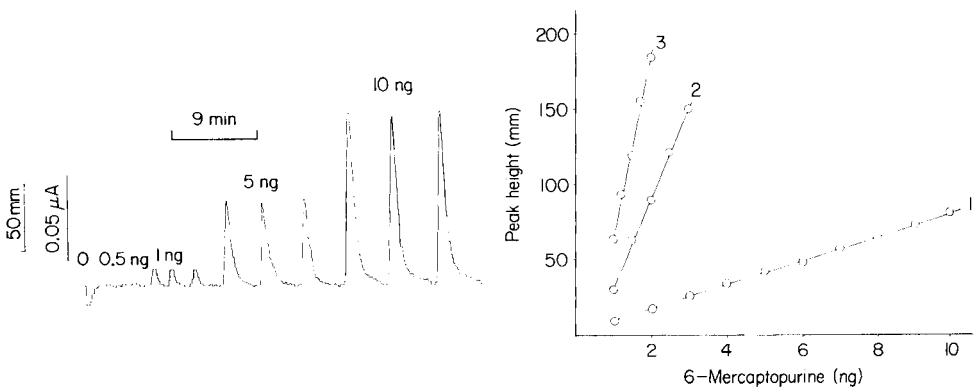

Fig. 3. Recorded peaks for thiosulphate. For reaction conditions, see Fig. 2, plot 4.

Fig. 4. Calibration plots for 6-mercaptopurine with 2×10^{-4} M iodine in the reagents. Current sensitivity: (1) 6×10^{-8} A/2.5 mm; (2) 12×10^{-9} A/2.5 mm; (3) 6×10^{-9} A/2.5 mm. Flow rate 1.4 ml min^{-1}; 10-μl injections.

TABLE 2

Determination of thiosulphate in presence of sulphite (Conditions: 2×10^{-4} M I_2 in 0.15 M KI, pH 5.9, with and without 2 g NaN_3/100 ml; flow rate 1.4 ml min^{-1}; current sensitivity 4×10^{-8} A/2.5 mm)

Reduction reaction		Induced reaction		
Sulphite		Thiosulphate		Thiosulphate + sulphite
Taken (ng)	Peak height (mm)	Taken (ng)	Peak height (mm)	Peak height (mm)
1000	13 ± 1	22.5	22 ± 1	36 ± 2
2000	31 ± 2	22.5	22 ± 1	54 ± 3
1000	13 ± 1	45	43 ± 2	57 ± 3
2000	31 ± 2	45	43 ± 2	76 ± 4

on the basis of triple measurements on at least eight concentrations of the test compound. The linear ranges were similar to those shown in Table 1 for thiosulphate; the correlation coefficients for the linear ranges were >0.99. Relative standard deviations were 20% for 1 ng of 6-mercaptopurine or 2-thiobarbituric acid, 15% for 2 ng of 2-thiouracil or 2-mercaptopyrimidine, and 13% for 3 ng of sulphide, cysteine, glutathione, or thiourea (n = 5) when the concentrations were read from these plots.

Selectivity. Inductors with long induction times do not interfere with the determination of the above-mentioned compounds. The influence of compounds that reduce iodine but do not induce the iodine/azide reaction, can be eliminated by evaluating the difference of the peak heights obtained in the induced and reduction reactions. The reduction reaction is evaluated under the same conditions as the induced reaction except that azide is omitted from the pumped solution. An example is the determination of thiosulphate in the presence of sulphite (Table 2). When the amount of sulphite in the sample is >100 times the amount of thiosulphate, a separate standard plot is needed. The presence of a large amount of sulphite in the sample considerably decreases the iodine concentration in the reaction zone so that the induced reaction conditions become significantly different from those pertaining to the absence of sulphite; a positive deviation from linearity was observed.

The author thanks Prof. Z. Kurzawa for his encouragement and helpful discussions. This work was done within the MR.I-32 project coordinated by the Institute of Chemistry, Warsaw University.

REFERENCES

1 Z. Kurzawa, Chem. Anal., 5 (1969) 551.
2 Z. Kurzawa and J. Kurzawa, Chem. Anal., 19 (1974) 755.
3 Z. Kurzawa, H. Matusiewicz and K. Matusiewicz, Chem. Anal., 19 (1974) 1175.
4 H. Weisz, W. Meiners and G. Fritz, Anal. Chim. Acta, 107 (1979) 301.

5 S. Pantel, Anal. Chim. Acta, 152 (1983) 215.
6 J. Kurzawa, Quim. Anal., in press.
7 N. Kiba, Talanta, 28 (1981) 115.
8 W. Jedrzejewski and W. Ciesielski, Chem. Anal., 26 (1981) 743.
9 W. Puacz and Z. Kurzawa, Mikrochim. Acta, II (1978) 263.
10 Z. Kurzawa, J. Kurzawa and Z. Swit, Chem. Anal., 21 (1976) 791.
11 N. Kiba and M. Furusawa, Talanta, 23 (1976) 637.
12 Z. Kurzawa, Chem. Anal., 5 (1960) 741.

Analytica Chimica Acta, 173 (1985) 349—353
Elsevier Science Publishers B.V., Amsterdam — Printed in The Netherlands

Short Communication

COULOMETRIC TITRATION OF SULPHIDE WITH MERCURY(II) IN AN AMMONIACAL BUFFER

J. L. PISÓN GARCÉS, L. M. POLO DÍEZ* and C. AVELLANAL CALZADILLA

Department of Analytical Chemistry, Faculty of Chemistry, Complutense University, 28040 Madrid (Spain)

(Received 19th November 1984)

Summary. An accurate method is described for the coulometric titration of low sulphide concentrations (8×10^{-5}—8×10^{-3} M) with mercury(II) in a pH 9 ammoniacal buffer at room temperature. The electrochemical reactions involved are explained. Cyanide does not interfere at cyanide/sulphide ratios below 3. Accurate precise results were obtained for a lithopone sample.

Many methods, often indirect, are available for the determination of sulphide in small concentrations [1]. Edwin et al. [2] developed a coulometric titration of sulphide with electrochemically generated mercury(II) in potassium hydroxide medium using a mercury pool working electrode. However, a temperature of 80°C was necessary in order to minimize adsorption phenomena and to attain suitable rates for the chemical reactions involved; the mechanisms of the reactions were not very clear.

In the present communication, an accurate selective method is proposed for the coulometric titration of sulphide with electrogenerated mercury(II), in an ammonium nitrate/ammonia buffer solution at room temperature. Results are fully explained on the basis of the electrode reactions involved.

Experimental

Apparatus. An Amel-831 coulometer was used for the constant-current coulometric titrations. Current/potential curves were recorded by using an Amel-551 potentiostat with an Amel-560 interface, an Amel function generator and a Hewlett-Packard 7035B x/y recorder. A Metrohm E-516 pH meter/millivoltmeter was used, to measure the pH and to follow the potential of an amalgamated gold indicator electrode during the titration. A thermostatted Metrohm EA-875-20 electrolytic cell was used.

Electrodes. The working electrode (anode) for the coulometric titration was a pool of 25 ml of twice-distilled mercury in the electrolytic cell; its surface area was 10.7 cm^2. A dropping mercury electrode (DME) with a drop time of 3 s was used to obtain the polarograms of solutions containing sulphide in order to study the electrochemical reactions involved. The amal-

gamated gold indicating electrode (surface area 25 mm^2) for the coulometric titration was obtained by dipping a cylindrical gold electrode into twice-distilled mercury for 15 min.

An auxiliary electrode consisting of a platinum microelectrode dipped in a small tube with a porous fritted bottom containing a saturated sodium nitrate solution was used as the counter electrode (cathode) in the coulometric circuit and as a third electrode in the potentiostatic circuit. A conventional saturated calomel electrode (SCE) served as reference electrode. All experimental potential are referred to this electrode.

Reagents. The 0.198 M sodium sulphide stock solution was standardized by potentiometric titration, in a 1 M ammonia/ammonium nitrate buffer at pH 10, against: (a) a standard silver nitrate solution with a silver indicator electrode, and (b) a standard mercury(II) nitrate solution with the amalgamated gold electrode. The above-mentioned ammoniacal buffers were prepared at pH 9 and 10. A 0.5 M potassium cyanide solution was used to study the cyanide interference. All the chemicals used were of analytical grade.

Lithopone standard sample. The lithopone sample had the following certified composition: 29.5 ± 0.16% ZnS (9.71% in sulphide), 69.8 ± 0.30% $BaSO_4$ and 0.66 ± 0.18% ZnO.

Coulometric titration of sulphide. Pure nitrogen was bubbled for 15 min in the usual way through 25 ml of the ammoniacal buffer solution at pH 9 in the electrolytic cell. Then, 25 ml of twice-distilled mercury and an aliquot of the sulphide sample solution (a few μl to obtain sulphide concentrations in the range 7.9×10^{-5}—7.9×10^{-3} M) were added. The solution was stirred by using a helix stirrer and the potential of the amalgamated gold electrode was measured. For the coulometric titration, a constant current (in the 5—100 mA range) was applied to the mercury pool anode and the potential of the indicator electrode was measured every 1—20 s. The end-point of the titration was evaluated from the sigmoidal potential/time curve. Titrations were also done in the ammoniacal buffer solution at pH 10, but at 80°C.

Determination of sulphide in the lithopone sample. A suitable amount of the lithopone sample, accurately weighed, was heated in 9 M sulphuric acid and the hydrogen sulphide evolved was collected in the ammoniacal buffer (pH 9). The concentration of sulphide was determined as indicated above.

Results and discussion

Current/potential curves during the coulometric titration. Sulphide in the ammoniacal buffer at pH 9 shows two oxidation waves at the dropping mercury electrode (curves 1 and 2, Fig. 1). The first wave, having $E_{1/2} \approx -0.75$ V, not referred to previously [2], does not conform with Fick's law. The wave involves an exchange of one electron per sulphide ion and, according to the results shown below, the electrode reaction seems to be

$$Hg^0 + 2\,HS^- + 2\,NH_3 - 2e^- \rightarrow HgS_2^{2-} + 2\,NH_4^+ \qquad (1)$$

The height of the combined waves increases linearly with sulphide concentra-

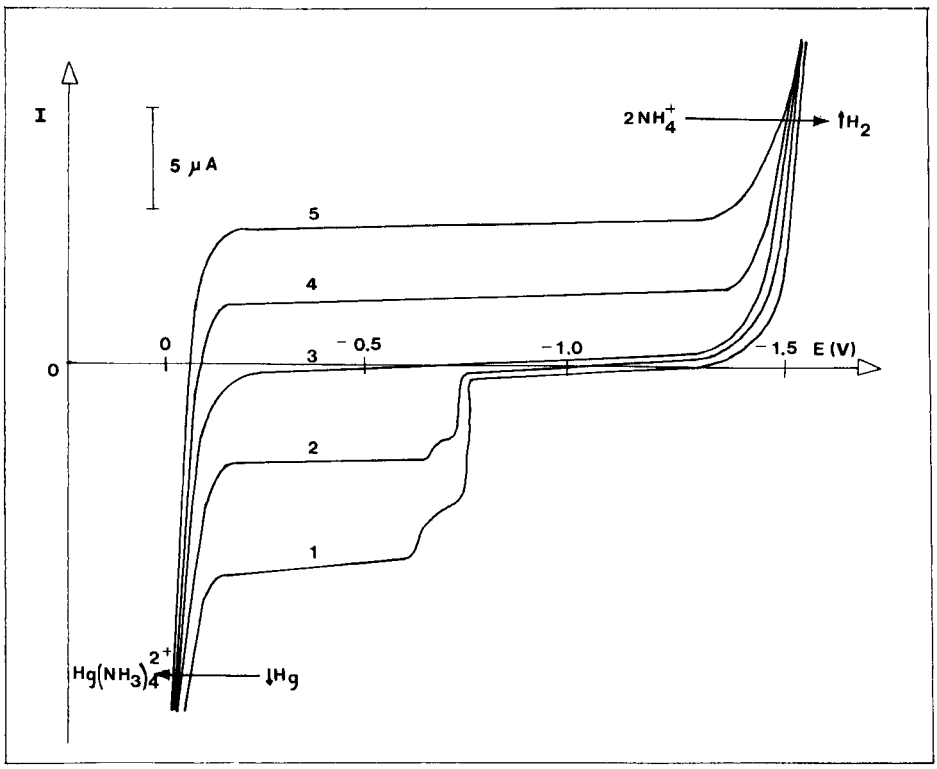

Fig. 1. Current/voltage curves during the coulometric titration. Conditions: 1 M NH_4NO_3/NH_3 buffer, pH 9, 25°C; total sulphide concentration 7.92×10^{-4} M; electrolysis current 40 mA. Titration time (s): (1) initial; (2) 25; (3) 50—100; (4) no; (5) 120.

tion and involves two electrons per sulphide ion corresponding to the reaction

$$Hg^0 + HS^- + NH_3 - 2e^- \rightarrow HgS + NH_4^+ \quad (2)$$

Results obtained in 0.2 M phenol at pH 11 and in potassium hydroxide at pH 13 showed somewhat similar trends, but neither the reduction of the dithiomercurate(II) ion, HgS_2^{2-}, nor the oxidation of the mercury electrode in the presence of this species was observed. Probably, at such pH, the HgS_2^{2-} species is unstable at low concentrations, decomposing by dilution as it diffuses from the electrode. These two waves were observed only when relatively high sulphide concentrations were present, e.g., a solution obtained by adding sodium sulphide to mercury(II) sulphide until total solubilization was obtained at about 2×10^{-2} M.

The reduction of the ammine-mercury(II) complex did not appear until electrolysis times twice those needed to attain the equivalence point corresponding to the formation of the dithiomercurate(II) ion (curve 2). This is probably due to reactions between this complex and either the dithiomer-

curate(II) ion or the sulphide ions coming from its decomposition, which produce a mercury sulphide precipitate, experimentally observed, according to reactions such as

$$Hg(NH_3)_4^{2+} + HgS_2^{2-} \rightarrow 2\ HgS + 4\ NH_3 \quad (3)$$

$$Hg(NH_3)_4^{2+} + HS^- \rightarrow HgS + 3\ NH_3 + NH_4^+ \quad (4)$$

Reproducible potential jumps (of about 550 mV, from 600 to 50 mV in 10^{-4} M sulphide) were obtained at the end-point of the coulometric titration. As can be deduced from Fig. 1, any mercury electrode may be used as indicator electrode to detect the end-point of the coulometric titration; an amalgamated gold electrode was used here because of its well known advantages over a mercury ring electrode.

Determination of sulphide in prepared sample solutions. The procedure specified under Experimental was applied to several samples prepared from the stock sulphide solution under different experimental conditions, as shown in Table 1. Results obtained at pH 9 and room temperature for sulphide concentrations above about 10^{-4} M show very good agreement between the sulphide concentrations added and found. This accuracy indicates that current efficiency is close to 100% under these working conditions. It also confirms that the reaction (1) proposed for the oxidation of the mercury electrode involves one electron per sulphide ion, according to the Faraday law.

At higher pH values and room temperature, negative errors are caused by the slowness of the chemical reactions involved in the titration. Significant amounts of the ammine-mercury(II) complex remain at the theoretical

TABLE 1

Coulometric titration of sulphide in ammoniacal buffers under different conditions

Constant current (mA)	t_1[a] (s)	Sulphide (10^{-5} mol/25 ml)		t_2[c] (s)
		Added	Found[b]	
pH 9 at 25°C				
100	20	19.8	19.79(0.10)	191.0
40	5	1.98	1.973(0.006)	47.6
20	10	1.98	1.980(0.002)	95.5
5	5	0.198	0.222(0.004)	42.9
pH 10 at 80°C				
100	20	19.8	19.82(0.13)	191.3
20	10	1.98	1.972(0.006)	95.1
5	5	0.198	0.197(0.0003)	38.1
1	15	0.158	0.155(0.0009)	150.0

[a]Time between successive potential measurements. [b]Mean of five determinations with standard deviation in parentheses. [c]Time at the equivalence point.

equivalence point, as indicated by the reduction wave of this complex, which disappeared after the system had been left for about two hours. At higher temperatures, around 80°C, this problem was minimized (Table 1) although it remained at pH values higher than 10; e.g., in a phenol/phenolate buffer at pH 11, the coulometric titration was not viable.

Effect of dissolved oxygen. The presence of dissolved oxygen in the test solution leads to oxidation of the mercury pool anode:

$$2\ Hg + O_2 + 2\ H_2O + 8\ NH_3 \rightarrow 2\ Hg(NH_3)_4^{2+} + 4\ OH^-$$

causing negative errors in the titration. It was observed experimentally that a wave corresponding to the reduction of this mercury complex at the DME appeared when a non-deaerated ammoniacal buffer solution (pH 9) was kept in contact with the working electrode. It is thus necessary to remove the dissolved oxygen by bubbling with nitrogen in the usual way, before the mercury pool is placed in the cell. Similar results were obtained in ammoniacal buffer of pH 10.

Effect of the cyanide concentration. According to the literature, the most important interference on sulphide determinations comes from cyanide. Current/voltage curves of 7.92×10^{-4} M sulphide solutions with increasing concentrations of cyanide showed that the oxidation wave of mercury in the presence of cyanide occurs at more positive potentials than in the presence of sulphide. From a qualitative point of view, cyanide seems to interfere only for cyanide/sulphide ratios above 3, which produce significant distortions on the oxidation wave of mercury to form the mercury(II) complex. Quantitatively, for the above concentration of sulphide, significant errors were not observed for cyanide concentrations in the range 9.0×10^{-7}—9.0×10^{-4} M, which corresponds to cyanide/sulphide ratios below about 1. A relative error of +1.5% was observed for 5.0×10^{-3} M cyanide, i.e., a cyanide/sulphide ratio of about 6, which means that sulphide can be determined in the presence of relatively large amounts of cyanide without large errors.

Determination of sulphide in the lithopone sample. The content of sulphide in the lithopone sample was determined by applying the procedure detailed under Experimental. The sulphide concentration in the tested solution was 1.01×10^{-3} M. The mean value of five determinations was 9.71% of sulphide with a standard deviation of 0.05%. The agreement of this value with the certified value shows the validity of the proposed method.

REFERENCES

1 See, e.g., B. Morris, M. Jacobs, M. Braverman and S. Hochheiser, Anal. Chem., 29 (1957) 1349.
2 P. Edwin, E. P. Przybylowicz and L. B. Rogers, Anal. Chem., 30 (1958) 1064.

Analytica Chimica Acta, 173 (1985) 355—360
Elsevier Science Publishers B.V., Amsterdam — Printed in The Netherlands

Short Communication

COMPUTER GRAPHICS-ASSISTED APPLICATIONS OF FIRST-ORDER CHEMICAL KINETICS IN THE DETERMINATION OF INORGANIC COMPLEXES

LEE HIN-FAT*, HIN-CHEUNG LEE, WING-YI WU and WING-YEE KWONG
Hong Kong Baptist College, 224 Waterloo Road, Kowloon (Hong Kong)
HIN-KWEN LI
Hong Kong Buddhist College, 325 Lai Chi Kok Road, Kowloon (Hong Kong)
(Received 26th July 1984)

Summary. Computer graphics-assisted applications of first-order chemical kinetics are applied to absorbance data from spectrophotometric measurements of the decomposition of di-μ-hydroxobis[dioxalatocobaltate(III)] (at pH 4.0) and trioxalatocobaltate(III) (in 1.0 M perchloric acid) in order to estimate the purity of the complexes. A program called KINFIR is used.

In recent years work has continued in applying chemical kinetics to analyses of various materials [1—4]. In one type of application, advantage is taken of the relationship between rate of reaction (or differential rate) and concentration of reactants; in the other, catalysis by trace amounts of certain species gives perceptible differences in reaction rates. In most of these analytical applications, absorbances of reactants are measured at fixed times. However, the reaction order with respect to the reactant concerned must be found before the rate constant and the initial concentration of the reactant can be computed. Based on the initial concentration found, the purity of material can be determined. Kinetic plotting by hand in order to find the reaction order is lengthy and tedious, but these disadvantages can be removed by using a microcomputer. Computers have been used generally in chemical kinetics but they have not been applied in chemical analysis of the kind presented here [5—8]. The present communication describes the application of a program written in BASIC for use in making such plots. The determination of two inorganic complexes by means of their thermal decomposition kinetics is used to demonstrate the application.

Experimental

Reagents and apparatus. All chemicals were of analytical grade, and the solutions for kinetic analysis were kept in a thermostat. The pH of the solutions was measured with an Orion research digital pH/mV meter (type 611) at the end of the reaction. All absorbances were measured with a Shimadzu UV-240 recording spectrophotometer. The temperature of the cell holder

0003-2670/85/$03.30

was maintained constant with a Haake FE circulating thermostat. A NEC PC 8801B microcomputer system was used for the graphics and computation; it consists of a central processor unit with 64 kbyte of memory, floppy disk drive unit, printer and monitor.

Potassium trioxalatocobaltate(III) and di-μ-hydroxo-bis[dioxalatocobaltate(III)] were prepared and analysed as described by Palmer [9]. The results obtained confirmed their formulae to be $K_3Co(C_2O_4)_3 \cdot 3\frac{1}{2}H_2O$ (found: Co = 11.6 ± 0.2%; oxalate = 52.5 ± 0.2%) and $K_4CO_2(C_2O_4)_4(OH)_2 \cdot 3H_2O$ (found: Co = 16.4 ± 0.1%; oxalate = 49.1 ± 0.2%). The former exhibits absorbance maxima at 425 nm (ϵ = 219 l mol^{-1} cm^{-1}) and 601 nm (ϵ = 169 l mol^{-1} cm^{-1}), while the latter shows only one maximum at 608 nm (ϵ = 260 l mol^{-1} cm^{-1}). These results are in close agreement with earlier data [10]. An aqueous 4.0 M sodium perchlorate solution was used; its concentration was determined by ion exchange (Amberlite IR-120) and titration of the alkali produced. Perchloric acid (4.0 M) was prepared from the concentrated acid and standardized with 0.1 M sodium hydroxide. Acetate buffer was prepared by mixing 100 ml of 2.0 M sodium acetate and 100 ml of 6.0 M acetic acid and diluting to 1 l.

Purity of di-μ-hydroxo-bis[dioxalatocobaltate(III)]. An accurately weighed sample of the complex was dissolved in 15 ml of water in a 50-ml volumetric flask, 12.0 ml of 4.0 M sodium perchlorate and 10 ml of acetate buffer were added with shaking, and the mixture was diluted to 50 ml. The reaction was followed to completion spectrophotometrically at 608 nm, with absorbances measured every 4 min.

Purity of trioxalatocobaltate(III). An accurately weighed sample of the complex was dissolved in 15 ml of water in a 50-ml volumetric flask, 12.5 ml of 4.0 M perchloric acid was added, and the mixture was diluted to 50 ml. The reaction was followed spectrophotometrically at 425 nm, with absorbances measured every 4 min until the end of the reaction.

Results and discussion

Kinetic principle. Complexes of cobalt(III), rhodium(III) etc. are chemically inert [11]. The decomposition of di-μ-hydroxo-bis[oxalatocobaltate(III)] giving cobalt(II) has been found to be first order in the complex. The following mechanism has been suggested [12]

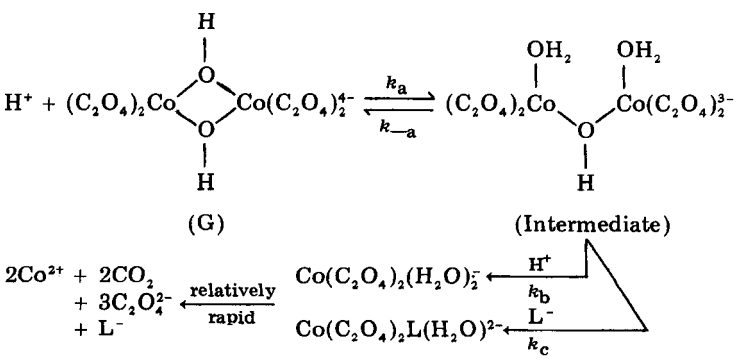

where L represents the base form of the buffer used, i.e., the acetate ion. By applying a steady-state approximation to the intermediate indicated above and integrating, $\ln[G] = -k_{obs}t + D$ is obtained, where $k_{obs} = (k_a k_b + k_a k_c[L])/(k_{-a} + k_b + k_c[L])$, and D is the integration constant. From this equation, it can be seen that a plot of $\ln[G]$ vs. t should be linear; $-k_{obs}$ is the gradient and the integration constant D is the intercept.

The $Co(C_2O_4)_3^{3-}$ complex ion has been found to decompose in accordance with the following mechanism [12]

$$Co(C_2O_4)_3^{**3-} \underset{k_{-1}}{\overset{k_1}{\rightleftharpoons}} Co(C_2O_4)_2^{**}(C_2O_4)^*(H_2O)^{3-}$$

(A) (B)

$$Co(C_2O_4)_3^{**3-} + Co(C_2O_4)_2^{**}(C_2O_4)^*(H_2O)^{3-} \xrightarrow{k_2} 2Co^{2+}aq + 5C_2O_4^{2-} + 2CO_2$$

where superscripts ** and * represent bidentate and monodentate oxalate binding, respectively. By applying a steady-state approximation to intermediate B and integrating, the result is $\ln[A] - k_{-1}/k_2/[A] = -k'_{obs}t +$ integration constant, where k'_{obs} represents $2k_1$. Experiments showed that plots of $\ln[A]$ vs. t were linear up to 80% reaction; thus the reaction is first order in the complex.

During these reactions, the total absorbance $A_t = \epsilon_{Co(III)}[Co(III)]_t + \epsilon_{Co(II)}[Co(II)]_t$. Also $[Co(III)]_0 = [Co(III)]_t + [Co(II)]_t$ and $A_\infty = \epsilon_{Co(II)}[Co(II)]_\infty = \epsilon_{Co(II)}[Co(III)]_0$ or $A_\infty = \epsilon_{Co(II)}[Co(III)]_t + \epsilon_{Co(II)}[Co(II)]_t$. Therefore, $(A_t - A_\infty) = [\epsilon_{Co(III)} - \epsilon_{Co(II)}][Co(III)]_t$, where $\epsilon_{Co(III)}$ and $\epsilon_{Co(II)}$ are the molar absorptivities for the complex and for the product of decomposition, respectively, $[Co(III)]_t$ and $[Co(II)]_t$ are the concentrations of the complex and product of decomposition at time t, $[Co(II)]_\infty$ is the concentration of the decomposition product at the end of the reaction, and $[Co(III)]_0$ is the initial concentration of the complex. The last equation gives:

$$\ln(A_t - A_\infty) = \ln[\epsilon_{Co(III)} - \epsilon_{Co(II)}] + \ln[Co(III)]_t$$

or the initial concentration $[Co(III)]_0$ of the complex can be calculated from:

$$[Co(III)]_0 = \exp\{\ln[A_{t=0} - A_\infty] - \ln[\epsilon_{Co(III)} - \epsilon_{Co(II)}]\}$$

and the % purity of the complex is therefore $[Co(III)]_0 \times$ relative molecular mass of complex $\times 100$/sample weight.

Computer program for kinetic plotting and computing. The program called KINFIR written in BASIC contains approximately 120 statements. Details are available from the authors. The general flow of this program is illustrated in Fig. 1. The numbers in the Figure are the block numbers. The blocks are self-explanatory except for the following [13]: (2) input data which means time → A(array), $\log(A_\infty - A_t)$ → B(array); (4) sort out minimum and maximum values in x and y scales; (5 and 6) set up the decision to explore whether automatic range or manual input minimum and maximum range is

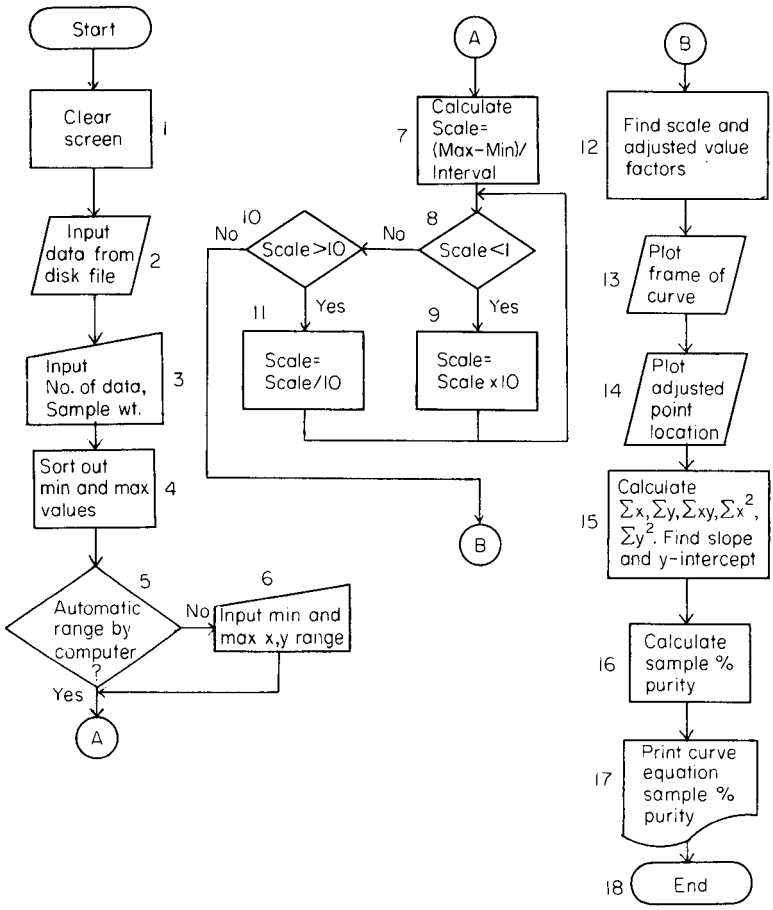

Fig. 1. Flowchart for KINFIR program.

adopted; (7) calculate the scale range from the maximum values of x and y minus the minimum values of x and y, then divide by 10 in order to have 10 scales in the plot later; (12) establish the scales and adjustment scale factors so that the experiment points can be located properly inside the frame on the screen; (14) plot the actual experiment points; (15) use least-squares fit technique.

This program was used to treat all data obtained from kinetic determination of the two complexes. The results are given in Table 1. Use of this program on the 8801B system for the decomposition of di-μ-hydroxo-bis-[dioxalatocobaltate(III)] at pH 4.06 generated Fig. 2 as part of the output.

TABLE 1

Kinetic determination of inorganic complexes (35° C, 1.00 M $NaClO_4$)

pH	Taken (g)	Rate constant k_{obs} ($\times 10^{-2}$ min^{-1})	Found (g)	Purity (%)
$K_4Co_2(C_2O_4)_4(OH)_2 \cdot 3H_2O$				
4.05	0.1108	5.99	0.1096	98.9
4.02	0.1271	6.08	0.1257	98.9
4.06	0.1275	6.12	0.1274	99.9
4.02	0.1343	6.09	0.1331	99.1
$K_3Co(C_2O_4)_3 \cdot 3\frac{1}{2}H_2O$[a]				
	0.0788	2.13	0.0780	99.0
	0.0791	2.15	0.0788	99.6
	0.0782	2.11	0.0774	99.0
	0.0613	2.19	0.0606	98.9

[a] 1.0 M $HClO_4$ solution; in this case k'_{obs} (= $2k_1$) is used.

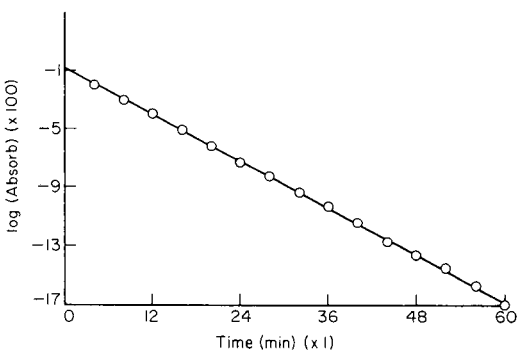

Fig. 2. Complete plot of $\ln(A_t - A_\infty)$ vs. time for the decomposition of di-μ-hydroxo-bis[dioxalatocobaltate(III)] at pH 4.06 (acetate buffer), 35° C and ionic strength 1.00 M (perchlorate). The initial concentration of the complex was 3.566×10^{-3} M. The equation of the line is $y = -0.0266x - 0.0891$; k is thus 0.0612 min^{-1} and the purity of the sample is 99.92%.

REFERENCES

1 A. Aleksiev and K. Mutafchev, Anal. Lett., 16 (1983) 769.
2 J. L. Ferrer-Herranz and D. Perez-Bendito, Anal. Chim. Acta, 132 (1981) 157.
3 L. Ballesteros and D. Perez-Bendito, Analyst (London), 108 (1983) 443.
4 M. Ternero, F. Pino, D. Perez-Bendito and M. Valcarcel, Michrochem. J., 25 (1980) 102.
5 D. D. Perrin, Talanta, 24 (1977) 339.
6 J. L. Hogg, J. Chem. Educ., 51 (1974) 109.
7 P. B. Kelter and J. D. Carr, Anal. Chem., 51 (1979) 1828.
8 M. L. Nase and K. Seidman, J. Chem. Educ., 60 (1983) 734.
9 W. G. Palmer, Experimental Inorganic Chemistry, Cambridge University Press, 1954.

10 A. W. Adamson, H. Ogata, J. Crossman and R. Newbury, J. Inorg. Nucl. Chem., 6 (1958) 319.
11 J. Burgess, Metal Ions in Solution, Ellis Horwood, England, 1981.
12 Lee Hin-Fat and W. C. E. Higginson, J. Chem. Soc. A, (1971) 2589.
13 J. B. Morton, Introduction to BASIC, Pitman, London, 1979.

Analytica Chimica Acta, 173 (1985) 361—365
Elsevier Science Publishers B.V., Amsterdam — Printed in The Netherlands

Short Communication

DETERMINATION OF DISSOLVED ARSENIC IN WATERS AT $\mu g\ l^{-1}$ LEVELS BY PRECIPITATION AND ENERGY-DISPERSIVE X-RAY FLUORESCENCE SPECTROMETRY

N. S. C. BECKER, V. M. MCRAE[a] and J. D. SMITH*

Marine Chemistry Laboratory, Department of Inorganic Chemistry, University of Melbourne, Parkville 3052, Victoria (Australia)

(Received 6th November 1984)

Summary. Arsenic is precipitated as magnesium ammonium arsenate with magnesium ammonium phosphate as carrier. The precipitate is collected on a glass-fibre filter and arsenic is measured by energy-dispersive x-ray fluorescence spectrometry with a silver secondary target. With 200-ml water samples and 100-s counting times, the limit of detection is 0.7 μg As l^{-1}. The method is applicable to all types of natural water including sea waters.

Gravimetric methods are of no value for the determination of traces of elements but the classical methods still find use in this field for preconcentration and for avoidance of interferences. The problems of interference are usually not serious in x-ray fluorescence spectrometry (x.r.f.) whereas preconcentration is often important. The classical gravimetric determination of arsenic by precipitation as magnesium ammonium arsenate [1] can be adapted to provide preconcentration. The arsenic compound is precipitated in the presence of a magnesium salt by addition of ammonia; phosphate forms the related magnesium ammonium phosphate. If excess of phosphate is added to solutions containing microgram amounts of arsenic, the magnesium ammonium phosphate precipitated acts as carrier. The method is attractive in that x-ray fluorescence spectrometry is very selective for arsenic, and provides a simple alternative to the various methods dependent on atomic absorption spectrometry. The standards are stable, are easily stored and can be repeatedly used. The procedure can be used for determination of arsenic in a wide range of natural waters.

Experimental

Reagents and filtration equipment. Distilled-deionized water was used in preparation of solutions. Analytical-grade concentrated ammonia, concentrated hydrochloric acid and ammonium chloride were used. Arsenic(III)

[a]Present address: Department of Physical Chemistry, University of Melbourne.

0003-2670/85/$03.30

chloride standard solution for atomic absorption spectroscopy (BDH Chemicals) was used as the arsenic standard solution (1000 mg l^{-1}).

For the magnesium chloride solution (10 g Mg l^{-1}), dissolve 42 g of magnesium chloride hexahydrate in water and dilute to 500 ml. For the phosphate solution (1 g P l^{-1}), dissolve 2.2 g of potassium dihydrogen phosphate in water and dilute to 500 ml.

Precipitates were collected on 2.5-cm diameter Gelman Type A-E glass-fibre filters, using a glass vacuum filtration unit exposing a filter area of 3.14 cm^2. The polyester film was Spectro-film (<4 μm thick; Somar Laboratories, New York).

Precipitation procedure. Transfer 200 ml of filtered acidified water sample to a 400-ml beaker. With continuous stirring add 1 ml of hydrogen peroxide solution (30% w/v), 20 ml of the magnesium chloride solution and enough ammonia to make the solution alkaline (about pH 10). Add 3.5 g of ammonium chloride, continue stirring until it dissolves, and allow the solution to stand for at least 5 h, preferably overnight. Acidify the solution with 5 ml of concentrated hydrochloric acid, and add 5 ml of aqueous 7% (w/v) EDTA (disodium salt) solution and 3 ml of the phosphate solution. Slowly add concentrated ammonia solution until the pH is about 11 (this requires about 10 ml). After an hour, collect the precipitate by filtration on a glass-fiber filter. Dry the filter and precipitate at 110° C for 2 h. Mount the filter between two layers of polyester film stretched flat in a 35-mm slide mount and store in a desiccator.

Preparation of standards. Prepare calibration solutions by adding aliquots of the arsenic(III) standard solution to 200-ml volumes of water, and include duplicate blanks. Treat these solutions as described above. The precipitates on these filters are stable and may be used repeatedly with no deterioration in the x-ray beam.

X-ray fluorescence spectrometry. Mount the filter holders in the sample changer of the x-ray spectrometer with the precipitate facing the x-ray source and detector. Measure the integrated fluorescence intensity in the arsenic K_α peak and subtract the intensity of the blank in the same region. Calculate the amount of arsenic in each sample by comparison with the standards.

In this work, a Kevex 0700 series energy-dispersive x-ray spectrometer was used with a rhodium primary target operated at 60 kV and 2 mA and a silver secondary target. The samples were counted for 100 s live time and the arsenic K_α peak was integrated over the range 10.38—10.70 keV.

Results and discussion

There are various methods for precipitating arsenic from solution including the use of hydrated iron(III) oxide and dithiocarbamates. The method described here has the advantages of being highly selective for arsenic, and giving a stable precipitate that is easily collected and adheres well to the filter.

The silver secondary target gives efficient excitation of arsenic, and background intensities much lower than those resulting from use of direct

excitation. The low background aids in achieving the low limit of detection [2]. The x-ray spectrum is remarkably simple with the arsenic K_α peak at 10.543 keV. No interference was observed, and the only possible overlap is from the lead L_α peak at 10.549 keV. The presence of lead would be recognised by the simultaneous presence of its L_β peak clearly separated at 12.620 keV.

The precipitation of magnesium ammonium arsenate and magnesium ammonium phosphate has been used analytically for over a century [3]. The stoichiometric precipitates form only if there is an excess of ammonium chloride over magnesium ion (magnesia mixture) and in a limited pH range (ca. 9.5—10.6) [4]. Optimum arsenic recovery was obtained with 3.5 g of ammonium chloride and 0.2 g of magnesium, giving a mole ratio of 8:1. For sea water (1.3 g Mg l^{-1}), no magnesium need be added. For highly saline waters containing more than 300 mg of magnesium in the 200-ml aliquot, the amount of ammonium chloride should be increased to keep the mole ratio at 8:1. A large excess of ammonium chloride did not affect arsenic recovery. During the precipitation, the pH must be controlled as the magnesium ammonium arsenate and phosphate are significantly soluble at pH less than 9.4, whereas at pH values above 10.6 there can be formation of basic magnesium arsenate and magnesium hydroxide. After standing overnight the solution is acidified to dissolve any metal hydroxides that might have precipitated, and EDTA is added to keep these metals in solution when the pH is raised after addition of the phosphate. The solubilities of the magnesium ammonium arsenate and phosphate decrease with increasing pH, and a pH of about 11 is needed to maximize arsenic recovery. The precipitate forms rapidly and may be collected after about an hour. It is not necessary to wash the precipitate on the filter; this eliminates a major source of loss in the gravimetric procedure.

Optimum phosphate concentration. The amount of phosphate added as carrier was varied and the effect on arsenic recovery noted. Six 200-ml solutions, each containing 10 μg of arsenic but different amounts of phosphate, were treated as described in the precipitation procedure. The recovery did not increase when the volume of phosphate solution added was greater than 3 ml (Table 1); the slight decrease in arsenic fluorescence intensity with greater amounts of phosphate is probably due to increasing deviation from thin-film behaviour.

Effect of sample volume. The amounts of reagents used were optimized for 200-ml sample volumes. Volumes of 100 and 200 ml containing 25 μg of arsenic gave identical (100%) arsenic recoveries; when the sample volume was

TABLE 1

Effect of added phosphate solution (1 mg ml^{-1}) on recovery of 10 μg of arsenic

Phosphate added (ml)	0.5	1.0	3.0	5.0	8.0	10.0
Arsenic peak (counts s^{-1})	6.0	44.2	63.8	58.6	57.7	57.5

increased to 400, 600 or 1000 ml, the recovery fell to 95, 84 or 64% respectively. Loss of arsenic from the higher volumes probably results from the solubility of the product, and might be overcome by increasing the amounts of reagents.

Calibration and limit of detection. A calibration prepared using 2—300 μg of arsenic (200-ml volume) was linear over the whole range (9.9—1670 counts s^{-1}). The apparent recovery of arsenic, estimated by comparison of the fluorescence intensities of arsenic in films of the precipitates and the intensities of arsenic in accurately known thin-film standards prepared as methyl cellulose films, was about 85%. This decrease in fluorescence intensity is probably due to solubility losses and to the precipitates not behaving strictly as thin films.

The limit of detection was calculated from the integrated fluorescence intensity of the background of five replicate blanks taken through the recommended procedure. Using the average background (b), and the sensitivity (m) calculated from the slope of the regression line fitted to the calibration results, the limit of detection for counting time t is $(3/m)(b/t)^{0.5}$ [5]. Sensitivity, limit of detection, and estimates of precision at three levels of arsenic are summarized in Table 2. The limit of detection would be improved by increasing the counting time; with 1000 s, the calculated limit of detection becomes 0.045 μg arsenic in 200-ml sample aliquots, or 0.2 μg l^{-1}.

Arsenic(III) and arsenic(V). The gravimetric method depends on formation of magnesium ammonium arsenate and is selective for arsenic(V). In the presence of the large amount of magnesium ammonium phosphate used as carrier in the x-ray method, some precipitation of arsenic(III) is expected. To examine this, two 100-ml solutions each containing 25 μg of arsenic(III) were prepared. One solution was analysed after the arsenic(III) had been oxidised to arsenic(V) with hydrogen peroxide; the other was analysed without this treatment. Recovery of arsenic(III) was 95% of the recovery of arsenic(V). At microgram levels, the method does not distinguish between arsenic(III) and arsenic(V), but it is recommended that hydrogen peroxide be added to sample solutions to ensure that all the arsenic is present as arsenic(V).

TABLE 2

Sensitivity, background, limit of detection, and precision for 100-s acquire times

Background	6.54 c s^{-1}
Sensitivity	5.36 c s^{-1} μg^{-1}
Limit of detection	0.7 μg l^{-1}
Precision[a]	
5 μg As	7%
10 μg As	6%
25 μg As	3%

[a]Relative standard deviation for five replicate determinations at each arsenic level.

TABLE 3

Recovery of arsenic from sea water of salinity 35

As added (μg)	0	5	10	25
As found (μg)	<0.1	4.7	9.7	25.5
Recovery (%)	—	94	97	102

Interferences. Some elements, including copper, iron, manganese and zinc, could form insoluble hydroxides under the experimental conditions, and be included in the final precipitate. Whilst these elements do not cause spectral interference, they could lead to low results for arsenic by increasing the mass of precipitate thus causing deviation from thin-film conditions. Addition of EDTA to the sample solution before precipitation prevented the precipitation of hydroxides of these elements. Up to 5 mg of iron in a 200-ml water sample caused no problems with collection of the precipitate or with x-ray counting efficiency.

The effect of salinity on arsenic determination was examined by comparing recoveries of arsenic added to sea water with the calibration obtained with distilled water. Standard additions of arsenic(III) were made to sea water (salinity 35, from Bass Strait, Victoria) that had been stored for several weeks in a polyethylene bottle to remove the naturally occurring arsenic. The added arsenic(III) was oxidised to arsenic(V) and determined as in the recommended procedure. Results of duplicate determinations (Table 3) showed recoveries of 94–102% indicating that the method is well suited to the analysis of natural waters up to the salinity of sea water.

REFERENCES

1 J. W. Mellor and H. V. Thompson, A Treatise on Quantitative Inorganic Analysis, Charles Griffin, London, 1938, p. 282.
2 D. E. Porter, X-Ray Spectrometry, 2 (1973) 85.
3 A. Levol, Ann. Chim. Phys., 17 (1846) 501.
4 L. Erdey, Gravimetric Analysis, Part 2, Pergamon, Oxford, 1965, p. 174.
5 E. P. Bertin and I. Bertin, Introduction to X-ray Spectrometric Analysis, Plenum Press, New York, 1978, p. 316.

Analytica Chimica Acta, 173 (1985) 367—372
Elsevier Science Publishers B.V., Amsterdam — Printed in The Netherlands

Short Communication

LASER FLUORIMETRY OF POLYNUCLEAR AROMATIC HYDROCARBONS BASED ON TIME-RESOLVED FLUORESCENCE DETECTION

YUJI KAWABATA, TOTARO IMASAKA and NOBUHIKO ISHIBASHI*
Faculty of Engineering, Kyushu University, Hakozaki, Fukuoka 812 (Japan)
(Received 22nd February 1985)

Summary. Three polynuclear aromatic hydrocarbons are quantified from the pre-exponential factor of the fluorescence decay curve, instead of the integrated fluorescence intensity. The slopes of the calibration plots are independent of the oxygen concentration in the solvent as predicted. Deaeration of sample solutions gives lower detection limits (around 10^{-10} M); the extent of improvement depends on the fluorescence lifetime.

Airborne particulates produced in combustion processes are emitted into the atmosphere from various industrial plants. They may contain various polynuclear aromatic hydrocarbons (PAHs), which are known to be strongly carcinogenic. Fluorimetry is an attractive method for quantifying traces of PAHs, most of which are fluorescent. The PAHs often have long fluorescence lifetimes, so that fluorescence is readily quenched by oxygen dissolved in the solution [1—3]. The fluorescence intensity measured under air-saturated conditions can be much smaller than that measured under deaerated conditions. Thus, accurate and sensitive determinations can be achieved only by complete deaeration of sample solutions. Freeze/pump/thaw cycles remove oxygen completely, but they are tedious and sometimes change the concentration of the sample by vaporization of the solvent. Removal of oxygen is easily achieved by bubbling nitrogen, but complete removal of dissolved oxygen can be time-consuming and the degree of deaeration may not be identical in each run. Incomplete removal of oxygen can cause quite serious errors in the determination of PAHs, so that new approaches are necessary.

The integrated fluorescence intensity (F) can be expressed by the product of the concentration (c) and the fluorescence quantum yield (ϕ) of a sample: $F = K\phi c$, where K is a constant. If the fluorescence decay curve can be expressed by a single exponential function, then the quantum yield can be represented by the observed lifetime (τ_m) and the intrinsic lifetime (τ_0): $\phi = \tau_m/\tau_0$. Thus $F = K\tau_m c/\tau_0$. The fluorescence intensity I_t at time t is expressed by $I_t = I_0 \exp(-t/\tau_m)$, where I_0 is the pre-exponential factor of the decay curve, and t the time after excitation. From this equation, the integrated fluorescence intensity is calculated from I_0 and τ_m: $F = \int_0^\infty I_t dt = I_0\tau_m$. Thus

0003-2670/85/$03.30

$$F/\tau_m = (K/\tau_0)c = I_0 \quad (1)$$

Hieftje and Haugen [4] proposed the idea of using the value obtained by dividing the integrated fluorescence intensity by the fluorescence lifetime, because the value obtained is not affected by the quenching caused by collision of the sample molecules with dissolved oxygen. Equation 1 indicates that the pre-exponential factor of the decay curve is independent of dynamic fluorescence quenching and that a calibration plot can be constructed directly from the pre-exponential factor. Furthermore, measurement of the decay curve allows multicomponent determinations, and components with short-lived emissions such as Raman scattering and impurity fluorescence can readily be removed by suitable processing of the decay curves.

In this communication, ultratrace determinations of some PAHs by using a laser fluorimetric system are demonstrated and the advantages of time-resolved fluorimetry for sensitive and accurate determinations are discussed.

Experimental

Apparatus. A block diagram of the equipment is shown in Fig. 1. A transversely-excited atmospheric-pressure (TEA) nitrogen laser (Nippon Dynamic Distribution Company, JH-500A) was operated at 20 Hz, and used as a pumping source for a dye laser. The dye used, 4,4″-bis(butyloctyloxy)-*p*-quaterphenyl, was dissolved in toluene/ethanol (1:1). The wavelength and the linewidth of the dye laser were 386 nm and 5 nm, respectively. The output power of the dye laser was 40 μJ/pulse.

The dye laser beam is split by a quartz plate. The reflected laser beam is detected with a photodiode (NEC, LSD-39A) to trigger a sampling oscilloscope (Iwatsu, SS601B), and the transmitted beam is introduced into a non-fluorescent sample cuvette (10 mm × 10 mm, height 45 mm) from the bottom window. Fluorescence of the sample is focused onto the entrance slit of a monochromator (Jasco, CT-10) and is detected by a microchannel plate photomultiplier (Hamamatsu, R-1294U). The wavelength of the monochromator was adjusted to the emission maximum of the sample [benzo(ghi)-perylene 420 nm, benzo(a)pyrene 406 nm, benzo(k)fluoranthene 408 nm].

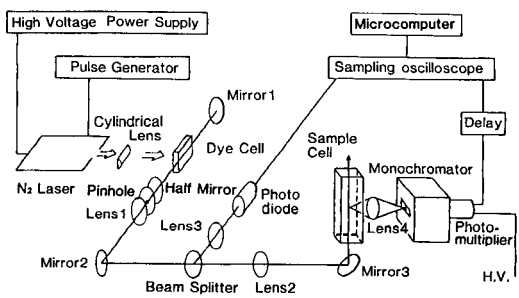

Fig. 1. Schematic diagram of the equipment.

The horizontal output of the sampling oscilloscope is introduced into a home-made comparator circuit and its output triggers the analog-to-digital converter of a microcomputer (SORD M223III). The vertical output is amplified and digitized by the microcomputer.

The fluorescence intensities were digitized at one hundred points in the decay curve and fifty decay curves were accumulated by the microcomputer to improve the signal-to-noise (S/N) ratio. It took five minutes to measure a decay curve. Least-squares fits are commonly used for calculation of the fluorescence lifetime [5, 6]. The fluorescence lifetimes and the pre-exponential factors were obtained from the slope and the intercept of the semilog plot of the decay curve, respectively. The time resolution of the instrument was 1 ns. All experiments were done at room temperature.

Procedure. Benzo(ghi)perylene (Aldrich Chemical Company), benzo(a)pyrene (Wako Pure Chemical Industries), and benzo(k)fluoranthene (RK Chemical Co.) were used as received. These standards were dissolved in benzene (fluorescence-spectroscopy grade; Merck). For deaeration, nitrogen was bubbled through the sample solutions for 2 min before the measurement, and the sample solution was isolated from the atmosphere with a glass cap. Leakage of oxygen into sample solutions was confirmed to be negligible.

Results and discussion

Deaeration. Calibration plots for deaerated and air-saturated PAH samples were constructed by using conventional fluorimetry. The fluorescence of benzo(ghi)perylene is strongly quenched by oxygen dissolved in the solution; the intensity for deaerated samples was about five times larger than that for air-saturated samples. Thus it is clear that deaeration will greatly improve the limit of detection, and that incomplete deaeration can cause serious errors in quantifying PAHs. Fluorescence decay curves were measured for the air-saturated and deaerated PAH samples by using time-resolved fluorimetry. The observed fluorescence lifetimes are listed in Table 1. The increased total signals (fluorescence enhancement) obtained by deaeration of the sample solutions are also indicated in Table 1. The values of F/τ_m are identical for

TABLE 1

Fluorescence lifetimes of polynuclear aromatic hydrocarbons

Compound	Fluorescence lifetimes (ns)		Fluorescence enhancement[a]
	Deaerated	Air-saturated	
Benzo(ghi)perylene	100	20	5.0
Benzo(a)pyrene	36	13	2.6
Benzo(k)fluoranthene	9	8	1.3

[a]Fluorescence enhancement is the ratio of the fluorescence intensities for the deaerated and air-saturated samples; it was measured with a conventional fluorimeter.

the deaerated and air-saturated samples and the left-hand side of Eqn. 1 is verified. These results are consistent with previously reported data [4, 7].

The decay curves for benzo(ghi)perylene measured at different concentrations are shown in Fig. 2. Deaeration of the sample solution increases the fluorescence lifetime, but the pre-exponential factor, i.e., the fluorescence intensity immediately after excitation, remains unchanged on deaeration. The pre-exponential factor is proportional to the sample concentration, and the slopes of the calibration plots measured under deaerated and air-saturated conditions are identical within an experimental error of 6%. These results verify the right-hand side of Eqn. 1. Similar results were obtained for benzo(a)pyrene and benzo(k)fluoranthene. It should be emphasized that the sample concentration can be determined accurately from the pre-exponential factor without being affected by dissolved oxygen.

Background correction. At concentrations below 1×10^{-9} M PAH solutions, background emission mainly originated from Raman scattering of benzene and from short-lived fluorescence of impurities in the solvent. The peak height of Raman scattering in the decay curve was 20—40 times larger than the pre-exponential factors of the fluorescence decay curves for 1×10^{-9} M PAH solutions. Figure 3 shows the decay curves for benzo(ghi)perylene obtained by subtracting the background emission data with the microcomputer. The signal intensities of the decay curves for both the sample solution and the blank solution exceeded the dynamic range of the analog-to-digital converter in the time region from 6 to 9 ns, and then the subtracted data showed zero signal intensity. The pre-exponential factor was calculated by extrapolating the data from 13 to 158 ns, and a calibration plot was constructed.

Detection limits. The detection limits for the PAHs in this study were evaluated from the precision of the observed pre-exponential factor. The fluorescence signal from the photomultiplier was large enough, and precision in the measurements was limited by the drift noise from the oscilloscope. The input voltage was usually adjusted to 1.4 V so as not to exceed the

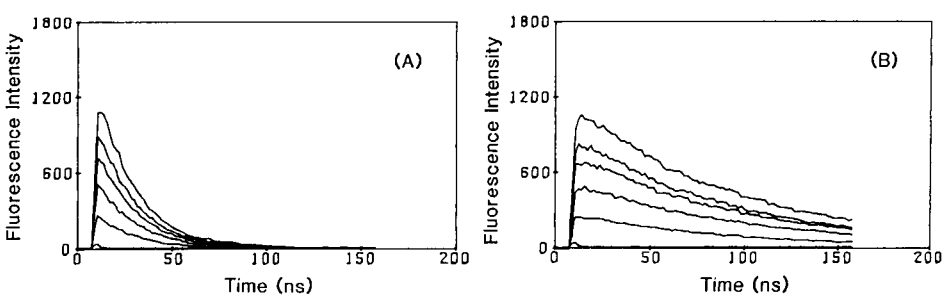

Fig. 2. Fluorescence decay curves for benzo(ghi)perylene in benzene: (A) air-saturated; (B) deaerated by bubbling nitrogen. Concentrations (from the top curve down): 5, 4, 3, 2, 1, and 0×10^{-7} M.

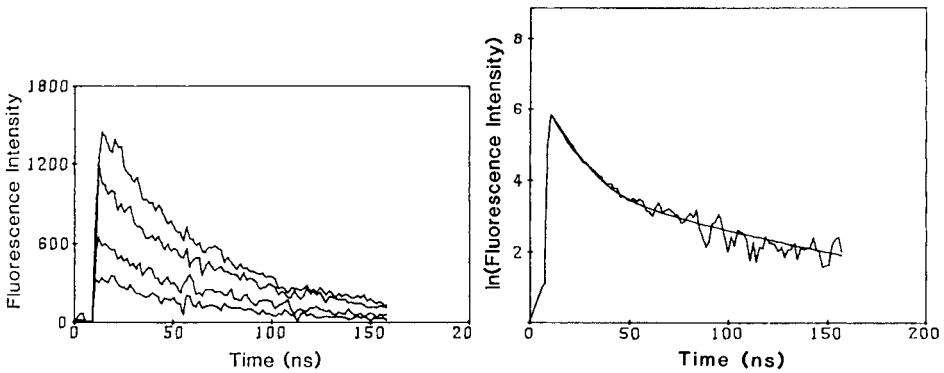

Fig. 3. Fluorescence decay curves for nitrogen-bubbled benzo(ghi)perylene solutions obtained by subtracting background emission. Concentrations (from the top curve down): 10, 7.5, 5.0, and 2.5 × 10^{-10} M.

Fig. 4. Fluorescence decay curve of a sample extracted from airborne particulates. See text for explanation.

maximum rating (±4.5 V), and the inherent noise was ±3 mV for the present equipment. Thus, the dynamic range was about 1500. The S/N ratio could be improved sevenfold by accumulation of signals over 50 measurements. The theoretical detection limits calculated from this evaluation and the observed pre-exponential factors for the sample are shown in Table 2. Short fluorescence lifetimes produce less accurate pre-exponential factors because the S/N ratio decreases after excitation; thus the actual detection limit can become high for species with short fluorescence lifetimes. The observed detection limits for the deaerated and air-saturated samples are also shown in Table 2. Deaeration of the sample solution improves the detection limits for benzo(ghi)perylene and benzo(a)pyrene, but scarcely affects the limit for benzo(k)fluoranthene. The improvement apparently comes from lengthening of the fluorescence lifetime (see Table 1) as predicted. These results are consistent with the observed error of ±39% in the pre-exponential factor for the air-saturated solution and of ±3% for the deaerated benzo(ghi)perylene solution at 2.5 × 10^{-9} M. The determination of benzo(k)fluoranthene is little affected by deaeration, because the fluorescence quenching effect is so small.

Application to airborne particulates. Samples obtained from the airborne particulates can include various PAHs [8—12] ; their determination is difficult by conventional fluorimetry. The fluorescence decay curve for a deaerated solution extracted from airborne particulates sample is shown in Fig. 4. The solid line represents the best-fit curve obtained by assuming the presence of three components with lifetimes of 100, 40 and 10 ns. This implies that benzo(ghi)perylene, benzo(a)pyrene, and benzo(k)fluoranthene are present, but this is not conclusive because the observed fluorescence lifetimes are not very accurate (±20 ns for the latter two components). For more reliable assignment, separation by high-performance liquid chromatography would

TABLE 2

Detection limits[a] for some polynuclear aromatic hydrocarbons

Compound	DL_1 (M)	DL_2 (M)	DL_3 (M)
Benzo(ghi)perylene	6×10^{-11}	9×10^{-11}	6×10^{-10}
Benzo(a)pyrene	4×10^{-11}	1×10^{-10}	4×10^{-10}
Benzo(k)fluoranthene	3×10^{-11}	5×10^{-10}	4×10^{-10}

[a]DL_1: theoretical detection limit calculated from the noise level of the sampling oscilloscope on the assumption of infinite fluorescence lifetimes. DL_2: observed detection limit for the deaerated sample. DL_3: observed detection limit for the air-saturated sample.

be necessary. Time-resolved fluorimetry is useful even in the chromatographic system not only for the temporal removal of unwanted emissions, but also for sensitive and precise determinations of the components from the observed pre-exponential factor of the decay curve.

The authors thank Kazumi Fukamachi for his gift of the real PAH sample extracted from airborne particulates in Omuta City. This research was supported by Grant-in-Aid for Environmental Science from the Ministry of Education of Japan.

REFERENCES

1 B. Stevens and B. E. Alger, J. Phys. Chem., 72 (1968) 2582.
2 C. S. Parmenter and J. D. Rau, J. Chem. Phys., 51 (1969) 2242.
3 A. P. Darmanyan, Chem. Phys. Lett., 86 (1982) 405.
4 G. M. Hieftje and G. R. Haugen, Anal. Chim. Acta, 123 (1981) 255.
5 E. Blatt, E. F. Treloar, K. P. Ghiggino and R. G. Gilbert, J. Phys. Chem., 85 (1981) 2810.
6 F. Heisel, J. A. Miehe and B. Sipp, Rev. Sci. Instrum., 52 (1981) 992.
7 I. B. Berlman, Handbook of Fluorescence Spectra of Aromatic Molecules, Academic Press, New York, 1971, p. 58.
8 T. Imasaka, K. Ishibashi and N. Ishibashi, Anal. Chim. Acta, 142 (1982) 1.
9 J. M. Daisey and M. A. Leyko, Anal. Chem., 51 (1979) 24.
10 K. Ogan, E. Katz and W. Slavin, Anal. Chem., 51 (1979) 1315.
11 J. R. Maple, E. L. Wehry and G. Mamantov, Anal. Chem., 52 (1980) 920.
12 G. Grimmer, J. Jacob, K. W. Naujack and G. Dettbarn, Anal. Chem., 55 (1983) 892.

Analytica Chimica Acta, 173 (1985) 373—375
Elsevier Science Publishers B.V., Amsterdam — Printed in The Netherlands

Short Communication

ANOMALOUS INFRARED SPECTRA OF CODEINE FREE BASE IN POTASSIUM BROMIDE PELLET

HIROMITSU KANAI*, VERONICA INOUYE and REGINALD GOO[a]

Chemistry Section, Laboratories Branch, Hawaii State Department of Health, Honolulu, HI 96813 (U.S.A.)

(Received 27th February 1985)

Summary. When codeine free base is incorporated into a potassium bromide pellet, its infrared spectrum can show anomalous phenomena between approximately 1100 cm^{-1} and 750 cm^{-1}. Investigation of the problem indicated that the anomalies are related to rapid formation of the codeine free base monohydrate during sample preparation.

Depending on the type of forensic infrared (i.r.) analysis required, the sample may need to be processed as a salt or as the free acid or base [1, 2]. Most basic drugs are first dissolved in 0.1 M sodium hydroxide or 5% (w/v) sodium hydrogencarbonate solution and are later extracted into chloroform as part of sample preparation [3]. During routine drug analysis, it was sometimes observed that codeine free base when extracted as above and incorporated into potassium bromide pellets produced anomalous phenomena from about 1100 cm^{-1} to 750 cm^{-1}. The bands at 1105, 1087, 1012, 955, 806, and 769 cm^{-1} changed to shoulder-like shapes, and the ratio of the 955 cm^{-1} to 968 cm^{-1} bands changed from 1.6 to 0.14.

The effect of moisture on the i.r. spectra from KBr pellets has been described [4—6]. The codeine free base is known to form a monohydrate [7]. This study showed that the anomalous behavior of codeine free base incorporated into KBr pellets is probably related to its monohydrate formation.

Experimental

The rapid KBr pellet method [8] was used. All the pellets were pressed at 15000 psi and scanned from 4000 cm^{-1} to 400 cm^{-1} on a Perkin-Elmer model 467 i.r. spectrometer with a 4X beam condenser attachment. The concentration of codeine free base in KBr was 1%. A codeine free base monohydrate was prepared as described in the Merck Index [7].

[a]Present address: Dept. of Public Works, City and County of Honolulu, Honolulu, HI, 96813.

0003-2670/85/$03.30

Results and discussion

Figure 1 shows the relevant portions of the i.r. spectra of codeine as free base, free base monohydrate, and as a mixture of these substances. Although most routine i.r. spectra of codeine free base in KBr pellets were identical to the spectrum as shown in Fig. 1C, some samples which were similarly prepared produced the spectra shown in either Fig. 1A or 1B.

To study this problem, a few microliters of distilled water were added to the 1% (w/w) codeine free base in KBr which had previously shown the i.r. spectral characteristic of the free base. This sample was air-dried, and recrystallized from chloroform; the KBr pellet of this sample showed an i.r. spectrum identical to that in Fig. 1A. Other portions of the sample were heated at 100°C for 5 min and 15 min, respectively. After the samples had cooled in a desiccator, the KBr pellets gave spectra similar to those shown in Fig. 1B and 1C, respectively. In further tests, codeine free base monohydrate was prepared in a KBr pellet. The spectrum was identical to that shown in Fig. 1A. The spectrum of another portion of codeine free base monohydrate

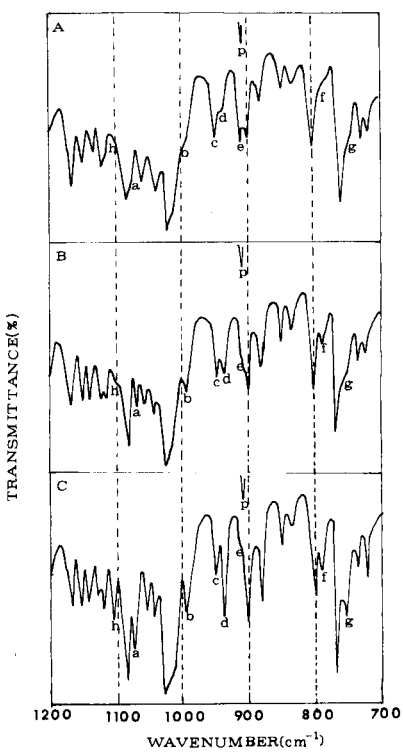

Fig. 1. The i.r. spectra of different codeine compounds incorporated in KBr pellets: (A) codeine free base monohydrate; (B) mixture of codeine free base and its monohydrate; (C) codeine free base. Bands: (p) polystyrene film calibration at 906.5 cm^{-1}; (h) 1105 cm^{-1}; (a) 1087 cm^{-1}; (b) 1012 cm^{-1}; (c) 968 cm^{-1}; (d) 955 cm^{-1}; (e) 925 cm^{-1}; (f) 806 cm^{-1}; (g) 769 cm^{-1}.

which had previously been heated for 15 min at 100°C and pelleted (KBr) was identical to the spectrum shown in Fig. 1C.

On the basis of these data, the anomalous i.r. spectral phenomenon of codeine free base is related to the formation of its monohydrate. Just as the monohydrate is rapidly formed, it can be removed by briefly heating the sample.

REFERENCES

1 J. A. Heagy, Anal. Chem., 42 (1970) 1459.
2 A. G. Allen, D. A. Cooper, W. O. Kiser and R. D. Cottrell, J. Forensic Sci., 26 (1981) 12.
3 E. G. C. Clarke, Isolation and Identification of Drugs, The Pharmaceutical Press, London, 1969, p. 27.
4 G. Duyckaerts, Analyst (London), 84 (1959) 201.
5 M. J. de Faubert Maunder, Practical Hints on Infra-red Spectrometry, Adam Hilger, London, 1971, p. 19.
6 H. A. Szymanski, Theory and Practice of Infrared Spectroscopy, Plenum Press, New York, 1964, p. 80.
7 P. G. Stecher, The Merck Index, 8th edn., Merck, Rahway, NJ, 1968, p. 276.
8 C. E. Meloan, Elementary Infrared Spectroscopy, Macmillan, New York, 1963, p. 29.

Analytica Chimica Acta, 173 (1985) 377—380.
Elsevier Science Publishers B.V., Amsterdam — Printed in The Netherlands

Short Communication

COMPARISON OF SECONDARY-ION MASS SPECTROMETRY AND COMPLEXIMETRIC TITRATION FOR THE DETERMINATION OF LEACHING OF MAGNESIUM FROM CHRYSOTILE ASBESTOS

I. M. SWENTERS, J. K. DE WAELE, J. A. VERLINDEN and F. C. ADAMS*
Department of Chemistry, University of Antwerp (U.I.A.), B-2610 Wilrijk (Belgium)
(Received 11th December 1984)

Summary. The dissolution of chrysotile asbestos in 0.05 M oxalic acid is evaluated by secondary-ion mass spectrometry and by titration of magnesium with EDTA. The results of the two methods agree closely; thus matrix effects in the utilization of sputtering depth profiles of the mass spectrometric determination do not influence the final results.

Chrysotile asbestos belongs to the serpentine group and has a hollow cylindrical structure caused by the disproportionately large brucite layers on a silicate framework [1, 2]. Most of its surface properties are similar to those of brucite (natural magnesium hydroxide). There is relatively little substitution of Mg^{2+} ions by Fe^{3+}, Fe^{2+} and Al^{3+} ions [3]. In recent years, much work has been devoted to understanding the relation between asbestos minerals and the diseases asbestosis and mesothelioma in the lungs [4, 5]. Leaching and partial dissolution by body fluids, with their many organic and inorganic components, is considered to be a complication in the understanding of the surface-related phenomena. It is assumed that the structural and compositional modifications are dominated by the release of magnesium ions from the chrysotile surface, which modifies the crystalline structure with the production of an ordered fibrous silica-gel layer as was indicated by infrared and nuclear magnetic resonance spectroscopy [6].

Recently, measurements of the dissolution kinetics of chrysotile asbestos in 0.05 M oxalic acid over the temperature range 0—80° C have been reported [7]. After treatment, the fractional release of magnesium from the fibres was determined from depth-profile measurements by secondary-ion mass spectrometry (s.i.m.s.). Diffusion coefficients were calculated by assuming a plane sheet model. The activation energy of 72.1 kJ mol^{-1} found is in agreement with earlier, less precise, data (60—80 kJ mol^{-1}) which relied on x-ray photoelectron spectroscopy [8, 9], although in both studies the instrumental techniques were not used quantitatively. In this communication, verification of the s.i.m.s. results by results obtained by compleximetric titration of the leached magnesium ions in solution is reported.

0003-2670/85/$03.30

Experimental

Materials and reagents. The asbestos mineral studied was Zimbabwean chrysotile A, supplied by the UICC (International Union Against Cancer) [10]. The oxalic acid was pro Analysi grade (Merck). Titriplex-III solution (0.1 M Titrisol from disodium-EDTA; Merck) was used with an aqueous 0.1% (w/v) solution of calmagite (3-hydroxy-4-(2-hydroxy-5-methylphenylazo)-1-naphthalene sulphonic acid; Janssen Chimica, Belgium) as indicator. The buffer solution (pH 10.00 ± 0.05, 20°C) was prepared by diluting 570 ml of ammonia liquor (d = 0.90) and 70 g of ammonium chloride (both pro Analysi, Merck) to 1 l with water.

Fibre treatment. About 60 mg of the chrysotile fibres was suspended in 30 ml of 0.05 M oxalic acid. Treatment times were between 5 min and 312 h while treatment temperatures ranged from 0 to 80°C. At the end of each experiment, the suspensions were filtered on Schleicher & Schüll filters (no. 589, 110-mm diameter, Schwarzband) and washed with 45 ml of twice-distilled water.

Titrimetric procedure. Aliquots (1 ml) of the filtrate were diluted to 25 ml, buffered with 10 ml of the buffer solution and titrated with a 10^{-3} M EDTA solution to the colour change from red to pale blue in the presence of 2—4 drops of the calmagite solution [11].

Secondary-ion mass spectrometry. Depth profiles were obtained with a Cameca IMS-300 ion microscope equipped with an electrostatic sector and an on-line microcomputer [12]. Asbestos fibres were suspended in twice-distilled water and deposited onto a gold-coated glass substrate. After drying, the samples were mounted into the sample chamber where they were bombarded with a 5.5-keV O_2^+ primary ion beam, which was rastered over an area of 500 × 500 μm^2. A mechanical aperture placed in the image plane of the secondary ion extraction lens restricted the sampled area to a diameter of 200 μm. The primary ion density was 10^{-6}—10^{-5} A cm^{-2} which provided an erosion rate of ca. 0.5 nm min^{-1}. The $^{24}Mg^+$ ion was measured at a residual oxygen pressure of ca. 2×10^{-3} Pa. The $^{28}Si^+$ signal was used for normalization of the data.

Results and discussion

The diffusion coefficients were determined with s.i.m.s. by measurement of the fractional release of magnesium from the fibre through depth profiling. Figure 1 gives an example showing the relative intensity ratio as a function of sputtering time. Measured profiles are shown for treatments with 0.05 M oxalate for 1, 2 and 5 h, respectively, all at room temperature. The intensity ratio for untreated fibres was 3.4 ± 0.2. From such depth profiles, the fractional release of magnesium from the fibres can be precisely determined and from these the diffusion coefficients can be calculated. Their accuracy depends on the assumption that the intensity ratios used are linearly proportional to the concentration ratios, i.e., that matrix effects are the same for raw and leached fibres and are not a function of depth in the fibres after

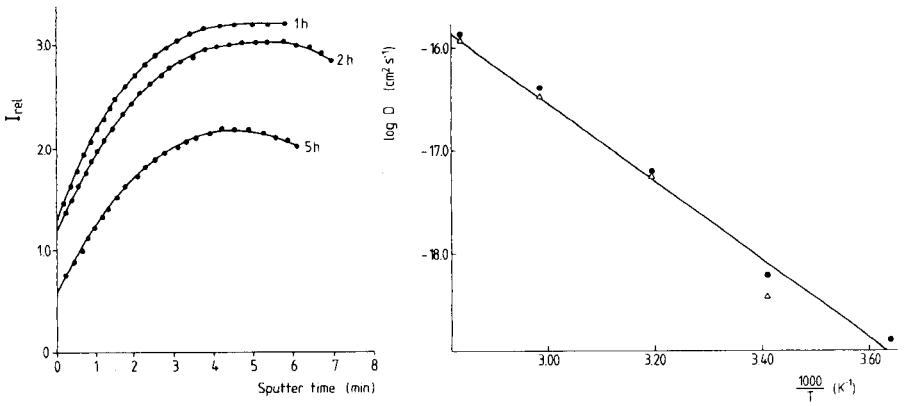

Fig. 1. Concentration/depth profiles of magnesium in chrysotile, measured after treatment in 0.05 M oxalate at room temperature for 1, 2 and 5 h. I_{rel} (= I_{Mg^+}/I_{Si^+}) is plotted as a function of sputtering time.

Fig. 2. Arrhenius plot of the logarithmic diffusion coefficient of magnesium in chrysotile determined by (•) s.i.m.s.; (△) complexim etric titration.

leaching. The existence of a matrix-dependent sensitivity, however, is common in s.i.m.s. An independent analytical method was therefore used to verify this assumption.

The relative fractional release of magnesium (% F) obtained by complexim etric titration as a function of the treatment time in seconds (t) was found to correspond to the relationship % $F = a + bt^{1/2}$, with a regression coefficient $r = 0.995$ and with $a = 6.94 \pm 0.084$ and $b = 0.0703 \pm 0.0002$ when the bulk magnesium concentration was 27.4%, derived from bulk analysis by energy-dispersive x-ray spectrometry [13]. The slight deviation from the origin is due to an overestimation of this bulk concentration by ca. 1.9% magnesium. This relationship was followed up to a time of ca. 300 h.

The diffusion coefficients obtained by complexim etric titration are compared with those obtained by s.i.m.s. in Fig. 2 as a plot of log D versus the inverse absolute temperature. The results obtained by both methods agree remarkably well with an activation energy of 70.1 kJ mol^{-1} by the titrimetric method compared with 72.1 kJ mol^{-1} by s.i.m.s. Other published data are 75.6 kJ mol^{-1} obtained by Bleiman and Mercier [14], 63.0 kJ mol^{-1} obtained by Papirer et al. [15], both using wet chemical methods, and the range of 60—80 kJ mol^{-1} given by Thomassin et al. [9].

The data obtained prove that s.i.m.s., despite its strong matrix-dependent sensitivity can provide accurate results for relative depth profiling based on signal intensities. It has the advantage that only small amounts of material are required.

This research was funded by the EEC (through research grant ENV-620-B(RS)) and by the Interministerial Commission for Science Policy, Belgium,

through research grant 80-85/10. J. D. W. is indebted to the Instituut tot Aanmoediging van het Wetenschappelijk Onderzoek in Nijverheid en Landbouw for financial support.

REFERENCES

1 S. Speil and J. A. Leineweber, Environ. Res., 2 (1969) 166.
2 J. E. Chisholm, in S. S. Chissick and R. Derricott (Eds.), Asbestos, Vol. 2, Properties, Applications and Hazards, Interscience-Wiley, New York, 1983, Chap. 4.
3 S. Chowdhury, J. Appl. Chem. Biotechnol., 25 (1975) 347.
4 S. Chowdhury, Surface Chemical Studies of Asbestos Minerals, Ph.D. Thesis, University of London, 1973.
5 G. Monchaux, J. Bignon, M. C. Jaurand, J. Lafuma, P. Sebastien, R. Masse, A. Hirsch and J. Goni, Carcinogenesis, 2 (1981) 229.
6 F. Paco, L. Van Gaugh and J. J. Fripiat, Bull. Soc. Chim. Fr., 7—8 (1976) 1022.
7 J. A. Verlinden, J. K. De Waele, I. M. Swenters and F. C. Adams, Surf. Interf. Anal., 6 (1984) 286.
8 J. Goni, J. H. Thomassin, M. C. Jaurand and J. C. Touray, in L. H. Ahrens (Ed.), Origin and Distribution of the Elements, Pergamon Press, Oxford, 1979, p. 807.
9 J. H. Thomassin, J. Goni, P. Baillif, J. C. Touray and M. C. Jaurand, Phys. Chem. Minerals, 1 (1977) 385.
10 V. Timbrell and R. E. Rendall, Powder Technol., 5 (1971—1972) 279.
11 D. A. Skoog and D. M. West, Fundamentals of Analytical Chemistry, 3rd edn., Holt, Rinehart and Winston, New York, 1976, p. 738.
12 Z. Johan, J. Goni, C. Sarcia, G. Bonnaud and J. Bignon, Proceedings of the 6th International Congress on Organic Geochemistry, Rueil, France, 1973, p. 883.
13 M. J. Luys, G. De Roy, E. F. Vansant and F. C. Adams, J. Chem. Soc., Faraday Trans. 1, 78 (1982) 3561.
14 C. Bleiman and J. P. Mercier, Bull. Soc. Chim. Fr., 3—4 (1975) 529.
15 E. Papirer, G. Dovergne and P. Leroy, Bull. Soc. Chim. Fr., 5—6, 651 (1976).

Analytica Chimica Acta, 173 (1985) 381—386
Elsevier Science Publishers B.V., Amsterdam — Printed in The Netherlands

Short Communication

ASSAY OF D-CYCLOSERINE BY CHLORAMINE-B, BROMAMINE-T, AND BROMAMINE-B

B. JAYARAM

Department of Chemistry, V.V. Pura College of Science, Bangalore-560 004 (India)

N. M. MADE GOWDA

Division of Biochemistry, Department of Human Biological Chemistry & Genetics, The University of Texas Medical Branch, Galveston, TX, 77550 (U.S.A.)

(Received 19th November 1984)

Summary. The reaction between D-cycloserine (DCS) and aromatic *N*-haloamines proceeds quantitatively over a wide range of experimental conditions. Simple titrimetric procedures for the assay of DCS are described. Oxidation of DCS involves an eight-electron change and the oxidation products are identified. The methods can be used for the assay of the antibiotic in medicinal preparations as well as for calculating the number of ligand molecules present in metal complexes of DCS.

Aromatic sulfonyl haloamines are useful as redox titrants [1, 2]. D-Cycloserine (DCS; 4-amino-3-isoxazolinone) is one of the simplest structures to possess antibiotic activity. The reported methods for the assay of DCS involve colorimetric, potentiometric, and chromatographic techniques [3—6]. The mechanism of oxidation of DCS at a glassy carbon electrode has been reported [7]. There are no simple titrimetric methods for DCS. The present communication reports on titrations of DCS with chloramine-B (CAB), bromamine-B (BAB) and bromamine-T (BAT). The methods described are simple and reasonably rapid. They are suitable for the assay of DCS in pharmaceutical preparations and for estimating the number of DCS ligands in metal complexes.

Experimental

D-cycloserine (Sigma Chemicals) was used as received. Colorimetric assay [5] showed the purity to be 99.9%. Aqueous solutions (1 mg ml^{-1}) were prepared by dissolving the required amount of DCS in triple-distilled water or standard buffer solution [8].

Chloramine-B ($C_6H_5SO_2NClNa\ 1.5\ H_2O$) was prepared [9] by chlorination of benzenesulfonamide dissolved in 4 M sodium hydroxide at 70°C. The compound was recrystallized from water; its purity was checked by iodimetric titration of the active chlorine (theor. 14.7%; found 14.2%) present, and by recording its Fourier-transform ^1H- and ^{13}C-n.m.r. spectra (obtained

0003-2670/85/$03.30

on a Varian 60-MHz and a Brucker WH 270-MHz nuclear magnetic resonance spectrometer, respectively) in $CDCl_3$ solvent with tetramethylsilane (TMS) as the internal standard. [^{1}H-spectrum (δ relative to TMS): 7.86 (doublet corresponding to H ortho to hetero atom), 7.72 (multiplet corresponding to H meta to hetero atom); the latter integrates to three protons; the coupling constant $J_{o,m}$ is 8.0 Hz. ^{13}C-spectrum (ppm relative to TMS): 142.48 (C-1 attached to S atom), 134.37 (C-4, para to the hetero atom); 131.26 (C-2,6) and 129.37 (C-3,5).]

Bromamine-T (p-$CH_3C_6H_4SO_2NBrNa\ 3H_2O$) was obtained [10] by dissolving 20 g of dibromamine-T (prepared by brominating chloramine-T [11] with stirring in 30 ml of 4 M sodium hydroxide at 25 ± 2°C and cooling the solution in ice. Pale yellow crystals of BAT that formed were filtered under suction, washed quickly with a minimum quantity of cold water and dried over phosphorus pentoxide. Their purity was checked by iodimetric determination of the active bromine content (theor. 24.5% Br; found 24.4% Br) and by recording its ^{1}H- and ^{13}C-n.m.r. spectra in $CDCl_3$ solvent. [^{1}H-spectrum (δ relative to TMS): 2.4 (singlet corresponding to $-CH_3$); 7.8 (doublet for ortho H); 7.4 (doublet for meta H); the coupling constant $J_{o,m}$ is 8.0 Hz. ^{13}C-spectrum (ppm relative to TMS): 145.39 (C-1, carbon attached to S atom); 140.50 (C-4); 131.75 (C-2,6); 129.40 (C-3,5); 23.0 (methyl carbon).]

Bromamine-B ($C_6H_5SO_2NBrNa\ 1.5H_2O$) was prepared [12] by dissolving about 32 g of dibromamine-B in about 50 ml of 4 M sodium hydroxide, as above, and cooling in ice. Pale yellow crystals were filtered, washed with a little cold water, dried over anhydrous calcium chloride, and recrystallized from hot water at 50°C. Their purity was checked as for bromamine-T (theor. 28.0% Br; found 27.9% Br) and by recording the F.t. n.m.r. spectra in D_2O. [^{13}C-spectrum: (ppm relative to TMS) 143.38 (C-1, carbon attached to S atom), 134.30 (C-4, para to hetero atom), 131.26 (C-2,6) and 129.31 (C-3,5).]

Approximately 0.025 M solutions of the oxidants were prepared in distilled water and standardized by the iodimetric methods. Compounds of acceptable grades of purity were used in preparing other solutions.

Preparation of the complexes. The palladium(II) and platinum(II) complexes ($Pd(DCS)_2Cl_2\ 2H_2O$, $Pd(DCS)_3Br_2\ H_2O$, $Pt(DCS)_2Cl_2$, and $Pt(DCS)_3Br_2\ 3H_2O$) were obtained [13] by reaction of MX_4 (M = Pt or Pd; X = Cl or Br) with the ligand (DCS) in molar ratios of 1:2 and 1:3. The complexes were precipitated by addition of ethanol and diethyl ether. The compounds were purified by repeated washing with water, ethanol and diethyl ether and were dried over phosphorus pentoxide. Results for carbon, hydrogen and nitrogen agreed with the above formulae; melting points agreed with literature data [13]. A known amount of the sample was dissolved in anhydrous acetic acid.

Preliminary studies. Portions (5 ml) of DCS solution were added to known volumes (40—60% in excess) of the oxidant solution containing enough acid,

base or buffer (Table 1) in glass-stoppered Erlenmeyer flasks. The reaction mixtures were shaken and set aside for different intervals of time. Then 10 ml of 1 M sulfuric acid and 10 ml of 10% (w/v) potassium iodide solution were added and the liberated iodine was titrated with standard sodium thiosulfate solution to a starch end-point. A blank titration was done with the oxidant under identical conditions. Based on the reproducible stoichiometry of eight-electron change per mole (Table 1) observed in these experiments for the oxidation of DCS by each of the three haloamines, the following methods are recommended.

Assay of DCS with CAB. Add 25 ml of 0.025 M CAB solution to an aliquot of DCS solution containing enough hydrochloric acid to give an overall concentration of 0.001—0.01 M. After 30 min, titrate the unreacted CAB iodimetrically, as above.

Assay with BAT. Add aliquots of the DCS solution to 25 ml of 0.025 M BAT solution containing 0.5—1.0 M sodium hydroxide. After 30 min, titrate the unconsumed BAT iodimetrically.

Assay with BAB. Add 25 ml of 0.025 M BAB solution to aliquots of DCS solution containing sodium hydroxide (final concentration of 0.1—0.5 M). After 20 min, titrate the unreacted BAB iodimetrically.

Assay of DCS in pharmaceutical samples and in metal complexes. For tablets, grind about 20 tablets to a fine powder. Dissolve about 100 mg of the powder in 150 ml of water in a beaker with sitrring [6]. Filter. Dilute the filtrate and washings to 250 ml in a volumetric flask. Take 10 ml of the solution for the assay as described above. For capsules, remove the shell from about 20 capsules and grind the contents to a fine powder. Shake 100 mg of the powder with 150 ml of water for about 30 min [6]. Filter. Dilute the filtrate and washings to 250 ml, and proceed as above. For metal complexes of DCS, use an aliquot of the solution of the metal complex in the above general procedures.

The numbers of electrons exchanged per mole are 8 for DCS, 16 for

TABLE 1

Extent of oxidation of D-cycloserine with *N*-haloamines in various media[a]

Medium	Mol oxidant/mol DCS			Medium	Mol oxidant/mol DCS			Medium	Mol oxidant/mol DCS		
	CAB	BAT	BAB		CAB	BAT	BAB		CAB	BAT	BAB
0.1 M HCl	3.65	2.21	2.94	pH 1	3.71	2.22	2.95	pH 8	0.65	2.25	2.92
0.1 M H_2SO_4	3.43	2.15	2.68	pH 2	3.48	2.81	2.25	pH 9	0.38	2.31	3.32
0.1 M $HClO_4$	3.32	2.10	2.48	pH 3	3.36	2.76	1.25	pH 10	0.12	2.42	3.68
0.001 M HCl	4.00	—	—	pH 4	3.30	3.12	3.43	0.1 M NaOH	0.00	—	4.00
0.005 M HCl	4.00	—	—	pH 5	3.20	3.25	3.20	0.25 M NaOH	0.00	—	4.00
0.01 M HCl	4.00	—	—	pH 6	2.81	2.83	3.14	0.5 M NaOH	0.00	4.00	4.00
0.01 M H_2SO_3	3.14	—	—	pH 7	2.20	2.29	2.87	1.0 M NaOH	0.00	4.00	—

[a]Reaction for 30 min at 25°C of 5 ml of (1 mg ml^{-1}) DCS solution with 25 ml of 0.025 M oxidant.

$Pd(DCS)_2Cl_2$ $2H_2O$ and $Pt(DCS)_2Cl_2$, and 24 for $Pd(DCS)_3Br_2$ H_2O and $Pt(DCS)_3Br_2$ $3H_2O$.

Results and discussion

Table 1 shows the extent of oxidation of DCS with the *N*-haloamines in various media in 30 min at 25 ± 2°C. The oxidation of DCS by CAB is stoichiometric only in the presence of hydrochloric acid (0.001—0.01 M); the extent of oxidation decreases with increase in pH and is very slow in alkaline solutions. Oxidation by BAT or BAB is slow and incomplete in mineral acids and in buffers, but the required stoichiometry is obtained in 0.5—1.0 M sodium hydroxide with BAT. However, a reproducible stoichiometry is observed in 0.1—0.5 M sodium hydroxide with BAB. The time-dependence of the oxidation with different haloamines is shown in Fig. 1; 100% completion of the reaction occurs in about 30 min.

The results of DCS determinations are given in Table 2. A comparison of the standard deviations shows that the precision of the results is in the order:

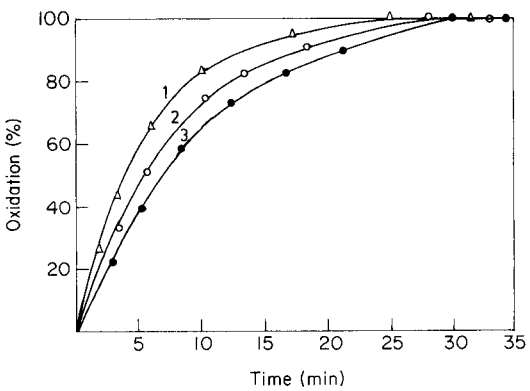

Fig. 1. Variation of % oxidation of D-cycloserine by *N*-haloamines with time. Curves: (1) CAB, 0.01 M HCl; (2) BAB, 0.1 M NaOH; (3) BAT 0.5 M NaOH. (1×10^{-3} M DCS, 1×10^{-2} M Oxidant.)

TABLE 2

Performance data for determination of D-cycloserine with *N*-haloamines

DCS taken (mg)	DCS found (mg)[a]		
	CAB	BAB	BAT
2.10	2.10 ± 0.01	2.11 ± 0.015	2.10 ± 0.015
7.28	7.28 ± 0.025	7.28 ± 0.02	7.28 ± 0.02
12.51	12.50 ± 0.04	12.55 ± 0.01	12.51 ± 0.03
22.25	22.26 ± 0.045	22.26 ± 0.04	22.25 ± 0.04

[a]Average of five trials for each sample size with standard deviation.

TABLE 3

Assay of the antibiotic in formulations and in metal complexes

Sample	Antibiotic present (mg)	Antibiotic found (mg)[a]		
		CAB	BAB	BAT
Tablet[b]	10.26	10.27	10.23	10.24
Capsule[b]	10.54	10.52	10.56	10.53
$Pt(DCS)_2Cl_2$	5.15	5.14	5.12	5.16
$Pd(DCS)_2Cl_2 \cdot 2H_2O$	5.23	5.26	5.21	5.22

[a]Samples from Acichem Labs, Bombay, India, with nominal contents. [b]Average of five trials for each oxidant.

BAB > BAT > CAB. Table 3 shows the recoveries of DCS obtained with tablets, capsules and the metal complexes. The results are accurate within about 1%.

With the proposed procedures, DCS undergoes an eight-electron oxidation (Table 1). It is known that DCS, in aqueous hydrochloric acid, undergoes hydrolysis [14] giving hydroxylamine and serine. Therefore, one could expect subsequent oxidation of these hydrolyzed products. In these reactions, the oxidants, CAB, BAB, and BAT, undergo two-electron reductions forming the corresponding sulfonamides. The stoichiometry of oxidation of DCS by the *N*-haloamines can be represented by

$$2C_3H_6N_2O_2 + 8RNXNa + 3H_2O \rightarrow 2HCOCN + N_2O + 2CO_2 + 8RNH_2 + 8Na^+ + 8X^-$$

where R = $C_6H_5SO_2^-$ and X = Cl or Br for CAB and BAB; and R = p-$CH_3C_6H_4SO_2^-$ and X = Br for BAT. The presence of *p*-toluenesulfonamide, the reduction product of BAT, was identified by paper chromatography [15]. Benzenesulfonamide formed in the reaction with CAB and BAB was detected [16] by thin-layer chromatography. The nitrile formed in the reaction was detected by the Werner's test [17].

The stoichiometry of oxidation was unaffected by the reversal of the order of addition of the reagents. The presence of foreign ions such as Na^+, K^+, Zn^{2+}, Ba^{2+}, sulfate, perchlorate and phosphate (up to 0.2 M) had no influence on the rate of oxidation. Addition of chloride ions slightly accelerated the rate of oxidation. Because with CAB (Table 1) the stoichiometric oxidation takes place in 0.001—0.010 M hydrochloric acid but not in buffers at pH 2—3 (84—87% reaction) or in 0.01 M sulfuric acid (79% reaction), the chloride ion effect seems to be responsible for the completion of the reaction in hydrochloric acid.

The authors are grateful to the authorities of India Institute of Science, Bangalore, India, for the ^1H- and ^{13}C-F.t. n.m.r. spectra.

REFERENCES

1 V. J. Jennings and E. Bishop, CRC Crit. Rev. Anal. Chem., (1974) 407.
2 M. M. Campbell and G. Johnson, Chem. Rev., 78 (1978) 66.
3 K. Tadeusz, K. G. Zuzanna and K. Wlodzimierz, Antibiotics, Vol. 1, Pergamon Press, London, 1967, p. 729.
4 F. D. Snell and C. L. Hilton, Encyclopedia of Industrial Chemical Analysis, Vol. 5, Interscience, New York, 1967, pp. 510—513.
5 F. D. Snell and C. T. Snell, Colorimetric Methods of Analysis, Vol. IV, Van Nostrand, New York, 1971, p. 193.
6 British Pharmacopoeia, Vol. II, Department of Health and Social Security: Ministry of Health and Social Services for Northern Ireland, 1980, p. 528.
7 M. Masaichiro and Shigeko, Chem. Pharm. Bull., 27 (1979) 142.
8 A. Findlay, Practical Physical Chemistry, Longmans, London, 1954, p. 268.
9 Chrzaszczewska, Bull. Soc. Sci. Lett. Lodz. Cl., III 3 (1962).
10 C. G. R. Nair, R. L. Kumari and P. Indrasenan, Talanta, 25 (1978) 525.
11 C. G. R. Nair and P. Indrasenan, Talanta, 23 (1976) 239.
12 D. S. Mahadevappa and M. S. Ahmed, Talanta, 27 (1980) 669.
13 C. Preti and G. Tosi, J. Coord. Chem., 9 (1979) 125.
14 R. M. Evans, The Chemistry of Antibiotics Used in Medicine, Pergamon Press, New York, 1965, p. 10.
15 D. S. Mahadevappa and N. M. M. Gowda, Talanta, 22 (1975) 771.
16 H. S. Yathirajan, D. S. Mahadevappa and Rangaswamy, Talanta, 27 (1980) 62.
17 E. A. Werner, J. Chem. Soc., 123 (1923) 2577.

AUTHOR INDEX

(continued from inside back cover)

(continued from outside back cover)

(continued on facing page)

CONTENTS

(Abstracted, Indexed in: Anal. Abstr.; Biol. Abstr.; Chem. Abstr.; Curr. Contents Phys. Chem. Earth Sci.; Life Sci., Index Med.; Mass Spectrom. Bull.; Sci. Citation Index; Excerpta Med.)

(continued on inside back cov